

INTERNATIONAL MINERALOGICAL ASSOCIATION

**PAPERS AND PROCEEDINGS**  
OF THE  
**FIFTH GENERAL MEETING**

Cambridge, England

August 30—September 3, 1966

THE MINERALOGICAL SOCIETY, LONDON

1968

# International Mineralogical Association

An Association of 24 National Mineralogical Societies

* President	C. E. Tilley
First Vice-President	H. Strunz
Second Vice-President	D. S. Korzhinski
* Secretary	A. Preisinger
* Treasurer	L. G. Berry
Councillors	T. F. W. Barth
	J. Kutina
	T. Watanabé
Past President	D. Jerome Fisher

\* Member of the Executive Committee.

---

## COMMISSIONS

### *Abstracts*

Th. Hügi, Chairman  
R. A. Howie, Secretary

### *Cosmic Mineralogy*

D. P. Grigoriev, Chairman  
E. P. Henderson, Secretary

### *Mineral Data*

H. Strunz, Chairman  
J. R. Butler, Secretary

### *Museums*

C. Frondel, Chairman  
P. C. Zwaan, Secretary

### *Ore Microscopy*

W. Uytendogaardt, Chairman  
S. H. U. Bowie, Secretary

### *Teaching*

C. S. Hurlbut, Chairman  
E. den Tex, Secretary

### *New Minerals and Mineral Names*

M. Fleischer, Chairman  
C. Guillemin, Secretary

Unesco subvention—1968—DC/2.1/414/26

Printed by Adlard & Son Ltd., Dorking

## Foreword

THE fifth general assembly of the International Mineralogical Association was held at Cambridge, August 30 to September 3, 1966, sponsored by the Mineralogical Society of Great Britain and Ireland and the Department of Mineralogy and Petrology, University of Cambridge.

The programme Chairman for the meeting was T. F. W. Barth and the Chairmen for each of the three main sessions were: M. J. Buerger and R. Kern, Symposium I on Crystal Growth, with special reference to minerals, and Bonding Forces in Mineral Structures; P. Gay and J. Zussman, Symposium II on Pyroxenes and Amphiboles; B. H. Mason and H. Neumann, General Session. The programme included two special lectures: Theory of Chemical Valence and its relation to Bonding in Silicates by D. W. J. Cruickshank, and The Relation of Lattice Dynamics to Chemical Bonding by W. Cochran. In all 102 papers were presented (23 in Symposium I, 31 in Symposium II, 42 in the General Session, with 6 papers presented at an extra session, devoted to Methods in Reflected Light, under the Chairmanship of N. F. M. Henry).

Publication of papers submitted for the two Symposia has been undertaken jointly by the International Mineralogical Association and the Mineralogical Society and has been aided by a generous grant from the International Union of Geological Sciences. Other papers are printed by title and abstract. Editing of papers has been carried out by P. Gay, A. F. Seager, H. F. W. Taylor, and J. Zussman, who wish to express their thanks to numerous colleagues for their help. The Association is especially appreciative of the work of M. H. Hey, Editor of the Mineralogical Magazine, in seeing the volume through the press.

C. E. TILLEY.

## Table of Contents

<i>Proceedings of the International Mineralogical Association</i>	<i>page vii</i>
<i>Symposium I: Bonding Forces and Crystal Growth in Minerals</i>	
Paramagnetic resonance of electron-hole centres in minerals L. V. Bershov and A. S. Marfunin	1
The strength of bonding forces in mineral structures A. S. Povarennykh	6
The influence of dislocation-strain energy on crystal morphology P. J. Shlichta	13
Measurement and interpretation of infra red pleochroism in minerals J. Zemann	20
Crystal-field spectra and chemical bonding in manganese minerals K. L. Keester and W. B. White	22
Applications of the Mössbauer effect to mineralogy G. M. Bancroft and R. G. Burns	36
Growth of diamond and cubic boron nitride from multi-component systems P. J. Gielisse	43
La croissance du quartz lamellaire sur l'exemple des cristaux de la Gardette (Isère, France) B. Poty	54
Macro- and micro-morphology of quartz and pyrite I. Sunagawa and Y. Endo	63
Growth of phlogopite crystals in marble from Quebec R. Kretz	85
Comparison between theoretical and observed morphology of crystals with the rutile type structure P. Hartman	94
Notation and genetic significance of crystal habits I. Kostov	100
Crystal growth of galena J. Banfield and A. F. Seager	110
Inclusions of gases in minerals H. Arming and A. Preisinger	117
An investigation of natural and synthetic quartz by the Hilger-Chance refractometer V. B. Tatarsky and V. F. Chernyshova	123
Substitutional and interstitial impurities in quartz and their mineralogical significance V. A. Frank-Kamenetsky and I. E. Kamentsev	131
The geochemical significance of dendritic-skeletal crystallization in polymetallic ore deposition processes R. O. Radkevich	140
Vergleichende Untersuchungen der Farb- und Lumineszenzeigenschaften natürlicher und gezüchteter definiert dotierte Fluorite K. Recker, A. Neuhaus, and R. Leckebusch	145

Thermodynamique et cinétique de formation d'une texture par nucléation dans un champ de tension . . . . .	M. Bienfait and R. Kern	153
The relative orientation of solid mineral inclusions in diamond . . . . .	J. W. Harris	163
Summaries of other papers presented in Symposium I . . . . .		169

*Symposium II: Amphiboles and Pyroxenes*

Crystal-field phenomena and iron enrichments in pyroxenes and amphiboles . . . . .	R. G. Burns	170
Étude magnétique de pyroxènes et d'amphiboles . . . . .	M. M. Babkine, J. Bolfa, J. C. Reithler, and C. Zeller	184
The use of amphiboles to illustrate trends in contact metamorphism . . . . .	B. J. Cahill (née Macara)	189
Nature des hornblendes et types de métamorphisme . . . . .	J. Fabriès	204
An attempt to rationalize the classification of natural pyroxenes of space group $C2/c$ . . . . .	I. V. Ginzburg	212
The $\alpha$ - $\beta$ -LiAlSi <sub>2</sub> O <sub>6</sub> (spodumene) transition from 5 000 to 45 000 lb/in <sup>2</sup> $P_{H_2O}$ . . . . .	A. D. Edgar	222
Classification of the amphiboles . . . . .	E. J. W. Whittaker	232
Hydrothermal investigations and stability relations of synthetic gedrites . . . . .	Th. J. Hinrichsen	243
Studies on synthetic alkali amphiboles . . . . .	R. Phillips and G. Rowbotham	249
Synthesis and stability field of cummingtonite . . . . .	K. Schürmann	255
On the chemical composition, properties, and mineral paragenesis of riebeckite-arfvedsonite . . . . .	V. I. Kovalenko	261
On the amphiboles of the hastingsite-pargasite series . . . . .	D. P. Serdyuchenko	285
Chemistry of the hastingsitic amphiboles from the Marangudzi igneous complex, Southern Rhodesia . . . . .	C. M. B. Henderson	291
Redox behaviour of amosite . . . . .	W. E. Addison and J. H. Sharp	305
The alkalic amphibole of the Lueshe carbonatite . . . . .	H. Jans and P. de Béthune	312
On the pleochroic formula of alkalic amphiboles . . . . .	P. de Béthune and H. Jans	315
Some aspects of the chemical composition of non alkaline monoclinic pyroxenes from effusive rocks . . . . .	G. V. Gvakharia	319
Phase transitions of enstatite in the Earth's mantle . . . . .	V. A. Kirkinskii	323
Über Kosmochlor (Ureyit) . . . . .	A. Neuhaus	329
Summaries of other papers presented in Symposium II . . . . .		334
<i>Titles and authors of other papers presented in Open Sessions at the Meeting</i> . . . . .		340

## **Proceedings of the I.M.A.**

*Fifth General Business Meeting of Delegates*

Cambridge, August 31 to September 3, 1966

Anton Preisinger, Secretary

THE *first session* of the fifth General Business Meeting of Delegates of the 24 Member Societies of the I.M.A. was held in the Department of Mineralogy and Petrology, University of Cambridge, England, on August 31, 1966 at 5.15 p.m.

The delegates of 23 Member Societies were present: Austria, Belgium, Brazil, Bulgaria, Canada, Czechoslovakia, Denmark, Egypt, Finland, France, Germany, Hungary, India, Italy, Japan, Netherlands, Norway, Spain, Sweden, Switzerland, United Kingdom, U.S.A., and U.S.S.R., New Zealand was not represented. Algeria, Australia, Eire, Malaysia, Sudan, and Turkey were represented by observers.

*Opening remarks.* The President, Prof. C. E. Tilley, and Dr. Claringbull, President of the Mineralogical Society of Great Britain and Ireland, welcomed the delegates and other participants.

The President said the Association was greatly indebted to the Mineralogical Society and the Department of Mineralogy and Petrology for their invitation to hold the sessions of the I.M.A. at Cambridge. The preparatory work of the Local Committee ensured that this was to be a most successful meeting. Altogether 311 mineralogists with 54 accompanying members, from twenty-nine countries, had registered, the meeting thus forming the largest gathering of mineralogists in the Association's history.

### *Reports of the officers*

The *Secretary*, Prof. A. Preisinger, reported that within the short time, since December 1964, when he became secretary, no important business was handed over to him except the preparation of the business of the present meeting. The proceedings and 29 papers of the New Delhi Meeting would be published in October, 1966. Reprints of the proceedings of the Fourth General Business Meeting of Delegates in New Delhi, December 1964, were given to the main delegates and were approved by the Assembly. One new member, Hungary, has been accepted in the I.M.A. It was suggested that, in order to guarantee a better co-operation of member societies with the I.M.A., it would be desirable to send letters not only to the National Representative but also a copy to the

Secretariat of each National Mineralogical Society, and the Secretary asked for the address of the Secretariats before the Second Session of this Business Meeting.

The *Treasurer*, Prof. L. G. Berry, submitted a report covering receipts and disbursements from November 1, 1964, to July 31, 1966 (p. xv).

#### *Appointment of the Auditors*

The delegates nominated Profs., M. Font-Altaba and O. Mellis as auditors and scrutineers for this Meeting of the Association.

#### *Next Meeting*

President Prof. C. E. Tilley announced that the next Meeting will be held in Prague at the end of August 1968. Further the President told the Assembly that an invitation had been received from the Mineralogical Society of Japan to hold the 7th General Meeting of I.M.A. in Japan in 1970. He asked Prof. T. Watanabe to explain the situation. The Meeting should take place at the end of August or the beginning of September. The invitation was accepted with acclamation.

#### *New Business*

There was a brief discussion about the publication of the papers of this Meeting. Prof. C. E. Tilley informed the Assembly of a resolution of the Council of the Mineralogical Society to print the papers of the two symposia (pyroxenes and amphiboles; crystal growth) and the titles of the papers in the open session, together with the proceedings of the general Meeting, in one or two separate volumes. This was made possible by a substantial award for this purpose given by the International Union of Geological Sciences. The President announced a second edition of the World Directory of Mineralogists and asked Prof. Font-Altaba for remarks. Prof. M. Font-Altaba believed that the second edition could be published in spring of 1968. He asked the National Representatives to send a list of the names and addresses of the members of the National Mineralogical Societies of all non-English speaking countries to him, Prof. M. Font-Altaba, Dept. of Crystallography and Mineralogy, University of Barcelona; all English speaking countries should send the lists to Miss M. Hooker, U.S. Geological Survey, Washington 25, D.C., U.S.A. There being no further business, the first session of the fifth General Meeting was adjourned by the President.

#### *Second session*

The second session of the Business Meeting of the Delegates was held on September 3, at 16.15 at the same place. The President opened the session and asked the Chairmen of the Commissions to give their reports:

A most interesting thing is the change of the parameter  $c$  of the quartz lattice, which is connected with the presence of aluminium in the lattice. The data show that the quartz crystallized under higher temperatures (from pegmatites and magmatic rocks) contains but little  $\text{Al}_2\text{O}_3$  (about 0.01%) and has the minimum values of the unit cell. On lowering of the temperature of crystallization (quartzes from hydrothermal veins) the content of  $\text{Al}_2\text{O}_3$  increases (up to about 0.018%). Synthetic quartz contains the maximum amount of  $\text{Al}_2\text{O}_3$  (up to about 0.025%), which is probably due to the conditions of its crystallization in laboratories. The data obtained for microisomorphic correlations in quartzes of various parageneses are confirmed by the investigations of A. I. Belkovsky (1964).

Thus all the data point to the fact that when the temperature of crystallization decreases crystals of quartz absorb a relatively large amount of microisomorphic aluminium, which is accompanied by the insertion of alkali cations into the voids of the quartz structure. If the originally formed quartz is subjected to recrystallization (without additional absorption of contaminants) there will be a decrease of impurities in it (self-purification during recrystallization); this is supported by the study of the products of recrystallization of synthetic quartzes. Crystals of quartz with 0.05% of structural aluminium, after being used as a charge, contained only 0.03% of  $\text{Al}_2\text{O}_3$ . Deviations observed in some samples of natural quartz (fig. 4) are probably due to recrystallization. This must be the case with the crystals of quartz from the pegmatite veins of Volign, which have an almost constant parameter  $c$  from different zones of the pegmatite body ( $\Delta c = 0.0002 \text{ \AA}$ , Kamentsev, 1962). Mineralogical and geological investigations confirm the intensive recrystallization of the pegmatite body in that region (Prikazchikov, 1962).

*Conclusions.* The results of the investigations indicate that the fluctuations in the unit-cell parameters of quartz are in direct dependence on the inclusion of impurities in its structure: Al replacing Si in silicon-oxygen tetrahedra affects mainly the parameter  $c$  of the lattice, while uni- and divalent ions, compensating the aluminium charge, enter the canals of the quartz structure and increase the parameter  $a$ . The inclusion of impurities depends on the conditions of crystal growth. The effects of the rate of growth and of the chemical composition of the solution were observed in crystals of synthetic quartz. Correlating the variations in the lattice parameters of natural quartz with the conditions of formation, a definite dependence emerges between the temperature of crystallization and the content of structural aluminium, as well as variations in the parameters of the unit cell in quartzes of magmatic and hydrothermal origin. Yet other factors (chemical composition of the medium, rate of growth, etc) cannot be ignored, as they are likely to affect the amounts of impurities in the lattice. Any variation in the conditions of crystallization of quartz causes changes in the parameters of the unit cell, which may be observed by means of precision X-ray methods.

The studies of microisomorphic replacements in natural and synthetic

*Reports from Commissions*

*Commission on Abstracts.* Prof. Hügi, Chairman of the Commission, reported that the full commission met on two occasions. Reports were presented on three developments in the abstracting field: The proposed abstract programme of the Geological Society of America and the American Geological Institute covering the whole field of geology including mineralogy, at an estimated cost of production per abstract 10 times greater than that of the "Mineralogical Abstracts"; the proposal of the Deutsche Mineralogische Gesellschaft for computer-style abstracts and documentation based on key-words; and the proposal of Prof. Preisinger for a complete abstracting service based on a computer (e.g. IBM 360) using key-words plus data and text. The last two proposals would involve the co-operation of the Editors of journals in requiring their authors to prepare abstracts in conformity with rules to be formulated by the I.M.A.

The Commission decided that we should actively explore the possibility of developing a computer-based abstract system and the members present voted unanimously for this to be on the lines of Prof. Preisinger's proposal for key-words plus data and text. It was also decided to set up a sub-Committee of six who, together with the Chairman, Prof. Hügi, and the Secretary, Dr. Howie, would go into the details of the proposed scheme and formulate rules for abstracts in the various fields, and who would report progress to the National Delegates and invite co-operation from the Member Societies. The six members are: Dr. Olive Bradley (U.K.), Dr. Isa Kubach (Germany), Prof. A. Preisinger (Austria), Prof. J. Wyart (France), Dr. D. E. Appleman (U.S.A.) and Prof. Zakharov (U.S.S.R.).

It is emphasized that the decision is to explore the possible creation of such a computer key-word system and that in any event the present mineralogical abstracting journals will continue to be produced for some years. During this period a trial run of the proposed key-word abstracts should enable a comparison to be made.

*Commission on cosmic mineralogy.* Dr. Sandréa, in the name of Prof. Grigoriev, reported that The Commission met twice under the Chairman Prof. Grigoriev (U.S.S.R.); France, Germany, Hungary, India, Italy, Japan, and U.S.A. were represented. At the first meeting it was decided to ask the national delegates for a quick reproduction of the publications on cosmic mineralogy in their countries and to send 10 to 12 copies either to Prof. Grigoriev or to the Secretary of the Commission. The second meeting was devoted to reports of the work done in the different countries: Grigoriev for U.S.S.R., Sunagawa for Japan, Sztrokay for Hungary, and Sandréa for France.

*Commission on Mineral Data.* Prof. Strunz, Chairman, reported that as in earlier years the Commission has issued a classified list of the new minerals from 1964 to 1966 and of new data important for the classification of known minerals. About 70 copies of the list have been distributed (for internal use only).

The national delegates were asked to send their comments to the chairman by December 1, 1966. The Commission expressed the hope that further classified lists would be available at biennial intervals.

It is hoped to reach agreement on the format of proposed data sheets for the Mineral Data File by February 1967 and to have ready by September 1967 data sheets on some 50 minerals for distribution to national delegates. Dr. El-Hinnawi is preparing alternative formats and copies will be sent also to the Commission on Ore Microscopy for its comments.

The Commission expressed its thanks again to Dr. Fleischer, Chairman of the Commission on New Minerals and Mineral Names, for his memoranda on new minerals and for copies of his translations of certain Russian papers.

*Commission on Museums.* One meeting of the Commission has been held, and the principal topic of discussion has been the proposed World List of Mineral Collections. Response to the questionnaires sent out in 1959 is far from complete, but all the replies have been partially edited and put on index cards. A majority of delegates present agreed that the List should be published, although incomplete, and that Messrs Embrey and Jobbins should edit and prepare the copy for printing as soon as they received the data from the Chairman. Details of the layout should be left to the editors, except that a separate listing should be made of all meteorite collections, however small. It was also agreed that a draft should be submitted to each national delegate for checking before going to press, and that a limited time be allowed for late entries. The question of numbers and publication costs is to be considered later, but Prof. Frondel undertook to ask the I.M.A. for a preliminary cash grant to cover editorial and typing costs.

Other topics discussed more briefly included: the preparation by curators of lists of type and described specimens in their collections, for limited circulation; the need for an interest to be taken in computerized cataloguing; the starting of an informal newsletter for the benefit of curators, to include the current availability of specimens and prevailing prices, methods of conservation, display techniques, etc. Mr Desautels offered to edit such a newsletter.

Prof. Frondel tendered his resignation as Chairman of the Commission, and the delegates agreed that Dr. C. Guillemin should be approached and asked to accept nomination as Chairman. Dr. Guillemin agreed and was briefed at an informal meeting.

*Commission on New Minerals and Mineral Names.* Dr. Guillemin, Secretary of the Commission, reported: The commission was founded in 1959. Its essential task consists in checking the publication of new species, so as to avoid the proliferation of useless names; we must not forget that with less than 2 500 mineral species, mineralogical nomenclature lists about 20 000 names. The commission is well aware of this; accordingly, it has also undertaken a revision of nomenclature, in order to avoid as much as possible the use of synonyms in

mineralogical literature. One of its first tasks was to provide rules for descriptions, necessary and sufficient for a new species to be considered valid.

Here is a brief account of the progress of our work:

The commission investigates, before publication, the new species that are submitted for its approval. The members vote, and the description of the new species may then be published with the I.M.A.'s agreement; in other instances further studies are carried out at our request, or we discard the species as non-valid. I must lay stress on our growing efficiency. 6 species were submitted to us in 1962, 42 in 1965, and this year, at the end of August, we have already examined 32 new names. Generally, about 16 or 17 members out of 24 take part in the votes. The commission seldom rejects new names, but criticisms from members have often led to withdrawals, changes of names, or correction of descriptions.

Unfortunately, names are still published without having been previously investigated by the Commission (however, several societies refuse to publish new species without approval by the Commission. For instance in 1964, we did check 33 new names, but 21 were still published without previous investigation. For this reason, we issue an annual review of new names and changes in nomenclature, in which the members of the commission express their approval or disapproval of the published names. In 1964, for instance, out of the 33 names submitted to the Commission by 13 countries, 16 were agreed upon, 1 was rejected, and 15 were withdrawn for further investigation. But 54 names were published during that same year, 37 without approval by the Commission; and 14 out of these 37 were objected to by our Commission after they had been published.

We hope these annual reviews will help us to dissuade mineralogists from publishing without our agreement. In order to achieve this, we have asked that the periodicals of the Societies in the Commission publish each year the results of the votes on new names. We have secured agreement from our Russian colleagues by settling an important matter: the transcription of Latin names with Cyrillic letters. The Commission stresses the importance of this annual review; it is to be desired that all the members should answer the list of questions sent to them.

It is evident that far too many bad names are being published. Several countries have set up their own national committees to screen proposed names. We hope that this becomes more widespread and acts as a deterrent, to some degree, for the publication of disapproved names.

*Nomenclature revision.* Using different names for the same mineral causes confusion and difficulty in indexing. The Commission has tried, with some success, to bring about some measure of agreement. Taking into account the names investigated during this session, we now have agreed on over 50 names of important species, and this should eliminate more than 200 synonyms. We hope that the societies will publish these results, that mineralogists will follow these recommendations, and that the discarded names will slowly vanish from the literature.

*Names of mineral groups.* Proposals for new names of members of large mineral groups have given the Commission much difficulty, since they require careful study of the entire group. At its 1964 meeting in Delhi, the Commission authorized the formation of two sub-committees, one to study the amphibole group, the other for the pyrochlore group. Setting-up these committees was a difficult task, but that on pyrochlores is almost complete, with Mr. A. H. Van der Veen as chairman. A preliminary meeting has taken place, and proposals on nomenclature will probably be ready for examination by the Commission before the meeting in Prague.

The Commission has undertaken no work on the nomenclature of the clays, but has maintained close contact with the committee of the International Clay Minerals group.

A proposal by A. A. Levinson (United States) on the nomenclature of the rare-earth minerals has been approved by the Commission. It has been published in *Amer. Min.*, 1966, **51**, 152-158.

Other subjects have been discussed during the two sessions held in Cambridge by the Commission. Both these sessions brought forth a remarkable spirit of conciliation from the representatives of the 14 countries attending: Belgium, Bulgaria, Denmark, Finland, France, Germany, Great Britain, Italy, Japan, Netherlands, Norway, Spain, Switzerland, U.S.S.R.

Among these subjects, I shall emphasize the importance of examining the nomenclature of isomorphic series. Members have agreed to suggest that only the end terms of the series should be called by specific names; the varieties originating from isomorphic substitution would keep the same name, with the addition, in brackets, of the symbol for the replacing element. According to this scheme, the varieties will be listed in an index immediately after the name of the species, and not under the substituting element.

The Commission examined, and adopted with only slight changes, Dr. Hey's proposals and Dr. Permingeat's remarks about the rules that should be followed in selecting names for minerals and defining type-samples. It recommended close contacts with the Commission on Museums, in order to set up quickly a locality-index of existing type-samples.

Finally, the Commission decided to make widely known its decisions of 1959 and 1960 on the validity of description of new mineral species and of changes in the mineralogical nomenclature (see *Bull. Soc. franç. Min. Crist.*, 1966, **84**, 96–105). The representatives from each country should especially forward these decisions to the editors of those periodicals in which descriptions of new minerals are bound to appear. In addition, the Commission will consider the changes that should be introduced eventually into the minimal description of a mineral; these changes could be examined during the Prague meeting in 1968.

*Commission on Ore Microscopy.* Prof. Uytendogaardt, Chairman of the Commission, reported that an informal meeting of the Commission was held in Paris on May 1, 1965, since 7 representatives, the Secretary and the Chairman were present at a joint meeting of the Société française de Minéralogie et de Cristallographie and the Mineralogical Society of Great Britain. The minutes of this meeting were afterwards circulated to all national representatives and the recommendations accepted with minor reservations. The main conclusions and agreements reached were:

*Standards.* The National Physical Laboratory (Gt. Britain) will calibrate standard material over the wavelength range of from 440 to 660  $m\mu$  at intervals of 20  $m\mu$  for a charge of £12 per sample. The requirements are that the sample should be: roughly circular in section and 3 mm or more in diameter; the total surface area together with coplanar surround should be between 10 and 50  $mm^2$  in diameter; the overall depth perpendicular to the reflecting surface should be less than 27 mm; the surface should be flat—less than five fringes (546  $m\mu$ ) per cm; and a minimum of ten samples at a time would be required for measurement in order to keep the cost down to £12 per sample.

A minimum of five standards should comprise a set. Initially, standards would be made available on request from the National Representative who would hold a set for use in his country. Subsequently, additional sets of standards would be made more generally available. One set of standards would be held by the Secretary of the Commission for reference purposes.

*Publication of reports and data.* It was agreed to approach the Society of Economic Geologists for approval to publish data and reports of the Commission in *Economic Geology*. Assent was immediately forthcoming, and the minutes of the Delhi meeting, together with the proposed scheme of tables of quantitative data, were published in the issue of September–October, 1965.

*Standard materials.* The position concerning suitable standards was reviewed and it was agreed that no new information was available that seemed to necessitate any change in the

series of standards accepted at Delhi. Germanium was proposed by Prof. Cameron and there was general agreement that this metal might replace pyrite if a sufficient quantity of the required purity could be obtained. The importance of being able to make direct measurements of reflectivity in oil was stressed and it was requested that the National Physical Laboratory look into this possibility.

*Measurement of spectral reflectivity.* The most suitable half-height band-widths for spectral filters was discussed; also the tolerance permissible on the stated peak wavelength. It was accepted that the half-height band-width should be no greater than  $25 \text{ m}\mu$  and that the tolerance of the peak wavelength should be  $\pm 1\%$  or better. Following the Paris meeting, a concerted effort was made to get suitable material for standards, and early in 1966 23 specimens of neutral glass, provided by Dr. Piller, 10 specimens of carborundum, provided by Dr. Henry, and 12 specimens of silicon, provided by the Chairman, had been prepared for measurement in the laboratory of the Secretary. These 45 standards were submitted to the National Physical Laboratory. More recently, 12 additional silicon specimens and 20 germanium specimens have been prepared for measurement as well as 10 oriented sections of Elba pyrite provided by the secretary. Provisional data on silicon indicate a reflectivity range of 43 to 50% for wavelengths between 589 and 570  $\text{m}\mu$ , while for germanium the range is 53 to 48%. Germanium is less dispersive than silicon or pyrite and may make a good standard in the 45 to 65% range. Satisfactory high reflectivity standards have not yet been found, but provisional work on chromium (about 65%) and rhodium (75 to 80%) seems promising.

On February 1, 1966, an interim report on the progress made by the Commission was distributed to all members of the Commission. Different international meetings in Finland and Western and Eastern Germany provided the opportunity to continue personal contact with many representatives, and to have informal discussions on Commission business.

Finally, the second list of recent literature on quantitative methods in ore microscopy was issued in August 1966, together with a summary of the progress to date.

*Commission on Teaching.* Prof. Hurlbut, Chairman of the Commission, reported: During the 22nd Session of the International Geological Congress at New Delhi in December 1964 the Commission on Teaching of the International Mineralogical Association met twice under the Chairmanship of Prof. J. Orcel.

The activities of the Commission up to December 1964 were discussed and, in particular, the results of its enquiry into the Content of the elementary Mineralogy course at university level. Some outstanding contributions to this question had been received, notably from C. S. Hurlbut, W. Kleber, and J. Orcel, and it was decided not to press for more information on this particular score. No decision has been reached as to the future activities of the Commission. The General Assembly of the I.M.A., in its final session at New Delhi, elected as the Commission's Chairman: C. S. Hurlbut and as its Secretary: E. den Tex.

The national working groups, through their delegates, suggested that an international list of teaching aids currently used in departments and institutes of Mineralogy and Petrology be compiled from national lists to be prepared by individual members. This suggestion met with a reasonable measure of response.

By August 3, 1966 information had been received from the delegates of the U.S.A., U.K., Canada, France, Italy, Denmark, Norway, Sweden, Bulgaria, and the Netherlands. There was, however, considerable variation in both quantity and quality of the information furnished. The most complete and best classified lists of pertinent material were obtained from the U.S.A., the U.K., and France. Owing to the short interval between the date of availability of most of the said information and of the present I.M.A. meeting, it has not been possible for the secretary to append a complete international list of teaching aids to this report. It is hoped that such a list can be made available at a date in the near future.

*All the reports of the Commissions were discussed and approved by the Assembly.*

#### *Report of the Auditors*

The Auditors, Profs. M. Font-Altaba and O. Mellis, reported: We have examined the Treasurer's books and records and the bank statements of the International Mineralogical Association for the period November 1, 1964, to July 31, 1966, and find them to be in order and in agreement with the financial statement presented by the Treasurer.

The report was approved by the Assembly by unanimous vote.

#### *Other Business*

The President announced that the papers of the symposia presented at this meeting should be sent not later than December 1 to Prof. M. Buerger, Cambridge, U.S.A., for Bonding Forces, to Prof. R. Kern, Marseille, France, for Crystal Growth, or to Dr. P. Gay, Cambridge, England, for Pyroxene and Amphiboles.

Prof. H. G. F. Winkler expressed the thanks of the Assembly to Dr. Claringbull, Prof. Tilley, Dr. Gay, and the Local Secretary of this meeting, Dr. Henry, and his co-workers for this wonderfully organized meeting.

The President thanked the Secretary, the Treasurer, and the Council members and closed the Fifth General Meeting of the I.M.A. in Cambridge.

ANTON PREISINGER, Secretary

<i>Receipts</i>		\$
Cash on hand November 1, 1964.		
Current account (51-90819-E)		1768.10
Savings account (1966584)		2652.07
Dues for 1963		
Egypt 15.00	15.00	
Dues for 1964		
Egypt 15.00, India 15.00, Spain 15.00	45.00	
Dues for 1965		
Austria 30.00, Belgium 30.00, Brazil 30.00, Bulgaria 15.00, Canada 60.00, Czechoslovakia 30.00, Denmark 30.00, Egypt 14.89, Finland 30.00, France 120.00, Germany 120.00, India 15.00, Italy 90.00, Japan 90.00, New Zealand 15.00, Norway 15.00, Spain 15.00, Sweden 60.00, Switzerland 60.00, United Kingdom 90.00, U.S.A. 150.00, U.S.S.R. 150.00	1259.89	
Dues for 1966		
Austria 30.00, Belgium 30.00, Bulgaria 15.00, Canada 60.00, Czechoslovakia 30.00, Denmark 30.00, Finland 29.75, France 120.00, Germany 120.00, Italy 90.00, Japan 90.00, Netherlands 15.00, New Zealand 15.00, Norway 15.00, U.S.A. 150.00, U.S.S.R. 150.00	989.75	
Dues for 1967		
Austria 30.00	30.00	
Interest on savings account 1965		113.42
Interest on savings account 1966		114.09
Sale of directories (Washington)		121.50
Sale of directories (Germany)		47.50
Receipts	2736.15	2736.15
Total		\$7156.32

<i>Disbursements</i>		\$
Travel grant to secretary		900.00
President's office 1964		26.10
1965		30.00
Secretary's office 1965		176.05
Treasurer's office 1965		21.62
Disbursements		<u>1153.77</u>
Bank balance ac 51-90819-E		2122.97
Bank balance ac 1966584		<u>3879.58</u>
Cash on hand July 31, 1966		6002.55
Total		<u>6002.55</u>
		\$7156.32

*Note:* The dues for all member countries have been paid to the end of 1965. Dues for 1966 for seven countries remain unpaid as at August 15 (payment was received from Sweden on August 4).

# Paramagnetic resonance of electron-hole centres in minerals

By L. V. BERSHOV and A. S. MARFUNIN  
(Л. В. Бершов и А. С. Марфунин)

Institute of the Geology of Ore Deposits, Petrology,  
Mineralogy, and Geochemistry, Moscow, U.S.S.R.

*Summary.* It has been shown that electron-hole centres are rather common in natural coloured and non-coloured minerals; that the results of EPR spectra suggest models for these centres; that different types of centres may be observed in the same mineral; and that hole centres are more common in minerals than electron centres.

UP to about the middle of this century, extensive data had been obtained from investigations of colour-centres in minerals, but these investigations had a number of limitations. First of all they dealt with colour-centres but not with electron-hole centres in general, which occur both in coloured and non-coloured minerals; the colour was taken as an initial indication of the presence of a centre and the latter was assumed to be the cause of colour. The list of minerals with colour-centres included not more than twenty to thirty names and the centres were considered as particular phenomena. Only for the simplest compounds (e.g. halides) were models of the centres proposed, and even for quartz their interpretation was not unambiguous. For most of the minerals the type of centre (electron or hole centre) present was not determined. The methods of investigation of centres were: the decolorization of samples on heating, the reconstruction of colour by irradiation, the investigation of optical absorption spectra, and luminescence and thermoluminescence spectra. In more recent years the application of electron paramagnetic resonance (EPR) techniques to the study of electron-hole centres in minerals has resulted in accurate descriptions of the structure of these centres (table I). This report presents the results of an investigation on the EPR spectrum of electron-hole centres in non-irradiated natural minerals. EPR spectra were taken at room temperature on a RE-1301 spectrometer at frequencies of 9 400 Mc/sec (X-band). The data obtained from the measurements, the  $g$ -values and the hyperfine splitting constants, for some minerals, are given in table II.

On the basis of the measured  $g$ -values it is possible to distinguish electron and hole centres: the first have a  $g$ -value close to the free-electron value (2.0023) or less, and the second have  $g$ -values more than the free-electron value. Qualitative features of the EPR spectra have suggested models for the electron-hole centres. In general three kinds of atom may be involved: atoms (or vacancies)

TABLE I.

Mineral	Natural or synthetic	Irradiation	Type of centre	Ref.
Quartz	natural	X-ray irradiated and not irradiated	electron	(1)
Quartz	natural	X-ray irradiated	hole	(2)
Corundum	synthetic	$\gamma$ -irradiated	hole and electron	(3)
Corundum	synthetic	reactor-irradiated	hole	(4)
Cancrinite	natural and synthetic	X-ray irradiated and not irradiated	hole	(5)
Zeolites	synthetic	$\gamma$ - and X-ray irradiated	hole and electron	(6)
Calcite	natural	X-ray irradiated and not irradiated	electron	(7)
Diamond	natural	not irradiated	electron	(8)
Sphalerite	synthetic	light-irradiated	electron	(9)
Topaz	natural	X-ray irradiated and not irradiated	electron	(10)
Fluorapatite	synthetic	X-ray irradiated	electron and hole	(11)

TABLE II.  $g$ -value and  $hfs$  constant  $A$  (gauss) in some minerals.

	$g_1$	$g_2$	$g_3$	$A_1$	$A_2$	$A_3$
Danburite	2.0060	2.0109	2.0474	9.7	9.7	1.5
Apophyllite	2.0041	2.0106	2.0451	—	—	—
Beryl	—	0.9988	—	—	7.4	—
Scapolite	2.0072	2.0099	2.0155	—	—	—
	—	2.0036	—	—	—	—
Baryte	2.0036	2.0082	2.0037	6.8	6.0	5.4
	2.0096	2.0145	2.0462	0.2	1.5	5.6
	2.0105*	—	2.0145†	0.2*	—	0.1†
	2.0000	2.0026	2.0032	—	—	—
	2.0093	2.0122	2.0255	—	—	—
Celestine	2.0100	2.0241	2.060	2.8	—	4.2
	2.0076	2.0105	2.0193	—	—	—
	2.0093	2.0105	2.0180	—	—	—
	2.0025	2.036	2.0051	—	—	—
Anhydrite	2.0018*	—	2.0063†	0.2*	—	0.27†
Calcite	2.0105*	—	2.0163†	12.8*	—	8.0†
Aragonite	1.9981	2.0020	2.0036	2.2	2.2	1.9
	1.9959	2.0020	2.0036	0.5	0.2	0.2
	2.0036*	—	2.0038†	0.5*	—	0.5†
Cerussite	2.0030	2.0053	2.0107	—	—	—
	2.0068	2.0149	2.0200	—	—	—
Amblygonite	—	2.0096	—	—	8.1	—

\*  $g_{\parallel}, A_{\parallel}$ .†  $g_{\perp}, A_{\perp}$ .

that trap electrons or holes, atoms related to these electrons or holes, and atoms that act as charge compensators.

The hyperfine structure (*hfs*) may be exhibited by atoms with magnetic nuclei. We call this structure, according to the atom types mentioned above, 1st, 2nd, or 3rd-order *hfs*. The magnitude of the *hfs* splitting constant ( $A$ ) indicates the fraction of time the unpaired electron spends at the atom, and for the 1st order  $A$  is about  $100\text{--}400 \times 10^{-4} \text{ cm}^{-1}$ . This *hfs* is analogous to the *hfs* observed for paramagnetic ions such as  $\text{Mn}^{2+}$ , and arises from the interaction of an unpaired electron with the magnetic moment of the  $^{57}\text{Mn}$  nucleus. The magnitudes of the 2nd and 3rd order hyperfine splitting constants are about 0.2 to  $20 \times 10^{-4} \text{ cm}^{-1}$ . This is comparable with the super-*hfs* constant arising from the interaction of electrons of paramagnetic ions (for example  $\text{Mn}^{2+}$ ) with magnetic moments of the nuclei of neighbouring ions (for example  $^{19}\text{F}$ ). The relative magnitudes of the *hfs* constants of different orders is:  $A_1 > A_2 > A_3$ . For hole centres localized on neighbouring oxygen ions that have no magnetic moment, no *hfs* is shown. 3rd order *hfs* may be superimposed on the 2nd order *hfs* (i.e., there may be additional splitting of the 2nd-order *hfs* lines). For the hole centres in quartz with 5 to 15 ppm Ti, the hole is trapped at charge-deficient cation sites ( $\text{Ti}^{3+}$ ) and localized on neighbouring anions (i.e.  $\text{O}^-$  ions). In this case 1st order and 3rd order *hfs* are present but 2nd order *hfs* is absent; 3rd order *hfs* splits the 1st order *hfs* lines and the 3rd order *hfs* arises from compensating atoms of hydrogen located in structural channels.

A knowledge of the nuclear spin allows the number of *hfs* lines to be determined; their number and their relative intensities allow the determination of the number of equivalent atoms with equal interatomic distances. These data together with the angular dependences of the  $g$ -tensors and *hfs* constants, the symmetry of centres, and the number of non-equivalent positions usually provide the interpretation of the centre.

Let us consider from the minerals listed in table II some characteristic types of hole centres. Danburite single crystals of optical quality were obtained from Tetyukhe and an EPR spectrum of a hole centre ( $g$  value  $> 2.0023$ ) has been observed (fig. 1a). The spectrum consists of two sets of four *hfs* lines in accordance with two equally populated  $^{11}\text{B}$  sites in the danburite structure. A hole localized on  $^{11}\text{B}$  is consistent with the four *hfs* lines observed (the nuclear spin of  $^{11}\text{B}$  is  $I = \frac{3}{2}$  and the number of *hfs* lines is  $2I + 1 = 4$ ). Absorption lines have total widths of the order of 3 gauss. Taking into account the orthorhombic symmetry and the angular orientation of the spectra we conclude that the hole is trapped at a charge-deficient cation site ( $\text{B}^{3+} \rightarrow \text{Si}^{4+}$ ) and is shared among neighbouring anions. This is typical also for charge-deficient  $\text{SiO}_4$  tetrahedral substitution such as  $\text{AlO}_4$  (smoky quartz),  $\text{FeO}_4$  (amethyst),  $\text{GeO}_4$ ,  $\text{TiO}_4$  (rose quartz), and  $\text{BO}_4$ .

In baryte from Kuli-Kolon, Slyudyanka, Tyuya Muyun, and Kola Peninsula, the EPR spectra were considerably more complex: there are approximately 50 to 70 lines, which are very narrow (0.2 to 1.5 gauss). In these specimens three

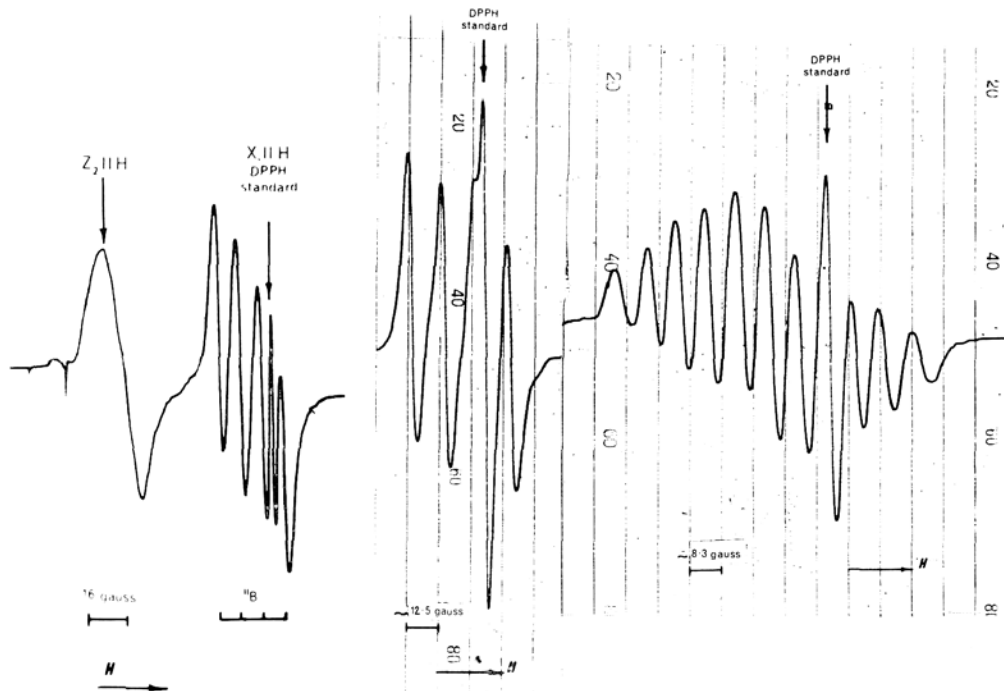


FIG. 1. Paramagnetic resonance spectra for: *a* (left), danburite ( $^{11}\text{B}$  centre); *b* (middle), blue calcite ( $^{23}\text{Na}$  centre); and *c* (right) amblygonite ( $^{27}\text{Al}$  centre).

hole-centres and one electron-centre were established. The first two spectra were attributed to a hole localized on ( $^{31}\text{P}$ ) substituting for sulphur in  $\text{SO}_4$  tetrahedra. The nuclear spin of  $^{31}\text{P}$  is  $\frac{1}{2}$ , thus explaining the doublet structure of the *hfs* lines.

In natural blue calcite from Slyudyanka an axial hole centre is present. This centre produces four *hfs* lines (fig. 1b) and the average width of each line is about 3 to 4 gauss. The EPR centre is related to the  $\text{Na}^+$  impurities substituting for  $\text{Ca}^{2+}$ , as shown by the four *hfs* lines due to  $^{23}\text{Na}$  ( $I = \frac{3}{2}$ ).

In amblygonite from Kazakhstan the observed EPR spectrum (fig. 1c) corresponds to an isotropic hole centre. Such centres are formed from a hole trapped at an *F*-vacancy and localized on two aluminium atoms (the nuclear spin of  $^{27}\text{Al} = \frac{5}{2}$ ).

The results obtained have shown that electron-hole centres are rather common for natural coloured and non-coloured minerals; that the construction of models for these centres using the results of EPR spectra is possible; that different types of centres may be observed in the same mineral; and that hole centres are more common in minerals than electron centres.

Electron-hole centres may be considered as an easily measurable general property of minerals due to the defect structure of natural crystals. The centres

give information about the structure and about the isomorphous replacement of non-paramagnetic atoms in minerals. The relative stabilities of different centres can indicate the distribution of bond strengths between pairs of atoms in the crystal.

#### References

- GAMBLE (F. T.), BARTRAM (R. H.), YOUNG (C. G.), and GILLIAM (O. R.), 1964. *Phys. Rev.*, **134**, 589.
- , and LEVY (P. W.), 1965. *Ibid.*, **138**, 577.
- GRIFFITHS (J. H. E.), OWEN (J.), and WARD (I. M.), 1955. "Magnetic resonance in irradiated diamond and quartz" in Rept. of Conference on Defects in crystalline Solids (Bristol 1954), p. 81, Phys. Soc.
- KASAI (P. H.), 1965. *Journ. Chem. Phys.*, **43**, 3322.
- MARSHALL (S. A.), REINBERG (A. R.), SERWAY (R. A.), and HODGES (J. A.), 1964. *Molec. Phys.*, **8**, 225.
- [NOVOZHILOV (A. I.), SAMOILOVICH (M. I.), MIKULSKAYA (E. K.), and PARUSNIKOVA (L. I.)  
НОВОЖИЛОВ (А. И.), САМОЙЛОВИЧ (М. И.), МИКУЛЬСКАЯ (Е. К.), и ПАРУСНИКОВА  
(Л. И.), 1966 Зап. Всесоюз. Мин. Общ. (*Mem. All-Union Min. Soc.*), **95**, 736.
- PIPER (W. W.), KRAVITZ (L. C.), and SWANK (R. K.), 1965. *Phys. Rev.*, **138**, 1802.
- [SAMOILOVICH (M. I.) and NOVOZHILOV (A. I.)] САМОЙЛОВИЧ (М. И.) и НОВОЖИЛОВ (А. И.),  
1965. Журн. Структ. Хим. (*Journ. Struct. Chem.*), **6**, 438.
- SCHNEIDER (J.), RÄUBER, (A.), and DISCHLER (B.), 1965. *Journ. Chem. Phys.*, **42**, 1839.
- SMITH (W. V.), SOROKIN (P. P.), GELLES (I. L.), and LASHER (G. J.), 1959. *Phys. Rev.*, **115**, 1546.
- WRIGHT (P. H.), WEIL (G. A.), BUCH (T.), and ANDERSON (J. H.), 1963. *Nature*, **197**, 246.

give information about the structure and about the isomorphous replacement of non-paramagnetic atoms in minerals. The relative stabilities of different centres can indicate the distribution of bond strengths between pairs of atoms in the crystal.

#### References

- GAMBLE (F. T.), BARTRAM (R. H.), YOUNG (C. G.), and GILLIAM (O. R.), 1964. *Phys. Rev.*, **134**, 589.
- , and LEVY (P. W.), 1965. *Ibid.*, **138**, 577.
- GRIFFITHS (J. H. E.), OWEN (J.), and WARD (I. M.), 1955. "Magnetic resonance in irradiated diamond and quartz" in Rept. of Conference on Defects in crystalline Solids (Bristol 1954), p. 81, Phys. Soc.
- KASAI (P. H.), 1965. *Journ. Chem. Phys.*, **43**, 3322.
- MARSHALL (S. A.), REINBERG (A. R.), SERWAY (R. A.), and HODGES (J. A.), 1964. *Molec. Phys.*, **8**, 225.
- [NOVOZHILOV (A. I.), SAMOILOVICH (M. I.), MIKULSKAYA (E. K.), and PARUSNIKOVA (L. I.)  
НОВОЖИЛОВ (А. И.), САМОЙЛОВИЧ (М. И.), МИКУЛЬСКАЯ (Е. К.), и ПАРУСНИКОВА  
(Л. И.), 1966 Зап. Всесоюз. Мин. Общ. (*Met. All-Union Min. Soc.*), **95**, 736.
- PIPER (W. W.), KRAVITZ (L. C.), and SWANK (R. K.), 1965. *Phys. Rev.*, **138**, 1802.
- [SAMOILOVICH (M. I.) and NOVOZHILOV (A. I.)] САМОЙЛОВИЧ (М. И.) и НОВОЖИЛОВ (А. И.),  
1965. Журн. Структ. Хим. (*Journ. Struct. Chem.*), **6**, 438.
- SCHNEIDER (J.), RÄUBER, (A.), and DISCHLER (B.), 1965. *Journ. Chem. Phys.*, **42**, 1839.
- SMITH (W. V.), SOROKIN (P. P.), GELLES (I. L.), and LASHER (G. J.), 1959. *Phys. Rev.*, **115**, 1546.
- WRIGHT (P. H.), WEIL (G. A.), BUCH (T.), and ANDERSON (J. H.), 1963. *Nature*, **197**, 246.

## The strength of bonding forces in mineral structures

By A. S. POVARENYYKH  
(A. C. Поваренных)

Institute of Geological Sciences, Academy of Sciences of the Ukrainian  
S.S.R., Kiev

*Summary.* The various factors that determine interatomic forces in minerals are considered, and are combined in a single quantitative expression. From this the relative strengths of bonds in different directions and the degree to which the bonding is isodesmic or anisodesmic are estimated for a number of minerals with chain and sheet structures. Results may be usefully correlated with mechanical properties.

THE bonding forces between atoms in mineral structures differ, first of all, in their nature, as well as in their direction in space and multiplicity.

The strength of these forces depends primarily on the predominance in the mineral of one of four types of chemical bond: ionic, covalent, metallic, and Van der Waals. They may be manifested in the mineral in pure and mixed form, the latter state ordinarily predominating.

Calculations of the hardness of minerals (Goldschmidt, 1933; Povarennykh, 1959) show that the strongest is the covalent bond, followed by the ionic, metallic (Povarennykh, 1963a), and, lastly, the Van der Waals or residual bond (Evans, 1964), which possesses the least strength. The last, its strength being inversely proportional to the sixth power of the interatomic distance, is typical of the softest, plastic minerals, such as graphite, molybdenite, talc, pyrophyllite, etc. Purely metallic bonding is considerably stronger, since it depends directly on the effective valence of the atoms (Povarennykh, 1963a; Hume-Rothery and Rayner, 1956), but the nature of the forces of attraction and repulsion is not quite clear in this case (Cottrell, 1955), and this type of bond occurs infrequently among minerals.

We shall consider the ionic-covalent bond, the most widespread among minerals, which is in most cases intermediate (or mixed) between purely ionic and purely covalent and may vary, depending on the chemical composition of the minerals, within very wide limits. The proportion of ionic (or covalent) bonding in minerals of binary composition may be determined by a nomogram on the basis of the difference in electronegativity of the elements (Povarennykh, 1963a and b). During the transition from ionic to covalent bonding in minerals a relative increase in bonding strength is observed, due to the gradual replacement of polar (Coulomb) interaction between atoms (ions) by quantum-mechanical (atom-atomic) interaction. This increase in bonding strength is easily calculated,

since during the transition from purely ionic bond to the most widespread purely covalent hybrid  $\sigma$ -bond of  $sp^3$ -type, its relative strength is doubled (all other conditions being equal) (Povarennykh, 1963a; Pauling, 1960).

A detailed study of the hardness of various substances (Povarennykh, 1963a) showed that the bonding strength in minerals with ionic-covalent bond depends on many crystallochemical factors. The most important of these factors are the properties of the atoms: valence, co-ordination number, and electron shell structure, then the interatomic distances, the forces of repulsion between the nearest neighbouring atoms, and the degree of shielding (or valence saturation) of the atoms in co-ordinational polyhedrons.

With the hardness equation for a crystalline substance as a basis (Povarennykh, 1963a), and taking into consideration the fact that for some crystallochemical factors the effects on breaking and compression strengths differ, a formula may be derived that permits calculation of the breaking strength of the bonds. It should be kept in mind that the number and direction of the bonds from any atom in the structure is determined by the shape and orientation of its coordination polyhedron. The atoms concerned are usually electropositive.

The relative strength of a single bond of an electropositive atom in the structure of any mineral of binary composition with ionic-covalent bonds may be calculated approximately by the formula:  $\sigma = rK\beta(W_k - W_a)Cd^2$ , where  $r$  is the coefficient of repulsion between the electron shells of neighbouring atoms, represented in a simplified way in the form of a factor equal to the square root of the reciprocal value of the product of the atom charges ( $r$  varies for different valent types of bonding from 1 to 0.25);  $K$  is the bonding strength coefficient, taking into account the share of covalent bond between opposite atoms (its value varies from 1 to 2);  $W_k$  and  $W_a$  are the valences of electropositive (cation) and electronegative (anion) atoms;  $C$  is the co-ordination number of the electropositive atom (for minerals it varies from 2 to 12);  $d$  is the interatomic distance in Å;  $\beta$  is bonding strength relaxation coefficient, which depends on the number and state of orbits of valence electrons not involved in the chemical bond (varying from 0.7 to 1.0).

The repulsion forces between neighbouring atoms depend chiefly on their charges (valencies), as was ascertained when studying the hardness of minerals (Povarennykh, 1963a). These forces are approximately proportional to the square root of the product of the charges. For convenience of calculation the repulsion coefficient  $r$  is introduced into the equation as a factor with a reciprocal value, i.e.  $r = 1/\sqrt{(W_k \cdot W_a)}$ , and not in the form of a difference term. For various valence ratios of  $W_k : W_a$  it has the values:  $1/1 = 1$ ,  $1/2 = 0.71$ ,  $1/3 = 0.58$ ,  $2/2 = 0.50$ ,  $2/3 = 0.41$ ,  $2/4 = 0.35$ ,  $3/3 = 0.33$ ,  $2/5 = 0.31$ ,  $2/6 = 0.29$ ,  $4/4 = 0.25$ .

The value of the coefficient  $K$  is calculated by a special nomogram or table (Povarennykh, 1963a, p. 58), while the value of the coefficient  $\beta$  is found from the table (*ibid.*, p. 77), being different for the same element for an essentially ionic or a covalent bond.

Table I presents the values of the relative strengths of single bonds of the

most important elements for various anion coordinations. The range of these values for various chemical elements is very great—from 0.01 ( $\text{CsCl}_8$ ,  $\text{CsO}_{12}$ ) to 1.0 or 1.3 ( $\text{CO}_3$ ,  $\text{NO}_3$ ); i.e. the bonding strength in the polyhedrons of various elements may differ by over 100 times. It is true that for the most widespread elements encountered in oxides and silicates this difference is markedly less, about 0.02 ( $\text{NaO}_{12}$ ,  $\text{KO}_{12}$ ) to 0.41 ( $\text{SiO}_4$ ), which corresponds to a change in bonding strength of 20 times.

TABLE I. Relative strengths of single bonds of some elements in different anionic co-ordination

Element and co-ordination	Relative strength of bond	Element and co-ordination	Relative strength of bond	Element and co-ordination	Relative strength of bond	Element and co-ordination	Relative strength of bond
$\text{LiO}_6$	0.09	$\text{Cu}^{2+}\text{Cl}_6$	0.07	$\text{As}^{3+}\text{O}_3$	0.31	$\text{AsO}_4$	0.45
$\text{NaCl}_6$	0.03	$\text{ZnO}_6$	0.11	$\text{As}^{\text{III}}\text{S}_3$	0.31	$\text{AsS}_4$	0.30
$\text{NaO}_6$	0.04	$\text{ZnS}_4$	0.16	$\text{Sb}^{3+}\text{O}_3$	0.23	$\text{SbO}_6$	0.21
$\text{NaO}_{12}$	0.02	$\text{ZnCl}_6$	0.08	$\text{Sb}^{\text{III}}\text{S}_3$	0.19	$\text{SbS}_4$	0.28
$\text{AgS}_4$	0.07	$\text{Pb}^{2+}\text{O}_3$	0.16	$\text{CO}_3$	1.00	$\text{NbO}_4$	0.32
$\text{BeO}_4$	0.25	$\text{PbS}_6$	0.05	$\text{SiO}_4$	0.41	$\text{NbO}_6$	0.19
$\text{MgO}_4$	0.17	$\text{BO}_3$	0.66	$\text{SiF}_6$	0.14	$\text{TaO}_6$	0.18
$\text{MgO}_6$	0.10	$\text{BO}_4$	0.41	$\text{TiO}_6$	0.18	$\text{VO}_4$	0.48
$\text{CaO}_6$	0.07	$\text{AlO}_4$	0.28	$\text{SnS}_6$	0.14	$\text{VS}_4$	0.32
$\text{CaO}_{12}$	0.03	$\text{AlO}_6$	0.16	$\text{ZrO}_8$	0.10	$\text{SO}_4$	0.71
$\text{CaF}_8$	0.04	$\text{AlF}_6$	0.10	$\text{Mn}^{4+}\text{O}_6$	0.18	$\text{CrO}_4$	0.58
$\text{Fe}^{2+}\text{O}_6$	0.09	$\text{Fe}^{3+}\text{O}_4$	0.21	$\text{ThO}_{12}$	0.05	$\text{MoO}_4$	0.41
$\text{Fe}^{\text{II}}\text{S}_6$	0.08	$\text{Fe}^{3+}\text{O}_6$	0.12	$\text{U}^{4+}\text{O}_8$	0.09	$\text{WO}_4$	0.40
$\text{Cu}^{2+}\text{O}_4$	0.15	$\text{Fe}^{3+}\text{Cl}_6$	0.08	$\text{NO}_3$	1.28	$\text{WO}_6$	0.23
$\text{Cu}^{\text{II}}\text{S}_2$	0.19	$\text{Fe}^{\text{III}}\text{S}_4$	0.22	$\text{PO}_4$	0.53	$\text{UO}_6$	0.19

A comparison of the values of the relative bonding strength in various atomic co-ordinations (with the same anion) permits an assay of the degree of inhomogeneity of the bonds (anisodesmicity) between the atoms in compounds of complex composition. Thus, for instance, in spinel  $\text{MgAl}_2\text{O}_4$  the ratio of the values  $\sigma_{\text{MgO}_4}$  and  $\sigma_{\text{AlO}_6}$  is 0.17 : 0.16, which is close to unity and is evidence of the completely isodesmic nature of this mineral. Some silicates are close to being isodesmic, for example, phenakite  $\text{Be}_2\text{SiO}_4$  and andalusite  $\text{AlAlSiO}_4\text{O}$ ; for the first  $A$ , the ratio of the values of  $\sigma$ , is equal to 1.64, while for the second it is about 1.80. However, an orthosilicate such as larnite  $\text{Ca}_2[\text{SiO}_4]$  is a markedly anisodesmic mineral ( $A \approx 4.2$ ). Even more anisodesmic are calcite  $\text{Ca}[\text{CO}_3]$  ( $A \approx 7.3$ ), baryte  $\text{Ba}[\text{SO}_4]$  ( $A \approx 12$ ) and nitre  $\text{K}[\text{NO}_3]$  ( $A \approx 20$ ).<sup>1</sup> Thus, all compounds may be classified by the degree of their anisodesmicity (Povarennykh, 1963a; 1966).

Such a classification would, however be too approximate. It may be improved by taking more strictly into account the number and direction of the various

<sup>1</sup>The ratios of the bonding strength values determining the anisodesmicity coefficient ( $A = \sigma_{\text{max}}/\sigma_{\text{min}}$ ) are calculated for these minerals, taking into account atomic co-ordination and the number and distribution of single bonds in space.

TABLE II. Relative strengths of bonds in different directions in crystal structures of some chain minerals

Mineral and formula	Direction of section of crystal	Atoms participating in the bond	$C$	$W_k$	$W_a$	$K$	$r$	$d$	$n$	$\beta$	$\sigma$	Degree of anisodesmicity of bonds	
Cinnabar HgS	{	0001	Hg-S	6	2	2	1.80	0.50	2.3	1	1.0	0.114	1.00
		10 $\bar{1}$ 0	Hg-S	6	2	2	1.80	0.50	3.1	1	1.0	0.063	0.55
		1 $\bar{2}$ 10	Hg-S	6	2	2	1.80	0.50	3.3	1	1.0	0.055	0.48
Stibnite Sb <sub>2</sub> S <sub>3</sub>	{	001	Sb-S	7	3	2	1.73	0.41	2.80	2	0.8	0.124	1.00
		010	Sb-S	7	3	2	1.73	0.41	3.47	1.5	0.8	0.061	0.49
		100	Sb-S	7	3	2	1.73	0.41	3.11	2.5	0.8	0.126	1.02
Chalcostibite CuSbS <sub>2</sub>	{	001	(Cu, Sb)-S	5	2	2	1.72	0.50	2.75	1.5	0.9	0.124	1.00
		100	(Cu, Sb)-S	5.3	2.3	2	1.73	0.48	2.78	1	0.85	0.079	0.64
		010	Sb-S	6	3	2	1.73	0.41	3.11	2	0.8	0.117	0.94
		010	Cu-S	4	1	2	1.71	0.71	2.29	1	1.0	0.116	0.93
Rutile TiO <sub>2</sub>	{	001	Ti-O	6	4	2	1.51	0.35	1.94	2	1.0	0.375	1.00
		110	Ti-O	6	4	2	1.51	0.35	1.99	1	1.0	0.179	0.48
Diaspore AlOOH	{	001	Al-O	6	3	2	1.41	0.41	1.88	4	1.0	0.640	1.00
		010	Al-O	6	3	2	1.41	0.41	2.12	2	1.0	0.259	0.39
		210	(Al, H)-O	4	2	2	1.52	0.50	2.41	4	1.0	0.525	0.82
		100	(Al, H)-O	4	2.5	2	1.46	0.45	2.16	4	1.0	0.706	1.10
Diopside CaMg[Si <sub>2</sub> O <sub>6</sub> ]	{	001	Si-O	4	4	2	1.54	0.35	1.62	4	1.0	1.65	1.00
		110	(Ca, Mg)-O	6.7	2	2	1.27	0.50	2.25	6	1.0	0.465	0.28
		100	(Ca, Mg)-O	7	2	2	1.24	0.50	2.32	14	1.0	0.92	0.56
Tremolite Ca <sub>2</sub> Mg <sub>5</sub> [Si <sub>4</sub> O <sub>11</sub> ] <sub>2</sub> (OH) <sub>2</sub>	{	001	Si-O	4	4	2	1.54	0.35	1.62	8	1.0	3.29	1.00
		110	(Ca, Mg)-O, OH	6.2	2	1.83	1.28	0.55	2.18	18	1.0	1.53	0.46
		100	(Ca, Mg)-O, OH	6.6	2	1.87	1.26	0.54	2.22	23	1.0	1.80	0.55

TABLE III. Relative strengths of bonds in different directions in crystal structures of some sheet minerals

Mineral and formula	Direction of section of crystal	Atoms participating in the bond	<i>C</i>	<i>W<sub>k</sub></i>	<i>W<sub>a</sub></i>	<i>K</i>	<i>r</i>	<i>d</i>	<i>n</i>	$\beta$	$\sigma$	Degree of anisodesmicity of bonds
Arsenic As	⊥ (0001)    (0001)	As-As	6	3	3	2.00	0.33	2.51	3	0.8	0.564	1.00
		As-As	6	3	3	2.00	0.33	3.15	3	0.8	0.360	0.64
Covellite Cu <sub>2</sub> CuS <sub>2</sub> S	⊥ (0001)    (0001)    (0001)	(Cu <sup>I</sup> , Cu <sup>II</sup> )-S	3.7	1.3	2	1.76	0.57	2.26	6	0.9	0.746	1.00
		Cu <sup>I</sup> -S	4	1	2	1.71	0.58	2.35	5	1.0	0.453	0.61
		S-S	4	2	2	2.00	0.50	2.05	4	1.0	0.950	1.27
High-chalcocite Cu <sub>2</sub> S	⊥ (0001)    (0001)	Cu-S	3	1	2	1.71	0.71	2.24	2	1.0	0.320	1.00
		Cu-(Cu, S)	3	1	2	1.71	0.71	3.34	2	0.85	0.121	0.38
Litharge PbO	⊥ (001)    (001)	Pb-O	4	2	2	1.28	0.50	2.30	4	0.9	0.485	1.00
		Pb-O	8	2	2	1.28	0.50	3.10	4	0.9	0.120	0.25
Gibbsite Al(OH) <sub>3</sub>	⊥ (001)    (001)	Al-OH	6	3	1	1.41	0.58	1.86	4	1.0	0.476	1.00
		OH-OH	3	1	1	2.00	1.00	2.79	3	1.0	0.260	0.55
Brucite Mg(OH) <sub>2</sub>	⊥ (0001)    (0001)	Mg-OH	6	2	1	1.29	0.71	2.10	4	1.0	0.277	1.00
		OH-OH	6	1	1	2.00	1.00	3.22	3	1.0	0.100	0.36
Quenselite PbMnO <sub>2</sub> OH	⊥ (100)    (100)    (100)    (100)	(Pb, Mn)-(O, OH)	4.5	2.5	1.5	1.39	0.52	2.06	2	0.86	0.244	1.00
		Pb-O	3	2	2	1.28	0.50	2.24	1	0.9	0.155	0.63
		Pb-OH	3	2	1	1.28	0.71	2.13	2	0.9	0.242	0.99
		OH-OH	3	1	1	2.00	1.00	2.84	1	1.0	0.080	0.33
Muscovite KAl <sub>2</sub> [AlSi <sub>3</sub> O <sub>10</sub> ](OH) <sub>2</sub>	⊥ (001)    (001)	(Si, Al)-O	4.7	3.7	2	1.49	0.37	1.72	8	1.0	2.340	1.00
		K-O	12	1	2	1.12	0.71	3.10	14	1.0	0.192	0.08
Margarite CaAl <sub>2</sub> [Al <sub>2</sub> Si <sub>2</sub> O <sub>10</sub> ](OH) <sub>2</sub>	⊥ (001)    (001)	(Si, Al)-O	4.7	3.3	2	1.45	0.39	1.76	8	1.0	2.060	1.00
		Ca-O	12	2	2	1.19	0.50	2.72	14	1.0	0.375	0.18

bonds in the mineral structure. The latter is particularly important in determination of bonding strength in various plane sections of minerals possessing chain and sheet structures. Such calculations can be used to determine the degree of strong anisotropic bonding in the principal directions in the mineral structure, which is of great importance for determination of the cleavage planes and for ascertaining the relationship between the mineral structure and the appearance of its crystalline individuals (Povarennykh, 1965a).

However, the task of taking into consideration all angles between bonds in the structure, and to compute the specific number of bonds per  $\text{\AA}^2$  of the selected section of the crystal is very laborious, and can be solved only for highly symmetrical minerals of simple composition. In most cases it is sufficient to take into consideration only the number of bonds intersected by some imaginary plane in order to calculate the degree of anisotropy of the bonds.<sup>1</sup> The formula presented in the foregoing can be used for computations, adding in the numerator the value  $n$ , which designates the number of single bonds of the given atom extending in the same direction.

Tables II and III present data on the calculation of the relative bonding strengths between atoms in various crystallographic directions for a number of the most important minerals with chain and sheet structures. The highest degree of anisotropy of the bonds is possessed by sheet silicates (muscovite, margarite) and sheet hydrates (brucite, gibbsite, quenselite). The anisotropy coefficient of the bonds varies between 3 and 12. Lower anisotropy of the bond is found in chain silicates (diopside, tremolite) and in sheet and chain sulphides and oxides; for these minerals the bond anisotropy coefficient is between 1.5 and 3, which is as expected, since the bonding strength along the most important sections is determined in their case chiefly by the differences in the number and lengths of the bonds, which cannot vary much.

The quantitative expression of anisotropy of the bonds in mineral structures makes possible a clearer representation of the difference between the most important structural motifs, the consideration of which can serve as a basis for the revision of the systematics of minerals (Povarennykh, 1956, 1963b, 1965b). In addition, it gives a better idea of the degree of anisotropy of certain properties of minerals, especially the mechanical properties (for instance, hardness, tension, and compression of minerals). These data may also be of importance for crystallographical investigations.

#### References

- COTTRELL (A. H.), 1955. *Theoretical Structural Metallurgy*. London.  
EVANS (R. C.), 1964. *An Introduction to Crystal Chemistry*. Cambridge.  
GOLDSCHMIDT (V. M.), 1933. *Coll. The Main Ideas in Geochemistry*. Moscow, I, 166.  
HUME-ROTHERY (W.) and RAYNOR (G. V.), 1956. *The Structure of Metals and Alloys*. London.  
PAULING (L.), 1960. *The Nature of the Chemical Bond*. Ithaca.

<sup>1</sup> The difference here is within the limits of error; thus for rutile the difference between  $\sigma$  calculated by the exact and approximate methods is 2%.

- [POVARENNYKH (A. S.)] Поваренных (А. С.), 1956. Изв. Акад. Наук СССР (*Bull. Acad. Sci. URSS, sér. geol.*), **12**, p. 91.
- 1959. *Min. Colloq. (Lvov)*, **13**, 84.
- 1963a. *Hardness of Minerals*. Kiev.
- 1963b. *Geologie*, **4**, 377.
- 1965a. *Min. Colloq. Morphology, Properties and Genesis of Minerals*. Kiev, p. 3.
- 1965b. *Geologie*, **2**, 153.
- 1966. *Reports of Carpatho-Balkan Geol. Assoc.*, Kiev (in press).

# The influence of dislocation-strain energy on crystal morphology

By P. J. SHLICHTA

6026 Springvale Drive, Los Angeles, California, U.S.A.

*Summary.* Analyses are presented of three different models of crystal growth, which assume isotropic surface-energy parameters. These analyses indicate that dislocation-strain energy can affect growth rate. There is ample evidence, however, that surface-energy parameters usually have the predominant role in determining crystal growth rate and morphology and that dislocation-strain energy has only a minor effect. None the less, any detailed theory of crystal growth must take this factor into account.

BRAVAIS' observation (1851) that the most prominent faces of a crystal lie parallel to the lattice planes of highest reticular density (i.e., the planes with widest interplanar spacing) has since been confirmed by G. Friedel (1905) and reinterpreted and extended in terms of screw axes and glide planes by Donnay and Harker (1937). Explanations have been attempted in terms of chains of strong bonds (Hartman and Perdok, 1955) or the minimization of surface energy (Wulff, 1901; Zadumkin, 1964), but these have considered only the equilibrium form of the crystal. However, since crystal growth is not a morphologically reversible process,<sup>1</sup> equilibrium models are of doubtful value. Kinetic explanations, based on the adsorption and diffusion of molecules on the crystal surface (Amelinckx, 1950) or on the surface area created by the nucleation of new growth steps (Buerger, 1947), have considered only the growth of perfect crystals. Bravais' rule, however, is of necessity confined to euhedral crystals and therefore to crystals grown from vapor or solution. Under these conditions, at least at low supersaturations, growth depends on the nucleation of new steps from emerging screw dislocations (Frank, 1949). Detailed kinetic analyses of this model (Burton, Cabrera, and Frank, 1951; Chernov, 1961) have not specifically discussed Bravais' rule, but it is evident that according to these models, Bravais' rule would be a direct consequence of the assumption that the most closely packed faces have optimum activation and evaporation energies for atoms at steps and kinks. These quantities are in turn related to equilibrium surface

<sup>1</sup> For a dramatic demonstration of this, see the film "Sugar Crystal Studies" by H. E. C. Powers (Tate & Lyle, Ltd., London). In this connection, it has also been observed that when crystals having an atypical habit are immersed for long periods in saturated solution, there is no tendency to change to the "equilibrium form" unless opportunity is provided for macroscopic growth (Wells, 1946).

energy or bond strengths or both, thereby somewhat justifying explanations of Bravais' rule in terms of the latter parameters.

There is, however, another aspect of the growth-spiral model that also depends on lattice spacing, namely the free energy of formation of the screw dislocations. This has been shown to be equivalent to the dislocation strain energy (Cottrell, 1953), which is proportional to the square of the Burgers vector. Presumably, this strain energy is capable of influencing crystal growth, either by affecting the population of growth spirals or by inhibiting the growth rate near the centre of the spirals.

In this paper, a qualitative examination of various simple models of crystal growth is made to determine the effect of dislocation-strain energy on growth kinetics. In each of the cases considered, it is assumed that the surface energy per unit area and the adsorption and diffusion parameters are isotropic, i.e., the same on all faces.

#### *Case A. Growth spiral formation is the rate-limiting process*

A relation between Burgers vector and growth rate can be deduced from the following premises: The free energy of a screw dislocation is proportional to the square of its Burgers vector; dislocations with the highest free energy have the lowest probability of formation; crystal faces with the lowest concentration of emerging screw dislocations have the slowest growth rate; and the slowest growing faces are the most prominent ones on the crystal.

Of these premises, the first and fourth are well established. The second is not obviously true, since dislocations do not as a rule exist in dynamic equilibrium with the lattice. It is however, at least approximately true for dislocations moving under stress or at high temperatures, since dislocations with large Burgers vectors can under these conditions decompose, with an overall decrease in free energy, to form two or more dislocations with the same total Burgers vector. Other mechanisms of dislocation formation in seed crystals, such as the incorporation of dirt particles, may involve similar mechanisms; but the formation of dislocations by the growing together of two seed crystals is probably a non-equilibrium process. Therefore the second premise is, at best, difficult to substantiate.

The third premise is also extremely doubtful. In theory, one dislocation per face is sufficient to provide growth steps (J. Friedel, 1964), and real crystals usually contain numerous dislocations on all faces. Therefore, although Kirksinghe, Morris, and Strickland-Constable (1966) have recently demonstrated that dislocation density can, in certain cases, profoundly affect growth rate, it seems unlikely that the third premise is generally applicable.

Hence the foregoing argument is untenable for most crystals. In crystals with highly anisometric unit cells, however, dislocations may be entirely absent in all but the shortest unit cell dimension(s). Such crystals will obey Bravais' rule in an exaggerated manner, i.e., by forming whiskers or platelets. The habits

of numerous minerals such as millerite and jamesonite tend to substantiate this prediction.

*Case B. Abundant kinks—surface diffusion as the rate-limiting process*

For crystals with approximately equidimensional unit cells having emerging screw dislocations on all low-index faces, the growth rate can be related to the dislocation strain energy by the following assumptions: The surface energy per unit area is the same on all faces. Each face grows by the linear advance of a series of monolayer growth steps. Abundant kinks are available at each step; hence the surface diffusion of adsorbed molecules to the kinks is the rate-limiting process. The surface diffusion parameters are the same on all faces (this is to some extent a consequence of the first premise). The spacing  $L$  between steps is much greater than the diffusion zone around each step (Fig. 1); hence there is no interaction or competition between adjacent steps (This appears to be a valid assumption at low supersaturations; J. Friedel, 1964).

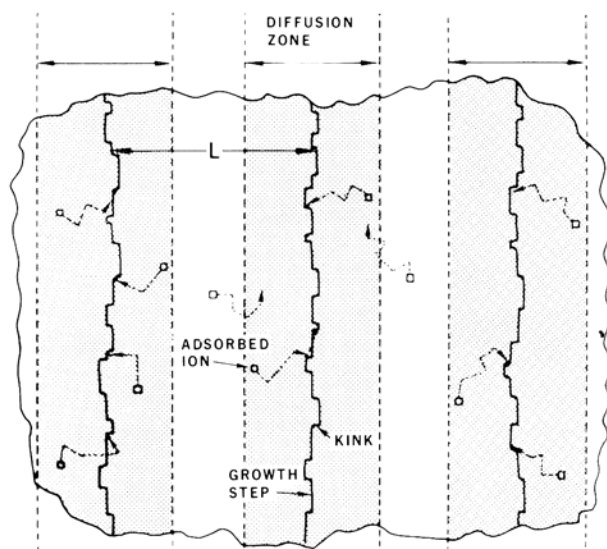


FIG. 1. Case B: Growth of crystal by steps with abundant kinks.

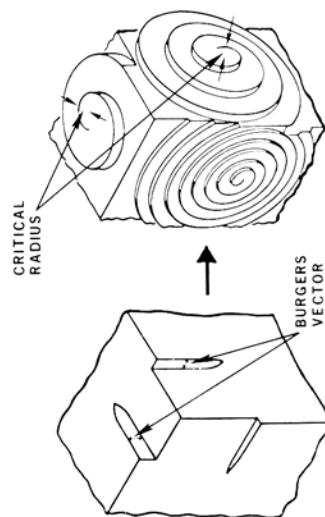


FIG. 2. Case B: Effect of dislocation strain energy on spacing between steps.

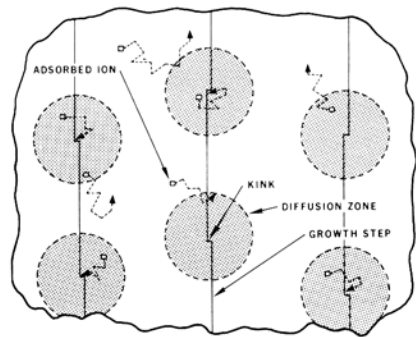
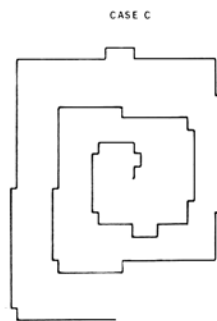
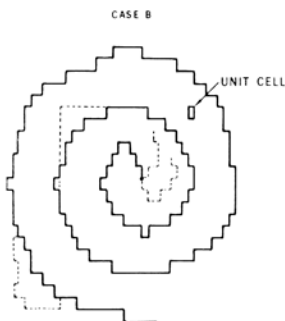
Under these assumptions, molecules are adsorbed at the same rate on each step; and the linear velocity of each step varies inversely as the step height. Therefore the perpendicular growth rate of each face is proportional only to the reciprocal of the distance between steps. If the steps are derived from screw-dislocation growth spirals, the step spacing depends on the rate of growth of the curved portion of the step in the immediate vicinity of the dislocation. The spacing is then approximately proportional to the critical radius  $r_c$  for two-

dimensional nucleation (Verma, 1953):  $L \approx 4\pi r_c \approx 4\pi\sigma/\epsilon$ . If we assume that surface energy ( $\sigma$ ) and edge energy ( $\epsilon$ ) are isotropic, then  $r_c$  and  $L$  should be the same on all faces and the crystal should grow at the same rate on all faces. It is proposed, however, that the dislocation-strain energy causes an anomalously high surface energy near the dislocation core. Assuming typical values for the critical radius ( $\sim 1000 \text{ \AA}$  at one percent supersaturation), the strain energy at  $r \approx r_c$  amounts to 10 to 40% of the yield stress of the average material; this should be sufficient to appreciably increase the surface energy and hence the critical radius at any given supersaturation. This assumption is substantiated by the size of etch pits formed during the evaporation of crystals.

Faces with dislocations having the largest Burgers vector will therefore have the highest surface energy near the dislocation cores. Such faces will have growth spirals with the largest critical radius, the largest spacing between steps, and hence the slowest growth rate (fig. 2).

### *Case C. Kink formation as the rate-limiting process*

Case B was based on the assumption of Burton, Cabrera, and Frank (1951) that, even on low-energy steps, kinks are abundant and occur on approximately every fourth atomic site. It is unlikely, however, that this model can account for the polygonal growth spirals that are observed on many types of crystals at low supersaturations. If, for example, we assume that on a given face the steps have minimum energy in two directions, it is plausible to conclude that the growth spiral will be composed of steps in the minimum-energy directions. If kinks are abundant, however, it is always possible to construct a circular spiral out of minimum energy step segments (fig. 3a). This configuration will have a lower edge energy than a polygonal spiral having the same frequency of kinks. Therefore, crystals growing as in case B will always have circular or elliptical growth spirals.



FIGS. 3. Round versus polygonal growth spirals.  
a. Case B: abundant kinks; b. Case C: few kinks.

FIG. 4. Case C: Growth of crystal by steps with few kinks.

Polygonal growth spirals will occur only if kink formation is extremely rare (i.e., is the rate-limiting process) and if a kink, once formed, grows rapidly until it comes to another kink or to a corner of the spiral (fig. 3b). According to this model, the molecules for growth come from isolated circular diffusion zones centred around each kink (fig. 4), the radius of these diffusion zones being of the order of the average diffusion distance of an adsorbed molecule before evaporation (J. Friedel, 1964).

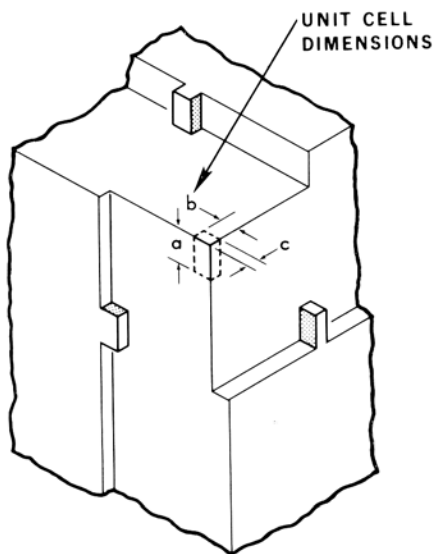


FIG. 5. Case C: Creation of new kinks.

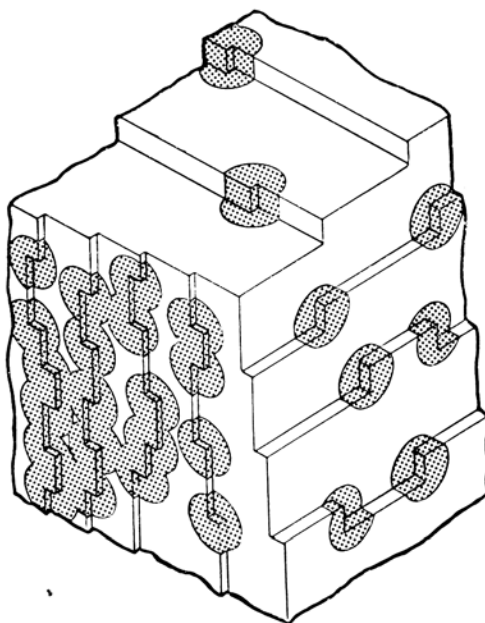


FIG. 6. Case C: Relation between step height and growth rate.

If  $a$ ,  $b$ , and  $c$  are the unit cell axial lengths, and  $\bar{S}_a$  is the average value for the surface created by the formation of one kink on a face normal to the  $a$ -axis (fig. 5), then:  $\bar{S}_a \approx (a \cdot b) + (a \cdot c)$ ,  $\bar{S}_b \approx (a \cdot b) + (b \cdot c)$  and  $\bar{S}_c \approx (a \cdot c) + (b \cdot c)$ . Then if  $a > b > c$ ,  $(a \cdot b) > (a \cdot c) > (b \cdot c)$ , and therefore  $\bar{S}_a > \bar{S}_b > \bar{S}_c$ .

If we again assume that the surface energy per unit area is the same for all principal faces, then the faces having the highest step height will have the highest average energy of kink formation. The steps on these faces will therefore have the lowest density of kinks per unit step length.<sup>1</sup> Moreover, these faces will also have the largest spacing between steps, inasmuch as kink formation (necessary for each quarter-turn advance of the innermost segment of the spiral) will be inhibited by the dislocation-strain energy for reasons similar to those set forth

<sup>1</sup> Note the resemblance of this model to the one proposed by Buerger (1947) for ideal crystals.

in case B. Therefore, faces with the largest step height (i.e., Burgers vector) will have the fewest kinks per unit area and hence (if diffusion and adsorption parameters are the same on all faces) the slowest rate of growth (fig. 6).

### *Conclusions*

It has thus been shown that, according to several models, the strain energy of the dislocations from which growth spirals emerge tends to inhibit the growth rate of the corresponding crystal faces, and that the effect is greatest for the faces with the greatest step height (i.e., Burgers vector). There are several reasons, however, for doubting whether this effect has a significant influence on crystal morphology:

The models proposed herein are extremely simplified and involve only elementary steps. It appears plausible, however, that the basic concept—the inhibition of the growth rate at the centre of the spiral, with a consequent retardation of the rotation rate of the spiral—is general enough to be applicable to sophisticated models involving macroscopic steps (e.g., Chernov, 1961).

Even if the foregoing models are valid, it is evident that the surface-energy anisotropy, either of itself or in conjunction with dislocation-strain energy, would also result in anisotropy of growth rate. Moreover, there is considerable evidence that surface-energy anisotropy is of itself sufficient to account quantitatively for crystal morphology. For example, well-developed faces occur on many dislocation-free crystals, such as metal whiskers and flux-grown BeO crystals (Newkirk and Smith, 1965). It is also noteworthy that, in many materials, thermal etching causes facets corresponding to the principal growth faces, even in cases, such as NaCl, that apparently violate Bravais' rule (e.g., Krasnopolsky de Grinberg and Grinberg, 1965). Therefore, it appears that the dislocation-strain energy causes only a minor modification of the surface energy term.

Growth-rate anisotropies predicted solely on the basis of dislocation-strain energies conform to Bravais' rule only in a few instances, such as prismatic faces in simple tetragonal, hexagonal, or orthorhombic lattices. As a rule, there is no simple correlation between Burgers vector and interplanar spacing. For example, screw dislocations normal to high-index faces with small interplanar spacings tend to have very large Burgers vectors; the absence of such faces can therefore be explained only in terms of surface energy. That most crystals do conform to Bravais' rule is additional evidence that the contribution of dislocation-strain energy is at most quite small.

Despite these objections, however, it would seem advisable to consider the effect of dislocation-strain energy in any detailed quantitative treatment of crystal growth. For this purpose, Nenow's results (1963) can be used to calculate the equilibrium form of a dislocation-step line as a function of the Burgers vector. In conjunction with this, some experimental evidence might be adduced from correlations of relative prominence versus growth spiral spacing for different faces on the same crystal.

*Acknowledgments.* The author is indebted to Drs. A. Chase, W. Wilcox, and G. Wolten of the Aerospace Corporation for valuable criticisms and comments. Earlier portions of this research were carried out at the Jet Propulsion Laboratory, Pasadena, California, under contract NAS7-100 with the National Aeronautics and Space Administration.

#### References

- AMELINCKX (S.), 1950. *Journ. Chem. Phys.*, **47**, 213.  
BRAVAIS (M. A.), 1851. *Études Crystallographiques, Journ. de L'Ecole Polytechnique*, 167.  
BUERGER (M. J.), 1947. *Amer. Min.*, **32**, 593.  
BURTON (W. K.), CABRERA (N.), and FRANK (F. C.), 1951. *Phil. Trans., ser. A*, **243**, 299.  
[CHERNOV (A. A.)] ЧЕРНОВ (А. А.), 1961. *Soviet Physics—Uspekhi*, **4**, 116.  
COTTRELL (A. H.), 1953. *Dislocations and Plastic Flow in Crystals* Oxford. pp. 38–40.  
DONNAY (J. D. H.) and HARKER (D.), 1937. *Amer. Min.*, **22**, 446.  
FRANK (F. C.), 1949. *Discussions Faraday Soc.*, **5**, 48.  
FRIEDEL (G.), 1905. *Bull. Soc. franç. Min.*, **28**, 6.  
FRIEDEL (J.), 1964. *Dislocations* (Pergamon), 195–196.  
HARTMAN (P.) and PERDOK (W. G.), 1955. *Acta Cryst.*, **8**, 49 and 521.  
KIRTSINGHE (D.), MORRIS (P. V.), and STRICKLAND-CONSTABLE (R. F.), 1966. *I.U.C. Symposium on Crystal Growth*, Abstract S2-14, Moscow.  
KRASNOPOLSKY DE GRINBERG (D.) and GRINBERG (A.), 1965. *Czech. Journ. Phys.*, **15**, 363.  
NENOW (D.), 1963. *Phys. Stat. Sol.*, **3**, 654.  
NEWKIRK (H. W.) and SMITH (D. K.), 1965. *Amer. Min.*, **50**, 22 and 44.  
VERMA (A. R.), 1953. *Crystal Growth and Dislocations*. London, (Butterworth), pp. 18 and 62.  
WELLS (A. F.), 1946. *Phil. Mag.*, **37**, 184.  
WULFF (G.), 1901. *Zeit. Krist.*, **34**, 449.  
[ZADUMKIN (S. N.)] ЗАДУМКИН (С. Н.), 1964. *Soviet Physics—Solid State*, **5**, 3429.

*Note added in proof:* This paper was also presented at the Symposium on Crystal Growth of the 7th Congress of the International Union of Crystallography (Moscow, 1966). An unauthorized version in Russian has been published in Рост Кристаллов (Growth of crystals), 1967, **7**, 91–97.

## Measurement and interpretation of infrared pleochroism in minerals

By JOSEF ZEMANN

(Inst. Min. Krist., Göttingen)

*Summary.* An account is given of two examples illustrating the conclusions that can be drawn from infra-red measurements.

WHILE powder absorption spectroscopy in the infrared is now rather extensively used in mineralogy, only relatively few papers in this field report on the use of polarized infrared (cf. e.g. 1-3), although it is evident that polarized radiation should be appropriate when dealing with crystals. The first experiments in this field date back to the end of the last century, but technical difficulties have prevented rapid development of this kind of work. Recently the difficulties have been partly overcome by commercial polarizers (e.g. with sets of Se-foils) and by different kinds of "infrared-microscopes", which concentrate the radiation onto a small sample. To work in convergent light is of course a disadvantage compared with the use of parallel light, but it is often necessary when examining objects of only some few square millimetres in area.

Since 1964 the infrared-pleochroism of the OH-stretching frequency has been measured for several minerals in the Institute for Mineralogy and Crystallography in Göttingen (5-10). Several oriented thin sections of each of the minerals were cut. The absorption spectrum was recorded in the region of the OH-stretching frequency with the axis of the incident convergent beam perpendicular to the plate and with a known vibration direction of the electric vector. Another spectrum was recorded after the plate had been turned  $10^\circ$  around the axis of the beam, and the whole procedure was repeated often enough to be able to draw the absorption figure.

Two examples illustrate the conclusions that can be drawn from such measurements.

In riebeckite (8) the absorption figures on thin sections parallel to (100), parallel to (010), and perpendicular to [001] show that the absorption figure for the OH-stretching frequency ( $\lambda = 2.76 \mu$ ) has the shape of a dumb-bell with its axis perpendicular to (100). The result is in accordance with expectations from space-group considerations, since all OH-groups are parallel to each other and to (010). The angle between the direction of the OH-dipoles and [001] is not determined by symmetry—the infrared pleochroism proves that it is  $90 \pm 3^\circ$ .

For topaz (7) the absorption figure in space, as derived from the absorption figures on thin sections parallel to (100), (010), and (001), resembles a lemniscate rotated around its short axis; the rotation axis is parallel to [010] for the usual orientation ( $a$  4.65 Å,  $b$  8.80 Å,  $c$  8.39 Å). The only interpretation of this pleochroic behaviour is that the four OH-groups in the unit-cell all lie practically parallel to (010) but are crossed in this plane by pairs. From the known position of the oxygens of the OH-groups approximate parameters for the hydrogens could be derived.

For details, and for the results for azurite, tourmaline, epidote, and datolite the reader must be referred to the literature (5 to 10). The method is especially useful if the crystal contains groups of strong pleochroic efficiency, and for cases in which the structure does not contain more than one such group in the asymmetric unit.

#### References

1. TSUBOI (M.), 1950. *Bull. Chem. Soc., Japan*, **23**, 83.
2. PETCH (H. E.), SHEPPARD (N.), and MEGAW (H.), 1956. *Acta Cryst.*, **9**, 29.
3. VEDDER (W.), 1964. *Amer. Min.*, **49**, 736.
4. MERRIT (E.), 1895. *Ann. Physik*, **55**, 49.
5. TILLMANNS (E.) and ZEMANN (J.), 1965. *Neues Jahrb. Min., Monatshefte*, 228 [M.A. **18**-124
6. GEBERT (W.) and ZEMANN (J.), 1965. *Ibid.*, 232.
7. ———, 1965. *Ibid.*, 380.
8. HANISCH (K.) and ZEMANN (J.), 1966. *Ibid.*, 19.
9. SAHL (K.), 1966. *Ibid.*, 45.
10. HANISCH (K.), 1966. *Ibid.*, 109.

# Crystal-field spectra and chemical bonding in manganese minerals

By KENNETH L. KEESTER and WILLIAM B. WHITE

Materials Research Laboratory and  
Department of Geochemistry and Mineralogy  
Pennsylvania State University  
University Park, Pennsylvania

*Summary.* Optical absorption spectra have been obtained on a suite of bivalent manganese minerals either by transmission through single crystals or by diffuse powder reflection techniques. The spectra exhibit 5 to 7 weak absorption bands in the visible range that can be assigned in terms of the energy level diagram of  $Mn^{2+}$ . The manganese spectrum is particularly useful in that the easily recognizable sharp bands due to  ${}^6A_{1g} \rightarrow {}^4A_{2g} : {}^4E_g(G)$  and  ${}^6A_{1g} \rightarrow {}^4E_g(D)$  transitions can be used to calculate exactly values for the Racah parameters  $B$  and  $C$ . The Racah  $B$ -parameter is a possible measure of the extent of covalent bonding in the manganese-oxygen bonds in the mineral. The Nephelauxetic ratio ( $B/B$  free ion) varies from 73 to 83% in the various silicates (rhodonite, leucophoenicite, tephroite, glaucochroite, etc.) and is less than its values in the carbonate, sulphate, borate, phosphate, and oxide minerals, thus indicating a higher degree of covalent bonding in the silicates.

THE colour of a mineral is perhaps its most ubiquitous property and might very well be expected to contain some information about the mineral's internal structure. To extract this information requires first the quantification of the colour by expressing it in terms of the absorption spectrum and then in turn interpreting the spectrum by the relatively new theoretical technique of the crystal-field theory. The end products of the analysis are some parameters that can be correlated with structural properties.

The two most common transition metal ions that occur in minerals are iron and manganese. The application of crystal-field theory to iron in silicates has been treated by Burns (1966) and White and Keester (1966). The present paper is a parallel study of the spectra of manganese ions in minerals.

Literature on the spectra of  $Mn^{2+}$  in oxide hosts is sparse. Of interest is the work of Heidt, Koster, and Johnson (1958) on the hexaquo complex, of Pratt and Coelho (1959) on  $MnO$ , of Ford *et al.* (1963) on manganese sulphides, and of Bates, White, and Roy (1966) on the spectra of synthetic zincites.

The object of this paper is to describe the spectra of manganese ions in other oxide hosts, to assign correctly the spectral bands by crystal-field theory, and to use the derived crystal-field parameters to draw some tentative conclusions about the chemical bonding in these minerals.

Both natural and synthetic minerals were used in this study:

*Glaucochroite*, Franklin, New Jersey. Hand-picked, pale blue, glassy grains. Spectra obtained by diffuse reflectance.

*Hübnerite*, synthetic. Prepared by reacting  $\text{Na}_2\text{WO}_4 \cdot 2\text{H}_2\text{O}$  and  $\text{MnCl}_2 \cdot 4\text{H}_2\text{O}$  in water solution, washing, drying, and sintering at  $1000^\circ\text{C}$ . Spectra obtained by diffuse reflectance of the bright olive powder.

*Ilesite*, synthetic. Crystals were grown by slow evaporation of water solution. Spectra obtained by transmission through single crystal plates.

*Inesite*, Kwaduzu mine, Shimoda Township, Shidzoka Prefecture, Japan. Diffuse reflectance spectra were obtained from crushed, unaltered bright pink fibres and laths. This mineral occurs as pink fibrous to radial vein fillings in quartz.

*Leucophoenicite*, Franklin, New Jersey. Purplish-pink massive material crushed and grains hand-picked to avoid zincite contaminant, ground to obtain diffuse reflectance spectra.

*Lithiophilite*, Custer Mountain mine, Custer, South Dakota, and White Picacho district, Yavapai Co., Arizona. The former is a dull orangish-tan, massive but glassy material and the latter has a bright salmon coloured, fine grained, semi-opaque appearance. Thin translucent slices of these minerals were used to obtain spectra by diffuse transmission.

*Manganosite*, synthetic. Dull green stoichiometric oxide powder. Made by heating  $\text{MnO}_2$  in vacuum at  $900^\circ\text{C}$ . Diffuse reflectance spectra.

*Pyrophanite*, synthetic. Prepared by heating pelletized, equimolar  $\text{MnO}_2$ - $\text{TiO}_2$  powders in vacuum, first at  $970^\circ\text{C}$ , then regrinding and reacting at  $990^\circ\text{C}$  to remove all traces of the orthotitanate. Spectra obtained from the bright olive coloured powder by diffuse reflectance.

*Rhodochrosite*, Moose mine, Gilpin County, Colorado. Transmission spectra obtained from transparent, bright rose, cleavage rhombs; the rhombohedron faces were polished.

*Rhodonite*, North mine, Broken Hill, New South Wales, Australia. Transparent, cherry-red sections produced by cleaving and polishing. Transmission spectra.

*Sussexite*, Sterling Hill, New Jersey. Massive, pink. Spectra were obtained by diffuse reflectance on powdered hand-picked grains.

*Tephroite*, Franklin, New Jersey. Pure grey, massive, with zincite and franklinite. Pure powder obtained by crushing the material and selecting grains under magnification, then pulverizing to obtain a diffuse reflectance sample.

The natural specimens were obtained through commercial sources or from personal collections and their identity checked by microscopic examination and by X-ray powder diffraction. Quantitative emission spectrographic analyses were obtained in order to determine the presence of interfering ions such as

ferrous and ferric iron and other transition metals; these results are given in Table I.

All spectra were obtained on a Beckman DK-2A spectrophotometer over the range of 300–3500  $m\mu$ . Three techniques of sample mounting were used as appropriate: transmission through a cleaved or polished single crystal when possible, diffuse transmission through a translucent slab of mineral mounted directly in front of the detector, and diffuse reflectance from powders utilizing a MgO-coated integrating sphere attachment and an MgO plate in the reference beam.

TABLE I. Emission spectrographic analyses of manganese minerals

Sample*	FeO†	MnO	CaO	MgO	Al <sub>2</sub> O <sub>3</sub>	ZnO	TiO <sub>2</sub>	V <sub>2</sub> O <sub>5</sub>
Glaucocroite	0.06%	>3%	36%	0.15%	0.45%	8.5%	<0.02%	<0.02%
Inesite	0.52	>3	7.7	0.26	1.8	<0.2	0.04	<0.02
Leucophoenicite	0.11	>3	3.6	2.2	0.3	<0.2	<0.02	0.02
Lithiophilite (Arizona)	0.43	>3	1.7	0.11	1.7	<0.2	<0.02	<0.02
Lithiophilite (South Dakota)	8.2	>3	2.5	1.3	0.2	<0.2	<0.02	<0.02
Rhodochrosite	0.21	>3	2.2	1.2	0.3	3.7	<0.02	0.02
Rhodonite	13	>3	4.8	0.13	0.45	<0.2	<0.02	<0.02
Tephroite	0.05	>3	2.6	0.65	0.30	5–10%	0.02	—

\* All results in weight percent. In all samples: Cr<sub>2</sub>O<sub>3</sub> < 0.04, CuO < 0.01, Ag<sub>2</sub>O < 0.01, and NiO < 0.03. CoO not determined since it was used as an internal standard.

† Total iron calculated as FeO.

### Theory

The absorption bands in the visible and near infrared parts of the spectrum due to transition metal ions in oxide hosts are usually best interpreted by the crystal-field theory. The theory has been reviewed in detail in several books such as McClure (1959), Griffiths (1961), and Ballhausen (1962) and needs no further review here.

In the weak-field scheme of the crystal-field theory, which is appropriate for most oxide materials, the spectral bands arise from transitions between energy levels derived from the crystal-field splitting of the free-ion energy levels. The degree of splitting can be described by a parameter  $Dq$  and effects of inter-electronic repulsion can be described by the Racah parameters  $B$  and  $C$ . It is thus the object of the analysis here to select the values of the three crystal-field parameters that give the best fit with the observed spectra and then to use these parameters to draw certain conclusions about the structure and bonding of the minerals.

The Mn<sup>2+</sup> ion has a  $d^5$  electron configuration with a <sup>6</sup>S ground term which does not split in any crystal field. The excited states are quartet or doublet states so all transitions are spin forbidden and the resulting absorptions are very weak. It is these weak transitions that give divalent manganese compounds

their typical pale pink colours. Since the ground state is not split, the near infrared region of the spectrum is devoid of features.

The energy level diagram of  $Mn^{2+}$  is extremely complicated. Exact solutions for the excited-state energy levels in terms of  $Dq$ ,  $B$ , and  $C$  may be obtained from the Tanabe–Sugano matrices; however, these are very large (up to  $10 \times 10$ ) matrices and hand calculations are not feasible. For this reason the Tanabe–Sugano diagrams given in many places in the literature (e.g., McClure, 1959) are very incomplete and in fact are not sufficiently complete to allow the assignment of all the observed bands. Dr. J. S. Berkes in this laboratory has written a set of computer programs to solve the Tanabe–Sugano secular equations for any selected values of  $B$  and  $C$  and plot the energy levels as a function of  $Dq$ . Such a computer print-out is shown in fig. 1.

With the computer program it is only necessary to have obtained values for  $B$  and  $C$  and the complete scheme for any  $Dq$  can be quickly calculated. Fortunately  $B$  and  $C$  can be obtained analytically rather easily if a sufficiently complete spectrum can be obtained.

It can be seen from the energy level diagram of fig. 1 that the  ${}^4A_{1g}$ ,  ${}^4E_g(G)$  and  ${}^4E_g(D)$  levels plot as horizontal straight lines on the weak-field side of diagram. These levels are independent of the crystal field strength,  $Dq$ , and can be used for a calculation of  $B$  and  $C$ . The Tanabe–Sugano equations for these levels are:

$$\begin{array}{l} {}^6A_{1g}(S) - 35B - E = 0 \\ {}^4A_{1g}(G) - 25B + 5C - E = 0 \end{array} \quad \begin{array}{l} {}^4E_g(G) \\ {}^4E_g(D) \end{array} \left| \begin{array}{cc} -22B + 5C - E & -2\sqrt{3}B \\ -2\sqrt{3}B & -21B + 5C - E \end{array} \right| = 0$$

For convenience in labelling we make the following definitions:

$$\begin{array}{ll} E_1 = {}^6A_{1g}(S) \text{ (ground state),} & \nu_1 = E_2 - E_1, \\ E_2 = {}^4A_{1g}(G) = {}^4E_g(G), & \nu_2 = E_3 - E_1, \\ E_3 = {}^4E_g(D), & \end{array}$$

where  $\nu_1$  and  $\nu_2$  are the observed wavenumbers of the absorption bands arising from transitions between these states. By solving the Tanabe–Sugano equations and taking advantage of the fact that the  ${}^4A_{1g}(G)$  and  ${}^4E_g(G)$  levels are accidentally degenerate in an octahedral field, the following equations are obtained:

$$\nu_1 = 10B + 5C, \quad \nu_2 = 17B + 5C.$$

If  $\nu_1$  and  $\nu_2$  can be observed and correctly identified in the spectrum,  $B$  and  $C$  can immediately be calculated. Identification is particularly easy in these cases because of the sharpness of the bands. Since these levels are independent of  $Dq$ , the band broadening that usually results from thermal vibrations does not occur.



*Spectra and band assignments*

In this section are presented the spectra of twelve manganese minerals. Two common manganese minerals, rhodochrosite and rhodonite, were available in high quality single crystals, therefore much better spectra were obtained, and the results on these minerals are presented in greater detail. The analysis of all other minerals closely parallels the treatment given to these two.

*Rhodochrosite.* The near IR-spectrum of  $\text{MnCO}_3$  exhibits only a group of bands at the long-wave end of the spectrum, which can be assigned to overtones of the carbonate ion vibrational modes. There is a profusion of detail in the visible and ultraviolet region as shown in fig. 2. This is a particularly detailed spectrum of  $\text{Mn}^{2+}$  and the features present cannot all be accounted for by the energy level diagram of fig. 1. A listing of band wavenumbers and their assignments is given in table II. There are six strong bands, which correspond to the first six quartet states in the energy-level diagram. The two low-energy broad bands can be assigned to the strongly  $Dq$ -dependent  ${}^4\text{T}_{1g}(\text{G})$  and  ${}^4\text{T}_{2g}(\text{G})$  levels. The sharp band at  $24\,750\text{ cm}^{-1}$  is assigned to the field-independent  ${}^4\text{A}_{1g}$ ,  ${}^4\text{E}_g(\text{G})$  level and provides a reference point for the assignment of the higher levels. These assignments agree well with the calculated energy-level diagram except for the  ${}^4\text{T}_{1g}(\text{P})$  level which is calculated to be about  $1\,500\text{ cm}^{-1}$  higher than the highest energy band observed in the ultraviolet. The  $Dq$  value estimated from the diagram is  $750\text{ cm}^{-1}$ . A second check on the assignments can be made by comparing table II with the spectrum of  $\text{MnF}_2$  published by Stout (1959). The assignments for the quartet states agree with those proposed by Stout.

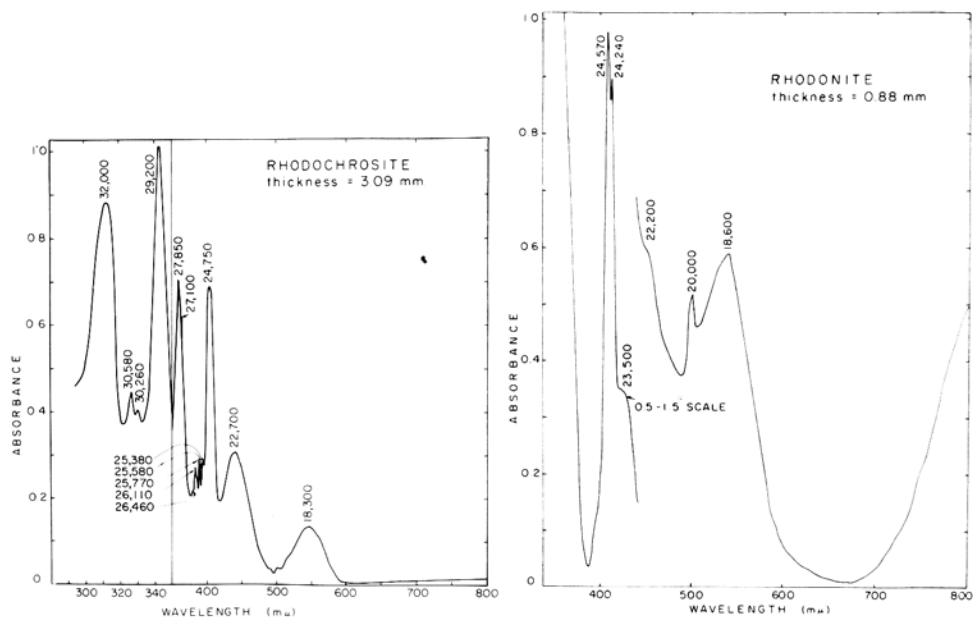
TABLE II. Band positions and assignments for rhodochrosite

Wavenumber ( $\text{cm}^{-1}$ )	Description	Assignment
18 300	broad, strong	${}^6\text{A}_{1g}(\text{S}) \rightarrow {}^4\text{T}_{1g}(\text{G})$
22 700	broad, strong	$\rightarrow {}^4\text{T}_{2g}(\text{G})$
24 750	sharp, v. strong	$\rightarrow {}^4\text{A}_{1g}, {}^4\text{E}_g(\text{G})$
25 380	sharp, weak	} $\rightarrow {}^2\text{T}_{2g}(\text{I})$
25 580	sharp, weak sh.	
25 770	sharp, weak	
26 110	sharp, weak	
26 460	sharp, weak sh.	
27 100	sharp, weak	
27 850	sharp, strong	$\rightarrow {}^4\text{T}_{2g}(\text{D})$
29 200	sharp, v. strong	$\rightarrow {}^4\text{E}_g(\text{D})$
30 260	sharp, weak	$\rightarrow {}^2\text{A}_g(\text{I})$
30 580	sharp, weak	$\rightarrow {}^2\text{T}_{1g}(\text{I})$
32 000	broad, strong	$\rightarrow {}^4\text{T}_{1g}(\text{P})$

The very sharp lines near  $26\,000\text{ cm}^{-1}$  and near  $30\,000\text{ cm}^{-1}$  pose a problem that is not solved here. The high-energy pair assigns rather well to the  $\text{A}_{2g}(\text{I})$  and  $\text{T}_{1g}(\text{I})$  doublet states according to the energy-level diagram. The centre of the family of lines at  $26\,000\text{ cm}^{-1}$  lies near the doublet  $\text{T}_{2g}(\text{I})$  level, which becomes

the ground state of  $\text{Mn}^{2+}$  at the strong field limit. The high degree of splitting may be due to spin-orbit coupling, vibronic coupling, trigonal field splitting, or a combination of all three. The spin-orbit splitting of the  ${}^2\text{T}_{2g}$  term yields only a  $\Gamma_7$  and  $\Gamma_8$  level so at least one additional factor must be operating.

*Rhodonite.* The specimen of rhodonite used in this investigation contains a considerable amount of ferrous iron and the spectral bands of  $\text{Fe}^{2+}$  dominate the near-infrared spectrum. The spectrum of ferrous iron in pyroxenes has become a subject of some debate (White and Keester, 1966; Bancroft and Burns, 1967; White and Keester, 1967). For this reason the present discussion will be limited to those features due to  $\text{Mn}^{2+}$  and a treatment of the near infrared  $\text{Fe}^{2+}$  bands will be deferred to a later paper.



FIGS. 2 and 3: FIG. 2 (left). Visible-ultraviolet spectrum of single-crystal rhodochrosite.

FIG. 3 (right). Visible-ultraviolet spectrum of single-crystal rhodonite.

The assignment of the various bands in the visible part of the spectrum (fig. 3) is now somewhat more difficult since the intensities of the spin-forbidden bands of the ferrous iron will be of comparable intensity to the bands of  $\text{Mn}^{2+}$ . The assignments given in table III were obtained by using a comparison with the pure  $\text{Mn}^{2+}$  spectrum of rhodochrosite as a guide to the  $\text{Mn}^{2+}$  bands and using a computer print-out of the energy-level diagram for  $d^6$  to locate the spin-forbidden bands of  $\text{Fe}^{2+}$ . A match of the observed values for the  ${}^4\text{T}_{1g}(\text{G})$  and  ${}^4\text{T}_{2g}(\text{G})$  levels with the calculated energy level diagram gives an approximate  $Dq$  value of  $825 \text{ cm}^{-1}$  for  $\text{Mn}^{2+}$  in rhodonite. The field-independent  ${}^4\text{A}_{1g}$ ,  ${}^4\text{E}_g$

level is easily recognized by its sharpness, but strong charge-transfer absorption in the ultraviolet obscures the other  ${}^4E_g(D)$  field-independent level and makes the exact calculation of B and C impossible.

TABLE III. Band positions and assignments for rhodonite

Wavenumber (cm <sup>-1</sup> )	Ion and co-ordination	Assignment
18 600	$\left\{ \begin{array}{l} (Mn^{2+})^{VI} \\ (Fe^{2+})^{VI} \end{array} \right.$	${}^6A_{1g}(S) \rightarrow {}^4T_{1g}(G)$
20 000		${}^5T_{2g}(D) \rightarrow {}^3T_{1g}(H)$
22 200	$(Fe^{2+})^{VI}$	${}^5T_{2g}(D) \rightarrow {}^1A_{1g}(I)$
23 500	$(Mn^{2+})^{VI}$	${}^6A_{1g}(S) \rightarrow {}^4T_{2g}(G)$
24 240	$(Fe^{2+})^{VI}$	${}^5T_{2g}(D) \rightarrow {}^3T_{1g}(H)$
24 570	$(Mn^{2+})^{VI}$	${}^6A_{1g}(S) \rightarrow {}^4A_{1g}, {}^4E_g(G)$

*Other silicate minerals.* The spectra of tephroite, glaucocroite, and leucophoenicite are shown in fig. 4 and the spectrum of inesite in fig. 6. These spectra were all obtained by diffuse reflectance techniques and only the quartet states are observed. The important  $\nu_1$  and  $\nu_2$  transitions are recognizable by their sharpness and most of the assignment is easily done by direct comparison of the spectra with the spectrum of rhodochrosite. The quartet levels of these silicates are tabulated in table IV; the near-infrared spectra of these minerals show few features except for hydroxyl and water bands and are not reproduced.

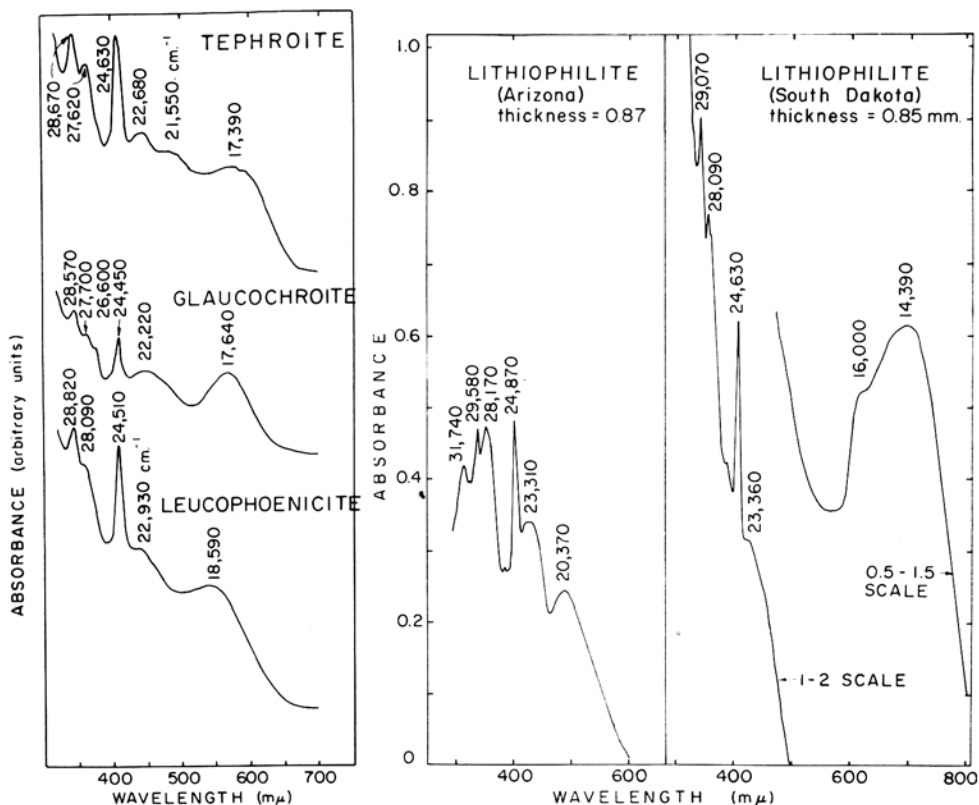
TABLE IV. Band positions and assignments for manganese silicates

Tephroite	Glaucocroite	Leucophoenicite	Inesite	Assignment
17 390	17 640	18 590	18 970	${}^6A_{1g}(S) \rightarrow {}^4T_{1g}(G)$
21 550	—	—	—	
22 680	22 220	22 930	22 880	$\rightarrow {}^4T_{2g}(G)$
24 630	24 450	24 510	24 570	$\rightarrow {}^4A_{1g}, {}^4E_g(G)$
—	26 600	—	—	
27 620	27 700	28 090	27 780	$\rightarrow {}^4T_{2g}(D)$
28 670	28 570	28 820	29 150	$\rightarrow {}^4E_g(D)$
31 340	—	—	—	$\rightarrow {}^4T_{1g}(P)$

*Borate minerals.* The spectrum of sussexite is shown in fig. 6 and the band wavenumbers and assignments in table VI. The spectrum of  $Mn^{2+}$  in the borate compound does not differ in any important respect from the spectrum of  $Mn^{2+}$  in the silicates. The spectrum of a synthetic jimboite,  $Mn_3(BO_3)_2$ , was also examined but the spectral features of  $Mn^{3+}$  obliterated those of  $Mn^{2+}$ .

*Phosphate minerals.* The spectra of two specimens of lithiophilite are shown in fig. 5. Band positions and assignments are tabulated in Table V. The spectra of  $LiMnPO_4$  are interesting in that the Arizona specimen has a clean well-developed  $Mn^{2+}$  spectrum whereas the spectrum of the South Dakota specimen seems to be mainly due to ferric iron. This is borne out by the analyses given in table I.

Two other manganese phosphate minerals, purpurite and hureaulite, were examined. The purpurite spectrum is not easily interpretable and the hureaulite specimen had no observable absorption bands in the region of the spectrum examined.



FIGS. 4 and 5: FIG. 4 (left). Visible-ultraviolet spectra of tephroite, glaucochroite, and leucophoenicite. FIG. 5 (right). Visible-ultraviolet spectra taken by diffuse transmission of two specimens of lithiophilite.

TABLE V. Band positions and assignments for lithiophilite

Arizona specimen	South Dakota specimen	Assignment
20 370	14 390 (Fe <sup>3+</sup> )	${}^6A_{1g}(S) \rightarrow {}^4T_{1g}(G)$
23 310	16 000, (23 360)(Fe <sup>3+</sup> )(Mn <sup>2+</sup> )	$\rightarrow {}^4T_{2g}(G)$
24 870	24 630 (Fe <sup>3+</sup> )	$\rightarrow {}^4A_{1g}, {}^4E_g(G)$
28 170	28 090 (Fe <sup>3+</sup> , Mn <sup>2+</sup> )	$\rightarrow {}^4T_{2g}(D)$
29 580	29 070 (Fe <sup>3+</sup> , Mn <sup>2+</sup> )	$\rightarrow {}^4E_g(D)$
31 740	—	$\rightarrow {}^4T_{1g}(P)$

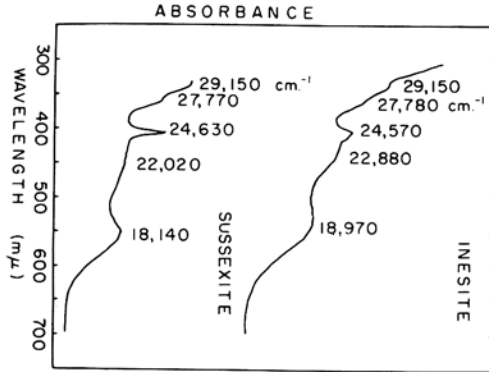


FIG. 6. Visible-ultraviolet spectra taken by diffuse reflectance of inesite and sussexite.

*Oxide and sulfate minerals.* The spectra of ilesite, manganosite, hübnerite, and pyrophanite are shown in fig. 7 and the band positions tabulated in Table VI

The ilesite spectrum was obtained from a thick single crystal and it is not clear why the bands should be weak. The field-independent level in this structure is split into three components with frequencies of 24 750, 25 190, and 26 650  $\text{cm}^{-1}$  when observed under high resolution.

TABLE VI. Band positions and assignments for oxide and sulfate minerals

Ilesite	Manganosite	Hübnerite	Pyrophanite	Sussexite	Assignment
19 800	16 530	17 980	17 980	18 140	${}^6A_{1g}(S) \rightarrow {}^4T_{1g}(G)$
23 470	20 830	—	—	22 020	$\rightarrow {}^4T_{2g}(G)$
25 000	23 920	—	—	24 630	$\rightarrow {}^4A_{1g}, {}^4E_g(G)$
28 330	—	—	—	27 770	$\rightarrow {}^4T_{2g}(D)$
29 850	—	—	—	29 150	$\rightarrow {}^4E_g(D)$

The spectrum of MnO is incomplete because the optical absorption edge cuts off the spectrum just above the  $A_{1g}$ ,  $E_g(G)$  level. The bands that are observed are in good agreement with the values measured by Pratt and Coehlo (1959) on an MnO single crystal. Because the higher levels are not observed,  $B$  and  $C$  cannot be calculated exactly.

In  $\text{MnTiO}_3$  and  $\text{MnWO}_4$  the optical absorption edge is still lower and only the first quartet state of  $\text{Mn}^{2+}$  is observed. No further conclusions can be drawn concerning these minerals.

#### Discussions and conclusions

*Calculation of crystal field parameters.* Racah  $B$  and  $C$  parameters were calculated for all minerals for which a complete spectrum could be observed by use of the formulae previously derived and the experimental values of  $\nu_1$  and  $\nu_2$ . These data are listed in Table VII. The  $Dq$  values listed were derived by fitting

the observed  $T_{1g}(G)$  and  $T_{2g}(G)$  transitions to the energy-level diagram and scaling off  $Dq$ . Thus, the  $Dqs$  can be regarded only as approximations and are certainly not accurate to better than  $\pm 25 \text{ cm}^{-1}$ . The only check possible was for the case of MnO where the present  $Dq$  of  $975 \text{ cm}^{-1}$  agrees remarkably and perhaps fortuitously with Pratt and Coehlo's (1959) value of  $979 \text{ cm}^{-1}$ .

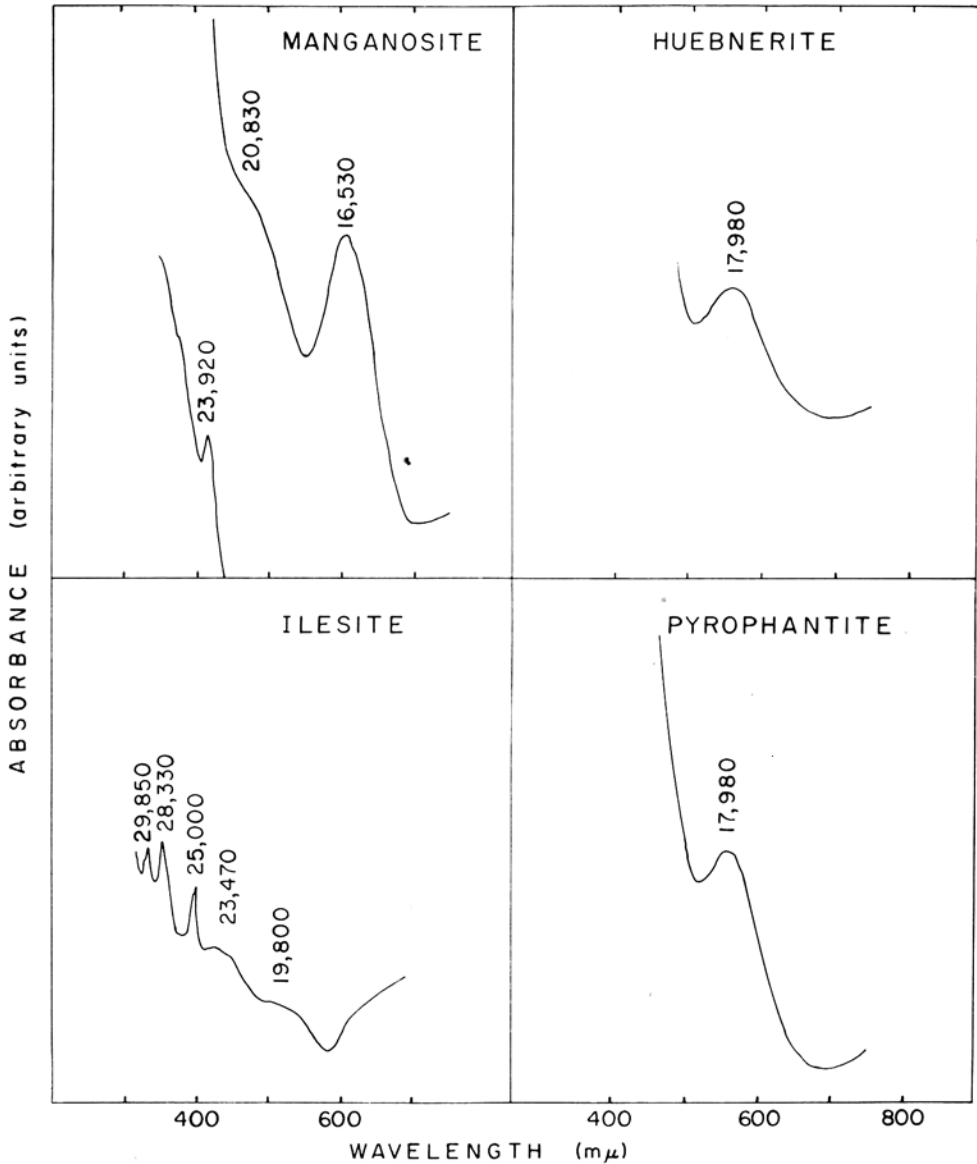


FIG. 7. Visible-ultraviolet spectra for manganosite, ilesite, hübnerite, and pyrophanite.

Also listed in table VII are selected literature data pertinent to the discussion. The values of the crystal-field parameters listed are those given by the authors except for Stout's (1959) data on  $\text{MnF}_2$ . Stout treated his spectra in terms of a covalency parameter,  $\epsilon$ , and thus his results were not directly comparable. The values in table VII were calculated using Stout's reported values for the various absorption bands and the methods discussed above. Some doubt must be expressed concerning Pratt and Coehlo's values for the Racah parameters of  $\text{MnO}$  since the value of  $B$  is much closer to the free ion value than would be expected. At least some lowering of the free ion levels due to covalency effects is expected.

TABLE VII. Crystal field parameters for manganese minerals

Mineral	$\nu_1(\text{cm}^{-1})$	$\nu_2(\text{cm}^{-1})$	$B(\text{cm}^{-1})$	$C(\text{cm}^{-1})$	$Dq(\text{cm}^{-1})$	$C/B$	$\beta(\%)$
$\text{MnO}$ (Manganosite) <sup>†</sup>	23 810		786	3210	979	4.08	100
$\text{MnF}_2$ <sup>‡</sup>	25 180	30 230	721	3594	780	4.98	92
$\text{MnSO}_4 \cdot 4\text{H}_2\text{O}$ (Ilesite)	25 000	29 850	693	3614	750	5.22	88
$\text{LiMnPO}_4$ (Lithiophilite)	24 870	29 580	673	3628	680	5.39	86
$\text{Mn}(\text{H}_2\text{O})_6^{2+}$ <sup>§</sup>	25 115	29 750	$\left\{ \begin{array}{l} 671 \\ (621)^* \end{array} \right.$	$\left\{ \begin{array}{l} 3710 \\ (3781)^* \end{array} \right.$	848	$\left\{ \begin{array}{l} 5.53 \\ (6.09)^* \end{array} \right.$	$\left\{ \begin{array}{l} 85 \\ (79)^* \end{array} \right.$
$\text{Mn}_7\text{Ca}_2\text{Si}_{10}\text{O}_{28}(\text{OH})_2$ (Inesite)	24 570	29 150	654	3606	780	5.51	83
$\text{H}(\text{Mn}, \text{Mg}, \text{Zn})\text{BO}_3$ (Sussexite)	24 630	29 760	646	3634	875	5.62	82
$\text{MnCO}_3$ (Rhodochrosite)	24 750	29 200	636	3678	750	5.78	81
$\text{Mn}_6\text{Mn}(\text{OH})_2(\text{SiO}_4)_3$ (Leucophoenicite)	24 510	28 820	616	3670	830	5.96	78
$\text{Mn}_4\text{CaSi}_5\text{O}_{15}$ (Rhodonite)	24 400		590	3700	825	6.27	75
$\text{CaMnSiO}_4$ (Glaucocroite)	24 450	28 570	588	3714	875	6.32	75
$\text{MnS}$ (Alabandine) <sup>  </sup>	21 600		583	3125	730	5.36	74
$\text{Mn}_2\text{SiO}_4$ (Tephroite)	24 630	28 670	577	3772	875	6.54	73

\* Values calculated by the present methods using the author's experimental data.

† Pratt and Coehlo, 1959.

‡ Stout, 1959.

§ Heidt *et al.*, 1959.

|| Ford *et al.*, 1963.

Crystal-field parameters for rhodonite were calculated using the measured value of  $\nu_1$  and a  $C/B$  ratio of 6.27 obtained by averaging the  $C/B$  ratios of tephroite, glaucocroite, and leucophoenicite. The results must, therefore, be regarded as approximate.

In the usual construction of Tanabe–Sugano diagrams (McClure, 1959) it is often assumed that the  $C/B$  ratio remains constant for any given ion ( $C/B=4.48$  in the Tanabe and Sugano's original and widely copied diagram for  $d^5$ ). From the tabulation in table VII, it can be seen that this ratio varies over a wide range and should not be assumed constant.

*The nephelauxetic effect and covalent bonding.* Jørgensen (1962) has written at great length on what he calls the nephelauxetic or “cloud-expanding” effect. It has long been known that the Racah  $B$  parameters of ions incorporated into crystals are smaller than the Racah  $B$ -parameters of free ions. Since the  $B$ -parameter measures the inter-electronic interaction among the electrons in the  $d$ -orbitals, Jørgensen attributes the decrease in  $B$  to a decrease in interelectronic interaction due to the formation of partially covalent bonds. He proposes that the ratio,  $\beta$ , of the crystal  $B$ -parameter to the free ion  $B$ -parameter is a measure of covalent bonding, the covalence increasing as  $\beta$  decreases.

We have applied Jørgensen's hypothesis to the manganese minerals with the hope of at least comparing the degree of covalence with the bonding in related materials and evaluating its usefulness.

The free ion  $B$ -parameter is obtained from published tables of free-ion energy levels (Moore, 1952) using Griffiths' equations for the free-ion levels in terms of the Racah parameters. The free-ion  $B$  for  $Mn^{2+}$  is  $785\text{ cm}^{-1}$ . The values of  $\beta = B_{\text{crystal}}/B_{\text{free-ion}}$  are tabulated in table VII, and the minerals are arranged in order of decreasing  $\beta$ , leading to a reasonable array. The highest values are exhibited by  $MnO$  and  $MnF_2$ , which are expected to be the most ionic. In the range of 80 to 90% are compounds in which  $Mn^{2+}$  is co-ordinated by groups that themselves are highly covalent such as the sulphate, carbonate, borate, phosphate, and the hexaquo ions. Also included in this group is the mineral inosite for reasons that are not clear at the present time. In the range of 70 to 80% are the silicates and alabandine, the rocksalt form of  $MnS$ . It would thus appear that in the silicates,  $Mn^{2+}$  is more strongly covalently bonded than in the other compounds.

The results, unfortunately, are not as precise as one would like if one wanted to make a detailed ranking within the groups. As can be seen from the Table,  $B$  is derived from a difference term and is very sensitive to the absolute value of  $\nu_2$ . The spectra obtained on powders, which include most of the silicates, are weak and somewhat broadened so that the maximum precision of the band positions is no better than  $\pm 1\text{ m}\mu$ . This uncertainty introduces an uncertainty of  $\pm 20\text{ cm}^{-1}$  in  $B$  and about  $\pm 2$  in  $\beta$ . No significance, therefore, should be attached to the relative covalency of minerals whose  $\beta$  values differ by only a few percent. There would be some value in repeating these measurements on single crystals using a higher precision spectrometer.

One further complication to the Jørgensen hypothesis presents itself.  $MnS$  has a  $\beta$ -value of 74 and falls among the silicates. However,  $\nu_1$  is much lower than  $\nu_2$  for the silicates and this is reflected in the Racah  $C$ -parameter, which is

much lower than the  $C$ -parameter of the silicates. It is apparent that the electronic behavior of the sulfide is different from that of the silicates and that the value of  $B$  alone is not sufficient to describe it.

It is concluded that the application of the Nephelauxetic Ratio concept to the manganese minerals gives results more or less in agreement with expectation. Much more work, both theoretical and experimental, is needed to determine whether this approach will yield a more quantitative statement than could be obtained by chemical intuition.

*Acknowledgements.* This work was supported by the National Science Foundation under Grant No. GP3232.

#### References

- BALLHAUSEN (C. J.), 1962. *Introduction to Ligand Field Theory*. McGraw Hill, New York.
- BANCROFT (G. M.) and BURNS (R. G.), 1967. Interpretation of the electronic spectra of iron in pyroxenes. *Amer. Min.*, **52**, 1278.
- BATES (C. H.), WHITE (W. B.), and ROY (R.), 1966. The solubility of transition metal oxides in zinc oxide and the reflectance spectra of  $Mn^{2+}$  and  $Fe^{2+}$  in tetrahedral fields. *Journ. Inorg. Nucl. Chem.*, **28**, 397.
- BURNS (R. G.), 1966. Origin of pleochroism in orthopyroxenes. *Min. Mag.*, **35**, 715.
- FORD (R. A.), KAUER (E.), RABENAU (A.), and BROWN (D. A.), 1963. The electronic states of octahedral and tetrahedral  $Mn^{++}$  in  $\alpha$ ,  $\beta$ , and  $\gamma$  manganous sulphide. *Ber. Bunsengesell. Phys. Chem.*, **67**, 460.
- GRIFFITH (J. S.), 1961. *The Theory of Transition Metal Ions*. Cambridge.
- HEIDT (L. J.), KÖSTER (G. F.), and JOHNSON (A. M.), 1959. Experimental and crystal field study of the absorption spectrum at 2 000 and 8 000 Å of manganous perchlorate in aqueous perchloric acid. *Journ. Amer. Chem. Soc.*, **80**, 6471.
- JØRGENSEN (C. K.), 1962. The nephelauxetic series. *Prog. Inorg. Chem.*, vol. 4, p. 73. John Wiley, New York.
- MOORE (C. E.), 1952. Atomic energy levels. *Nat. Bur. Std. Circ.*, 467, vol. 2.
- MCCLURE (D. S.), 1959. Electronic spectra of molecules and ions in crystals. In *Solid State Physics*, **9**, 399. Academic Press, New York.
- PRATT (G. W. J.) and COEHLO (R.), 1959. Optical absorption of CoO and MnO above and below the Neel temperature. *Phys. Rev.*, **116**, 281.
- STOUT (J. W.), 1959. Absorption spectrum of manganous fluoride. *Journ. Chem Phys.*, **31**, 709.
- WHITE (W. B.) and KEESTER (K. L.), 1966. Optical absorption spectra of iron in the rock-forming silicates. *Amer. Min.*, **51**, 774.
- 1967. Selection rules and assignments for the spectra of ferrous iron in pyroxenes. *Ibid.*, **52**, 1508.

# Applications of the Mössbauer effect to mineralogy

By G. MICHAEL BANCROFT

University Chemical Laboratories, Cambridge

and ROGER G. BURNS<sup>1</sup>

Department of Mineralogy and Petrology, Cambridge

*Summary.* The Mössbauer spectra of a number of iron silicate minerals of known crystal structure and three iron silicate minerals of unknown crystal structure have been recorded at room temperature. The two Mössbauer parameters, the chemical isomer (C.I.) shift and the quadrupole splitting, are sensitive to changes in the oxidation state, electronic configuration, and the co-ordination symmetry in the minerals. Using the Mössbauer parameters from the silicates of known crystal structure, information on the oxidation state, electronic configuration, and co-ordination symmetry of iron in the unknown crystal structures has been obtained.

Mössbauer measurements have also been used to detect cation ordering in minerals of the orthopyroxene and cummingtonite-grunerite series. Quantitative results for the cummingtonite-grunerite series show that  $\text{Fe}^{2+}$  preferentially occupies the  $M_4$  position, and discriminates against the  $M_2$  position.

THE Mössbauer effect (for a review, see Wertheim, 1964) has found widespread applications in chemistry and physics following its discovery in 1957. In applying this effect to mineralogical problems, two important applications have been found in the study of iron-containing minerals. First, Mössbauer spectroscopy provides a rapid method for obtaining information on the state of iron in minerals. Second, Mössbauer measurements may be used to estimate site populations in complex crystal structures.

The present study was aimed at investigating the variations of Mössbauer parameters with changes in electronic configuration, oxidation state, and co-ordination symmetry of iron in various minerals of known crystal structure. It was hoped that these data could be used to obtain information on the state of iron in three minerals for which the structures are unknown: zussmanite, howieite, and deerite. The reference minerals studied included the following with high-spin  $\text{Fe}^{2+}$ : staurolite (tetrahedral); gillespite (square planar); olivines, pyroxenes, amphiboles (octahedral with various distortions); and almandine garnet (distorted cubic). Epidote (distorted octahedral) and andradite (octahedral) provided parameters for high spin  $\text{Fe}^{3+}$ . These parameters are compared with those of a few inorganic compounds containing low-spin Fe II and Fe III in octahedral co-ordination.

<sup>1</sup> Present address: Department of Geology and Mineralogy, Parks Rd., Oxford.

There are several advantages of working with silicate minerals. Firstly, the crystal structures of the reference silicates are known with moderate to high degrees of precision. Secondly, the minerals provide co-ordination symmetries not readily available to the synthetic inorganic chemist. Thirdly, solid-solution phenomena enable measurements on a phase with a range of iron concentrations.

The Mössbauer parameters are sensitive to changes in the environment about the iron atom. Since in many silicate minerals iron can enter two or more sites differing structurally and energetically, the Mössbauer technique may be used to estimate site populations in ferromagnesium silicates (Bancroft, Burns, and Maddock, 1967). In these studies, computer-calculated areas under peaks (Stone, 1967) are used to determine the ratio of the amounts of iron in two distinct sites in a mineral.

*Experimental.* The Mössbauer instrumentation and technique are described elsewhere (Bancroft, Maddock, and Ward, 1965). A two millicurie source of  $^{57}\text{Co}$  in stainless steel was used. This gives a minimum line-width of 0.35 mm/sec with sodium nitroprusside as the absorber. All the spectra in the present study were measured with both the source and absorber at room temperature. Total counts in excess of  $2 \times 10^5$  per channel were obtained for each spectrum.

Absorbers were prepared by mixing the finely ground mineral (150 mesh) with two grams of ground perspex and pressing the mixture into a disc about 2 mm thick. Each disc contained an iron concentration of about 10 mg/cm<sup>2</sup>.

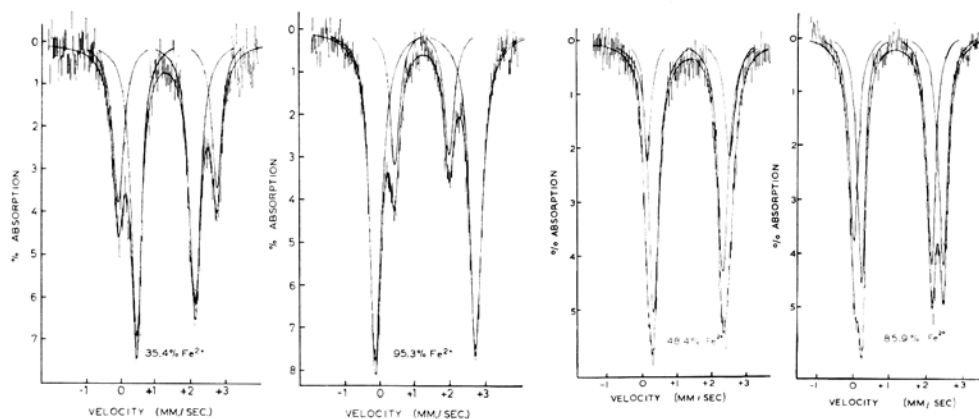
The mirror image spectra obtained from the spectrometer were fitted by computer to Lorentzian line shapes (the theoretical line shapes). A good fit, defined by the value of  $\chi^2$  (Stone, 1967), was obtained for most of the spectra.

The two principal parameters measured in the present study were the C.I. shift and quadrupole splitting. The quadrupole splitting is the separation between the doublet peaks in a Mössbauer spectrum. The chemical isomer shift is the displacement of the midpoint of a quadrupole doublet from zero velocity (relative to a standard, which was stainless steel).

### *Results and discussion*

*The reference silicates.* The C.I. shifts and quadrupole splittings obtained for the reference silicates are summarized in table I, along with parameters for low-spin iron compounds. Four peaks were resolved in the cummingtonite, grunerite, staurolite, and orthopyroxene spectra, but only two were resolved in the other spectra. In the olivine, orthopyroxene, and cummingtonite-grunerite spectra, the C.I. shift and quadrupole splitting varied with  $\text{Fe}^{2+}/\text{Mg}^{2+}$  ratio. Table I quotes the range of these parameters. This variation of Mössbauer parameters with increasing  $\text{Fe}^{2+}$  concentration demonstrates the sensitivity of the parameters to small changes in the structure.

The computer plots of the Mössbauer spectra of two members of the cummingtonite-grunerite series (35.4% and 95.3%  $\text{Fe}^{2+}$ ) and two members of the orthopyroxene series (48.4% and 85.9%  $\text{Fe}^{2+}$ ) are shown in figs. 1 and 2.



FIGS. 1 and 2: FIG. 1 (left). Computer plots of the Mössbauer spectra of the 35.4% Fe<sup>2+</sup> cummingtonite and the 95.3% Fe<sup>2+</sup> grunerite. FIG. 2 (right). Computer plots of the Mössbauer spectra of the 48.4% Fe<sup>2+</sup> and 85.9% Fe<sup>2+</sup> orthopyroxenes.

TABLE I. Mössbauer parameters for the reference minerals and compounds

Mineral or compound	Type of Iron	Position in the structure	Symmetry of the co-ordination polyhedra	C.I. shift mm/sec.	Quadrupole splitting mm/sec.
Olivines	Fe <sup>2+</sup>	$M_1$ and $M_2$	~octahedral	1.25-1.27	2.81-3.02
	Fe <sup>2+</sup>	$M_2$	distorted six fold	1.24-1.27	1.91-2.13
Orthopyroxenes	Fe <sup>2+</sup>	$M_1$	~octahedral	1.24-1.27	2.35-2.65
	Fe <sup>2+</sup>	$M_4$	distorted six fold	1.14-1.20	1.50-1.64
Cummingtonites and grunerites	Fe <sup>2+</sup>	$M_1, M_2, M_3$	~octahedral	1.23-1.27	2.76-2.90
	Fe <sup>2+</sup>		distorted eight fold		
Garnet	Fe <sup>2+</sup>		~square antiprism	1.40	3.55
Gillespite	Fe <sup>2+</sup>		four fold square planar	0.86	0.51
Staurolite*	Fe <sup>2+</sup>		four fold ~tetrahedral	1.05	2.29
Epidote	Fe <sup>3+</sup>	(Al, Fe) site	distorted six fold	0.43	2.01
Andradite	Fe <sup>3+</sup>		octahedral	0.50	0.58
Fe II compounds†	Fe II		octahedral	0-0.45	0-1.0
Fe III compounds†	Fe III		octahedral	-0.25-+0.25	0-1.5

\* Another quadrupole doublet was resolved in this spectrum.

† Parameters taken from Duncan and Golding, 1965.

In both series, the inner two peaks arise from  $\text{Fe}^{2+}$  in the most distorted site, which is the  $M_4$  site in the cummingtonite structure (Ghose, 1961) and the  $M_2$  site in the orthopyroxene structure (Ghose, 1965). The outer two lines in fig. 2 are due to  $\text{Fe}^{2+}$  in the  $M_1$  position in orthopyroxene, and in fig. 1 the outer two lines represent a composite plot for iron in the  $M_1$ ,  $M_2$ , and  $M_3$  positions in cummingtonite. Figs. 1 and 2 indicate that ordering occurs in both the cummingtonite–grunerite series and orthopyroxene series, and that  $\text{Fe}^{2+}$  ions favour the most distorted site in each structure.

TABLE II. Percentage of each position in the amphibole structure occupied by iron in the cummingtonite–grunerite series

Mole % $\text{Fe}^{2+}$	Percentage of position occupied by $\text{Fe}^{2+}$			Mole % $\text{Fe}^{2+}$	Percentage of position occupied by $\text{Fe}^{2+}$		
	$M_1 + M_3$	$M_2$	$M_4$		$M_1 + M_3$	$M_2$	$M_4$
35.4	24.0	5.5	82.5	87.5	85.3	80.5	98.0
51.8	50.0	33.0	73.5	95.3	98.3	96.0	90.0
63.0	65.3	36.0	86.5	19.7*	14.7	28.5	18.5
85.0	87.3	83.0	83.5				

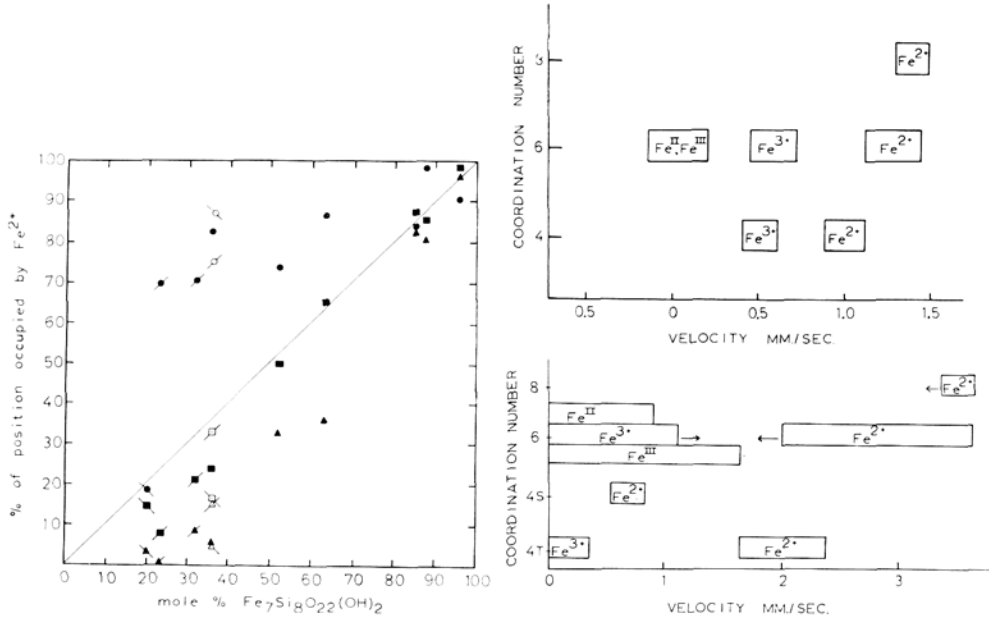
\* Manganoan cummingtonite containing 23.7%  $\text{Mn}_7\text{Si}_8\text{O}_{22}(\text{OH})_2$ .

The computer-calculated areas under the peaks in the Mössbauer spectra enable site populations to be estimated in orthopyroxenes directly (Bancroft, Burns, and Howie, 1967). Total site populations in the cummingtonite–grunerite series may also be estimated from the Mössbauer spectra (Bancroft, Burns, and Maddock, 1967) in conjunction with data from infrared spectroscopy (Burns and Strens, 1966). The results for the cummingtonite–grunerite series are summarized in table II and fig. 3. This method gives site populations in good agreement with X-ray results (Fischer, 1966). These quantitative results confirm the qualitative observations from figs. 1 and 2 that  $\text{Fe}^{2+}$  ions enter preferentially the cummingtonite  $M_4$  and orthopyroxene  $M_2$  positions.

Fayalitic olivines, almandine garnet, and epidote gave simple two-line spectra. The spectra of olivine and epidote are similar to those published earlier (de Coster *et al.*, 1963; Sprenkel-Segel and Hanna, 1964). No ordering was detected in olivine and epidote, although electronic spectral measurements of olivines (Burns, unpublished work) and optical data of epidotes (K. Mills, personal communication) suggest that cation ordering may occur also in these structures.

The four-line spectrum of staurolite indicates that this mineral contains  $\text{Fe}^{2+}$  in two distinct structural positions. This was not found by X-ray diffraction studies (Náray-Szabó and Sasvári, 1958).

The results in table I show that the quadrupole splitting and chemical isomer shift are sensitive not only to the electronic configuration and oxidation state of iron, but also to the number and symmetry of the co-ordinating ligands. The changes in C.I. shift and quadrupole splitting are illustrated in fig. 4 for the different electronic configurations, oxidation states, and co-ordination



FIGS. 3 and 4: FIG. 3(left). Percentages of each position in the amphibole structure occupied by iron in the (Fe, Mg, Mn)-Si-O<sub>22</sub>(OH)<sub>2</sub> series. A line at 45°, representing random distribution, is drawn for reference. ● M<sub>4</sub> position; ■ M<sub>1</sub>, M<sub>3</sub> positions; ▲ M<sub>2</sub> position. ● ■ ▲ cummingtonite-grunerite series; ● ■ ▲ anthophyllite series; ● ■ ▲ manganese cummingtonite; ∅ □ △ Ghose (1961); ∅ □ △ Fischer (1966). FIG. 4 (right). Variations of (top) the chemical isomer shift; and (bottom) the quadrupole splitting with changes in the oxidation state and electronic configuration of iron, and the coordination number about iron. 4S square planar co-ordination, 4T tetrahedral co-ordination.

symmetries of iron. The quadrupole splitting for epidote lies outside the normal range for Fe<sup>3+</sup> compounds. This may be due to the very large distortion of the oxygen environment about iron in the epidote structure (Ito, Morimoto, and Sadanaga, 1954). It should be noted that in "high spin" Fe<sup>2+</sup> compounds, the quadrupole splitting becomes smaller with increasing distortion from octahedral symmetry of the co-ordinating oxygens (Ingalls, 1964), whereas the reverse is true for "high-spin" Fe<sup>3+</sup> compounds. Few "low-spin" Fe II and Fe III compounds have been studied. Values of the C.I. shift and quadrupole splitting for these species are taken from Duncan and Golding (1965). Fig. 4 shows that Mössbauer spectra will generally indicate the state of iron (including the oxidation state, electronic configuration, co-ordination number, and site distortion) in a silicate of unknown or complex crystal structure.

*The silicates of unknown crystal structure.* The Mössbauer spectra of zussmanite, howieite, and deerite are shown in fig. 5, together with the computer-plotted best-fit to the spectra. Table III summarizes the Mössbauer parameters for these three minerals.

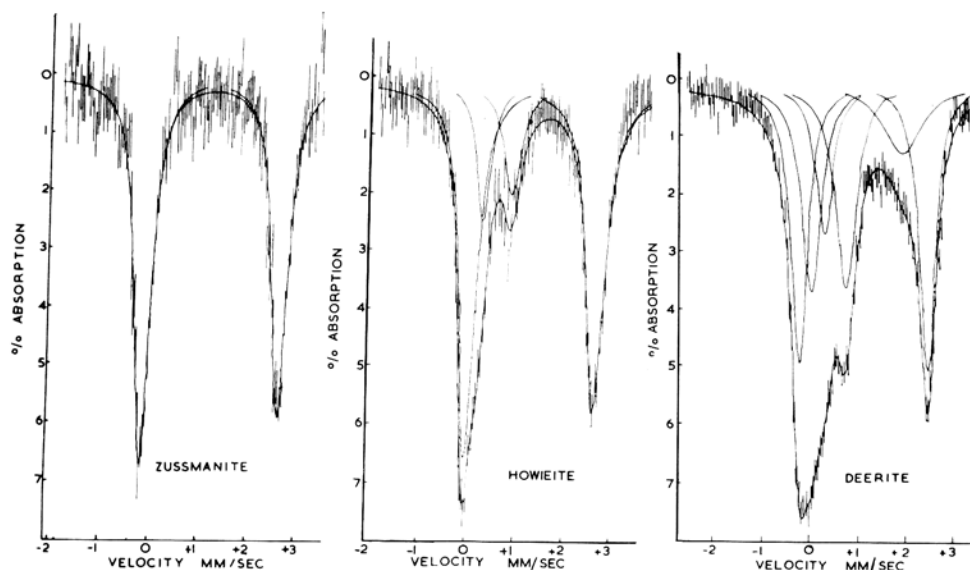


FIG. 5. Computer plots of the Mössbauer spectra of zussmanite, howeite, and deerite.

In view of the sensitivity of the Mössbauer parameters to changes of electronic configuration, oxidation state, and co-ordination symmetry of iron (fig. 4) the C.I. shift and quadrupole splitting may be used to characterize the iron in these three minerals.

Thus, zussmanite contains "high-spin"  $\text{Fe}^{2+}$  ions in an octahedral environment similar to that in olivine (Hanke, 1965). Howeite contains "high-spin"  $\text{Fe}^{2+}$  ions in octahedral co-ordination, and "high-spin"  $\text{Fe}^{3+}$  ions in a slightly distorted six-fold co-ordination site. Deerite appears to contain three distinct "high-spin" iron species: Two of these, one  $\text{Fe}^{2+}$  and the other  $\text{Fe}^{3+}$ , are present in sites similar to those in howeite; the third, consisting of  $\text{Fe}^{2+}$  ions, occur in distorted six-fold co-ordination sites similar to the  $M_4$  site in the cummingtonite structure. However, the large width of the peaks due to the latter  $\text{Fe}^{2+}$  species (fig. 5) cannot be explained at the present time. It may be related to the anomalously low magnetic susceptibility of deerite reported by Fyfe *et al.*, (1966),

TABLE III. Mössbauer parameters for the unknown crystal structures

Mineral	Type of iron	Symmetry of the co-ordination polyhedra	C.I. shift mm/sec.	Quadrupole splitting mm/sec.
Zussmanite	$\text{Fe}^{2+}$	~octahedral	1.26	2.77
Howeite	$\text{Fe}^{2+}$	~octahedral	1.27	2.81
	$\text{Fe}^{3+}$	~octahedral	0.49	0.58
Deerite	$\text{Fe}^{2+}$	~octahedral	1.22	2.57
	$\text{Fe}^{2+}$	very distorted six fold	1.14	1.40
	$\text{Fe}^{3+}$	~octahedral	0.54	0.62

which has led them to postulate the presence of "low-spin" Fe II in deerite. In the present study, however, no peaks were found which could be attributed to "low-spin" Fe II.

### Conclusions

The Mössbauer effect gives valuable information on the electronic and molecular structure of iron in silicate minerals. Qualitative estimates may be made of the amount of distortion of a co-ordination polyhedron from octahedral symmetry, and information may be obtained on the state of iron in minerals of unknown crystal structure, such as deerite, howieite, and zussmanite. Other minerals to which Mössbauer spectroscopy may be applicable include sapphirine, neptunite, stilpnomelane, chloritoid, and yoderite. The Mössbauer technique is also useful for detecting cation ordering and estimating site populations in ferromagnesian silicates, such as in the orthopyroxene and cummingtonite-grunerite series. Other mineral series at present being studied include actinolite, anthophyllite, and pigeonite. The great advantage of the Mössbauer technique in studies of ordering is the speed and, in many cases, the improved accuracy over more conventional X-ray diffraction methods.

### References

- BANCROFT (G. M.), MADDOCK (A. G.), and WARD (J.), 1965. *Chem. and Ind.*, 423.  
 — BURNS (R. G.), and HOWIE (R. A.), 1967. *Nature*, **213**, 1221.  
 — — and MADDOCK (A. G.), 1967. *Amer. Min.*, **52**, 1009.  
 BURNS (R. G.) and STRENS (R. G. J.), 1966. *Science*, **153**, 890.  
 DE COSTER (M.), POLLAK (H.), and AMELINCKX (S.), 1963. *Phys. Stat. Sol.*, **3**, 283.  
 DUNCAN (J. F.) and GOLDING (R. M.), 1965. *Quart. Rev.*, **19**, 36.  
 FISCHER (K. F.), 1966. *Amer. Min.*, **49**, 963.  
 FYFE (W. S.), CARMICHAEL (I. S. E.), and MACHIN (D. J.), 1966. *Nature*, **211**, 1389.  
 GHOSE (S.), 1961. *Acta Cryst.*, **14**, 622.  
 — 1965. *Zeits. Krist.*, **122**, 81.  
 HANKE (K.), 1965. *Beitr. Min. Petr.*, **11**, 535.  
 INGALLS (R.), 1964. *Phys. Rev.*, ser. A, **133**, 787.  
 ITO (T.), MORIMOTO (N.), and SADANGA (R.), 1954. *Acta Cryst.*, **7**, 53.  
 MUELLER (R. F.), 1962. *Geochimica Acta*, **26**, 581.  
 NÁRAY-SZABÓ (I.) and SASVÁRI (K.), 1958. *Acta Cryst.*, **11**, 862.  
 SPRENKEL-SEGEL (E. L.) and HANNA (S. S.), 1964. *Geochimica Acta*, **28**, 1913.  
 STONE (A. J.), 1967. Appendix to:  
 BANCROFT (G. M.), MADDOCK (A. G.), ONG (W. K.), and PRINCE (R. H.), 1967. *Journ. Chem. Soc.*, 1966.  
 WERTHEIM (G. K.), 1964. *Mössbauer Effect: Principles and Applications*, Academic Press, New York.

## **Growth of diamond and cubic boron nitride from multi-component systems**

By P. J. GIELISSE

General Electric Company  
Specialty Materials Department  
Detroit, Michigan 48232, U.S.A.

*Summary.* The growth characteristics of diamond synthesized from multi-component systems under controlled conditions of high pressure and high temperature are contrasted with those of cubic boron nitride. Growth processes are found to be quite similar. The morphologies, although distinctly different, are crystallographically quite similar. In cubic boron nitride, tetrahedra replace the octahedron in diamond. As contrasted to the covalently bonded diamond, cubic boron nitride depends to an appreciable extent on direct coulombic interaction for its bonding energy.

AS the only hard non-metallic elemental mineral, diamond possesses a variety of very desirable qualities. Consequently, its physical properties have been widely investigated. In spite of this, and the fact that diamond constitutes one of the simplest crystallographic structures, little information about the actual crystal growth process has been derived from the study of the characteristics or genesis of diamond. The earliest, and, at the same time, very extensive observations on naturally occurring diamond were made by Fersman and Goldschmidt (1911) and Williams (1932). Though often very detailed, their conclusions regarding crystal growth processes had to remain speculative for the greater part since virtually nothing was known about the crystal growth parameters or the system from which they were derived. Laboratory-grown diamonds for the first time afforded an opportunity for the study of diamond crystal forms, habits, surface structure, and other properties with the possibility of relating them to the many variables in the growth process.

A distinct advantage is the possibility of comparing the results on diamond to those derived from crystal growth studies on cubic boron nitride, which is very similar to diamond in a great many respects. Some of the more recent results are reported in this paper.

Since the crystals of diamond and cubic boron nitride studied here were synthesized in high-pressure-high-temperature apparatus, using cells, systems, and catalysts described previously (Wentorf, 1961; Bundy, 1963; Bundy and Wentorf, 1963), further mention of any of the particulars need not be made here.

Fig. 1 shows, for ease of reference, the pressure and temperature regimes for the synthesis of both high pressure forms. The data are taken from Bundy (1963) and Bundy and Wentorf (1963).

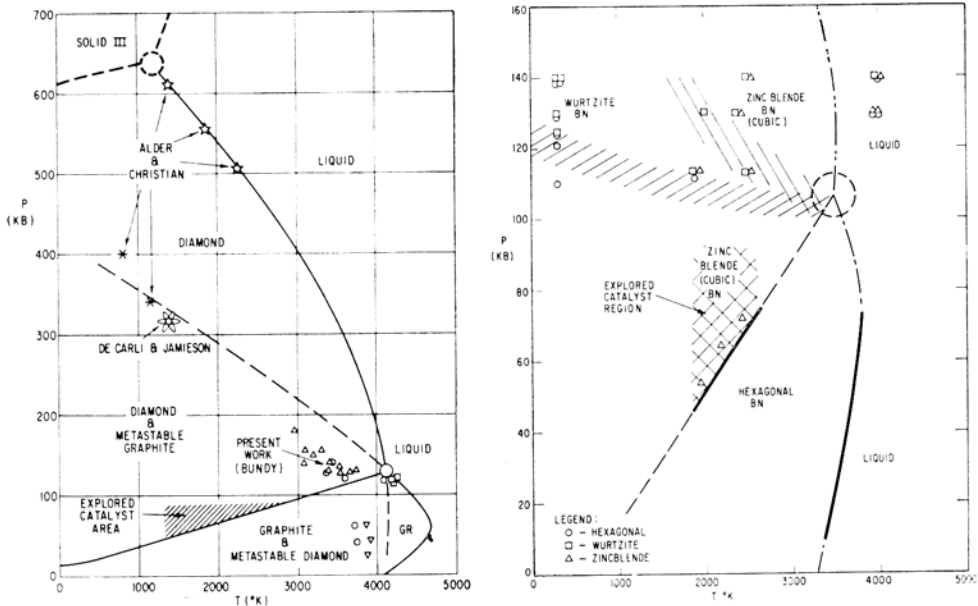


FIG. 1. The  $P$ - $T$  phase diagrams of carbon and boron nitride, after Bundy (1963) and Bundy and Wentorf (1963).

### Crystallography

**Diamond.** The high-pressure-stable form of carbon crystallizes in the cubic system with the structure based on the cubic space group,  $Fd\bar{3}m$ . The unit cell contains eight atoms, and each atom is surrounded by four equidistant neighbours at the corners of a regular tetrahedron.

An unusual aspect of the crystallography of mined diamond is that, although the rhombic dodecahedron and octahedron are most common, it crystallizes in virtually all of the forms that are allowed for its class. Considering any one crystal, this is not common since one or two habits are often representative of the species, and, as such, characteristic. The forms developed on laboratory-grown diamonds are almost exclusively the octahedron, the cube, or, more often, a combination of the two (Bovenkerk, 1961). This points to a difference in either the fundamental growth process or the conditions under which growth took place.

Under laboratory conditions, where growth takes place from a metal-carbon system, the low-temperature limit for diamond synthesis is usually set by the melting point (i.e. eutectic of the carbon-metal system), and the high-temperature limit by the conditions of thermodynamic stability of the diamond. If we

assume that pressures are low enough to prevent overgrowth, intergrowth, or extremely rapid nucleation, we shall find that cubic development is favoured at the lower temperature, gradually changing to cubo-octahedra and eventually octahedra at more elevated temperatures. This occurs for growth from apparently pure systems.

Doping, apart from possible changes in the electrical or optical properties of the resulting crystals, can drastically influence their morphological development. For example, addition of boron to the catalyst at concentrations as low as 200 p.p.m. does not significantly affect the above-described pattern. However, at constant pressure and with increasing concentration of boron, it becomes essentially impossible to synthesize a well-developed cube, and only cubo-octahedra and octahedra result. At concentrations of boron around 1 000 p.p.m. only octahedra are synthesized over the entire region between the lower and upper limits of diamond stability (fig. 2). Chemical analysis, progressively increasing conductivity, and change in colour confirm increasing boron content in the crystal itself. Similar effects, although not yet studied as fully, have been

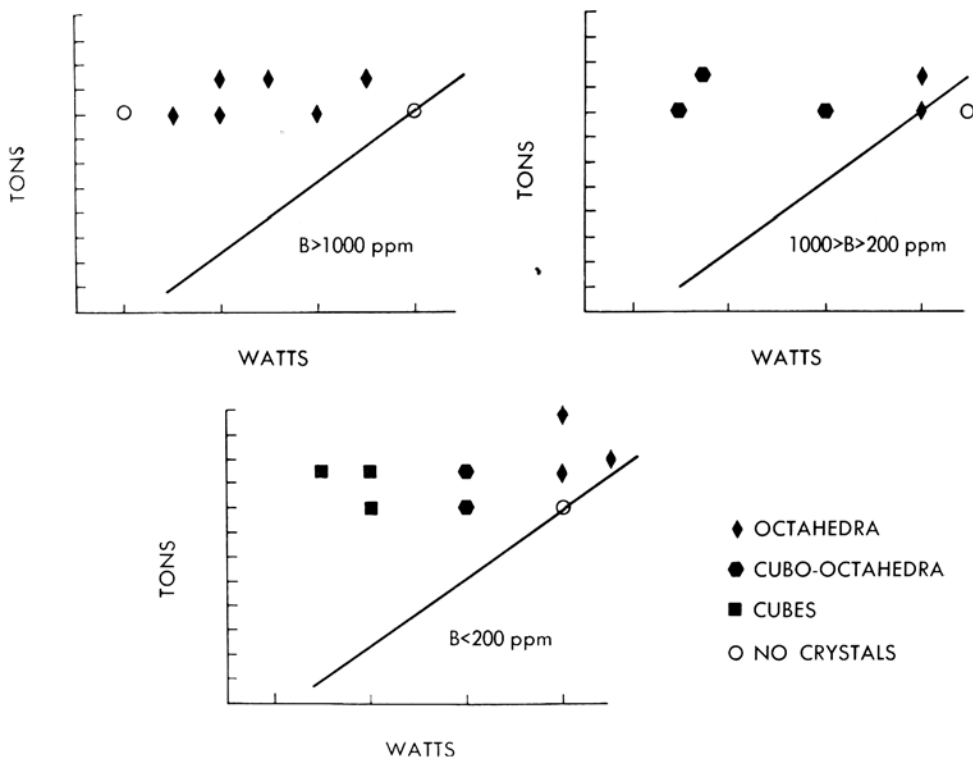


FIG. 2. Schematic representation of the crystal habit of diamond for systems with varying boron content: a,  $B < 200 \text{ p.p.m.}$ ; b,  $1\ 000 > B > 200 \text{ p.p.m.}$ ; c,  $B > 1\ 000 \text{ p.p.m.}$

observed with several elements other than boron. Cannon (1966) has recently described the greatly increased occurrence of contact twins when diamond is formed by catalysed reaction in the presence of decomposable silicon compounds.

Thus, whereas trace quantities of impurities do not appear to influence crystal habit significantly, laboratory growth of diamond from multicomponent systems may produce appreciably different results. In the case of boron, the apparent effect is that of a rise in synthesis temperature.

*Cubic boron nitride* is structurally similar to diamond and shares many of its physical properties. It is hard, inert, commonly a dielectric, has a high index of refraction and high dispersion, and is commonly synthesized as white, pale yellow to yellow crystals. It forms crystals with the B<sub>3</sub> (zinc blende) structure, the only difference from diamond being that the positions in the structure are alternately filled with boron and nitrogen atoms and each atom is surrounded by four atoms of the other kind. An important consequence of this is, however, that the space group is  $F\bar{4}3m$ , which lacks a centre of symmetry. This should give rise to vector properties and, more important in this context, the lower symmetry will affect the habit and face development of the crystals.

As in manufactured diamond, none of the more complex forms have been observed, and only  $\{100\}$ ,  $\{111\}$ , and  $\{1\bar{1}1\}$ , the cube and the positive and negative tetrahedra, could be identified (cf. P. Cannon, 1966). A recent report (K. Kudaka, H. Konno, T. Matoba, and S. Takahashi, 1965) on the morphology of cubic boron nitride describes frequent occurrence of the rhombic dodecahedron  $\{110\}$  as the most prominent form modifying the tetrahedron; the text is not explicit enough nor is the evidence sufficient to prove the occurrence of the dodecahedral faces. It seems likely that rhombic dodecahedral surfaces are formed by accumulation of growth layers on  $\{111\}$  and  $\{1\bar{1}1\}$ . It should be pointed out that dodecahedra are only rarely found in laboratory-grown diamonds and only under very special conditions where dissolution is suspected (H. P. Bovenkerk, 1961). The rhombic dodecahedron is not considered a true growth form of synthetic diamond, but since the dodecahedral form is very common in natural diamond, the natural growth environment may not be duplicated in our laboratory conditions. Since cubic boron nitride is not a mineral, no correlation is possible.

The more common forms and habits of cubic boron nitride are: the tetrahedron as a simple form, or more commonly as a combination of positive and negative tetrahedra, which resembles an octahedron when equally developed. Very often, however, growth in the third dimension is suppressed on these combined tetrahedra, resulting in platelets no thicker than  $20 \mu$ , which often appear like a more or less perfect hexagon. Due to variations in growth conditions and environment these platelets may take on almost any shape and vary widely in thickness as well.

The most complex morphology of untwinned crystal observed is the combination of cube and both tetrahedra, in which one tetrahedron is almost invariably

more developed than the other. Interestingly enough, this habit is very common with sphalerite (ZnS), the structural prototype of boron nitride.

In all our observations, the crystals have generally shown smooth plane faces. Curved faces are very rare if not nonexistent. However, fracture is very common and often produces fragments with curved faces. In general, tetrahedra are the most common form in boron nitride, with the cubo-tetrahedral habit also very pronounced. In no case has the development of a cube been observed as a simple form.

As is common for many crystals with the zinc blende structure, twinning is pronounced in cubic boron nitride. The twins in general have a  $[111]$  twin axis and a corresponding  $\{111\}$  twin or composition plane. The most abundant twin variety is a rotation twin in which the parts of the crystal on both sides of this composition plane are rotated  $180^\circ$  around  $[111]$ . On both sides positive and negative tetrahedra have been developed. Again, if both tetrahedra are equally developed, the geometrical shape will resemble the familiar twinned octahedron or spinel twin, common in both natural and synthetic diamond. The common occurrence of this type of twinning must be indicative of the relatively slight energy difference between such a twinned form and the regular or normally occurring form. Cannon (1966) has found that a very large amount of contact twinned diamond may be grown from systems containing decomposable silicon compounds, such as  $Mg_2Si$  and  $CaSi_2$ , and proposed the growth of a very thin SiC layer from which the twin would develop. It has been observed that Mg itself induces twinning in diamond, and since Mg and Ca as well as Li, Na, and K are used as catalysts in BN growth systems that produce abundant twins, these elements may be responsible for the twinning. Synthesis at elevated temperature, as contrasted with growth at low temperature, invariably produces a greater quantity of twinned crystals in boron nitride and diamond. It is therefore not yet clear whether the formation of twins depends on the presence of foreign atoms. Much less common is a contact twin on  $\{111\}$  with tetrahedra and cube developed.

Many crystals are far from perfect geometrically. They are often irregularly distorted giving rise to a wide variety of shapes. Penetration twins and intergrowths do not always appear as commonly as in diamond. Tetrahedral crystal faces are very smooth, with trigons not uncommon, while striations are quite common on cube faces, probably reflecting the higher reticular density in the tetrahedral face. In general, visual observation discloses no inclusions in crystals grown from pure catalysed BN systems, other than entrapped crystals of cubic BN itself. Symmetrically arranged impurities may be observed when deliberately introduced into the growth system. They are discussed later.

Evidence for a step-wise or layer-spreading growth mechanism in BN, as opposed to a continuous growth mechanism, may be found in the development of well-defined step surfaces on tetrahedral planes (fig. 3). The largest step in the particular example shown was estimated to have a height of  $30 \mu$ , with a similar width and a slope of 1 : 10 between the top and bottom edges.

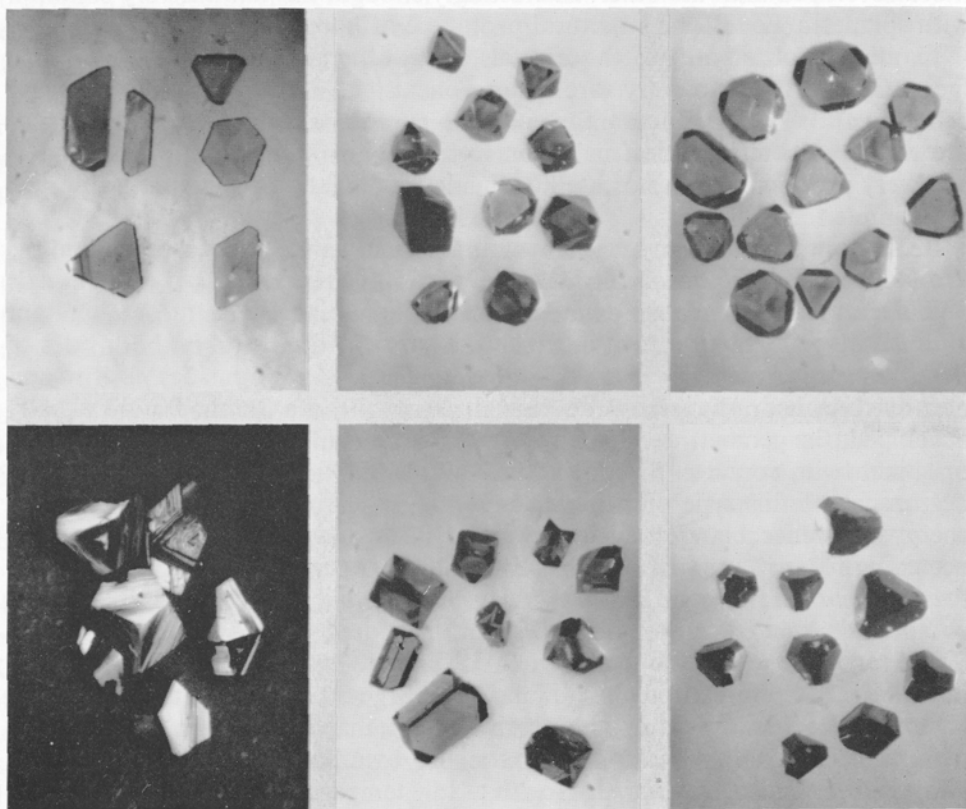


FIG. 3. Photomicrographs of cubic boron nitride. Top left, various habits of platelets; top middle and right, combinations of positive and negative tetrahedra; bottom left, evidence for stepped growth on (111); bottom middle, twinned crystals with (111) as composition plane; bottom right, combinations of cube and tetrahedra.

The habit of crystals is known to vary with the type of growth process, degree of supersaturation, amount and type of impurity, concentration, rate of diffusion, pressure, and temperature. In the BN system we again find many similarities with diamond. The development of the principal habits in boron nitride is chiefly a function of temperature. At moderate pressures and low temperatures, only the very smallest crystals appear, as tetrahedra. A slight increase in temperature or growth time immediately leads to the development of the cubic faces, while at increasingly higher temperatures twinned platelets develop, which show only tetrahedral forms. At higher temperatures the growth rate, as well as the amount of twinned crystals, is markedly increased. Both the prevalence of twinned crystals and the platelet development are assumed to be indicative of high rate of growth and surface nucleation under conditions of high supersaturation. This is confirmed by our observations in the higher temperature

regime, as described above. Evidently, growth mechanisms under these conditions are such that axial growth is very much suppressed while lateral growth is enhanced.

Increased pressure chiefly seems to increase the rate of nucleation and thus results in generating large numbers of much smaller crystals. Appreciably elevated pressures generate crystals with very poor morphological development, ultimately resulting in an essentially anhedral particle. It may thus be said that, in general, the most perfect crystals are grown close to the equilibrium line between the hexagonal and cubic forms of boron nitride.

Surface markings that resemble streams with tributary development, reflecting differential freezing of catalyst metal, are a very marked phenomenon on synthetic diamonds (Bovenkerk, 1961). No such markings appear on boron nitride faces, and we may in all likelihood conclude that the growth process is either more abruptly ended or precipitation of the high pressure form of boron nitride proceeds in a manner dissimilar to that in catalyzed diamond systems.

*Discussion.* When crystals of cubic boron nitride were grown from systems containing deliberately introduced carbonaceous material, it was observed that darker coloured bands or "streamers" developed, apparently symmetrically arranged, emanating from a point in the crystal and extending towards the tetrahedral faces. Since this phenomenon is only observed when carbon is present, it must be concluded that the inclusions are carbonaceous impurities, or a carbon complex, symmetrically and preferentially trapped in or between the growth layers.

Similar observations have been made on diamond (fig. 4). This type of occurrence is typical for conditions of minimum pressure and temperature, i.e. close to the equilibrium line, where growth is extremely rapid and inclusion of particles, possibly undissolved, is most likely. A very interesting point is the fact that in crystals showing both tetrahedra, the zones of inclusions extend only from what is believed to be the point of nucleation to one set of tetrahedral faces, preserving symmetry. It may, therefore, be indicated that the crystal is nucleated as a tetrahedron with the development of the other tetrahedron at a later stage. The tetrahedron thus appears to be the fundamental form immediately after nucleation, which is supported by the occurrence of very small ( $< 5 \mu$ ) tetrahedra at the very early stages of growth, with the development of the cubic faces only when conditions regulating relative growth rates are favourable, i.e. at low temperatures. From all evidence gathered from laboratory experiments, similar reasoning may be applied to the development of habit in diamond, with the octahedral form replacing the tetrahedra in cubic BN.

Growth of one crystal around another has been observed. This suggests interruption of the growth process by thermal or concentration gradients or actual movement and subsequent initiation of new growth. As in diamond, growth upon a seed always reveals a boundary and the crystal is never truly continuous structurally.

The development of many and often complex forms on any one crystal is frequently interpreted as evidence for very slow growth rates from very pure systems. The lack of development of crystal forms, other than the three simplest ones, might indicate growth conditions quite different from those attained in our experiments. There is evidence that very slow growth develops more complex forms in diamond. Very pure systems do affect the habit of boron nitride, producing multiple twins never observed in any standard system.

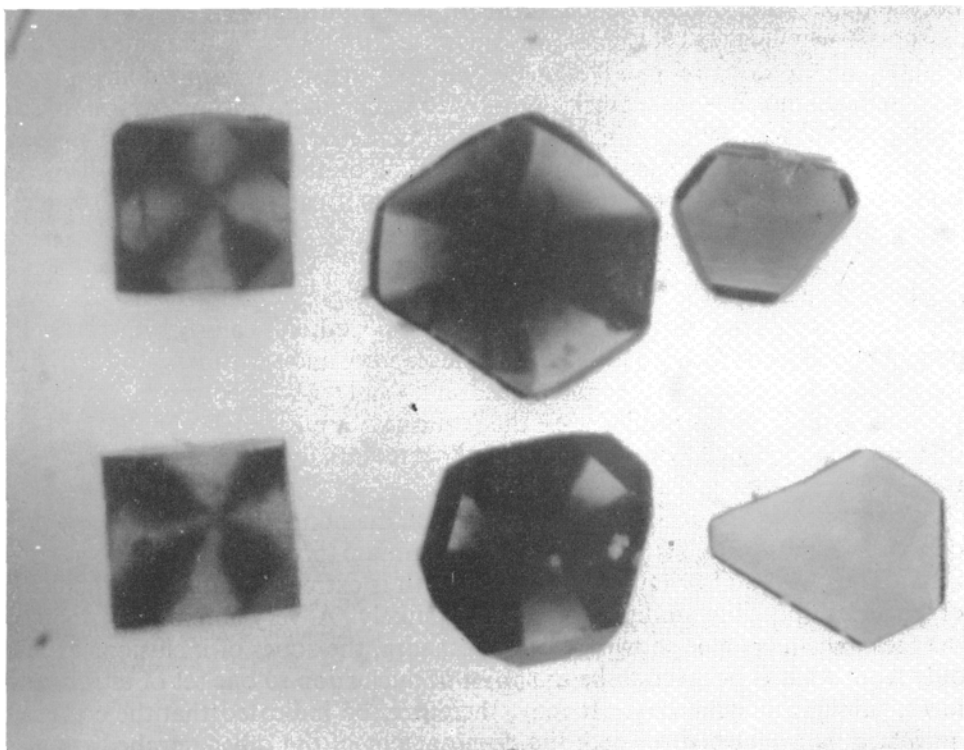


FIG. 4. Symmetrically oriented carbonaceous impurities in diamond (left), cubic boron nitride containing a little carbon (middle), and cubic boron nitride with very little carbon (right).

From experiments on the synthesis of cubic BN, from catalysed systems in the stability region of this high-pressure polymorph, we may thus conclude that: The principal forms developed on cubic BN are the tetrahedra and the cube; more complex forms have not been identified so far. The habit of cubic BN is dependent on pressure and temperature, but primarily on temperature. The first form after nucleation is probably the tetrahedron, with cubo-tetrahedral development at low temperatures, and tetrahedral habit, often composite and twinned, at high temperatures. At any given temperature, an increase in pressure results in higher nucleation rates, smaller crystals and eventually less perfect

particles. A combination of low pressure and temperature favours the cubo-tetrahedral habit. The habits described here are probably the result of very rapid growth from impure systems.

*Binding forces in diamond and cubic boron nitride.* Cubic boron nitride, through its similarities in structure and physical properties, is the solid most closely related to diamond. The relationship also holds true for the low-pressure polymorphs from which they are normally synthesized, graphite and hexagonal boron nitride, except that graphite is a conductor and hexagonal boron nitride

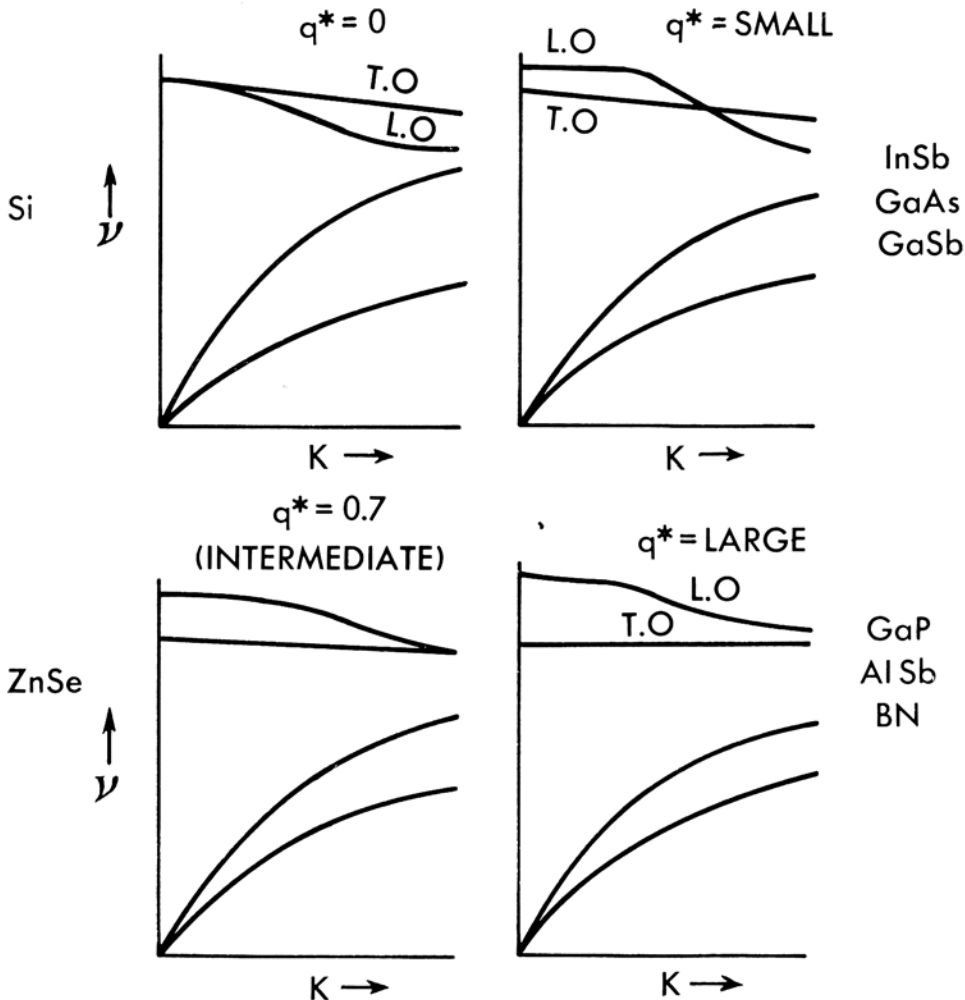


FIG. 5. The effect of ionicity on the dispersion curves (frequency as a function of wave vector) for solids with varying degrees of ionicity, adapted from Mitra and Marshall (1964). For cubic boron nitride  $q^*$  is large.

a dielectric. Graphite thus manifests an excess of free electrons, reflecting the difference in electronic structure between carbon on the one hand and boron and nitrogen on the other. Since binding forces in solids are the result of the electromagnetic interaction of the participating constituents, a difference in bond type between diamond and cubic boron nitride should be indicated. Following Pauling's (1960) concepts of chemical bonding, diamond, with zero electronegativity, has been classified as a covalent solid. Using Pauling's formula,  $1 - \exp[-1/4(X_a - X_b)^2]$  where  $X_a$  and  $X_b$  are the electronegativities of the participating atoms, we arrive at a value of 22% for the ionic character of cubic boron nitride. Part of the binding energy should, therefore, depend on direct coulombic or electrostatic interaction. Support for the fact that binding in cubic BN is partly ionic has recently been derived from our studies of the optical properties of BN in its lattice-vibrational region (Gielisse *et al.*, 1967). The maximum reflectivity in this region was found to be 84%, indicating the presence of an appreciable dipole moment between boron and nitrogen in the high-pressure structure. By comparison diamond shows no attenuation of the reflectivity in its vibrational region. Cubic boron monophosphide, another compound in the III-V series with an electronegativity of only 0.1 and consequently an essentially covalent character, shows a reflectivity of only 5% above the high-frequency background.

The polar character of the bond in cubic boron nitride, as measured by the effective charge  $q^*$  from an interrelation between the dielectric constants and the vibrational frequencies, according to Szigeti (1949), gave  $q^* = 1.14$ . This is the highest value for any compound in the III-V series. Similar results were derived from the difference between the longitudinal and transverse optical frequencies, which is known to increase with ionicity (Mitra and Marshall, 1964; Mitra and Gielisse, 1964). Furthermore, for crystals of high effective ionic charge the longitudinal optical frequencies are higher than the transverse optical frequencies at the zone boundary (Mitra and Gielisse, 1964). For cubic boron nitride L. O. was found to be  $1\,232\text{ cm}^{-1}$  and T. O. =  $1\,000\text{ cm}^{-1}$ . The reverse is true for a totally covalent material. Fig. 7 is a graphical presentation of the effect of ionicity on the dispersion curves.

The report of purely dipolar local fields in cubic boron nitride by Sundfors (1963), as a result of a nuclear magnetic resonance study, is correlated by the observation of sharp lines in the ESR spectra of the same material as determined by Cannon (personal communication, 1964).

### Conclusions

Laboratory evidence from growth phenomena of cubic boron nitride and diamond indicates very similar crystallization processes. Principal crystal forms are the cube and octahedron for diamond and cube and tetrahedra for cubic boron nitride. For any one given system, temperature is the most important in determining habit. Low temperature, preferably combined with low pressure, favours cubo-octahedral or cubotetrahedral habit while higher temperatures

result in octahedra and tetrahedra. The results reported here are due to rapid, sometimes, very rapid, growth from relatively impure systems under conditions of pressure and temperature very close to the respective equilibrium lines. Growth at much reduced rates and for extended periods of time from pure systems will probably result in more complex morphological development. From physical considerations, it was concluded that cubic boron nitride, although similar to diamond in many of its properties, is appreciably ionic. Any physical characteristics principally determined by this difference should, therefore, be significantly dissimilar.

*Acknowledgement.* I would like to thank H. P. Bovenkerk for his constructive comments on reading this text.

#### References

- BOVENKERK (H. P.), 1961. *Amer. Min.*, **46**, 952. [M.A. **15**, 513].  
BUNDY (F. P.), 1963. *Journ. Chem. Phys.*, **38**, 631.  
— and WENTORF (R. H. Jr.), 1963. *Ibid.*, **38**, 114.  
CANNON (P.), 1966. Morphology and properties of diamond, presented to the Amer. Chem. Soc. annual meeting.  
FERSMAN (A.) and GOLDSCHMIDT (V.), 1911. *Der Diamant*. Winter, Heidelberg.  
[FILONENKO (N. E.), IVANOV (V. I.), and FELDGUN (L. I.)] ФИЛОНЕНКО (Н. Е.), ИВАНОВ (В. И.), и Фелдгун (Л. И.), 1966. *Soviet Physics Doklady* (translation of Докл. акад. наук СССР, сер. Физ.), **16**, 899.  
GIELISSE (P. J.), MITRA (S. S.), PLENDL (J. N.), GRIFFIS (R. C.), MANSUR (L. C.), MARSHALL (R.), and PASCOE (E. A.), 1967. *Phys. Rev.*, **155**, 1039.  
KUDAKA (K.), KONNO (H.), MATOBA (T.), and TAKAHASHI (S.), 1965. *Japan. Journ. Appl. Phys.*, **4**, 767.  
MITRA (S. S.) and GIELISSE (P. J.), 1964. *Progress in infrared spectroscopy*, **2**, 47. Plenum Press, New York.  
— and MARSHALL (R.), 1964. *Journ. Chem. Phys.*, **41**, 3158.  
PAULING (L.), 1960. *The nature of the chemical bond*. Cornell University Press, New York.  
SUNDFORS (R. K.), 1963. *Thesis*, Cornell University.  
SZIGETI (B.), 1949. *Trans. Faraday Soc.*, **45**, 155.  
WENTORF (R. H. Jr.), 1961. *Journ. Chem. Phys.*, **34**, 809.  
WILLIAMS (A. F.), 1932. *The genesis of the diamond*. Benn, London.

# La croissance du quartz lamellaire sur l'exemple des cristaux de la Gardette (Isère, France)

par B. POTY

Centre de Recherches Pétrographiques et Géochimiques  
B. P. 682—54-Nancy

*Résumé*—Les cristaux de quartz lamellaire de la Gardette se sont formés dans un milieu dont les caractéristiques ont varié brutalement un grand nombre de fois. Ceci a engendré une structure zonaire des cristaux par adsorption irrégulière d'impuretés. La croissance est examinée ici à travers l'avancement du rhomboèdre positif. La vitesse d'avancement de la face est le facteur qui règle la teneur en impuretés (Al, Li) adsorbées dans le cristal. Les faces plagiédres *s* et *x* ne se forment que lorsque la vitesse de croissance est faible et tendent à disparaître dès que celle-ci augmente. Il en résulte qu'elles apparaissent et disparaissent plusieurs fois au cours de la formation d'un cristal.

LES anomalies optiques des cristaux de quartz sont signalées par Descloizeaux (1858) qui outre ses propres observations rapporte des observations antérieures aux siennes. Mais le premier travail moderne sur cette question est celui de Weil (1930). Weil décrit des cristaux de quartz de la Gardette formés d'un empilement de lamelles biréfringentes parallèles aux faces. Remarquant le même phénomène sur des cristaux d'autres gisements il en déduit que le quartz ne saurait avoir une symétrie hexagonale et devrait plutôt être considéré comme un empilement mimétique de lamelles de symétrie moindre. Bambauer, Brunner, et Laves (1961) ont décrit des lamelles comparables sur des cristaux de quartz de Madagascar. Ils considèrent que les lamelles biaxes résultent d'une formation secondaire mais admettent que leur disposition et leur répartition ont pu être prédéterminées dans une large mesure par une répartition zonaire et sectorielle des impuretés lors de la croissance des cristaux.

Cette idée d'une structure mimétique du quartz est issue de conceptions qui furent développées par Mallard (1876) à propos de toute une série de minéraux. On sait que d'autres points de vue furent adoptés: en particulier celui d'une adsorption d'impuretés par les différentes faces du cristal au cours de sa croissance. L'avancement de faces à propriétés de surface différentes entraîne une structure sectorielle du cristal, chaque secteur montrant des particularités induites par la face qui le forme compte tenu des caractéristiques du milieu (Lemlein, 1948).

Ce travail est une tentative de reconstitution des conditions de croissance des cristaux de quartz de la Gardette par des observations détaillées de leur structure zonaire et sectorielle. Les cristaux de la Gardette sont incolores,

mais on sait que l'irradiation du quartz par les rayons X provoque habituellement une coloration (Frondel, 1945). Cette coloration est particulièrement utile ici car elle met nettement en évidence la structure zonaire et sectorielle. Les lamelles biréfringentes prennent des teintes variées, elles sont en continuité rigoureuse d'un secteur du cristal à l'autre. Il est alors possible de délimiter le domaine d'un certain nombre de cristaux à l'intérieur de celui qu'on examine.

Les relations entre la croissance et les modifications du milieu telles qu'elles peuvent être cernées par l'étude des inclusions fluides ont été recherchées sur un grand nombre de cristaux. Cent trente individus particulièrement limpides ont été taillés en sections épaisses (2 mm) parallèles au plan de pseudosymétrie du cristal, (11 $\bar{2}$ 0). Une trentaine d'autres ont été taillés perpendiculairement à l'allongement du prisme. Ces sections ont été polies optiquement (oxyde de cerium) puis irradiées (Machlett, W, 38 KV, 20 ma, 2 h). L'exposé complet des résultats de cette étude sera fait ailleurs.<sup>1</sup> Ici on s'attache à montrer exclusivement le mode d'avancement du rhomboèdre positif ainsi que celui des faces plagiédres.

#### *Bandes de croissance du rhomboèdre positif*

Elles sont bien visibles sur les sections parallèles au plan de pseudosymétrie des cristaux. On constate alors le plus souvent une alternance de lamelles jaunes et de lamelles brunes, parfois de lamelles incolores. Quand on examine l'évolution de la couleur dans le sens d'avancement de la face on voit que souvent les lamelles jaunes passent progressivement aux lamelles brunes, mais que l'inverse ne se produit jamais: les lamelles brunes passent toujours brutalement aux lamelles jaunes. Ceci incite à ne pas dissocier l'ensemble formé par une lamelle jaune et la lamelle brune qui lui succède dans le sens d'avancement de la face: on appellera cet ensemble une *bande de croissance*.

Ces bandes possèdent dans un même cristal des épaisseurs et des intensités de coloration variées. Elles sont donc très facilement reconnaissables et on peut les numéroter (fig. 1). Les numéros partent de la fin de la croissance des cristaux et remontent en direction du germe. Le nombre des bandes diffère sur chaque cristal. Dans une même cavité les cristaux ne sont en effet pas tous nés au même instant et les déformations de leur base qui oblitèrent cette structure en bandes ne sont pas identiques sur tous les individus. Mais on constate que dans une même cavité la succession des bandes est la même pour tous les cristaux. Il en résulte que lorsqu'on examine sur deux cristaux prélevés dans la même cavité des bandes portant le même numéro on compare des phénomènes qui se sont produits rigoureusement au même moment.

Lorsqu'on suit la limite entre deux bandes en direction des faces du cristal qui dans le gisement regardaient vers le haut on constate que cette limite est jalonnée par un dépôt de petits cristaux de quartz ou autres minéraux dont la taille varie entre 1 et 30  $\mu$ . Ce dépôt de débris minéraux rigoureusement réglé

<sup>1</sup> Poty (B.) Recherches sur la croissance des cristaux de quartz dans les filons. Thèse—Nancy—à paraître 1967.

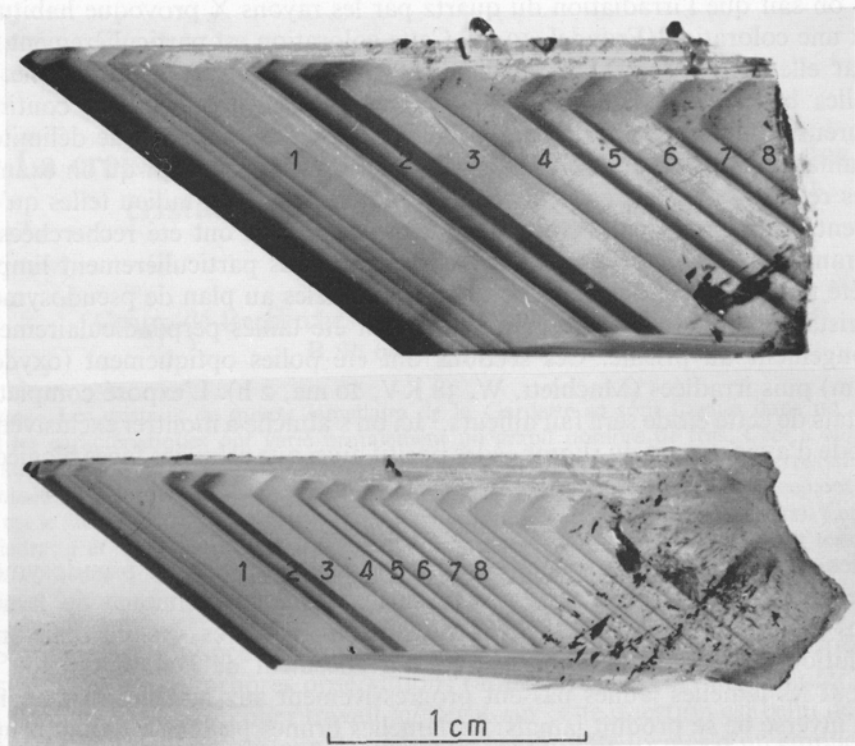


FIG. 1. Cristaux provenant de la même cavité et montrant des successions identiques de bandes de croissance.

par la direction de la verticale (Poty, 1966) trouve son origine très vraisemblablement dans les broyages successifs engendrés par les différents rejeux de la fracture dans laquelle le filon s'est mis en place. On peut observer de légers dépôts de cristaux au milieu d'une bande de croissance, mais ceci n'est pas général. De toutes façons les dépôts à l'intérieur des bandes sont faibles et la plus grande masse des débris a sédimenté à la limite entre les bandes. Il faut déduire de ce fait qu'une bande de croissance est la partie du cristal qui a poussé entre deux rejeux importants de la fracture.

*Signification de la division des bandes de croissance en lamelles.* Elle nous est donnée par l'examen des cristaux dans toute l'étendue du gisement. Le filon de la Gardette est constitué par une série de cavités échelonnées, sur une distance de plus de 300 m, dans des gneiss au contact de la surface de transgression triasique. Dans chaque cavité on trouve des cristaux de tailles très variées, allant de plusieurs cm de longueur à quelques mm. Mais les dimensions de la majorité des cristaux d'une cavité, comme celles des plus gros individus, ne sont pas distribuées au hasard: à une extrémité du gisement, au contact des

roches sédimentaires, les cristaux atteignent leur taille maxima pouvant dépasser parfois 20 cm de longueur alors qu'à l'autre extrémité, ils sont beaucoup plus petits, ne dépassant guère 5 cm de longueur, et prennent un faciès aciculaire. On note donc une évolution de faciès réglée par la distance à la surface de transgression triasique. Cette évolution de faciès témoigne des différences suivantes dans la croissance des cristaux: le quartz pousse rapidement en gros cristaux trapus près des roches sédimentaires, il pousse plus lentement, en cristaux allongés, lorsqu'on s'éloigne de la surface de transgression triasique.

Les individus montrent un nombre de bandes comparable d'un bout à l'autre du gisement mais la constitution des bandes varie. Dans le premier cas elles sont formées par une lamelle jaune épaisse et une fine lamelle brune, dans le deuxième cas le rapport des épaisseurs est inversé. On considère donc que les lamelles jaunes témoignent d'une croissance du quartz relativement rapide et que les lamelles brunes témoignent d'une croissance plus lente.

Des lamelles jaunes et des lamelles brunes ont été isolées et on a recherché les variations des teneurs en impuretés ainsi que les variations des paramètres du réseau.

*Recherche des impuretés.* De nombreux travaux (cf. Frondel, 1962) ont montré que Al était l'impureté rencontrée le plus fréquemment et avec la plus grande abondance dans les cristaux de quartz naturel. A côté de Al on trouve également H, Li, Na, Mg, Ti, Fe. Dans les lamelles analysées Al et Li sont les impuretés les plus abondantes et les plus régulièrement distribuées (tableau No I). Les lamelles jaunes contiennent 2 fois plus de Al que les lamelles brunes et la quantité de Li est liée à celle de Al aux erreurs d'analyse près. Na, Mg, Ti, Fe sont présents à des teneurs faibles ne dépassant pas le plus souvent 1 ppm. H a été décelé par spectrométrie de masse sur des cristaux entiers et limpides, ne contenant pas d'inclusions fluides visibles au microscope (Zimmermann, 1966). On ne peut malheureusement pas comparer les teneurs en H des deux types de lamelles.

TABLEAU No I. Teneurs en Al et Li des lamelles formant les bandes de croissance du rhomboèdre positif

No.	Lamelles brunes		No.	Lamelles jaunes	
	Al	Li		Al	L
1	120 p.p.m.	20 p.p.m.	6	410 p.p.m.	40 p.p.m.
2	250	35	21	310	40
4	190	30	42	420	50
8	310	30	94	460	55
93	160	25	95	470	80
			Moyennes		
p.p.m.	210	30		410	55
Atomes/10 <sup>6</sup> .Si	460	240		920	470

Les lamelles brunes ont été analysées au moins deux fois, les lamelles jaunes au moins trois fois. Précision de la méthode analytique,  $\pm 30\%$ .

Mesure précise des variations des paramètres  $a$  et  $c$ . Des diffractogrammes ont été réalisés pour quatre lamelles (2 jaunes et 2 brunes) à des angles proches de la diffraction en retour. Les raies utilisées pour le calcul furent 420 ( $\theta_{\text{Cu-K}\alpha_1} = 73^\circ 31'$ ) et 315 ( $\theta_{\text{Cu-K}\alpha_1} = 75^\circ 8'$ ). Les variations  $\delta a$  et  $\delta c$  des paramètres  $a$  et  $c$  sont consignées dans le tableau No II. On voit que le paramètre  $a$  croît lentement quoique irrégulièrement lorsque la teneur en impuretés s'accroît. La dimension du paramètre  $c$  est par contre une fonction nette de la teneur en Al.

TABLEAU No II. Variations des paramètres  $a$  et  $c$  dans les lamelles

No.	lamelle	Atomes/ $10^6$ .Si		Li/100 Al	$\delta a$	$\delta c$
		Al	Li			
4	brune	420	250	59	$10 \times 10^{-4} \text{ \AA}$	$3 \times 10^{-4} \text{ \AA}$
2	brune	560	300	53	7	6
6	jaune	910	350	38	13	10
94	jaune	1 020	480	47	13	11

Trois diffractogrammes ont été réalisés pour chaque échantillon. Reproductibilité,  $\pm 1.10^{-4} \text{ \AA}$ . Les constantes utilisées pour le calcul sont celles données par Frondel (1962, pp. 25 et 33).

*Contenu en impuretés et centres colorés.* On admet généralement (Frondel, 1962; Frank-Kamenetskii, 1964; Kamensksev, 1965) qu'une augmentation du paramètre  $c$ , parallèlement à une augmentation de la teneur en Al indique une substitution de Si par Al. De ceci on déduit que la quantité d'Al contenue dans les tétraèdres est plus grande dans les lamelles jaunes que dans les lamelles brunes.

Pourquoi alors ces lamelles contiennent-elles moins de centres colorés que les lamelles brunes? Les travaux de Bambauer (1961) ont montré que, dans le modèle de centre coloré d'O'Brien, les défauts Al-H, Al-Li et Al-Na n'étaient pas équivalents. Le défaut Al-Li semble bien être un centre coloré potentiel mais dans les cristaux des Alpes Suisses une teneur importante en H entraîne généralement une faible coloration après irradiation  $\gamma$ .

H a été décelé dans les cristaux de la Gardette mais non dosé. Na est par ailleurs une impureté peu abondante. Il faut donc croire que, outre leur plus grande teneur en impuretés, les lamelles jaunes se distinguent des lamelles brunes par une répartition différente de H et de Li. Dans les lamelles brunes Li doit être préférentiellement associé à l'Al des tétraèdres, et produit des centres colorés, alors que dans les lamelles jaunes il pourrait céder la place à H.

#### *Apparition et disparition des faces plagiédres $s$ et $x$*

*Observations sur la morphologie interne.* Sur des sections taillées spécialement et irradiées on peut examiner le comportement des faces plagiédres  $s$   $\{11\bar{2}1\}$  et  $x$   $\{51\bar{6}1\}$  au cours de l'histoire des cristaux. Sur de telles sections on remarque nettement la trace de ces faces sous forme de lamelles incolores à la fin de la croissance des bandes (lorsque se forment des lamelles brunes sur le rhomboèdre).

Elles sont visibles sur de nombreuses bandes (fig. 2), ce qui montre que les faces plagiédres, à la Gardette, ne se développent pas seulement à la fin de l'histoire du cristal. Si on n'observe plus leur trace dans les régions proches du germe c'est peut-être parce qu'il est difficile d'en deviner la position à l'intérieur du cristal et de tailler des sections adéquates.

Que deviennent les faces plagiédres au début de la croissance des bandes? Les différences de coloration sont alors plus ténues et l'observation est difficile. Seuls quelques cas sont démonstratifs. Sur la fig. 3 on voit le secteur de croissance d'un trapèzoïdre. Au niveau d'une lamelle jaune du rhomboïdre ce trapèzoïdre a adsorbé des impuretés qui ont formé des centres colorés. Au niveau des lamelles brunes et incolores



0,5 mm

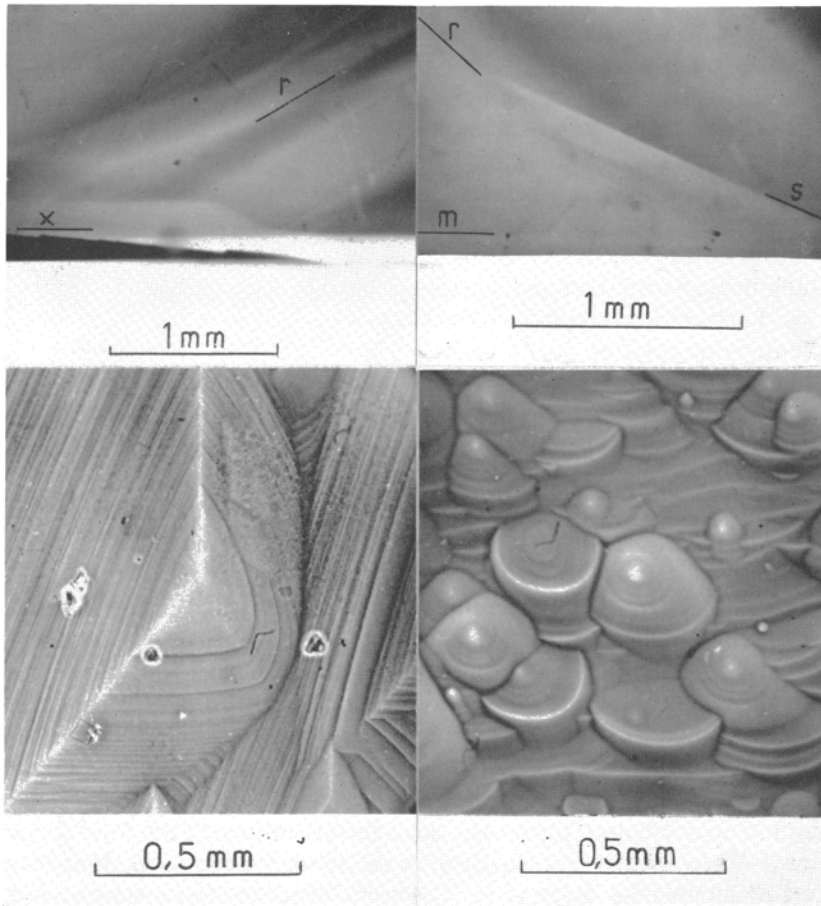
FIG. 2. Traces de la dipyramide trigonale  $s$  en fin de croissance des bandes.

qui suivent sur le rhomboïdre on voit que le trapèzoïdre n'a plus formé de centres colorés et que sa vitesse d'avancement par rapport au rhomboïdre a été beaucoup plus faible, 6 fois plus faible dans cet exemple. Sur la fig. 4 on voit la trace d'une dipyramide trigonale  $s$ . Elle est incolore au niveau d'une lamelle brune du rhomboïdre. Au niveau de la lamelle jaune qui suit on voit nettement que cette face est devenue de plus en plus petite puis a disparu tout en ensevelissant des impuretés sous forme de centres colorés.

On peut résumer ces observations de la manière suivante: les faces plagiédres  $s$  et  $x$  se développent en fin de croissance des bandes; à ce moment elles n'ensevelissent pas d'impuretés capables de former des centres colorés et leur vitesse d'avancement par rapport à celle du rhomboïdre est faible. Au début de la croissance d'une bande leur vitesse d'avancement est beaucoup plus grande et elles tendent à disparaître; à ce moment elles ensevelissent des impuretés dans des sites du réseau et des centres colorés se forment. Ce phénomène d'apparition et de disparition des faces plagiédres se produit pour de nombreuses bandes de croissance, c'est-à-dire pour une grande partie de l'histoire des cristaux.

Il est intéressant de rapprocher ces observations des conclusions de Hartman (1959) sur la formation du trapèzoïdre. A la suite d'une recherche sur les chaînes de liaisons intenses du quartz, Hartman prévoit que si l'apparition de la face  $x$  est liée à une adsorption d'impuretés ces impuretés ne doivent pas se loger dans des sites du réseau.

*Observations sur la morphologie externe.* A la Gardette un cristal de quartz n'est limité par des faces plagiédres que lorsque sa vitesse de croissance est très faible. Dès que celle-ci augmente les faces plagiédres tendent à disparaître. La morphologie externe des cristaux va nous donner une confirmation de cette hypothèse.



FIGS. 3 à 6: FIG. 3 (gauche, en haut). Croissance rapide du trapézoïde  $x$  au moment où se forme une lamelle jaune du rhomboèdre. FIG. 4 (droit, en haut). Avancement rapide et disparition de la dipyramide trigonale  $s$  au début de la croissance d'une bande. FIG. 5 (gauche). Figures de croissance du premier type sur le rhomboèdre positif. FIG. 6 (droit). Figures de croissance du deuxième type sur le rhomboèdre positif.

Les cristaux de ce gisement montrent un rhomboèdre particulièrement développé: celui qui, dans la cavité, regarde vers le bas. Comme cette face ne reçoit pas d'impuretés par sédimentation, sa croissance est très régulière et c'est sur elle que les figures de croissance doivent être observées. Ces figures de croissance sont, schématiquement, de deux types. Les figures du premier type (fig. 5) sont des pointements pyramidaux très réguliers et peu nombreux sur la face. Ils sont formés d'un empilement de couches, très facilement décelables au microscope à contraste de phase après métallisation. On n'a pas observé de dislocations en leur centre. D'autres pointements pyramidaux beaucoup plus

élevés et étendus en surface peuvent également être observés. Ils sont plus rares et au centre de chacun d'eux on voit toujours un défaut qui est vraisemblablement à l'origine de leur développement plus important. Les figures de croissance du deuxième type sont celles montrées par la fig. 6. On voit que les pointements ne sont plus pyramidaux mais au contraire globuleux. Ils sont beaucoup plus nombreux que les précédents sur la face et empiètent fréquemment les uns sur les autres de façon anarchique. On distingue également à leur surface les lisières de nombreuses couches de croissance, mais elles sont moins nettes que dans les pointements du premier type.

Comment interpréter ces phénomènes? Bienfait, Boistelle, et Kern (1965) ont montré sur des halogénures alcalins que les pointements pyramidaux apparaissent en dehors du phénomène de croissance réversible des faces. Ils seraient en quelque sorte issus d'une germination tridimensionnelle sur support étranger. Si les résultats de ces auteurs sont généralisables au quartz on a, par l'observation de ces pointements pyramidaux, un moyen de comparer les forces minéralisantes des solutions qui ont nourri les cristaux. Dans une cavité les cristaux montrent effectivement des figures de l'un ou de l'autre type, jamais un mélange des deux. Ceci signifie que lorsque les cristaux ont arrêté leur croissance celle-ci était lente dans certaines cavités, plus rapide dans d'autres. Or dans les cavités où la croissance était lente la quasi totalité des cristaux montrent des faces plagiédres et celles-ci sont de belles dimensions alors que dans les cavités où la croissance était plus rapide une grande proportion des cristaux ne possèdent pas de faces plagiédres et lorsqu'ils en montrent elles sont très petites. La morphologie externe des cristaux apporte donc une confirmation de ces interprétations tirées de l'examen de la morphologie interne.

Lemlein (1941) avait fait une observation similaire sur les cristaux de l'Oural subpolaire: il avait remarqué que les faces plagiédres ne se formaient qu'à la fin de la croissance des cristaux et en avait déduit que leur apparition nécessitait une sursaturation extrêmement faible.

### *Conclusions*

La croissance des cristaux de quartz lamellaires de la Gardette est un phénomène discontinu lié aux nombreuses réouvertures de la fracture dans laquelle le filon s'est mis en place. Chaque rejeu de cette fracture provoque la croissance d'une nouvelle bande. Dans chaque bande on distingue deux types différents de quartz: le premier se forme aussitôt après le rejeu, le deuxième plus tard.

Aussitôt après un rejeu de la fracture la vitesse de croissance est relativement élevée. Le rhomboèdre positif avance en adsorbant une grande quantité d'impuretés. La densité des centres colorés est faible. Les faces plagiédres avancent rapidement ce qui peut entraîner leur disparition. Elles adsorbent alors des impuretés dans des sites du réseau et produisent des centres colorés.

Après la croissance de ce premier quartz un deuxième quartz apparaît. Le passage du premier au deuxième quartz est fréquemment progressif. La vitesse

de croissance est faible. Ce quartz contient moins d'impuretés et la densité des centres colorés y est élevée. Les faces plagiédres avancent lentement et leur surface augmente. Elles n'adsorbent pas d'impuretés dans des sites du réseau de façon à produire des centres colorés.

La force minéralisante est renouvelée à chaque rejeu de la fracture. Mais elle est suffisamment faible, et les solutions suffisamment immobiles pour que les effets de ces rejeux s'estompent à mesure que l'on s'éloigne de la surface de transgression triasique au delà de laquelle il faut rechercher la source de silice.

*Remerciements.* Les analyses ont été effectuées au Centre de Recherches Pétrographiques et Géochimiques: les analyses spectrographiques sous la direction de K. Govindaraju, les études aux rayons  $x$  sous la direction de P. Leymarie. Les discussions sur ce travail avec R. Kern ont été enfin particulièrement utiles.

#### Références bibliographiques

- BAMBAUER (H. U.), 1961. *Schweiz. Min. Petr. Mitt.*, **41**, 335. [M. A. 15-463].  
 —, BRUNNER (G. O.), et LAVES (F.), 1961. *Zeits. Krist.*, **116**, 173.  
 BIENFAIT (M.), BOISTELLE (R.), et KERN (R.), 1965. *Colloque C.N.R.S.*, **152**, 515.  
 DESCLOIZEAUX (M.), 1858. *Mem. Acad. Sci. Paris*, **15**, 404.  
 [FRANK-КАМЕНЕЦКИЙ (V. A.)] Франк-каменецкий (В.А.), 1964. Природа структурных примесей и включений в минералах. Изд. Лен. Унив. (*Nature des impuretés structurales et incluses dans les minéraux*. Ed. Univ. Leningrad.)  
 FRONDEL (C.), 1945. *Amer. Min.*, **30**, 432 [M.A. 10-38].  
 —, 1962. *Dana's System of Mineralogy*, vol. 3. J. Wiley, New York.  
 HARTMAN (P.), 1959. *Bull. Soc. franç. Min. Crist.*, **82**, 335 [M.A. 14-470].  
 [КАМЕНЦЕВ (I. E.)], Каменцев (И. Е.), 1965. Зап. Всесоюз. Мин. Общ. (*Mem. All-Union Min. Soc.*), **94**, 687.  
 [LEMMLEIN (G. G.)] Леммлейн (Г. Г.), 1941. *Compt. Rend. (Doklady) Acad. Sci. URSS*, **33**, 415. [M.A. 9-128].  
 —, 1948. Секториальное строение кристалла. Изд. акад. наук СССР (*Structure sectorielle d'un cristal*. Ed. Acad. Sci. URSS.)  
 MALLARD (E.), 1876. *Ann. Mines*, **10**, 60.  
 POTY (B.), 1966. *Sciences de la Terre, Nancy*, **11**, 41.  
 WEIL (R.), 1930. *Compt. Rend. Acad. Sci. Paris*, **191**, 270, 380, et 935.  
 ZIMMERMANN (J. L.), 1966. *Ibid.*, **263**, Sér D, 461.

# Macro- and micro-morphology of quartz and pyrite

By I. SUNAGAWA and Y. ENDO

Geological Survey of Japan, 8 Kawada-cho, Shinjuku-ku, Tokyo, Japan

## PART I. A COMPARATIVE STUDY OF NATURAL AND SYNTHETIC QUARTZ CRYSTALS

(By I. Sunagawa)

*Summary.* A comparative study was made of the crystal morphology and surface structures of natural quartz (*A*), synthetic quartz grown on seed plates (*B*), and synthetic quartz spontaneously grown on the upper wall of the crucible (*C*). Crystal habits of *B* vary according to the rate and duration of crystal growth and the orientation of the seed plates. If an infinite time of growth were allowed their habits would be similar to those of natural crystals. Both *A* and *C* crystals show similar prismatic habit, except that on the *C* crystals only major rhombohedral faces develop, whereas on the former crystals both major and minor rhombohedral faces develop. It is also noticed that *C* crystals take on in general a longer prismatic habit than *A* crystals. Surface structures of the basal, rhombohedral, and prismatic faces of the two types of synthetic quartz are essentially the same, but very different from those of natural crystals, suggesting different growth conditions as between natural and synthetic crystals. Growth pyramids on rhombohedral faces of natural crystals and on prism faces of synthetic crystals show eccentric morphology, which is closely related with the hands of the crystals. Those on rhombohedral faces of synthetic crystals are different in number and size as between major and minor faces. These growth pyramids are considered to be formed either from screw dislocations or from the contact points of foreign minerals with the growing surfaces. Other growth features are also described in connection with the structure and growth conditions of quartz crystals. Characteristics of the crystal morphology of quartz are considered from the standpoint of growth mechanism.

CRYSTAL morphology and surface structures of both natural and synthetic quartz have been studied by several workers. Judging from their results, natural and synthetic quartz exhibit very different crystal habits and surface structures. It is, therefore, intended to make a comparative study between natural and synthetic quartz, with the hope of finding what are the main differences between the two. By doing so, it is hoped to clarify the mechanism of crystal growth of quartz and to analyse its crystal morphology from the standpoint of growth mechanism.

The characteristics of crystal habit of natural quartz are: hexagonal prismatic habit, non-appearance of the basal plane, asymmetrical appearance of trigonal pyramidal and trapezohedral faces depending on the hand of the crystal, and unequal development of two types of rhombohedral face. These can be partly accounted for by its structural characteristics such as the three-fold screw axis along *c* (Donnay and Harker, 1937). Hartman (1959, 1965) has

recently put forward an explanation of the unequal development of two types of rhombohedral face. In this paper, it is intended to account for these morphological characteristics, on the basis of the mechanism of crystal growth, which will be deduced from the studies of surface structures.

As to the surface structures of both natural and synthetic quartz, the following summarizes previous studies:

Rounded triangular growth spirals are observed on the  $\{0001\}$  face of synthetic quartz (Augustine and Hale, 1960). The profile of these spirals is not abrupt stepwise but has curved steps. This profile was due to a dissolution mechanism according to Joshi and Tolansky (1961), but the present writer is not in favour of their explanation.

On the  $\{10\bar{1}1\}$  faces of synthetic quartz, growth patterns suggesting the existence of growth spirals are observed, together with other growth features such as bubble-like and tadpole structures (Joshi, 1959).

Shallow isosceles triangular growth pyramids develop on the  $\{10\bar{1}1\}$  faces of natural quartz. These have been regarded as vicinal surfaces. There are several types of pyramids, and they are suggested to have close correlation with the hands of quartz crystals (Kalb, 1930, 1933). No definite evidence showing that they are spirals has been reported, except in a few cases reported by Joshi (1959). No clear difference has so far been reported on the nature of these structures as between major and minor rhombohedral faces.

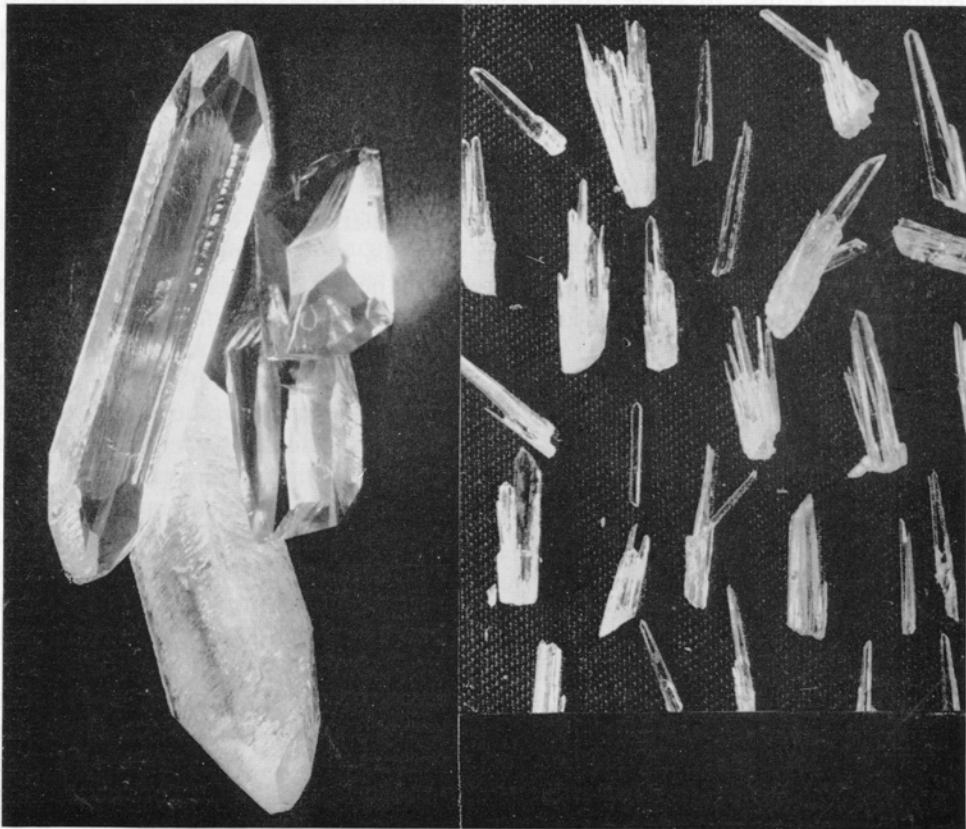
Characteristic surface structures of the  $\{10\bar{1}0\}$  faces of natural quartz are striations parallel to the horizontal axis. These are inferred to be due to an oscillatory growth between rhombohedral and prism faces (Dake, Fleener, and Wilson, 1938). Tetrahedral growth pyramids are observed on these faces (Praagh and Wills, 1952), and eccentric rhombic growth spirals are reported to occur on  $\{10\bar{1}0\}$  of synthetic quartz by Joshi (1964).

In the present study, natural quartz crystals from five localities and two different types of synthetic crystals made at Toyo Communication Equipment Co. were investigated by means of reflection and phase contrast microscopy as well as interferometry. Natural quartz crystals are from: Naegi, Gifu Pref.; Ishikawa, Fukushima Pref.; Kofu, Yamanashi Pref. (pegmatitic origin); Donsuiwa mine, Fukushima Pref. (hydrothermal vein) in Japan, and St. Gotthard, Switzerland. Synthetic crystals investigated are those grown on seed plates parallel to the  $Z$ -,  $Y$ - and  $R$ -cut, and those grown spontaneously on the wall of the crucible at the top portion. Their morphological characteristics were compared, and their surface structures were studied.

*Crystal morphology.* Synthetic crystals grown on seed plates show different crystal habits according to the type of the seed plates and the duration of growth, as shown by the examples in fig. 1. When a long plate parallel to  $\{0001\}$  is used as a seed, an elongated crystal consisting of  $\{0001\}$ ,  $\{10\bar{1}1\}$ ,  $\{10\bar{1}0\}$ , and  $\{11\bar{2}0\}$  faces is formed. If a seed plate parallel to a  $\{10\bar{1}1\}$  face is used, a rhombohedral platy crystal parallel to the seed plate is formed. However, the crystal

habit of synthetic quartz is also controlled by the duration of crystal growth. Let us take a crystal grown on the Z-cut seed plate as an example. At an earlier stage, the crystal is an elongated plate having a wide basal plane, together with small  $\{10\bar{1}1\}$ ,  $\{10\bar{1}0\}$ , and  $\{11\bar{2}0\}$  faces. The  $\{0001\}$  and  $\{11\bar{2}0\}$  faces have rough surfaces, whereas  $\{10\bar{1}1\}$  and  $\{10\bar{1}0\}$  have smooth surfaces. As growth proceeds, the latter two faces develop larger, whereas the former two faces tend to decrease in size. In the normal procedure of quartz syntheses, crystals are taken out from the crucible at this stage, and hence they show external forms as shown in fig. 1. However, if growth continues further, both  $\{0001\}$  and  $\{11\bar{2}0\}$  faces ultimately disappear, and the crystal takes on a short hexagonal prismatic form, which is an ordinary crystal habit of natural quartz. This process is more or less similar in the case of other types of seed plates being used, and their ultimate habit is similar to those of natural crystals.

The crystal habit of spontaneously grown synthetic quartz is very different



FIGS. 1 and 2: FIG. 1 (left). Synthetic quartz crystals grown on seed plates of different orientations. FIG. 2 (right). Spontaneously grown synthetic quartz crystals.

from the habit of quartz grown on seed plates, and is more or less similar to that of natural quartz. As can be seen in fig. 2, prismatic or acicular habits are adopted. However, a few distinct differences are noticed between these synthetic crystals and natural ones. In contrast to the well-balanced hexagonal prismatic forms of natural crystals, spontaneously grown synthetic quartz crystals take on trigonal prismatic forms with three well-developed and three narrow prism faces. On these synthetic crystals only major rhombohedral faces develop, except in a few cases where minute minor rhombohedral faces appear as well. Another important difference is that these crystals take on much more elongated forms than ordinary natural crystals. In the case of natural crystals, the ratio of width to length of the crystals as measured along the *a*- and *c*-axes generally falls within the range from 2 : 3 to 1 : 4, long prismatic crystals with an elongation of more than 1 : 6 are uncommon, and acicular habits are very rare (Dana 7th edn, vol. 3). In contrast, the spontaneously grown synthetic crystals take on a much more elongated prismatic habit, and acicular habit commonly occurs. In some cases, whisker-like crystals are found as well. It should be noted here that these spontaneously grown crystals must have grown by a growth mechanism similar to that of natural crystals, since no seed crystals are used, yet they take on different crystal forms, the forms that reflect the structural nature of quartz crystals more vividly.

#### *Surface structures*

*Natural quartz.* Rhombohedral faces are characterized by the development of slightly malformed triangular growth pyramids, an example being shown in fig. 3. They have usually a rounded corner on the left and point corners on the right and at the tops of the triangles, though on some crystals pyramids are

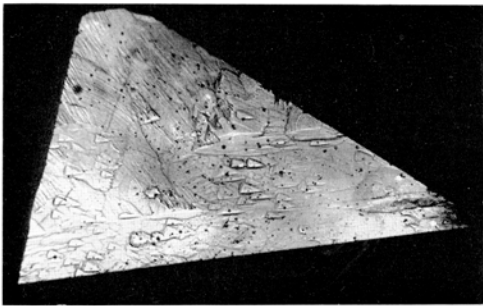


Fig. 3. Low magnification photomicrograph of  $(10\bar{1}1)$  face of natural quartz.  $\times 5$ .

circular or elliptical and in a few cases they have a flat top surface. These pyramids have long been regarded as vicinal surfaces. They consist of a pile up of thin triangular growth layers, the edges of which can be easily detected in most cases under low magnification with a reflection microscope. This shows that the spacings between neighbouring growth layers are relatively wide, suggesting low supersaturation conditions for the growth of natural quartz. Both the forms of the pyramids and the

spacings between successive layers vary from locality to locality, corresponding to different supersaturation conditions.

If the apex of these pyramids is carefully observed under high magnification with a phase contrast microscope, it is seen on some crystals that spiral growth

layers originate from screw dislocations that are situated at the apex, or on a few crystals it is seen that triangular growth layers originate from the point of intersections between an acicular foreign mineral and the surface of a rhombohedral face. The latter case was observed on the crystals from St. Gotthard, and an example is shown in fig. 4. As can be seen in this figure, an acicular crystal is situated at the summit of the pyramid. Growth layers may preferentially start from such a point, and will form a pyramid that has the appearance of a spiral pyramid. If such foreign crystals are enclosed in the crystal by further growth, no point for preferential growth will be left on the growing surface. Then the growth layers will not be newly created and a pyramid with a flat top surface will be formed.

On one surface of the rhombohedral face, one or a few growth centres,

i.e. triangular pyramids, are seen. In some cases, one surface is completely covered by growth layers originating from a single centre; in other cases, a large number of small pyramids occur on one surface. It is found to be a general tendency that major rhombohedral faces show a small number of pyramids, whereas minor rhombohedral faces show a large number of pyramids. A similar tendency is also noticed on the synthetic quartz in a more exaggerated form; this is described later. This is the only difference in surface structures as between major and minor rhombohedral faces that could be noticed; no fundamental difference was found as to the morphology of growth pyramids between the two types of rhombohedral face.

The apex of a triangular pyramid is usually not situated at the very centre of the triangle. Two types of eccentricity are noticed; one type has its apex nearly at the centre of the triangle or to the left, the other type has its apex to the right of the centre. Kalb and his co-workers (1930, 1933), as well as several other workers, have made extensive studies of the origin of this eccentricity. They recorded more than two types, though their observations were not made on individual pyramids but on a face as a whole. They consider that the attitude of the upper edge of triangular pyramids is useful for determining the hands of quartz. However, it has been suggested by Joshi (1959) that the eccentricity is related to the directional flow of ore solution, though according to the present observations his explanation is not valid, since pyramids of different eccentricity occur on one surface. It seems that Kalb's explanation is more likely. A similar tendency is also observed more clearly on the eccentricity of growth pyramids on the  $\{10\bar{1}0\}$  faces of synthetic quartz, which will be described later.

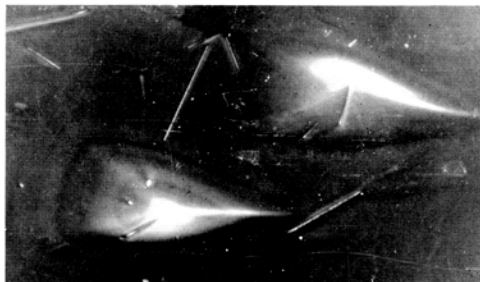
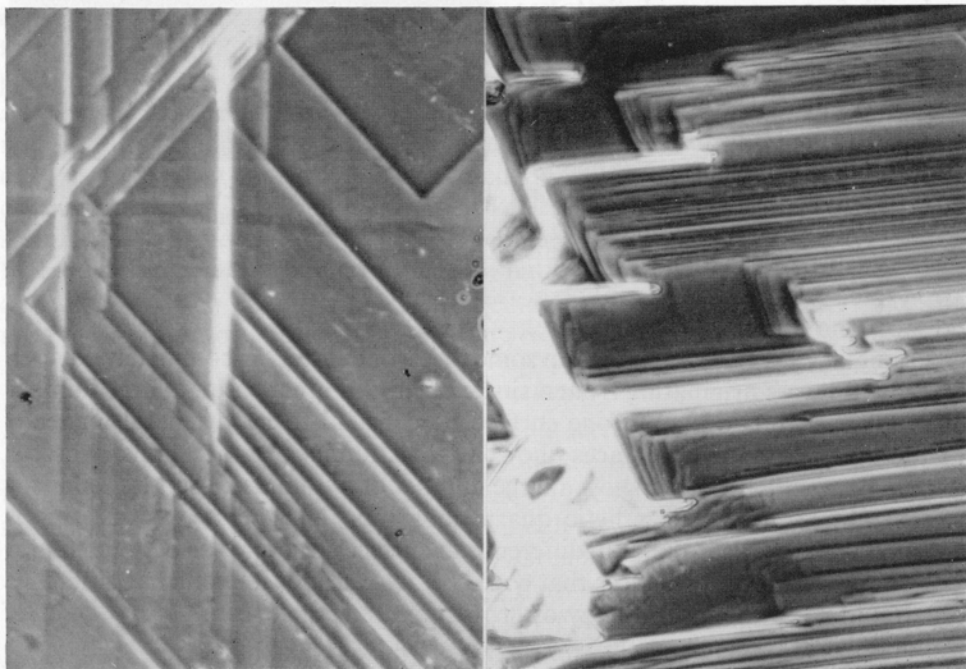


FIG. 4. Positive phase contrast photomicrograph showing the relation between acicular foreign minerals and growth pyramids on the  $(10\bar{1}1)$  face of natural quartz from St. Gotthard.  $\times 110$ .

Straight or irregular discontinuity lines are often observed to develop on the rhombohedral faces. They give shifts or kinks to the growth layers. The irregular discontinuity lines are considered to be twin boundaries, whereas straight lines are inferred to be slip lines formed during growth. An example of the latter lines is shown in fig. 5.

Under low magnification,  $\{10\bar{1}0\}$  faces of natural quartz exhibit only striations parallel to the horizontal axis, with a few exceptions where vertical or oblique discontinuity lines, which are boundaries of penetration twins, cut the former.



FIGS. 5 and 6: FIG. 5 (left). Slip lines formed during crystal growth.  $(10\bar{1}1)$  face of natural quartz, Kurobira, Kofu, Japan. Positive phase contrast.  $\times 160$ . FIG. 6 (right).  $(10\bar{1}0)$  face of natural quartz. Positive phase contrast.  $\times 160$ .

Under higher magnification with a phase contrast microscope, the striations are found to consist of steps with narrow bands of flat areas on which elongated growth pyramids occur. These pyramids have elongated rhombic forms rather than rectangular forms (fig. 6). It should be stressed here that these pyramids occur rarely, and in general only steps (which are not uni-directional) parallel to the horizontal axis are seen. This suggests that the development of growth layers on the prism face is strongly controlled by the growth on the rhombohedral faces.

Crystals from Ruby Mountain, Colorado, U.S.A. are the only natural quartz crystals that are reported to have a  $\{0001\}$  face. They are very small in size

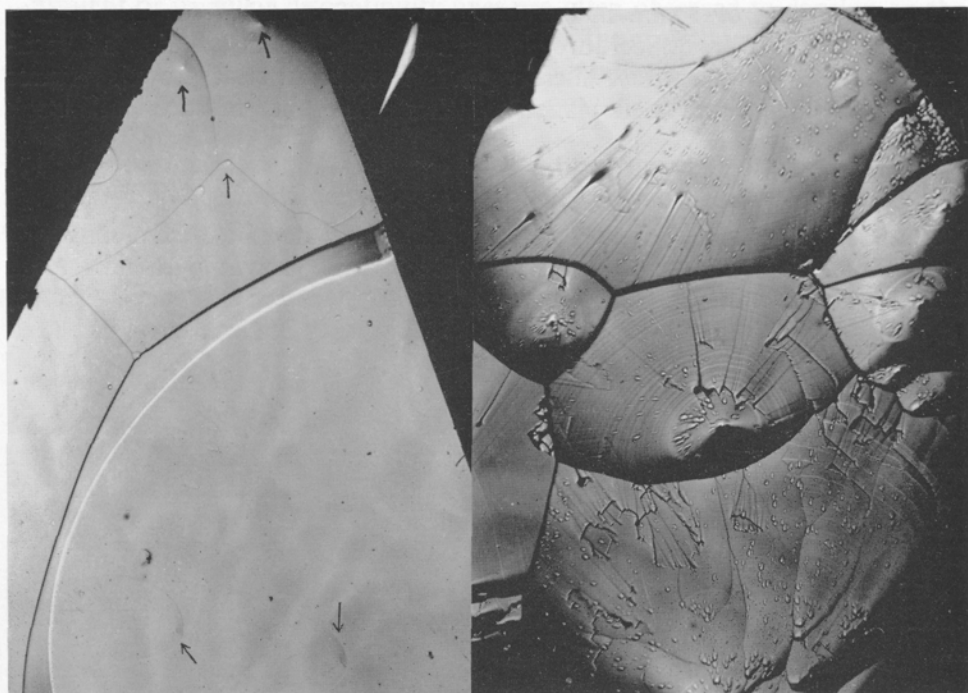
with a maximum of 1 mm. in length. A group of crystals from this locality was presented by Mr. P. Seel through Prof. J. D. H. Donnay, and was investigated using a phase contrast microscope. However, no clear growth features were observed on the basal planes, which showed only mottled and rough surfaces.

*Synthetic crystals grown on seed plates*

$\{0001\}$  faces. It can be seen even with the naked eye that these faces consist of many boules placed upside down. The boules are growth pyramids. As a general tendency, the number of boules decreases, whereas their sizes increase, as growth proceeds. As the crystals grow, neighbouring boules coalesce together to form larger ones.

As reported by Joshi and Tolansky (1961), Augustine and Hale (1960) and some other workers, some of these boules exhibit triangular spirals with rounded corners. However, such boules are rather exceptional, and in most cases they do not show clear spiral patterns. This does not mean that the boules are not formed by a spiral growth mechanism, but it is simply because they consist of spiral layers of too narrow a spacing to be disclosed by optical microscopes. There is no definite evidence that they are formed by mechanisms other than that of spiral growth. When they show spiral patterns, their profiles are not of an abrupt stepwise nature, but are of curved steps, which can be clearly seen on their interferograms. The curved steps, instead of ordinary abrupt steps, of these spirals were attributed by Joshi and Tolansky to a dissolution mechanism. However, such profiles can also be formed by rythmical bunching of a large number of thin spiral layers that are extremely closely spaced. Indeed, a similar profile of curved steps was reported on the basal plane of flux-grown synthetic emerald by the present author, and found to consist of extremely closely spaced mono-molecular spiral layers (Sunagawa, 1964). These were observed under very high magnification with a phase contrast microscope.

$\{10\bar{1}1\}$  faces. Two types of surface structure are noticed under low magnification, examples of which are shown in figs. 7 and 8. One has a rather smooth surface consisting of wide and flat domains, though a small number of minute hillocks are found as well (fig. 7); the apparently flat areas, under low magnification, in fact have shallow cone-like features, and there is always one summit in each flat area (shown by arrows in the photograph). Making a good contrast to the apparently flat surface of the first type, the second type is characterized by a large number of large and minute conical hills, a typical example being shown in fig. 8; circular growth layers are seen even under low magnification on the side surface of larger hills, and interferograms show that they have profiles of curved steps, similar to those on the basal plane. Another point of interest in this photograph is the area marked irregularly by short lines, which represent twin boundaries.



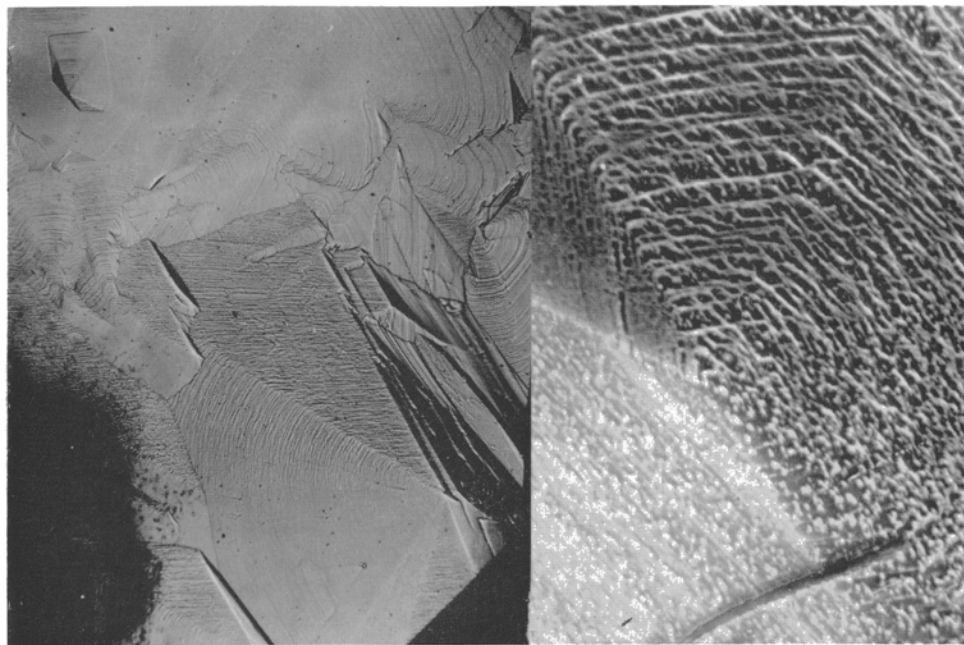
FIGS. 7 and 8: FIG. 7 (left). Low magnification photomicrograph of major  $(10\bar{1}1)$  face of seed-grown synthetic quartz.  $\times 7.3$ . FIG. 8 (right). Low magnification photomicrograph of minor  $(10\bar{1}1)$  face of seed-grown synthetic quartz.  $\times 7.3$ .

Under the phase contrast microscope, extremely closely spaced growth layers can be seen on the side surfaces of these hillocks and even on minute hills. Since these hillocks have curved surfaces due to closely spaced layers, a proper phase contrast effect was not secured at their summit or on their side surfaces. As a result, definite evidence showing the spiral nature of these hillocks was not obtained in this study. However, since they have singular summits and extremely closely spaced growth layers on the side faces, it is conjectured that they are also spiral hills.

The two different types of general surface structures of  $\{10\bar{1}1\}$  faces are considered to be derived from the difference between major and minor rhombohedral faces. The face that exhibits a smaller number of domains and apparent flat areas is considered to be the major rhombohedral face, whereas the second type may correspond to the minor rhombohedral face. Differences between the two types of rhombohedral faces in the number and steepness of growth hills suggest different growth velocities. The growth velocity of the first type is smaller than the second type, which will result in a larger development of the first type (major rhombohedral face) as growth proceeds. This is in fact an observed general tendency in the development of major and minor rhombohedral faces.

$\{10\bar{1}0\}$  faces. These faces of synthetic crystals exhibit entirely different surface structures from those of natural quartz. Striations parallel to the horizontal axis, which are characteristic patterns of the  $\{10\bar{1}0\}$  faces of natural crystals, are not seen at all on synthetic crystals. The prism faces of synthetic crystals are characterized by the development of eccentric five-sided growth pyramids. An example is shown in a low-magnification photomicrograph, fig. 9. These pyramids always have their apex at an off-centred position. There are two opposite types of this eccentricity; one has its apex on upper right side of the pyramid, the other on the lower left side in fig. 9. There is no doubt that this eccentricity is directly related to the hands of quartz crystals. Therefore, in a certain area on the surface, only one type occurs, and on twinned crystals two types occur on the same surface but in different areas, with discontinuity lines between them. It is also conjectured that this eccentricity has a close connection with the development of trapezohedral faces. A large number of these pyramids, large and small, occur on one surface. Individual growth layers are clearly seen on their side faces even under low magnification.

Fig. 10 is an example of the pyramids seen under higher magnification with the phase contrast microscope. Closely spaced thin growth layers can be seen



FIGS. 9 and 10: FIG. 9 (left). Low magnification photomicrograph of  $(10\bar{1}0)$  face of seed grown synthetic quartz. This crystal is twinned, as can be seen from the orientations of eccentric five-sided growth pyramids.  $\times 7$ . FIG. 10 (right). Phase-contrast photomicrograph of five-sided growth pyramids on the  $(10\bar{1}0)$  face of seed-grown synthetic quartz.  $\times 150$ .

clearly, though at the apex individual layers are difficult to see due to close spacings between the successive layers. As a result, no definite evidence showing the spiral nature of these pyramids was obtained, though they are considered to be spirals.

Another interesting feature is the universal occurrence of white lines or dots along the steps and on the surfaces of growth layers. Since they appear brighter than the actual surface of growth layers on the phase contrast photomicrographs, they are at a higher level than the surface of growth layers. They are considered to be impurities selectively adsorbed along growth fronts; detailed discussion about this has appeared elsewhere (Sunagawa, 1965).

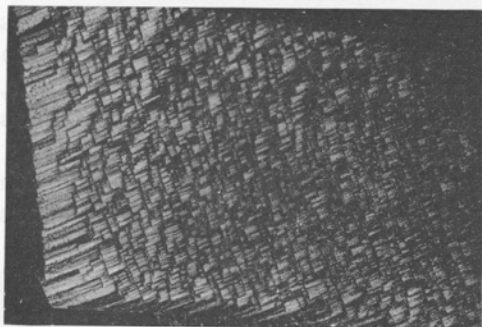


FIG. 11. Low magnification photomicrograph of  $\{11\bar{2}0\}$  face of seed-grown synthetic quartz.  $\times 6$ .

$\{11\bar{2}0\}$  faces. Fig. 11 is a low magnification photomicrograph of a  $\{11\bar{2}0\}$  face on a synthetic quartz. As can be seen on this photograph, this face exhibits two directions of striations, and no growth layers develop, which suggests that the growth of this face is not made by the addition of two-dimensional layers but by the attachment of chains or molecules. Therefore, the  $\{11\bar{2}0\}$  faces are transitional and will soon disappear as growth proceeds.

*Synthetic crystals grown spontaneously.* Since the crystal habit of synthetic quartz grown spontaneously on the inner wall of the upper part of the crucible has a close similarity with that of natural quartz, one may expect close resemblance between the surface structures of the two. However, surprisingly enough, these crystals have entirely different surface characteristics from those of natural crystals. Their surface structures are essentially the same as those of the synthetic quartz grown on seed crystals.

Instead of showing striations parallel to the horizontal axis on the prism faces, they exhibit similar five-sided growth pyramids to those observed on the prism faces of quartz grown on seed plates. Furthermore, clear growth layers as well as selective impurity adsorption along the growth fronts are seen as well on these faces. Fig. 12 shows an example. One will find little difference between this photomicrograph and those of the prism faces of seed-grown synthetic quartz. Similarly, rhombohedral faces (only major rhombohedral faces develop on these crystals) exhibit circular layers or shallow circular cones, an example of which is shown in fig. 13. These are again fundamentally similar to those on the major rhombohedral faces of seed-grown synthetic crystals.

These observations definitely show that the growth conditions are the governing factor of surface structures.

# Growth of phlogopite crystals in marble from Quebec

By RALPH KRETZ

Department of Chemistry, Imperial College, London

*Summary.* The edges of growth steps on certain phlogopite crystals may be straight, irregularly curved, or cusped. Straight step edges may or may not be parallel to lines of closely packed oxygen ions in the mica structure. Chemical processes that have participated in the crystallization of phlogopite are considered.

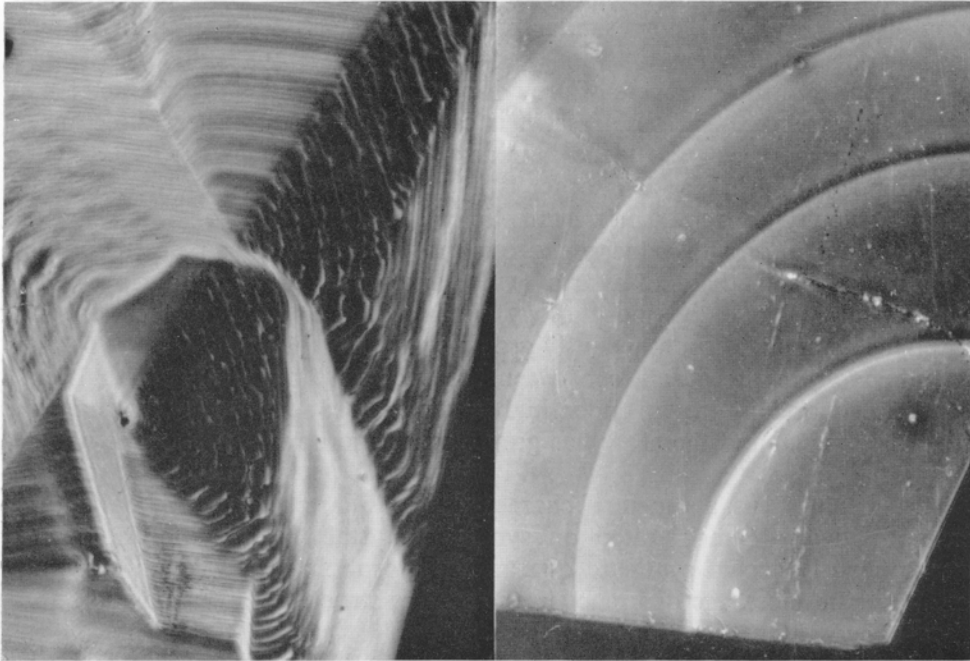
THE phlogopite crystals studied occur in marble from the Grenville region of Quebec. The marbles form layers and lenses in a terrain that consists mainly of various hornblende-, biotite-, garnet-, and sillimanite-bearing gneisses, veined gneisses, migmatites, and granitic rocks (Kretz, 1957). A selected specimen of marble consists largely of calcite, a small percentage of phlogopite, and very minor amounts of quartz, tremolite, diopside, tourmaline, magnetite, and graphite.

*Properties.* The phlogopite crystals are pale yellowish-brown and transparent. The position of the *a*-axis in many crystals could be determined from the interference figure; successive cleavage slices showed no variation in the optic orientation. A few crystals that yielded a slightly anomalous interference figure were found to be twins with composition plane (001) and twin axis [310]. Small variations in orientation of the optic axial plane, as found in synthetic fluor-phlogopite by Bloss, Gibbs, and Cummings (1963), were not found, nor do the crystals possess domains of different crystallographic orientation, as described by Sunagawa (1964).

The shape of a typical phlogopite crystal is shown in fig. 1. {001} faces are normally well developed and commonly contain growth steps and depressions. {010} and {110} faces, where present, are poorly developed; the sides of the crystals commonly consist of several curved or nearly planar rough surfaces.

The ratio of average diameter to height of these crystals varies from 1 to 8, with an arithmetic mean of 2.8 (Kretz, 1966a). The smallest crystals tend to be more equidimensional than larger ones, with a corresponding ratio of 2.1. Hence the growth rate in the direction [001] was less than growth rates in directions normal to [001], and the ratio of these rates may have varied slightly as the crystals became larger.

The crystals range in size from 0.10 mm diameter to 2.70 mm diameter, or from 0.00027 mm<sup>3</sup> to 3.3 mm<sup>3</sup> (Kretz, 1966b). The grain-size distribution



FIGS. 12 and 13: FIG. 12 (left).  $(10\bar{1}0)$  face of spontaneously grown synthetic quartz. Positive phase contrast.  $\times 160$ . FIG. 13 (right).  $(10\bar{1}1)$  face of spontaneously grown synthetic quartz. Positive phase contrast.  $\times 160$ .

### Conclusions

From the observations described above, several points emerge in connection with the relations between surface and internal structures of quartz crystals, between surface structures and growth conditions, between crystal morphology of quartz and the nature of growth layers and pyramids on each face, and especially the relationship between all these and the growth mechanism of quartz crystals. The results can be summarized as follows:

Each face of the basal, rhombohedral, and prism type shows its own characteristic surface structures, which are partly defined by the atomic arrangement and symmetry of the face.

The hand of a quartz crystal is manifested in the morphological eccentricity of growth pyramids on both rhombohedral and prism faces.

Major and minor rhombohedral faces show different numbers, types, and steepness of growth pyramids, from which it is deduced that the major rhombohedral face will develop larger than the minor rhombohedral face.

Characteristics of surface structures are different as between natural and synthetic crystals, but no fundamental difference was found between the two types of synthetic quartz. This shows that the surface structures reflect the

difference in growth conditions most vividly. If crystals grow under similar conditions, they will show similar surface structures, even if their growth mechanisms are different.

Judging from the steepness of growth pyramids as well as the characteristics of surface structures on each face, it is estimated that the fastest direction of growth is perpendicular to  $\{11\bar{2}0\}$ , the next  $\{0001\}$ , and then  $\{10\bar{1}0\}$  and major and minor  $\{10\bar{1}1\}$  faces. This order is in good agreement with the measured growth velocity of each face on synthetic crystals.

This order in growth velocity suggests that if growth takes place for a long duration in the synthesis of quartz,  $\{11\bar{2}0\}$  and  $\{0001\}$  faces will disappear and the crystal will take on morphology similar to that of natural crystals, or ultimately similar to spontaneously grown synthetic crystals.

Judging from the spacings between the successive arms of growth layers, synthetic quartz is grown under higher supersaturation conditions than the natural crystals, and therefore has grown much more rapidly than the natural crystals.

As a result of this, a structural characteristic of quartz, e.g. its trigonal nature, is more vividly demonstrated on synthetic crystals by the morphology of spontaneously grown synthetic quartz, the morphology of growth pyramids on the prism faces, the difference in the surface structures of major and minor rhombohedral faces, and other features.

Although the spiral nature at the apex of growth pyramids on both natural and synthetic quartz was in general not clear because of close spacings, it is conjectured that most of the pyramids on basal, rhombohedral, and prism faces are spirals. However, some of the growth pyramids on the  $\{10\bar{1}1\}$  faces of natural quartz are formed by preferential growth at the points where foreign crystals make contact with the growing surface.

In the case of synthetic quartz grown on seed, morphological development with growth is different according to the orientation of the seed used. In general, growth starts by spiral mechanism at a large number of locations on the seed. Spirals thus formed coalesce together forming bigger pyramids, but at the same time, morphologically predominant faces such as  $\{10\bar{1}1\}$  and  $\{10\bar{1}0\}$  will appear on the sides of these pyramids. Once these faces appear, growth takes place as a spiral layer spreading on them. Because of different growth velocities,  $\{10\bar{1}1\}$  and  $\{10\bar{1}0\}$  faces develop larger as growth proceeds, and the original faces, if they are other faces than the above two, will gradually disappear.

In the case of synthetic quartz grown spontaneously, growth layers develop on both  $\{10\bar{1}1\}$  and  $\{10\bar{1}0\}$  faces. As a result, elongated prismatic crystals are formed.

In the case of natural crystals, spiral growth layers mainly develop on  $\{10\bar{1}1\}$  faces, and the piling up of edges on these faces will form prism faces. On the prism faces thus formed, growth layers may develop, but their development is very weak, resulting in the formation of striations parallel to the horizontal axis, and also in shorter prismatic crystals.

Distinct differences in surface structures, in spite of similarity of crystal habit, as between natural and spontaneously grown synthetic quartz, suggest that the order of face importance calculated on the basis of the Bravais–Donnay–Harker Law or Hartman's theory can vary considerably according to the conditions of growth.

*Acknowledgements.* The writer expresses his thanks to Prof. J. D. H. Donnay, Mr. P. Seel, and the staffs of Toyo Communication Equipment Co. for the specimens.

#### *References*

- AUGUSTINE (F.) and HALE (D. R.), 1960. *Jour. Phys. Chem. Solid*, **13**, 344.  
 DAKE (H. C.), FLEENER (F. L.), and WILSON (B. H.), 1938. *Quartz family minerals*. McGraw Hill Co., London.  
 DONNAY (J. D. H.) and HARKER (D.), 1937. *Amer. Min.*, **22**, 446.  
 HARTMAN (P.), 1959. *Bull. Soc. franç. Min. Crist.*, **82**, 335.  
 —, 1965. *Zeits. Krist.*, **121**, 1.  
 JOSHI (M. S.), 1959. *Ph.D. Thesis*, London Univ.  
 — and TOLANSKY (S.), 1961. *Proc. Roy. Soc. Ser. A.*, **260**, 475.  
 — and VAGH (A. S.), 1964. *Amer. Min.*, **49**, 1771.  
 KALB (G.), 1930. *Zeits. Krist.*, **73**, 266.  
 — 1933. *Ibid.*, **86**, 439.  
 PRAAGH (G. VAN) and WILLS (B. T. M.), 1952. *Nature*, **169**, 623.  
 SUNAGAWA (I.), 1964. *Amer. Min.*, **49**, 785.  
 —, 1965. C.N.R.S. Coll. Intern. No. 152, Adsorption et croissance cristalline, 665.  
 TOLANSKY (S.), 1960. *Surface microtopography*. Longmans, London.

## PART II. SURFACE STRUCTURES OF PYRITE

(Y. Endo and I. Sunagawa)

*Summary.* The surface structures of pyrite crystals from many localities were studied by means of phase-contrast microscopy and multiple-beam interferometry. Both single and composite spirals were observed on {100}, {111}, and {210} faces, though their occurrence is not universal. Commonly observed growth features are growth tables, which are considered to be formed by two-dimensional nucleation or by the oriented settlement of minute crystals. Freely developed growth layers are observed mainly on {100} faces, sometimes on {111} faces, and rarely on {210} faces. The advance of growth layers on the latter two faces is strongly controlled by the directions parallel to the edges between these faces and the {100} face. Each of the three faces shows a different morphology of growth layers in accord with its symmetry. Morphology of growth layers on {100} faces varies according to the different combinations of crystal faces, whereas that of the other two faces is more or less uniform. These observations are discussed in relation to the growth mechanism and habit variation of pyrite crystals.

GROWTH features observed on the surfaces of pyrite crystals have been studied by several workers. Seager (1953) observed them under low magnification with an ordinary reflection microscope and discussed growth velocities, etc. He also reported an example of composite spirals on cube faces. Sunagawa (1957) summarized characteristics of the surface structures of {100}, {111}, and {210} faces of pyrite and tried to correlate them with the crystal habit variation. His observations also were made under low magnification with an ordinary

reflection microscope. Font-Altaba (1963) reported dislocation lines observed on pyrite crystals from Spain. However, the surface structures of pyrite crystals have not been studied in detail using modern and sensitive methods of observation such as phase-contrast microscopy or multiple-beam interferometry. Therefore, it seemed desirable to make detailed observations and to clarify the mechanism of crystal growth of pyrite. By doing so, at least three problems relating to crystal growth might be solved:

Causes of crystal habit variation, which is the result of crystal growth, and so should be studied in relation to growth mechanisms.

The mechanism of crystal growth which takes place in hydrothermal solution. The spiral growth theory was at first put forward for the case of growth from a vapour phase of low supersaturation. It is apparent from studies of many artificial crystals that the theory can also be applied to growth from the solution phase. However, at the same time there are many natural crystals grown from hydrothermal solution that do not show growth spirals. Detailed surface-structural studies on pyrite crystals will show to what extent the spiral growth mechanism can be applied to growth from hydrothermal solution, and what will be the other mechanism that governs the growth from this phase.

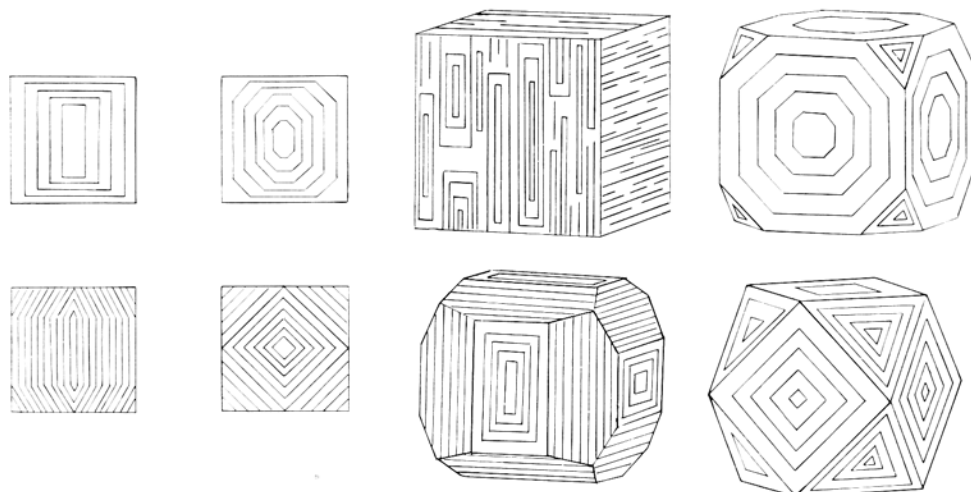
Hartman's theory on crystal morphology says that  $\{111\}$ ,  $\{100\}$ , and  $\{210\}$  are the *F*-faces of pyrite and that  $\{111\}$  has its position at the first place,  $\{100\}$  second, and  $\{210\}$  third in the order of predominance among the *F*-faces. This suggests that free growth layers will develop mainly on  $\{111\}$ , whereas on the other two faces their development will be controlled by the directions parallel to the edges between  $\{111\}$  and the other two faces. Whether this is true on natural crystals will be clarified by the detailed observations of their surface structures.

In view of the above, the present study mainly attempted to clarify whether growth spirals are observed universally on natural pyrite, to determine what types of growth layers will be found on the three *F*-faces and what will be the relations between the morphology of growth layers and crystal habits, and to determine on which face of the three *F*-faces growth layers will develop most freely. The pyrite crystals investigated in this study are from Kamikita mine, Aomori Pref.; Hanaoka, Osarizawa, Mizusawa, and Ani mines, Akita Pref.; Tsunatori mine, Iwate Pref.; Akiu mine, Miyagi Pref.; Chichibu mine, Saitama Pref.; Ogoya and Komatsu mine, Ishikawa Pref.; Kambe mine, Nara Pref.; and Ogasawara Island in Tokyo. They are either from epithermal vein deposits of Cu, Zn, and Pb or from Kuroko-deposits, which are massive-type ore deposits of Cu, Zn, and Pb. Only the three *F*-faces,  $\{100\}$ ,  $\{111\}$ , and  $\{210\}$  were studied, using an ordinary reflection microscope, a phase-contrast reflection microscope and a two-beam and multiple-beam interferometer.

#### *Observations*

$\{100\}$  faces exhibit a wide variety of surface structures, making a good contrast with the other two faces, which exhibit more or less uniform surface structures.

To the naked eye,  $\{100\}$  faces are either very flat or heavily striated. Under low magnification, however, every  $\{100\}$  face exhibits its own growth layers and pyramids. This is true even for cubic crystals with heavily striated faces. Fig. 16 is a typical example of such faces and clearly shows that the surface is covered by a large number of elongated rectangular growth pyramids, the morphology of which gives an effect of striated appearance.



FIGS. 14 and 15: FIG. 14 (left). Showing different forms of growth features observed on the  $\{100\}$  faces of pyrite. FIG. 15 (right). Schematic drawing to show the relation between different crystal habits and different forms of growth features on the  $\{100\}$  faces.

The morphology of growth layers and pyramids on the  $\{100\}$  face varies considerably from crystal to crystal and from locality to locality. It varies from irregular to polygonal, and from elongated rectangular to cubic patterns that are rotated  $45^\circ$  from the cubic ones. The different morphologies of growth layers and pyramids on the cube faces are summarized and shown schematically in fig. 14, and each of the different forms can be seen in figs. 16 to 18. No definite correlation between the morphology of growth pyramids and modes of occurrence was established in this study, whereas a close correlation was noticed between the morphology of pyramids and the crystal habits of pyrite. Although a few exceptions can be found, it is noticed as a general tendency that the forms of growth layers and pyramids vary according to different combinations of crystal faces, in a way shown schematically in fig. 15 and summarized below:

On simple cubic crystals, growth layers on  $\{100\}$  faces take on irregular or rectangular forms, the edges of which are parallel to  $\langle 001 \rangle$  and  $\langle 010 \rangle$ . They may be elongated or shortened, but are not in the form of a cube with edges parallel to  $\langle 011 \rangle$ .

On cubo-octahedral crystals or octahedral crystals with cube faces, rectangular growth layers on  $\{100\}$  faces are truncated at their four corners in the directions

of  $\langle 011 \rangle$ , and in an extreme case growth layers take on cubic form with their edges parallel to  $\langle 011 \rangle$ .

On cubo-pentagonal crystals or pentagonal crystals with cube faces, growth layers take on either elongated rectangular forms or the corners of the rectangles are truncated parallel to  $\langle 012 \rangle$ . Cubic forms parallel to  $\langle 011 \rangle$  are not observed on these crystals.

The above tendencies are noticed not only on the surface structures as a whole but also on individual growth pyramids that occur on a face in large numbers. It is another peculiarity of the surface structures of pyrite crystals that a large number of minute growth hills or tables occur on one face (fig. 19). The number of such growth features is much larger than that on other minerals such as hematite, which shows only a few growth centres on any one face.

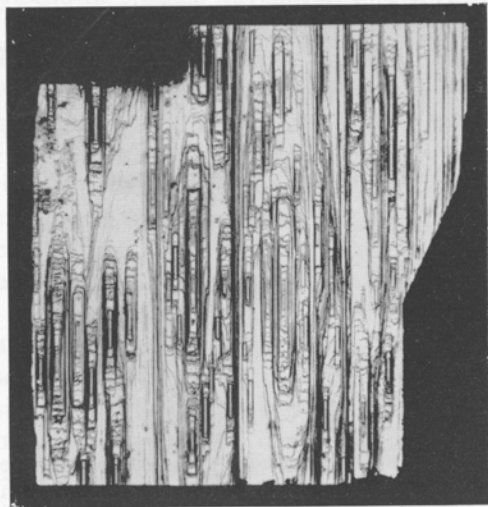
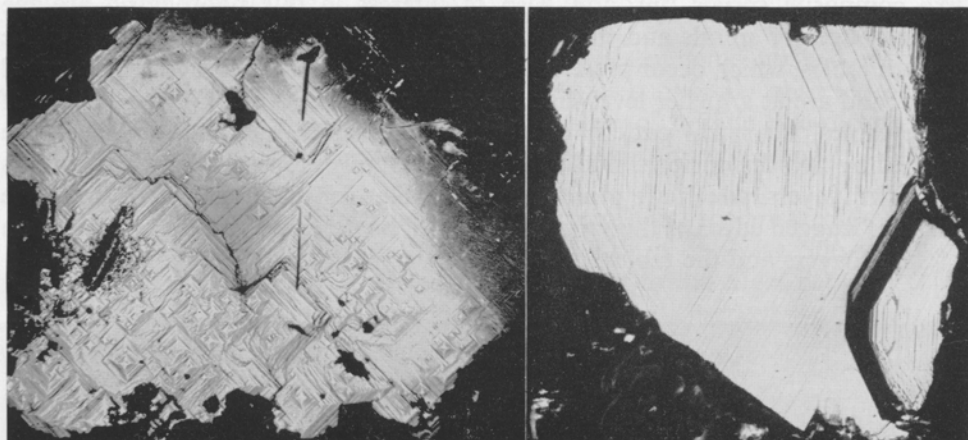


FIG. 16. An example of elongated rectangular growth features on the  $\{100\}$  face. Ohizumi mine.  $\times 7$ .

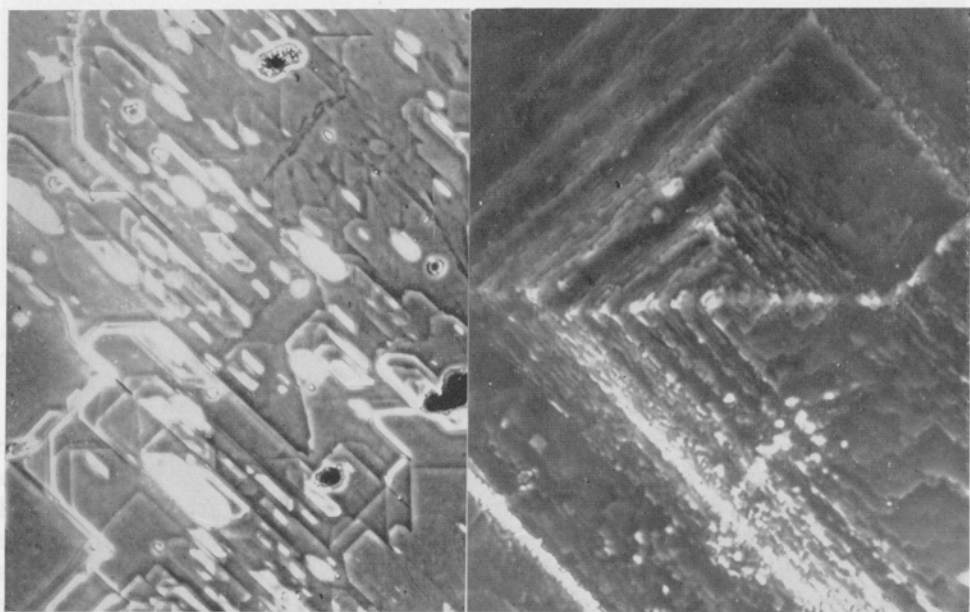
Under higher magnification with a phase contrast microscope, neither typical nor composite spirals are observed on either the surfaces of growth layers or on the apices of growth pyramids or tables, except in a few cases. Many of the minute growth hills seen under low magnification have a flat surface rather than a steep summit. This makes a good contrast to ordinary growth pyramids

observed on many other crystals, which have steep summits and consist of composite spirals originating from a cluster of screw dislocations. On these flat-topped growth hills, no spiral pattern can be found even if special care is taken to secure very high contrast to enable the detection of layers as thin as a few Ångströms. Therefore it is considered that these growth hills are not formed at screw dislocation points, but are formed by two-dimensional nucleation or by an epitaxial settlement of minute crystals on to the growing surface. The occurrence of a large number of minute growth hills or tables provides additional evidence to support this consideration.

In addition to the above, some crystals exhibit something like "twist boundaries" on the surface, and growth pyramids occur along these lines (see, for example, fig. 20). The twist boundaries are considered to be formed either from the coalescence of several growing crystals or from the distortion of a growing surface due to external or internal stresses. Under the phase contrast microscope, it is often observed that both large and minute pyramids formed along these lines exhibit a spiral nature, though they are not typical spirals but are rather



FIGS. 17 and 18: FIG. 17 (left). An example of cubic forms of growth features on the  $\{100\}$  face. The photograph is in the same orientation as fig. 16. Ashio mine.  $\times 7$ . FIG. 18 (right). Another type of growth features on the  $\{100\}$  face. Chichibu mine.  $\times 7$ .



FIGS. 19 and 20: FIG. 19 (left). Showing a large number of minute growth tables on a  $\{100\}$  face. Positive phase contrast. Ogasawara Island.  $\times 120$ . FIG. 20 (right). Composite spirals observed along a twist boundary on  $\{100\}$  face. Positive phase contrast. Ashio mine.  $\times 600$ .

like composite spirals (fig. 20). Also of interest in this photograph are the rugged edges of spirals and the occurrence of a large number of minute cubic growth tables, which occur preferentially along the steps or corners of the spiral layers and are at a higher level than the surface of the layers. On the surface of these tables, no spiral pattern can be noticed, which suggests that they are formed by two-dimensional nucleation preferentially along the edges or corners of growth layers, which are more favourable sites for nucleation than the plane surface. Rugged edges of the spirals might well be derived from the combination of spiral layers and the tables.

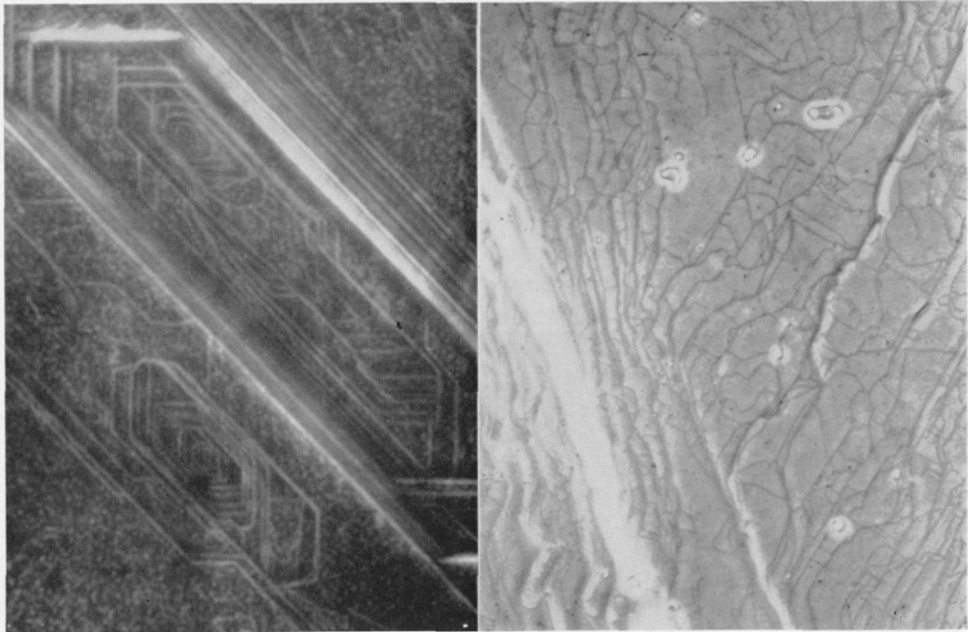


FIG. 21. Possible mono-molecular spirals observed on the {100} face. a (left), Ogasawara Island. Negative phase contrast.  $\times 3\,500$ . b (right), Tsunatori mine. Positive phase contrast.  $\times 880$ .

Two more examples of growth spirals seen under higher magnification are shown in figs. 21a and b. On both photomicrographs, one can see faint lines, on both sides of which no white diffraction bands are seen. They are ditches formed by preferential dissolution along steps of very thin growth layers. That no white diffraction bands appear along these lines suggests that their heights are as thin as a mono-molecular layer. Although no typical spiral pattern with many turns was observed, it was noticed on these photographs that many lines do not close themselves but originate from a point on the surface. When spiral layers originate from a large number of screw dislocations and interfere with each other, they often take on a pattern of this kind. It is, therefore, conjectured

that these are also spirals originating from single screw dislocation points with unit Burgers' vector.

Although growth spirals occur on the cube faces of some crystals, it should be stressed here that they are not growth features commonly observed on this face, which in most cases shows a large number of minute two-dimensional islands that are not considered to be formed by spiral mechanism.

$\{111\}$  faces. The characteristic surface structures of this face are well developed regular equilateral triangular markings, which are in opposite orientation to the triangle of the face, i.e. their edges are parallel to the edges between  $\{111\}$  and  $\{100\}$  faces (fig. 22). Triangular markings are observed on almost all octahedral faces of not only cubo-octahedral and penta-octahedral crystals but also of simple octahedral crystals, except in a few cases to be described later. The edges of the triangular markings are in most cases very straight, even on simple octahedral crystals, and the centre is generally situated at the centre of a face. Generally, there is only one centre on a face, though in some cases two or more centres occur, and in a few cases no centre is found on a face. If the surfaces of these centres are observed under the phase contrast microscope, neither composite nor single spirals are found, but only a pile up of triangular layers is noticed. This is surprising, since at such centres for other minerals one can usually find either composite or single spirals. It is also noteworthy that thinner layers

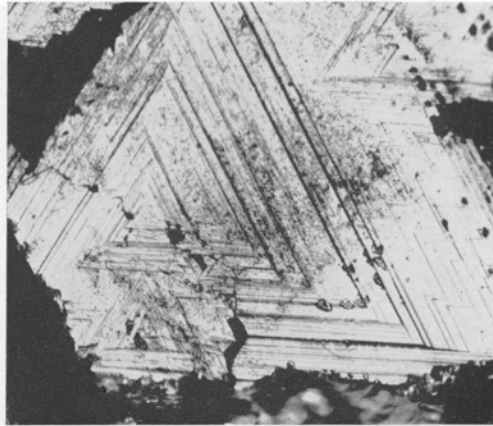


FIG. 22. Triangular markings on the  $\{111\}$  face. Ani mine.  $\times 7$ .

observed on the surface of triangular markings have more or less irregular or rugged edges, whereas thicker steps have very straight edges, which are too straight to be called ordinary growth layers. It looks as if the advance of thinner growth layers having irregular fronts is halted at linear discontinuities, resulting in the formation of regular equilateral triangular markings.

There are a few crystals that do not show these regular triangular markings on the octahedral faces. These are always simple octahedral crystals, and on such crystals only one can find growth spirals of both composite and typical nature, three examples of which are shown in fig. 23a, b, and c. Fig. 23a is a composite spiral observed on an octahedral crystal from Hanaoka mine. Small star-like patterns on the photograph represent gypsum crystals. The spiral is not regular equilateral triangular with straight edges but is malformed triangular with curved edges. Furthermore, its orientation is not the same as the

commonly observed triangular markings but is inclined to the latter by a small angle. Fig. 23b is another example of composite spirals observed on a crystal from Mizusawa mine. In this case, spiral layers originate from clusters of screw dislocations and again have curved steps instead of straight steps. Fig. 23c is the only example of possible typical spirals with monomolecular step height. The triangular pyramids have single apices and smooth side faces. Unfortunately the face of this crystal has been subjected to natural etching, and the apices of the pyramids cannot be seen clearly under high magnification with the phase contrast microscope. As a result, it was not possible to prove that the pyramids consist of spirals. However, it has been demonstrated on many crystals such as hematite, corundum, and spinel that this sort of pyramid is formed by closely spaced typical spiral layers of monomolecular height originating from a single screw dislocation.

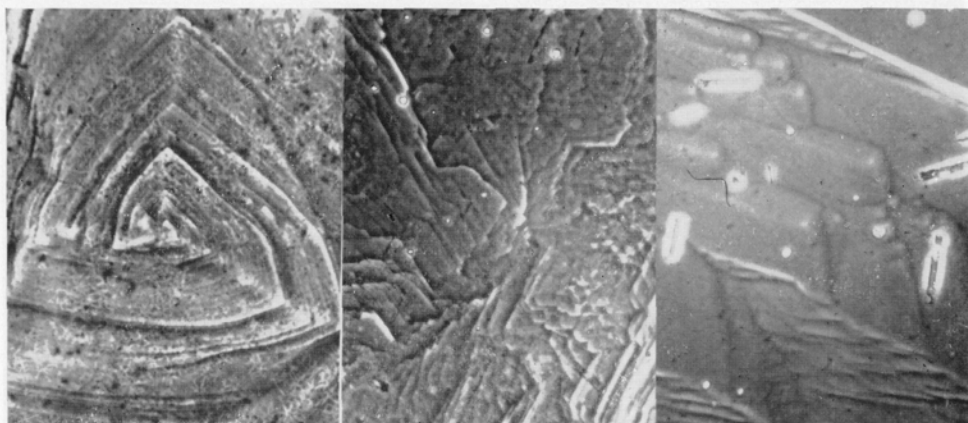


FIG. 23. Three examples of growth spirals observed on  $\{111\}$  faces. Positive phase contrast. a (left), Hanaoka mine.  $\times 175$ . b (middle), Mizusawa mine.  $\times 100$ . c (right) Hanaoka mine.  $\times 100$ .

$\{210\}$  faces are characterized by the good development of striations parallel to the edges with cube faces. Almost all  $\{210\}$  faces of pyrite crystals exhibit only striations under low magnification, irrespective of size or habit of crystals. Under higher magnification with the phase contrast microscope, the striated surfaces show only parallel lines, and only poor development of elongated growth layers can be observed. This suggests that on the  $\{210\}$  faces growth layers cannot develop as freely as on the  $\{100\}$  face, and even if they start to develop, their advance is strictly controlled by the  $\{100\}$  faces. On a few crystals, striations develop in different orientations, perpendicular to the edge between  $\{100\}$  and  $\{210\}$ . These crystals are regarded as negative crystals and can be found only rarely. It is interesting to note that negative crystals are only found in a special mode of occurrence and where they are found every pyrite crystal is negative.

On a few crystals, only when they take simple pentagonal habit, one can find  $\{210\}$  faces without well marked striations. On such surfaces, a few growth pyramids occur, and they are found, under high magnification with the phase contrast microscope, to consist of closely spaced growth layers. The pyramids have point apices, and at the tops of some pyramids a minute hole was found to occur (shown by an arrow in fig. 24). This shows that the pyramids are formed by spiral growth and the hole is a dislocation hole. The morphology of these spirals is in general trapezoidal, which is in good accord with the symmetry of the  $\{210\}$  face.

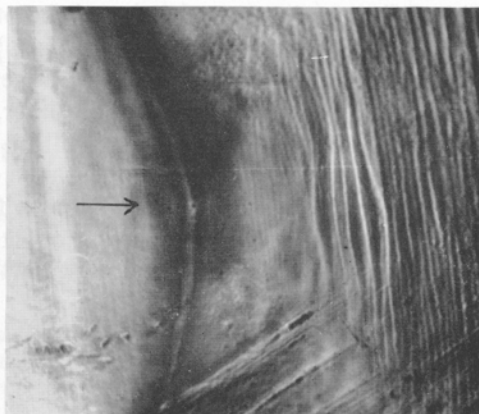


FIG. 24. Possible spiral pyramid observed on  $\{210\}$  face. Arrow shows dislocation hole. Hanaoka mine.  $\times 240$ .

#### Conclusions

From the observations described above, the following conclusions can be drawn regarding the mechanism of crystal growth of pyrite and crystal habit variations:

Spiral growth is not a universal feature in the growth of pyrite, though it takes place in special cases on all three dominant faces. Typical spirals originating from a single screw dislocation are found only exceptionally on pyrite crystals. Layer growth, originating either from two-dimensional nucleation or epitaxially settled crystallites, is more general than spiral growth from screw dislocations. If a similar argument to that for the growth from vapour phase can be applied in this case too, one can say that most of the pyrite crystals were grown in relatively high supersaturation conditions.

Growth layers, no matter how they originated, can develop on all of the three *F*-faces  $\{100\}$ ,  $\{111\}$ , and  $\{210\}$ . However, they develop freely only on  $\{100\}$ , sometimes on  $\{111\}$ , and rarely on  $\{210\}$ . Advance of growth layers on the latter two faces is in most cases strongly controlled by the directions parallel to  $\{100\}$  faces. In this sense, the most predominant *F*-face is  $\{100\}$ , next  $\{111\}$ , and the last  $\{210\}$ . This order of predominance is not the same as the theoretical order based on both Donnay-Harker's and Hartman's theories, but is in good accord with the observed order of predominance of crystal faces in pyrite (Sunagawa, 1957).

The forms of growth layers and pyramids on  $\{100\}$  faces vary considerably, and this variation is closely related to the variation of crystal habit. Growth layers and pyramids on the  $\{111\}$  and  $\{210\}$  faces show more or less uniform morphology, except in a few cases of simple octahedra or pentagonal crystals.

This difference between  $\{100\}$  and the other two faces suggests that the growth of pyrite will take place mainly on  $\{100\}$ , while the other two faces are in most cases formed by the pile up of the edges of growth layers on  $\{100\}$ , at least at the beginning of their appearance; later, growth layers start to develop spontaneously, though their advance will be controlled strongly by  $\{100\}$  faces.

It is conjectured that the appearance of  $\{111\}$  and  $\{210\}$  faces is conditioned by the morphology of growth layers on the  $\{100\}$  face. Which factor will govern the morphology of growth layers on  $\{100\}$  faces has not been clarified in this study. Impurity adsorptions along growth steps will certainly be one such factor.

#### References

- FONT-ALTABA (M.), 1963. *Min. Soc. America*, Sp. Paper 1, 186.  
SEAGER (A. F.), 1953. *Min. Mag.*, **30**, 1.  
SUNAGAWA (I.), 1957. *Rep. Geol. Surv. Japan*, No. 175.

is positively skewed, and hence the rate of nucleation increased for a longer period than it decreased. On the assumption of a constant rate of growth parallel to (001), the increase in nucleation rate was exponential.

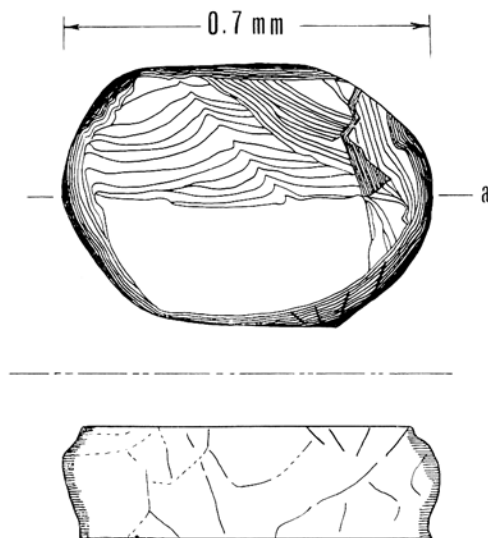


FIG. 1. Sketch showing plan and elevation of a typical phlogopite crystal. Growth steps are shown.

*Growth steps.* The basal surfaces of most of the phlogopite crystals contain growth steps, often giving rise to complex patterns. The steps are more common on large crystals than on smaller ones, and are concentrated at the margins of the faces.

Different patterns of steps may be described in relation to the shape of the line that defines the step edge, and differences are shown in figs. 1 and 2. Some step edges are straight (fig. 2b), others are irregularly curved (fig. 2c), while others are cusperate (figs. 1 and 2d).

The steps that appear in fig. 2 are much higher than the unit cell of phlogopite ( $10.3 \text{ \AA}$ ), reaching an upper limit of about  $15 \mu$ . On one surface (fig. 2d, bottom) the average step height is  $\frac{1}{2} \mu$ .

The straight or nearly straight steps tend to lie parallel to preferred crystallographic directions (fig. 3 and table I). The angles between the  $a$  axis and straight step edges in the crystals of fig. 2 are listed in table II. Many of the edges coincide with directions of relatively close packing of oxygen ions, presumably because the free energy of these edges is relatively low.

The complete step pattern of one face of a crystal is shown in fig. 2a. The top surface appears plane and free of steps. Along a line parallel to  $\{110\}$  at  $a$ , this surface gives way to one that is inclined and has a rough surface. Nearby is a depression with sides that are clearly stepped (f and g), and although the step

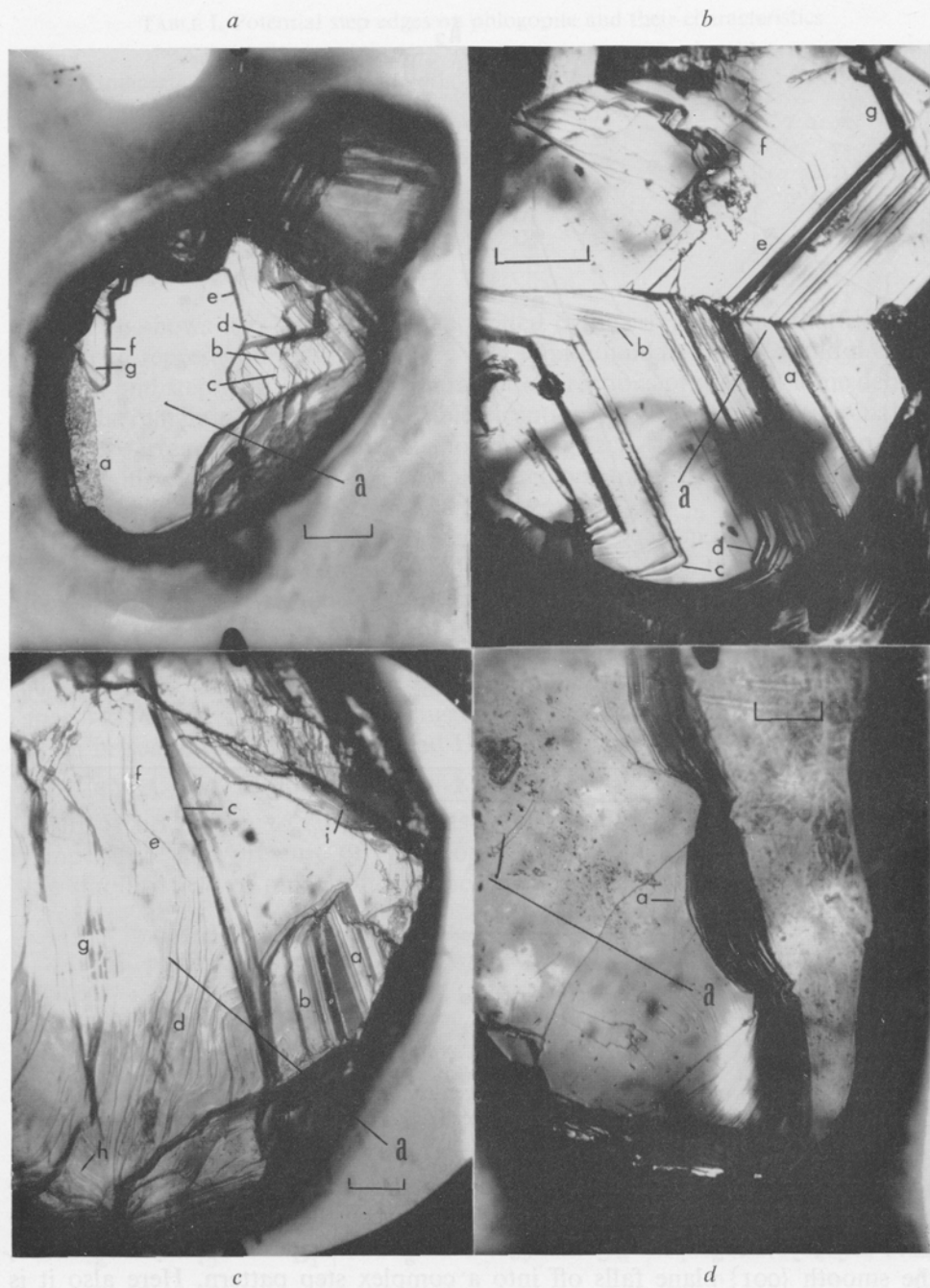


FIG. 2 *a-d*. Growth steps on phlogopite crystals; position of crystallographic *a* axis is indicated; scale bar = 0.1 mm.

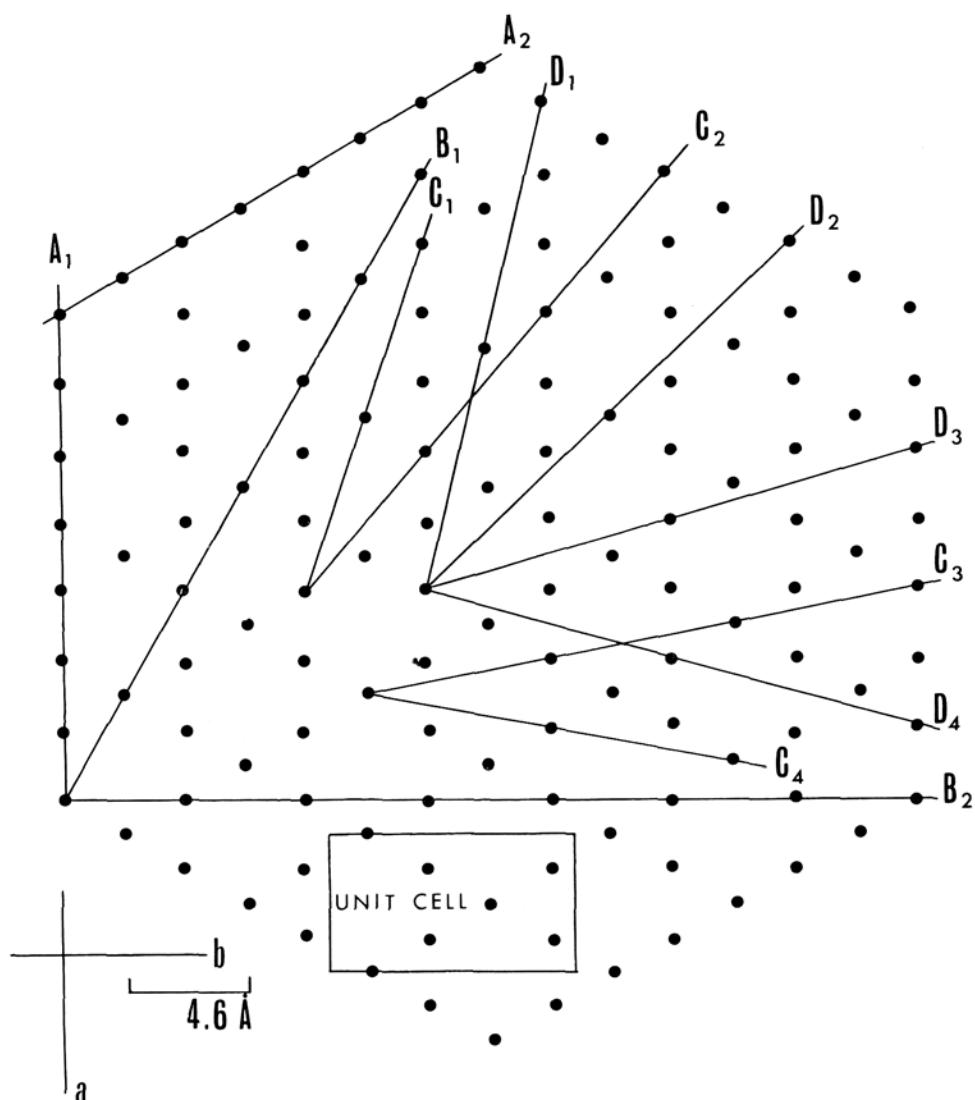


FIG. 3. Position of oxygen ions in the oxygen-rich plane of the phlogopite structure; potential positions of step edges (A<sub>1</sub>, A<sub>2</sub>, etc.) are indicated.

edges appear perfectly straight, they do not lie parallel to directions of close ionic packing (table II) nor does the angle between them (50 degrees) appear to have any crystallographic significance. On the other side of the crystal surface, the smooth {001} plane falls off into a complex step pattern. Here also it is difficult to relate step direction with crystallographic direction, as illustrated by the well-formed steps at b and c and the high steps at d and e (table II).

TABLE I. Potential step edges on phlogopite and their characteristics

Line (fig. 3)	Indices	Angle with <i>a</i> axis	O-O*	<i>d</i> <sub>hkl</sub>	Line (fig. 3)	Indices	Angle with <i>a</i> axis	O-O*	<i>d</i> <sub>hkl</sub>
A <sub>1</sub>	{01-}	0° 00'	2.65 Å	4.60 Å	C <sub>3</sub>	{31-}	79° 06'	7.01 Å	1.73
A <sub>2</sub>	{11-}	60° 00'			C <sub>1</sub>	{31-}	79° 06'		
B <sub>1</sub>	{13-}	30° 00'	4.60	2.65	D <sub>1</sub>	{17-}	13° 54'	9.55	1.28
B <sub>2</sub>	{10-}	90° 00'			D <sub>2</sub>	{35-}	46° 06'		
C <sub>1</sub>	{15-}	19° 06'	7.01	1.73	D <sub>3</sub>	{21-}	73° 54'		
C <sub>2</sub>	{12-}	40° 54'			D <sub>4</sub>	{21-}	73° 54'		

\* Spacing of oxygen atoms along line.

Fig. 2b shows two step patterns separated by an irregular line that does not appear to represent a grain boundary or a twin boundary. Steps a and d of one portion and step g of the other lie parallel to directions of greatest ionic density, while the remaining steps, with possible exception of c, are apparently anomalous.

A very irregular step pattern is shown in fig. 2c. Although some step edges are irregular in shape, they may locally become straight and parallel to a line of close ionic packing, as shown at d and e.

Peculiar cusped patterns are shown in fig. 2d. The cusp may be sharp and it invariably points in the "down hill" direction. Locally the two lines that extend from the point lie parallel to crystallographic directions. The points of the cusps may be obstacles that prevented the effective spreading of growth layers.

*The reaction.* The reactants that produce phlogopite in marbles are not easily specified (Tilley, 1920), and it is suggested that this mineral is the consequence of an introduction of  $\text{KAlSi}_3\text{O}_8$  and  $\text{H}_2\text{O}$  into magnesium-containing limestone

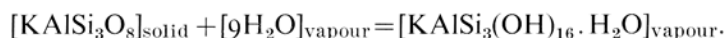
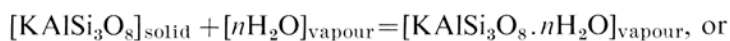


There is no reason to suspect metastable crystallization, since the estimated temperature and pressure of metamorphism lie well within the boundaries of the stability field of phlogopite, as located by Yoder and Eugster (1954).

TABLE II. Orientation of step edges on phlogopite crystals of fig. 2 and possible arrangement (*P*) of oxygen ions at step edge (fig. 3; table I)

Crystal and edge	Angle between edge and <i>a</i> axis	<i>P</i>	Crystal and edge	Angle between edge and <i>a</i> axis	<i>P</i>	Crystal and edge	Angle between edge and <i>a</i> axis	<i>P</i>
A a	60°	A <sub>2</sub>	B a	60°	A <sub>2</sub>	C a	30°	B <sub>1</sub>
b	23	—	b	70	—	b	35	—
c	72	D <sub>3</sub>	c	30	B <sub>1</sub>	c	31	B <sub>1</sub>
d	39	C <sub>2</sub>	d	~0	A <sub>1</sub>	d	60	A <sub>2</sub>
e	52	—	e	12	D <sub>1</sub>	e	~0	A <sub>1</sub>
f	65	—	f	85	—	f	49	—
g	15	D <sub>1</sub>	g	60	A <sub>2</sub>	g	42	C <sub>2</sub>
						h	~0	A <sub>1</sub>
						i	0	A <sub>1</sub>
						D a	60	A <sub>2</sub>

Little is known regarding the mechanism by which potassium, aluminium, silicon, and other elements are transported into rock bodies. It is presently suggested that H<sub>2</sub>O played an important role in the transport process, not as a solvent but as a reactant, giving rise to chemical transport reactions as described by Schäfer (1964). By analogy with SiO<sub>2</sub>, which under certain conditions is evidently transported as Si(OH)<sub>4</sub> (Brady, 1953), the transport reaction may possibly be



Although the phlogopite-forming material may be referred to as vaporous when contained by a vessel, the migration of this matter is thought to be more analogous to grain-boundary diffusion in metals than to the flow of a gas through a porous medium.

It is further suggested that the mobile material maintained at first a chemical potential sufficiently low to prevent reaction from taking place. Then, as the concentration of this material slowly and uniformly increased in the grain boundary phase, chemical reaction and nucleation of phlogopite were initiated at numerous points throughout the rock.

Slightly different reactions may be written depending on the choice of reactants. For a mobile reactant of composition KAlSi<sub>3</sub>(OH)<sub>16</sub>, the reaction is:



Whatever the exact nature of the reaction, there can be no doubt that at the time of reaction, a small proportion of the phlogopite existed as an activated complex (Kingery, 1959; Osipov, 1964; Burke, 1965), and that all of the material presently found in phlogopite passed through this transitional state. Since points of reaction in the rock could not have invariably coincided with points of crystal growth, the activated complex must have possessed an inherent mobility. It is postulated therefore that at the time of reaction and crystal growth, the activated complex was generally dispersed throughout the rock, especially along grain boundaries, where it mingled with other mobile constituents but moved independently of them.

Nucleation of the phlogopite crystals presumably occurred at certain favourable nucleation sites. These may possibly include the surface of illite or other sheet silicate impurities in the limestone, grain boundaries (Clemm and Fisher, 1955), and at imperfections (Bengus *et al.*, 1960; Hanke, 1961; Patel and Goswami, 1962) in the interiors of carbonate grains.

*Growth mechanism.* The crystal growth theory of Frank (1949) and Burton, Cabrera, and Frank (1951), which considers screw dislocations as favourable

sources from which growth layers may spread, has proved highly successful, and spiral growth steps have been found on several minerals. It is suggested that the steps observed on phlogopite crystals of the present study are true growth steps inasmuch as they represent edges of layers that were spreading but did not reach the edge of the crystal. Spiral step patterns, as found on phlogopite crystals from cavities in volcanic rocks by Amelinckx (1952) and Sunagawa (1964) were not detected on those of the present study, and it is not known to what extent the Frank mechanism was operative.

Although the basal faces of the phlogopite crystals evidently advanced by layer formation and layer spreading, the outward growth of the sides of the crystals evidently advanced by the accretion of material to the edges of the mica sheets in a fairly irregular manner. As soon as a small portion of a prismatic side advanced by accretion, the portions above and below could advance by continued spreading of the now deeply buried layers, and hence two growth mechanisms evidently brought about the advance of the prismatic surfaces.

The question of why steps on crystal faces are commonly many unit cells in height was considered by Bunn and Emmett (1949), who suggested that amalgamation of many steps may take place as a natural attempt to reduce the surface energy, while Frank (1958) suggested that impurities might cause amalgamation of steps, and Mason, Bryant, and Van der Heuvel (1963) considered the problem in relation to surface diffusion. With reference to the crystals of the present study, different layers may have spread at different rates owing to heterogeneities in the activity of the activated complex surrounding the crystals, which may be partly determined by heterogeneities in the calcite that surrounded the crystals. Different layers spreading at different rates would cause an amalgamation of layers, provided the variation in rates was sufficiently large.

The relative dimensions of mica crystals may provide information regarding relative growth rates in different crystallographic directions. Thus very small crystals of biotite in volcanic glass normally form thin plates (Ross, 1962), crystals of fluor-phlogopite grown from a vapour form tabular prisms (Anikin, 1960), crystals of phlogopite in marble may form relatively long prisms (Struwe, 1958), and it may be deduced that high "supersaturation" favours a relatively rapid growth of the prismatic sides of the mica crystals. In view of the fact that the diameter of the crystals of the present study exceed the thickness by a factor of about 3, brief consideration may be given to the activation energy associated with the accretion of matter on phlogopite under the particular conditions of growth.

Consider a phlogopite crystal of nearly cylindrical shape, one half of which is illustrated in fig. 4. Three contributions to crystal growth may be imagined: deposition on  $\{001\}$  (at d, fig. 4) causing an increase in thickness (two-dimensional nucleation); deposition on the edge of a spreading layer (at a, b, b', fig. 4) causing an increase in width; and deposition on the edges of layers that have spread as far as possible (at c, fig. 4), also increasing the width of the crystal.

Since the crystals are tabular in shape (fig. 1), the second and third processes

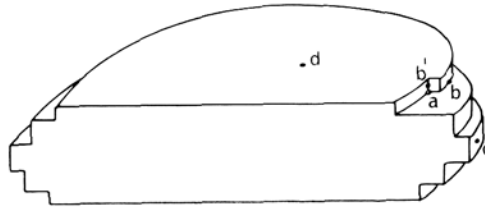


FIG. 4. Sketch of half a phlogopite crystal, showing different points where material may be added during growth.

in co-operation occurred more readily than the first, and the activation energies associated with them were less than that associated with the first process.

For a crystal of cylindrical shape it may be shown that in order to maintain a constant ratio of diameter to height, the volume of material deposited on the sides must exceed the volume of material deposited on the ends by a factor of 2. Hence it is suggested that of the total material deposited on a phlogopite crystal, a very small fraction was deposited by the first process, approximately  $\frac{1}{3}$  was deposited on the ends by the second, and approximately  $\frac{2}{3}$  was deposited on the sides by the second and third processes.

The conclusion that the activation energy associated with the first process is greater than that associated with the other two is in agreement with the expectation that the placing of ions to form new mica sheets on a mica substrate is more "difficult" than the placing of these ions on the edges of existing sheets.

*Displacement of matrix.* Crystals grow by displacement of their environment. The displacement of a solid environment may be a mechanical process in which the matrix becomes deformed plastically, or a physico-chemical process in which ions of the matrix are continuously removed from the interface. In certain instances, displacement of the matrix may possibly govern the rate of crystal growth.

It is postulated that, in the marbles of the present study, calcite was displaced from the interface by the diffusion of ions or larger units along grain boundaries and away from the phlogopite crystals. Such a process evidently operated in marbles described by Malakhova (1964), which clearly showed that growing quartz and feldspar crystals displaced foraminiferal shells by dissolution and removal of the carbonate portions of the shells, while the carbonaceous portions remained undisturbed.

#### Conclusion

The several processes that have participated in the crystallization of phlogopite in marble are as yet imperfectly understood. It is necessary to postulate a mobilization of several of the phlogopite-forming atoms, possibly by a chemical transport reaction, and migration of these into marble layers, possibly by diffusion along grain boundaries. Chemical reaction then occurred between

the mobile constituents and dolomite or magnesian calcite crystals to produce an activated complex. This resulted in the nucleation of phlogopite crystals at numerous points in the rock, and the diffusion of the phlogopite-forming portion of the activated complex to the sites of crystal growth. Growth of the phlogopite crystals evidently proceeded by the formation and spreading of layers on {001} faces and the accretion of matter on the prismatic surfaces. Meanwhile the calcite matrix was removed from the front of crystal growth, possibly by diffusion of calcium carbonate away from the interface.

*Acknowledgements.* Professor R. M. Barrer kindly provided laboratory facilities and Dr. I. S. Kerr was very helpful in obtaining the photographs. The study was supported by the Quebec Department of Natural Resources and a Royal Society and Nuffield Foundation Commonwealth Bursary.

#### References

- AMELINCKX (S.), 1952. *Compt. Rend. Acad. Sci. Paris*, **234**, 971-973.
- [ANIKIN (I. N.)] АНИКИН (И. Н.), 1960. [Труды Всес. Научн.—Исслед. Инст. Пьезоопгич, Мин., Сыр. 4, **1** 107-9]; abstr. in *Chem. Abstr.*, 1962, **57**, 12118e.
- [BENGUS (V. Z.), LAVRENT'EV (F. F.), SOIFER (L. M.), and STARTSEV (V. I.)] БЕНГУС (В. З.), Лаврентьев (Ф. Ф.), Соифер (Л. М.), и Старцев (В. И.), 1960. Кристаллография (*Crystallography*), **5**, 441-5.
- BLOSS (F. D.), GIBBS (G. V.), and CUMMINGS (D.), 1963. *Journ. Geol.*, **71**, 537-547.
- BRADY (E. L.), 1953. *Journ. physical Chem.*, **57**, 706-710.
- BURKE (J.), 1965. *The kinetics of phase transformations in metals*. Pergamon, London.
- BURTON (W. K.), CABRERA (N.), and FRANK (F. C.), 1951. *Phil. Trans.*, **243**, 299-358.
- CLEMM (P. J.) and FISHER (J. C.), 1955. *Acta Met.*, **3**, 70-73.
- FRANK (F. C.), 1949. *Disc. Faraday Soc.*, **5**, 48-54.
- , 1958. In *Growth and perfection of crystals*, Wiley, New York.
- HANKE (I.), 1961. *Acta Phys. Austriaca*, **14**, 1-21.
- KINGERY (W. D.), 1959. In *Kinetics of high temperature processes*, Mass. Inst. Tech.
- KRETZ (R.), 1957. *Prelim. Rept. Dep. Mines, Quebec*, 338.
- , 1966a. *Journ. Petrology*, **7**, 68-94.
- , 1966b. *Journ. Geol.*, **74**, 147-173.
- [MALAKHOVA (N. P.)] МАЛАХОВА (Н. П.), 1964. [Доклады акад. наук СССР (*Compt. Rend. Acad. Sci. URSS*)], **155**, 361-363]; abstr. in *Chem. Abstr.*, 1964, 15624e.
- MASON (B. J.), BRYANT (G. W.), and VAN DER HEUVEL (A. P.), 1963. *Phil. Mag.*, **8**, 505-526.
- OSIPOV (K. A.), 1964. *Activation processes in solid metals and alloys*. Elsevier, New York.
- PATEL (A. R.) and GOSWAMI (K. N.), 1962. *Acta Cryst.*, **15**, 417-449.
- ROSS (C. S.), 1962. *Amer. Min.*, **47**, 723-740.
- SCHÄFER (H.), 1964. *Chemical transport reactions*, Academic Press.
- STRUWE (H.), 1958. *Leidse Geol. Mededel.*, **22**, 237-349.
- SUNAGAWA (I.), 1964. *Amer. Min.*, **49**, 1427-1434.
- TILLEY (C. E.), 1920. *Geol. Mag.*, **57**, 449-462.
- YODER (H. S.) and EUGSTER (H. P.), 1955. *Geochimica Acta*, **6**, 179-182.

# Comparison between theoretical and observed morphology of crystals with the rutile type structure

By P. HARTMAN

Geologisch en Mineralogisch Instituut der Rijksuniversiteit,  
Garenmarkt, Leiden, The Netherlands.

*Summary.* For crystals with the rutile type structure the theoretical habit is  $\{110\}$ ,  $\{011\}$ . Natural and synthetic crystals often show  $\{100\}$  and  $\{111\}$  as prominent forms. Arguments are given that high supersaturation evokes mainly  $\{111\}$  and that adsorption of water molecules enhances  $\{100\}$ .

The adsorption of an epitactic layer of hematite enhances  $\{100\}$  and  $\{111\}$  on rutile, but  $\{100\}$  only on plattnerite.

The adsorption of an epitactic layer of quartz would promote  $\{100\}$  on rutile.

THE morphology of the rutile group can be derived from the crystal structure by applying the periodic bond chain method (Hartman and Perdok, 1955; Hartman, 1963). In short this method distinguishes three types of crystal faces: F-faces, which grow according to a layer mechanism. The minimum thickness of this growth layer or slice is  $d_{hkl}$  and the slice should contain at least two periodic bond chains (PBC's); S-faces, which cannot grow according to a layer mechanism, as they contain within a layer  $d_{hkl}$  only one PBC; and K-faces, which do not contain any PBC within a layer  $d_{hkl}$ .

A crystal that grows slowly from a slightly supersaturated vapour or solution should be bounded by F-faces exclusively. Other faces may occur through the influence of supersaturation or the presence of impurities upon crystal growth.

Kern (1955) has shown that a high supersaturation may induce a habit change in ionic crystals whereby the new faces are structurally characterized by alternating layers of positive and negative ions, as e.g. the  $(111)$  face of NaCl. Such faces are often K-faces.

The application of the PBC method to the rutile structure gives the following results (Hartman, to be published):

The PBC's are  $\langle 001 \rangle$  and  $\langle 111 \rangle$ . These determine the F-forms  $\{110\}$  and  $\{011\}$ . All other forms  $\{hko\}$  are S-forms. Densely packed K-faces are  $\{111\}$  and  $\{001\}$ , of which only the former has a polar surface structure.

From this we conclude that rutile crystals should be bounded by  $\{110\}$  and  $\{011\}$  only,<sup>1</sup> to which  $\{111\}$  may be added when crystallization took place from aqueous solutions at a high supersaturation. Impurities might be responsible for the appearance of S- and K-faces.

<sup>1</sup> Dana's settings (Syst. Min., 7th edn) are used throughout.

*Observed morphology.* Since the PBC method is a strong bond approximation, and since no specific atomic properties are considered, the predicted morphology should hold for all compounds with the rutile structure.

On natural crystals of rutile ( $\text{TiO}_2$ ), pyrolusite ( $\text{MnO}_2$ ), cassiterite ( $\text{SnO}_2$ ), and sellaite ( $\text{MgF}_2$ ) the main forms are  $\{110\}$ ,  $\{100\}$ ,  $\{011\}$ , and  $\{111\}$ . Plattnerite crystals ( $\text{PbO}_2$ ) have been described as having  $\{100\}$  dominant, and  $\{110\}$  absent.

In the last few years rutile type crystals have been grown hydrothermally (Harvill and Roy, 1964 and 1965).  $\text{TiO}_2$  was grown from 9*M.*  $\text{H}_2\text{SO}_4$  at  $640^\circ\text{C}$  and 60 000 lb./in.<sup>2</sup> and a supersaturation of a few percent. These crystals show  $\{100\}$ ,  $\{110\}$ , and  $\{011\}$ , with  $\{100\}$  consistently larger than  $\{110\}$ . Small  $\{111\}$  faces appear at higher supersaturation when spontaneous nucleation occurs.  $\text{GeO}_2$  was grown from aqueous solution at about  $500^\circ\text{C}$  and 60 000 lb./in.<sup>2</sup> and supersaturations of about 70–80%. On these crystals  $\{110\}$  and  $\{111\}$  dominated slightly over  $\{100\}$  and  $\{011\}$ .  $\text{SnO}_2$  was grown from 2*M.*  $\text{KOH}$  at  $700^\circ\text{C}$  and 60 000 lb./in.<sup>2</sup>. Supersaturation values are not known. The crystals are bounded by  $\{110\}$  and  $\{011\}$  only.

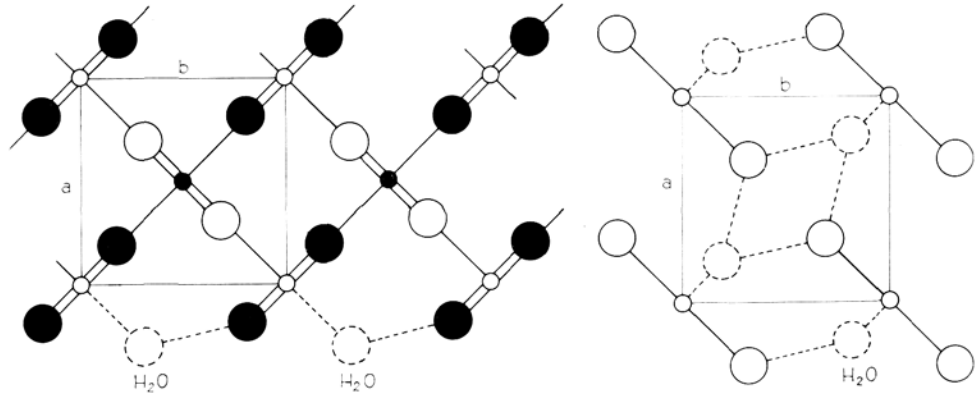
#### *Comparison between predicted and observed morphology*

If we compare the observed morphology with the predicted one, we see that indeed the two F-forms are among the main forms. Further,  $\{111\}$  is a prominent form, which might be explained as an influence of supersaturation, possibly combined with the influence of impurities.

The occurrence of  $\{100\}$ , an S-form in  $[001]$ , might have been expected on the equilibrium form, but not on the growth form. It can easily be shown that neighbouring chains  $[001]$  in a layer  $d_{200}$  have an attractive interaction energy, so that  $\{100\}$  should be present at least on the equilibrium form as rather narrow facets. But how to explain its often being the most prominent face? In the following it will be argued that water, ferric ions, and silica may favour the development of  $\{100\}$ :

*Water* will act as an impurity when it is adsorbed on the crystal from either the vapour or the liquid phase. In the outermost layer of (100) or of (110) the Ti ions are surrounded by 5 oxygens only. A water molecule can therefore be adsorbed on these faces in the site of the sixth oxygen atom, as shown in fig. 1. On the face (100) this water molecule can form a hydrogen bond with an oxygen atom of the next PBC  $[001]$ , the distance being 2.78 Å for rutile. Moreover the angle  $\text{Ti-H}_2\text{O-O}$  is about  $117^\circ$ . In this way the adsorbed water molecule links the two neighbouring PBC's  $[001]$  together, so that it forms a new PBC  $[010]$  or  $[011]$ . Formally it then changes the S-form into an F-form, so that layer growth becomes possible (Wolff, 1962; Hartman and Kern, 1964).

On the face (110) the adsorbed water molecule cannot be linked to an oxygen atom by means of a hydrogen bond. It appears therefore that this particular adsorption site for  $\text{H}_2\text{O}$  occurs on  $\{100\}$  only. A different adsorption site is



FIGS. 1 and 2: FIG. 1 (left). Projection of the rutile structure along  $[001]$ . Small circles, Ti; large circles, O. Open circles at height  $z=0$ ; filled circles,  $z=\frac{1}{2}$ . At the surface of (100) a water molecule can be adsorbed at the site of an oxygen atom of the next  $d_{200}$  slice. Through its hydrogen bond of  $2.78 \text{ \AA}$  new PBC's  $[010]$  and  $[011]$  are formed. FIG. 2 (right). A layer  $d_{002}$  of the rutile structure, projected along  $[001]$ . All atoms are coplanar at  $z=0$ . Adsorbed water molecules are drawn as dashed circles; they are at height  $z=\frac{1}{2}$ .

found on (001) as shown in fig. 2. A layer  $d_{002}$  consists entirely of coplanar Ti and O atoms, which means that the electrostatic field is rather weak. A water molecule may be adsorbed in the site of an oxygen atom as shown in the figure, but although the distance to a neighbouring oxygen is favourable for a hydrogen bond ( $2.78 \text{ \AA}$  in rutile), the angle Ti-H<sub>2</sub>O-O is not, since it is  $94^\circ$ , which is rather far from the ideal angle of  $125^\circ 16'$ .

The face (111) is a K-face. In a projection along  $[0\bar{1}1]$  (fig. 3) it is seen that its structure can be considered as consisting of alternating positive (Ti<sup>4+</sup>) and negative (TiO<sub>4</sub><sup>4-</sup>) layers. According to Kern (1955) such a face would be expected to develop on crystallization from highly supersaturated solutions in polar

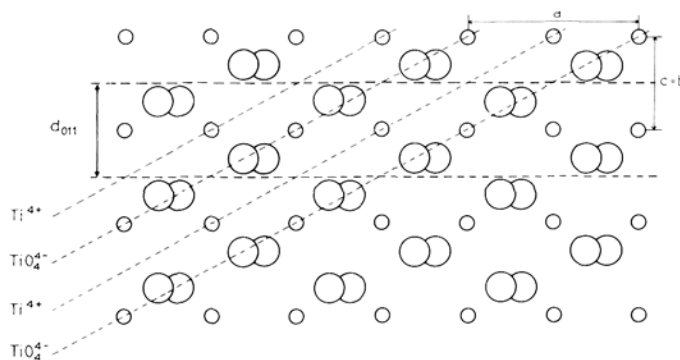


FIG. 3. Projection of the rutile structure along  $[0\bar{1}1]$ . Parallel to (111) the structure shows alternating positive and negative layers, so that the electrostatic field at the surface of (111) is high.

solvents. The electrostatic field is high for (111) so that the polar water molecules are well adsorbed. The fact that, according to Harvill and Roy, {111} appears on  $\text{TiO}_2$  and  $\text{GeO}_2$  at high supersaturations is in agreement with the results of Kern's experiments.

*Ferric iron* is present as an impurity in natural crystals of  $\text{TiO}_2$ ,  $\text{MnO}_2$ ,  $\text{SnO}_2$ , and  $\text{PbO}_2$ . When  $\text{Fe}^{3+}$  ions are present as an impurity in the noncrystalline phase, they may affect the crystal habit through the formation of an adsorbed epitactic layer of  $\text{Fe}_2\text{O}_3$ . The epitaxy of hematite on rutile follows the law: (100) [011] rutile  $\parallel$  (0001)  $[\bar{1}1.0]$  hematite. This brings the following faces nearly into coincidence (the indices of hematite are referred to the structural rhombohedral unit cell with  $a = 5.424 \text{ \AA}$  and  $\alpha = 55^\circ 17'$ ): (100) of rutile with (111) of hematite, (101) with (011), (001) with ( $\bar{2}11$ ), (011) with ( $\bar{1}10$ ), (111) with (021), and (010) with (01 $\bar{1}$ ). Now the most prominent PBC's of hematite are the same as those for corundum, namely [01 $\bar{1}$ ] and [100] (Hartman, 1962), which are parallel to [010] and [10 $\bar{1}$ ] of rutile, respectively. This means that through the adsorption of an epitactic layer with the hematite structure the zones  $\langle 010 \rangle$  and  $\langle 011 \rangle$  of rutile might become new PBC's.

In table I the misfits are given for the various combinations. A smaller misfit means a more stable adsorption of an epitactic layer and therefore a more pronounced change in habit. From the table it follows that for  $\text{MnO}_2$  and  $\text{TiO}_2$  the  $\langle 101 \rangle$  zones will be enhanced, that is, {111} and {100} will become more developed, as is indeed the case on natural crystals. For  $\text{SnO}_2$  not only  $\langle 101 \rangle$  but also  $\langle 010 \rangle$  would be enhanced, which would result in larger developments of {100}, {111}, and possibly {001}. This is exactly what is observed on natural crystals.

TABLE I. Misfit of hematite with rutile type crystals

Hematite [01 $\bar{1}$ ] (5.033 Å)			Hematite [100] (5.424 Å)		
Compound	compared with:		Compound	compared with:	
	[010]	Misfit		[10 $\bar{1}$ ]	Misfit
$\text{MnO}_2$	4.397 Å	+14.5%	$\text{MnO}_2$	5.250 Å	+3.3%
$\text{TiO}_2$	4.593	+9.6	$\text{TiO}_2$	5.464	-0.7
$\text{SnO}_2$	4.718	+6.7	$\text{SnO}_2$	5.679	-4.5
$\text{PbO}_2$	4.955	+1.6	$\text{PbO}_2$	6.000	-9.6

For  $\text{PbO}_2$  the misfit for  $\langle 010 \rangle$  is clearly much less than for  $\langle 101 \rangle$ , so that here the former zone is mainly enhanced. This is in excellent agreement with the habit of plattnerite crystals from Idaho, which show {100} large, {301} medium, and {101}, {001} small. Moreover these crystals are found together with limonite (cf. Hintze, 1915) so that this special habit may well be accounted for by the adsorption of  $\text{Fe}_2\text{O}_3$ .

The habit changes can be formulated in a formal way as follows: The S-face (100) of  $X\text{O}_2$  is transformed into an F-face by the adsorption of a slice of the F-face (111) of hematite, which produces the new PBC [010], or a slice of the F-face (01 $\bar{1}$ ) of hematite, which produces the PBC [10 $\bar{1}$ ]. The K-face (111) of

$XO_2$  is transformed into an F-face by the adsorption of a slice of the F-face (021) of hematite, which produces the new PBC  $[10\bar{1}]$ . As the zone  $[01\bar{1}]$  is equivalent with  $[10\bar{1}]$  two new PBC's are formed, assuring the F-character of the original K-face.

In a fluid containing *silica*, epitaxial adsorption of a layer of a silica polymorph on the (100) face of rutile may occur. It appears that the  $(10\bar{1}0)$  face of quartz has the best dimensional and structural fit on (100) of rutile. The misfits of the PBC's (Hartman, 1959) in the quartz  $d_{10\bar{1}0}$  slice are given in table II. The epitaxial quartz layer is shown in fig. 4. When the oxygen atom A is placed in the position of the missing oxygen around Ti, the nearest Si atom is at a distance of 1.79 Å from an oxygen of the rutile structure, somewhat larger than the Si-O distance of 1.61 Å in quartz. Minor displacements in the relative position of the two structures would certainly result in better agreement with normal Si-O, Ti-O, and O-O distances, but no attempt was made to calculate them. The periodic bond chain from A to B is  $[01\bar{1}1]$ , which has the smallest misfit (table II).

TABLE II. Misfits of PBC's in a  $d_{10\bar{1}0}$  slice of quartz on the (100) face of rutile

Quartz	Rutile	Misfit
$[01.0]=4.903 \text{ \AA}$	$[010]=4.593 \text{ \AA}$	+6.7%
$[00.1]=5.393 \text{ \AA}$	$2[001]=5.918 \text{ \AA}$	-8.9%
$[01.1]=7.289 \text{ \AA}$	$[012]=7.491 \text{ \AA}$	-2.7%

Hence the S-face (100) of rutile is formally transformed into an F-face by the adsorption of a slice of the F-face  $(10\bar{1}0)$  of quartz. For rutile the direction  $[012]$  has become a PBC through adsorption, so that  $\{100\}$  will be enhanced when silica is present.

Little is known about the influence of silica on the habit of rutile. It is known that rutile often occurs in quartz as needles. According to von Vultée (1955,

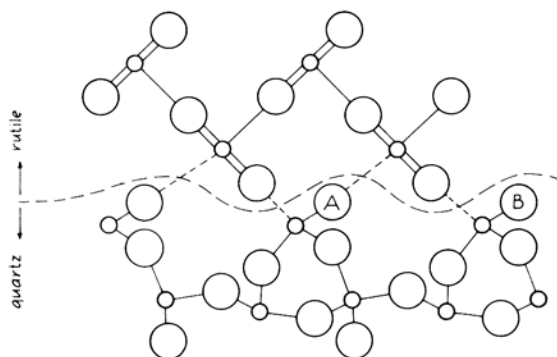


FIG. 4. Epitaxial layer of quartz on rutile  $(10\bar{1}0)$  of quartz on (100) of rutile. This layer has the structure of a  $d_{10\bar{1}0}$  slice and both crystals are projected along their  $c$ -axes. In the quartz slice is a PBC  $[01.1]$  from A to B, which fits well with  $[012]$  of rutile.

1956) these needles have a square cross section, but the indices of the prism could not be determined, owing to the small dimensions.

### Conclusions

The morphology of natural crystals with the rutile type structure differs from the theoretical  $\{110\}$   $\{011\}$  combination; the enhanced forms are  $\{100\}$  and  $\{111\}$ . The discrepancy can be understood if high supersaturations and adsorption of impurities occurred. High supersaturation would evoke  $\{111\}$ . The adsorption of  $H_2O$  would enhance  $\{100\}$  and  $\{111\}$ . The adsorption of ferric ions in the form of an epitactic hematite layer can account for the appearance of  $\{100\}$  and  $\{111\}$  on rutile and for the prominence of  $\{100\}$ ,  $\{001\}$ , and other  $\{hol\}$  forms on plattnerite. The adsorption of silica in the form of an epitactic quartz layer accounts for the development of  $\{100\}$ .

*Acknowledgements.* The author wishes to express his sincere thanks to Prof. R. Roy and to Dr. M. L. Harvill for their kind permission to use their experimental data prior to publication.

### References

- HARTMAN (P.) and PERDOK (W. G.), 1955. *Acta Cryst.*, **8**, 49 [M.A. 13-279].  
—, 1959. *Bull. Soc. franç. Min. Crist.*, **82**, 335 [M.A. 14-470].  
[—] ХАРТМАН (П.), 1962. Зап. Всесоюз. Мин. Общ. (Mem. All-Union Min. Soc.), **91**, 672.  
—, 1963. *Zeits. Krist.*, **119**, 65 [M.A. 17-24].  
— and KERN (R.), 1964. *Compt. Rend. Acad. Sci. Paris*, **258**, 4 591.  
HARVILL (M. L.) and ROY (R.), 1964. *Bull. Amer. Ceram. Soc.*, **43**, 255.  
— —, 1965. *Ibid.*, **44**, 297.  
HINTZE (C.), 1915. *Handb. Min. Bd. I Abt. 2*, p. 1 718.  
KERN (R.), 1955. *Bull. Soc. franç. Min. Crist.*, **78**, 461, 497.  
VULTÉE (J. VON), 1955. *Neues Jahrb. Min., Abh.*, **87**, 389, [M.A. 12-597].  
—, 1956. *Zeits. Krist.*, **107**, 1.  
WOLFF (G. A.), 1962. *Zeits. physikal. Chem.*, **31**, 1.

## Notation and genetic significance of crystal habits

By IVAN KOSTOV  
(ИВАН КОСТОВ)

Chair of Mineralogy and Crystallography  
University of Sofia, Bulgaria.

*Summary.* A system of classification for crystal habits is described, and the dependence of habit on genetic conditions and its uses as an indicator of genetic discussions are discussed.

A DETAILED analysis of the main crystal types was made by Niggli (1926a), on the basis of the fundamental work of Fedorov (1903), where all crystals are treated either as pseudotetragonal or pseudo-hexagonal. Niggli distinguished cubic or hypocubic, tetragonal or hypotetragonal, and hexagonal or hypohexagonal types, the latter two extending from tabular to pseudoisometric and finally to columnar subtypes. These he used as principal subdivisions in his well-known textbook of special mineralogy (Niggli, 1926b). Kalb (1927) suggested analogous subdivisions, viz. isoharmonic, tetraharmonic, and hexaharmonic, on the basis of corresponding harmonic point nets. Niggli (1941) provided also a detailed statistical analysis of crystal habits, later used extensively by many other authors. To Kalb and Koch (1929, 1931) and Kalb (1928), on the other hand, we owe excellent papers on habit types of minerals, derived chiefly by observation on crystals from natural occurrences.

As pointed out by Kalb (1927) the systematics of his crystal types concerns the basic crystal form (Kristallgrundgestalt) and not the crystal habit (Kristalltracht); the first is conceived as the mean of all possible habits of crystals of a given substance. Thus anatase is considered a basal-tetraharmonic, whereas its dimorph rutile is prismatic-tetraharmonic, with axial ratios  $a=b < c$  and  $a=b > c$ . The two minerals are similarly grouped by Niggli, the classifications of both authors obviously putting stress on the equilibrium and not on the growth forms.

The habit of the crystals of some minerals is fairly constant (e.g. those of spinel, siderite, etc.) but as a rule it varies considerably, as exemplified by calcite, tourmaline, apatite, anatase, and many others. For example, Niggli's classification of tourmaline with the columnar hexagonal types seems correct for its equilibrium form but not for its growth form. Therefore the manner of subdivision presented by both Niggli and Kalb, although structurally logical, seems rather incompatible with the morphogenetic systematics of crystal habits, which should also take their variability into account.

In an attempt to derive statistically the main habit types of the crystals of many minerals, certain generalizations were put forward by the present author. These concerned the nomenclature of types of habit taking into account the geometry of the crystal structure and its relationship to variation of crystal habit (Kostov, 1962, 1965). What follows is a further development of these ideas, evolving the notation of crystal habit, particularly for crystals of low symmetry. This is more suitable for the treatment of crystal habit, particularly its modification under different conditions.

*Structure and habit of crystals.* The direct relationship between structure and habit has been demonstrated by Donnay and Harker (1937), Niggli (1941), Kossel (1927), Stranski and Kaischew (1935), Kleber (1939, 1955), Hartman and Perdok (1955, 1956), Hartman (1953, 1963), Evzikova (1958), Kern (1953a, 1953b, 1955), and other authors, on the basis of the classic Law of Bravais, which relates interplanar spacing and reticular density. As stressed by Bragg (1937), there is a distinct reciprocity between shape of unit cell and basic crystal form, in the sense of Kalb. For instance, millerite, crystallizing in the space group  $R\bar{3}m$ , has an axial ratio  $c/a$  0.328 and its crystals are invariably long prismatic to acicular along the  $c$ -axis. Conversely, molybdenite, space group  $P6_3/mmc$ , has a ratio  $c/a$  3.899 and is normally micaceous in habit. If other examples are considered, it will be seen that crystal habit tends to become more isometric when the axial ratio approaches or is equal to unity. The latter case applies generally to crystals of the cubic system, the habits of which depend primarily on the type of Bravais lattice (primitive, body-centred, or face-centred).

The reciprocity between shape of unit cell and basic crystal form can be used successfully for differentiating the main habit types for crystals of all systems except the cubic, where details of the structure have to be considered. The axial ratio can be used as a measure of anisometricity of the structure, from which two fundamental types of structure can be derived, an *axial* or A-type, and a *planar* or P-type. The axial type is determined by a ratio  $c/a < 1$  the planar type by a ratio  $c/a > 1$ . Crystals with an axial ratio  $c/a \sim 1$  are *pseudo-isometric*, denoted as (I)-type, to distinguish them from true *isometric* or I-type crystals of the cubic system. Examples of pseudoisometric crystals are chabazite, space group  $R\bar{3}m$ , which has an axial ratio  $c/a$  1.086, mitscherlichite,  $K_2CuCl_4 \cdot 2H_2O$ , space group  $P4_2/mmm$  and axial ratio  $c/a$  1.059, zircon, space group  $I4_1/amd$  and  $c/a$  0.901, chloraluminite, space group  $R\bar{3}c$  and  $c/a$  1.00, and quartz, space group  $P3_121$  or  $P3_221$  and  $c/a$  1.10. Typical in this respect, pseudoisometric and pseudooctahedral in habit is stottite ( $FeGe(OH)_6$ ), space group  $P4_2/n$  and  $c/a$  0.989.

Crystals of lower symmetry can be referred to analogous types (orthorhombic, monoclinic, and triclinic). For instance stibnite, space group  $Pbnm$ , has  $a$  11.22,  $b$  11.30, and  $c$  3.84 Å, possesses a pseudotetragonal symmetry as regards the  $c$ -axis, and has a pseudotetragonal axial ratio  $2c/(a+b)$  0.34. The mineral is therefore distinctly of an axial A-type, which agrees with its invariably long-

prismatic to acicular habit. Because the structural anisotropy is due to elongation along the  $c$ -axis, the corresponding superscript  $A^c$  is used to distinguish this case from crystals with the higher rotational symmetry. Epidote, space group  $P2_1/m$ , with  $a$  8.98,  $b$  5.64,  $c$  10.22 Å, and  $\beta$   $115^\circ 24'$ , is an example of an axial pseudo-hexagonal type, since  $2b/(a+c)=0.58$ ; the mineral is usually elongated along  $[010]$  and is thus of the  $A^b$ -type. Metavariscite, space group  $P2_1/m$  with  $a$  5.16,  $b$  9.47,  $c$  8.47 Å,  $\beta \sim 90^\circ$  is a further example of an axial  $A^a$ -type with  $2a/(b+c)$  0.57 and crystals that are prismatic along  $[100]$ .

Similarly, analogous planar types can be derived. Muscovite and the micas in general possess a typically layered structure and are of the  $P^c$ -type, the first having a unit cell with  $a$  5.19,  $b$  9.04,  $c$  20.08 Å, and  $\beta$   $95^\circ 30'$ , hence anisotropy  $2c/(a+b)$  2.82. Gypsum can be taken as an example of the  $P^b$ -type, with space group  $A2/a$ ,  $a$  5.68,  $b$  15.18,  $c$  6.29 Å,  $\beta$   $113^\circ 50'$ , with  $2b/(a+c)=2.65$ ; the layered structure gives rise to its tabular habit  $\{010\}$  and perfect cleavage parallel to that plane. Finally, clinoclase, space group  $P2_1/a$ ,  $a$  12.38,  $b$  6.46,  $c$  7.24 Å,  $\beta$   $99^\circ 30'$  is a good example of a planar  $P^a$ -type, with crystals often elongated parallel to  $[001]$  but having prominent  $\{100\}$  face.

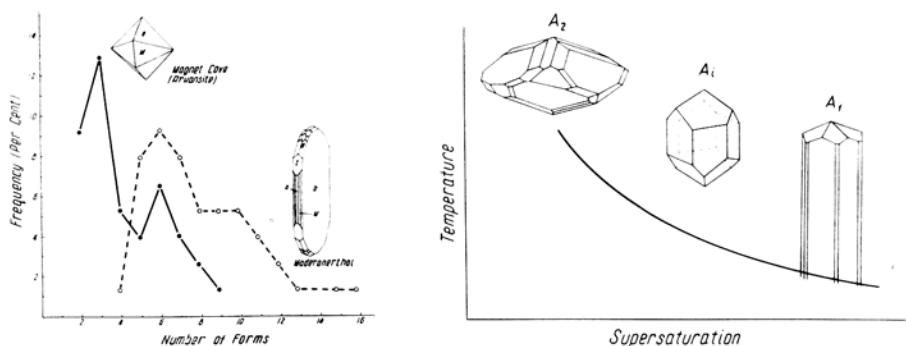
The examples cited are typical and many others could be added to them. There are, however, structures with unit cells, the  $a$ ,  $b$ , and  $c$  dimensions of which are either similar or vary with an almost equal step. The first case represents a pseudo-isometric (I)-type *sensu stricto*, as exemplified by monazite, space group  $P2_1/n$ ,  $a$  6.78,  $b$  6.99,  $c$  6.445 Å,  $\beta$   $76^\circ 22'$ , the crystals of which are often equant. The slight anisotropy,  $2c/(a+b)$  0.93, points to a tendency towards axial development. Barite is an example with the  $a$ ,  $b$ , and  $c$  parameters varying in a step-wise manner: 8.87, 5.45, and 7.14 Å respectively. The ratios  $2a/(b+c)$ ,  $2b/(a+c)$ , and  $2c/(a+b)$  are correspondingly 1.41, 0.68, and 0.99, so that as regards the first axis the structure is planar, as regards the second—axial, as regards the third—isometric. The usual habit of barite is tabular  $\{001\}$  and elongated  $[010]$ , a slight predominance of the axial pattern. Such instances are more complicated as far as habit variation is concerned, but they can rightly be treated as pseudo-isometric (I)-type *sensu lato*.

*Variation of crystal habit.* The habits of minerals are of greater importance in mineralogy than their forms, because they are indicative of more drastic changes in the conditions of crystallization than are the forms which trace only what can be called the polishing touch of the process.

From experimental work it is known that quick crystallization or higher supersaturation favours the development of simpler crystals, whereas slow crystallization or low supersaturation tends to the formation of more modified crystals. The first possess as a rule a habit compatible with their structure, i.e. reciprocal to it, the second display a tendency to concur in form with the general geometry of the structure. This can be used for a rough and ready differentiation of main habit types with definite genetic significance, as depicted in fig. 1 for crystals of brookite, which has space group  $Pcab$ , with  $a$  5.45,  $b$  9.18,  $c$  5.15 Å,

the ratio  $2b/(a+c)$  being 1.79. It belongs, therefore, to the planar  $P^b$ -type, and this is in good agreement with the frequent tabular habit on  $\{010\}$  shown by its crystals, which are usually rich in forms. Also well known, however, are the arkansite type of crystals, devoid of or with narrow  $\{010\}$  faces; these are less modified, as shown by statistical analysis on brookite crystals from different occurrences. The two tendencies of development, perpendicular to and along the axis of modification, which in this case is  $b$ , can conveniently be denoted as  $P_2^b$  and  $P_1^b$ , the subscripts here represent a tendency to development in two dimensions and in one dimension respectively.

Often crystals are of intermediate or pseudo-isometric habits; especially those of the tetragonal and hexagonal systems, such habits are denoted with the subscript 'i'. Whether we deal with crystals of higher symmetry (excluding cubic) or lower symmetry, the major variations of habit for the basic A, P, and (I)-type can be designated:  $A_1 \rightleftharpoons A_i \rightleftharpoons A_2$ ,  $P_2 \rightleftharpoons P_i \rightleftharpoons P_1$ , and  $(I)_1 \rightleftharpoons (I)_i \rightleftharpoons (I)_2$ .



FIGS. 1 and 2: FIG. 1 (left). Evolution of the main habit types of brookite by using forms cited in Goldschmidt's Atlas (1913-23). FIG. 2 (right). Main habit types of phenakite as dependent on temperature and supersaturation.

The tendency of variation can run either way depending on whether we start from higher or lower supersaturations. Crystals of tourmaline, which are of a typical axial A-type ( $c/a$  0.45) can be either acicular  $A_i$  or strongly flattened (platy) perpendicular to the  $c$ -axis, i.e.  $A_2$ -type. In pegmatitic veins tourmaline crystals of a pseudo-isometric or short-prismatic  $A_i$ -type are sometime overgrown by later acicular crystals. The latter apparently formed at lower temperature and higher supersaturation, the former at higher temperature and lower supersaturation. Crystals of phenakite behave similarly (fig. 2). The sequence here is therefore  $A_2 \rightarrow A_i \rightarrow A_1$ . At the end of crystallization of the  $A_1$ -type the supersaturation can naturally be lowered, so the final forms can appear more highly modified than even the  $A_2$ -type, which is normally richer in forms than the  $A_1$ -type.

Crystals of lower symmetry display further variations in habit. In addition to variation along the axis of major modification, variations are also discernable

along other crystallographic directions. A structural  $A^c$ -type for instance can be  $A_1^c$ ,  $A_2^c$  if the habit varies along the  $c$ -axis only; but if variation goes in other directions, for instance along the  $b$ -axis, then we have  $A_{1b}^c$  and  $A_{2b}^c$  types, or along the  $a$ -axis  $A_{1a}^c$  and  $A_{2a}^c$  types. Minor variations can be detailed when "two-dimensional" habits vary along one or other of the two directions. This is indicated by enclosing the additional subscript in brackets, e.g.  $A_{2(a)}^c$  and  $A_{2(b)}^c$ , for crystals of the structural  $A^c$ -type, which are flattened perpendicular to the  $c$ -axis, but elongated in the first case along the  $a$ -direction, and in the second along the  $b$ -direction. Similarly we have  $A_{2b(a)}^c$  and  $A_{2b(c)}^c$  for crystals flattened perpendicular to the  $b$ -axis, and  $A_{2a(b)}^c$  and  $A_{2a(c)}^c$  for crystals flattened along the  $a$ -axis. All possible variations of the habits of low symmetry crystals are schematically depicted in fig. 3 for crystals with a predominant prismatic development. To denote pinacoidal or pyramidal development a bar or circumflex respectively is used.

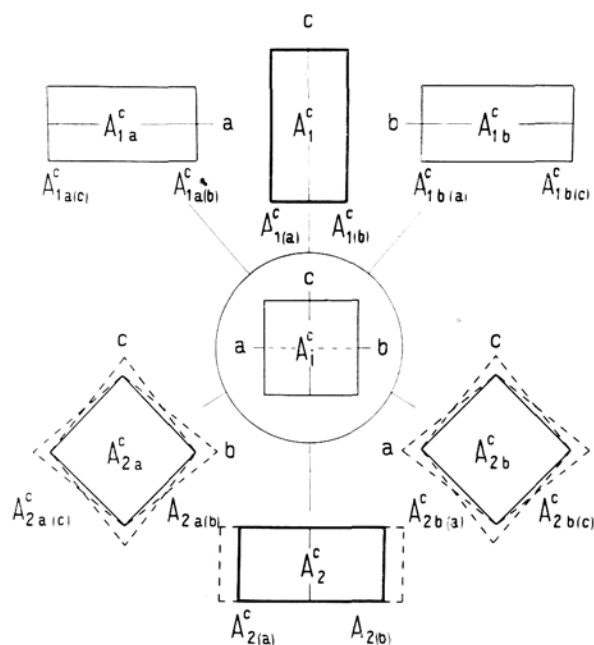
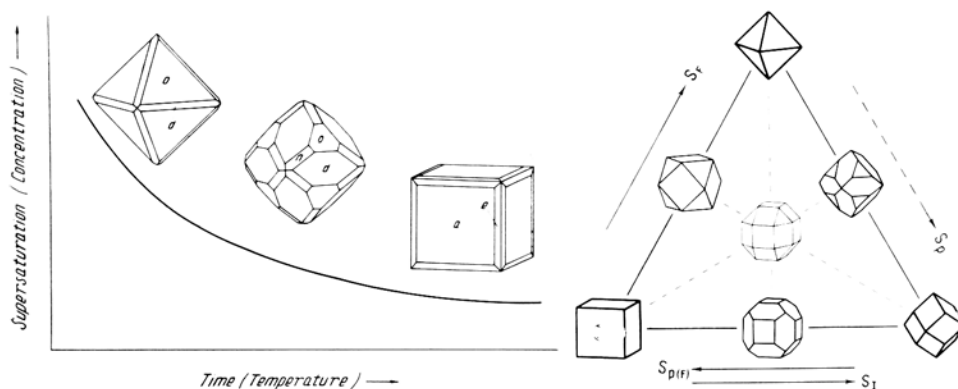


FIG. 3. Schematic representation of prismatic habit types of low symmetry crystals. For pinacoidal habits, a bar is placed over the subscript figures, and for pyramidal habits, a circumflex.

Such a notation is not overburdened and logically unites basic structural features with variation of habit of minerals. The capital letter together with the superscript in the habit symbol has a structural significance, whereas the subscript underlines morphological modification.

Three main symbols are used for crystals of the cubic system,  $I_c$ ,  $I_d$ , and  $I_o$ , for habits in which the principal forms have indices  $\{100\}$ ,  $\{hko\}$ , or  $\{hkl\}$  respectively. The variation  $I_c \rightleftharpoons I_d \rightleftharpoons I_o$  depends first of all on the type of space lattice (primitive, body-centred, or face-centred) and then on conditions of crystallization. Magnetite, for instance, possesses an F-lattice, and is usually octahedral in habit, but can also be rhombododecahedral or cubic. The sequence of variation is  $I_o \rightarrow I_d \rightarrow I_c$ , possibly due to lowering of supersaturation, as inferred from observations on natural occurrences (fig. 4).



FIGS. 4 and 5: FIG. 4 (left). Habit variation of franklinite (and magnetite).

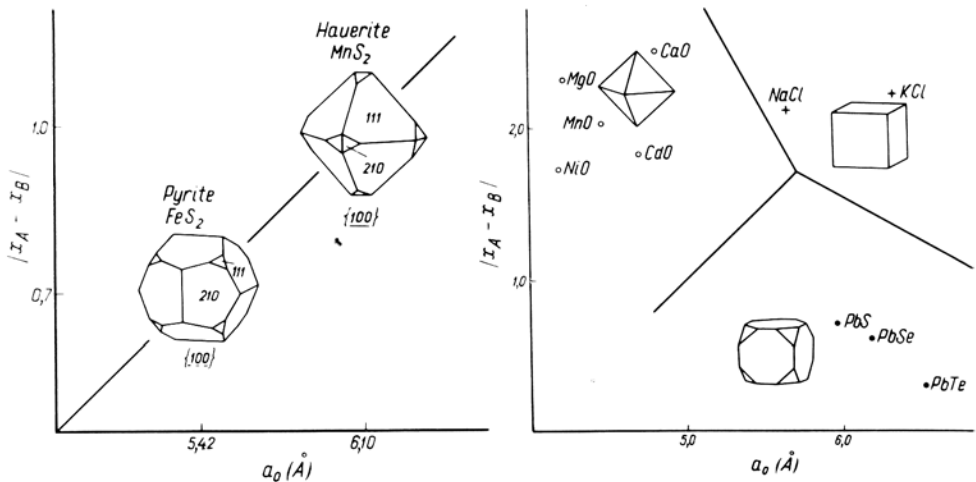
FIG. 5 (right). Principal habit modifications of cubic crystals.

Fig. 5 illustrates the sequence of appearance of the basic habit types in the cubic system, in accordance with the type of space lattice ( $P$ ,  $I$ ,  $F$ ) and increasing supersaturation. More highly modified crystals are obtained under intermediate supersaturations, as is demonstrated by experimental work and by statistical analysis. This should be taken into account when deductions of habit types and their conditions of formation are sought. Intermediate supersaturations also seem to favour the development of twin crystals. Other factors that play a definite role in certain cases, apart from supersaturation, are impurities, temperature, pressure, pH, etc. Impurities have proved to be a major habit modifying factor for a considerable number of minerals, therefore a good knowledge of the exact composition of the minerals is a condition sine qua non for a proper interpretation of their habit variation.

*Crystal habit and bond type.* The type of bonds between constituent atoms in the crystal structure plays an important part in the development of crystal habit in addition to the external factors. This becomes clear when crystals of the same crystallochemical type are considered. An example is provided by pyrite and hauerite, both possessing an  $AX_2$  pyrite type of structure with  $a$  5.42 and 6.10 Å respectively. The electronegativity differences  $|X_A - X_B|$  are 0.7 and 1.0, accentuating the more ionic character of hauerite, which accounts apparently

for its perfect cleavage along  $\{100\}$ , whereas pyrite is practically devoid of cleavage. Although occurring as octahedra, pyrite is found predominantly as cubes or pentagonal dodecahedra, the latter being obviously the 'structure-image' form. Hauerite is commonly octahedral in habit (fig. 6).

Crystals of the  $AX$  type possessing the true NaCl structure provide an additional example. The oxides (periclase, manganosite, bunsenite, monteponite, and lime) have a high electronegativity difference and small cell dimensions, the halides (halite and sylvine) also have a high electronegativity difference but larger cell dimensions, whereas the sulphide and similar compounds (galena, clausthalite, and altaite) have a low electronegativity difference and large cell dimensions. Their predominant habits are correspondingly octahedral, cubic, and cubo-octahedral (fig. 7).



FIGS. 6 and 7: FIG. 6 (left). Influence of electronegativity difference and cell dimension on the habit of crystals with the pyrite structure. FIG. 7 (right). Influence of electronegativity difference and cell dimension on the habit of crystals with the NaCl structure.

Influence of bond type on habit can also be traced in crystals of other than cubic symmetry, as in crystals of the  $AX_2$  type having a rutile type of structure (sellaite, rutile, cassiterite, plattnerite, and paratellurite). The first of these has an electronegativity difference of 2.8, the last of 1.4. The cleavage of this series varies as follows: sellaite perfect  $\{010\}$  and  $\{110\}$ , rutile distinct  $\{110\}$  only, cassiterite indistinct  $\{010\}$  and  $\{110\}$ , and paratellurite and plattnerite none. Crystals of paratellurite, which have a structure of distorted rutile type, are as a rule equant or short-prismatic, whereas those of rutile are often long-prismatic to acicular along the  $c$ -axis.

From these examples, which are not the only ones, it appears that the degree of ionic and covalent character of the bonds should be taken into account when strong bonds in the structure of minerals are used to explain predominant

forms and habit types. The effect of bonds, which are an internal factor, should be considered together with the principal external factors. The most important of these for genetic mineralogy seem to be concentration of constituents and supersaturation, temperature, and impurities. The inclusion of impurities by isomorphous substitution, on the other hand, depends to a great extent on the first mentioned factors, which can be successfully applied for tackling morphogenetic problems.

*Significance of genetic habit types.* If we consider the genesis of the principal habit types in the way mentioned, it is but logical to assume that rough and ready conclusions can be drawn about the conditions of crystallization of minerals on the basis of their habit variations. The following examples show the validity of applying the study of crystal habits of minerals derived statistically and by using their structural anisometricity to the elucidation of their genesis.

The first example concerns certain observations made by Varlamoff (1949) on the crystal habit of cassiterite from the Kalima tin deposit in the Congo. Bipyramidal crystals ( $A_2$ -type) are found in the deeper levels within a granitic intrusion, short-prismatic crystals ( $A_1$ -type), as a rule more modified and often twinned, at intermediate levels, whereas at higher levels and away from the intrusion the crystals tend to be prismatic ( $A_1$ -type). The trend of crystallization can be interpreted in terms of falling temperature and rising supersaturations. Finally, impurities (Fe, Nb, Ta) can also play a role in shortening the habit of the higher temperature types (fig. 8).

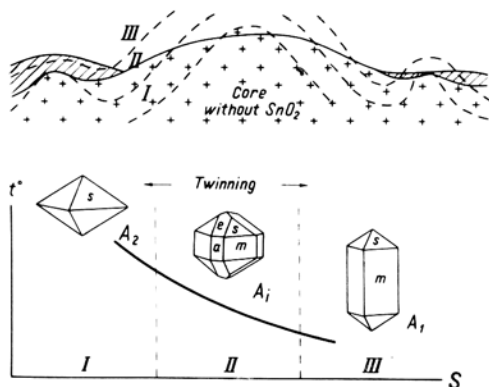


FIG. 8. Variation of habit in cassiterite from the Kalima tin deposit, Congo.

The second example is quoted from Babkin (1962), but in the light of what was already said. Cinnabar crystals from a deposit in the north-eastern part of the U.S.S.R. occur with a prismatic habit in the deeper levels with a rhombohedral habit at intermediate depths, and as tabular crystals near the surface. The ratio  $c/a$  of cinnabar is 2.29, the mineral is therefore of the planar P-type, although the screw axes in its structure may play a role for corresponding

change in anisometricity. The variation of its habit is  $P_1 \rightarrow P_i \rightarrow P_2$ . As the tabular habit is found at the intersections of mineral veins, it is presumed that it is formed by quick crystallization under higher supersaturations.

Quartz has the same space group as cinnabar ( $P_{3_121}$ , or  $P_{3_221}$ ), but is pseudo-isometric with  $c/a$  1.10. The electronegativity difference of quartz  $|X_A - X_B|$  is 1.7, against 0.6 for cinnabar, and its habit varies from bipyramidal and short-prismatic to long-prismatic and acicular. The tendency of variation is thus  $(I)_2 \rightarrow (I)_i \rightarrow (I)_1$ . Prismatic quartz of the common varieties is often capped by water-clear or amethystine quartz, which is usually short-prismatic or equant. Judging by quartz habits in pegmatitic veins and hydrothermal deposits, it seems logical to assume that the latter formed under higher supersaturations so that the normal sequence of the habit development should be as given above. Diminished supersaturation at some final stages of crystallization might cause a reverse trend towards shortening of the habit along the  $c$ -axis.

In conclusion it is suggested that the proposed manner of deriving and denoting the genetic habit types of minerals seems to supply a better foundation for unified interpretation of their variability. The method can also indicate approximately the conditions under which crystals were formed.

#### References

- [BAVKIN (P. V.)] Бабкин (П. В.), 1962. Зап. всесоюз. мин. общ. (*Mem. All-Union Min. Soc.*) **91**, 337.
- BRAGG (W. L.), 1937. *Atomic structure of minerals*. London.
- DONNAY (J. D. H.) and HARKER (D.), 1937. *Amer. Min.*, **22**, 446 [M.A. 7-241].
- [EVZIKOVA (N. Z.)] Евзикова (Н. З.), 1958. Зап. всесоюз. мин. общ. (*Mem. All-Union Min. Soc.*), **87**, 647 [M.A. 14-251].
- FEDOROV (E. S.) [Федоров (Е. С.)], 1903. *Zeits. Kryst. Min.*, **38**, 321.
- GOLDSCHMIDT (V.), 1913-1923. *Atlas der Kristallformen*, Bd. 1 to 9. Heidelberg.
- HARTMAN (P.), 1953. *Relations between structure and morphology of crystals*. Dissertation, Groningen. [M.A. 12-314].
- and PERDOK (W. G.), 1955. *Acta Cryst.*, **8**, 49, 521, and 525 [M.A. 13-279].
- , 1956. *Amer. Min.*, **41**, 449 [M.A. 13-280].
- , 1963. *Zeits. Krist.*, **119**, 65 [M.A. 17-24].
- HONIGMANN (B.), 1958. *Gleichgewichts- und Wachstumsformen von Kristallen*. Darmstadt.
- KALB (G.), 1927. *Centr. Min., Abt. A*, 158.
- , 1928. *Ibid.*, 337.
- and KOCH (L.), 1929. *Ibid.*, 267.
- , 1931. *Zeits. Krist.*, **78**, 169.
- KERN (R.), 1953a. *Bull. Soc. franç. Min. Crist.*, **76**, 325.
- , 1953b. *Ibid.*, 391.
- , 1955. *Ibid.*, **78**, 461 and 497.
- KLEBER (W.), 1939. *Neues Jahrb. Min., Abt. A, Abh.*, **75**, 72.
- , 1955. *Naturwiss.*, **42**, 170.
- KOSSEL (W.), 1927. *Nachr. Ges. Wiss. Göttingen, Math.-phys. Kl.*, 135.
- [KOSTOV (I.)] Костов (И.), 1962. Мин. сборн. Львов. геол. общ. (*Min. Mag. Lvov Geol. Soc.*), **16**, 75.
- , 1965. Изв. геол. инст. Българ. акад. наук (*Bull. Inst. Geol., Bulgar. Acad. Sci.*), **14**, 48.

NIGGLI (P.), 1926a. *Zeits. Krist.*, **63**, 49 and 295.

—, 1926b. *Lehrbuch Min.*, **2**, Berlin.

—, 1941. *Lehrbuch Min. Kristallchem.*, Berlin.

STRANSKI (I. N.) and KAISCHEW (R.), 1935. *Ann. Physik.*, **23**, 330.

VARLAMOFF (N.), 1949. *Ann. (Bull.) Soc. Géol. Belg.*, **72**, B289 [M.A. 11-48].

## Crystal growth of galena

By Dr. J. BANFIELD<sup>1</sup> and Dr. A. F. SEAGER

Department of Geology, Birkbeck College, London, W.C.1.

*Summary.* The lineage structure of galena was studied by optical and X-ray methods. Elements of the structure are rotated about [100] and [110] axes, which themselves have a small angular dispersion. Growth spirals were observed on a specimen from Trepča, Yugoslavia. Galena near a fault plane in the Sherburn Hill colliery, Co. Durham, had suffered mechanical deformation, which produced lamellar twinning and a parting on {441}. Other twin laws are discussed. Translation lamellae and etching were also observed.

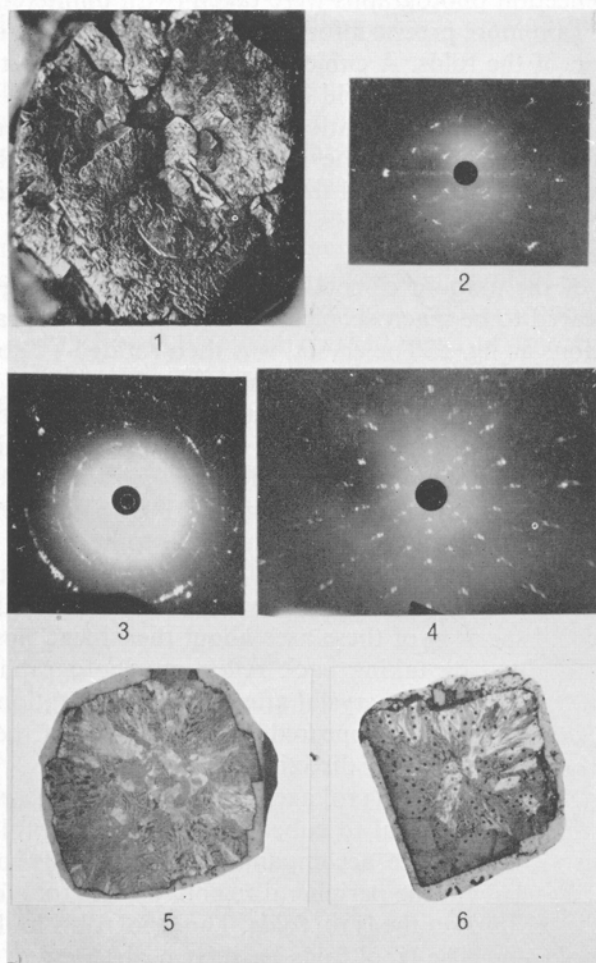
THE primary object of the work to be described was to make a further study of the lineage structure of galena, which has been previously investigated by M. J. Buerger.<sup>2</sup> In the course of the work observations were also made on the growth, deformation, twinning, and etching of galena.

Fig. 1 shows a cubo-octahedron of galena from Alston, Cumberland, England, in which misalignment of both large and small elements of the structure is immediately apparent. Qualitative and quantitative observations of the nature of such structures have been made by serial grinding of the crystal in fig. 1, by studying the external growth surfaces and cleavage surfaces of crystals in reflected light, and by X-ray back reflections from cleavages. An extensive study was made of specimens in the British Museum (Mineral Department) and two very fine specimens were lent by the University of Durham. Some specimens were collected *in situ* by one of the authors (J. B.).

A visual examination of the cleavage surfaces of galena shows that very few specimens have plane surfaces, and those exceeding an area of half a square inch are exceptional. The commonest type of deformation appears like a series of small folds, with their length (fold axes) in [110] directions. The word "fold" will be used as a convenient descriptive term, without any genetic significance. Folds may extend from the nucleus of the crystal to its surface, or they may be present only in the peripheral part of the crystal. Observation of the folds by incident light shows that the axes are not all strictly in [110] directions, but have a dispersion of up to 10° about these directions. Some of the folds are seen to be discontinuous and others have curved axes. In the British Museum specimen 173 (BM 1968, 62, which probably comes from Alston, Cumberland), the average width of the folds is  $\frac{1}{4}$  mm, but they may exceed 1 mm, and their length seems to vary from  $\frac{1}{2}$  mm to about 20 mm, although microscopic examination showed

<sup>1</sup> This paper forms part of a thesis approved for the degree of Ph.D. by the University of London.

<sup>2</sup> Buerger (M. J.), *Amer. Min.*, 1932, 17, 177.



FIGS. 1 to 6: FIG. 1. Cubo-octahedral crystal of galena from Alston, Cumberland.  $\times 2$ . FIG. 2. X-ray back reflection photograph of cubic cleavage surface of galena, with  $[110]$  fold axes set vertical. Dispersion of the fold axes and rotation about them approximately  $2^\circ$ . FIG. 3. Similar to fig. 2, but showing a more strongly folded region. Optical examination suggests dispersion of the  $[110]$  fold axes up to  $10^\circ$ . The  $[110]$  axes lie NE.-SW. FIG. 4. X-ray back reflection photograph of cubic cleavage of galena, with  $[100]$  folds set vertical. Elements of the structure are rotated some  $2^\circ$ - $3^\circ$  about these axes. FIG. 5. Ground surface of the cube of galena shown in fig. 1. This surface is approximately half way between the original crystal face and the centre of the crystal.  $\times 1.5$ . FIG. 6. Similar to fig. 5, but this plane passes almost through the centre of the crystal. The development of folds with  $[100]$  and  $[110]$  axes is clearly seen in the upper and right hand parts of the figure.  $\times 1.2$ .

that in the longer folds a distinct change of orientation usually takes place within 2 mm.

X-ray back reflection photographs were taken (with unfiltered Cu radiation) in an attempt to gain more precise information about the nature of the deformation in the region of the folds. A cubic cleavage surface was set normal to the X-ray beam and one of the [110] fold axes placed vertical. The photograph of fig. 2 was taken with the crystal stationary, but there is some resemblance to a rotation photograph, owing to the rotation of elements of the structure in the region of the fold. In this crystal there appears to be a rotation of up to  $2^\circ$  about the [110] fold axis, and the axis itself has a dispersion of about  $2^\circ$  from its mean direction.

The estimate of the amount of rotation was made by taking a fragment of galena that appeared to be macroscopically perfect and photographing it under the same conditions as fig. 2. The crystal was then rotated  $1^\circ$  about its vertical [110] axis and a second exposure made on the same plate; finally the crystal was rotated a further  $1^\circ$  and a third exposure made on the plate. A stationary X-ray back reflection photograph was then taken of a crystal that appeared to have more intense curvature about the [110] fold axes (Birkbeck College, SD 15); this is shown in fig. 3 with the fold axes running NE.-SW. There is obviously a greater degree of misorientation, which is difficult to interpret. Optical examination suggests that the [110] axes may suffer a dispersion of up to  $10^\circ$ . For less distorted parts of specimen SD 15 it was proved that rotation about the [110] axes, and the dispersion of these axes about their mean position, was less than  $5^\circ$ . This was done by taking back reflection photographs of a macroscopically "good" portion of the crystal after successive rotations of  $1^\circ$ . It was found that the  $K\alpha$  reflections disappeared from each side of the photographic film within  $5^\circ$  of rotation in either direction.

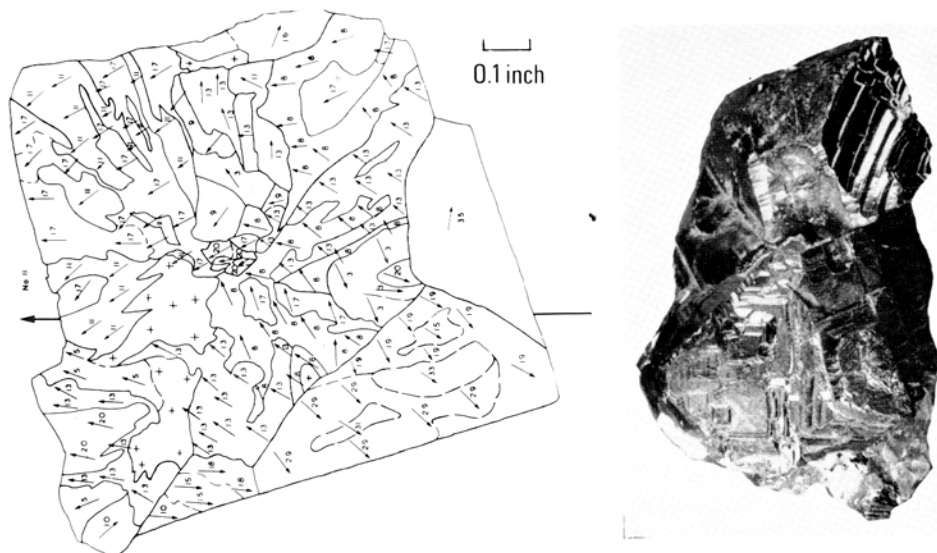
In addition to the folds about [110] axes there are often present very similar folds that have their axes normal to cube faces. These [100] folds may extend from the nucleus to the surface accompanied by [110] folds, or both sets of folds may be present only in the peripheral region, or the [100] folds may begin further from the nucleus than the [110] folds. The [100] folds look like branches at  $45^\circ$  to the [110] folds. The [110] folds have been observed to exist alone, or with the [100] folds, but the latter have not so far been observed without the [110] folds. Fig. 4 shows an X-ray back reflection photograph of a region with [100] fold axes set vertical and a cubic cleavage plane normal to the X-ray beam, for the specimen BM 173. There is a rotation of elements of the structure about the [100] axes, amounting to some 2 to  $3^\circ$ .

The distortion produced by angular dispersion of the [110] and [100] axes, and by rotation about them, can be detected by looking at the surface features of crystals of galena. Those from Alston are particularly rugged and show a fairly extreme degree of misorientation. In marked contrast were some crystals from the Stari Trg mine, Trepča, Yugoslavia (which were kindly lent by the University of Durham); these had exceptionally plane faces for galena. One

specimen had translation lamellae, which indicated the directions of traces of cube planes and made it possible to detect small rotations in the plane of the face, the measured values ranging from  $2^\circ$  to  $5^\circ$ . The latter produced a grain with marked discontinuities at its boundary. These crystals are described and figured later.

The orientation of the two sets of folds axes agrees with the known translation properties of galena. All the fold axes  $f$  lie in translation planes  $T \{100\}$  and are normal to one or other of the translation directions  $t [100]$  or  $[110]$ <sup>1</sup>. Thus a fold axis  $[100]$  might be formed by translation on  $(001)$  in the direction  $[010]$ .

An attempt was made to obtain detailed information about the lineage structure by grinding serial sections. These were usually made at intervals of 1 mm, but when changes in the structure were taking place at short intervals, only 0.1 or 0.2 mm was removed by grinding. A crystal from Alston, Cumberland, England, was chosen that had marked signs of misorientation on the surface (fig. 1). The ground surfaces were photographed; fig. 5 shows a section practically half-way from the surface to the centre and fig. 6 is a section almost passing through the centre of the crystal. The linear elements clearly show the presence of  $[100]$  folds directed towards adjacent cube faces, and of  $[110]$  folds at approximately  $45^\circ$  to the other folds. A map showing the domain of each



FIGS. 7 and 8: FIG. 7. Map of the ground section of fig. 6, showing the position of constituent grains. The arrows give the direction of dip of the cubic cleavage and the amount is indicated in degrees. Note the very large angular discordance between some of the grains, particularly in the left hand half of the crystal. FIG. 8. Crystals of galena from Trepča, Yugoslavia (University of Durham No. 11471). These crystals have exceptionally plane cube faces, which are steeply terraced.  $\times 1.3$ .

<sup>1</sup> Buerger (M. J.) *Amer. Min.*, 1930, **15**, 45.

grain was prepared, to which was added the direction and amount of dip for every grain of appreciable size, determined with a two-axis stage. Some of the grains had sharp boundaries, with a marked angular discordance between the grain and its neighbours, but in other cases deformation often made it difficult to decide what constituted a grain. Fig. 7 is a map of the section shown in fig. 6. Arrows indicate the direction of dip of the cleavage and the inclination is given in degrees, with + signs on horizontal cleavages. Black dots in fig. 6 mark the points at which measurements were taken. Fig. 7 shows some very large angles between adjacent grains, in one case amounting to  $42^\circ$ , much larger than the  $8^\circ$  maximum quoted by D. P. Grigor'ev<sup>1</sup> for galena from the Berezovsk gold deposit in the Urals.

The serial sections were used in an attempt to trace lineage structures through the crystal. The textural features of the ground sections were so complex that this could not be done in detail, but some of the larger grains could be traced.

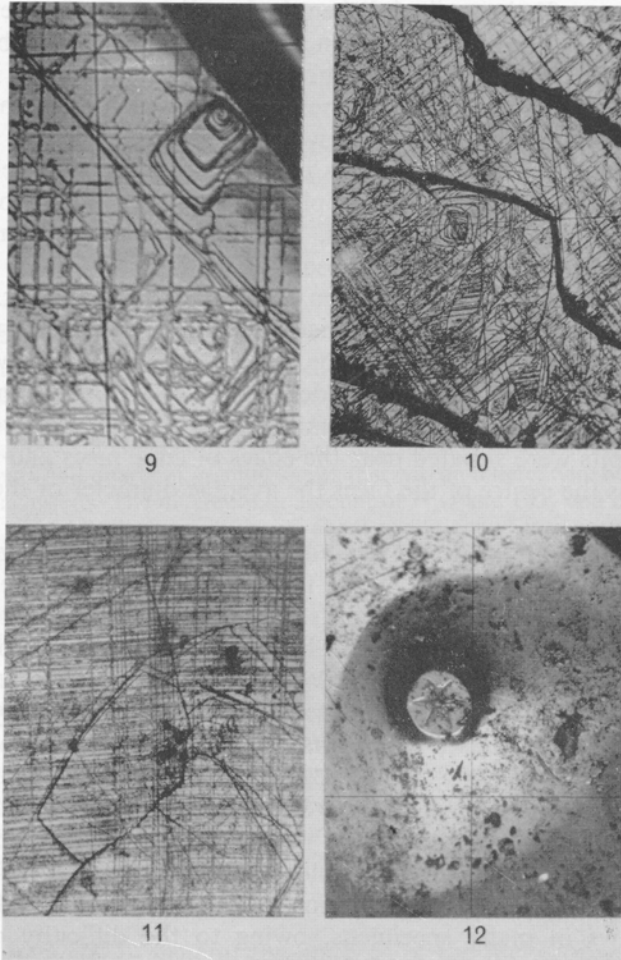
The folds and misorientated grains described above all seem to have arisen during growth. This conclusion is suggested by two kinds of evidence: Firstly, the growth surface of many crystals shows individual grains or elements that are differently oriented to their neighbours and may project above them. Secondly, it may sometimes be observed that the central region of a cleavage surface is free, or almost entirely free, from folds and visible misorientation, but that these features start more or less abruptly along lines parallel to the edges of the crystal (presumably traces of former faces) and continue from there to the surface of the crystal. This seems to suggest that the early growth of the crystal was free from these macroscopic defects, the onset of which began at a particular moment and continued until the end of growth. This in no way denies that folding, block structure, and similar defects are also caused by mechanical deformation after growth.

#### *Galena from Trepča, Yugoslavia*

Two specimens of galena from the Stari Trg mine, Trepča, Yugoslavia were lent by the University of Durham. They had exceptionally well preserved surfaces, which are rarely seen in a mineral as soft as galena. These specimens gave evidence of growth spirals, of translation lamellae, and of etching.

The general appearance of the crystals is seen in fig. 8. The cubes have very plane faces, which are interrupted by steep terraces up to 1.5 mm high. The best spirals are found at the foot of terraces where they have been protected from physical damage and the more severe effects of etching. The position of the spirals made it necessary to take photomicrographs with low-power objectives of long working distance and to magnify photographically, with consequent loss of definition. Away from the terraces similar growth pyramids are present, but it is not possible to prove the presence of spiral growths on them. The best spiral is shown in fig. 9. Precise measurement of the step heights of the spirals was not

<sup>1</sup> Grigor'ev (D. P.) [Д. П. Григорьев] *Ontogeny of minerals*, p. 125. English translation 1965.



FIGS. 9 to 12: FIG. 9. Cube face of galena from Trepča, showing a growth spiral, translation lamellae, and growth layers (at  $45^\circ$  to lamellae).  $\times 165$ . FIG. 10. Galena from Trepča. Growth pyramids on a cube face are centred on a grain boundary. Steep growth terraces and translation lamellae are also seen.  $\times 55$ . FIG. 11. Galena from Trepča. Cube face has translation lamellae, which show that two coplanar grains have a relative rotation of  $5^\circ$  about  $[100]$  axes.  $\times 55$ . FIG. 12. Octahedral face of galena from Trepča. The flat base of a large etch pit bears a six-rayed star.  $\times 60$ .

possible, but estimates made by measuring the height microscopically and counting the number of turns indicated heights of the order of  $1\,000\text{ \AA}$  to  $2\,500\text{ \AA}$ . Fig. 10 shows the general relationship of growth pyramids or spirals: these are often connected by curved discontinuities, which form notches on the thick terraced growth layers.

Fig. 10 also gives a good view of the translation lamellae. At high magnification it can be seen that they vary in width in an irregular manner, and have

every appearance of being etched. When the lamellae traverse unetched portions of the surface they become invisible in ordinary incident light, but can still be traced with phase contrast illumination. The translation lamellae in fig. 11 show the presence of two grains with coplanar surfaces, which are rotated  $5^\circ$  relative to each other about a  $[100]$  axis. Growth layers can be seen at approximately  $45^\circ$  to the lamellae. Elsewhere grains can be seen that have relative rotation about a  $[100]$  axis but do not have coplanar surfaces. Translation lamellae are also present on the octahedral faces, but the general prevalence of etching makes the lamellae less clear than those on cube faces.

Both of the specimens from Trepča showed natural etching. On the cube faces of DU 11469, the square pits had arcuate sides, the tangents to which are set at  $45^\circ$  to the edges of the cube, as observed by Ichikawa.<sup>1</sup> The larger pits had diameters of 0.2 mm and a depth of 0.01 mm, and the smaller pits were typically about 0.1 mm in diameter and approximately 0.005 mm in depth. These pits were situated near the edges of cube faces and had very steep sides. Towards the centre of the faces the average diameter of the pits was only 0.075 mm.

On the octahedral faces the (rounded) triangular growth layers have the same orientation as the edges of the face, which truncates the cube corners. On DU 11471 there are triangular pits, with straight or arcuate sides meeting in a point at the base of the pit, and having a width of 0.005 to 0.01 mm. The specimen DU 11469 has deeper and larger pits than DU 11471. The average diameter of the pits is 0.25 mm and their depths vary from 0.005 to 0.025 mm. These pits have a flat base, which may be minutely etched or may have a complex pattern such as the six-rayed star in fig. 12.

Since the translation lamellae have been subjected to natural etching, they could have been formed during growth as Buerger has suggested (1932).<sup>2</sup>

The misorientation that the component parts of a crystal can suffer and the continuous deformation of single grains make it particularly difficult to determine twin laws in many specimens, owing to the difficulty of goniometry. Some laws seem to be well established, such as growth twinning on  $\{111\}$  and  $\{441\}$ . A specimen was obtained by one of the authors, (J. B.) from a fault plane in the Five-quarter seam in the Sherburn Hill colliery (Co. Durham). This showed lamellar mechanical twinning on  $\{441\}$  and it had also developed a parting parallel to faces of this form, which appears to be a new feature for galena.

*Acknowledgements.* The authors gratefully acknowledge the loan of two specimens from the University of Durham, and permission to examine specimens in the Department of Mineralogy, British Museum (Natural History). They are greatly indebted to members of the Museum staff for assistance, especially Mr. J. Fuller and Mr. R. F. Symes.

<sup>1</sup> Ichikawa (S.) *Amer. Journ. Sci.*, 1916, ser. 4, 42, 111.

<sup>2</sup> Buerger (M. J.) *Amer. Min.*, 1932, 17, 177.

## Inclusions of gases in minerals

By H. ARMING und A. PREISINGER

Mineralogisches Institut, Univ. Wien  
Vienna, Austria

*Summary.* The method of decrepitation by heating crystals in ultra-high vacuum is used in combination with a mass-spectrometer for the qualitative and quantitative determination of minute inclusions of gases in minerals. The method is suited for the determination of amounts of gases up to  $0.1 \text{ mm}^3$  quantitatively in very small crystals. The determination of  $\text{H}_2\text{O}$  and  $\text{CO}_2$  in the feldspars and quartz of granites shows that we can differentiate between epigenetic and syngenetic inclusions. The difference in amount of  $\text{H}_2\text{O}$  and  $\text{CO}_2$  in a zoned plagioclase is discussed and some conclusions are drawn about conditions of formation.

SINCE the beginning of the 19th century scientists have investigated inclusions of gases and liquids in minerals, as they rightly supposed that these inclusions were formed at the time of crystallization of these minerals, and could therefore yield information about the composition of gases and liquids at the time of formation. In order to draw conclusions about the formation of crystals and their changes in the course of time, it appears necessary to differentiate between syngenetic and epigenetic inclusions. According to Yermakov (1965) syngenetic inclusions are considered to be those that are formed during crystallization while epigenetic inclusions are those formed after crystallization is complete.

*Experimental methods.* In general the analysis of the inclusions shows primary  $\text{H}_2\text{O}$  and  $\text{CO}_2$ , and in addition  $\text{H}_2$ ,  $\text{N}_2$ ,  $\text{H}_2\text{S}$ ,  $\text{HCl}$  etc. (an historical review is given by Wahler, 1956). The size of the inclusions vary greatly. Starting from the size of the order of a cm they reach into the submicroscopic region. Determinations have been made:

Mechanically, by drilling or puncturing into the inclusions under a sealing solution (Davy, 1822), or by crushing or grinding of the crystals in vacuo (Suess, 1952; Khitarov and Rengarten, 1956; Roedder, 1958; Goguel, 1963); chemically, by dissolving the crystals in vacuo (Ramsay, 1895; Chamberlin, 1908; Karlik, 1939), or by dissolving the crystals, the solvent serving as sealing solution (Tamman and Seidel, 1932); and thermally, by melting the crystals in vacuo (Shepard, 1938), by decrepitation of crystals by heating in vacuo (Ross and Smith, 1955; Wahler, 1956; Chaigneau and Debrune, 1961; Preisinger and Huber, 1963), or by decrepitation of crystals by freezing in vacuo (Taber, 1950).

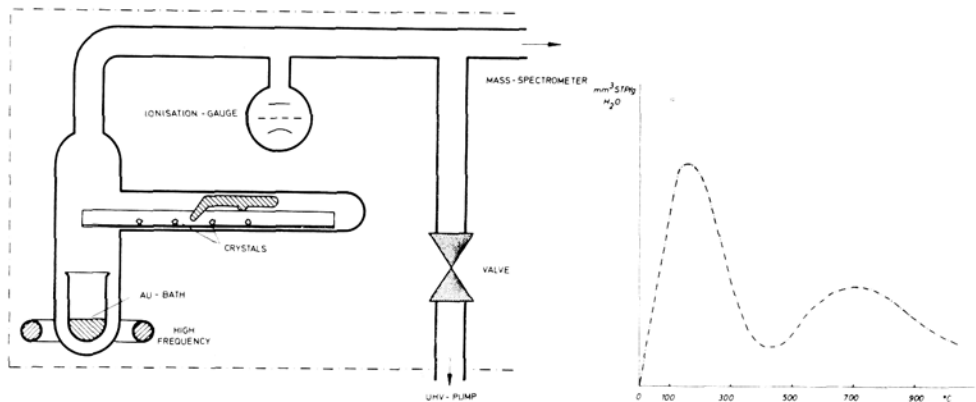
In carrying out qualitative and quantitative gas analyses the sizes of the inclusions and the chemical composition of the mineral will determine the method of decomposition and analysis.

We were interested in inclusions in silicate minerals, especially in the minerals of granites. Inclusions in these minerals lie within the micron range and below (Deicha, 1961; Goguel, 1963). We therefore decided to use the method of decrepitation by heating the crystals in ultra-high vacuum in combination with a mass-spectrometer for accurate gas analysis (Preisinger and Huber, 1963; Arming, 1966).

The principal of the method lies in the fact that at a sufficiently high temperature the gas pressure within inclusions in the crystal increases until the crystal bursts and the gases are set free. These can be directly measured by means of the mass-spectrometer.

The advantages of this method are that one can proceed without adding foreign material, that by ultra-high vacuum clean and defined environmental conditions are provided, and that by means of the mass-spectrometer even very small amounts of gas can be rapidly analysed.

The apparatus for decrepitation (fig. 1) consists of a pyrex tube connected on one side by a valve to a ultra-high vacuum (UHV) pump and on the other side to a mass-spectrometer. The UHV-pump used and the double-focusing Cycloid mass-spectrometer were products of Baltzers AG.



FIGS. 1 and 2: FIG. 1 (left). Apparatus for decrepitation.

FIG. 2 (right). Curve of dehydration of alkali feldspar.

The decrepitation furnace itself consists of a quartz crucible filled up to a third with gold, which is placed in UHV in the pyrex tube and is heated by means of a high-frequency generator (12 KW) up to 930°C. The crystals lie in the attached socket of the pyrex tube in UHV and can be thrown into the decrepitation furnace by means of a simple magnetic slot mechanism. The whole apparatus can be heated to 500°C.

The procedure was as follows: 10 to 15 samples of crystals of 0.15–0.30 mm diameter, selected microscopically, were wrapped in gold foil and put into the socket attached to the pyrex tube. A single sample amounted to 0.1–1.0 mg. In order to clean up the internal surface of the system and the surface of the samples the whole system was brought to a vacuum of  $10^{-7}$  mm. Hg. and heated for 12 hours up to 100, 200, or 300°C. After examining the residual gases by means of the mass-spectrometer individual samples could be thrown into the decrepitation furnace, which was heated up to 930°C, and the gases set free could be analysed in the mass-spectrometer.

By this method even 0.1 mm<sup>3</sup> of included gas can be investigated quantitatively and qualitatively.

The calibration was done with solids under the same conditions as described above; muscovite was used for calibrating H<sub>2</sub>O, and calcite crystals for calibrating CO<sub>2</sub> (Arming, 1966).

*Results and discussion.* Putting alkali feldspars from granites in the decrepitation furnace and heating them gradually in the UHV in a temperature range of 0° to 1 000°C, two H<sub>2</sub>O maxima result, one being at about 150°C and another at about 700°C (fig. 2).

For accurate quantitative analyses the samples had been heated before in the apparatus for decrepitation in UHV up to temperatures of 100, 200, 300, 400, or 500°C. Afterwards they were brought into the decrepitation furnace at 930°C. The dependence on temperature of H<sub>2</sub>O and CO<sub>2</sub> was determined by

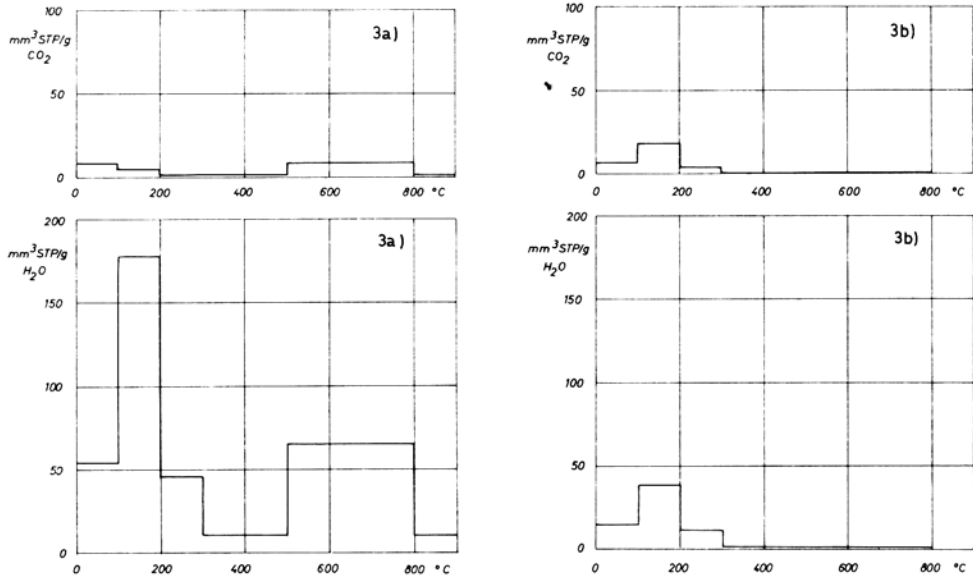


FIG. 3. Discharge of H<sub>2</sub>O and CO<sub>2</sub> (a) of an alkali feldspar from a granite, (b) of a quartz crystal.

the difference in the amounts obtained. Fig. 3 shows the H<sub>2</sub>O and CO<sub>2</sub> released by the alkali feldspar (3a) from a granite (Albtal, Schwarzwald, Germany) and by a quartz crystal (3b) (Ankogel, Salzburg, Austria). The alkali feldspar shows two maxima, the quartz crystal only one.

In the case of the quartz crystal, which was of hydrothermal origin, the inclusions of H<sub>2</sub>O and CO<sub>2</sub> are syngenetic. The temperature of the maxima of H<sub>2</sub>O and CO<sub>2</sub> corresponds to the temperature of formation.

In the case of the alkali feldspar there are two different kinds of inclusions. Considering the conditions of formation of granites (Makart and Preisinger, 1965) the inclusions of H<sub>2</sub>O and CO<sub>2</sub> of the second maximum (~700°C) are probably syngenetic, those of the first maximum (~150°C) surely epigenetic. It appears probable that the H<sub>2</sub>O of the first maximum originates from the phase boundaries of the finely lamellated unmixed albite in the microcline-perthite.

In order to be able to compare gas inclusions in feldspars of granites and to

TABLE I. The contents of H<sub>2</sub>O and CO<sub>2</sub> of feldspars (K<sub>f</sub>), quartzes (Qu), and plagioclase (Pl).

Rock	Mineral	H <sub>2</sub> O STP/g mm. <sup>3</sup>	CO <sub>2</sub> STP/g mm. <sup>3</sup>
Granite, Albtal, Schwarzwald, Germany	K <sub>f</sub>	235	44 (14)
Weinsberger granite, Kollmitzberg, Austria (Kurat, 1965)	½K <sub>f</sub> ½Qu	970 446	940 (314) 117
Weinsberger granite, Naarntal, Perg, Austria (Kurat, 1965)	½K <sub>f</sub> ½Qu	213 107	245 (47) 17
Mauthausner granite, Naarntal, Perg. Austria (Makart and Preisinger, 1965; Richter, 1965)	½K <sub>f</sub> ½Qu	2030 507	72 56
Mauthausner granite, Weitersfelden, Austria	½K <sub>f</sub> ½Qu	1770 257	65 27
Eisgarner granite, Groß-Eibenstein, Austria (Scharbert, 1966)	½K <sub>f</sub> ½Qu	3120 528	95 25
Seebacher granite, Wernberg, Villach, Austria	K <sub>f</sub>	2370	62
Granodiorite, St. Oswald, Freistadt, Austria	½K <sub>f</sub> ½Qu	712 173	19 17
Weinsberger granite, Pulgarn, Austria	Pl <sup>rim</sup>   <sub>core</sub>	146 115	17 57

draw conclusions on the conditions of formation, only those inclusions can be considered that are set free at temperatures above 300°C.

No relationship between amounts and composition of gases and the formation of feldspars has been detected from the gas analyses of feldspars of granites carried out up to the present.

Table I shows the H<sub>2</sub>O and CO<sub>2</sub> contents of feldspars and quartzes, which were pre-heated to 300°C in vacuo. In three alkali feldspars, (Albtal granite, Weinsberger granites) the origin of the CO<sub>2</sub> content, whether from gaseous inclusions or from finely intergrown carbonates, was investigated. For this purpose the samples were treated with *N/10* HClO<sub>4</sub> before heating. Thus the carbonate finely intergrown with the feldspar is destroyed. The CO<sub>2</sub> values determined by means of decrepitation then originate from the inclusions only. The values obtained are quoted in brackets with the respective samples.

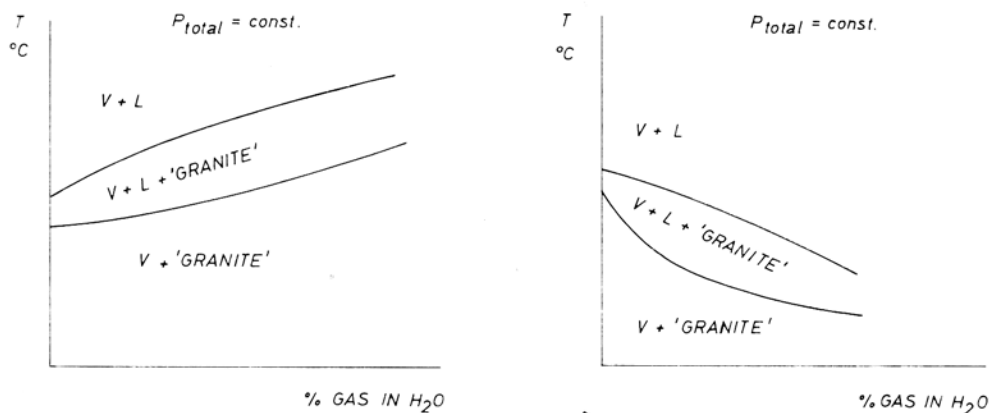


FIG. 4. Influence of a second gaseous phase besides water vapour on the melting temperature of "granite".

As shown by Wyllie and Tuttle, 1960, a second gaseous phase besides water vapour influences the melting temperature of "granite". Fig. 4 shows two extreme possibilities of influencing the melting temperature: addition of a second gaseous phase may increase or decrease the melting point. For example, the former applies for CO<sub>2</sub>, the latter for HF. If the total pressure during the formation of crystals remains constant the CO<sub>2</sub> content of the first crystallization must exceed that of the final crystallization. We investigated a zoned plagioclase from a Weinsberger granite (Pulgarn, Austria) with an An-content of the core of 34% and of the rim of 26% (Kurat, 1965). With a nearly constant total gas amount the core plagioclase, in accordance with the curves of Wyllie and Tuttle (fig. 4), showed a higher CO<sub>2</sub> content than the marginal plagioclase (Table I).

*Acknowledgements.* We wish to express our thanks to Dr. W. Kaltenecker for his valuable critical discussions and to Ing. W. Bochschanl for technical assistance. We would also like to thank Prof. Dr. F. Machatschki and the Österreichischen Forschungsrat for lending us apparatus.

## References

- ARMING (H.), 1966. *Diss. Univ. Wien*
- CHAIGNEAU (M.) and DEBRUNE (M.), 1961. *Compt. Rend. Acad. Sci. Paris*, **252**, 2 427 and 3 842.
- CHAMBERLIN (R. T.), 1908. *Carnegie Inst. Publ.* 106, Washington.
- DAVY (H.), 1822. *Ann. Chim. Phys.*, ser. 2, **21**, 132-144.
- DEICHA (G. A.), 1961. *Cursillos y Conferencias del Inst. "Lucas Mallada"*, fasc. 8, 31-32.
- GOGUEL (R.), 1963. *Geochimica Acta*, **27**, 155-181.
- KARLIK (B.), 1939. *Mikrochemie*, **27**, 216-230.
- [KHITAROV (N. I.) and RENGARTEN (E. V.)] Хитаров (Н. И.) и Ренгартен (Е. В.), 1956 *ГЕОХИМИЯ* 7, 74-84. (*Geochem.*, 1958, engl. transl.)
- KURAT (G.), 1965. *Tschermaks Min. Petr. Mitt.*, **9**, 202-227.
- MAKART (J.) and PREISINGER (A.), 1965. *Ibid.*, **9**, 315-344.
- PREISINGER (A.) and HUBER (W.), 1963. *Fortschr. Min.*, **41**, 183.
- RAMSAY (W.), 1895. *Proc. Roy. Soc.*, **58**, 65-89.
- RICHTER (W.), 1965. *Tschermaks Min. Petr. Mitt.*, **9**, 265-296.
- ROEDDER (E.), 1958. *Econ. Geol.*, **53**, 235-269.
- ROSS (C. S.) and SMITH (L. S.), 1955. *Amer. Min.*, **40**, 1071-1089.
- SCHARBERT (S.), 1966. *Diss. Univ. Wien*
- SHEPARD (E. S.), 1938. *Amer. Journ. Sci.*, ser. 5, **35A**, 311-351.
- SUESS (H. E.), 1952. *Geochimica Acta*, **2**, 76-79.
- TABER (S.), 1950. *Journ. Geol.*, **58**, 37-48.
- TAMMAN (G.) and SEIDEL (K.), 1932. *Zeits. anorg. Chem.*, **205**, 209-229.
- WAHLER (W.), 1956. *Geochimica Acta*, **9**, 105-135.
- WYLLIE (P. J.) and TUTTLE (O. F.), 1960. *Amer. Journ. Sci.*, **258**, 498-517.
- YERMAKOV (N. P.), 1965. *Research on the Nature of Mineral-forming Solutions*, Pergamon Press.

## An investigation of natural and synthetic quartz by the Hilger-Chance refractometer

By V. B. TATARSKY and V. F. CHERNYSHOVA

(В. Б. Татарский и В. Ф. Чернышова)

Department of Geology, The Leningrad State University, Leningrad, USSR

*Summary.* A Hilger-Chance precision refractometer equipped with a vertical slit diaphragm (0.1 mm in width) mounted immediately behind the refractometer prism was used, a rack-and-pinion furnished with scale and vernier was added to move the crystal under investigation. These devices permitted measurements to be made of the refractive indices of a single crystal in separate narrow zones at desired intervals. One crystal of natural quartz and the growth zones of 13 synthetic crystals were studied.

THE refractive indices of colourless natural quartz, at room temperature, according to the most reliable data available, lie in the range of  $\omega$  1.54411 to 1.54441;  $\epsilon$  1.55325 to 1.55363. These indicate that the fluctuations in the refractive indices of natural quartz do not exceed 3 to  $4 \times 10^{-4}$ . Sosman (1927), who made a comprehensive review of the optical properties of quartz, considers the most probable values for  $\omega$  and  $\epsilon$  of quartz at  $18^\circ$  to be 1.544246 and 1.553355 (unless specifically stated, optic constants quoted here refer to  $\text{Na}_D$  illumination, and to the same room temperature,  $18^\circ\text{C}$ ). Shubnikov (1940) gives similar values, as do A. N. Winchell and H. Winchell (1951), quoting the values to  $1 \times 10^{-5}$ . The birefringence of quartz, calculated as the difference  $\epsilon - \omega$  shows but little fluctuation, probably not exceeding the measurement errors. Most measurements give  $\epsilon - \omega = 0.00911$ . Direct measurements of birefringence (see Sosman, 1927, p. 642) showed it to be 0.009129 at  $0^\circ\text{C}$  and 0.009109 at  $18^\circ\text{C}$ ; the latter being in accord with the difference  $\epsilon - \omega$ . The temperature coefficient of refractivity for quartz,  $dn/dt$ , like that of most substances, is negative. Fizeau (1864, quoted by Le Chatelier, 1913), gives  $d\omega/dt = -5.37 \times 10^{-6}$ ,  $d\epsilon/dt = -6.28 \times 10^{-6}$ ; Gifford (1902) gives  $-5.19 \times 10^{-6}$  and  $-6.35 \times 10^{-6}$ ; Micheli (1902, quoted by Sosman, 1927) gives  $-5.39 \times 10^{-6}$  and  $-6.42 \times 10^{-6}$ . If refractive indices measured at various room temperatures are compared, one may take  $d\omega/dt = -5.3$  to  $5.4 \times 10^{-6}$ ,  $d\epsilon/dt = -6.3$  to  $6.4 \times 10^{-6}$ .

We have hardly any data on the variation in the refractive indices of quartz within a single crystal. Buisson (1906) used the interference method to measure the refractive indices of two cubic blocks cut from an optically homogeneous quartz crystal, the block edges being 5 cm and 4 cm long. The difference in

the values obtained on the opposite sides of the larger block was  $5 \times 10^{-6}$ , and that in the values between the two blocks  $1 \times 10^{-7}$ . The authors assume the error in their measurements not to exceed 2 to  $3 \times 10^{-7}$ .

The present investigations were carried out with a Hilger–Chance precision refractometer, designed for measuring the refractive index of optical glasses. Light in this refractometer passes through a complex glass prism (V-block), its parallel planes facing the collimator and the optic tube.

The sample to be investigated must have two mutually perpendicular polished faces (the quality of polishing is not important). It is placed inside the right angle formed by the middle part of the V-block, the faces of the sample being first moistened with a contact liquid of a similar refractive index. The signal in the form of a fine line is placed symmetrically in relation to the two shorter lines seen in the observation tube.

The readings were made accurately to  $0.01'$  of arc, which corresponds with a variation of about  $1.5 \times 10^{-6}$  in the refractive index. With quartz of high optic homogeneity and correspondingly distinct signals, a series of repeated determinations of the signal gave a scattering of readings in the range of  $0.05'–0.08'$ , the value of refractive index calculated as an average of 5 or 6 such readings being reproduced in repeated measurements with a precision of 2 to  $3 \times 10^{-6}$ .

The accuracy of the results obtained with good signals, and the correspondingly small scatter in the readings depends on the closeness of approach of the prism angle to  $90^\circ$  and of the refractive index of the contact liquid to that of the substance under investigation. If the deviation from a right angle does not exceed  $0.5'$ , the accuracy of the results obtained is  $\pm 1 \times 10^{-5}$ , provided that the indices of the sample and of the contact liquid do not differ by more than 0.02. B. V. Ioffe (1960, p. 127) showed that an accuracy of  $\pm 1 \times 10^{-5}$  may be attained even with a prism angle deviating by one degree from a right angle provided that the indices of the sample and of the contact liquid coincide within  $\pm 1 \times 10^{-4}$ .

The deviation from a right angle in our specimens lay in the range of 1 to  $3'$ . The contact liquid was a mixture of  $\alpha$ -monochloronaphthalene and a high-boiling fraction of kerosene,  $n_D^{20} = 1.545$ . The closeness of this refractive index to  $\omega$  of quartz permits us to disregard the error of the prism angle.

The position of the apparatus limb was determined by two independent methods: by passing the light beam from the collimator directly into the observation tube (with the V-block removed); and by means of a standard prism of optical glass with a known refractive index, this being near to that of the quartz.<sup>1</sup> The zero position located by both these methods coincided at  $0^\circ 2.52'$ .

A vertical slit diaphragm (0.1 mm in width) was mounted immediately behind the V-block in order to transmit only the narrow central part of the light-beam. The sample was moved by means of a rack-and-pinion, furnished with a scale and vernier. These devices<sup>2</sup> permitted measurements to be made of

<sup>1</sup> We are deeply grateful to N. F. Tomofeeva for placing the prisms at our disposal.

<sup>2</sup> This idea and its application was first suggested by T. G. Petrov.



The results of measurement (Table I) are of interest not only in determining the homogeneity of the sample in question, but also in enabling the precision and reproducibility of the results obtained to be assessed. The table shows that most series of measurements give a difference between the greatest and smallest values as low as 2 to  $3 \times 10^{-5}$ . The mean indices obtained in each series coincided within  $\pm 0.5 \times 10^{-5}$  (if an allowance for temperature differences was taken into account).

The refractive indices of the Polar Urals quartz lie in the middle range of the values listed for natural quartz in the literature and are very close to the values quoted above, which are taken as being the most probable ones.

The crystals of synthetic quartz investigated may be divided into two groups: experimental crystals, grown in small autoclaves, and industrial ones, grown in large autoclaves. The former show, as a rule, much larger fluctuations in refractive indices, asymmetry of thickness, and in the optical properties of the substance grown on both sides of the seed plate. This can probably be explained as the result of lower heat inertia and of larger fluctuations in the growth regime in small autoclaves compared with large ones.

TABLE II. Refractive indices ( $n_D$ ) of sample 353-9

Points	I measurement 18°C		II measurement 18-19°C		Points	I measurement 18°C		II measurement 18-19°C	
	$\omega$	$\gamma'$	$\omega$	$\gamma'$		$\omega$	$\gamma'$	$\omega$	$\gamma'$
1	1.54451	1.55176	1.54456	1.55172	16	—	—	—	—
2	48	71	49	69	17	50	70	49	69
3	53	74	48	72	18	75	93	72	91
4	54	71	52	72	19	53	68	53	69
5	53	71	55	74	20	41	57	40	60
6	52	71	53	73	21	49	68	48	66
7	52	74	52	73	22	36	54	33	53
8	52	74	54	74	23	32	50	30	50
9	55	75	53	73	24	36	56	34	55
10	51	69	57	75	25	39	59	39	59
11	(06)	(40)	51	67	26	42	61	40	60
12	(17)	(53)	(04)	(40)	27	45	65	43	62
13	57	75	(16)	(42)	Means				
14	50	70	55	74	(without				
15	49	66	41	61	seed				
					plate)	1.54449	1.55168	1.54448	1.55167

Refractive indices given below are typical of the crystals of both groups. The "experimental" sample 353-9 was measured twice, the measurements agreeing with each other (see table II and fig. 1). The seedplate of this sample made an angle of about  $27^\circ$  with the plane  $\{0001\}$  and, instead of  $\epsilon$  the intermediate index  $\gamma'$  was measured, its values being of interest only in that they change in strict accordance with the value of  $\omega$ . This is clearly seen in fig. 1.

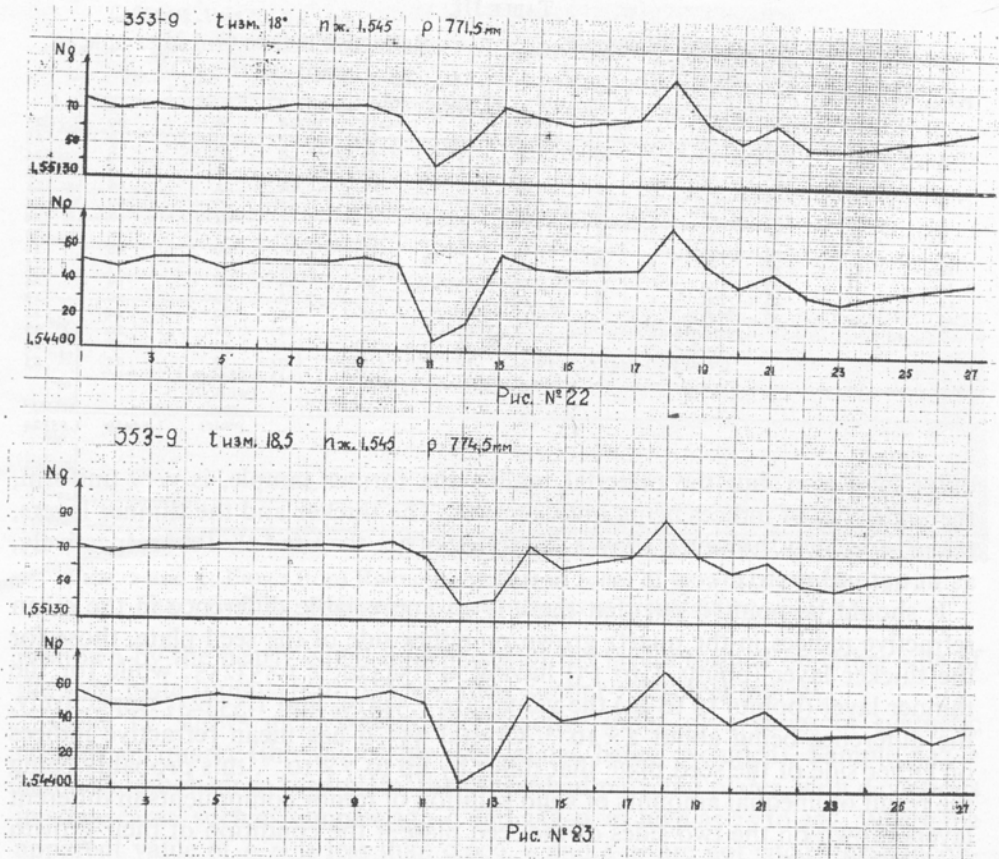


FIG. 1. Refractive indices in zones of growth of crystal 353-359:  
A, 1st measurement; B, 2nd measurement.

Points 11 and 12 (first measurement) and 12 and 13 (second measurement) refer to the seed plate cut from quartz of lower refractive indices than the quartz grown on it (these being in brackets in the tables).

The layers of quartz grown on either side of the seed plate differ in thickness in the ratio 1 : 1.5, the thicker one having zones exhibiting a sharp difference in refractive indices, exceeding  $40 \times 10^{-5}$ . The signals deteriorated acutely in some places; this was the cause of the absence of measurements at point 16. The thinner layer on the opposite side of the seed plate is more homogeneous, its index fluctuations lying in the range  $5$  to  $9 \times 10^{-5}$ , and those of the middle zone, 6 to 7 mm thick, (points 3 to 8), only  $2$  to  $3 \times 10^{-5}$ , like those of the natural Polar Urals quartz described above.

In the "industrial" sample C-95-p points 14 and 15 (table III and fig. 2) refer to the seed plate. The thickness of the layers grown on either side of it

TABLE III.

Refractive indices ( $n_D$ ) of sample C-95-P (at 21 °C)						Refractive indices ( $n_D$ ) of sample C-85 (at 18.5 °C)					
Points	$\omega$	$\epsilon$	Points	$\omega$	$\epsilon$	Points	$\omega$	$\epsilon$	Points	$\omega$	$\epsilon$
1	1.54419	1.55326	14	(17)	(23)	1	1.54419	1.55324	18	20	25
2	20	25	15	(13)	(16)	2	18	29	19	19	25
3	21	24	16	20	23	3	20	28	20	18	24
4	22	25	17	19	24	4	19	25	21	19	23
5	22	25	18	19	24	5	19	24	22	18	25
6	21	26	19	19	23	6	21	25	23	19	24
7	20	27	20	18	23	7	22	27	24	18	24
8	20	26	21	19	25	8	20	26	25	19	23
9	21	26	22	19	24	9	20	26	26	18	22
10	21	25	23	20	23	10	18	24	27	17	23
11	21	25	24	19	23	11	20	24	28	19	24
12	21	26	25	18	24	12	19	23	29	20	23
13	20	26	Means (without seed plate)	1.54420	1.55324	13	18	25	30	20	22
						14	19	24	31	20	23
						15	(17)	(21)	32	18	23
						16	(15)	(19)	33	21	23
						17	(18)	(24)	Means (without seed plate)	1.54419	1.55324

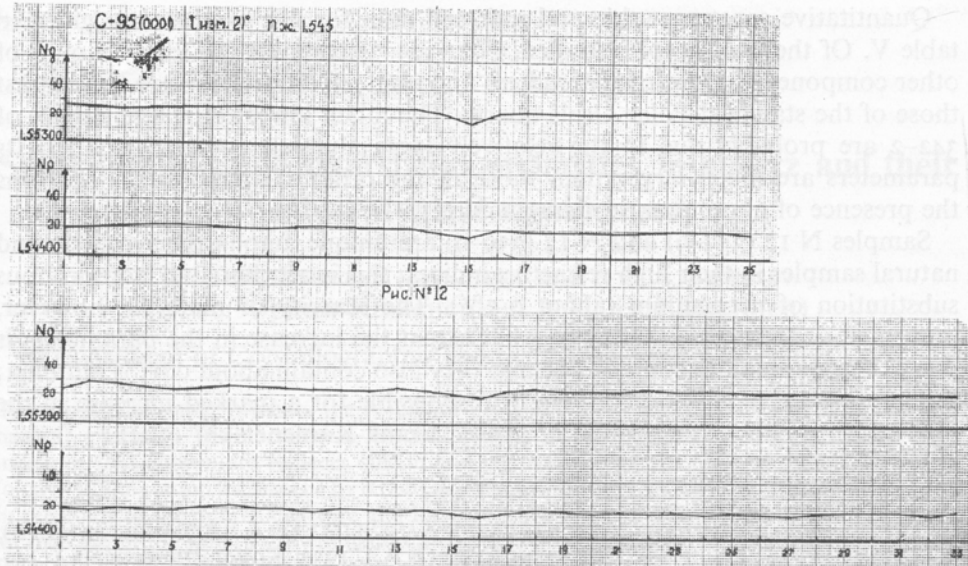
differ here also, but the material, unlike the former sample, is very uniform, the scattering of indices being only  $4 \times 10^{-5}$ . The thicker and the thinner layers, taken separately, however, show a scattering of  $3 \times 10^{-5}$  and  $2 \times 10^{-5}$  respectively, as in natural quartz.

It should be pointed out that there is an appreciable difference in the mean refractive indices in the quartz grown on either side of the seed plate, those for the thicker layer (points 1 to 13) having  $\omega$  1.54420;  $\epsilon$  1.553255; while for the thinner layer (points 16 to 25) the values are 1.54419<sub>0</sub> and 1.55323<sub>7</sub> respectively, the difference being about  $2 \times 10^{-5}$ . Crystal 353-9 has mean refractive indices on either side of the seed plate that differ by up to  $7 \times 10^{-5}$ , this probably being the result of unequal amounts of solid solution of minor components in different layers grown on the two sides of the seed plate if the condition of their growth was slightly different.

The crystals C-85 (table III and fig. 3) and G-95-p were, apparently, grown under constant conditions that were the same on either side of the plate; this

TABLE IV. Mean refractive indices ( $n_D$ ) of synthetic quartz

Samples	$t$	$\omega$	$\epsilon$	$\epsilon - \omega$
1	342-2	18 °C	1.54401	—
2	190-6	18	01	0.00905
3	014-1-7	19	01	907
4	383-3	19.6	14	912
5	C-95-2	21	15	—
6	201-1	18	17	0.00910
7	309-3	19.5	18	912
8	C-85	19.5	19	905
9	C-75	18.5	19	909
10	C-95-NP	21	20	905
11	385-3	19.6	23	910
12	353-9	18	48	—
13	339-9	19	52	—



FIGS. 2 and 3: FIG. 2 (top) Refractive indices in zones of growth of crystal C-95-p.  
 FIG. 3 (bottom) Refractive indices in zones of growth of crystal C-85.

is shown by the nearly equal thicknesses of the layers formed on either side of the seed plate (points 15 to 17) and their similar refractive indices.

Table IV shows mean values of refractive index of a series of synthetic crystals of quartz (the values for seed plates being excluded). Sample 343-2 had a rhombohedron seed plate, the others had pinacoid plates, with deviations in some cases, such as samples 339-9 and 353-9, as high as 25 to 27°. Where the apparent value of  $\epsilon - \omega$  is less than 0.009,  $\epsilon$  and  $\epsilon - \omega$  are not cited; these inconsistencies between  $\omega$  and  $\epsilon - \omega$  suggest that the fluctuations in the latter are accidental and are due to faulty orientation of the samples, not to variations in their composition.

TABLE V. Refractive indices ( $\omega_D$ ), parameters of the unit cell at  $18^\circ \pm 2^\circ\text{C}$ , and impurities (weight %) in samples of synthetic quartz

No.	Sample	$\omega$	$t$	$a$	$c$	$\text{Fe}_2\text{O}_3$	$\text{Al}_2\text{O}_3$
1	342-2	1.54401	18°C	4.91346, Å	5.40499, Å	0.00031	0.08
4	383-3	1.54414	19.6	4.91260	5.40417 <sub>7</sub>	0.02	0.01
7	309-3	1.54418	19.5	4.91253 <sub>5</sub>	5.40416	0.0003	0.0033
12	353-9	1.54448	18	4.91298 <sub>8</sub>	5.40499 <sub>8</sub>	0.002	0.03
13	339-9	1.54452	19	4.91318 <sub>7</sub>	5.40469	0.0006	0.025

No.	MgO	$\text{Mn}_3\text{O}_4$	CaO	$\text{TiO}_2$	$\text{Na}_2\text{O}$	CuO	PbO	$\text{GeO}_2$
1	0.0001	0.00004	0.0001	0.0005	0.0001	0.0005	0.00007	0.03
4	0.001	0.001	0.002	—	—	0.02	0.0002	—
7	0.00025	—	0.0003	0.00015	0.0078	—	—	—
12	0.0002	—	0.0006	0.0002	0.018	—	—	0.43
13	0.0003	—	0.00075	0.0002	0.013	—	—	0.52

Quantitative spectrographic and unit cell data for five samples are given in table V. Of the five samples studied, N 7 (309-3) contains the least amount of other components, its refractive indices and unit cell parameters are the nearest those of the standard Polar Urals quartz. The much lower refractive indices of 342-2 are probably due to the relatively large alumina content (0.08%). Its parameters are much larger than those of the other samples, which confirms the presence of aluminium in the structure.

Samples N 12 (353-9) and N 13 (339-9) are unique among the synthetic and natural samples in their high refractive indices; this is attributed to isomorphous substitution of germanium (about 0.5%). The scarcity of material, however, prevented us from ascertaining to what extent the increase in the parameters is due to the germanium content, because they also contain about 0.03% alumina; the latter, even in small quantities, is responsible for a marked increase in the unit cell of quartz (Afansieva *et al.*, 1959; Frank-Kamenetskii, 1964).

#### References

- [AFANAS'eva (I. A.), KAMENTSEV (I. E.), and FRANK-KAMENETSKY (V. A.)] Афанасьева (И.А.), Каменцев (И.Е.), и Франк-Каменецкий (В.А.), 1959, Кристаллография (*Crystallography*), **4**, 382.
- BUISSON (H.), 1906. *Compt. Rend. Acad. Sci. Paris*, **142**, 881.
- [FRANK-KAMENETSKY (V. A.)] Франк-Каменецкий (В.А.), 1964. Природа структурных примесей и включений в минералах (*The nature of structural admixtures and inclusions in minerals*). Leningrad University.
- GIFFORD (J.), 1902. *Proc. Roy. Soc. London*, **70**, 329.
- [IOFFE (B. V.)], Иоффе (Б. В.), 1960. Рефрактометрические методы химии (*Refractometric methods of chemistry*). State Chem. Publishing House, Leningrad.
- LE CHATELIER (H. L.), 1913. *La silice et les silicates*.
- [SHUBNIKOV (A. V.)] Шубников (А.В.), 1940. Кварц и его применение (*Quartz and its application*). Acad. Sci. USSR.
- SOSMAN (R. B.), 1927. The Properties of silica. *Amer. Chem. Soc. Monograph.*, series N 37, New York.
- WINCHELL (A. N.) and WINCHELL (H.), 1951. *Elements of optical mineralogy*, Vol 2. New York.

## Substitutional and interstitial impurities in quartz and their mineralogical significance

By V. A. FRANK-KAMENETSKY and I. E. KAMENTSEV  
(В. А. Франк-Каменецкий и И. Е. Каменцев)

Department of Crystallography, The Leningrad State University, USSR

*Summary.* The paper presents the results of precision X-ray investigations of synthetic and natural quartzes. The correlation of quantitative spectroscopic analyses and X-ray data indicates that aluminium replaces silicon and changes the parameter  $c$  of the quartz lattice (0.0035% aluminium increases  $c$  by 0.0001 Å). The impurities (Na, Ca, Fe, Mg) are distributed in the voids of the quartz structure and increase the parameter  $a$ . In synthetic quartz crystals an increase in the rate of growth causes a decrease in  $c$  and an increase in  $a$ . Natural quartz from various types of rocks shows minimal values of the lattice parameters, the amount of substitution being negligible. An increase of the parameters accompanies the lowering of the temperature of crystallization. Quartz from hydrothermal veins has a greater parameter  $c$  than quartz from pegmatites and magmatic rocks.

QUARTZ is considered to be a comparatively pure substance, with but small fluctuations of chemical composition and properties. Nevertheless, precise determinations of the refractive indices, lattice parameters, chemical composition,  $\alpha \rightleftharpoons \beta$  transition temperature, specific gravity, etc. show that different specimens of natural and synthetic quartz have slight fluctuations in their properties, mostly due to the presence of other elements in the structure of the mineral (Sosman, 1927; Keith and Tuttle, 1952; Cohen and Sumner, 1958; Semenov, 1958).

Precision determination of the unit cell parameters  $a$  and  $c$  of various natural and synthetic quartzes shows appreciable fluctuations (table I), depending on the elements present (Keith, 1950; Keith and Tuttle, 1952; Cohen and Sumner, 1958).

Fluctuations in the composition of quartzes formed under different conditions,

TABLE I. Lattice parameters of quartz at 18°C obtained by different authors

Author	$a$	$c$	Author	$a$	$c$
<i>Natural quartz</i>			<i>Synthetic quartz</i>		
Bradley and Jay, 1933	4.90288 kx	5.39327 kx	Keith, 1950, grown at:		
Cohen, 1935	4.90287	5.39314	{ 290°C	4.90322 kx	5.39382 kx
Miller and Du Mond, 1940	4.90228	5.39334	{ 380°C	4.90284	5.39353
Wilson and Lipson, 1941	4.90320	5.39371	{ 390°C	4.90273	5.39350
Keith and Tuttle, 1952	4.9033-4.9074	5.3928-5.3961	Sabatier and Wyart, 1954,		
Frondel and Hurlbut, 1955	4.90311	5.39382	{ pure quartz	4.9040	5.3932
Cohen and Sumner, 1958	4.9032-4.9042	5.3938-5.3943	{ quartz with Na+	4.9025	5.3932
Afanas'eva, Kamentsev, and Frank-Kamenetsky, 1959 (from the Polar Urals)	4.90275	5.39350	Cohen and Sumner, 1958	4.9033-4.9040	5.3940-5.3943
Cooper, 1962	4.90276	5.39360	Frank-Kamenetsky and Kamentsev, 1961	4.9026-4.9038	5.3933-5.3945
Belkovsky, 1964	4.9022-4.9025	5.3930-5.3940			

and the presence of various contaminants in them, throw light on some peculiarities of the crystal growth and the conditions of their formation; X-ray analyses of natural quartzes of different parageneses and of synthetic quartzes (where we can control the experiments and obtain crystals with only the desired impurities) are of great interest in this connection.

This paper deals with the results of X-ray investigations of some specimens of synthetic quartz obtained by the temperature drop method (Butuzov, 1962) and of natural quartzes from many deposits. The parameters of 47 samples of synthetic quartz are correlated with precision spectroscopic analyses (the latter carried out at the Research Institute of Glass in Moscow by N. N. Semenov's method, 1958).

Structural variations observed in quartz are connected with the inclusion of small amounts (not exceeding 0.1%) of impurities, which requires precision measurements of the unit cell parameters. X-ray examinations were made in the focusing camera (designed by S. S. Kvitka and M. M. Umansky, 1951), with copper radiation, quartz being used as the standard. The parameters were determined with a precision of  $\pm 0.0001 \text{ \AA}$  from measurements of the  $\alpha_1$  diffractions  $23\bar{5}4(2\theta 153.6^\circ)$  and  $21\bar{3}6(2\theta 157.2^\circ)$ .

Transparent crystals of quartz from the Polar Urals were taken as standard, impurities being very small in them ( $\text{Al}_2\text{O}_3$ , 0.0085%;  $\text{FeO}$ , 0.0008%;  $\text{MgO}$ , 0.002%;  $\text{Na}_2\text{O}$ , 0.00016%; according to Afanas'eva, Kamentsev, and Frank-Kamenetsky, 1959); their parameters at  $18^\circ\text{C}$  are:  $a 4.91265 \pm 0.00007 \text{ \AA}$ ;  $c 5.40441 \pm 0.00005 \text{ \AA}$ . These values are near to the data given in literature for quartz containing only small amounts of impurities (table I).

Measurements of the lattice parameters of 106 samples of synthetic quartz allowed us to determine their deviations as falling into in the range:  $a = 4.91210$  to  $4.91390 \text{ \AA}$ ,  $c = 5.40377$  to  $5.40550 \text{ \AA}$ , the amount of  $\text{Al}_2\text{O}_3$  in these specimens being in the range 0.002–0.1%, and that of  $\text{Na}_2\text{O}$  in the range 0.00003–0.1%.

The causes of the parameter fluctuations emerge when we correlate the values for  $a$ ,  $c$ , or  $V$  of the unit cell with the amount of impurities ( $\text{Ge}$ ;  $\text{Al}$ ;  $R^+ = \text{Na}$ ;  $R^{2+} = \text{Ca}$ ,  $\text{Mg}$ ,  $\text{Fe}$ ) (Frank-Kamenetsky, 1964; Frank-Kamenetsky and Kamentsev, 1961). The diagram (fig. 1) shows the changes of the parameters of the 47 specimens of synthetic quartz studied to be in direct relation to the amount of impurity, mainly of aluminium. In most cases, however, there is a large scattering of the points, which makes it difficult to find out the precise correlations in each individual case.

Quantitative correlations were established by correlation analysis (Kamentsev, 1965b), single and general correlation coefficients being determined and regression equations solved. The data obtained reveal a direct dependence of the parameter  $c$  ( $r = 0.520$ ) upon the aluminium content and of  $a$  on the presence of uni- and divalent cations ( $r = 0.497$ ). The data suggest that Al replacing Si in the tetrahedra generally effects an increase of  $c$ , while ions of alkali (Na) or of Ca, Mg, or Fe, occupying channels along  $[0001]$  in the quartz structure, slightly increase the parameter  $a$  (fig. 2).

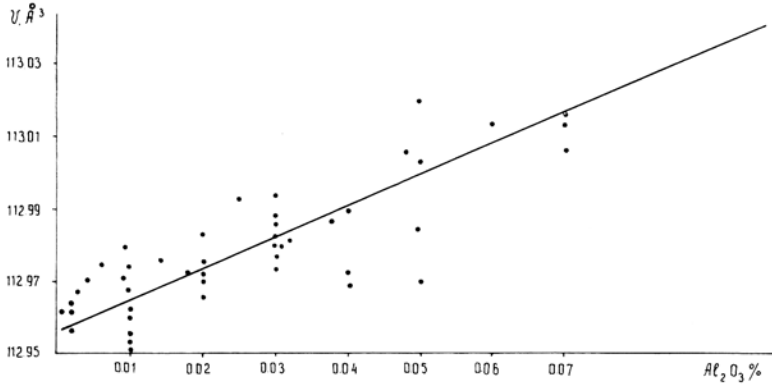
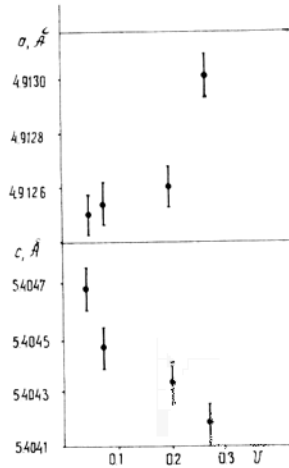
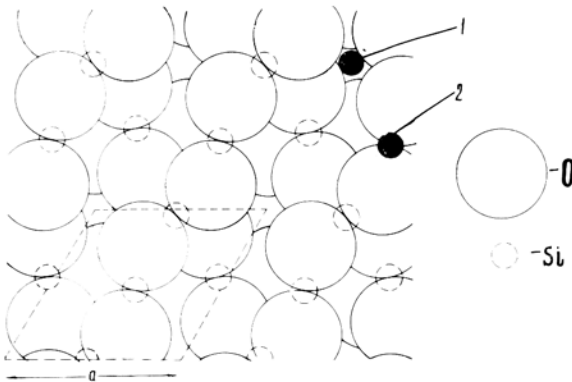


FIG. 1. Dependence of the volume of a unit cell ( $V$ ) on the content of  $Al_2O_3$ .

It is established (Kamentsev, 1965b) that 0.0035% of  $Al_2O_3$  increases the parameter  $c$  by 0.0001 Å, while 0.002% of  $Na_2O$  does the same to the parameter  $a$ . The parameters of the unit cell of pure quartz are:  $a = 4.91242$  Å,  $c = 5.40395$  Å, and the amount of aluminium included in the quartz structure may be calculated by the formula:  $\%Al_2O_3 = (c - 5.40395) \times 35.36$ , where  $c$  is the parameter of the unit cell of the quartz under investigation (in Å).

Simultaneous changes in the  $a$  and  $c$  parameters of the samples of synthetic and natural quartz studied show the microisomorphic replacement as occurring according to the following scheme:  $Si^{4+} \rightleftharpoons Al^{3+} + Na^+$ . The second row of microisomorphism  $2Si^{4+} \rightleftharpoons 2Al^{3+} + R^{2+}$ , where  $R^{2+} = Ca, Mg, Fe$ , is probably



FIGS. 2 and 3: FIG. 2 (left). Projection of the structure of quartz on (0001). Large circles are oxygen, smaller silicon. 1, ion of an impurity in one of the canals of quartz; 2, ion of aluminium replacing silicon in a  $SiO_4$  tetrahedron. FIG. 3. Dependence of the parameters  $a$ , and  $c$  on the rate of crystallization of synthetic quartz,  $V$  (mm/day).

of less importance because of the small quantity of divalent cations in quartz. The absence of an equivalent change in the parameters  $a$  and  $c$ , however, suggests the presence of aluminium and of uni- and divalent ions in non-equivalent quantities. In such cases a compensation of valency is possible due to some deficiencies, the intrusion of hydrogen, of hydroxyl ions, or oxygen vacancies (Kamentsev, 1965b; Tsinober, Khadzhi, Gordienko, and Samoilovich, 1965).

The crystals of synthetic quartz studied in our laboratory were grown under fixed experimental conditions, with the exception of the charge (the content of impurities) and the temperature drop, which determines the speed of crystal growth. Experiments show that quartz grown in a medium with a high content of aluminium contains much Al in its lattice (Tsinober, 1960), as is shown both by the spectroscopic analyses and by an increase in the parameter  $c$  of the unit cell. We further note that the pyramid of growth of the rhombohedron usually contains more aluminium than that of the basal plane (Frank-Kamenetsky and Kamentsev, 1961; Tsinober, 1960), its maximum, according to our data, approaching 0.04% in the synthetic quartz structure.

To observe the rate of growth four crystals of synthetic quartz were grown under identical conditions on seed plates parallel to the rhombohedron, but with various temperature drops and consequently with various speeds of growth (Tsinober and Kamentsev, 1964). The investigation showed a decrease of the parameter  $c$  of the quartz lattice with increase of the speed of growth, this being also confirmed by a regular decrease in the intensity of colour of these samples under X-ray irradiation. On the other hand, increased speed of growth results in an increase of the parameter  $a$  of the quartz lattice, which points to an increased amount of impurity entering the canals of the quartz structure (fig. 3).

An increase of the speed of crystallization from 0.06 mm. to 0.26 mm. a day resulted in a threefold increase of the aluminium included in the structure of the crystal, from 0.008% to 0.025%, though its amount in the medium in which the crystal was growing remained unchanged. This shows the speed of growth to be an important factor affecting the quantity of impurity included in the structure of quartz. It also affects its properties, e.g. aluminium results in the appearance of dot-like defects and in a smoky colour under X-irradiation (Zilbershtein, Ioffe, and Fedorov, 1965; Tsinober, 1960).

In some cases an irregular absorption of impurities into the quartz structure is connected with some defects involving fracturing and curvature in some parts of the crystal (*heterometry*), X-ray investigation of such crystals showing the mechanism of the appearance of macrodefects of such a kind. (Frank-Kamenetsky and Kamentsev, 1961; Sheftal, 1961; Shternberg, 1962).

Quartz is a major rock-forming mineral, occurring in rocks of widely differing parageneses. This led us to study specimens of quartz from magmatic rocks of various origins (Kamentsev and Priyatkin, 1963). The parameters were measured on quartz from the granites of various intrusive facies, from quartz porphyries, quartz diorites, quartz syenites, greisens, aplites, pegmatites, and from quartz

veins (14 specimens), these showing insignificant but easily detectable variations in their lattice parameters ( $\Delta a = 0.00036 \text{ \AA}$ ,  $\Delta c = 0.00057 \text{ \AA}$ ).

Correlating petrological data on the conditions of formation of various rock types of the Bolshoi Khingan complex (chemical composition of the medium, speed of growth, temperature of crystallization, pressure) with changes in the parameters of quartz, we find a definite connection between the temperature of crystallization of the rocks and the parameters of quartz. For instance, in the quartz samples from rocks of various intrusive facies, whose temperature decreased from the earlier facies to the later ones, a regular increase of the parameter  $c$  of the quartz lattice is observed, which indicates an increase of structural aluminium in the quartz crystallizing during the period of falling temperature.

But the part played by the medium in which the quartz crystallization was taking place still remains undetermined. Quartzes were also examined from various quartz veins of the Pamir granites: from conformable sheet veins, from intersecting veins, and from veins of complicated form with mineralized cavities. Their geological characteristics and conditions of formation were studied by I. Zakharchenko (1955). The data obtained by the method of homogenization of inclusions with bubbles and that of fracturing were used to calculate the most probable temperatures; these are not the true temperatures of crystallization but their comparative differences, which, though slightly erroneous, are sufficiently clear. The correlation (coefficient 0.80) obtained in this way between the temperature of crystallization and the changes in the parameter  $c$  (affected by the amount of structural aluminium, see fig. 4) is given by the relation (Kamentsev, 1963):  $\log(c - c_0) = 256/T - 5.7477$ , where  $c$  is the parameter of the quartz under investigation,  $c_0$  is the parameter of pure quartz, and  $T$  is the absolute temperature of crystallization.

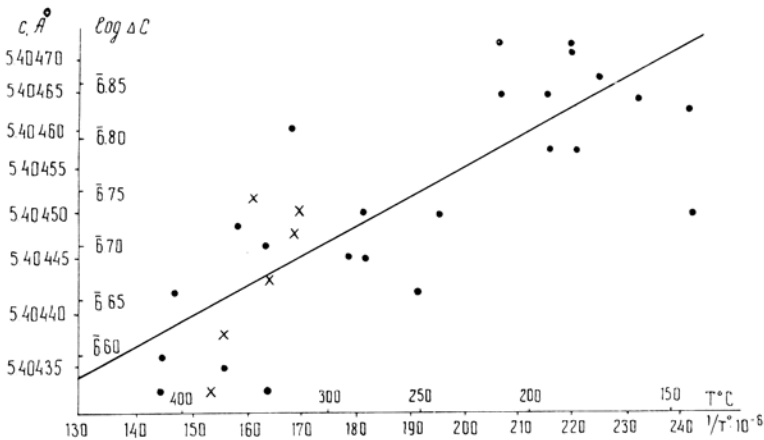


FIG. 4. Dependence of  $\log(c - c_0)$  on  $1/T$  for the quartz from the veins of the Pamir. Crosses mark the specimens from the quartz veins of Kounrad and Karoba. The straight line covers the data for the specimens of quartz of the Pamir.

Of course, such a correlation holds good only for the specific conditions that held during the formation of the quartz veins of the Pamir. Analogous regularities were found in the quartz from hydrothermal veins of the quartz-tungsten and quartz-molybdenum stage of mineralization of the Kounrad and Karoba deposits and from pegmatite bodies and granites of these areas. Thus the study of various samples of quartz differing in their genesis shows that the amount of structural aluminium in them is primarily connected with the temperature of crystallization.

To determine the microisomorphic compounds in natural quartz of various parageneses, it would be interesting to correlate the mean values of the parameters of the unit cell of natural quartz of magmatic and hydrothermal origin and synthetic quartzes (Kamentsev, 1965a). Mean values (at 95% significance) according to the criterion of 'Student' (Rumshinsky, 1966) are given in fig. 5.

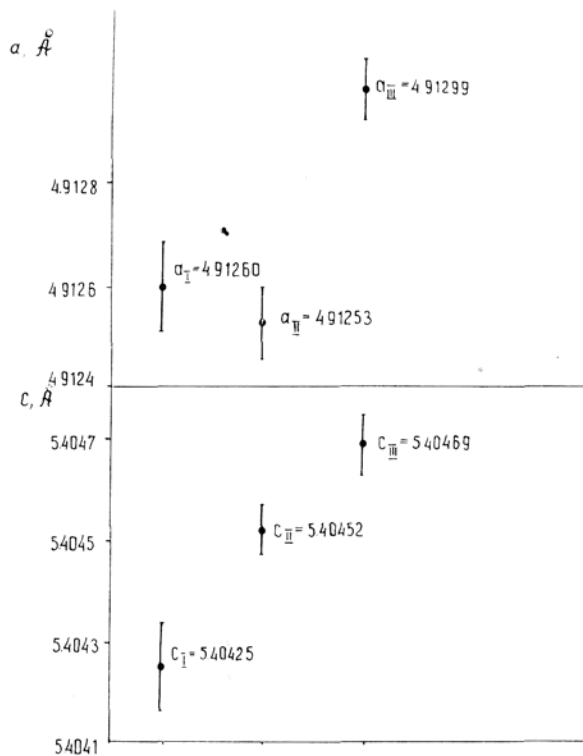


FIG. 5. Mean values for the parameters  $a$  and  $c$  for the quartz from rocks (type I), hydrothermal veins (type II), and synthetic quartz (type III). The length of the line shows the precision of determination of the mean value of a parameter.

These data were obtained in precision determinations of the parameters of 14 samples of quartz from magmatic rocks (type I), 31 samples of quartz from hydrothermal veins (type II), and 106 samples of synthetic quartz (type III).

quartzes of various parageneses, described above, clearly, show the widespread occurrence replacement and its connection with the conditions of quartz formation. Detailed X-ray analysis of natural quartzes gives valuable information about their structural characteristics and may assist in solving a number of mineralogenetic problems, such as the mode of formation of zonal deposits and the conditions of crystal growth in them. X-ray methods may be useful in determining the substitutions in natural and synthetic quartz crystals.

*Acknowledgements.* The authors express their heartfelt gratitude to E. E. Kostileva, A. A. Priyatkin, A. A. Shternberg, A. I. Zakharchenko, and L. I. Tsinober for the provision of samples of quartz.

#### References

- [AFANAS'eva (N. A.), KAMENTSEV (I. E.), and FRANK-KAMENETSKY (V. A.)] Афанасьева (Н.А.), Каменцев (И. Е.), и Франк-Каменецкий (В. А.), 1959. Кристаллография (*Kristallografiya*), **4**, 382 [M.A. 15-261].
- [BELKOVSKY (A. I.)] Белковский (А. И.), 1964. Доклады Акад. наук СССР (*Compt. Rend. Acad. Sci. URSS*), **154**, 111.
- BRADLEY (A. J.) and JAY (A. H.), 1933. *Proc. Phys. Soc.*, **45**, 507.
- BUTUZOV (V. P.), 1962. *Umely kremen "Cehosl. Casop. Fys."* **A12**, (2), 105.
- COHEN (A. J.) and SUMNER (G. G.), 1958. *Amer. Min.*, **43**, 58 [M.A. 14-177].
- COHEN (M. U.), 1935. *Rev. Scient. Instrum.*, **6**, 68.
- COOPER (A. S.), 1962. *Acta Cryst.*, **15**, 578 [M.A. 16-246].
- [FRANK-KAMENETSKY (V. A.)] Франк-Каменецкий (В. А.), 1964. Природа структурных примесей и включений в минералах. Издание Ленинградского университета. (*The nature of structural admixtures and inclusions in minerals*. Publ. Leningrad Univ.).
- [— and KAMENTSEV (I. E.)] — и Каменцев (И. Е.), 1961. Сборник "Рост кристаллов". (Symposium on *Crystal Growth*, **3**, 468.
- FRONDEL (C.) and HURLBUT (C. S., Jr.), 1955. *Journ. Chem. Physics.*, **23**, 1 215 [M.A. 13-298].
- [KAMENTSEV (I. E.)] Каменцев (И. Е.), 1962. Вестник Ленинград. госуд. унив. (*Bull. Leningrad State Univ.*), **18**, 109.
- — —, 1963. Геохимия (*Geochemistry*), по. 6, р. 586 [M.A. 16-623].
- — —, 1965a. *Ibid.*, по. 3, р. 366.
- — —, 1965b. Зап. Всесоюз. мин. общ. (*Mem. All-Union Min. Soc.*), **94**, 687.
- [— and PRIYATKIN (A. A.)] — и Прияткин (А. А.), 1963. Рентгенография минерального сырья (*X-ray studies of mineral resources*), **3**, 44.
- KEITH (H. D.), 1950. *Proc. Phys. Soc., Sect. B*, **63**, 208 [M.A. 11-535].
- and TUTTLE (O. F.), 1952. *Amer. Jour. Sci.*, Bowen vol., 203. [M.A. 12-122].
- [KVITKA (S. S.) and UMANSKY (M. M.)] Квитка (С. С.) И. Уманский (М. М.), 1951. Известия Акаде. наук СССР, сер. физ. (*Bull. Acad. Sci., U.S.S.R., phys. ser.*), **15**, 2.
- MILLER (P. H.) and DU MOND (Y. W.), 1940. *Phys. Review*, **57**, р. 198.
- [PRIKAZCHIKOV (L. A.)] Приказчиков (А. А.), 1962. Мин. сборник Львов. геон. общ. (*Min. Mag. Lvov Geol. Soc.*), **16**, 373.
- [RUMSHINSKY (L. Z.)] Румшинский (Л.З.), 1966. Элементы теории вероятности (*Fundamentals of the theory of probability*).
- SABATIER (G.) and WYART (J.), 1954. *Comp. Rend. Acad. Sci. Paris*, **239**, 1 053 [M.A. 12-499].
- [SHEFTAL (N. N.)] Шефтал (Н. Н.), 1961. Сборник "Рост кристаллов". (Symposium on *Crystal Growth*, **3**, 9.
- [SHTERNBERG (A. A.)] Штернберг (А. А.), 1962. Кристаллография (*Kristallografiya*), **7**, 114.

- [SEMENOV (N. N.)] Семенов (Н. Н.), 1958. Спектральный анализ кварцевого сырья (*Spectrochemical analysis of quartz material*). Промстройиздат, Москва.
- SOSMAN (R. B.), 1927. *The Properties of Silica*. New York.
- [TSINOBER (L. I.)] Цинобер (Л. И.), 1960. Труды Всесоюзного научно-исследовательского института пьезооптического минерального сырья (*Proceedings All-Union Scientific Research Institute of piezo-optic mineral resources*), 3, (2), 95.
- [— and КАМЕНТСЕВ (I. E.)] — и Каменцев (И. Е.), 1964. Кристаллография (*Kristallografiya*), 9, 448, [М.А. 17-373].
- [—, КНАДЖИ (V. E.), ГОРДИЕНКО (L. A.), and САМОЙЛОВИЧ (M. I.)] —, Хаджи (В. Е.), Гордиенко (Л. А.) и Самойлович (М. И.), 1965. Сборник "Рост кристаллов" Symposium on *Crystal growth*, 6.
- WILSON (A. J.) and LIPSON (R.), 1941. *Proc. Phys. Soc.*, 53 (3), 297.
- [ЗАХАРЧЕНКО (A. I.)] Захарченко (А. И.), 1955. Материалы Всесоюзного научно-исследовательского геологического института Минералогия и геохимия (*Proceedings All-Union Scientific Research Institute of geology, mineralogy and geochemistry*), no. 6.
- [ЗИЛЬБЕРШТЕЙН (Kh. I.), ИОФФЕ (V. A.), and ФЕДОРОВ (Yu. R.)] Зильберштейн (Х. И.), Иоффе (В. А.), и Федоров (Ю. Р.), 1965. Кристаллография (*Kristallografiya*) 10, p. 727.

## **The geochemical significance of dendritic-skeletal crystallization in polymetallic ore deposition processes**

By R. O. РАДКЕВИЧ  
(Р. О. Радкевич)

Vernadsky Institute of Geochemistry, Academy of Sciences,  
Moscow, U.S.S.R.

*Summary.* The problem of dendritic-skeletal crystal growth is known to be of great interest for geochemists in connection with the fact that the morphology of these crystals is a sensitive indicator of the kinetics of changes in the physico-chemical conditions of ore-deposition processes.

The polymetallic ore deposit under investigation is that of Tators (North Caucasus) and has been formed near the surface under complex tectonic conditions. The principal ore minerals of the Tators ores are often observed in a dendritic-skeletal form. Dendritic-skeletal galena crystals are found included in botryoidal sphalerite formations. These may be classified as follows: dendritic needles, chrysanthemum-like, tree-like, vermicular, box-like, and latticed forms. Some of them resemble the galena crystals described by H. Rouvier (1962) from the Bellericq mines (France). The dendritic-skeletal sphalerite forms in the Tators ores are not as wide-spread and varied as the galena forms. The morphology of the dendritic-skeletal galena from Tators displays a fairly obvious dependence on the concentration of admixed elements in sphalerite. The conclusions drawn are in good agreement with Tilmans' experiments (1952).

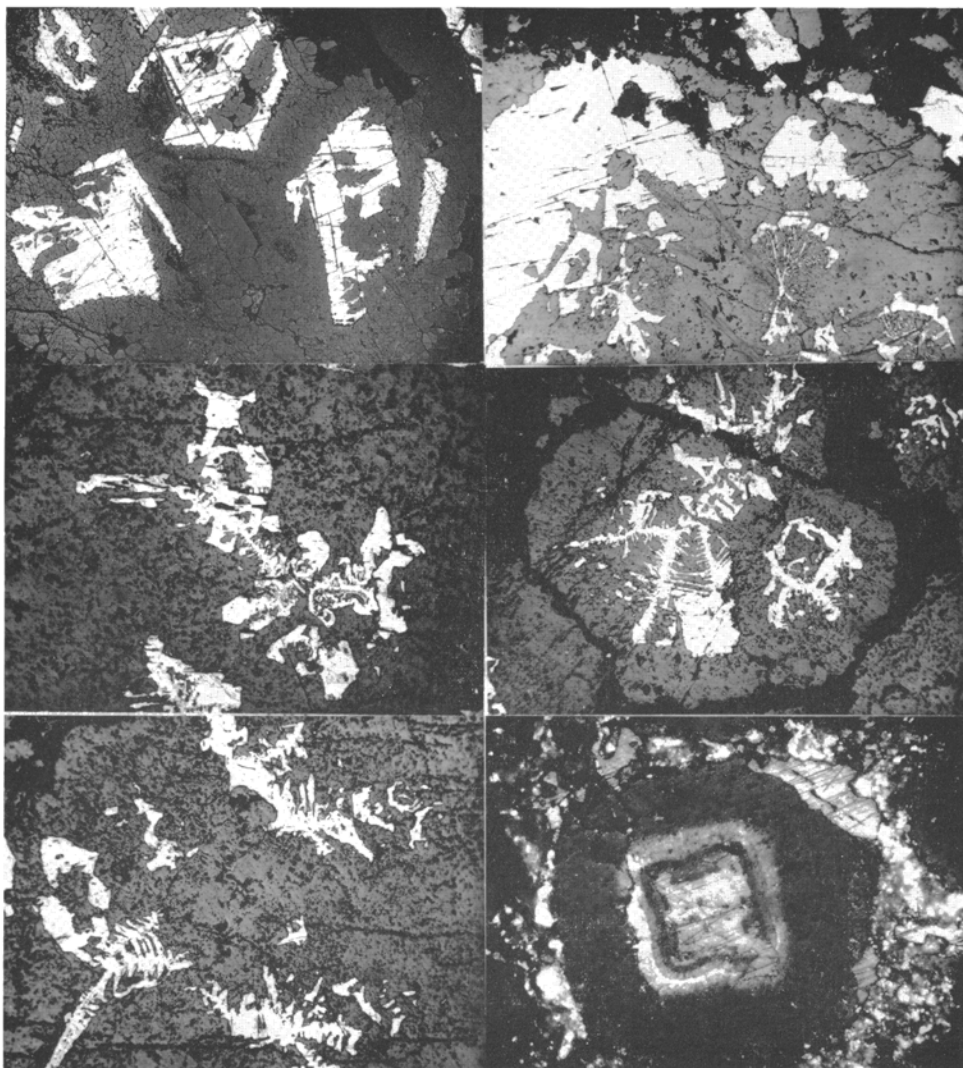
THE dendritic crystallization problem has a century-old history. It has to be noted here that the foundations of modern dendritic-skeletal crystallization theory, being developed successfully in the U.S.S.R. at present by D. D. Saratovkin, had been laid in the last century by the famous Russian metallurgist D. K. Chernov.

In studying dendritic-skeletal forms, a mineralogist can distinctly see the dependence of crystal morphology on the crystal structure and the physico-chemical conditions. Thus it should be possible to attempt a reconstruction of the geochemical conditions in being during the ore deposition process. In this respect the most interesting ore deposits are those where dendritic-skeletal crystallization is strongly pronounced not only in minor minerals but also in the main ore minerals.

Among the North Caucasian polymetallic vein deposits, one of the most interesting for studying the dendritic and skeletal forms of galena and sphalerite crystals is the Tators deposit. This is localized in the rocks of the Palaeozoic crystalline basement close to the Upper Jurassic (Callovian) carbonaceous

formation that overlaps them. The basal level of Upper Jurassic carbonaceous rocks marks the upper age limit of the polymetallic mineralization in the region. The ores of the deposit are of a comparatively simple composition: sphalerite, galena, pyrite, chalcopyrite, tetrahedrite, quartz, calcite. The main minerals are sphalerite, galena, and quartz. Colloform structures are widespread in the ores.

Among the various forms of dendritic-skeletal crystals the following groups may be noted the forms of minerals deposited together, and the forms of intra-ore and post-ore replacement of minerals (figs. 1 and 2). The most interesting from the point of view of the present paper are the dendritic-skeletal forms of galena and sphalerite that have been deposited together. The dendritic-skeletal crystals are produced, as a rule, by minerals present in relatively small amounts in the ore. Sphalerite was observed in the ore mainly as irregular and botryoidal masses, more rarely as dendritic needles (fig. 2) and dendrites among the galena. The dendritic-skeletal forms of galena are more varied, this variety being conditioned by the fact that the corners, edges, and faces not only of the cube but also of the cubo-octahedron are realized by growing crystals. The following morphogenetic types were observed: dendritic needles, chrysanthemum-like, arborescent vermicular, box-like, and latticed forms (figs. 2 to 5). The crystals of these types are met both in a pure form and in regular intergrowths. Some of them resemble the crystals studied and reported by H. Rouvier (1962) from the ores of the Bellericq mine (France). The skeletons and dendrites of galena from the Tators deposit are enclosed as a rule in the colloform sphalerite masses (fig. 6). The botryoidal masses often have a concentric zonal structure conditioned by an alternation of differently coloured botryoidal layers of microcrystalline sphalerite. Sometimes elements of a radiate-fibrous structure are observed in these masses. At the intersection of differently coloured layers with dendritic axes it can be seen distinctly that the most favourable conditions for the crystallization of galena existed during the deposition of brown sphalerite zones. In the yellowish-brown and colourless zones there was apparently a marked decrease in the degree of oversaturation of the hydrothermal solutions and, in these zones, a decrease, or cessation, of crystallization of galena is observed. According to our spectral analysis the sphalerite of Tators in the brownish-black zones is, like all dark sphalerites, the richest in foreign elements. In these zones, the growth of galena dendrites ceases, and the mineral forms crystals of cubic and/or octahedral habit. The suppression of dendritic-skeletal crystallization by other minerals, deposited synchronously and at the same place, is distinctly seen in cases where there are "lines" of microscopic sphalerite inclusions in galena. The sphalerite "lines" are parallel both to one another and to the growing galena crystal face. In each separate "line" the size of sphalerite inclusions is uniform. As the galena crystal face grows, the size of the inclusions regularly increases in each of the "lines" until they become so large that the crystallization of galena ceases. Such "lines" are obviously a sufficiently reliable criterion of dendritic-skeletal crystallization character.



FIGS. 1 to 6: FIG. 1 (top left). Galena (white) is replaced along cleavage directions by microcrystalline quartz (grey); galena pseudoskeletons are formed. Reflected light,  $\times 3$ . FIG. 2 (top right). Chrysanthemum-like forms of synchronously crystallized galena (white) and sphalerite (dark-grey); sphalerite dendritic needles in the galena; the galena is replaced by quartz (black) more intensively than sphalerite; metacrystals of pyrite (brightly white, relief) in the quartz. Reflected light,  $\times 30$ . FIG. 3 (middle left). A complex dendritic-skeletal crystal form of galena (white) in sphalerite (dark-grey). Reflected light,  $\times 30$ . FIG. 4 (middle right). The character of the dendritic-skeletal galena formations (white) in sphalerite (dark-grey). The spaces between the botryoidal sphalerite masses and veins are filled by quartz (black). Reflected light,  $\times 30$ . FIG. 5 (bottom left). Dendritic needles and dendritic-skeletal forms of galena (white) in sphalerite (dark-grey). Reflected light,  $\times 30$ . FIG. 6 (bottom right). A galena dendritic-skeletal crystal (white to grey) is in the central part of the concentric-zoned sphalerite botryoidal mass. The external sphalerite zone is enriched in microscopic chalcopyrite emulsion. On the periphery of this zone the galena is not dendritic and skeletal. Combined light,  $\times 25$ .

All the above observations are in good agreement with Yu. Ya. Tilmans' experiments (1952) on the modifying of dendritic crystals of some salts by different foreign substances. Our observations also corroborate the dendritic crystallization theory developed by D. D. Saratovkin (1950, 1957). According to this, the common cause of both the dendritic and skeletal crystallization types is the different rate at which growth is stopped in different parts of the crystal by the interfering foreign substances and even by the solvent itself. Indeed the studied galena crystals are surrounded on all sides by microscopic sphalerite particles and admixtures extraneous for galena, both hindering the lead diffusion. This is why the galena crystals can crystallize in the botryoidal sphalerite masses mainly in radial directions in the form of dendritic needles, which react sensitively upon the concentration of the surrounding admixtures in the solution. Naturally the energetically most profitable direction of the dendritic crystal growth is towards the corners or edges of the crystal, where, as is known, there exists the maximum possibility of forming new growth centres. If the concentration of interfering substances increases somewhat, the crystallization of galena will be difficult even in these directions. If the concentration of the interfering substances increases, due to a total oversaturation of the solution, and exceeds a certain limit, the dendritic growth will be suppressed. Hence under favourable conditions a galena crystal may form with only slowly growing equilibrium faces, i.e. cube faces. The regular change of the dendritic orientation of some crystals with the NaCl-type structure from  $\langle 111 \rangle$  through  $\langle 110 \rangle$  and to  $\langle 100 \rangle$  depending on the degree of oversaturation of the solution has been studied by J. Schlipf (1960).

In itself the presence of foreign substances in the solution is apparently not the only reason for dendritic-skeletal crystallization. The kinetics of the process has a decisive significance, and the ratio of the precipitation rate to the crystallization rate is most important for dendritic-skeletal crystallization. Such sudden and repeated oversaturation of the hydrothermal solution is in good agreement with the near-surface conditions and the geotectonic history of the Tators deposit. From the point of view of the Gibbs-Curie-Woulf's principle the crystal forms described are not equiponderous upon the whole. However we may speak about a discontinuous-continuous equilibrium only in relation to the tops of trunks and branches of a dendrite, which actually could be in equilibrium with the solution. After the completion of such a botryoidal mass with the dendritic-skeletal galena crystals buried in it the surrounding microscopic sphalerite crystals and other interfering substances hindered the recrystallization of the galena into the equilibrium crystal form. In the subsequent processes of collective recrystallization some signs of dendrite disintegration are revealed. The completely recrystallized sphalerite no longer contains galena inclusions. An interesting aspect of a subsequent study of dendritic-skeletal crystals is the possibility of estimating the time required for dendrite transformation. The first encouraging results along these lines have been obtained by M. O. Kliya and A. A. Chernov (1956).

Finally, in conclusion, we will dwell on the question of terminology: what difference is there between a dendrite and a skeletal crystal? There are more than six different answers to this question in the literature. Hence there is at present no sufficiently sharp distinction between them. Undoubtedly the International Mineralogical Association will take steps to put an end to this terminological confusion. Taking into account the data from the literature and the results of the above investigations, the following possible formulations are proposed: Dendritic crystals are crystals which grow mainly along the crystallographic symmetry axes of a lower order. Skeletal crystals are crystals which grow mainly along the crystallographic symmetry axes of a higher order. The order of the dendrite or skeleton must be singled out according to the order of the crystallographic symmetry axes. It would be expedient to work out quantitative criteria for their classification because dendrites and skeletal crystals are mutually interdependent and almost always co-existing.

#### References

- [CHERNOV (A. A.)] Чернов (А. А.), 1956. Кристаллография (*Kristallografia*), **1**, 583.  
[GRIGOR'EV (D. P.)] Григорьев (Д. П.), 1965. Известия высших учебных заведений (Publications of the University) Геология и разведка, (*Geology and prospecting*) по. 8.  
[KLIYA (M. O.)] Клия (М. О.), 1956. Кристаллография (*Kristallografia*), **1**, 577.  
[MOKIEVSKY (V. A.) and SEMENYUK (S. N.)] Мокиевский (В. А.), и Семенюк (С. Н.), 1952. Зап. Всесоюз. Мин. Общ. (*Mem. All-Union Min. Soc.*), **81**, 100.  
ROUVIER (H.), 1962. *Bull. Soc. Geol. France*, ser. 7, **4**, 816.  
[SARATOVKIN (D. D.)] Саратовкин (Д. Д.), 1957. Дендритная Кристаллизация. (Dendritic crystallization). Moscow, Металлургиздат.  
SCHLIPF (J.), 1960. *Fortschr. Min.*, **38**, 74.  
[SHAFRANOVSKY (I. I.) and MOKIEVSKY (V. A.)] Шафрановский (И. И.) и Мокиевский (В. А.), 1956. Зап. Всесоюз. Мин. Общ. (*Mem. All-Union Min. Soc.*), **85**, 171.  
[TILMANS (YU. YA.)] Тильманс (Ю. Я.), 1952. Журн. Общ. Хим. (*Journ. general Chem.*), **22**, по. 3.

# Vergleichende Untersuchungen der Farb- und Lumineszenzeigenschaften natürlicher und gezüchteter, definiert dotierter Fluorite

K. RECKER, A. NEUHAUS, und R. LECKEBUSCH

(Mineralogisch-Petrologisches Institut und Museum, Bonn)

*Summary.* Green natural fluorites show the absorption spectrum of  $\text{Sm}^{2+}$ , and some, in addition, show the luminescence spectrum of  $\text{Sm}^{3+}$ . Yellow fluorites show an electron-band spectrum that suggests the presence of a yet unknown incorporated complex. Blue, red, and violet fluorites have absorption spectra that can be related to the spectra of synthetic  $\text{CaF}_2$  crystals doped with non-colouring impurities (like  $\text{KF}$ ,  $\text{NaF}$ , and  $\text{YF}_3$ ) and then treated with X-rays. No colouring due to uranium ions ( $\text{U}^{3+}$ ,  $\text{U}^{4+}$  or  $\text{U}^{6+}$ ) was found in distinctly uranium bearing fluorites. Natural fluorites with violet fluorescence show the absorption and luminescence spectra of  $\text{Eu}^{2+}$ .

ALS zentrale Ursache der Farb- und Lumineszenzeigenschaften homogener natürlicher Fluorite werden, sehen wir von Sonderfällen wie Kolloidfärbung und organischen Einlagerungen ab, eingebaute Fremdionen (Ionenfärbung) und Farbzentren (Strahlungsverfärbung) angenommen. Über die zugehörigen Farbvarianten und -Mechanismen ist vielfältig gearbeitet worden, i.allg. jedoch ohne zu befriedigenden Deutungen zu gelangen (Przibram, 1953; Feofilov, 1958; Adler, 1959; Recker, 1961, 1962; Schulman u. Compton, 1962; Montoriol *et al.*, 1962). Alle bisherigen Untersuchungen zeigen überdies, daß das Problem Farbe und Lumineszenz der natürlichen Flußspäte wegen der Vielfalt an Fremdioneneinlagerungen und der Komplexheit der Anregungsmechanismen auf rein analytischem Wege überhaupt nicht zu lösen ist. Seit Jahren laufende neue Untersuchungen zu diesem mineralogisch, kristallchemisch und kristallphysikalisch gleich wichtigen Problem sind daher von vornherein analytisch und synthetisch angelegt worden. Hierzu wurden folgende Untersuchungsprogramme durchgeführt:

Qualitative und quantitative Spektralanalyse farbverschiedener und lumineszierender Naturfluorite auf Spurenverunreinigungen, Bestimmung der Absorptions- und Emissionsspektren dieser Fluorite mit leistungsfähigen Geräten (Beckman DK 2, Cary 14 R und Leitz IR-Gerät) und thermische Ausbleichungsversuche.

Züchtung reiner  $\text{CaF}_2$ -Einkristalle als Wirtkristalle für Dotierungen. Dotierungen mit Fluoriden und Oxiden von 1-, 2-, 3-, 4- und 6-wertigen Kationen, insbesondere der Übergangselemente, Seltenen Erden und Aktiniden.

Qualitative und quantitative Kontrolle der Dotierungszusätze und Studium der Absorptions- und Lumineszenzspektren der definiert dotierten  $\text{CaF}_2$ -Einkristalle. Definierte Röntgenbestrahlung der dotierten  $\text{CaF}_2$ -Zuchtkristalle und erneutes Studium ihrer Absorptions- und Lumineszenzspektren.

Synopsis der Absorptions- und Lumineszenzspektren der natürlichen Fluorite mit den Spektren der definiert dotierten, unbestrahlten und bestrahlten Zuchtfluorite.

Über einige Ergebnisse dieses Arbeitsprogramms wird hier berichtet.

### *Natürliche Flußspäte*

Zur Untersuchung gelangten bisher ca. 80 visuell homogene natürliche Fluorite verschiedener Farbe, Lumineszenz und Fundorte. Etwa 80% dieser Kristalle zeigten bei UV-Bestrahlung blaue Lumineszenz.

*Spektrochemische Untersuchungen.* Zur Aussonderung aller Flußspäte, deren Färbung bzw. Lumineszenz auf Gehalte an Fremdionen zurückgeführt werden können, wurden sämtliche Fluorite mit Hilfe eines 1.5 m-ARL-Gitterspektrographen + Projection Comparator Densitometer qualitativ und halbquantitativ spektrochemisch geprüft.

Die Seltenen Erden wurden allgemein nach einem von Hegemann und Wilk (1964) angegebenen Verfahren angereichert. Zum Nachweis von Sm, Eu und U wurde neben der üblichen Spektralanalyse auch die empfindlichere Lumineszenzanalyse benutzt. Hierzu wurden die Fluoritproben zerkleinert und die Pulver 10 min bei  $950^\circ\text{C}$  an Luft getempert. Oxidierend erhitztes  $\text{CaF}_2(\text{Sm})$  besitzt nach eigenen Untersuchungen Hauptmaxima der Lumineszenz bei 571 und 605  $\text{m}\mu$ ,  $\text{CaF}_2(\text{Eu})$  solche bei 575 und 612  $\text{m}\mu$  und  $\text{CaF}_2(\text{U})$  ein solches bei 529  $\text{m}\mu$ . Die Lumineszenzintensität dieser Maxima wurde mit einem Beckman DK2-Spektralphotometer gemessen und mit der Lumineszenzintensität von Eichproben verglichen. Der Uran-Gehalt der Fluorite interessierte besonders, da Uran einmal als Strahlungsquelle für die Erzeugung von Farbzentren, zum andern als eigenfärbendes und lumineszierendes Ion wirkt. Uran wurde deshalb quantitativ bestimmt durch Vergleich der Lumineszenzintensität der erhitzten natürlichen Fluorite mit der von  $\text{CaF}_2(\text{U})$ -Eichserien bekannten U-Gehaltes.

Tab. 1 enthält die Ergebnisse der spektrochemischen Untersuchungen für einige ausgesuchte Fluoritfarbvarianten. Tab. 1 verzeichnet außer Sm, Eu und Yb keine Seltenen Erden, da ihre Konzentration trotz der benutzten Anreicherungsmethode (s.oben) für einen sicheren Nachweis nicht ausreichte. Seltene Erden sind somit, ausgenommen Sm und Eu, als Ursache für eine ionogene Färbung für alle untersuchten Beispiele auszuschließen. Das gilt natürlich nicht für die Lumineszenz der Fluorite. Hierzu: Sehr viele Fluorite enthalten Eu. Besonders hoch ist der Eu-Gehalt der visuell blau fluoreszierenden Fluorite, sodaß wahrscheinlich Eu Ursache der blauen Fluoreszenz ist. Nur in grünen Fluoriten ließ sich Sm nachweisen. Dies läßt vermuten, daß Sm Ursache der grünen Farbe ist. Uran fand sich einerseits in rot- bis rotviolett

TAB. I. Fremdelemente in natürlichen Fluoriten. Spalte 1 enthält eine Aufstellung sämtlicher in den 80 Fluoriten gefundenen Fremdionen

	Kongsberg	Wölsendorf	Hesselbach	Kongsberg	Minas del Pinneo
	farblos	violett	hellblau	grün	gelb
Ag	< 10 p.p.m.	—	< 10 p.p.m.	—	< 10 p.p.m.
Al	< 10	< 10 p.p.m.	< 10	< 10 p.p.m.	< 10
Ba	—	+	+	—	—
Be	< 10	< 10	< 10	?	< 10
Cr	—	—	< 10	—	—
Cu	< 10	10–50	10–50	< 10	< 10
Fe	10–50	10–50	< 10	< 10	< 10
La	—	—	—	—	—
Mg	10–50	100–200	< 10	10–50	10–50
Mn	—	—	—	< 10	—
Na	10–50	10–50	10–50	50–100	10–50
Ni	—	—	—	—	10–50
Pb	—	—	—	—	—
Si	—	—	+	—	—
Sr	10–50	< 10	< 10	10–50	< 10
Sn	—	—	—	+	—
Ti	—	—	< 10	10–50	—
Y	< 10	10–50	10–50	100–200	< 10
Yb	—	—	—	+	—
U	—	—	—	—	—
Eu	—	—	?	—	—
Sm	—	—	—	+	—

+ = nur qualitativ in Spuren nachgewiesen.

gefärbten, andererseits in farblosen Fluoriten. Den höchsten U-Gehalt ( $\sim 10$  p.p.m.) besitzen die rot gefärbten Fluorite von Göschenen, dann folgen ein farbloser Fluorit von Münstertal ( $\sim 5$  p.p.m.) und der Stinkspat von Wölsendorf ( $< 5$  p.p.m.). Alle Uranmengen sind so gering, daß auch sie als Ursache ionogener Färbung hier auszuschließen sind.

*Absorptions- und Lumineszenzspektren natürlicher Fluorite.* Es wurden die Absorptionsspektren im Bereich von  $200\text{--}2700\text{ m}\mu$  und die Lumineszenzspektren im Bereich von  $400\text{--}800\text{ m}\mu$  aufgenommen und miteinander verglichen. Abb. 1 zeigt als Beispiel einige Absorptionsspektren verschieden gefärbter Naturfluorite.

Der Vergleich der Absorptionsspektren ergab, daß die Spektren visuell gleichgefärbter Kristalle verschiedener Herkunft weitgehend nach Anzahl und Lage der Absorptionsmaxima übereinstimmen. Es gleichen sich also die Spektren aller grünen Fluorite, aller gelben Fluorite, aller roten Fluorite etc. Fluorite einer bestimmten Farbe besitzen also wesentlich die gleiche Färbungsursache. Im einzelnen:

Etwa 80% der Fluorite zeigen ein Fluoreszenzspektrum mit einem Maximum bei  $422.5\text{ m}\mu$ . Dieses Maximum wird durch  $\text{Eu}^{++}$ -Ionen im Gitter der Fluorite

hervorgerufen (Adler u. Kveta, 1958). Das bedeutet, daß mit der verwendeten UV-Quelle (Osram-Quecksilberdampf Lampe Hg 3) nur ein, vermutlich das dominierende Element zur Lumineszenz angeregt wurde. Für die Fluoreszenz-anregung der in vielen Fluoriten sicherlich noch vorhandenen weiteren Seltenen Erden bedarf es offenbar stärkerer Lichtquellen.

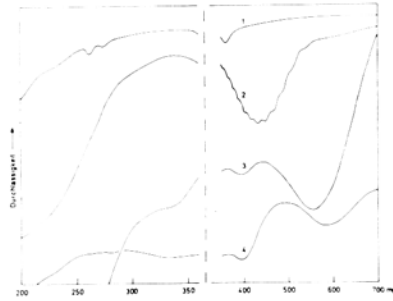


ABB. 1. Absorptionsspektren natürlicher Fluorite. Kurve 1, Huallapon, farblos; Kurve 2, Minas del Pinneo, gelb; Kurve 3, Wölsendorf, violett; Kurve 4, Todtnau, blau.

*Thermische Ausbleichung.* Langsames Erhitzen der natürlichen Fluorite bis ca. 300°C ergab: Fluorite mit grüner Farbe lassen sich nicht entfärben; blau fluoreszierende Fluorite bewahren ihre Fluoreszenz. Gelbe, blaue, violette und rote Fluorite hingegen entfärben sich. Aus diesem verschiedenartigen thermischen Verhalten der Fluorite läßt sich schließen, daß die Farbe der gelben, blauen, violetten und roten Fluorite wesentlich auf Bestrahlungsanregung (Farbzentren) beruhen dürfte, während die Farbe der grünen Fluorite und die Fluoreszenz der blau fluoreszierenden Fluorite auf Fremdionen beruhen muß.

#### *Züchtung und Untersuchung von reinen und dotierten $\text{CaF}_2$ -Einkristallen*

*Züchtung hochreiner, undotierter  $\text{CaF}_2$ -Einkristalle.* Um die Auswirkungen von Fremdkationen, insbesondere der in den natürlichen Flußspäten analytisch nachgewiesenen, und von Bestrahlungseinflüssen auf das Absorptions- und Lumineszenzspektrum des  $\text{CaF}_2$  studieren zu können, wurden homogen gewachsene, undotierte und definiert mit Fluoriden und Oxiden von 1-, 2-, 3-, 4- und 6-wertigen Kationen, insbesondere der Übergangselemente, Seltenen Erden und Aktiniden, dotierte  $\text{CaF}_2$ -Einkristalle gezüchtet.

Die undotierten  $\text{CaF}_2$ -Einkristalle wurden hergestellt durch zweimalige Einkristallzüchtung in Graphittiegel und Feinvakuum nach einem modifizierten Stockbarger-Bridgman-Verfahren (Neuhaus, 1951; Recker u. Liebertz, 1962). Ausgangsmaterial für die Erstzüchtung war  $\text{CaF}_2$ -Pulver vom Reinheitsgrad "für optische Zwecke", dem als Fluorierungsmittel 3 Gew.-%  $\text{PbF}_2$  und 2 Gew.-%  $\text{CdF}_2$  zugesetzt wurden. Der erhaltene Einkristall wurde wieder zerkleinert und nochmals unter Zusatz von Fluorierungsmittel zum Einkristall gezüchtet. Nach dieser Zweitzüchtung erfüllten die  $\text{CaF}_2$ -Einkristalle die

folgenden vier Reinheitskriterien: UV-Durchlässigkeit an der Meßgrenze (bei 200 m $\mu$ ) ca. 80–90%; keine selektive Absorption im Spektralbereich von 200 m $\mu$  bis 9  $\mu$  (IR-Absorptionskante), also OH-frei; Verfärbbarkeit durch Röntgenstrahlung auch bei stundenlanger Bestrahlung sehr gering; spektralanalytisch nachweisbare Fremdkationen nur Sr-Spuren (< 10 p.p.m.).

*Züchtung dotierter CaF<sub>2</sub>-Einkristalle.* Die Züchtung der dotierten CaF<sub>2</sub>-Einkristalle wurde nach dem Stockbarger-Verfahren im Hochvakuum durchgeführt. Als CaF<sub>2</sub>-Ausgangsmaterial dienten die durch zweimalige Vorzüchtung gewonnenen Einkristalle. Die Dotierungssubstanzen besaßen mindestens den Reinheitsgrad "p.a." oder wurden aus p.a.-Substanzen hergestellt. Tab. II enthält eine Auswahl der 200 bisher dotiert gezüchteten CaF<sub>2</sub>-Einkristalle mit Angabe ihrer Farbe, visueller Lumineszenz und Durchsichtigkeit.

TAB. II. Zusammenstellung einiger gezüchteter, dotierter CaF<sub>2</sub>-Einkristalle mit Angabe ihrer Farbe, visuellen Lumineszenz und Durchsichtigkeit. Dotierungen in Mol. %.

Kristall	Farbe	Durchsichtigkeit	Kristall	Farbe	Durchsichtigkeit
CaF <sub>2</sub> + 0,2 % NaF	farblos	wasserklar	CaF <sub>2</sub> + 0,1 % Sm <sub>2</sub> O <sub>3</sub>	stark grkn	leicht getrübt
CaF <sub>2</sub> + 1 % MgF <sub>2</sub>	farblos	wasserklar	CaF <sub>2</sub> + 0,1 % SmF <sub>3</sub>	grün	wasserklar
CaF <sub>2</sub> + 10 % CrF <sub>3</sub>	(s. schw. rotviol.)	wasserklar	CaF <sub>2</sub> + 0,1 % Eu <sub>2</sub> O <sub>3</sub>	farblos*	leicht getrübt
CaF <sub>2</sub> + 1 % MnF <sub>2</sub>	farblos	wasserklar	CaF <sub>2</sub> + 0,1 % EuF <sub>3</sub>	farblos†	wasserklar
CaF <sub>2</sub> + 1 % NiF <sub>2</sub>	farblos	wasserklar	CaF <sub>2</sub> + 0,1 % Ho <sub>2</sub> O <sub>3</sub>	schw. gelblich	leicht getrübt
CaF <sub>2</sub> + 0,1 % YF <sub>3</sub>	farblos	wasserklar	CaF <sub>2</sub> + 0,1 % ErF <sub>3</sub>	schw. rötlich	wasserklar
CaF <sub>2</sub> + 0,1 % Y <sub>2</sub> O <sub>3</sub>	farblos	leicht getrübt	CaF <sub>2</sub> + 1 % ThF <sub>4</sub>	farblos	wasserklar
CaF <sub>2</sub> + 0,1 % LaF <sub>3</sub>	farblos	wasserklar	CaF <sub>2</sub> + 0,1 % UF <sub>3</sub>	rot	wasserklar
CaF <sub>2</sub> + 0,1 % La <sub>2</sub> O <sub>3</sub>	farblos	leicht getrübt	CaF <sub>2</sub> + 0,1 % UF <sub>4</sub>	grün	wasserklar
CaF <sub>2</sub> + 0,1 % CeF <sub>3</sub>	farblos	wasserklar	CaF <sub>2</sub> + 0,1 % CaUO <sub>4</sub>	braungelb‡	z.T. leicht getrübt
CaF <sub>2</sub> + 0,1 % Nd <sub>2</sub> O <sub>3</sub>	s. schw. rotviol.	leicht getrübt			

\* Stark blaue visuelle Lumineszenz bei UV-Bestrahlung.

† Blaue visuelle Lumineszenz bei UV-Bestrahlung.

‡ Gelbgrüne visuelle Lumineszenz bei UV-Bestrahlung.

Von den gezüchteten CaF<sub>2</sub>-Einkristallen sind nur die mit Cr-, Nd-, Sm-, Er-, Ho- und U-Salzen dotierten visuell gefärbt, und zwar sind die Cr-dotierten sehr schwach rotviolett, die Nd-dotierten violett, die Sm-dotierten grün, die Er-dotierten rötlich, die Ho-dotierten gelblich, die UF<sub>3</sub>-dotierten rot, die UO<sub>2</sub>-dotierten rotviolett, die UF<sub>4</sub>-dotierten grün und die CaUO<sub>4</sub>-dotierten braungelb.

Visuelle Lumineszenz zeigen bei UV-Bestrahlung (Hg-Lampe) nur die mit Eu-, Tb- und U(VI)-Salzen dotierten CaF<sub>2</sub>-Einkristalle. Sämtliche mit Oxiden dotierten CaF<sub>2</sub>-Kristalle weisen geringe Trübung auf, deren Stärke von der Dotierungsmenge abhängt, während alle mit Fluoriden dotierten CaF<sub>2</sub>-Kristalle klar durchsichtig sind.

*Absorptions- und Lumineszenzspektren dotierter CaF<sub>2</sub>-Einkristalle.* Von den dotierten CaF<sub>2</sub>-Einkristallen wurden mit dem Beckman DK2-Spektralphotometer im Bereich von 200–2700 m $\mu$  Absorptionsspektren und im Bereich von 400–800 m $\mu$  Lumineszenzspektren aufgenommen. Hierbei wiesen die (und nur die) mit Seltenen Erden oder U-Salzen dotierten Kristalle selektive Absorption auf. Die mit Nd-, Dy-, Ho- und Er-Salzen dotierten CaF<sub>2</sub>-Einkristalle zeigen zahlreiche schwache, scharfe Linien. Letztere sind nach Weybourne (1965) charakteristisch für dreiwertige Seltene Erden, sodaß Nd, Dy, Ho und Er im

3-wertigen Valenzzustand im  $\text{CaF}_2$  vorliegen müssen. Die mit Eu-, Yb-, Ce- und Tb-Salzen dotierten  $\text{CaF}_2$ -Einkristalle hingegen besitzen Absorptionsspektren mit starken breiten Maxima teils im Sichtbaren, teils im UV, sodaß für diese Dotierungselemente im  $\text{CaF}_2$  die 2-wertige Valenzstufe anzunehmen ist. Die mit Pr- und Sm-Salzen dotierten  $\text{CaF}_2$ -Einkristalle besitzen Absorptionsspektren, die sowohl starke breite Maxima als auch schwächere scharfe Linien aufweisen. Bei ihnen liegen somit 2- und 3-wertige Valenzzustände der entsprechenden Seltenen Erden vor. Die mit Verbindungen des 3-, 4- oder 6-wertigen Urans dotierten  $\text{CaF}_2$ -Einkristalle besitzen sehr komplexe Spektren mit zahlreichen teils sehr scharfen, teils breiten Maxima im UV, Sichtbaren und IR, die sich in Abhängigkeit von Dotierungssubstanz und Zuchtbedingungen in Anzahl, Lage und Intensitäten unterscheiden.

Lumineszenzspektren lieferten die mit Ce-, Eu-, Tb-, Dy-, Er- und U(VI)-Salzen dotierten  $\text{CaF}_2$ -Einkristalle.

*Absorptionsspektren röntgenbestrahlter reiner und dotierter  $\text{CaF}_2$ -Einkristalle.* Die gezüchteten reinen und dotierten  $\text{CaF}_2$ -Einkristalle wurden zur Erzeugung von Farbzentren nacheinander erst 2, dann 10, dann 30 und schließlich 500 min mit Röntgenlicht durchstrahlt (Cu-Strahlung, 45 kV, 15 mA). Nach jeder Bestrahlung wurde das Absorptionsspektrum im Bereich von 200–2700  $m\mu$  aufgenommen. Abb. 2 zeigt als Beispiel einige Absorptionsspektren dieser bestrahlten  $\text{CaF}_2$ -Kristalle im Bereich von 200–700  $m\mu$ , und zwar  $\text{CaF}_2$  ohne Zusatz,  $\text{CaF}_2(\text{Na})$ ,  $\text{CaF}_2(\text{Mg})$ ,  $\text{CaF}_2(\text{Y})$ .

Die aufgenommenen Absorptionsspektren wurden miteinander verglichen. Einige Ergebnisse:

In Abhängigkeit von Dotierungssubstanz und Bestrahlungsdosis entstehen die verschiedenartigsten Absorptionsspektren mit Maxima im UV, Sichtbaren und nahen IR. Entsprechend treten auch zahlreiche verschiedene visuelle Färbungen auf. Diese Spektren ließen sich bisher jedoch noch nicht syste-

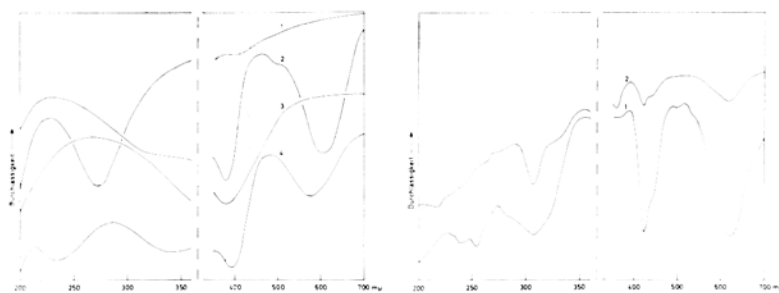


ABB. 2 u. 3: ABB. 2 (links). Absorptionsspektren synthetischer, röntgenbestrahlter  $\text{CaF}_2$ -Einkristalle. Kurve 1,  $\text{CaF}_2$  ohne Zusatz (Bestr. 64 h.); Kurve 2,  $\text{CaF}_2$  mit 0.2% NaF (Bestr. 10 m.); Kurve 3,  $\text{CaF}_2$  mit 1%  $\text{MgF}_2$  (Bestr. 500 m.); Kurve 4,  $\text{CaF}_2$  mit 0.1%  $\text{YF}_3$  (Bestr. 10 m.). ABB. 3 (rechts). Absorptionsspektren von  $\text{CaF}_2$ -Einkristallen. Kurve 1,  $\text{CaF}_2$ , synth., + 0.1%  $\text{Sm}_2\text{O}_3$ ; Kurve 2, Naturfluorit, Dalcoath mine, grün.

matisieren, was wiederum auf die ungewöhnliche Komplexität der Farb- und Lumineszenzphänomene dotierter  $\text{CaF}_2$ -Kristalle hinweist. Im einzelnen:

Alle mit Oxiden dotierten  $\text{CaF}_2$ -Kristalle zeigen nach der Bestrahlung Absorptionsspektren, die sich in ihrer Struktur weitgehend gleichen. Diesen Spektrentyp möchten wir deshalb Sauerstoffionen im  $\text{CaF}_2$ -Gitter zuordnen. Adler und Kveta (1957) erhielten ähnliche Spektren von farblosen natürlichen Fluoriten, die sie im Sauerstoffstrom erhitzt hatten. Die Bestrahlungsspektren der mit Alkalifluoriden dotierten  $\text{CaF}_2$ -Kristalle zeigen vor allem zwei Absorptionsmaxima; die Bestrahlungsspektren der mit  $\text{MgF}_2$  und  $\text{SrF}_2$  dotierten  $\text{CaF}_2$ -Kristalle besitzen ein Maximum bei ca.  $380 \text{ m}\mu$ ; die Bestrahlungsspektren der mit dreiwertigen Selten-Erd-Fluoriden dotierten  $\text{CaF}_2$ -Kristalle weisen die Maxima der zweiwertigen Valenzstufe dieser Seltenen Erden auf. Die Seltenen Erden wurden hiernach also durch die Bestrahlung reduziert.

*Synopsis der Absorptions- und Lumineszenzspektren der natürlichen und synthetischen Calciumfluoride*

Die Absorptions- und Lumineszenzspektren der untersuchten natürlichen und synthetischen, undotierten und dotierten, unbestrahlten und röntgenbestrahlten Flußspäte wurden miteinander verglichen. Einige der verglichenen Spektren sind in den Abb. 3–5 wiedergegeben.

Ergebnisse dieser Spektrenvergleiche:

Die Absorptionsspektren der grün gefärbten Naturfluorite sind identisch mit den Absorptionsspektren der gezüchteten  $\text{Sm}^{2+}$ -haltigen  $\text{CaF}_2$ -Einkristalle. Die grüne Farbe der Naturfluorite dürfte also durch zweiwertiges Sm im  $\text{CaF}_2$  hervorgerufen werden (Abb. 3).

Der UV-Teil des Absorptionsspektrums der roten Naturfluorite ist identisch mit den Absorptionsspektren der gezüchteten  $\text{Yb}^{2+}$ -haltigen  $\text{CaF}_2$ -Einkristalle

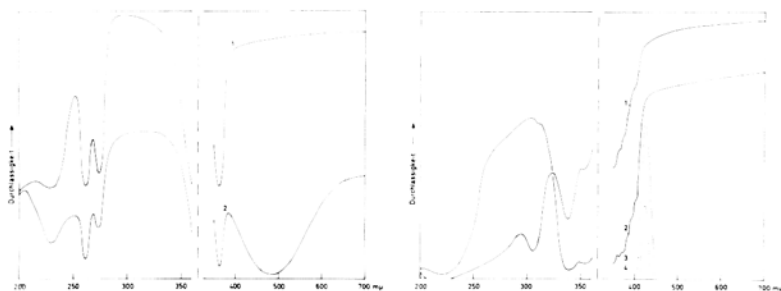


ABB. 4 u. 5: ABB. 4 (links). Absorptionsspektren von  $\text{CaF}_2$ -Einkristallen. Kurve 1,  $\text{CaF}_2$  synth. + 0.1%  $\text{Yb}_2\text{O}_3$ ; Kurve 2, Naturfluorit, Göschenen, rot. ABB. 5 (rechts). Absorptions- und Lumineszenzspektren von  $\text{CaF}_2$ -Einkristallen. Kurve 1, Absorptionsspektrum von  $\text{CaF}_2$  synth. + 0.1%  $\text{Eu}_2\text{O}_3$ ; Kurve 2, Absorptionsspektrum von Naturfluorit, Weardale, farblos; Kurve 3, Lumineszenzspektrum von Naturfluorit, Weardale, farblos; Kurve 4, Lumineszenzspektrum von  $\text{CaF}_2$  synth. + 0.1%  $\text{Eu}_2\text{O}_3$ .

(Abb. 4). Die UV-Maxima in den Spektren der roten Naturfluorite können somit auf einem diadochen Einbau von zweiwertigem Yb beruhen. Das  $\text{Yb}^{2+}$  ist jedoch nicht für die rote Farbe verantwortlich! Diese ist eine Strahlungsverfärbung, deren Farbzentrenart noch nicht geklärt ist. Die gleichen UV-Maxima treten auch in den Absorptionsspektren vieler farbloser und verschieden gefärbter Naturfluorite auf, sodaß auch in diesen Fluoriten  $\text{Yb}^{2+}$  vorliegen dürfte.

Die blau fluoreszierenden Naturfluorite besitzen Absorptions- und Lumineszenzspektren, die denen der gezüchteten  $\text{Eu}^{2+}$ -haltigen  $\text{CaF}_2$ -Einkristalle sehr gleichen (Abb. 5). Die blaue Fluoreszenz dieser Fluorite und ihre UV-Absorption kann somit auf zweiwertiges Eu zurückgeführt werden.

Die Farbe der gelben Naturfluorite wird, obwohl thermisch ausbleichbar, wahrscheinlich nicht durch "Farbzentren" verursacht, da die Struktur der zugehörigen Absorptionsbande (Elektronenbandenspektrum) das Vorliegen eines noch nicht bekannten Komplexes nahelegt.

Auch deutlich Uran-haltige Naturflußspäte weisen kein Absorptions- oder Lumineszenzspektrum auf, das denen der gezüchteten  $\text{U}^{3+}$ -,  $\text{U}^{4+}$ - oder  $\text{U}^{6+}$ -haltigen  $\text{CaF}_2$ -Einkristalle wesentlich gleicht. Uran-Ionen spielen als direkte Farb- oder Lumineszenzursache der Naturfluorite somit offenbar keine Rolle.

Wie bei den roten, so ist auch bei den hellblauen und violetten Naturfluoriten die Art der farbgebenden Bestrahlungszentren noch nicht bekannt. Einige Maxima in den Absorptionsspektren dieser Kristalle entsprechen jedoch in der Lage den Maxima von Absorptionsspektren synthetischer, röntgenbestrahlter Fluorite mit Gehalten an nicht farbgebenden Fremdionen.

Der Deutschen Forschungsgemeinschaft möchten wir an dieser Stelle für die Bereitstellung der Spektralphotometer (Beckman DK 2 und Cary 14 R) herzlich danken.

#### Literatur

- ADLER (H.) und KVETA (I.), 1957. *Sitzungsber. Österr. Akad. Wiss., Math.-Naturwiss. Kl.*, Bd. **166**, s. 199.  
 ——— 1958. *Ibid.*, Bd. **167**, s. 213.  
 ——— 1959. *Acta Physica Austriaca*, Bd. **12**, s. 356.  
 FEOFILOV (P. P.), 1958. *Chem. Zentr.*, Bd. **15**, s. 4088.  
 HEGEMANN (F.) und WILK (G. W.), 1964. *Neues Jahrb. Min., Monatsh.*, s. 147.  
 MONTORIOL (P. J.), SAN MIGUEL (A.), und FONT ALTABA (M.), 1962. *Amer. Min.*, Bd. **47**, s. 200.  
 NEUHAUS (A.), 1956. *Chem. Ing. Techn.*, s. 155–161 u. 350–365.  
 PRZIBRAM (K.), 1953. *Verfärbung und Lumineszenz*. Springer Verlag, Wien.  
 RECKER (K.), 1961. *Fortschr. Min.*, Bd. **39**, s. 72.  
 ——— 1962. *Ber. geol. Gesell.*, Bd. **7**, s. 515.  
 ——— 1963. *Zeits. Krist.*, Bd. **118**, s. 161.  
 ——— und LIEBERTZ (J.), 1962. *Naturwiss.*, Bd. **49**, s. 391.  
 SCHULMAN (J. H.) und COMPTON (W. D.), 1962. *Color Centers in Solids*. Pergamon Press, London.  
 WEYBOURNE (B. G.), 1965. *Spectroscopic Properties of Rare Earths*. Interscience Publishers, London.

## Thermodynamique et cinétique de formation d'une texture par nucléation dans un champ de tension

M. BIENFAIT et R. KERN

Laboratoire de Minéralogie-Cristallographie,  
Université de Marseille, France

*Summary.* The authors have studied the mechanisms of the formation of a crystalline texture through the nucleation of a new phase. When a tension field is applied to material that is in the process of phase-transformation or of chemical reaction, the equilibrium form of the new-forming crystals is very sensitive to the orientation of the crystal relative to the field. Moreover, the activation energy of germination, which is controlled by the kinetics of the formation of the new phase, is itself very sensitive to this form. Thus the germs of the new phase that appear in such a field suffer a selection according to their crystal orientation relative to that of the field; from this there can result a texture through nucleation.

The values that enter into such a process are essentially: the magnitude and the sign of the variation of the molar volume  $\Delta V$  during the reaction or the change of phase; the sign and the anisotropy of the principal axes of the field. The elastic energy contained in the new phase is of negligible magnitude within the elastic limit.

One can take it as a rule that for a negative tension field (i.e. positive pressure), the equilibrium form of the crystal has its faces normal to the field when  $\Delta V < 0$ ; during the nucleation crystals are favoured in growth when they have their largest surface normal to the field. When  $\Delta V > 0$ , or when the tension field is positive, the opposite takes place.

*Résumé.* Les auteurs s'intéressent aux mécanismes de formation d'une texture cristalline par nucléation d'une nouvelle phase. Lorsqu'un champ de tension est appliqué à une matrice qui est le siège d'une transformation de phase ou d'une réaction chimique, la forme d'équilibre des cristaux qui naissent est très sensible à l'orientation relative du cristal par rapport au champ de tension. Par ailleurs, l'énergie d'activation de germination, qui dicte la cinétique de formation de la nouvelle phase, est elle-même très sensible à cette forme. Ainsi les germes de la nouvelle phase qui apparaît dans un champ de tension, subissent-ils une sélection suivant l'orientation relative des cristaux dans le champ. Il peut en résulter une texture par nucléation.

Les grandeurs qui interviennent dans un tel processus sont essentiellement, la valeur et le signe de la variation du volume molaire  $\Delta V$  durant la réaction ou le changement de phase, le signe et l'anisotropie des tensions principales. L'énergie élastique emmagasinée par la nouvelle phase est une grandeur négligeable dans le domaine de limite élastique.

On peut retenir comme règle que pour une tension négative (surpression positive) la forme d'équilibre du cristal voit ses faces normales à la tension se développer si  $\Delta V < 0$ . Durant la nucléation sont favorisés les cristaux qui présentent leur plus grande surface à la tension. Il se produit l'inverse, si  $\Delta V > 0$ , ou si la tension est positive.

UNE texture, c'est à dire l'orientation privilégiée des cristaux dans une matrice, peut avoir plusieurs origines. Elle peut être causée par une sédimentation, un écoulement plastique, une épitaxie, un champ de tension élastique, etc. Dans cette étude, nous nous intéressons seulement à ce dernier cas, c'est à dire l'orientation qu'un cristal peut acquérir à la suite d'une déformation élastique

lorsqu'une tension (pression anisotrope) agit sur lui par l'intermédiaire d'une matrice.

La formulation thermodynamique du problème remonte à Gibbs (1875-1878) et elle a été reprise par MacDonald (1957; 1960; 1961) et Kamb (1959; 1961a, b). D'une manière générale un cristal placé dans un champ de tension voit son potentiel chimique modifié par "l'énergie élastique" emmagasinée. Ce potentiel chimique dépend, d'une part de l'orientation du cristal dans le champ, d'autre part, pour une orientation donnée du cristal, de la face cristalline considérée.

MacDonald et Kamb adoptent au départ deux points de vue différents.<sup>1</sup> Le premier considère un système sur lequel agit une tension constante et le second choisit le cas d'une déformation constante. Les équilibres qui en résultent sont de ce fait complémentaires les uns des autres; c'est à dire dans le premier cas, l'équilibre est réalisé pour le maximum de l'énergie élastique et dans le second pour le minimum (Nye 1961). Ces cas correspondent à deux problèmes physiques différents. La tension constante décrit, par exemple, le cas d'un cristal sur lequel repose librement un poids. La déformation constante est réalisée, par exemple, lorsque ce cristal est serré d'une manière définitive entre les mâchoires d'un étau. Il est évident que dans la nature ces deux cas pourraient exister.

Kamb applique ses équations à plusieurs minéraux dont le quartz. Les résultats qu'il obtient sont en accord avec certaines textures observées dans la nature. Les calculs de Kamb ont été repris par Hartman et den Tex (1966) et appliqués à l'olivine. Là encore, les résultats permettent d'expliquer certaines textures naturelles de l'olivine. Les résultats de MacDonald ont été appliqués par Brace (1960) à l'étude théorique des textures du quartz, de la calcite, et de la glace.

Cependant l'anisotropie de "l'énergie élastique" est faible lorsque change l'orientation du cristal. La différence d'énergie pour deux orientations différentes du cristal par rapport aux tensions est inférieure à 1 cal. mole<sup>-1</sup> si une surpression uniaxiale de 10<sup>3</sup> Kg. cm<sup>-2</sup> agit sur le cristal. Cette valeur très faible semble difficilement pouvoir assurer une orientation du cristal.

C'est pourquoi nous avons complètement reformulé le problème thermodynamique de la formation d'un cristal dans un champ de tension. Nous nous posons la question suivante: *Peut-il y avoir une sélection en orientation des germes pendant la nucléation dans une matrice solide supportant une tension anisotrope constante?*

#### *Thermodynamique*

*Formulation.* Lorsqu'une tension anisotrope constante agit sur un cristal qui modifie sa taille et sa forme, la variation d'enthalpie libre s'écrit:<sup>2</sup>

$$dG = -V \epsilon_{uv} df_{uv} + V dP + \mu dn + \sigma ds \quad \text{à } T, C^e \quad (1)$$

<sup>1</sup> MacDonald, par ailleurs, omet de tenir compte de la variation de volume molaire avec la direction des tensions.

<sup>2</sup> Nous utilisons à quelques variantes près ( $f_{uv}$  au lieu de  $\sigma_{uv}$  pour le tenseur des tensions) les notations de Nye (1961).

où  $V$ ,  $s$ ,  $n$  sont le volume, la surface, le nombre de particules;  $\epsilon_{uv}$ ,  $f_{uv}$  sont les tenseurs des déformations et des tensions;  $\mu$ ,  $P$ ,  $\sigma$  sont le potentiel chimique, la pression, l'enthalpie libre spécifique de surface.

La relation (1) étant une différentielle totale exacte on a :

$$(\partial\mu/\partial f_{uv})_{n, s, T} = -(\partial V \epsilon_{uv} / \partial n)_{f_{uv}, s, T} = -\epsilon_{uv} \Omega \quad (2)$$

$$(\partial\mu/\partial P)_{n, s, T} = (\partial V / \partial n)_{f_{uv}, s, T} = \Omega = \Omega_0(1 + \epsilon_{uv}) \quad (3)$$

où  $\Omega$  est le volume d'une particule du cristal subissant la tension,  $\Omega_0$  le volume de la même particule sans tension.

Lorsque le cristal échange un seul constituant avec une matrice solide homogène qui l'entoure, la variation d'enthalpie libre comprend deux contributions, l'une volumique, l'autre de surface :

$$dG = \sum_{\alpha} \sum_j \mu_j^{\alpha} dn_j^{\alpha} + \sum_j \sigma_j ds_j \quad (4)$$

La phase  $\alpha$  est soit le cristal ( $c$ ), soit la matrice ( $m$ ). L'indice  $j$  caractérise les propriétés des faces  $j$  du cristal.

A l'aide de (2) et (3) nous explicitons (4), en admettant que la loi de Hooke est vérifiée, soit  $\epsilon_{uv} = s_{uvkl} f_{kl}$  avec  $s_{uvkl}$  les coefficients d'élasticité, et que  $f_j = -P_j$  est la tension (surpression au dessus de 1 atmosphère) dans la direction  $j$ , perpendiculaire à la face  $j$ :

$$dG = \sum_j [W_{el}^c - W_{el}^m - f_j(\Omega^c - \Omega^m) - \Delta\mu] dn_j^c + \sum_j \sigma_j ds_j \quad (5)$$

où l'énergie élastique par particule du cristal  $W_{el}^c$  vaut  $-\frac{1}{2}s_{uvkl}f_{uvkl}\Omega^c$  et  $W_{el}^m$  est l'énergie élastique dans la matrice.  $\Delta\mu = \mu^m - \mu^c$  est la différence de potentiel chimique en l'absence de tension entre la matrice et un cristal semi-infini, c'est à dire, un cristal ne présentant pas de variation de surface lorsqu'il augmente son volume;  $\Delta\mu$  est alors le dépassement ou la sursaturation thermodynamique. L'équation (5) décrit toutes les propriétés de notre système. On voit que l'action d'un champ de tension modifie le dépassement ou la sursaturation d'une quantité  $W_{el}^c - W_{el}^m - f_j(\Omega^c - \Omega^m)$ .

*Equilibres.* On peut décomposer la condition d'équilibre en deux conditions partielles, l'une donnant un équilibre relatif pour une *orientation quelconque* du cristal :

$$(\partial G / \partial a_{um})_{n^c, s_j} = 0, \quad (6)$$

où  $a_{um}$  sont les cosinus directeurs du repère des tensions, l'autre donnant un équilibre relatif pour une *orientation donnée*,

$$(\partial G / \partial s_j)_{a_{um}} = 0. \quad (7)$$

Cette dernière condition donne la forme d'équilibre du cristal.

Pour un polyèdre convexe dont les faces ont des distances centrales  $h_j$ , on a

$$dn_j^c = (h_j ds_j) / 2\Omega^c \quad (8)$$

La relation (5) peut être transformée et la condition (7) donne avec (8) selon une méthode analogue à celle de Volmer (1939):

$$\sigma_j/h_j = \Delta\mu/2\Omega^c + f_j\Delta\Omega/2\Omega^c - \Delta W_{el}/\Omega^c = b_j \quad (9)$$

avec  $\Delta\Omega = \Omega^c - \Omega^m$ ;  $\Delta W_{el} = W_{el}^c - W_{el}^m$

La relation (9) indique que pour une orientation donnée du cristal, l'équilibre est réalisé lorsque les énergies interfaciales compensent sur chaque face le potentiel chimique que cette face subit sous l'effet de la tension. La forme d'équilibre du cristal ne dépend plus seulement des énergies interfaciales, mais aussi du champ de tension.

La forme d'équilibre du cristal peut être construite de la manière suivante. Selon (9) on porte suivant les normales à toutes les faces imaginables  $j$  du cristal des vecteurs de module  $\sigma_j/b_j$ ; on mène les plans perpendiculaires à ces vecteurs, ce qui donne un ensemble de polyèdres concentriques. Le plus petit polyèdre est la forme d'équilibre.<sup>1</sup>

*Effet du champ de tension sur la forme d'équilibre.* Considérons un cristal se formant dans une matrice solide homogène par changement de phase ou réaction chimique. A titre d'exemple, étudions la modification de faciès sous

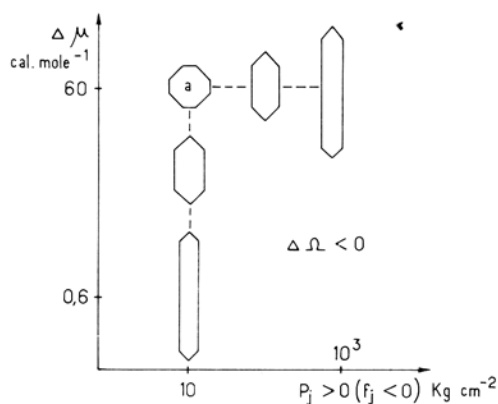


FIG. 1. Influence de la tension sur la forme d'équilibre d'un cristal; tension dirigée suivant l'abscisse, ordonnée sursaturation.

l'influence d'une tension uniaxiale d'un cristal cubique, composé d'une forme  $\{10\}$  et d'une forme  $\{11\}$  (on pose  $\sigma_{10}/\sigma_{11} \sim 1$ —fig. 1 en (a)). Nous prenons une valeur usuelle de  $\Delta V = N\Delta\Omega = -3 \text{ cm}^3$  ( $N$  nombre d'Avogadro). Nous faisons d'abord le calcul quand la tension est fixe ( $f_j < 0$ ;  $P_j > 0$ ) dirigée suivant l'abscisse de la fig. 1 et quand  $\Delta\mu$  varie; le cristal s'allonge aux faibles sursaturations  $\Delta\mu$ , perpendiculairement à la tension uniaxiale. Ensuite, le calcul est établi quand  $\Delta\mu = C^{te}$  et  $P_j$  varie en intensité (fig. 1). Il y a encore allongement pour les fortes tensions, dans une direction normale à l'axe de la tension uniaxiale.

Notons que pour les mêmes tensions l'allongement du cristal est inversé si le changement de phase ou la réaction a lieu avec  $\Delta\Omega > 0$ .

Le calcul numérique permet de montrer aussi que pour les sursaturations et les tensions utilisées  $\Delta\mu$  et  $f_j\Delta\Omega$  sont du même ordre de grandeur. Par contre,

<sup>1</sup> La relation (9) et la construction invoquée se simplifient en  $\sigma_j/h_j = \Delta\mu/2\Omega^c$  lorsqu'il n'y a pas de tension. Cette relation est appelée théorème de Wulff (Wulff, 1901; Volmer, 1939; Herring, 1951).

le terme  $\Delta W_{el}$  est toujours négligeable sauf au voisinage de la limite d'élasticité du cristal (usuellement  $f_j \sim 10^4 \text{ Kg. cm}^{-2}$ ).

### Cinétique de Nucléation

Considérons un milieu fermé homogène subissant une tension anisotrope et contenant  $n_0$  particules d'un constituant à partir duquel se forme le cristal. La sursaturation initiale  $\Delta\mu_0$  est définie, si les phases sont parfaites, par la relation:

$$\Delta\mu_0 = kTLn(n_0/n_\infty), \quad (10)$$

où  $n_\infty$  est la concentration dans le système à saturation du constituant qui forme le cristal ( $k$  est la constante de Boltzmann,  $T$  la température).

Lorsque le cristal a atteint une taille  $n^c$ , la sursaturation du système vaut seulement:

$$\Delta\mu = kTLn(n_0 - n^c/n_\infty). \quad (11)$$

*Germe critique.* Nous cherchons à expliciter  $dG$  en fonction de la seule variable  $n^c$ . C'est pourquoi nous introduisons (11) dans (5). Mais il reste à trouver une relation liant  $s_j$  à  $n^c$  et une autre relation liant  $n_j^c$  à  $n^c$ . Nous utilisons pour cela deux facteurs géométriques  $c_j$  et  $c'_j$  qui sont définis, pour une forme donnée du cristal, par les relations

$$s_j = (n^c)^{2/3} c_j \quad (12)$$

et

$$c'_j = dn_j^c/dn^c. \quad (13)$$

On obtient alors à l'aide de (5), (11), (12), (13) la valeur  $dG(n^c)/dn^c$

$$dG(n^c)/dn^c = \Delta W_{el} - \sum_j f_j c'_j \Delta\Omega - kTLn(n_0 - n^c)/n_\infty + \frac{2}{3}(n^c)^{-1/3} \sum_j \sigma_j c_j \quad (5')$$

On peut, après avoir intégré (5') tracer la variation d'enthalpie libre  $\Delta G(n^c)$  lorsque se forme le cristal (voir Bienfait et Kern, 1964; Bienfait, 1966).

Cette équation est représentée fig. 2. Elle montre qu'il existe un *équilibre stable* de taille  $n_E$  et un *équilibre instable* qui correspond au germe critique de taille  $n^*$ . Pour les deux équilibres ( $n^*$  et  $n_E$ ) l'équation (9) donnant la forme d'équilibre du cristal est vérifiée. Les valeurs de  $n^*$  et de  $n_E$  sont dérivées dans un appendice.

*Fréquence de germination.* Le germe critique  $n^*$  nécessite pour se former une énergie de germination  $\Delta G^*$  (fig. 2) qui est établie à partir de (5') en introduisant dans cette équation la valeur de  $n^*$ :

$$\Delta G^* = 4/27(\sum_j \sigma_j c_j)^3 / (\Delta\mu - \Delta W_{el} + \sum_j f_j c'_j \Delta\Omega)^2 \quad (14)$$

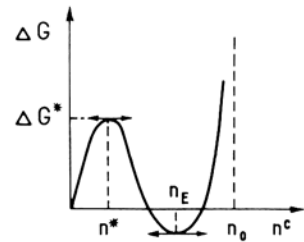


FIG. 2. Variation de l'enthalpie libre de formation d'un cristal.  $n^*$  et  $n_E$  dimensions du germe critique et du cristal à l'équilibre absolu.

Dans cette équation la forme du cristal intervient par les deux facteurs géométriques  $c_j$  et  $c'_j$ .

Cette énergie d'activation de germination  $\Delta G^*$ , permet de calculer la fréquence de germination  $J$ . Selon Turnbull (1949) on a dans un système condensé:

$$J = (nkT/h) \exp(-U^*/kT) \exp(-\Delta G^*/kT) \quad (15)$$

où  $n$  est le nombre de particules du constituant dans le milieu fermé,  $U^*$  une énergie d'activation de diffusion,  $h$  la constante de Planck et  $kT/h$  une constante qui est de l'ordre de  $10^{13} \text{ sec}^{-1}$ .

A l'aide de (14) on peut calculer (15) c'est à dire la fréquence de germination dans la matrice. Nous avons vu en haut que  $\Delta\mu$  est habituellement du même ordre de grandeur que  $f_j\Delta\Omega$  et que  $\Delta W_{el}$  est négligeable. Ici, on a toujours  $\Delta\mu$  du même ordre que  $\sum_j f_j c'_j \Delta\Omega$ . On peut donc escompter un effet de la forme du cristal, par l'intermédiaire de  $c_j$  et  $c'_j$  sur la fréquence de germination. Mais avant de développer cette question il faut s'assurer que l'ordre de grandeur de  $J$  est raisonnable. Si ce n'est pas le cas, la phase nouvelle (le cristal) ne pourra apparaître dans la matrice. En prenant  $T = 3 \cdot 10^2 \text{ }^\circ\text{K}$ ,  $\sum_j \sigma_j c_j = 10^{-13} \text{ erg}$  (énergie interfaciale de la plupart des substances minérales),  $\Delta\mu + \sum_j f_j c'_j \Delta\Omega = 150 \text{ cal}$ . (sursaturation usuelle pour les phases solides),  $U^* = 40 \text{ Kcal mole}^{-1}$ , on trouve que pour un milieu fermé contenant une mole du constituant qui forme les cristaux, la fréquence de germination est de l'ordre de  $J \sim 10^{-2} \text{ germes sec}^{-1}$ . Puisque la germination existe dans la matrice qui subit la tension, il reste à préciser les effets de la forme du cristal sur la fréquence de germination. Cette forme, comme nous le verrons par la suite, est responsable de l'orientation privilégiée des germes.

### Exemples

Rappelons que l'anisotropie des propriétés élastiques (énergie élastique  $W_{el}^c$ , volume molaire  $N\Omega^c$ ) est excessivement faible. Elle est toujours inférieure à une calorie par mole; ce qui est négligeable devant les sursaturations habituelles, de l'ordre d'une centaine de calories, qui conduisent effectivement à une germination.

Par contre, l'effet de la forme qui est appréciable est la cause de la sélection des germes pendant la nucléation. Considérons d'abord l'exemple simple d'un cristal tabulaire, le cas d'un cristal aciculaire s'en déduisant immédiatement.

*Cristal tabulaire.* Un cristal tabulaire est placé dans deux positions différentes par rapport à une tension uniaxiale  $f_0$ . Dans la première position, la face principale est normale à la tension. Puisque  $c'_j$  est selon (13) le nombre relatif de particules sur la face  $j$ , on a  $\sum_j f_j c'_j \simeq f_0$ . Dans la seconde orientation la face principale est parallèle à la tension; on a dans ce cas  $f_j c'_j \simeq 0$ . L'effet de l'orientation n'est alors plus négligeable car on a vu que  $f_j \Delta\Omega$  est du même ordre

de grandeur que  $\Delta\mu$ . Calculons le rapport des fréquences de germination dans le 1<sup>er</sup> et le 2<sup>ème</sup> cas. Suivant (15) on a

$$J_1/J_2 = \exp -(\Delta G_1^* - \Delta G_2^*)/kT \quad (16)$$

Nous développons les calculs grâce à (14). On prend à nouveau  $T = 3 \cdot 10^2$  °K,  $\Sigma \sigma_j c_j = 10^{-13}$  erg,  $N\Delta\Omega = -3$  cm<sup>3</sup>,  $f_0 = -10^3$  Kg cm<sup>-2</sup>. Si on pose dans un premier calcul  $N\Delta\mu = 60$  cal. mole<sup>-1</sup>, puis dans un second  $N\Delta\mu = 300$  cal. mole<sup>-1</sup>, on trouve respectivement  $J_1/J_2 = 10^6$  et  $10^2$ . Suivant la valeur de  $\Delta\mu$ , la fréquence de germination des cristaux qui ont leur face principale normale à la pression uniaxiale est  $10^6$  ou  $10^2$  fois plus grande que celle de ceux dont la face principale est parallèle à l'axe de pression. On voit que, pour une tension donnée, l'effet très sensible à la sursaturation.

On conçoit que de cette manière, il puisse y avoir orientation privilégiée des germes dans la matrice. Il faut noter que l'orientation est due à la forme des germes et non aux propriétés élastiques des cristaux.

*Cristal hexagonal.* On recherche maintenant l'orientation sous tension uniaxiale d'un cristal prismatique hexagonal  $\{11\bar{2}0\}$  limité par une bipyramide  $\{11\bar{2}1\}$  (fig. 3a, b). Ce modèle ressemble grossièrement à un cristal de quartz. On détermine la fréquence relative de germination selon (14), (15), et (16) pour les deux zones  $[10\bar{1}0]$  et  $[0001]$  qui sont dessinées fig. 3a, b; la direction de la pression principale est donnée dans chaque cas par l'angle  $\omega$  (fig. 3a) ou  $\psi$  (fig. 3b). (On admet pour simplifier les calculs numériques que dans la direction perpendiculaire au dessin, les faces sont infiniment développées).

On procède comme suit. La forme d'équilibre sans champ est indiquée sur les fig. 3a, b. On détermine pour chaque orientation la modification de cette

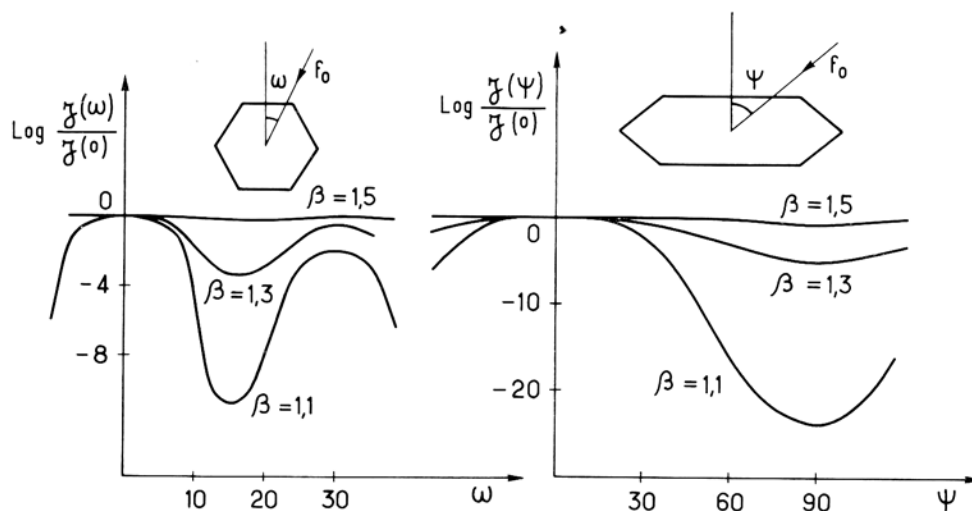


FIG. 3a, 3b. Fréquence de germination d'un cristal prismatique hexagonal surmonté d'une pyramide hexagonale en fonction de l'orientation du champ de tension uniaxiale.

forme d'équilibre sous l'action de la pression uniaxiale à l'aide de la construction géométrique indiquée en haut (p. 156). Cela permet d'évaluer les coefficients  $c_j$  et  $c'_j$ . Les valeurs numériques utilisées pour développer le calcul sont les suivantes: pression principale  $f_0 = 10^3 \text{ Kg. cm}^{-2}$ ,  $\sigma$  de la face du prisme  $= 100 \text{ erg. cm}^{-2}$ ,  $\sigma$  de la bipyramide  $= 200 \text{ erg. cm}^{-2}$ ,  $T = 3 \cdot 10^2 \text{ }^\circ\text{K}$ ,  $N\Delta\Omega = -3 \text{ cm}^3$ . On trace les fréquences relatives  $J(\omega)/J(0)$  pour diverses orientations du cristal par rapport à la pression principale et pour différents dépassements initiaux  $\Delta\mu_0 = kTLn(n_0/n_x) = kTLn\beta$  avec  $\beta = 1.1; 1.3; 1.5$ . Les résultats sont résumés fig. 3a, b.

La fig. 3a montre que pour la zone [0001], une orientation privilégiée existe de manière à ce que la face du prisme soit perpendiculaire à la pression principale ou, dans une moindre mesure, fasse un angle de  $30^\circ$  avec elle; ces orientations ne sont pas strictes; il y a une certaine latitude autour des directions précitées. Si  $\beta > 1.5$ , il n'y a plus d'effet dû à la tension. (Les germes critiques ont d'ailleurs, pour cette sursaturation, des dimensions atomiques).

La figure 3b montre les mêmes courbes que précédemment mais pour la zone [1100]. Il existe une fréquence de germination maximum lorsque la pression principale a une direction voisine (à  $\pm 20^\circ$ ) de la normale à la face du prisme.

Donc, si de tels cristaux se forment à partir d'une matrice solide subissant une tension uniaxiale, la fréquence de germination des cristaux ayant une face de prisme normale (ou voisine de la normale) à la pression principale sera bien plus élevée que celle des cristaux ayant une position différente. Il s'ensuivra que, macroscopiquement, lorsque les cristaux auront poussé, il existera une texture uniaxiale due à une sélection pendant la germination. L'approximation faite en considérant pour chaque zone un développement infini des faces dans la direction parallèle à l'axe de zone, ne porte pas à conséquence et ne change pas le sens du résultat.

Si on avait appliqué une tension principale ( $P < 0$ ) au lieu d'une pression, l'orientation se serait établie de manière à ce que l'axe d'ordre 6 soit parallèle à cette tension. Le même résultat aurait été obtenu avec  $P > 0$  si  $\Delta\Omega$  était positif.

Dans le cas général d'une tension triaxiale, il existe des effets analogues mais plus compliqués. Le calcul des fréquences relatives de germination devient alors laborieux.

#### *Domaine de Validité de la Théorie*

Peut-on appliquer ces résultats aux textures naturelles observées? Malheureusement, le corps le plus étudié, le quartz, ne possède pas de textures uniaxiales (Turner, 1960). Elles ont, soit une symétrie monoclinique qui est due à un écoulement ou à une surimpression de diverses textures, soit une symétrie orthorhombique qui est causée par une tension triaxiale. Nous ne pouvons donc pas interpréter ces textures puisque les modèles que nous avons utilisés conduisent à une orientation ayant une symétrie uniaxiale.

Par contre, les minéraux aciculaires (amphiboles) et lamellaires (micas)

possèdent très souvent une texture uniaxiale. Les premiers sont toujours allongés parallèlement à l'axe de pression la plus faible, les seconds se forment en plaquettes perpendiculaires à l'axe de pression la plus forte. Ceci correspond aux résultats déduits de la cinétique de germination.

Dans le cas particulier d'un système monominéral, la variation de volume molaire  $N\Delta\Omega$  est très faible. Elle n'est due qu'à la variation de celui-ci avec l'orientation. Le terme  $\sum_j f_j c_j' \Delta\Omega$  est donc négligeable. L'effet de la forme du cristal n'intervient plus que par le facteur  $c_j$ . Le calcul fait dans le cas du cristal hexagonal (en haut, p. 159) montre que les résultats obtenus pour l'orientation des germes ne sont pas modifiés mais que les maximum des fréquences de germination sont moins prononcés.

La théorie précédente doit trouver son domaine d'application lorsque l'espèce cristalline apparaît comme une nouvelle phase (nucléation), et lorsque le système est déformé élastiquement.

Si ces conditions sont réalisées, l'orientation des cristaux formés, n'est pas due, comme le pensent Kamb (1959) et MacDonald (1960), aux propriétés élastiques des solides. Bien que l'application des théories des deux auteurs précédents rende compte de quelques faits expérimentaux nous pensons que l'origine des textures doit être cherchée aussi dans une sélection pendant la germination. Cette sélection serait due à l'anisotropie de la forme des cristaux qui elle même est très sensible au champ de tension.

Nous remercions M. P. Hartman (Leiden) pour les discussions que nous avons eues avec lui.

#### Bibliographie

- BIENFAIT (M.) et KERN (R.), 1964. *Bull. Soc. franç. Min. Crist.*, **87**, 604.  
 — 1966. *Thèse. Forme d'équilibre d'un cristal dans un champ. Nancy.*  
 BRACE (W. F.), 1960. *Geol. Soc. Amer., Mem.* **79**, 9.  
 GIBBS (J. W.), 1875–1878. *Sci. Papers, Trans. Connecticut Acad.*, **3**, 343 et 524.  
 HARTMAN (P.) et DEN TEX (E.), 1967. *Proc. internat. geol. Congress. New Dehli*, 1964.  
 KAMB (W. B.), 1959. *Journ. Geol.*, **67**, 153.  
 — 1961a, b. *Journ. Geophys. Res.*, **66**, 259 et 3 985.  
 MACDONALD (G. J. F.), 1957. *Amer. Journ. Sci.*, **255**, 266.  
 — 1960. *Geol. Soc. Amer., Mem.* **79**, 1.  
 — 1961. *Journ. Geophys. Res.*, **66**, 2 599.  
 NYE (J. F.), 1961. *Propriétés physiques des cristaux. Leur représentation par des tenseurs et des matrices.* Dunod. Paris.  
 TUNNBULL (D.) et FISCHER (J. C.), 1949. *Journ. Chem. Phys.*, **17**, 71.  
 TURNER (F. J.) et VERHOOGEN (J.), 1960. *Igneous and Metamorphic Petrology.* McGraw-Hill Book Co., New York.  
 VOLMER (M.), 1939. *Kinetik der Phasenbildung.* Leipzig.

*Appendice.* On annule (5) pour trouver les extrêmes. La recherche des valeurs de  $n^*$  et de  $\mu_E$  n'est cependant possible qu'à l'aide de certaines approximations.

Pour un milieu ambiant de dimensions linéaires supérieures à  $10^{-5}$  cm on peut poser dans tous les cas  $n^* \ll n_0$ . On obtient alors

$$n^* = 8/27(\sum_j \sigma_j c_j)^3 / (-\Delta W_{el} + \Delta\mu + \sum_j f_j c_j \Delta\Omega)^3$$

La taille du germe critique  $n^*$  peut être augmentée ou diminuée par rapport à la forme classique ( $W_{el}=f_j=0$ ) suivant les signes des tensions principales et de  $\Delta\Omega$ .

La taille d'équilibre  $n_E$  s'obtient également en faisant une approximation. Lorsque, pour une direction  $j$ , on a  $|f_j| > 100 \text{ Kg cm}^{-2}$ , le terme  $\frac{2}{3}(n^c)^{-1/3} \sum_j \sigma_j c_j$  est négligeable devant les autres termes de l'équation d'équilibre. Il vient alors

$$n_E = n_0 - n_\infty \exp(\Delta W_{el} - \sum c_j f_j \Delta\Omega) / kT.$$

Le terme en exponentielle est une mesure de l'influence de la tension sur la solubilité à saturation; c'est le rapport suivant: solubilité à saturation avec tension/solubilité à saturation sans tension.

## The relative orientation of solid mineral inclusions in diamond

By J. W. HARRIS, M.Sc.

Dept. of Chemistry, University College, London W.C.1

*Summary.* The observed parallel alignment of certain directions in olivine inclusions and the diamond matrix has been explained in terms of the  $\text{SiO}_4$  and carbon tetrahedra of the two structures, and a number of suggestions have been offered in connection with other observations made on diamonds that contain inclusions. It is hoped that by improving the experimental technique certain anomalies mentioned may be explained.

A study of the solid mineral inclusions that occur in diamonds is being made in order to define more precisely the pressure and temperature conditions present during the genesis of natural diamonds, and to obtain greater understanding of the mineralogy of the Earth's Upper Mantle. As part of this work the relative crystallographic orientations of the various types of inclusion and the host diamonds have been studied using X-ray diffraction techniques.

The first X-ray identification of inclusions in diamonds was made by Mitchell and Giardini (1953) who found that at least one of the olivine inclusions was preferentially oriented with respect to the diamond structure. More recently, Futergendler and Frank-Kamenetsky (1961) have found that several of the silicates show preferential orientation. In both cases the periodic bond chain vector theory of Hartman (1953, 1954) has explained the orientation observed. So far, thirteen crystals of olivine, two of garnet, and two of enstatite have been found in thirteen diamonds, all of African origin and varying in size from 1.0 to 2.5 mm.

*Experimental procedure.* Usually a preliminary optical study is made of the diamond in order to determine where possible the type of inclusion present. Complete identification is established by random-rotation photographs, and then the inclusion is oriented about some major crystallographic axis using Laue photographs. A  $\theta$ ,  $\Phi$  chart (International Tables for X-ray Crystallography, Vol 2, p. 174) is then used to obtain the co-ordinates of a major zone of the diamond, usually  $[110]$ , which is plotted on a 5" stereographic net, and the positions of the three principal axes of the diamond are determined. A computer programme has been devised which, using this information, relates the orientation of the inclusion structure relative to the diamond structure in such a way that one can, by inspection, see if any poles of faces of either the diamond or the inclusion lie parallel to one another. The programme gives all possible poles from  $(hkl)$  planes, where the maximum value of  $h$ ,  $k$ , or  $l$  is 3,

but this can be varied. The spacings of the planes are also recorded. The computer programme has been tested using a known orientation of an olivine inclusion in a diamond. However, in view of the two graphical methods employed to obtain the above information, a maximum error of about  $2^\circ$  may result and this point is discussed later.

The use of accurate scale models of diamond and the silicate minerals found as inclusions has proved to be of considerable value in determining possible epitaxial relationships, once the common zones have been found.

### Results

*Epitaxial orientation.* Of the seventeen inclusions studied only one, an olivine, showed a good epitaxial relationship with its diamond host. Two of the parallel zones can clearly be seen from the Laue photograph (fig. 1), but these and further information, such as interfacial angles between zones and the percentage misfit of the relevant spacings, are tabulated in Table I, which shows that the percentage misfits of the spacings obey the conditions suggested by Hartman (1953) for oriented overgrowth.

Parallelism of the (010) and (111) poles of olivine and diamond respectively was first observed by Mitchell and Giardini (1953) and also by Futergendler and Frank-Kamenetsky (1961). Fig. 8 of the latter paper contains a stereogram<sup>1</sup> of olivine; the position of the pole (101) at  $38^\circ$  from the pole (100) shows that the axial lengths used were  $a=4.76 \text{ \AA}$ ,  $b=10.28 \text{ \AA}$ , and  $c=6.00 \text{ \AA}$ . Fig. 9, on the other hand, shows  $c=10.28 \text{ \AA}$  and  $b=6.00 \text{ \AA}$  and this does not correspond to the stereogram, nor to the associated Laue photograph, which closely resembles fig. 1 and corresponds to the orientation defined in table I.

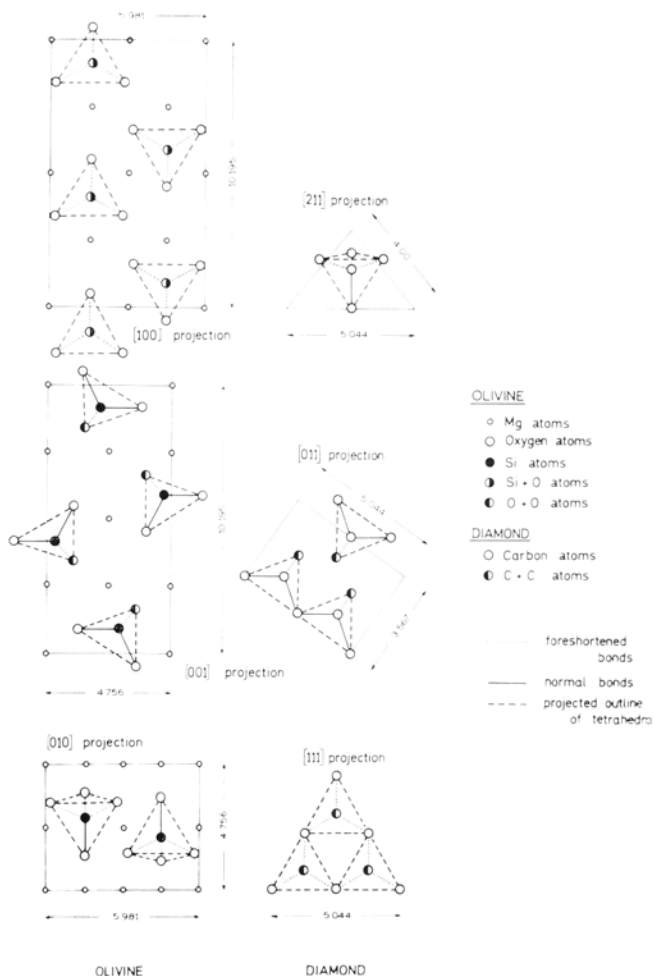
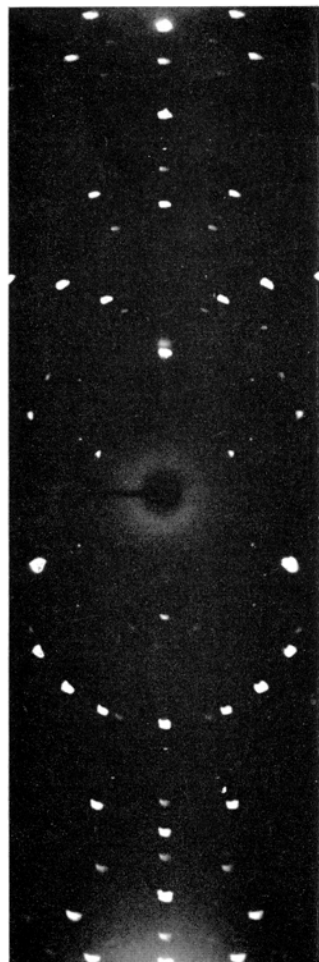
TABLE I.

Parallel zones		Interfacial angles		Parameters		Misfit
olivine	diamond	olivine	diamond	olivine	diamond	
[001]	[011]	[001] $\wedge$ [010] = $90^\circ$	[011] $\wedge$ [11 $\bar{1}$ ] = $90^\circ$	5.981 $\text{\AA}$	$2.522 \times \frac{5}{2} \text{ \AA}$	5.14%
[010]	[11 $\bar{1}$ ]	[010] $\wedge$ [100] = $90^\circ$	[11 $\bar{1}$ ] $\wedge$ [2 $\bar{1}$ 1] = $90^\circ$	10.195	$2.059 \times 5$	1.0%
[100]	[2 $\bar{1}$ 1]	[100] $\wedge$ [001] = $90^\circ$	[2 $\bar{1}$ 1] $\wedge$ [011] = $90^\circ$	4.756	$1.456 \times \frac{7}{2}$	6.67%

However, the suggestion made by Futergendler and Frank-Kamenetsky (1961), that it is the similarity of the  $\text{SiO}_4$  and carbon tetrahedra of these structures that governs epitaxial overgrowth, is still valid, for if the respective parallel planes of the zones in table I are considered, with reference to fig. 2, some features of interest emerge, based on the tetrahedral units of both structures:

There is identical geometrical orientation of the  $\text{SiO}_4$  and carbon tetrahedra on the planes (001) of olivine and (011) of diamond, when other zones in the crystal are parallel.

<sup>1</sup> In a book by V. A. Frank-Kamenetsky (1964), the same stereogram appears, but the associated projection has been corrected. (Pages 167 and 168.)



FIGS. 1 and 2: FIG. 1 (left). A Laue photograph of an olivine inclusion in a diamond, showing the exact parallelism of certain zones in both crystals on the centre line of the photograph. See also table I. FIG. 2 (right). Projections of the silica tetrahedra of olivine on the planes (100), (001), and (010), and the carbon tetrahedra of diamond on the planes (211), (011), and (111).

On correctly relating the planes (100) of olivine to (211) of diamond, an exact fit between the tetrahedra is only obtained if a relative tilt of the tetrahedra of 20° takes place either in the (001) plane of olivine or the (110) plane of diamond.

A similar relative amount of movement is also found to be necessary before the two types of tetrahedra in the planes (010) of olivine and (111) of diamond can be related exactly, and the planes involved in the tilt are the same as in the previous case.

A further consideration of fig. 2 shows that if the [211] and [111] projections of diamond were interchanged, there would be ideal geometrical orientations of the tetrahedra for all three sets of parallel zones. Since this is not found from our experiments, it suggests that, in this case, the oriented overgrowth is nucleated in one plane only, and in the other directions adjustments between the structures have to be made.

The exact geometrical orientation of the carbon and  $\text{SiO}_2$  tetrahedra on the planes (001) of olivine and (011) of diamond does not imply that such a perfect fit will be obtained on other planes that are observed to be parallel. It is, however, likely that forces exist across these planes and in order for a new face to grow, dislocations in or distortion of the structure must occur in the initial layers of the overgrowth. It is observed that the diamond immediately surrounding the inclusion is always in a state of strain, and this strain may be partly the result of the above type of phenomenon.

*Other types of orientation.* Of the remaining orientations, six specimens showed small misalignments of inclusion and diamond major zone axes, as observed from X-ray photographs, the angular deviation varying from  $3^\circ$ – $7.5^\circ$ . For example, the [001] of one of the enstatites is  $3^\circ$  from the diamond [110] (fig. 3); the [110] of a garnet is  $5^\circ$  from the diamond [110]; and the [100] of an olivine is  $3^\circ$  from the diamond [110].

The near parallelism of the above directions could indicate that elsewhere in the two structures there is another pair of common directions, but from the experimental results it does not appear that any other major directions are exactly parallel.

These observations, therefore, may indicate another form of epitaxy in which there is an angular deviation between planes before epitaxy can occur. Equally, however, these observations could indicate a purely random orientation of the two structures. It is hoped that by devising a better experimental technique that will reduce the error of  $2^\circ$  mentioned earlier, and possibly by increasing the number of zones to be considered by the computer, this present anomaly may be explained.



FIG. 3. A Laue photograph of enstatite in diamond showing the near, but not exact, parallelism of the [001] zone of enstatite and the [110] zone of diamond on the centre line of the photograph.

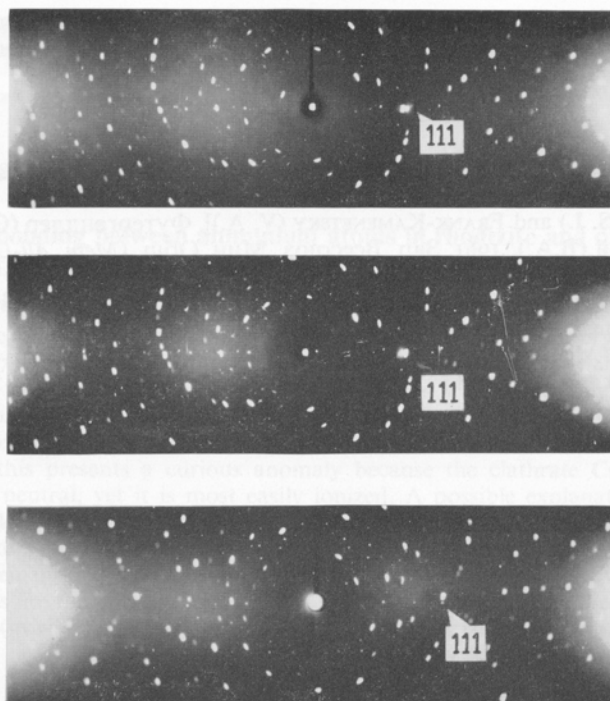


FIG. 4. Three Laue photographs of three olivine inclusions in one diamond. Note, in each case, the close parallelism between the poles of faces of the olivines and a (111) pole of the diamond.

*Orientations of multiple inclusions.* From one transparent octahedral diamond, it was possible to determine the orientation of three out of four olivine inclusions relative to the diamond. The olivines were not elongated in any specific direction, and no particular orientation was observed under the microscope, but this was due to a series of disc fractures surrounding three of the inclusions. The (111) pole of the diamond was observed in each case to be nearly parallel to certain faces in the olivine. Two of the olivines were similarly (though not exactly) oriented relative to the diamond, but the third was differently oriented, except for the relationship in the diamond (111) plane. The close parallelism of the respective poles can be seen from the Laue photographs of fig. 4.

These observations have not yet been explained. They may be due to some form of epitaxy, or they may result from a random orientation of the two structures.

*Acknowledgements.* My thanks are due to Professor Dame Kathleen Lonsdale, in whose laboratory this work is being done, to Drs. H. Judith Milledge and H. O. A. Meyer for their keen interest in and advice concerning the problem and to my colleague Mr. R. C. Henriques, who has allowed me to include some of his photographs and with whom I have had much stimulating discussion. I am indebted also to Mr. D. Walley for the computer programme

mentioned; to Ferranti Ltd. and to International Computers and Tabulators for the gift and servicing of the computer PEGASUS on which the calculations were made, and to Industrial Distributors for a grant supporting this research.

*References*

- FRANK-KAMENETSKY (V. A.), 1964. *The Nature of Structural Impurities and Inclusions in Minerals*, Leningrad State University.
- [FUTERGENDLER (S. I.) and FRANK-KAMENETSKY (V. A.)], Футергендлер (С. И.) и Франк-Каменецкий (В. А.), 1961. Зап. Всесоюз. Мин. Общ. (*Mem. All-Union Min. Soc.*), **90**, 230. [M.A. 16-437].
- HARTMAN (P.), 1953. *Relations between Structure and Morphology of Crystals*, Cryst. Inst. Univ. Groningen. [M.A. 12-314].
- 1954. *Amer. Min.*, **39**, 674.
- MITCHELL (R. S.) and GIARDINI (A. A.), 1953. *Amer. Min.*, **38**, 136. [M.A. 12-166].

## Summaries of other papers presented in Symposium I

**The possible bonding between aluminium atoms in rhodizite and other crystals.** By M. J. BUERGER and W. A. DOLLASE, Dept. of Geology and Geophysics, Massachusetts Institute of Technology, Cambridge, Massachusetts.

The structure of rhodizite has been recently solved. This isometric crystal has symmetry  $P\bar{4}3m$  with  $a=7.32 \text{ \AA}$  and one formula unit of  $\text{CsB}_{12}\text{Be}_4\text{Al}_4\text{O}_{28}$  per cell. The non-alkali part is a network in which oxygen atoms in close packing are held together by Be and B in tetrahedral co-ordination, and Al in octahedral co-ordination. A void in the network, due to omission of 4 oxygen atoms, provides a hole for the alkali. The network itself appears to be neutral. If so this presents a curious anomaly because the clathrate Cs atoms would be required to be neutral, yet it is most easily ionized. A possible explanation is that it may contribute its electron to a bond between the four Al atoms, thus permitting the network to have a charge of  $-1$ . The four Al atoms occur together, occupying 4 of the 8 corners of a cube so that their mutual distances are all  $2.95 \text{ \AA}$ , which is only about  $0.1 \text{ \AA}$  larger than the Al-Al distances in the metallic state. This same cluster occurs in the pharmacosiderite structural type (in which there is also an abnormal valence situation) as well as in the spinel structures.

**The crystal structure of olivine with reference to inclusions in diamond.** By R. HENRIQUES, Dept. of Chemistry, University College, London W.C.1.

The crystal structure of the synthetic end-member of the olivine series ( $\text{FO}_{100}$ ) has been refined by least squares, using X-ray diffraction data that was recorded photographically. There are no significant differences from the published results for naturally occurring forsterite. Olivine has been identified as a mineral inclusion in diamond. The crystal structure of one of these inclusions has been determined and compared with those of the synthetic and naturally occurring olivines mentioned above.

**Vectorial growth rates, statistical morphology, and the internal structure of crystals.** By C. J. SCHNEER and R. SILVA, Dept. of Geology and Geography, University of New Hampshire, Durham, New Hampshire, U.S.A.

Time-lapse photography of oriented cubes of Rochelle salt growing in saturated solution yields vectorial growth rates along the crystal axes of the order of  $0.4 \times 10^{-3} \text{ in./hr.}$  and  $3.0 \times 10^{-3} \text{ in./hr.}$  at  $0^\circ\text{C}$  and  $35^\circ\text{C}$ . If the ratio of the growth rates ( $R_{ij}$ ) along two axes  $i$  and  $j$  is determined by the difference in specific surface energies  $\Delta\epsilon_{ij}$ ,  $R_{ij} = \exp(-\Delta\epsilon_{ij}/kT)$ , then the difference in surface energies for different pinacoids of Rochelle salt crystals is of the order of  $10^2 \text{ cal./mol.}$  With increase in temperature, the empirical  $R_{ij}$  approach unity.

If each of the forms making up a crystal habit is characterized by a definite surface energy, the assemblage of forms may be taken as a set of points of the reciprocal lattice of the crystal. Each point may be characterized by a definite weight. Using the frequency of occurrence of forms in nature (Niggli) for weight, Fourier syntheses may be prepared that locate, with poor definition, the periodically distributed concentrations of the sources of energy for growth. These Fourier maps agree closely with Fourier maps using the corresponding intensity space given by X-ray diffraction.

# Crystal-field phenomena and iron enrichments in pyroxenes and amphiboles

By ROGER G. BURNS,

Department of Mineralogy and Petrology,  
University of Cambridge, England

*Summary.* Thermodynamic data estimated from measurements of electronic absorption spectra are summarized for suites of minerals of the following ferromagnesian silicate series: orthopyroxene, pigeonite, diopside–hedenbergite, anthophyllite, cummingtonite–grunerite and tremolite–actinolite. The energies of the absorption bands have been used to estimate crystal-field stabilization energies of the  $\text{Fe}^{2+}$  ion in various co-ordination sites in each mineral. The relative stabilization energies for each site correlate with preferred occupation by iron measured experimentally by X-ray diffraction, infrared spectroscopy, and the Mössbauer effect.

The compositional variations of crystal-field stabilization energies for each series, together with observed cation ordering, show that few ferromagnesian silicate series are ideal solid-solutions of magnesium and iron silicate components. The order of decreasing crystal-field stabilization energies between series correlates with decreasing relative iron enrichments in coexisting pyroxenes and amphiboles.

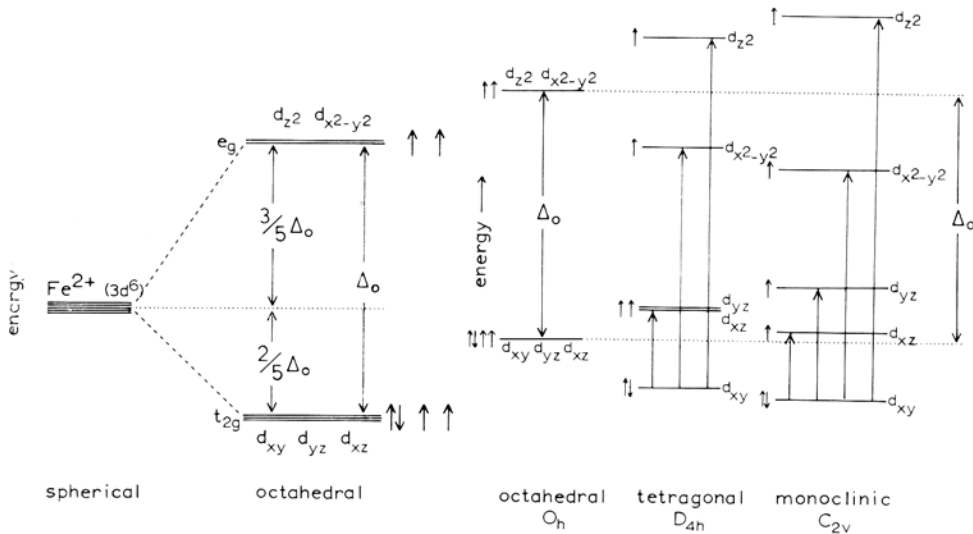
CONSIDERABLE data have been obtained recently on ordering of  $\text{Fe}^{2+}$  ions in crystal structures and relative iron enrichments in co-existing silicate minerals. These results may be explained semi-quantitatively by crystal-field theory (Orgel, 1960; Burns, Clark, and Fyfe, 1964; Burns and Fyfe, 1967) using data derived from measurements of electronic absorption spectra of ferromagnesian silicate minerals (Burns, 1965; White and Keester, 1966).

The present paper summarizes results of spectral measurements on over one hundred minerals of the following series: orthopyroxene (49); pigeonite (4); diopside–hedenbergite (16); cummingtonite–grunerite (29); anthophyllite (2); and tremolite–actinolite (10). Estimated relative crystal-field stabilization energies of the  $\text{Fe}^{2+}$  ion are used to interpret ordering of iron in crystal structures, and iron–magnesium ratios in co-existing pyroxenes and amphiboles.

*Theory.* Absorption bands in the visible (4 000 to 7 000 Å) and short-wave infrared (7 000 to 30 000 Å) regions in the spectra of transition-metal compounds usually represent electron transitions between the five  $3d$  orbital energy levels

<sup>1</sup> Present Address: Department of Geology and Mineralogy, Oxford.

of the transition-metal ion. These transitions in the visible region lead to coloured transmitted light in many minerals. The five  $3d$  orbitals have identical energies (i.e. are degenerate) when a transition-metal ion is in a spherically symmetric electrostatic field. In octahedral co-ordination in oxide structures three orbitals, designated  $t_{2g}$ , are stabilized relative to the other two orbitals, designated  $e_g$  (fig. 1). This resolution is caused by differential repulsion of electrons in the orbitals by the negatively charged, co-ordinating oxyanions or dipolar  $H_2O$  molecules. The energy separation between the  $t_{2g}$  and  $e_g$  groups is designated by  $\Delta_0$  and, according to crystal-field theory, the  $t_{2g}$  set is stabilized by  $\frac{2}{5}\Delta_0$  and the  $e_g$  set de-stabilized by  $\frac{3}{5}\Delta_0$  relative to the energy levels in a spherical electrostatic field. Electron transfer between the  $t_{2g}$  and  $e_g$  energy levels results in absorption of radiation. Measurements of absorption spectra enable  $\Delta_0$  to be estimated. Techniques for measuring the spectra of minerals have been described by Clark (1957), Burns (1965, 1966), and White and Keester (1966).



FIGS. 1 and 2: FIG. 1 (left). Energy-level diagram for the  $3d$  orbitals of the  $Fe^{2+}$  ion in an octahedral crystal-field. FIG. 2 (right). Relative energy levels of the  $Fe^{2+}$  ion in octahedral, tetragonal and monoclinic crystal-fields. Possible electron transitions are shown for each co-ordination.

The  $Fe^{2+}$  ion has six  $3d$  electrons. When iron occurs in octahedral co-ordination in oxides, five of the  $3d$  electrons occupy singly each of the  $3d$  orbitals, and the sixth fills one of the low-energy  $t_{2g}$  orbitals. This sixth electron induces a crystal-field stabilization energy (CFSE) of  $\frac{2}{5}\Delta_0$  on the  $Fe^{2+}$  ion relative to random filling of the degenerate orbitals in a spherically symmetric electrostatic field. The four unpaired electrons lead to paramagnetism in ferrous compounds.

Co-ordination sites in structures of ferromagnesian silicates frequently have symmetries lower than octahedral. This leads to further resolution of the energy levels for  $3d$  orbitals. For example, one of the  $t_{2g}$  orbitals is stabilized and one of the  $e_g$  orbitals de-stabilized in a tetragonally distorted octahedron compressed along one of the tetrad axes (fig. 2). In co-ordination sites of lower symmetries, the  $3d$  orbitals are separated into five energy levels (fig. 2).

Two important consequences of iron in distorted co-ordination sites are: first, additional electron transitions are possible between the resolved  $3d$  orbital energy levels. These transitions are polarization-dependent (Burns, Clark, and Stone, 1966) and lead to pleochroism, which may occur both inside and outside the visible region; measurements of absorption spectra enable the energy separations to be estimated. Second, increased stabilization of one orbital occurs with increased distortion of a site from octahedral symmetry (fig. 2); the sixth  $3d$  electron of the  $\text{Fe}^{2+}$  ion fills this most stable orbital, and induces additional CFSE. Relative stabilities of iron in two or more co-ordination sites in a crystal structure may be deduced from the geometries of the co-ordination sites.

*Ordering of iron in ferromagnesian silicate crystal structures.* The energy level diagrams for iron in co-ordination sites of octahedral, tetragonal and monoclinic symmetries (fig. 2) suggest that  $\text{Fe}^{2+}$  ions will favour the most distorted site in a crystal structure.<sup>1</sup> Co-ordination site symmetries and distortions may be obtained from crystal-structure analyses. Two designations of site symmetry need to be distinguished, however. The point symmetry gives the overall symmetry of a position with respect to all atoms in the structure. The molecular symmetry or co-ordination site symmetry refers to the symmetry of the next-nearest neighbour environment about a given atom. For the purposes of the present discussion, the approximate molecular symmetries of the oxygen co-ordination polyhedra about iron in the various ferromagnesian silicate structures will be considered, and no account taken of next-nearest neighbour interactions.

Approximate configurations and symmetries of co-ordination sites in ferromagnesian silicates are summarized in table I. These descriptions are based on geometries and metal–oxygen distances obtained from crystal structure measurements of the following silicates: enstatite (Byström, 1943), hypersthene (Ghose, 1965), orthoferrosilite (Burnham, 1968); pigeonite (Morimoto, Appleman, and Evans, 1960); diopside (Warren and Bragg, 1928); cummingtonite (Ghose, 1961), grunerite (Ghose and Hellner, 1959); anthophyllite (Warren and Modell, 1930; Ito, 1950); actinolite (Zussman, 1955); olivine (Hanke, 1965; Gibbs, Moore, and Smith 1963).

On the basis of site distortion alone, inspection of table I leads to the prediction that iron will be enriched in the following positions: orthopyroxene  $M_2$ ,

<sup>1</sup> This correlation holds provided the bond-type of the oxygens are identical and average metal–oxygen distances are approximately equal in the various co-ordination sites.

TABLE I. Approximate configurations of co-ordination sites occupied by iron in ferromagnesian silicate crystal structures

Structure	Position occupied by $\text{Fe}^{2+}$	Configuration of co-ordination site	Reference
Orthopyroxene	$\begin{cases} M_1 \\ M_2 \end{cases}$	approx. octahedral very distorted polyhedron, six co-ordinate	Byström, 1943; Ghose, 1965; Burnham, 1968
Pigeonite	$\begin{cases} M_1 \\ M_2 \end{cases}$	approx. octahedral very distorted polyhedron, six or seven co-ordinate	Morimoto, Appleman and Evans, 1960
Diopside	$M_1$	distorted octahedron	Warren and Bragg, 1928
Cummingtonite (anthophyllite)	$\begin{cases} M_1 \\ M_2 \\ M_3 \\ M_4 \end{cases}$	approx. octahedral distorted octahedron approx. octahedral very distorted polyhedron, six co-ordinate	Ghose, 1961; Ghose and Hellner, 1959; (Warren and Modell, 1930; Ito, 1950)
Actinolite	$\begin{cases} M_1 \\ M_2 \\ M_3 \end{cases}$	approx. octahedral distorted octahedron approx. octahedral	Zussman, 1955
Olivine	$\begin{cases} M_1 \\ M_2 \end{cases}$	tetrag. distorted octahedron trigon. distorted octahedron	Hanke, 1965; Gibbs, Moore and Smith, 1963

pigeonite  $M_2$ , cummingtonite  $M_4$ , anthophyllite  $M_4$ , actinolite  $M_2$  and olivine  $M_1$ . In general, there is excellent agreement between predicted iron enrichments and observed ordering of  $\text{Fe}^{2+}$  ions in crystal structures determined experimentally by X-ray diffraction, infrared spectroscopy, and the Mössbauer effect. These correlations are shown in table II.

Some inconsistencies may be noted, however. The actinolite  $M_2$  and cummingtonite  $M_2$  sites show similar distortions, and each site is more distorted than the corresponding  $M_1$  and  $M_3$  sites. Iron favours the actinolite  $M_2$  site, as predicted by crystal-field theory, but iron is depleted in the cummingtonite  $M_2$  site relative to the  $M_1$  and  $M_3$  sites, which is contrary to expectation. A similar distribution occurs between the anthophyllite  $M_2$  and  $M_1$ ,  $M_3$  sites. These results indicate that next-nearest neighbour interactions, such as those between cations in the adjacent  $M_4$  and  $M_2$  positions in amphiboles, must also be considered. Thus, the different influences of iron and calcium in the  $M_4$  position have been used to explain the large variation in Mössbauer spectra of iron in the actinolite  $M_2$  and cummingtonite  $M_2$  positions (Bancroft, Burns, and Maddock, 1967).

Implicit in the correlations in table II is the assumption that oxygen bond-types are identical in each co-ordination site. In the amphibole structure,

TABLE II. Predicted and observed ordering of Fe<sup>2+</sup> ions in ferromagnesian silicate crystal structures

Ferromagnesian silicate series	Predicted (crystal-field theory)	Observed	Reference
Orthopyroxene	$M_2 > M_1$	$M_2 > M_1$	Ghose (1965)—X-ray; Bancroft and Burns (1967, 1968)—Mössbauer
Pigeonite	$M_2 > M_1$	$M_2 > M_1$	Morimoto, Appleman, and Evans (1960)—X-ray
Cummingtonite	$M_4 > M_2 > M_1, M_3$	$M_4 > M_1, M_3 > M_2$	Ghose (1961)—X-ray; Ghose and Hellner (1959)—X-ray; Fischer (1966)—X-ray; Bancroft, Burns, and Maddock (1967)—Mössbauer + infrared
Anthophyllite	$M_4 > M_2 > M_1, M_3$	$M_4 > M_1, M_3 > M_2$	Burns and Strens (1966)—infrared
Actinolite	$M_2 > M_1, M_3$	$M_2 > M_1, M_3$	Bancroft, Burns, Maddock, and Strens (1966)—infrared + Mössbauer
Diopside	$M_1$ only	$M_1 = M_2 = M_3$	Burns and Strens (1966)—infrared; Zussman (1955)
Olivine	$M_1 > M_2$	$M_1$ only	Bancroft, unpublished—Mössbauer; Gibbs (pers. comm.)—X-ray
		no ordering detected	Hanke (1965)—X-ray; Gibbs, Moore, and Smith (1963)—X-ray; Bancroft and Burns (1968)—Mössbauer

however, three types of oxygen ligand may be distinguished: “ionic” oxygens constituting OH<sup>-</sup> and Si-O<sup>-</sup> groups, and “neutral” or bridging oxygens of Si-O-Si linkages. Similarly, two oxygen atoms, “ionic” Si-O<sup>-</sup> and “neutral” Si-O-Si, may be differentiated in the pyroxene structure. Differences in oxygen bond-type may also influence the iron distribution between co-ordination sites. Thus, increased covalent bonding with “neutral” oxygens of the pyroxene  $M_2$  and amphibole  $M_4$  sites probably contribute to the iron enrichments in these sites (table II).

*Crystal-field stabilization energies of iron in pyroxene and amphibole structures.* The enrichment of iron in certain structural positions of pyroxenes and amphiboles may be explained quantitatively by the relative CFSE's attained by the

$\text{Fe}^{2+}$  ion in each co-ordination site. These stabilization energies are calculated from the  $3d$  orbital energy levels of iron in the appropriate sites, which are determined from measurements of absorption spectra.

The procedure for evaluating CFSE's is illustrated by results for orthoferrosilite. The polarized spectra of an orthoferrosilite,  $\text{Fs}_{86.4}$ , are shown in fig. 3. Absorption bands are located in four regions of the spectrum between  $4\,000\text{ \AA}$  and  $24\,000\text{ \AA}$  at the following positions:  $6\,900\text{ \AA}$  ( $14\,500\text{ cm}^{-1}$ ),  $9\,340\text{ \AA}$  ( $10\,710\text{ cm}^{-1}$ ),  $10\,680\text{ \AA}$  ( $8\,570\text{ cm}^{-1}$ ), and  $20\,400\text{ \AA}$  ( $4\,910\text{ cm}^{-1}$ ).

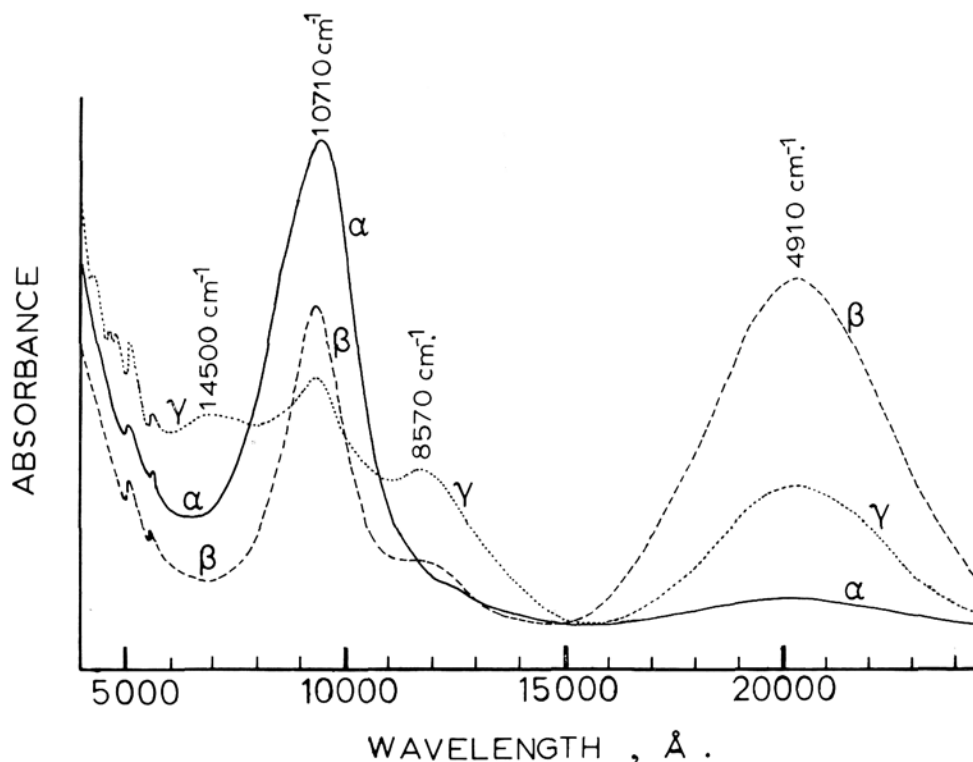


FIG. 3. Polarized absorption spectra of an orthoferrosilite,  $\text{Fs}_{86.4}$ . Measurements were made with a Cary model 14 spectrophotometer, using a polarizing microscope with universal stage attachment (Burns, 1966).

A fifth band at  $32\,200\text{ \AA}$  ( $3\,100\text{ cm}^{-1}$ ) was observed in enstatite by White and Keester (1966). The corresponding band is estimated to lie at  $2\,830\text{ cm}^{-1}$  in orthoferrosilite. The spectra of orthoferrosilite (fig. 3) represent electron transitions within  $\text{Fe}^{2+}$  ions in the  $M_1$  and  $M_2$  positions of the orthopyroxene structure. The bands at  $14\,500\text{ cm}^{-1}$  ( $\gamma$  spectrum),  $10\,710\text{ cm}^{-1}$  ( $\alpha$  spectrum),  $4\,910\text{ cm}^{-1}$  ( $\beta$  spectrum), and  $2\,830\text{ cm}^{-1}$  are due to iron in the  $M_2$  position, and the bands at  $10\,740\text{ cm}^{-1}$  ( $\beta$  spectrum) and  $8\,570\text{ cm}^{-1}$  ( $\beta$  spectrum) to iron in the  $M_1$  position. From the positions of these absorption bands, the energy level dia-

grams shown in fig. 4 may be constructed for iron in each site (Bancroft and Burns, 1967a; White and Keester, 1967). The values of  $\Delta_0$  for the  $\text{Fe}^{2+}$  ion in the  $M_1$  and  $M_2$  sites are estimated as  $9\,600\text{ cm}^{-1}$  and  $10\,025\text{ cm}^{-1}$ , respectively, and the CFSE's as  $11.1\text{ k. cal.}$  and  $18.8\text{ k. cal.}$ , respectively. Similarly, CFSE's may be estimated for other orthopyroxenes of the enstatite–orthoferrosilite series from absorption spectra. Thus, iron in hypersthene  $\text{Fs}_{50}$  receives CFSE's of  $11.2$  and  $20.1\text{ k. cal.}$  in the  $M_1$  and  $M_2$  sites, respectively. The values obtained by extrapolation for orthoferrosilite  $\text{Fs}_{100}$  are  $11.0$  and  $18.2\text{ k. cal.}$  for the  $M_1$  and  $M_2$  sites, respectively, and for enstatite  $\text{Fs}_1$  the CFSE's are  $11.4$  and  $22.0\text{ k. cal.}$  for the  $M_1$  and  $M_2$  sites. The higher stabilization energies for the  $M_2$  site account for the observed enrichment of iron in the  $M_2$  position of the orthopyroxene structure (Ghose, 1965; Bancroft and Burns, 1968, 1967b).

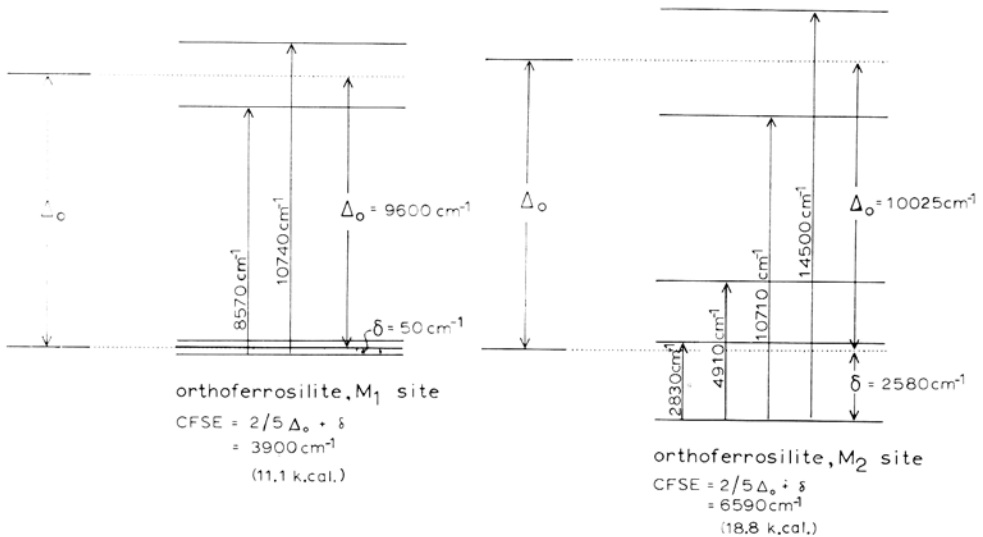


FIG. 4. Energy level diagrams for  $\text{Fe}^{2+}$  in the  $M_1$  and  $M_2$  co-ordination sites of orthoferrosilite. Energy separations are estimated from the spectra (fig. 3). The crystal-field stabilization energies calculated for  $\text{Fe}^{2+}$  in each site are shown. Transitions between the lowest energy levels of iron in the  $M_1$  site have not been observed, and the maximum separation is estimated to be  $100\text{ cm}^{-1}$ .

In principle, the CFSE's of iron in each co-ordination site of all ferromagnesian silicate structures may be calculated from energies of absorption bands in the spectra. In practice, however, it is often impossible to resolve individual absorption bands originating from iron in two or more sites having small structural, and hence energetic, differences. Thus, broad composite absorption bands are observed in the spectra of actinolites and grunerites (Burns, 1965). In addition, group theoretical selection rules (Cotton, 1963) show that certain transitions between the resolved  $3d$  orbital energy levels are forbidden. In these cases,

certain absorption bands are absent from the spectra, and some energy separations cannot be determined. Nevertheless, estimates of the CFSE's may be made (Burns, 1965; to be published). Ranges of approximate CFSE's for iron in pyroxene and amphibole structures are shown in fig. 5. The values vary with composition in most ferromagnesian silicate series. In the orthopyroxene, pigeonite, and cummingtonite series, CFSE's decrease with increasing iron content of all positions. A similar trend is shown in the actinolite series for iron in the  $M_1$ ,  $M_3$  sites, but values for the  $M_2$  site increase with rising iron concentration. The diopside-hedenbergite series shows little compositional variation.<sup>1</sup>

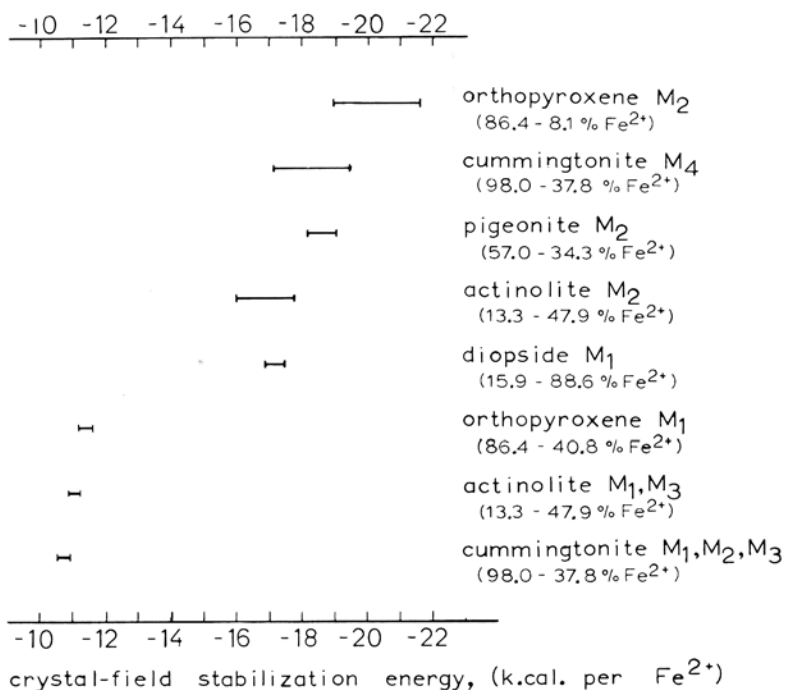


FIG. 5. Crystal-field stabilization energies of the  $Fe^{2+}$  ion in pyroxene and amphibole structures. Composition ranges (mole %  $Fe^{2+}$  component) measured for each series are shown.

The ranges of CFSE shown in fig. 5 indicate that the  $Fe^{2+}$  ion receives highest stabilization in the orthopyroxene  $M_2$ , pigeonite  $M_2$  and cummingtonite  $M_4$  sites. This may be correlated with the observed iron enrichments in these positions (table II).

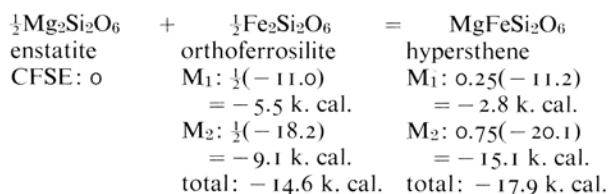
<sup>1</sup> Spectral measurements of augites (Burns, 1965) show that positions of absorption bands depend on Ca and Al contents. With increasing  $Al_2O_3$  and decreasing CaO concentrations, band maxima move to shorter wavelengths.

*Ideal solution behaviour.* One consequence of the compositional variations of CFSE's shown by pyroxenes and amphiboles (fig. 5) is that few ferromagnesian silicate series conform with criteria for ideal solid-solution behaviour. A similar conclusion may be drawn from the ordering of iron in crystal structures (table II) and from the non-linearity of unit cell volumes.

The criteria for ideal solution behaviour (Guggenheim, 1959; Denbeigh, 1957; Lewis and Randall, 1961) are: First,  $a_i = x_i \cdot a_i^\circ$ , for all values of  $x_i$  ( $0 < x_i < 1$ ), where  $a_i$ ,  $a_i^\circ$  are the activities of component  $i$  in solution and pure substance, respectively, and  $x_i$  is the mole fraction of component  $i$  in solution; secondly,  $\mu_i = \mu_i^\circ + RT \cdot \ln x_i$ , where  $\mu_i$ ,  $\mu_i^\circ$  are the chemical potentials of component  $i$  in solution and pure phase, respectively; thirdly, the free energy of mixing is given by  $\Delta_m G = RT \cdot \sum (x_i \cdot \ln x_i)$ ; and fourthly, the entropy of mixing or configurational entropy, which is given by  $\Delta_m S = -R \cdot \sum (x_i \cdot \ln x_i)$ , must have the maximum value.

From these relationships arise the necessary criteria that both the heat of mixing,  $\Delta_m H$ , and volume of mixing,  $\Delta_m V$ , must be zero.

*Heat of mixing criterion.* Variation of CFSE within a particular ferromagnesian silicate series implies a heat of mixing term. For example, consider the formation of hypersthene  $Fs_{50}$ , in which 75% of the  $M_2$  positions and 25% of the  $M_1$  positions are occupied by iron (Bancroft and Burns, 1967), and CFSE's are 20.1 and 11.2 k. cal. for the  $M_2$  and  $M_1$  positions, respectively. The process is represented as follows:



Therefore, according to this calculation, there is an excess CFSE of mixing of about -3.3 k. cal. in the formation of hypersthene  $Fs_{50}$  from enstatite and orthoferrosilite. Similarly, the formation of all orthopyroxenes of intermediate compositions results in an excess CFSE or heat of mixing term, indicating that the orthopyroxene series is not an ideal solid solution of  $Mg_2Si_2O_6$  and  $Fe_2Si_2O_6$ .

Similarly, the formation of intermediate members of the pigeonite, cummingtonite-grunerite, actinolite, and forsterite-fayalite series by mixing of iron and magnesium components produces an excess CFSE or heat of mixing term. The diopside-hedenbergite series was the only one studied where little or no compositional variation of CFSE is observed and no excess CFSE term appears.

Note that in a multi-site substitution where cation ordering occurs, a heat of mixing term could arise without compositional variation of CFSE (Whittaker, personal communication). Thus, if the CFSE's of  $Fe^{2+}$  in the orthopyroxene  $M_1$  and  $M_2$  positions were constant (for example,  $M_1$  position = 11.0 k. cal.,

orthopyroxene series is not an ideal solid solution of  $Mg_2Si_2O_6$  and  $Fe_2Si_2O_6$  components.

*Iron–magnesium ratios in coexisting pyroxenes and amphiboles.* The variation of CFSE of the  $Fe^{2+}$  ion between ferromagnesian silicate series (fig. 5) may be used to explain iron–magnesium ratios in coexisting pyroxenes and amphiboles. If it is assumed that  $Fe^{2+}$  ions are enriched in the phase giving highest CFSE and that equilibrium distribution of iron takes place during mineral formation, the following order of decreasing relative  $Fe^{2+}$  enrichment is predicted in magnesium-rich phases from the data in fig. 5: orthopyroxene > pigeonite > cummingtonite > diopside = actinolite. In iron-rich phases variations in this

TABLE III. Relationships between iron–magnesium ratios in coexisting ferromagnesian silicate minerals

Assemblage	Type	Order of decreasing $Fe^{2+}/Mg^{2+}$ ratio	Reference
Orthopyroxene–pigeonite	volcanic	orthopyroxene $\approx$ pigeonite	Kuno and Nagashima, 1952
Orthopyroxene–cummingtonite	iron formation	orthopyroxene > cummingtonite	Kranck, 1962
Orthopyroxene–clinopyroxene	metamorphic	orthopyroxene > clinopyroxene	Eskola, 1952; Howie, 1955; Clavan <i>et al.</i> , 1954, 1959; Muir and Tilley, 1958; Wilson, 1960; Kranck, 1961; Davidson, 1965
	igneous	orthopyroxene > clinopyroxene	Hess, 1949, 1960; Brown, 1957, 1960;
	ultramafic	orthopyroxene < clinopyroxene	Ross <i>et al.</i> , 1954; Kranck, 1962; White, 1965
Pigeonite–clinopyroxene	igneous	pigeonite > clinopyroxene	Muir and Burns, 1968
Anthophyllite–hornblende	metamorphic	anthophyllite > hornblende	Tilley, 1957
Cummingtonite–actinolite	iron formation	cummingtonite > actinolite	Mueller, 1960; Kranck, 1961
Cummingtonite–clinopyroxene	iron formation	cummingtonite > clinopyroxene	Mueller, 1960; Kranck, 1961
Actinolite–clinopyroxene	iron formation	actinolite > clinopyroxene	Meuller, 1960; Kranck, 1961
Orthopyroxene–cummingtonite–clinopyroxene	iron formation	orthopyroxene > cummingtonite > clinopyroxene	Kranck, 1961
Cummingtonite–actinolite–clinopyroxene	iron formation	cummingtonite > actinolite > clinopyroxene	Mueller, 1960

order are to be expected as a result of different crystal field stabilization energies of the sites in each phase. Although several assumptions are involved, there is good agreement between the iron enrichments predicted by crystal-field theory and those observed in coexisting minerals. Some of these correlations are shown in table III.

The predicted order of  $\text{Fe}^{2+}$  ion enrichment is valid strictly for mineral formation at  $25^\circ\text{C}$  and 1 atmosphere, the conditions under which the absorption spectra measurements were made. In order to apply the data of fig. 5 to igneous and metamorphic assemblages, it must be assumed that all phases show the same variation of CFSE with temperature and pressure.

*Conclusion.* Arguments based on crystal-field theory suggest that  $\text{Fe}^{2+}$  ions should be enriched in the most distorted co-ordination site in a crystal structure. Measurements of iron distribution in ferromagnesian silicates by X-ray diffraction, infrared spectroscopy, and Mössbauer techniques show that  $\text{Fe}^{2+}$  ions strongly favour the distorted amphibole  $M_4$  and pyroxene  $M_2$  sites. The enrichments are explained quantitatively by the relative CFSE's of the  $\text{Fe}^{2+}$  ion in each site, which are estimated from the positions of absorption bands in the electronic spectra.

The values of the CFSE's show compositional variations for each ferromagnesian silicate series. This variation, together with the observed  $\text{Fe}^{2+}$  ordering in crystal structures, indicates that few ferromagnesian silicate series conform with criteria for ideal solution behaviour: variation of CFSE within a series implies a heat of mixing term, and cation ordering reduces the configurational entropy from the ideal, maximum value.

The crystal-field stabilization energies for each series have been used to interpret iron-magnesium ratios in coexisting pyroxenes and amphiboles. Increasing relative  $\text{Fe}^{2+}$  enrichment can be correlated with increasing CFSE in coexisting phases.

*Acknowledgments.* This work is portion of a Ph.D. dissertation compiled at the University of California, Berkeley. The author gratefully acknowledges scholarship support from the Royal Commission for the Exhibition of 1851, London, the University of New Zealand, and the University of California. I wish to thank sincerely the following people who generously provided analysed specimens: Dr. S. O. Agrell, Dr. W. Clavan, Dr. L. R. Davidson, Prof. R. A. Howie, Prof. C. S. Hurlbut Jr, Dr. C. Klein Jr, Prof. H. Kuno, Dr. B. Mason, Dr. R. F. Mueller, Dr. E. H. Watson, Dr. W. A. Watters, and Dr. R. White. The work was supported by grants from the National Science Foundation and the Petroleum Research Fund of the American Chemical Society. The author has benefited from helpful criticisms by Dr. E. J. W. Whittaker.

#### References

- BANCROFT (G. M.) and BURNS (R. G.), 1968. This vol., p. 6.  
— — —, 1967a. *Amer. Min.*, **52**, 1278.  
— — —, 1967b. *Nature*, **213**, 1221.

- BANCROFT (G. M.), BURNS (R. G.) and MADDOCK (A. G.), 1967a. *Amer. Min.*, **52**, 1009.  
 ———, 1967b. *Geochimica Acta*, **31**, 2219.  
 ——— and STRENS (R. G. J.), 1966. *Nature*, **212**, 913.
- BROWN (G. W.), 1957. *Min. Mag.*, **31**, 511.
- BURNHAM (C. W.), 1968. This vol., p. 334.
- BURNS (R. G.), 1965. Electronic spectra of silicate minerals: applications of crystal-field theory to aspects of geochemistry. Ph.D. diss., University of California, Berkeley, California.  
 ———, 1966. *Journ. Sci. Instr.*, **43**, 58.  
 ——— CLARK (M. G.), and STONE (A. J.), 1966. *Inorg. Chem.*, **5**, 1268.  
 ——— and FYFE (W. S.), 1964. Crystal-field theory and applications to problems of geochemistry. In *Chemistry of the earth's crust. Proc. Vernadsky Cent. Sympos.*, **2**, 88.  
 ——— and FYFE (W. S.), 1967. Crystal-field theory and the geochemistry of the transition elements. In *Researches in Geochemistry* (P. Abelson, ed.), vol. 2, p. 259.  
 ——— and STRENS (R. G. J.), 1966. *Science*, **153**, 890.
- BYSTRÖM (A.), 1943. *Ber. deut. keram. Gesell.*, **24**, 2.
- CLARK (S. P.), 1957. *Amer. Min.*, **42**, 732.
- CLAVAN (W.), MCNABB (W.), and WATSON (E. H.), 1954. *Ibid.*, **39**, 566.  
 ——— and NORTON (D. A.), 1959. *Ibid.*, **44**, 844.
- COTTON (F. A.), 1963. *Chemical Applications of Group Theory*. Interscience Publ., New York.
- DAVIDSON (L. R.), 1965. The chemistry and paragenesis of some metamorphic pyroxenes. Ph.D. diss., Cambridge.
- DENBIGH (K.), 1937. *The Principles of Chemical Equilibrium*. Cambridge Univ. Press.
- ESKOLA (P.), 1952. *Amer. Journ. Sci.*, Bowen Vol., 133.
- FISCHER (K. F.), 1966. *Amer. Min.*, **49**, 963.
- GHOSE (S.), 1961. *Acta Cryst.*, **14**, 622.  
 ———, 1965. *Zeits. Krist.*, **122**, 81.  
 ——— and HELLNER, 1959. *Journ. Geol.*, **67**, 691.
- GIBBS (G. V.), MOORE (P. B.), and SMITH (J. V.), 1963. Crystal structure of olivine. *Progr. Abstr. Geol. Soc. Amer. Ann. Meeting*, 66.
- GUGGENHEIM (E. A.), 1959. *Thermodynamics*. North Holland Publ. Co., Amsterdam.
- HANKE (K.), 1965. *Beitr. Min. Petr.*, **11**, 535.
- HESS (H. H.), 1949. *Amer. Min.*, **34**, 621.  
 ———, 1960. *Mem. Geol. Soc. Amer.*, 80.
- HOWIE (R. A.), 1955. *Trans. Roy. Soc. Edinburgh*, **62**, 725.
- ITO (T.), 1950. *X-ray studies on Polymorphism*. Maruzen Co., Tokyo.
- KRANCK (S. H.), 1961. *Journ. Petrology*, **2**, 137.
- KUNO (H.) and NAGASHIMA (K.), 1952. *Amer. Min.*, **37**, 1000.
- LEWIS (G. N.) and RANDALL (M.), 1961. *Thermodynamics*. Revised by K. S. Pitzer and L. Brewer; McGraw-Hill Book Co., New York.
- MORIMOTO (N.), APPLEMAN (D. E.), and EVANS (H. T., Jr.), 1960. *Zeits. Krist.*, **114**, 120.
- MUELLER (R. F.), 1960. *Amer. Journ. Sci.*, **258**, 449.
- MUIR (I. D.) and BURNS (R. G.), 1968. This vol., p. 337.  
 ——— and TILLEY (C. E.), 1957. *Amer. Journ. Sci.*, **255**, 241.
- ORGEL (L. E.), 1960. *An Introduction to Transition-metal Chemistry: Ligand-field Theory*. Methuen and Co., London.
- ROSS (C. S.), FOSTER (M. D.), and MYERS (A. T.), 1954. *Amer. Min.*, **39**, 693.
- STEPHENSON (D. L.), SMITH (J. V.), and HOWIE (R. A.), 1968. This vol., p. 338.
- TILLEY (C. E.), 1957. *Amer. Min.*, **42**, 412.
- WARREN (B. W.) and BRAGG (W. L.), 1928. *Zeits. Krist.*, **69**, 168.  
 ——— and MODELL (D. I.), 1930. *Ibid.*, **75**, 161.

- WHITE (W. B.) and KEESTER (K. L.), 1966. *Amer. Min.*, **51**, 774.  
—— —, 1967. *Ibid.*, **52**, 1508.  
WHITE (R.), 1965. *Contr. Min. Petr.*, **12**, 245.  
WILSON (A. F.), 1960. *Geol. Mag.*, **97**, 1.  
ZUSSMAN (J.), 1955. *Acta Cryst.*, **8**, 301.

# Étude magnétique de pyroxènes et d'amphiboles

par MM. J. BABKINE, J. BOLFA, J. C. REITHLER, et C. ZELLER

Laboratoire de Minéralogie et de Cristallographie de la Faculté  
des Sciences de Nancy

*Summary.* Magnetic measurements have been made on some pyroxenes and amphiboles separated from rocks using a magnetic balance constructed by one of us (J. C. R.). By finding for each specimen the law of magnetization, values of magnetic susceptibility have been determined. In addition full and precise analyses of these pyroxenes and amphiboles have shown that the only magnetic ions present are  $\text{Fe}^{2+}$ ,  $\text{Fe}^{3+}$ , and  $\text{Mn}^{2+}$ . Assuming that these ions are free and without interaction, it is possible by using their known magnetic moments, derived from the Langevin relation for paramagnetics ( $\chi = C/T$ ), to calculate the susceptibilities of these amphiboles and pyroxenes at  $20^\circ\text{C}$ . Comparison with the measured susceptibilities shows good agreement for substances with a small proportion of magnetic ions. Measurements at low temperatures down to  $95^\circ\text{K}$  have shown that in general these materials obey the Curie-Weiss law,  $\chi = C(T - \theta)$ . An attempt is made to relate the value and the sign of  $\theta$  to the concentration of magnetic ions and to the mineral structure.

LES pyroxènes et amphiboles qui font l'objet de cette étude ont été extraits par Nicolas (1966) d'une quarantaine de roches différentes provenant des Alpes internes (Val de Suiza, Italie). Cet auteur se propose de mieux connaître les modalités du métamorphisme dans les roches vertes de cette région, puis de mettre en évidence l'unité éventuelle de cette série et dans ce cas de préciser les transformations primaires à l'intérieur de cet ensemble.

L'analyse chimique complète des échantillons a été effectuée au Centre de Recherches Pétrographiques et Géochimiques du CNRS de Nancy-Vandoeuvre (France).

Il nous a paru particulièrement intéressant d'étudier sur ces échantillons les relations qui existent entre les propriétés magnétiques et leurs constitutions.

*Travaux antérieurs.* Depuis 1957 plusieurs auteurs ont essayé de relier les propriétés magnétiques des silicates ferro-magnésiens à leur chimisme. Nous rappellerons les études de Nagata et ses collaborateurs (1957) sur les olivines, Chevallier et Mathieu (1958) sur les pyroxènes monocliniques du Skaergaard, Akimoto et ses collaborateurs (1958) sur des orthopyroxènes, Syono (1960) sur des cordiérites, biotites, amphiboles, et grenats, Petruk (1965) sur des chlorites.

Dans la plupart de ces travaux, les expériences ont été effectuées à  $20^\circ\text{C}$ . Les mesures de susceptibilités à cette température ont montré qu'elles étaient

pratiquement les mêmes que celles calculées à partir de la concentration en ions magnétogènes en admettant la loi de Curie.

*Composition chimique des amphiboles et des pyroxènes.* Les analyses chimiques, en ce qui concerne les ions magnétogènes, de nos échantillons sont données dans tableau I. Les teneurs en ions magnétogènes  $\text{Fe}^{2+}$ ,  $\text{Fe}^{3+}$ , et  $\text{Mn}^{2+}$  de ces substances présentent une assez grande variété.

TABLEAU I. Analyses chimiques des pyroxènes et des amphiboles  
(Teneurs en  $\text{Fe}^{2+}$ ,  $\text{Fe}^{3+}$ , et  $\text{Mn}^{2+}$ )

<i>Pyroxenes</i>	52	53	54	55	56	57	58	164	165	168	179	183
$\text{Fe}_2\text{O}_3$	2,01	2,87	1,77	1,06	0,75	1,79	0,55	1,05	0,38	0,00	1,35	1,70
$\text{FeO}$	7,34	7,21	4,85	3,30	8,73	4,70	3,76	10,39	6,87	4,63	1,30	2,60
$\text{MnO}$	0,36	0,31	0,15	0,09	0,11	0,12	0,10	0,14	0,15	0,13	0,19	0,07
<i>Amphiboles</i>	75	76	78	80	84	86	88	89	90	169	177	186
$\text{Fe}_2\text{O}_3$	1,00	1,82	2,52	7,13	5,29	0,00	1,93	1,95	1,62	10,50	6,27	1,26
$\text{FeO}$	4,90	8,93	3,14	8,13	8,47	4,24	7,79	5,45	2,78	2,26	9,27	10,46
$\text{MnO}$	0,14	0,16	0,12	0,14	0,19	0,08	0,16	0,16	0,03	0,17	0,09	0,02

*Susceptibilité magnétique théorique.* Si les trois ions magnétogènes  $\text{Fe}^{2+}$ ,  $\text{Fe}^{3+}$ , et  $\text{Mn}^{2+}$  sont considérés comme indépendants dans la structure, hypothèse qui a été formulée par la plupart des chercheurs, le calcul de la susceptibilité magnétique théorique est immédiat d'après la loi de Curie Langevin. Rappelons ce calcul (Chevallier, 1958).

L'aimantation d'un ion gramme à la température  $T$  est  $\sigma_i = M_B^2 p_B^2 H / 3RT$  ( $M_B$  est la valeur du magnéton gramme de Bohr,  $p_B$  le nombre de magnétons de Bohr relatif à l'ion,  $R$  la constante des gaz parfaits,  $T$  la température absolue, et  $H$  le champ appliqué). Si nous désignons respectivement par  $x$ ,  $y$ ,  $z$  les nombres d'ions grammes de  $\text{Fe}^{2+}$ ,  $\text{Fe}^{3+}$ , et  $\text{Mn}^{2+}$  contenus dans un gramme de silicate, l'aimantation d'un gramme de cette substance s'écrira  $\sigma = M_B^2 H (xp_B^2 + yp_B'^2 + zp_B''^2) / 3RT$  ( $p_B$ ,  $p_B'$  et  $p_B''$  sont respectivement les moments magnétiques des ions  $\text{Fe}^{2+}$ ,  $\text{Fe}^{3+}$ , et  $\text{Mn}^{2+}$  exprimés en magnétons grammes de Bohr).

Si les trois ions magnétogènes  $\text{Fe}^{2+}$ ,  $\text{Fe}^{3+}$ , et  $\text{Mn}^{2+}$  ne peuvent pas être considérés comme indépendants dans la structure, il convient de reprendre le calcul en faisant intervenir leur interaction par le champ moléculaire de Weiss. Nous admettons alors que les ions magnétiques sont soumis à un champ vrai  $H = H' + n\sigma$ , le champ  $H'$  étant augmenté d'un champ moléculaire proportionnel à l'aimantation spécifique du silicate ( $n$  est le coefficient de champ moléculaire).

Nous avons  $\sigma = CH/T = C(H' + n\sigma)/T$  où  $C$  est la constante de Curie Weiss rapportée à un gramme de silicate. Si nous posons  $\chi = \sigma/H'$  (susceptibilité spécifique du silicate que fournit la mesure) et  $nC = \theta$  ( $\theta$  étant la température de Curie paramagnétique), la loi d'aimantation prend la forme  $\chi(T - \theta) = C$  (loi de Curie-Weiss), où  $C = M_B^2 (xp_B^2 + yp_B'^2 + zp_B''^2) / 3R$ .

Les valeurs de la constante de Curie données dans le tableau II ont été calculées en prenant pour les moments magnétiques des ions, respectivement

les nombres suivants: pour  $\text{Fe}^{2+}$   $p_B = 5,20$  (Chevallier, 1958), pour  $\text{Fe}^{3+}$  et  $\text{Mn}^{2+}$   $p'_B = p''_B = 5,92$  (moments théoriques).

*Les mesures magnétiques.*<sup>1</sup> Pour effectuer nos expériences nous avons utilisé une balance de mesures magnétiques réalisée par l'un d'entre nous (Reithler, 1965) basée sur un principe dû à Weiss et Foëx (1921) et comportant un certain nombre de perfectionnements. Cette balance a été complétée par l'adjonction d'un cryostat (Reithler, 1966) qui nous permet d'effectuer des mesures isothermes de susceptibilité magnétique à basse température.

Les résultats de nos mesures à  $95^\circ\text{K}$  et à  $290^\circ\text{K}$  sont donnés dans le tableau II.

TABLEAU II. Constante de Curie calculée d'après l'analyse chimique, et susceptibilités magnétiques mesurées à  $290^\circ\text{K}$  et à  $95^\circ\text{K}$

<i>Pyroxènes</i>	52	53	54	55	56	57	58	164	165	168	179	183
$10^4 C$	47,81	51,60	33,47	21,91	45,91	32,69	21,34	55,55	35,37	22,61	14,69	21,99
$10^6 \chi_{290^\circ\text{K}}$	12,9	14,5	8,5	4,4	11,3	8,1	5,5	16,0	9,2	6,0	3,4	5,5
$10^6 \chi_{95^\circ\text{K}}$	36,2	37,2	23,5	15,7	29,2	22,4	15,6	50,7	29,1	20,2	10,9	18,7
<i>Amphiboles</i>	75	76	78	80	84	86	88	89	90	169	177	186
$10^4 C$	29,42	49,94	29,34	78,23	70,06	20,46	48,25	37,34	22,16	69,23	77,45	56,29
$10^6 \chi_{290^\circ\text{K}}$	10,6	18,4	9,1	28,3	24,2	7,1	16,4	13,3	5,6	21,1	28,7	20,4
$10^6 \chi_{95^\circ\text{K}}$	29,1	44,2	29,2	81,8	70,6	23,6	43,3	35,0	17,6	61,8	69,0	62,8

*Essais d'interprétation des résultats.* Sur les figures 1 et 2 nous avons porté les susceptibilités magnétiques mesurées en fonction de la constante de Curie calculée d'après l'analyse chimique. On constate que la susceptibilité magnétique mesurée varie linéairement avec la constante de Curie. En appliquant la méthode des moindres carrés aux points expérimentaux, nous avons déterminé les relations suivantes:

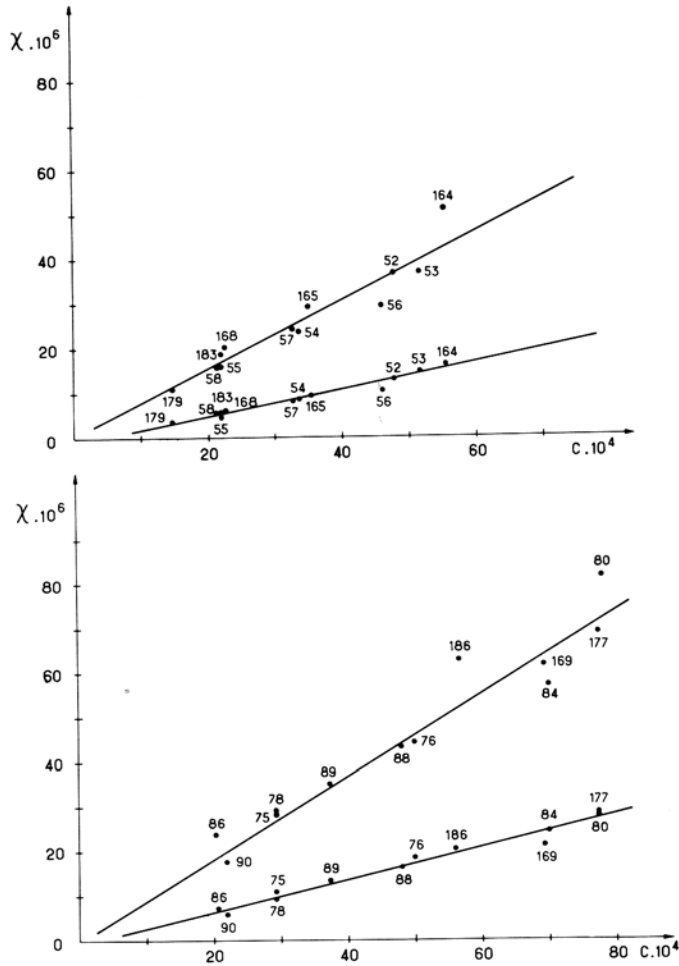
$$\text{Pyroxènes: } \chi_{95^\circ\text{K}} = C/127 - 0,7 \times 10^{-6}; \chi_{290^\circ\text{K}} = C/335 - 1,3 \times 10^{-6}.$$

$$\text{Amphiboles: } \chi_{95^\circ\text{K}} = C/105 - 0,9 \times 10^{-6}; \chi_{290^\circ\text{K}} = C/273 + 1,5 \times 10^{-6}.$$

Des mesures à une température de  $210^\circ\text{K}$  ont donné pour les amphiboles la relation:  $\chi_{210^\circ\text{K}} = C/222 - 0,7 \times 10^{-6}$ .

L'exploitation des mesures à la température ambiante et à basse température permet de calculer les constantes  $C$  et  $\theta$  de la loi de Curie-Weiss. Les valeurs de  $C$  déterminées par les propriétés magnétiques sont sensiblement les mêmes que celles calculées d'après l'analyse chimique ce qui tend à prouver que l'ion ferreux présent dans ces pyroxènes et amphiboles a le même moment magnétique que celui trouvé par Chevallier (1959) dans des pyroxènes monocliniques. En ce qui concerne  $\theta$ , cette grandeur semble indépendante de la constante de

<sup>1</sup> Ces mesures ont été effectuées avec la collaboration de Monsieur Pierre Menaert, collaborateur technique au (CNRS) Centre National de la Recherche Scientifique.



FIGS. 1 et 2: FIG. 1 (haut). Susceptibilités magnétiques mesurées à  $95^{\circ}\text{K}$  et à  $290^{\circ}\text{K}$  en fonction de la constante de Curie calculée d'après la teneur en ions magnétogènes. Cas des Pyroxènes. FIG. 2 (bas). Susceptibilités magnétiques mesurées à  $95^{\circ}\text{K}$  et à  $290^{\circ}\text{K}$  en fonction de la constante de Curie calculée d'après la teneur en ions magnétogènes. Cas des Amphiboles.

Curie, donc de la concentration en ions magnétogènes; pour les pyroxènes cette grandeur est de l'ordre de  $-40^{\circ}\text{K}$  et pour les amphiboles elle varie de  $+20^{\circ}\text{K}$  (température déterminée à l'aide des mesures effectuées à la température ambiante) à  $-10^{\circ}\text{K}$  pour  $95^{\circ}\text{K}$ .

Ces résultats préliminaires, en ce qui concerne les points de Curie, sont assez surprenants. Nous nous proposons de poursuivre ces recherches sur un plus grand nombre d'échantillons pour voir s'ils sont généralisables. Cette

étude montre, en outre, la possibilité de déterminer, à partir des mesures magnétiques, l'ordre de grandeur des teneurs en ions magnétogènes.

*Bibliographie*

- AKIMOTO (S.), HORAI (K.), et BOKU (T.), 1958. *Journ. Geomag. Geoelect.*, **10**, 7-11.  
CHEVALLIER (R.) et MARTIN (R.), 1959. *Bull. Soc. Chim. Fr.*, 3-10.  
— —, 1958. *Ibid.*, 726-729.  
FOËX (G.), 1921. *Ann. Phys. Fr.*, ser. 9, **16**, 200.  
NAGATA (T.), YUKUTAKE (T.), et UYEDA (S.), 1957. *Journ. Geomag. Geoelect.*, **9**, 51-56.  
NICOLAS (A.), 1966. Sous presse.  
PETRUK (W.), 1965. *Can. Min.*, **8**, 372-76.  
REITHLER (J. C.), 1965. *Bull. Soc. franç. Min. Crist.*, **88**, 399-403.  
—, 1966. *Ibid.*, **89**, 277-78.  
SYONO (Y.), 1960. *Journ. Geomag. Geoelect.*, **11**, 85-93.

# The use of amphiboles to illustrate trends in contact metamorphism

BRENDA J. CAHILL (née MACARA)

School of Applied Geology, University of N.S.W.,  
Sydney, Australia

*Summary.* This paper describes the paragenesis of the amphiboles of a basic igneous intrusion during its contact metamorphism. There are two remarkable features about the metamorphism of this intrusion, which make it well suited to a study of the detailed changes in amphibole mineralogy:

Metamorphism has been nearly isochemical, a feature that is rather unusual in contact metamorphism, where metasomatism often plays such a large part.

Although one unmetamorphosed phase and three distinct metamorphic grades can be recognised within the rocks studied, the structure of the essential mineralogy remains unchanged; i.e. in the unmetamorphosed rock, representatives of two primary mineral groups make up over 95% of the total volume,—an amphibole and a plagioclase feldspar. Members of these two series remain as the two principal stable phases at all stages of metamorphism, the plagioclase varying widely in composition, twinning, and zoning and the amphibole in colour, habit, and optical properties.

The above features allow a correlation of amphibole changes depending directly upon metamorphic grade to be made without worry about variation in the chemical components. Here, too, the amphiboles appear to have been particularly sensitive index minerals during the contact metamorphism.

They may all be regarded as “normal” calcium-rich amphiboles. Representatives from each metamorphic grade have been chemically analysed and a detailed examination of their optical properties made. The latter, including refractive indices,  $2V_z$ , and density, were determined as accurately as possible. Correlation of these results, both with each other and with selected chemical ratios, was also made.

THE Bathurst Batholith of southern New South Wales is a large high-level igneous complex of supposed Middle Carboniferous age, dominated by acid rock types. However, at its most easterly extension, known as the Hartley Granite, a number of small, apparently unconnected basic igneous bodies of varying sizes occur.

One of these, the Budthingeroo Metadiabase, has been intruded prior to, and near the SE margins of the granitic rocks in the area of the Jenolan Caves and Kanangra Plateau, about 130 miles west of Sydney (see fig. 1). This is a sheet- or dyke-like body of basaltic composition, some six miles in length and up to a half a mile in width. It is a homogeneous rock of fine to medium grain size (1.0 to 1.5 mm), which has a fine-grained marginal phase (0.5 mm) ranging from a few feet to over 20 yards in width. The marginal rocks often show evidence of flow, and contain lenticular, calcite-filled vesicles and veins.

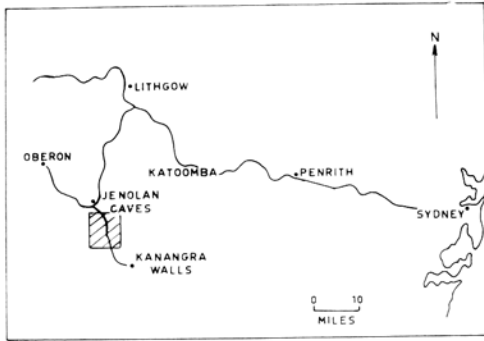


FIG. 1. Geographic location of the Budthingeroo Metadiabase.

an almost unique opportunity for an evaluation of the factors influencing the changes in the constituent amphiboles during the contact metamorphism:

Chemical analyses show that the introduction of chemically active fluids from the surrounding granitic rocks into the Metadiabase during the metamorphism was severely restricted. Consequently, the formation of metasomatic mineral assemblages is very limited, and thus it is possible to regard a major portion of the series of changes as taking place under isochemical conditions, to a first approximation, for the purposes of considering the individual minerals involved. This is a very important factor in the interpretation of results as it allows one to make a direct correlation of amphibole composition with metamorphic grade under the same chemical conditions, without having to worry about the continuously changing chemical concentrations of various ions.

The basic rock outside the contact aureole, although chemically a basalt, contains an unusually large amount (39.8%) of primary amphibole—common hornblende—for a rock of this composition. There is evidence, too, to indicate that this hornblende has crystallized directly from the basic magma, and has not resulted from the later alteration of clinopyroxenes or olivine in the solid state (Macara, *in press*). There is thus a good opportunity to observe the transformation of igneous hornblende to a low-grade metamorphic amphibole at the edge of the contact aureole.

Although one non-metamorphic and three distinct metamorphic zones can be distinguished, corresponding to progressive stages in the recrystallization of basaltic to metabasaltic rocks, representatives of only two main mineral groups, an amphibole and a plagioclase, are the principal stable phases in all stages, making up over 90% of the total rock volume. Depending upon the metamorphic grade of the rock, however, the character of these two minerals does change considerably—the amphibole in colour, form, and optical properties, and the plagioclase in composition and structure, including zoning and twinning.

The intrusion invades Upper Devonian sediments (quartzites and siltstones), but contact metamorphism by the later Hartley Granite has affected almost its entire length.

A detailed chemical and mineralogical study has been made of the progressive trends shown by the amphiboles of this intrusion, in response to increasing grade of contact metamorphism.

The Budthingeroo Metadiabase has several features that provide

*Petrography of the rocks*

The Budthingeroo Metadiabase may be subdivided into four main groups, according to the type of amphibole and the composition of the plagioclase feldspar present: Hornblende diabase—the parent rock outside the contact aureole, tremolite hornfelses, low-grade amphibolite hornfelses, and high-grade amphibolite hornfelses. Average modal and optical data for each zone are given in table I.

TABLE I. Average modal and optical data for the Budthingeroo Metadiabase

*Mode (volume %):*

	1	2	3	4
Amphibole	39.8	45.5	50.6	53.6
Plagioclase	44.9	39.3	37.1	32.2
Clinopyroxene	4.5	—	—	2.6
Olivine	2.6	—	—	—
Biotite	1.1	4.1	6.4	3.2
Epidote	—	2.8	0.9	—
Chlorite	—	1.4	—	—
Garnet	—	—	—	1.8
Magnetite	4.9	3.9	2.8	4.5
Apatite	1.2	—	—	—
Others	1.0	3.0	2.2	2.1

*Average optical data:*

Amphibole $\begin{cases} \gamma \\ \gamma : [001] \end{cases}$	1.675 23°	1.662 17°	1.669 24°	1.675 26°
Plagioclase $\beta$	1.559	n.d.	1.552	1.565

1. Hornblende diabase.
2. Tremolite hornfels.
3. Low-grade amphibolite hornfels.
4. High-grade amphibolite hornfels.

*Hornblende diabase.* This subdivision represents those portions of the igneous intrusion outside the contact aureole. The rocks are homogeneous and fine-grained and have the chemical composition of a high-alumina basalt (as defined by Yoder and Tilley, 1962). There is, however, a rather high water content ( $H_2O=4.06\%$ ). The rocks are composed principally of amphibole (common hornblende), 39.8%, and plagioclase (sodic labradorite, An 54–57%), 44.9%. These two minerals show typical diabasic textural relations. The plagioclase is mostly clear and unaltered, though rather fractured.

The hornblende is prismatic, though the prisms are quite short and stumpy. It is typically subhedral and appears to have crystallized somewhat later than the plagioclase. It is strongly pleochroic from pale yellow to a deep green-brown,  $\alpha < \beta < \gamma$ , and is nearly always fresh, with no signs of any alteration.

Olivine and clinopyroxene are present only in small discrete grains (total vol. 7.1%); where they are fresh, they are invariably euhedral. However, they are much more commonly altered to chlorite with some iron oxides.

At the edge of the contact aureole, quite distinctive mineralogical and textural changes have taken place.

*Tremolite hornfels*. This group of rocks represents the lowest grades of contact metamorphism of the Metadiabase. The assemblages are typical of the Albite–Epidote Hornfels Facies (as defined by Fyfe, Turner, and Verhoogen, 1958, p. 203). The principal minerals are amphibole (Al-bearing tremolite), 45.5%, and plagioclase (albite, An 9–13%), 39.3%. In some specimens, relicts of calcic plagioclase phenocrysts are preserved, but more commonly, all traces of the original mineral have been obliterated and all that remains is a fine xenoblastic mosaic of albitic material, containing clouds of tiny amphibole needles. The amphibole is a fine, fibrous variety, which has grown in a prismatic habit, forming the typical criss-cross or decussate texture, common in low-grade thermally metamorphosed rocks. It appears to be a true tremolite, as defined by Phillips and Layton (1964), though some of its optical properties are more consistent with those of a common hornblende. The tremolite is colourless to a pale green, with distinctly lower birefringence and extinction angles than in the Hornblende Diabase.

A characteristic feature of this zone is the universal occurrence of clouds of tiny amphibole needles, having the same optical properties as the tremolite. These almost obscure the other mineral phases. Fine granular epidote and calcite are constant minor accessories in these rocks; also, a fine Ca-bearing zeolite is commonly present, which is probably the breakdown product of the calcic plagioclase. Accessory magnetite, while abundant in some specimens, has almost disappeared in others. The latter contain a fine brown micaceous mineral.

Between the Hornblende Diabase and the Tremolite Hornfels there is an abrupt optical transition between the two kinds of amphibole. No crystals with intermediate properties were observed. At the very outer limits of the contact aureole there are some rocks where both amphiboles are present, each showing the distinctive properties of its respective zone.

With increase in the grade of contact metamorphism, the rocks very closely resemble regionally developed amphibolites. Thus, the higher-temperature rocks are termed “amphibolite hornfels”.

*The low-grade amphibolite hornfels*. Here the major mineral phases are amphibole (common hornblende), 50.6%, and plagioclase (andesine, An = 37–43%), 37.1%. The amphibole is a true hornblende. It is well formed and shows a complete lack of preferred orientation. Fibrous edgings are present on most crystals. The tiny acicular amphibole needles are again present, but to a lesser extent than in the lower-grade rocks. Optical properties of the hornblende vary somewhat within this zone, with  $\alpha$  pale green,  $\beta$  and  $\gamma$  green,  $\gamma$  : [001]  $22^\circ$  on the lower temperature portions, and  $\alpha$  and  $\beta$  green,  $\gamma$  green to bluish green,  $\gamma$  : [001]  $26^\circ$  near the higher-temperature regions.

Plagioclase is not well formed and is only poorly twinned. There are few accessory minerals. A little brown biotite and some rather ragged magnetite are the only common minor constituents.

The rocks of this zone are considered to have developed under conditions similar to the lower temperature regions of the Hornblende Hornfels Facies.

*The high-grade amphibolite hornfels.* The two principal mineral phases remain stable once more in this group of rocks. The composition is amphibole (pargasite), 53.6% and plagioclase (calcic labradorite, An 61–68%), 32.2%. The amphibole is again a true hornblende. It has deepened in colour in the  $\gamma$  direction, which now shows a distinct blue-green. Chemical analyses and refractive index work reveal the hornblende to be a member of the pargasite–ferrohastingsite series (Deer, Howie, and Zussmann, 1963, p. 264). The amphibole is optically homogeneous and has a prismatic to tabular habit, having completely lost its fibrous edgings. The tiny amphibole needles, so common in the lower grade rocks, are only of rare occurrence.

The plagioclase is well crystallized, but still almost untwinned. Textures are the typical granoblastic ones of high-grade contact hornfels. Accessories in this zone are magnetite, diopsidic pyroxene, and a little Ca–Al bearing garnet.

The rocks in this zone are representative of the upper temperature portions of the Hornblende Hornfels Facies and probably their conditions of formation actually overlap into the  $P$ – $T$  field of the Pyroxene Hornfels Facies (Macara, in press).

#### *Optical variation in the amphiboles*

Optically, the most striking variation shown by the amphiboles in response to increasing grade of contact metamorphism is the change in colour and habit. The correlation of the colour of the  $\gamma$  optical direction in amphiboles with grade of regional metamorphism has been noticed by several researchers (e.g. Shidô, 1958; Layton, 1963). Table II shows the relation between amphibole colour and habit and grade of contact metamorphism.

At the onset of metamorphism, a rather stumpy green-brown amphibole is transformed into a prismatic, almost acicular, pale-green variety, which gradually deepens in colour and becomes less attenuated with increasing temperature,

TABLE II. Relation of amphibole colour and habit to grade of contact metamorphism

Rock type	Amphibole $\gamma$ colour	Habit
Hornblende Diabase	Deep brown-green	Fairly equant to tabular crystals
Tremolite Hornfels	Very pale green to pale green	Long fibrous crystals, often acicular
Low-grade Amphibolite Hornfels	Green to light blue-green	Long prismatic crystals, fibrous edgings
High-grade Amphibolite Hornfels	Blue-green to very deep blue-green	Prismatic or tabular crystals. Not fibrous

until at the highest levels of metamorphism it is again in tabular crystals, but of a deep blue-green colour.

As might be expected, these results are not identical with those observed in regional terrains, where the more common tendency is toward a brown-green amphibole with increasing grade of regional metamorphism.

Also, the observations are similar to, but not identical with those made by Binns on the hornblendes in basic hornfelses of the New England region (Binns, 1965). Though he has found that the first indications of metamorphism are the crystallization of an amphibole with a "ragged or fibrous actinolitic habit" that with increase of grade becomes less ragged and finally granular, as has happened here, the colour changes he has observed differ quite considerably from those noted in the Budthingeroo Metadiabase.

In the New England basic hornfelses a pale bluish green "actinolite" gradually deepens to deep bluish green, then deep green and finally brown with rising metamorphic grade. In the Metadiabase there is no tendency at all toward greeny-brown tints. Instead it is a deep bluish colouring that indicates the highest metamorphic grades in the amphiboles.

Modal and optical data also reveal that a distinct correlation between the modal volume of plagioclase, its composition, and its metamorphic grade, does exist (see table I). The plagioclase becomes markedly more calcic with increasing grade. This is, in fact, one of the most striking features of the rocks. The proportion of plagioclase decreases however, with rising temperature, while that of hornblende increases.

The last observation again differs from that made by Binns for the New England basic hornfelses. However, the difference is most probably due to the initial dissimilarity in the mineral composition of the basic rocks outside the

contact aureole. In New England a clinopyroxene and plagioclase reaction occurred at the edge of the contact aureole to form the actinolite, thus decreasing by half the proportion of plagioclase, which gradually reconstituted with rising temperatures. Here, a large amount of hornblende was already present in the unmetamorphosed rock, and clinopyroxene was only a very minor constituent. Thus the formation of tremolite was mainly a result of a direct conversion of igneous hornblende.

The results of a comparison of optical measurements of axial angle ( $2V_x$ ) and refractive index ( $\gamma$ )

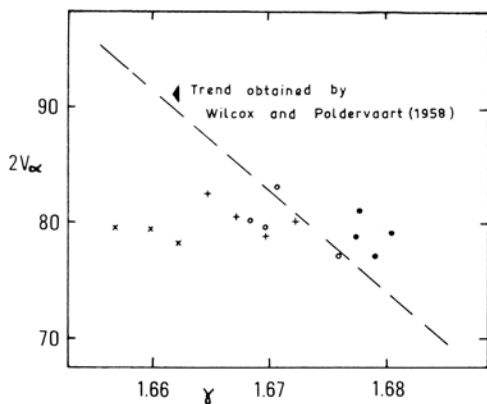


FIG. 2. Optical data for the amphiboles: ○, from the Hornblende Diabase; ×, from the Actinolite Hornfels; +, from the low-grade Amphibolite Hornfels; ●, from the high-grade Amphibolite Hornfels.

of the amphiboles are given in fig. 2. These do not reveal any single linear trend, such as that obtained on calciferous amphiboles by Wilcox and Poldervaart (1958), which is also given in fig. 2. The main optical variation here has been the change in  $\gamma$ . Optic axial angle is obviously not a diagnostic property; there is a range of  $2V_\alpha$  values for each different group, but no difference between groups.

The progressive changes in both optical and density measurements will be considered in detail later, in conjunction with the results of chemical work.

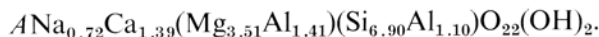
#### *Amphibole chemistry*

Chemical analyses, structural formulae (calculated after Phillips, 1963), and chief optical properties of the different amphiboles are given in table III. All of these amphiboles may be considered as calcium-rich amphiboles having the general formula of  $AX_2Y_3Z_8O_{22}(OH)_2$ , where  $A = Na, K$ ;  $X = Ca, Na, K$ ;  $Y = Mg, Fe^{2+}, Mn, Fe^{3+}, Ti, Al^{vi}$ , etc.; and  $Z = Si, Al^{iv}$ .

It has been found satisfactory to express all the compositions in terms of one or the other of two simple ionic substitutions into an initial "tremolite" formula of " $ACa_2Mg'_5Si_8O_{22}(OH)_2$ " where  $A$  is a vacant lattice position and  $Mg'$  is equivalent to  $(Mg + Fe^{2+} + Mn)$ . This form of systematization was derived by Sundius (1946) for calcium-bearing amphiboles in general.

The two types of ionic substitution used are the filling of the vacant  $A$  site in the lattice with Na, the electrical neutrality of the formula being maintained by the substitution of  $Al^{iv}$  for Si (i.e.  $Si \rightarrow Na, Al^{iv}$ ) and a substitution of the type  $Mg, Si \rightarrow Al^{vi}, Al^{iv}$  leaving the  $A$  space vacant.

These principles of ionic substitution will now be used to evaluate the chemical changes taking place in the amphiboles of the Budthingeroo Metadiabase in response to increasing grade of contact metamorphism. For the sake of simplicity, the following ions are grouped together,<sup>1</sup> Na, K; Mg,  $Fe^{2+}$ , Mn; and  $Fe^{3+}$ , Ti,  $Al^{vi}$ . Using Table III the chemical formula for the amphibole from the Hornblende Diabase (no. 1A) may be written as follows:



The formula of this amphibole can be considered as an almost straightforward variation of the pure "tremolite" formula, following the substitution  $MgSi \rightarrow AlAl$  to a value of 1.10 atoms/formula unit (atoms/f.u.). A portion of the sites usually occupied by Ca are, however, also vacant. Their place is taken by Na, but as it requires 2 Na to balance the charge of each Ca there remains a deficiency of 0.3 charges/f.u. in the  $X$  sites. Now it will be noticed that there is an excess of Al in the  $Y$  positions to an amount of 0.3 atoms/f.u. This balances the deficiency of the  $X$  valencies. The main variation from an initial theoretical tremolite formula is thus the substitution  $MgSi \rightarrow AlAl$  to an amount just over 1 atom/f.u.

<sup>1</sup> The grouping of  $Ti^{4+}$  with Al means that the charge balances referred to do not appear to be exact.

TABLE III. Chemical analyses, structural formulae, and optical data of the amphiboles

<i>Analyses:</i>					<i>No. of ions on a basis of 24(O, OH):</i>					
	1A	2A	3A	4A						
SiO <sub>2</sub>	48.20	52.40	47.50	43.50	Z	Si	6.90	7.47	6.79	6.27
Al <sub>2</sub> O <sub>3</sub>	11.51	5.95	10.69	13.02		Al <sup>iv</sup>	1.10	0.53	1.21	1.73
TiO <sub>2</sub>	2.22	0.89	0.56	0.63			} 8.00		} 8.00	
Fe <sub>2</sub> O <sub>3</sub>	3.03	4.35	3.73	4.76	Y	Al <sup>vi</sup>	0.84	0.47	0.59	0.48
FeO	10.10	7.57	8.12	8.45		Ti	0.24	0.10	0.06	0.07
MnO	0.22	0.16	0.17	0.32		Fe <sup>3+</sup>	0.33	0.47	0.40	0.51
MgO	10.65	14.33	14.43	14.01		Mg	2.27	3.05	3.07	3.02
CaO	9.08	10.20	11.03	11.04		Fe <sup>2+</sup>	1.21	0.90	0.97	1.02
Na <sub>2</sub> O	2.48	1.40	1.76	2.89		Mn	0.03	0.02	0.02	0.04
K <sub>2</sub> O	0.18	0.16	0.45	0.84	X	Ca	1.39	1.56	1.69	1.72
H <sub>2</sub> O	2.21	1.98	2.06	2.03		Na	0.69	0.39	0.49	0.81
Totals:	99.88	99.39	100.50	101.49		K	0.03	0.03	0.08	0.16
Analyst: B. J. Macara							} 2.11		} 1.98	
							} 2.26		} 2.68	
					(OH)		2.11	1.88	1.96	1.96
					O		21.89	22.12	22.04	22.04
					mg*		59.1	68.7	68.8	65.7
<i>Optical data:</i>					Specimens:					
D	3.18	3.12	3.16	3.20	1A	Hornblende from the Hornblende Diabase				
α	1.656	1.634	1.642	1.655	2A	Tremolite from the Tremolite Hnflses				
γ	1.679	1.657	1.665	1.678	3A	Hornblende from Low grade Amphib. Hnflses				
γ : [001]	25°	19°	22°	27°	4A	Pargasite from High grade Amphib. Hnflses				
2 V <sub>α</sub>	77°	79°	82°	80°						
α	yellow	colourless	pale green	yellow-green						
β	yellow-brown	pale green	yellow-green	green						
γ	deep green-brown	pale green	green	deep blue-green						

\* mg = 100 Mg / (Mg + Fe<sup>2+</sup> + Fe<sup>3+</sup> + Mn).

The amphibole is a member of the *common hornblende series* (as defined by Deer, Howie, and Zussman, 1963).

The formula for the amphibole in the Tremolite Hornfels (no. 2A) is  $ANa_{0.41}Ca_{1.56}(Mg_{3.97}Al_{1.04})(Si_{7.47}Al_{0.53})O_{22}(OH)_2$ . The main variation from a pure "tremolite" formula is once again the substitution  $MgSi \rightarrow AlAl$ . However, this time it is only to the amount of 0.53 atoms/f.u. The deficiency of charge in the *X* sites is compensated by the substitution of  $Al^{VI}$  in *Y*. The amphibole may be considered as chemically intermediate between the tremolites and the common hornblendes. Taking both optical and chemical factors into consideration, it is placed in the *tremolite series*, and may be classified as an Al-bearing tremolite.

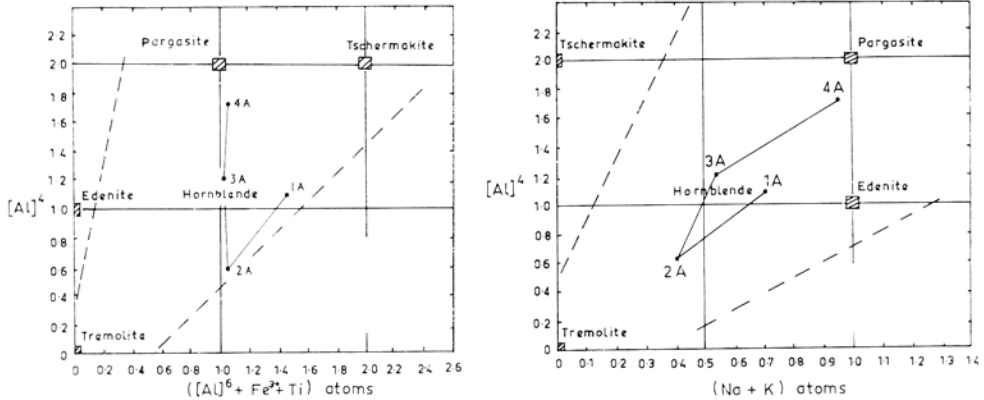
The amphibole in the Low-grade Amphibolite Hornfels (no. 3A) has a formula  $Na_{0.57}Ca_{1.69}(Mg_{4.06}Al_{1.09})(Si_{6.79}Al_{1.21})O_{22}(OH)_2$ . Once again, the main variation from an original "tremolite" formula is of the type  $MgSi \rightarrow AlAl$  to an amount of 1.09 atoms/f.u., leaving an excess  $Al^{IV}$  of 0.12 atoms/f.u. This is balanced by the net effect of a deficiency of 0.31 charges/f.u. in the *X* sites and 0.26 alkali atoms/f.u. in the *A* site. The actual amounts of both Ca and Na have increased and this amphibole may be considered as a member of the *common hornblende series*.

In the High-grade Amphibolite Hornfels the amphibole (no. 4A) has the formula  $Na_{0.97}Ca_{1.72}(Mg_{4.09}Al_{1.06})(Si_{6.27}Al_{1.73})O_{22}(OH)_2$ . To derive this formula from pure "tremolite" requires both types of ionic substitution recognised by Sundius (1946). The substitution  $MgSi \rightarrow AlAl$  has occurred to an amount of 1.06 atoms/f.u. Substitution of the type  $NaAl \rightarrow Si$  has also taken place. After filling the vacant *X* sites caused by a deficiency in Ca, an amount of Na equal to 0.69 atoms/f.u. is left over to fill the vacant *A* site. This balances the  $Al^{IV}$  of 0.67 atoms/f.u. left in excess after the other substitution. The amphibole may thus be considered as lying within the chemical boundaries of the *pargasite series* as defined by Deer, Howie, and Zussman (1963).

To illustrate the relations between end-member series of the calcium-rich amphiboles the above authors have expressed the two types of chemical variation in the form of two graphs. These graphs are reproduced in figs. 3 and 4 and plot the variation as numbers of  $(Na + K)$  and  $(Al^{VI} + Fe^3 + Ti)$  versus  $Al^{IV}$  respectively. The four analyses from the Metadiabase are plotted onto these two figures. Analyses 1A and 3A fall clearly into the field of the common hornblendes, neither showing any especial tendency toward either edenitic or tschermakitic types. Analysis 4A lies in the pargasite field, while analysis 2A falls close to what must be the boundary between the tremolites and the common hornblendes with respect to the amount of  $Al^{IV}$  in the lattice and to both the amounts of total alkalis and number of trivalent *Y* ions.

It is felt that the composition of this Al-bearing type of amphibole was probably influenced by the initial high alumina content of the igneous rock and the absence of any other possible Al-bearing mineral phases. The amphibole is thus considered to be a tremolite rather than a true hornblende.

Fig. 3 illustrates how the total number of trivalent ions in *Y* decreases quite



FIGS. 3 and 4: The chemical variation of the amphiboles in the Budthingeroo Metadiabase. FIG. 3 (left). Expressed as the numbers of Al<sup>vi</sup> + Fe<sup>3+</sup> + Ti and Al<sup>iv</sup> atoms per formula unit. FIG. 4 (right). Expressed as the numbers of Na + K and Al<sup>iv</sup> atoms per formula unit.

markedly at the commencement of metamorphism, till at the highest levels it regains approximately its initial content.

From fig. 4 it can be seen that the changes in the total amount of alkalis within the amphibole structure have been much greater, even when taking into account the fact that the abscissa scale in fig. 4 is twice that in fig. 3.

To appreciate the full significance of these changes it is necessary to look at them in more detail than this, however. Observations have thus been made, not only of the sums of various groups of ions, but also of the various ions themselves. This is done in Table IV.

It should perhaps be stressed once more, that, as the metamorphism is considered to be *mainly* isochemical, changes in amphibole composition are due entirely to direct response of the mineral to metamorphism and that they are not just a reflection of changes in total rock composition. There is one possible exception to this rule:

The greatest differences occur at the edge of the contact aureole in the conversion of the igneous hornblende to a tremolite. There are sharp changes in elements of all three structural groups of the amphibole formula. The drop in Al content in both four- and six-fold co-ordinate positions is quite large, totalling 1 atom/f.u. There has also been a high percentage decrease in the amount of total alkalis, amounting to 0.3 atoms/f.u. In the Y positions a large increase in Mg content has occurred (0.8 atoms/f.u.). However, this may be partly due to the 2% MgO increase in the whole rock and it is possible that this is the one case where a change in amphibole composition reflects a change in bulk composition.

In the conversion of tremolite into the metamorphic hornblende the Si → Al<sup>iv</sup> change is abrupt once more (0.7 atoms/f.u.), Al<sup>iv</sup> content increasing to just over the original amount. The Al<sup>vi</sup> gain is much lower (0.1 atoms/f.u.) and, in fact,

TABLE IV. Quantitative changes in amphibole chemistry during metamorphism

Atom groups in amphibole structure	Element	1A → 2A		2A → 3A		3A → 4A	
		Gain	Loss	Gain	Loss	Gain	Loss
Z	Si	0.6	—	—	0.7	—	0.5
	Al <sup>iv</sup>	—	0.6	0.7	—	0.5	—
Y	Al <sup>vi</sup>	—	0.4	0.1	—	—	—
	Fe <sup>3+</sup>	—	—	—	0.1	0.1	—
	Mg	0.8	—	—	—	—	0.1
	Fe <sup>2+</sup>	—	0.3	0.1	—	0.1	—
X	Ca	0.2	—	0.15	—	—	—
	Na	—	0.3	0.15	—	0.4	—
Net change in cations per change		—		+0.4		+0.5	

Na = total alkalis;

Fe<sup>2+</sup> includes Mn;

Fe<sup>3+</sup> includes Ti.

Conversions are: 1A → 2A = igneous hornblende to tremolite;

2A → 3A = tremolite to metamorphic hornblende;

3A → 4A = met. hornblende to pargasite.

all the changes in the Y positions are small. There is a small increase of both Ca and alkalis in the X positions.

The conversion of metamorphic hornblende to pargasite in the higher grades of metamorphism of the Metadiabase has, once more, brought about a number of changes in amphibole composition. The Si → Al<sup>iv</sup> substitution has increased by an amount of 0.5 atoms/f.u. The other major change is a sharp increase in the amount of total alkali by 0.4 atoms/f.u. Elements in the Y positions remain virtually unchanged, though this conclusion could be disturbed if the rather large analytical error in 4A were concentrated in one of the Y or Z elements.

Working on the regionally metamorphosed epidiorites of the South-west Highlands in Scotland, Wiseman (1934) found that with increasing metamorphic grade, there is a progressive increase in the amount of Al in the Z position. He thus postulated a continuous series of Si → Al<sup>iv</sup> substitution up to 2 atoms/f.u. (as in the pargasites). A number of writers disagree with this idea.

Shidô (1958) and Shidô and Miyashiro (1959), working on the regionally metamorphosed basic rocks of the Abukuma Plateau in Japan, showed that a progressive relationship between metamorphic grade and Si → Al<sup>iv</sup> replacement was not evident in that locality. However, they did demonstrate that the maximum possible content of alkali ions, of a particular metamorphic grade, increases with increasing grade.

Layton (1963) has indicated that "the conversion of actinolite to ferrohastingsite is not a simple matter of aluminium entering the molecule in response

to increasing metamorphic grade, but that there must be a concomitant increase in the Fe content".

There is a large increase in  $Al^{iv}$  content in the Metadiabase with increasing metamorphic grade, as predicted by Wiseman (1934). However, the changes are abrupt and owing to the lack of information on any intermediate types, results neither prove nor disprove the existence of continuous  $Si \rightarrow Al^{iv}$  replacement to the amounts present in the pargasite series.

Total alkalis increase in amount as predicted by Shidō and Miyashiro (1959). Evidence for a progressive increase in Fe content with increasing grade (Layton, 1963) is marginal.

#### *Trace element variations in the amphiboles*

The trace element content of the four analysed amphiboles was also determined (see table V). Amounts are given in parts per million of the relevant oxides. When metamorphism occurred, the trace element content of the igneous hornblendes altered markedly. The percentage of the elements Ba, Co, Cu, Mn, Sc, Sr, V, and Zr all decreased, while Ni and Cr increased.

TABLE V. Trace element content of the amphiboles, in parts per million

	1A	2A	3A	4A		1A	2A	3A	4A
BaO	600	150	250	300	NiO	110	270	240	180
CoO	70	45	55	50	Sc <sub>2</sub> O <sub>3</sub>	85	60	100	80
Cr <sub>2</sub> O <sub>3</sub>	300	800	1 000	400	SrO	500	250	200	350
CuO	200	75	200	90	V <sub>2</sub> O <sub>5</sub>	500	450	550	400
MnO	2 200	1 600	1 700	3 200	ZrO <sub>2</sub>	350	85	90	150

BaO, SrO, and ZrO<sub>2</sub> all show a sharp decrease on the transition from an igneous to a metamorphic amphibole. BaO goes from 600 to 150 p.p.m., SrO from 500 to 250 p.p.m., and ZrO<sub>2</sub> from 350 to 85 p.p.m. With increasing metamorphic grade this amount gradually rises again, BaO reaching 300 p.p.m., SrO 350 p.p.m., and ZrO<sub>2</sub> 150 p.p.m. In each case the last amount is about half of the original content.

MnO shows an initial sharp decrease, from 2 200 to 1 600 p.p.m., followed by an increase, until in the High-grade Amphibolite Hornfelses the Mn content is 3 200 p.p.m., or about half as great again as the original amount. Ni and Cr contents have both increased with metamorphism, NiO from 110 to 270 p.p.m. and Cr<sub>2</sub>O<sub>3</sub> from 300 to 800 p.p.m. Engel (1959) and Howie (1955) have found that these two elements tend to be concentrated in the more Mg-rich hornblendes. The MgO content of the igneous hornblende here is 10.65% and this rises to over 14% in all of the metamorphic amphiboles. The results thus are in accordance with both Engel and Howie's observations.

Howie (1955) has furthermore found that Co shows a small decrease in the Mg-rich amphiboles and this, too, is in agreement with the results here, Co content dropping from 70 to 50 p.p.m. with increase in Mg content. The elements

Cu, Sc, and V do not show any apparent trend, but form a “zig-zag” pattern, with an initial decrease, followed by a rise, then another decrease.

*Optical versus chemical data*

The amphibole variation with increasing grade of contact metamorphism may also be represented by comparing the optical measurements with the chemical composition. The relationship can be expressed in numerous ways. However, the complex chemistry makes a simple correlation impossible, as the presence or absence of so many individual ions can affect the optical results.

Thus, graphical means, although the most common form of expressing the relationship, are not really precise. To obtain maximum accuracy the optical results are generally plotted against a chemical ratio rather than a separate ion. Using the ratio  $100 \text{ Mg} / (\text{Mg} + \text{Fe}^{2+} + \text{Fe}^{3+} + \text{Mn})$ , Deer, Howie, and Zussmann (1963) have constructed separate charts relating this to the optical properties for each end-member series of the amphiboles. The correlation appears to be quite good.

In fig. 5 the optical data for the amphiboles in the Metadiabase are plotted onto these graphs. As only one chemical analysis was obtained from each zone, there is only one chemical ratio per group. Thus, the optical results fall into vertical columns, the abscissa value pertaining to the relative chemical analysis. Instead of plotting the charts of Deer, Howie, and Zussmann in full, each containing only one line of results, small portions were taken and all results are presented together.

For analyses of amphiboles 1A and 3A the standard curves are taken from the chart for the common hornblende series (op. cit. fig. 76). Analysis 2A uses

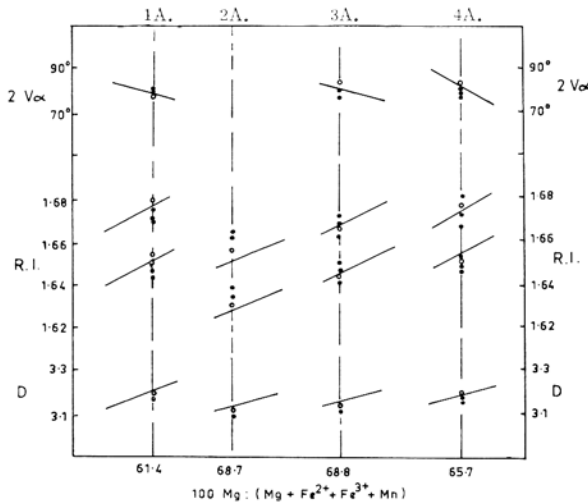


FIG. 5. Correlation of optical and chemical data for the amphiboles. ○, analysed specimens; ●, other specimens from the same rock.

the tremolite–actinolite series chart (op. cit. fig. 66) and analysis 4A the pargasite–ferrohastingsite chart (op. cit. fig. 78). Results of the amphibole specimens that were actually chemically analysed are given in small circles.

Refractive index results show the widest scatter from the plotted lines. In the Tremolite Hornfelses (2A) all indices are greater than the standard curves, yet fall well below the curves for the common hornblende series. (Plotted for 1A and 3A). This is another indication of their chemically intermediate position. 2 V results agree well with the standard curves. They are, however, not diagnostic. Density values have the closest correspondence of all.

### Conclusions

This paper has attempted to illustrate both mineralogical and chemical trends in the amphiboles of a basic igneous rock during its progressive contact metamorphism. The metamorphism has resulted in the formation of three different and distinct zones of amphibole-bearing basic hornfelses.

Changes have been quite distinct, both optically and chemically. Marked variation in colour and habit and a progressive alteration in both refractive index and density are the most striking physical changes.

Chemically, there have been distinct increases in the percentages of total alkalis and  $\text{Al}_2\text{O}_3$ , in both cases following an equally sharp initial decrease at the edge of the contact aureole. MgO increases sharply at the commencement of metamorphism, then remains fairly constant. The percentage of  $\text{SiO}_2$  decreases progressively with rising temperatures.

The trace element content of the constituent amphiboles also underwent some distinct changes. Mn increased markedly, while Ba, Sr, and Zr only gained slightly. The amount of Co remained fairly constant and Ni tended to decrease.

A fairly good correlation has been obtained for the optical results with their corresponding chemical compositions. It is sufficient to show that the amphiboles may be regarded as belonging to three separate solid-solution series, which are end-members of the calcium rich amphiboles.

*Acknowledgements.* I would like to thank Prof. J. J. Frankel and his staff in the School of Applied Geology at the University of N.S.W. for making available the facilities there. Especial thanks are also due to Dr. C. T. McElroy who first introduced the problem and to Mr. D. C. Craig whose aid made possible the chemical analyses.

### References

- BINNS (R. A.), 1965. *Min. Mag.*, **34**, 52.  
 DEER (W. A.), HOWIE (R. A.), and ZUSSMANN (J.), 1963. *Rock Forming Minerals*. Volume 2: Chain silicates. Longmans, London.  
 ENGEL (C. G.), 1959. *Bull. Geol. Soc. Amer.*, **70**, 951.  
 FYFE (W. S.), TURNER (F. J.), and VERHOOGEN (J.), 1958. *Geol. Soc. Amer.*, Mem. 73.  
 HOWIE (R. A.), 1955. *Trans. Roy. Soc. Edinburgh*, **62**, 725.  
 LAYTON (W.), 1963. *Journ. Geol. Soc. Aust.*, **10**, 261.  
 MACARA (B. J.), (in press): Petrology of the basic rocks in the Kanangra Plateau area, southern New South Wales, Australia.

- PHILLIPS (R.), 1963. *Min. Mag.*, **33**, 701.  
— and LAYTON (W.), 1964. *Ibid.*, **34**, 1097.  
SHIDÔ (F.), 1958. *Journ. Fac. Sci. Univ. Tokyo*, Sec. 2, **11**, 131.  
— and MIYASHIRO (A.), 1959. *Journ. Fac. Sci. Univ. Tokyo*, Sec. 2, **12**, 85.  
SUNDIUS (N.), 1946. *Arsbok. Sveriges Geol. Undersok.*, **40**, no. 4.  
WILCOX (R. E.) and POLDERVAART (A.), 1958. *Bull. Geol. Soc. Amer.*, **69**, 1323.  
WISEMAN (J. D. H.), 1934. *Quart. Jour. Geol. Soc.*, **90**, 354.  
YODER (H. S.) and TILLEY (C. E.), 1962. *Journ. Petrology*, **3**, 342.

# Nature des hornblendes et types de métamorphisme

Par J. FABRIÈS

Laboratoire de Géologie et de Minéralogie, Faculté des Sciences, ALGER

*Summary.* Although comparison of chemical analyses of amphiboles from different laboratories is unreliable, and there are few systematic studies of basic metamorphic rocks, it is possible to discern some crystallochemical trends as a function of some types of metamorphism, as defined by Miyashiro (1951).

Whatever the type of metamorphism, the hornblende compositions change more or less in the sense tschermakite  $\rightarrow$  edenite with the degree of metamorphism. The amount of  $Al^{iv}$  shows no definite change; the decrease in the substitution  $Al^{iv}Al^{vi} \rightarrow MgSi$  with increasing metamorphism is compensated by the reciprocal substitution of  $Na^A Al^{iv} \rightarrow Si$ . Hornblendes of the types disthene (kyanite)–sillimanite (DS) and andalusite–sillimanite (AS) are essentially distinguished by the relative quantities of  $Al^{vi}$  and  $Na^A$ , which are more important in amphiboles of the first type at the same metamorphic intensity (same temperature of formation); the total amount of Na does not, however, show any difference.

The chemical composition of the rock clearly influences that of the amphibole, and can sometimes mask certain of the crystallochemical characteristics of this mineral. Comparison of the ratio  $mg = Mg/(Mg + Fe^{2+})$ , which reflects the overall composition of the rock and which does not vary with the degree of metamorphism, and  $al = Al^{vi}/(Al^{vi} + Fe^{3+} + Ti)$  shows that hornblendes of the type DS are characterised statistically by the relation  $mg < al + 0.1$ ; an inverse relation exists for the AS type.

Crystallographic parameters are often different; hornblendes of the type AS have rather high values of  $b$  and  $V$ ; this phenomenon is due to the smaller quantity of  $Al^{vi} (+ Fe^{3+} + Ti)$  in the amphibole molecule.

DEPUIS quelques années, les pétrographes étudiant les séries métamorphiques s'intéressent de plus en plus à la nature chimique des minéraux constituants. C'est ainsi qu'ont été publiées récemment plusieurs études sur la composition des amphiboles provenant de roches métamorphiques basiques. Devant ces données nouvelles, nous sommes amenés tout naturellement à poser le problème des relations susceptibles d'exister entre les caractères cristallochimiques des hornblendes et les types de métamorphisme, tels que les a définis Miyashiro (1961).

Evidemment un tel essai soulève la question de la comparaison des données chimiques provenant de différents laboratoires d'analyses. D'autre part, comme l'ont déjà souligné Engel et Engel (1962) et Leake (1965), nous disposons actuellement de peu d'études systématiques sur les amphiboles des séries métamorphiques et à partir desquelles des comparaisons valables peuvent être établies. Aussi ces remarques préliminaires sont-elles nécessaires pour mettre l'accent sur le caractère d'essai que nous entendons donner simplement

aux considérations qui vont suivre, et auxquelles nous fûmes amenés après l'étude des roches métamorphiques basiques de la Province de Séville (Espagne du Sud) (Fabriès, 1963).

*Les Hornblendes des Amphiboles du NE de la Province de Séville (Espagne)*

La partie sévillane de la Sierra Morena est caractérisée par l'existence d'un complexe cristallophyllien d'âge hercynien (massif de Lora del Rio), dans lequel trois zones d'isométamorphisme peuvent être identifiées dans le faciès "amphibolite" à partir des roches pélitiques: zone I à grenat, zone II à andalousite, et zone III à sillimanite. Les nombreuses lentilles d'orthoamphibolites, contenues dans ces formations gneissiques, permettent également d'établir une zonéographie qui concorde bien avec la précédente et qui est basée sur l'habitus et la couleur des hornblendes:

<i>Zones</i>	<i>Habitus des amphiboles</i>	<i>Couleur de <math>\gamma</math></i>
Zone I	cristaux aciculaires en feutrage	bleu verdâtre
Zone II	cristaux aciculaires et prismatiques	vert
Zone III	cristaux prismatiques et trapus	brun verdâtre

Cette série métamorphique constitue un exemple du type andalousite-sillimanite, décrit par Miyashiro (1958) dans le plateau d'Abukuma (Japon).

Un certain nombre de ces amphiboles ont été séparées et analysées: les compositions chimiques et les constantes physiques sont indiquées dans le tableau I. Toutes ces amphiboles ont une forte teneur en alumine, même dans les roches de degré métamorphique peu élevé. Leurs compositions chimiques varient avec le métamorphisme croissant de la façon suivante: le rapport  $Mg/(Mg + Fe^{2+})$  reste sensiblement constant; le rapport  $Fe^{3+}/(Fe^{2+} + Fe^{3+})$  diminue; la quantité de  $Al^{vi}$  et la somme  $Al^{vi} + Fe^{3+}$  diminuent nettement; et la quantité de  $Na^+$  augmente dans les sites vacants  $A$  de la structure.

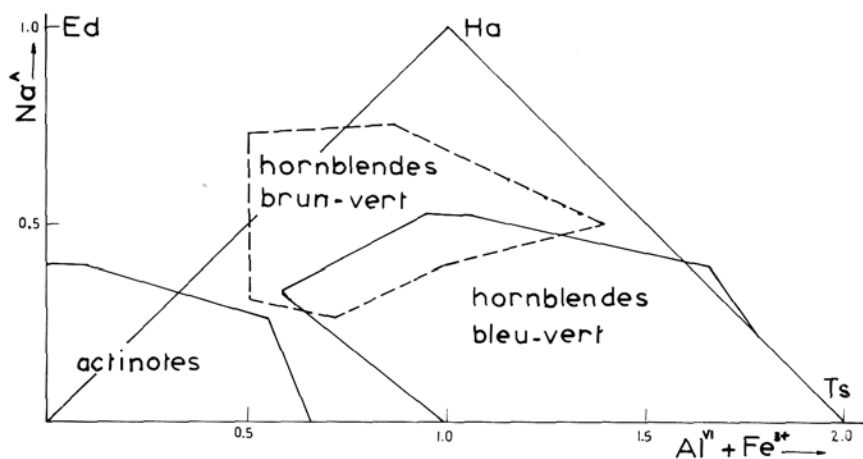
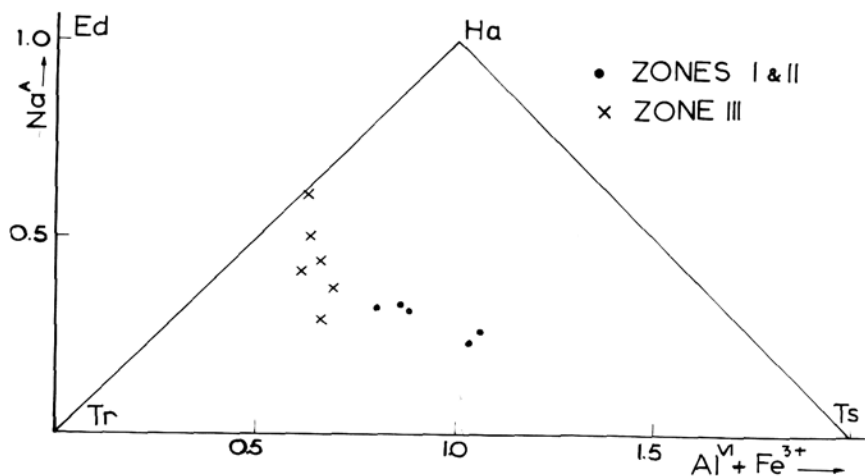
Ainsi les principales variations chimiques en fonction de l'intensité du métamorphisme correspondent à une diminution de la substitution isomorphique  $Al^{vi}Al^{iv} \rightarrow MgSi$ , en liaison avec une augmentation de  $Na^A$  dans les sites structuraux vacants. Cette évolution cristallochimique apparaît clairement dans le diagramme (fig. 1) de Boyd (1959), inspiré de celui de Hallimond (1943), et qui est le mieux adapté pour décrire les hornblendes ( $Ca > 1,5$ ) (Fabriès, 1966).

*La Nature des Hornblendes dans les Types Andalousite-Sillimanite et Disthène-Sillimanite*

La tendance mise en évidence dans le cas précédent semble générale et caractérise très souvent l'évolution cristallochimique des hornblendes, qui constituent les orthoamphibolites de différentes séries métamorphiques, du type andalousite-sillimanite (type A-S) comme du type disthène-sillimanite (type D-S). Comme

TABLEAU I. Compositions chimiques et propriétés physiques des hornblendes de la Province de Séville (Espagne)

Zones	Zone I			Zone II		Zone III et migmatites				Diorite		
	1	2	3	4	5	6	7	8	9	10	11	12
SiO <sub>2</sub>	45,44	43,43	44,26	44,30	43,30	38,91	45,68	44,12	44,35	44,40	47,21	39,60
Al <sub>2</sub> O <sub>3</sub>	12,49	12,30	11,25	10,30	11,60	11,85	10,71	10,58	10,08	8,36	9,78	10,71
Fe <sub>2</sub> O <sub>3</sub>	4,09	6,25	4,97	5,48	4,02	6,02	3,37	3,22	4,14	5,61	3,07	7,25
FeO	10,50	8,87	9,05	11,70	11,19	11,00	10,55	11,91	11,09	10,30	10,45	12,15
MnO	0,30	0,43	0,35	0,12	0,35	0,20	0,16	0,33	0,23	0,27	0,34	0,34
MgO	11,04	12,07	13,21	11,20	11,94	12,07	13,33	11,43	12,70	13,58	12,82	9,00
CaO	10,47	11,03	11,22	10,90	10,29	12,34	11,78	11,97	12,72	13,00	11,22	11,59
Na <sub>2</sub> O	1,72	1,61	1,17	1,90	1,48	1,24	1,50	1,57	1,39	1,75	1,30	1,12
K <sub>2</sub> O	0,58	0,30	0,85	0,45	0,71	0,50	0,45	0,50	0,75	0,65	0,95	1,33
TiO <sub>2</sub>	2,00	2,60	2,14	2,30	2,90	4,84	1,58	3,27	1,97	1,02	1,85	3,64
P <sub>2</sub> O <sub>5</sub>	0,09	0,05	0,07	0,19	0,08	0,22	0,09	0,07	0,05	0,06	0,08	0,32
H <sub>2</sub> O	0,92	0,92	1,24	0,35	1,58	0,64	0,48	0,88	0,76	0,32	0,64	2,60
F	tr.	0,03	0,24	0,20	0,40	tr.	0,25	0,15	0,37	0,07	0,07	0,20
O≡F	99,64	99,89	100,02	99,41	99,84	99,83	99,93	100,00	100,60	99,39	99,78	99,85
Total	—	0,01	0,10	0,08	0,17	—	0,11	0,06	0,16	0,03	0,03	0,08
	99,64	99,88	99,92	99,33	99,67	99,83	99,82	99,94	100,44	99,36	99,75	99,77
<i>Nombre d'ions pour 23 O<sup>2-</sup>:</i>												
Si	6,66	6,28	6,42	6,49	6,35	5,66	6,65	6,44	6,45	6,55	6,89	6,07
Al <sup>iv</sup>	1,34	1,72	1,58	1,51	1,65	2,34	1,35	1,56	1,55	1,38	1,11	1,93
Al <sup>vi</sup>	0,58	0,38	0,34	0,26	0,36	0,01	0,33	0,26	0,18	—	0,33	0,01
Fe <sup>3+</sup>	0,45	0,68	0,54	0,60	0,44	0,65	0,36	0,35	0,45	0,62	0,34	0,83
Ti	0,22	0,28	0,23	0,25	0,32	0,52	0,17	0,36	0,22	0,11	0,20	0,41
Fe <sup>2+</sup>	1,28	1,07	1,10	1,43	1,38	1,33	1,28	1,46	1,35	1,26	1,27	1,56
Mn	0,04	0,05	0,04	0,01	0,04	0,02	0,02	0,03	0,02	0,03	0,04	0,04
Mg	2,41	2,60	2,84	2,46	2,61	2,61	2,88	2,49	2,75	2,98	2,78	2,05
Ca	1,63	1,70	1,74	1,71	1,62	1,92	1,83	1,87	1,97	2,05	1,75	1,91
Na	0,48	0,45	0,33	0,54	0,42	0,35	0,42	0,44	0,39	0,49	0,37	0,33
K	0,11	0,05	0,15	0,08	0,13	0,09	0,08	0,09	0,14	0,12	0,17	0,26
Mg/(Mg+Fe)	0,65	0,71	0,72	0,63	0,65	0,66	0,69	0,63	0,67	0,70	0,68	0,56
Fe <sup>3+</sup> /(Fe <sup>2+</sup> +Fe <sup>3+</sup> )	0,26	0,39	0,33	0,30	0,24	0,33	0,22	0,19	0,25	0,33	0,21	0,34
Alc. in (A)	0,22	0,26	0,31	0,33	0,32	0,37	0,44	0,40	0,50	0,61	0,29	0,50
γ	1,668	1,662	1,665	1,675	1,674	1,676	1,670	1,683	1,675	1,666	1,667×	1,676
β	—	1,654	1,656	1,666	1,664	1,666	1,660	1,675	1,666	1,657	1,657	1,666
α	—	1,640	1,645	1,654	1,650	1,652	1,647	1,660	1,653	1,645	1,643	1,652
γ : [001]	17°	16°	20°	20°	19°-20°	16°	15°	18°	17°	18°-19°	18°	15°
2 V <sub>α</sub>	78°	80°	76°	79°-80°	82°	82°	85°	71°	80°	90°	80°	76°
a (Å)	9,897	9,898	9,896	9,934	9,916	9,893	9,914	9,922	9,933	nd.	nd.	nd.
b (Å)	18,129	18,100	18,162	18,170	18,173	18,100	18,139	18,160	18,175	nd.	nd.	nd.
c (Å)	5,328	5,331	5,331	5,316	5,324	5,333	5,331	5,337	5,331	nd.	nd.	nd.
β	104°,826	104°,883	104°,700	104°,858	104°,830	104°,933	104°,823	104°,858	104°,966	nd.	nd.	nd.
a sin β (Å)	9,568	9,566	9,573	9,603	9,586	9,559	9,584	9,591	9,597	nd.	nd.	nd.
V (Å <sup>3</sup> )	924,2	923,0	926,8	927,6	927,4	922,7	926,7	929,4	929,8	nd.	nd.	nd.



FIGS. 1 et 2. Diagrammes d'évolution cristallochimique, après Boyd (1959).

le montre le diagramme fig. 2, il existe généralement en fonction du métamorphisme croissant une compensation entre la diminution de la substitution  $Al^{VI}Al^{IV} \rightarrow MgSi$  (ou substitution tschermakitique) et l'augmentation réciproque de la substitution  $Na^4Al^{IV} \rightarrow Si$  (ou substitution édénitique). Cette compensation explique d'ailleurs pourquoi la quantité d'ions  $Al^{IV}$  ne présente en général aucune variation bien définie avec le degré métamorphique, contrairement aux idées de Harry (1950). Il est donc possible d'affirmer que l'évolution cristallochimique des hornblendes se fait plus ou moins dans le sens tschermakite  $\rightarrow$  édénite quand l'intensité du métamorphisme croît.

Ce phénomène s'explique par le fait que les hornblendes contenant des ions  $Na^+$  dans les sites vacants sont plus stables à températures élevées que celles

qui en sont dépourvues. Zussman (1955) a montré en particulier que l'introduction d'atomes alcalins dans les lacunes *A*, dont les dimensions sont plus grandes que celles de ces ions, augmente l'entropie du système. La comparaison des domaines de stabilité de la pargasite et de la trémolite (Boyd, 1959) en est une preuve supplémentaire. En outre dans les degrés faibles de métamorphisme, les gradients de pression sont relativement plus importants que les gradients de température, favorisant ainsi la co-ordination vi de l'aluminium.

Cette évolution cristallochimique des hornblendes varie-t-elle en fonction du type de métamorphisme? Quel que soit ce type, andalousite-sillimanite ou disthène-sillimanite, la quantité totale de Na ne montre pratiquement aucune différence, contrairement à l'affirmation de Shido et Miyashiro (1959). Mais les quantités d'ions  $Al^{vi}$  sont plus fortes dans les amphiboles du type disthène-sillimanite que dans celles de l'autre type, pour un même degré métamorphique, c'est à dire pour une température identique de cristallisation, qui est représentée approximativement par la teneur en ions  $Na^A$ . La figure 3 montre en effet que pour une valeur donnée de  $Na^A$ , la quantité de  $Al^{vi}$  est plus grande dans les hornblendes du type disthène-sillimanite. Remarquons aussi que les hornblendes du type andalousite-sillimanite sont assez comparables du point de vue chimique à celles des diorites et des tonalites. La co-ordination vi de l'aluminium étant favorisée par de fortes pressions, il est donc normal de trouver davantage d'ions  $Al^{vi}$  dans les amphiboles du type disthène-sillimanite qui est caractérisé par des pressions supérieures à celles qui conditionnent l'autre type.

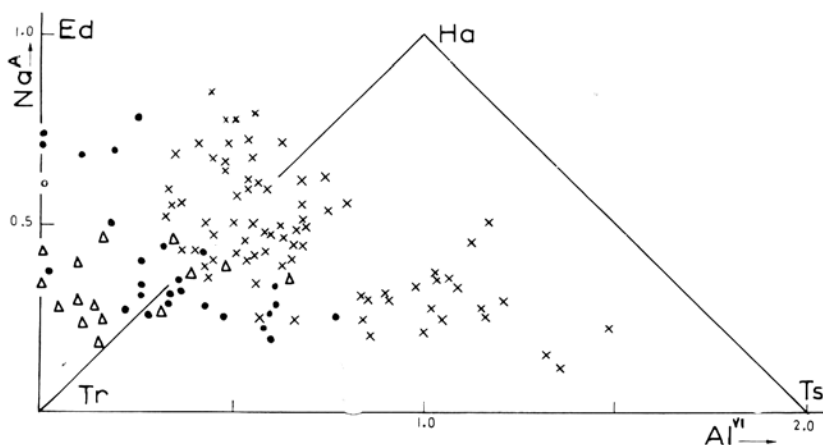
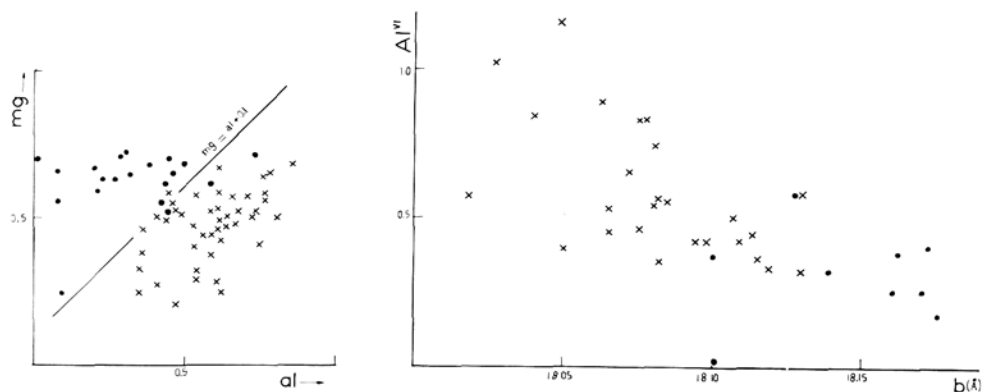


FIG. 3. Diagramme d'évolution: ×, hornblende du type disthène-sillimanite; ●, hornblende du type andalousite-sillimanite; Δ, hornblende des diorites et tonalites.

Cependant la composition des roches basiques influe sur celle des hornblendes et peut souvent masquer quelques unes de leurs caractéristiques cristallochimiques. Or comme nous l'avons indiqué dans le cas de la Province de Séville, le rapport  $mg = Mg/(Mg + Fe^{2+})$  ne varie généralement pas en fonction du degré de métamorphisme. Il reflète au contraire la composition globale de

la roche. Le diagramme  $mg/al$  (fig. 4) qui permet de comparer les rapports  $mg$  et  $al = Al^{vi}/(Al^{vi} + Fe^{3+} + Ti)$  montre alors que les points représentatifs des hornblendes du type disthène-sillimanite se situent dans un domaine de l'espace cartésien caractérisé par la relation  $mg \leq al + 0,1$ . Une relation inverse existe pour les amphiboles du type andalousite-sillimanite.



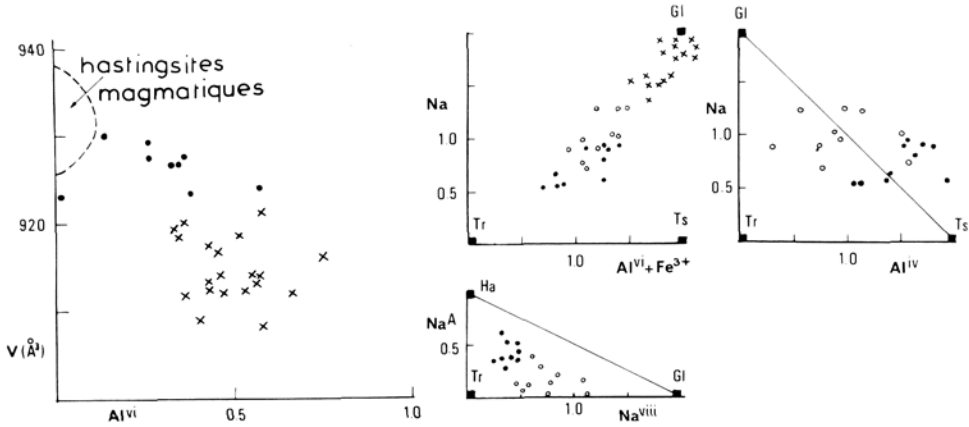
FIGS. 4 et 5: FIG. 4 (gauche). Mêmes symboles que dans la fig. 3.  
FIG. 5 (droit). Mêmes symboles que dans la fig. 3.

Enfin les hornblendes de ces deux types métamorphiques semblent se distinguer par les valeurs de leurs paramètres cristallographiques, bien que les informations sur cette question soient encore en nombre restreint. Ainsi dans les hornblendes du type andalousite-sillimanite, le paramètre  $b$  et le volume de la maille-unité ont des valeurs plus élevées que dans celles du type disthène-sillimanite (fig. 5 et 6). Probablement ce phénomène traduit le fait que de faibles quantités d'ions  $Al^{vi}$  ( $+Fe^{3+} + Ti$ ) remplacent les ions  $Mg^{2+}$  et  $Fe^{2+}$ . En effet ces paramètres cristallins sont très comparables à ceux des hornblendes de diorites et de tonalites, observation qui souligne encore l'analogie cristallochimique, signalée plus haut.

#### *La Nature des Hornblendes dans le Métamorphisme du Type Glaucophane-Jadeite*

Dans une récente note (Fabriès, 1966), nous avons montré que, dans le type glaucophane-jadeite ou le type intermédiaire de haute pression, les amphiboles bleu-vert qui accompagnent le glaucophane dans certaines roches basiques sont souvent des hornblendes subcalciques ( $Ca \leq 1,5$ ). Leur composition chimique est voisine de la formule idéale  $NaCaR_3^{2+}R_2^{3+}AlSi_7O_{22}(OH)_2$ , ( $R^{2+} = Mg + Fe^{2+}$ ;  $R^{3+} = Al^{vi} + Fe^{3+}$ ), dans laquelle une certaine proportion de  $R^{3+}$  serait remplacée par ( $Na^A + R^{2+}$ ) (fig. 7).

Deux évolutions cristallochimiques peuvent être mises en évidence, suivant que l'on a affaire à une variation du degré métamorphique dans l'espace ou dans le temps:



FIGS. 6 et 7: FIG. 6 (gauche). Mêmes symboles que dans la fig. 3. FIG. 7 (droit).  
 ×, glaucophane; ○, hornblende subcalciq.; ●, hastingsite.

*Dans l'espace.* S. Banno (1964) a décrit une séquence spatiale correspondant à l'apparition successive de glaucophane, de hornblende subcalciq., et d'hastingsite tschermakitique. Cette évolution se traduit par les remplacements isomorphiques suivants: augmentation des ions alcalins dans les sites vacants, de  $\text{Ca}^{2+}$  dans les positions structurales  $M_4$ , et diminution progressive de  $R^{3+}$  dans les lacunes octaédriques. Ces variations reflètent une augmentation progressive du gradient température/pression.

*Dans le temps.* Un deuxième type d'évolution se rencontre dans les roches plurifacielles (de Roever et Nijhuis, 1964), avec la succession dans le temps de paragenèse a glaucophane, à hornblende subcalciq., et a actinote. Elle se traduit par une diminution progressive des ions  $R^{3+}$  hexacoordonnés et une augmentation de  $\text{Ca}^{2+}$  à la place de  $\text{Na}^+$ , de sorte que les sites vacants  $A$  ne sont pratiquement jamais occupés par des alcalins tout au long de cette séquence plurifaciale. On peut en déduire que la température est restée à peu près constante lors de la cristallisation de ces trois types d'amphiboles; une diminution de la pression à température constante serait alors responsable de l'apparition de ces paragenèses successives.

*Conclusion.* Les considérations précédentes ne constituent qu'un essai pour distinguer les hornblendes provenant de roches basiques incluses dans des séries de différents types de métamorphisme. De nombreux travaux sont encore nécessaires pour confirmer ou non ces observations, mais dès à présent nous pensons que l'étude paragénetique des amphiboles peut rendre de grands services dans les recherches sur les terrains métamorphiques, en particulier dans les régions où font défaut des minéraux indicateurs classiques tels que les silicates d'alumine.

*References*

- BANNO (S.), 1964. *Journ. Fac. Sc. Univ. Tokyo*, Sect. 2, **15**, 203.  
BINNS (R. A.), 1965. *Min. Mag.*, **35**, 306.  
BOYD (F. R.), 1959. *Researches in Geochemistry*, (J. Wiley and Sons, New York), p. 377.  
COMPTON (R. R.), 1958. *Amer. Min.*, **43**, 890.  
ENGEL (A. E. J.) et ENGEL (C. G.), 1962. *Bull. Geol. Soc. Amer.*, **73**, 1 499.  
FABRIÈS (J.), 1963. *Sciences de la Terre, Mém.* 4, 267 pages.  
—, 1966. *Compt. Rend. Acad. Sc., Paris*, **262**, 1 824.  
—, 1966. *Ibid.*, **263**, 749.  
HALLIMOND (A. F.), 1943. *Amer. Min.*, **28**, 65.  
HARRY (W. T.), 1950. *Min. Mag.*, **36**, 142.  
LEAKE (B. E.), 1965. *Controls of Metamorphism*, (Oliver and Boyd, London), chap. 17, p. 299.  
MIYASHIRO (A.), 1961. *Journ. Petrology*, **2**, 277.  
RAYCHAUDHURI (B.), 1964. *Amer. Min.*, **49**, 198.  
DE ROEVER (W. P.) et NIJHUIS (H. J.), 1964. *Geol. Rundschau*, **53**, 324.  
SHIDO (F.), 1958. *Journ. Fac. Sc. Univ. Tokyo*, sect. 2, **11**, 131.  
— et MIYASHIRO (A.), 1959. *Ibid.*, **12**, 85.  
STEIGER (R.), 1961. *Schweiz. Min. Petr. Mitt.*, **41**, 127.  
ZUSSMAN (J.), 1955. *Acta Cryst.*, **8**, 301.

## An attempt to rationalize the classification of natural pyroxenes of space group $C2/c$

By I. V. GINZBURG  
(И. В. Гинзбург)

Mineralogical Museum, U.S.S.R. Academy of Sciences,  
Leninskii Prospect 14/16, Moscow V-71

*Summary.* Mineral species of the natural pyroxenes of space group  $C2/c$ , excluding spodumene and cosmochlorite (ureyite), form four assemblages: augite, diopside–hedenbergite, fassaite; johannsenite, diopside, hedenbergite; aegirine, diopside, hedenbergite; augite + diopside, omphacite, jadeite, aegirine. In each of these assemblages, each of the species named has more or less definite boundaries, which are discussed. The conclusions are based on considerations of chemical composition, X-ray powder patterns, optical properties, and paragenesis.

THE clinopyroxenes of space group  $C2/c$  cover a wide range of composition. They are commonly divided into several mineral species. Some of these species themselves show considerable variation in composition, but with others the variation is insignificant. The number of species, the limits of their compositions, and the characteristics of the breaks between them have not been established, and some of the species names are not universally accepted.

In order to rationalize the classification of these pyroxenes, published data have been surveyed. In addition, some ninety X-ray powder patterns of chemically analysed pyroxenes were obtained, and occurrence and paragenesis were taken into account. Special attention was paid to the establishment of species boundaries, for which the following four criteria were used: miscibility gaps, i.e., absence or rareness of natural representatives within a certain range of composition; specific features in the change of optical properties; general differences in X-ray powder patterns or the occurrence of diagnostic lines, following the principles described by Ginzburg and Sidorenko (1964); and difference in mode of occurrence or physico-chemical conditions of formation.

The results are summarized in crystal-chemical formulae for the species, which are written in such a way as to show the most probable distributions of ions among the various sites. The results are also illustrated by triangular diagrams, which show the compositional ranges of the species and the gaps between them. Priority and variety names, synonyms, and superfluous names are discussed where necessary. Structurally disordered varieties are not considered.

*The system clinoenstatite–clinoferrosilite–diopside–hedenbergite*

Clinoenstatite–ferrosilite (fig. 1, field 1) and pigeonite (field 2) have primitive lattices and thus lie outside the field of this paper. Augite and other calcic pyroxenes of this system occur widely in igneous and metamorphic rocks, and their classification is particularly important.

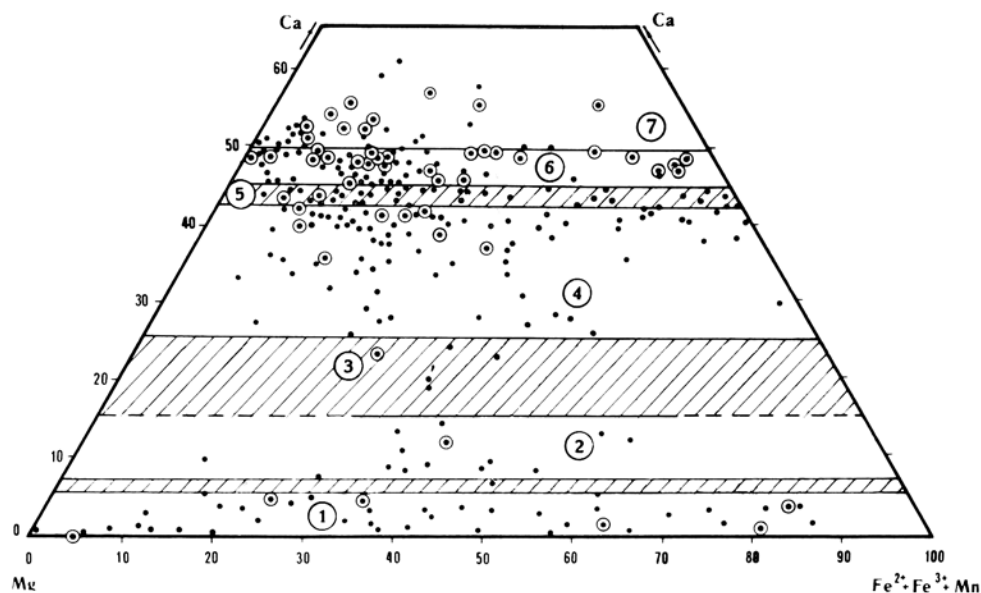


FIG. 1. The system clinoenstatite–clinoferrosilite–diopside–hedenbergite. Field 1: clinoenstatite–ferrosilite. Field 2: pigeonite. Field 3: subcalcic augite. Field 4: augite. Field 5: Ca-rich augite. Field 6: diopside–hedenbergite. Field 7: fassaite. Shaded areas denote boundary fields. Full circles represent chemically analysed pyroxenes (Veselovskaya, 1950; Deer, Howie, and Zussman, 1963; and other authors, 1950–1965). Open circles represent pyroxenes analysed chemically and studied by X-ray powder diffraction (Ginzburg and Sidorenko, 1964).

*Augites.* Subcalcic augites (field 3) with 9.56–11.10% CaO give X-ray powder patterns resembling those of augites with 14.3–20.8% CaO, but differing from those of pigeonites with 3.14–5.5% CaO (Kuno, 1955; Ginzburg and Sidorenko, 1964). They therefore probably have the space group  $C2/c$  assumed for augite, and not that of pigeonite ( $P2_1/c$ ). This structural difference gives rise to a narrow miscibility gap, pigeonites having up to 6 to 7% CaO and subcalcic augites 8 to 9% CaO or above. Cell parameters and optical properties (especially  $2V$ ) vary smoothly over the whole range of pigeonites and subcalcic augites.

The boundary between subcalcic augite and common augite (field 4) is arbitrary (Deer, Howie, and Zussman, 1963), neither optical properties, nor

X-ray powder patterns, nor any change in density of points on the composition diagram (fig. 1) showing any distinction. Modes of occurrence also show no clear difference, though Kuno (1955) considered that subcalcic augites may crystallize under specific, high-temperature conditions. Subcalcic augites can thus be considered a chemical, and perhaps also a structural subspecies of augite. The possibility is, however, not excluded that this compositional range is one in which metastable structures can exist, whose crystal chemical features can correspond to those of either of the neighbouring species. On this hypothesis, it is an extension of the miscibility gap, which, however, contains some representatives formed under specific conditions.

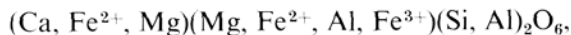
Pyroxenes with 42.5–45.0 moles percent  $\text{CaSiO}_3$  (field 5) will be termed Ca-rich augites. They are distinguished from those of lower CaO content by a diagnostic X-ray powder line near to the 260 reflection (Ginzburg and Sidorenko, 1964). These authors assigned them to their structural type VII, as opposed to common augites, which they assigned to type VI.

The Ca-rich augites can be regarded either as a subspecies of augite or as occupying a boundary zone between augite and diopside–hedenbergite (field 6). This can perhaps be regarded as a zone of structural instability, in which pyroxenes of almost identical composition can belong to different structural types (VI and VII).

The X-ray evidence might be taken as indicating a miscibility gap, but this does not seem to exist. Optical properties vary smoothly across the boundary, there is no change in the density of points on the composition diagram, and modes of occurrence are similar. Some points of distinction can, nevertheless, be noted. Ca-rich augites often occur in rapidly cooled zones of igneous rocks in which common augite is scarce. The  $\text{Al}_2\text{O}_3$  contents are more variable, and the  $\text{R}_2\text{O}_3$  and  $\text{TiO}_2$  contents higher, than for common augites. Dispersion is often high, perhaps due to  $\text{Fe}^{3+}$  and Ti. Abnormal values of 2 V occur in both common and Ca-rich augites, due to peculiarities of thermal history or to presence of Ti.

The arbitrary upper limit of 45 mol%  $\text{CaSiO}_3$  for the augites follows the proposals of Hess (1949) and Deer, Howie, and Zussman (1963). It may conveniently be retained; if the boundary between augites and diopside–hedenbergites were to be placed at 42.5 mol%  $\text{CaSiO}_3$ , many minerals formerly called augites (about one-third of those listed by Deer, Howie, and Zussman, 1963), would have to be re-named diopside–hedenbergites. This would be confusing. Sometimes, however, minerals that are really diopside–hedenbergites have been called augites only because they occurred in igneous rocks. This is incorrect.

The main conclusions about augites may now be summarized. Augites have CaO 8 to 22%,  $\text{Al}_2\text{O}_3$  0 to 6%, and  $\text{Fe}_2\text{O}_3$  0 to 5% by weight. The crystal-chemical formula of augite and its subspecies (ignoring Na, Ti and other minor constituents) is



with Ca 0.35 to 0.90 and  $Al^{iv}$  0 to 0.2 ( $Al^{vi} + Fe^{3+} = Al^{iv}$ ); the subspecies have the ranges:

subcalcic augite, Ca 0.35 to 0.47, $Al^{iv}$ 0 to 0.05;
common augite, 0.45 to 0.82 0 to 0.17;
Ca-rich augite, 0.80 to 0.90 0 to 0.14.

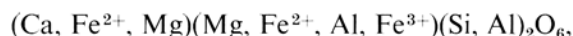
The following varietal names are self-explanatory: subcalcic ferroaugite; magnesian augite (enstatite–diopside); ferroaugite; ferroan hedenbergite. The following varieties, named after substituent ions, cause sharp changes in optical properties: nonaluminian augite, titanian augite, titanian ferroaugite, and ferrian augite.

*Diopside–hedenbergite and fassaite.* Fassaite (fig. 1, field 7) are characterized by high contents, not only of CaO, but also of  $R_2O_3$  (up to 15%  $Al_2O_3$  and 7%  $Fe_2O_3$ , Tröger, 1951; Deer, Howie, and Zussman, 1963). The boundary between diopside–hedenbergites (field 6) and fassaite is arbitrary. Usually, pyroxenes with over 6.5%  $Al_2O_3$  are called fassaite; this corresponds to replacement of over  $\frac{1}{8}$  of the Si by Al. The maximum  $Al_2O_3$  content corresponds to replacement of  $\frac{1}{4}$  of the Si. Like hornblendes and gedrites, which also have  $\frac{1}{8}$ – $\frac{1}{4}$  of the Si replaced by Al, fassaite can be regarded as aluminosilicates.

The only evidence of a miscibility gap between diopside–hedenbergites and fassaite is supplied by the dependence of cell parameters on the content of Al in the Z-sites in synthetic pyroxenes of this series (Sakata, 1957); the slope of the curve representing this dependence in the range  $Al_{0.00}$ – $Al_{0.20}$  (diopside) differs from that in the range  $Al_{0.25}$ – $Al_{0.50}$  (fassaite).

Powder patterns of natural fassaite and diopside–hedenbergites are identical; both species are of structural type VII. Optical properties of varieties of Ca-rich augites, diopsides, sahlites, and ferrosalites are similar to those of corresponding varieties of fassaite. In metamorphic and metasomatic rocks, diopsides, sahlites, and fassaite often form isomorphous series. These minerals occur in contact and regional metamorphic rocks, and also in igneous formations. Despite the absence of any sharp division between diopside–hedenbergites and fassaite, it is justifiable to regard the latter as a distinct species, because they are the only representatives of aluminosilicates among the pyroxenes. Fassaite occurs above diopside on fig. 1 because  $Al^{3+}$  occupies some of the octahedral sites and hence causes an increase in the ratio of Ca to the remaining octahedral cations.

The crystal-chemical formulae of diopside–hedenbergite and fassaite, ignoring minor constituents, are:



with the ranges:

diopside–hedenbergite, Ca 1.00 to 0.85, $Al^{iv} = (Al^{vi} + Fe^{3+})$ 0 to 0.24;
fassaite, 1.00 to 0.80 0.25 to 0.50.

The following varietal names may also be used: diopside, sahlite, hedenbergite, chrome-diopside, lavrovite (Cr, V). Fassaites especially high in Al may be called aluminian fassaites; titanian fassaites also exist.

*The system johannsenite–diopside–hedenbergite*

Within this system (fig. 2), there are no reliable analyses of uncontaminated pyroxenes with 30 to 40 mol%  $\text{CaMnSi}_2\text{O}_6$ . This points to the existence of a miscibility gap between diopside–hedenbergite and johannsenite, although

optical data (Zharikov and Vlasova, 1955) have been considered to provide evidence against any such gap. Iron-rich minerals in this system with 15 to 20 mol%  $\text{CaMnSi}_2\text{O}_6$  may be called manganhedenbergites (fig. 2, field 5), and Mg-rich minerals with 20 to 30 mol%  $\text{CaMnSi}_2\text{O}_6$  may be called manganian diopsides or schefferites (field 4). Minerals with 40 to 70 mol%  $\text{CaMnSi}_2\text{O}_6$  may be called ferrojohannsenites (field 2) or magnesian or zincian johannsenites (field 3). Two old analyses of jeffersonites show  $\text{MnO} + \text{ZnO}$  contents around 15 to 20%. Johannsenites proper (field 1) are defined as having at least 70 mol%  $\text{CaMnSi}_2\text{O}_6$ .

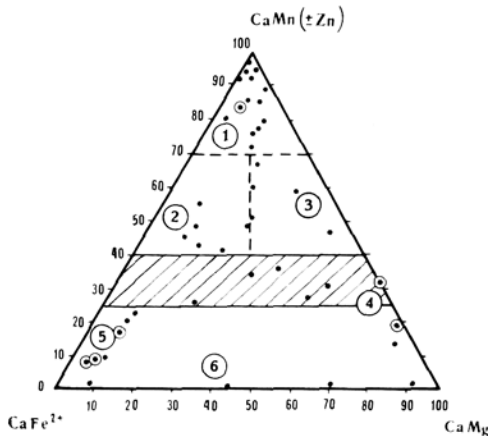


FIG. 2. The system johannsenite–diopside–hedenbergite. Field 1: johannsenite. Field 2: ferrojohannsenite. Field 3: magnesian (zincian) johannsenite. Field 4: schefferite (manganian diopside). Field 5: manganhedenbergite. Field 6: diopside–hedenbergite. Full circles represent chemically analysed pyroxenes (Palache, 1935; Zharikov and Vlasova, 1955; Padera *et al.*, 1964; other authors, 1950–1965); shaded areas and open circles have same meaning as in fig. 1.

Ginzburg and Sidorenko, 1964) was the same as those of Mn-hedenbergites from the U.S.S.R. This is readily explained by the similarity in ionic radii of  $\text{Mn}^{2+}$  and  $\text{Fe}^{2+}$ .

The paragenesis of johannsenite differs from those of manganhedenbergite and manganian diopside; johannsenite forms only at a high manganese potential, and this usually occurs only in the latest stages of deposit formation. The pronounced isolation of johannsenite in composition and occurrence makes it possible to regard this mineral as a separate species, despite the similarity between its X-ray pattern and those of diopside–hedenbergite.

Substitution of Mn for Mg in diopside causes the same changes in X-ray pattern as does that of Fe; the pattern of a johannsenite from Bulgaria (Padera, Mincheva-Stefanova, and Kirov, 1964;

The crystal chemical formula (ignoring Zn and other minor constituents) is:

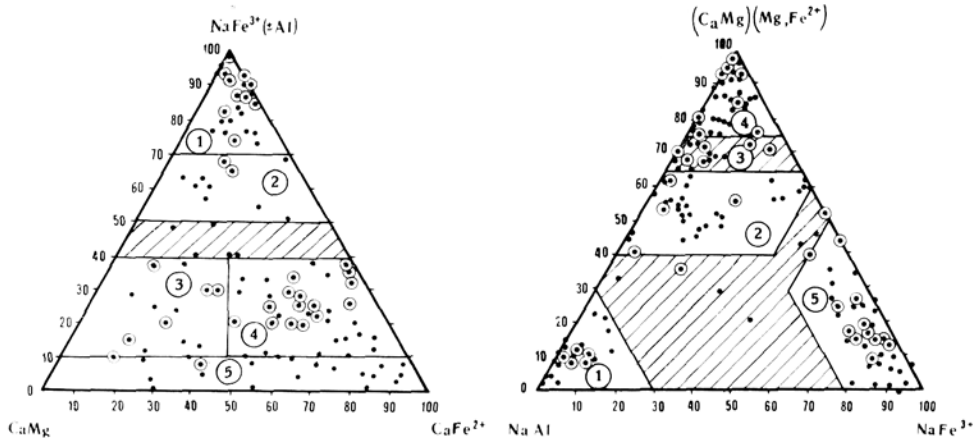


Mn-rich pyroxenes also occur in which the Ca content is under 0.85 per formula unit, and much Al is present in both octahedral and tetrahedral positions. These may be regarded as augites or Ca-rich augites.

*The system aegirine–diopside–hedenbergite*

Within this system (fig. 3), there are no reliable analyses for minerals with 40 to 50 mol%  $\text{NaFeSi}_2\text{O}_6$  and few for ones with 50 to 70 mol% (Iwasaki, 1960; Kostyuk, 1964). This suggests that a miscibility gap exists between aegirine and diopside–hedenbergite. This conclusion is supported by X-ray and optical evidence. Minerals containing over 50 mol%  $\text{NaFeSi}_2\text{O}_6$  give powder patterns typical of aegirines, even though some contain 7 to 8% CaO (specimens from the Urals and Kola peninsula). Minerals containing under 40 mol%  $\text{NaFeSi}_2\text{O}_6$  give patterns typical of diopside–hedenbergite; these may contain up to 5%  $\text{Na}_2\text{O}$  (specimen from the Enisei hills, Tuva). Synthetic preparations in the diopside–aegirine series show a gradual change in pattern (Nolan and Edgar, 1963).

The break at 40 to 50 mol% is also marked by a change in optic sign, which is negative for aegirine and positive for diopside–hedenbergite; this may be used diagnostically (Sabine, 1950). Minerals whose compositions are well



FIGS. 3 and 4: FIG. 3. The system aegirine–diopside–hedenbergite. Field 1: aegirine. Field 2: Ca-rich aegirine. Field 3: aegirine–diopside. Field 4: aegirine–hedenbergite. Field 5: diopside–hedenbergite. Closed circles represent chemically analysed pyroxenes (Kostyuk, 1964; other authors, 1950–1965); shaded areas and open circles have same meaning as in fig. 1. FIG. 4. The system jadeite–aegirine–diopside. Field 1: jadeite. Field 2: omphacite. Field 3: Ca-rich omphacite. Field 4: diopside–hedenbergite and augite. Field 5: aegirine. Closed circles represent chemically analysed pyroxenes (Iwasaki, 1964; Dobretsov and Ponomareva, 1964; Coleman *et al.*, 1965); shaded areas and open circles have same meaning as in fig. 1.

removed from the boundary zone occur under different conditions, but those with compositions neighbouring on this zone can be found under similar conditions.

It is proposed to include among the aegirines, aegirine proper (70 to 100 mol% NaFeSi<sub>2</sub>O<sub>6</sub>; field 1), and Ca-rich aegirine (50 to 70 mol% NaFeSi<sub>2</sub>O<sub>6</sub>; field 2). It is proposed to redefine the terms aegirine-diopside (Brögger, 1898) and aegirine-hedenbergite (Wolff, 1904) to comprise minerals with 10 to 40 mol% NaFeSi<sub>2</sub>O<sub>6</sub> and giving diopside-hedenbergite powder patterns (fields 3 and 4); these are separated by an arbitrary boundary at a Mg : Fe<sup>2+</sup> ratio of 1, and both are separated from the diopside-hedenbergites (field 5) by a further arbitrary boundary at 10 mol% NaFeSi<sub>2</sub>O<sub>6</sub> (1.5 ± 0.1% Na<sub>2</sub>O).

The uncertain term aegirine-augite is superfluous. The crystal-chemical formula of aegirine (including the manganiferous variety blanfordite), aegirine-diopside, and aegirine-hedenbergite is:



with the ranges:

aegirine,	Na 1.0 to 0.6,	Ca 0 to 0.3,	Fe <sup>3+</sup> 1.0 to 0.6,	Al <sup>vi</sup> 0 to 0.1;	
aegirine-diopside,	0.4 to 0.15	0.6 to 0.9	0.4 to 0.2	0 to 0.2,	0 to 0.1, Mg > Fe <sup>2+</sup> ;
aegirine-hedenbergite,	0.4 to 0.15	0.6 to 0.9	0.4 to 0.2	0 to 0.2	0 to 0.1, Fe <sup>2+</sup> > Mg.

#### *The system jadeite-aegirine-diopside*

Aegirines with more than 20 mol% NaAlSi<sub>2</sub>O<sub>6</sub> and jadeites with more than 10 mol% NaFeSi<sub>2</sub>O<sub>6</sub> are not known. Dobretsov and Ponomareva (1964) confirmed the existence of a miscibility gap by a statistical analysis. The X-ray patterns, optical properties, and conditions of formation of the two phases are quite distinct. There can be no doubt that a miscibility gap occurs between aegirine and jadeite. Two pyroxenes from Japan nevertheless fall near the middle of the zone of immiscibility; one had a powder pattern of intermediate character (Kanehira and Banno, 1960; Iwasaki, 1960). Both were found in unusual environments. The existence of even a wide zone of immiscibility, such as this, can under certain conditions favour the formation (probably metastable) of pyroxenes of unusual composition and intermediate structure.

A miscibility gap between aegirine (field 5) and omphacite (field 2) is visible in fig. 4 only as a slight decrease in the density of points; it occurs at compositions similar to those in the aegirine-diopside-hedenbergite system. Better evidence for a break is supplied by X-ray powder data; the pattern of omphacite differs from that of aegirine, and the two minerals belong to different structural types (Ginzburg and Sidorenko, 1964). They are also found in quite different environments, omphacites occurring in the eclogite facies, and aegirines (or aegirine-diopsides) in alkaline rocks. The compositions of omphacites may nevertheless approach closely those of aegirine-diopsides, and, within the ill-defined boundary zone, a typical aegirine-diopside (from the Urals) has been described whose powder pattern is of the omphacite type. This illustrates the structural instability of the pyroxenes of the boundary zone.

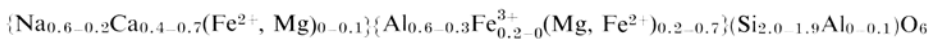
There is a clearly marked miscibility gap at 60 to 80 mol% NaAlSi<sub>2</sub>O<sub>6</sub> between jadeite (field 1) and omphacite (field 2), which was demonstrated both by the absence of intermediate compositions and differences in optical properties (Dobretsov and Ponomareva, 1964) and by differences in X-ray patterns (Ginzburg and Sidorenko, 1964). The differences in occurrence of omphacite and jadeite have been widely discussed. The only analyses falling within the gap are old ones, undoubtedly made on impure material. Omphacites approaching jadeite in composition are sometimes called diopside-jadeites; this term is not apt and should not be used. This also applies to the uncertain term, chloromelanite, which has been applied to many of these minerals. The crystal chemical formula of jadeite is:



Between omphacite (field 2) and the diopsides and augites (field 4), pyroxenes of intermediate composition are known (field 3). These will be called Ca-rich omphacites and can be regarded as a subspecies of omphacite. In general, omphacites occur under different conditions from diopsides and augites, but eclogites and similar rocks may contain, besides omphacites, pure diopside, chrome-diopside, or diopside approaching Ca-rich augite in composition, while augite has been found in kimberlites. Ginzburg and Sidorenko (1964) found the diffraction patterns of two omphacites (from the Urals and Yakutia) poor in Na(Al, Fe)Si<sub>2</sub>O<sub>6</sub> to be intermediate between those of omphacites and augites. Statistical treatment of chemical analyses (Dobretsov and Ponomareva, 1964) places the boundary zone at 75 to 85 mol% (Mg, Fe<sup>2+</sup>)Si<sub>2</sub>O<sub>6</sub>, while X-ray evidence places it at 65 to 75 mol%. Optical properties do not always distinguish the pyroxenes of eclogites from each other.

Omphacites and fassaites differ in conditions of occurrence, and the miscibility gap between them must be regarded as absolute. Sobolev and Kuznetsova (1965) found a pyroxene in an eclogite whose composition fell in the broad gap between them, though it more nearly approached the omphacites.

The crystal chemical formula of omphacite (including Ca-rich omphacite) is:



#### *Spodumene and ureyite (cosmochlore)*

Spodumene is separated from jadeite, the other pyroxene with octahedral Al, by both a very broad miscibility gap and also an utterly different diffraction pattern. The minerals form under entirely different conditions. The crystal chemical formula of spodumene is:



Ureyite (NaCrSi<sub>2</sub>O<sub>6</sub>), recently described by Frondel and Klein (1965) from meteorites, resembles aegirine and is separated from aegirine and jadeite by a complete absence of pyroxenes of intermediate composition, in spite of similarity in diffraction patterns.

*Conclusion*

The boundaries between the mineral species discussed are of varying character. Miscibility gaps of varying width are usually accompanied by differences in X-ray pattern (the johannsenite–diopside or hedenbergite gap is an exception). Within these “forbidden” fields, minerals are sometimes, but rarely, found, which are metastable and of intermediate structure.

Some species boundaries are zones in which there is no decrease in density of points on the composition diagram; the distinction between species is in such cases based on differences in X-ray powder patterns, or, as with the boundary between fassaite and diopside or hedenbergite, completely arbitrarily.

Based on these differing types of species boundary, varying degrees of isolation of the species may be established:

Pyroxenes of extreme compositions are the most isolated. They are separated from other pyroxenes by a miscibility gap. If spodumene and ureyite are excluded, the most isolated is jadeite, followed by aegirine and then johannsenite.

Pyroxenes of intermediate compositions with one distinct boundary. Thus augite is separated from pigeonite by a miscibility gap, but merges into diopside–hedenbergite through the subspecies or boundary zone of Ca-rich augites. Similarly, omphacite is distinguished sharply from jadeite, but merges into augite and diopside–hedenbergite.

Pyroxenes of intermediate compositions with less distinct boundaries. Thus diopside–hedenbergite merges into augite in a zone of transitional compositions and metastable structure, while it is separated from fassaite by an arbitrary boundary. Diopside–hedenbergite and fassaite are not isolated, but continuous mineral species.

*Acknowledgements.* The author thanks Dr. P. Gay for his kind help with the English text, and Professor G. P. Barsanov for his constant interest in the investigation.

*References*

- BRÖGGER (W. C.), 1898. *Skr. vid. Selsk. Christiania, Math.-natur. Kl.*, no. 6, p. 169.
- COLEMAN (R. G.), LEE (D. R.), BEATTY (L. B.), and BRANNOCK (W. W.), 1965. *Bull. Geol. Soc. Amer.*, **76**, 485.
- DEER (W. A.), HOWIE (R. A.), and ZUSSMAN (J.), 1963. *Rock-forming Minerals*, vol. 2. London (Longmans, Green & Co.)
- [DOBRETsov (N. L.) and PONOMAREVA (L. G.)] Добрецов (Н. Л.) и Пономарева (Л. Г.), 1964. Труды Инст. Геол. Геофиз. Сибирск. Отдел. Акад. Наук СССР (*Proc. Inst. Geol. Geophys. Siber. sect. Acad. Sci. U.S.S.R.*), **30**, 56.
- FRONDEL (C.) and KLEIN (C.), 1965. *Science*, **149**, 742.
- [GINZBURG (I. V.) and SIDORENKO (G. A.)] Гинзбург (И. В.) и Сидоренко (Г. А.), 1964. Труды Мин. Муз. (*Trav. Mus. Min. URSS*), **15**, 81.
- HESS (H. H.), 1949. *Amer. Min.*, **34**, 621–666 [*M.A.* **11-15**].
- IWASAKI (M.), 1960. *Journ. Geol. Soc. Japan*, **66**, 334.
- KANEHIRA (K.) and BANNO (S.), 1960. *Ibid.*, 654.
- [KOSTYUK (V. P.)] Костюк (В. П.), 1964. Доклады Акад. Наук СССР (*Compt. Rend. Acad. Sci. URSS*), **156**, 571.
- KUNO (H.), 1955. *Amer. Min.*, **40**, 70.

- NOLAN (J.) and EDGAR (A. D.), 1963. *Min. Mag.*, **33**, 625.
- [PADERA (K.), MINCHEVA-STEFANOVA (I.), and KIROV (G. K.)] Падера (К.), Минчева-Стефанова (И.) и Киров (Г. К.), 1964. Геол. Инст. "С. Димитров", Българ. Акад. Наук (*Bull. Geol. Inst. "S. Dimitrov", Acad. Sci. Bulgar.*), **13**, 5.
- PALACHE (C.), 1935. *U.S. Geol. Surv. Prof. Paper* no. 180 [M.A. 6-261].
- SABINE (P. A.), 1950. *Min. Mag.*, **29**, 113.
- SAKATA (Y.), 1957. *Japan Journ. Geol. Geogr.*, **28**, 161.
- [SOBOLEV (N. V.) and KUZNETSOVA (I. K.)] Соболев (Н. В.) и Кузнецова (И. К.), 1965. Доклады Акад. Наук СССР (*Compt. Rend. Acad. Sci. URSS*), **163**, 471.
- TRÖGER (E.), 1951. *Neues Jahrb. Min. Monatsh.*, **6**, 132.
- [VESELOVSKAYA (M. M.)] Веселовская (М. М.), 1950. Труды Геол. Инст. Акад. Наук СССР, сер. петрогр. (*Trav. Inst. Sci. Geol., Acad. Sci. URSS, sér. petrogr.*), **33**, 71.
- WOLFF (F. VON), 1904. *Centr. Min.*, 214.
- [ZHARIKOV (V. A.) and VLASOVA (D. K.)] Жариков (В. А.) и Власова (Д.К.), 1955. Доклады Акад. Наук СССР (*Compt. Rend. Acad. Sci. URSS*), **105**, 814.

[Manuscript received 8 July 1966; English text prepared 18 November 1966].

# The $\alpha$ - $\beta$ -LiAlSi<sub>2</sub>O<sub>6</sub> (spodumene) transition from 5 000 to 45 000 lb/in<sup>2</sup> P<sub>H<sub>2</sub>O</sub>

By A. D. EDGAR

Dept. of Geology  
University of Western Ontario  
London, Canada

*Summary.* The compound LiAlSi<sub>2</sub>O<sub>6</sub> exists as a low-temperature, or  $\alpha$ -form (the naturally occurring mineral spodumene), and a high-temperature, or  $\beta$ -form, whose structures and densities are radically different, the former having a dense pyroxene-type structure, the latter a much less dense keatite-type structure.

The  $\alpha$ - $\beta$  transition has been determined in the range 5 000 to 45 000 lb./in.<sup>2</sup> P<sub>H<sub>2</sub>O</sub> using three analysed natural spodumenes of high purity. In this range transition temperatures are between 555 and 630°C with  $dt/dp$  being positive. The transition is monotropic. There is some evidence to suggest that the determined curves represent equilibrium conditions.

Careful measurement of cell sizes of the  $\beta$ -form indicate that  $\beta$ -LiAlSi<sub>2</sub>O<sub>6</sub> contains SiO<sub>2</sub> in solid solution, and therefore that the  $\alpha$ - $\beta$ -LiAlSi<sub>2</sub>O<sub>6</sub> transformation cannot be regarded as strictly dimorphic. The transition can be approximately represented by the equation:  $\alpha$ -Li<sub>0.33</sub>Al<sub>0.33</sub>Si<sub>0.66</sub>O<sub>2</sub> + H<sub>2</sub>O (gas)  $\rightarrow$   $\beta$ -Li<sub>*x*</sub>Al<sub>*x*</sub>Si<sub>1-*x*</sub>O<sub>2</sub> + Li-Al-rich aqueous gas, where  $x < 0.33$ .

Comparison between the  $\alpha$ - $\beta$  transition for natural material and limited determinations for the transition using synthetic material indicates that the presence of very minor amounts of Na<sup>+</sup> and Fe<sup>3+</sup> in the natural spodumenes may increase the stability range of the  $\alpha$ -form. Using the Clapeyron equation, values of  $\Delta H$  for the transformation have been determined as 12 000  $\pm$  3 000 cal./mole as obtained from densities and unit-cell constants.

The crystallographic and petrologic implications of this transformation are discussed.

THE mineral spodumene (LiAlSi<sub>2</sub>O<sub>6</sub>) occurs in nature as the low-temperature or  $\alpha$ -form, crystallizing in the monoclinic system with probable space group C2/c. Warren and Bischof (1931) showed that its structure was similar to that of diopside although its axial ratios are different from those of other pyroxenes; it has a smaller cell volume and more closely packed chains of SiO<sub>4</sub> tetrahedra. Natural spodumene can readily be converted monotropically to the high-temperature or  $\beta$ -form, by heating at temperatures above 900°C at atmospheric pressure or at 700°C by fine grinding and prolonged heating (Roy and Osborn, 1949). Although Roy *et al.* (1950) suggest a maximum transformation temperature of 500°C at 10 000 lb./in.<sup>2</sup> P<sub>H<sub>2</sub>O</sub>, data on the effect of pressure on this transformation are scanty. Skinner and Evans (1960) have shown that  $\beta$ -spodumene<sup>1</sup> (space group P<sub>4<sub>3</sub>2<sub>1</sub></sub>) is isostructural with the tetragonal silica polymorph, keatite, and is thus one of the "stuffed silica structures" of Buerger

<sup>1</sup>  $\beta$ -LiAlSi<sub>2</sub>O<sub>6</sub> is a more appropriate name for this form since it does not have a pyroxene structure. However to conform with the terminology of previous workers the term  $\beta$ -spodumene is retained in this paper.

(1954). In  $\beta$ -spodumene, this structure consists of channels through which the lithium atoms can readily move under a suitable potential gradient and thus forms the basis for the cation exchange properties of this mineral used in the extraction of lithium by acid leaching.

The structures of the two polymorphs of LiAlSi<sub>2</sub>O<sub>6</sub> are radically different, the  $\alpha$ -form being a dense pyroxene-type structure (sp.gr. 3.2), the  $\beta$ -form a much less dense silica-type structure (sp.gr. 2.4). Because such transitions between major silicate structure types are not common, it was considered desirable to know the pressure-temperature dependence of these transitions and, using the Clapeyron equation, to attempt to calculate  $\Delta H$  transformation values from calculated  $\Delta V$  values obtained from specific gravities and cell constants.

Unfortunately reproducible synthesis of  $\alpha$ -spodumene is difficult. Isaacs and Roy (1958) attempted to determine the effects of pressure on the  $\alpha$ - $\beta$ -spodumene transition but were unable to synthesize  $\alpha$ -spodumene at pressures up to 4 000 atmospheres, obtaining instead mixtures of  $\alpha$ -eucryptite (LiAlSiO<sub>4</sub>) and petalite (LiAlSi<sub>4</sub>O<sub>10</sub>), and they suggest (p. 217) that failure to synthesize  $\alpha$ -spodumene may be due either to the absence of ions such as Na<sup>+</sup>, Fe<sup>3+</sup>, or F<sup>-</sup>, or because  $\alpha$ -spodumene is metastable under the conditions of synthesis. Stewart (1960) reported the synthesis of  $\alpha$ -spodumene and albite from a synthetic eucryptite-albite glass at pressures of 14 960 to 17 120 bars. Synthesis of  $\alpha$ -spodumene has also been achieved by Eppler *et al.* (1962).

In order to determine the  $P$ - $T$  conditions of the  $\alpha$ - $\beta$  transformation, the most suitable method is to use natural spodumenes. Fortunately, spodumenes show very little variation in chemical composition from the ideal formula LiAlSi<sub>2</sub>O<sub>6</sub>, there being no replacement of Si by Al and only minor replacement of Al by Fe<sup>3+</sup> (Deer, Howie, and Zussman, 1963, p. 93). Accordingly, three spodumene samples from the collections of the University of Western Ontario were selected largely on the basis of lack of alteration or inclusion or of variability in physical appearance. It was hoped that colour differences etc. might reflect variation in chemical properties, which, in turn, might affect the transformation temperatures. These samples, described below, were chemically analysed and their transformation temperatures determined in the pressure range 5 000 to 45 000 lb./in.<sup>2</sup>  $P_{\text{H}_2\text{O}}$ .

Under conditions of water-vapour pressure, the  $\alpha$ - $\beta$  spodumene transition cannot be considered as strictly dimorphic. Comparisons of  $d$  spacings and cell parameters of the  $\beta$ -spodumenes produced in this study with those given by Skinner and Evans (1960) indicate that the  $\beta$ -spodumenes are solid solutions containing about 4 wt. % SiO<sub>2</sub> in excess of the stoichiometric formula LiAlSi<sub>2</sub>O<sub>6</sub>. Thus the calculated  $\Delta H$  values are not exact  $\Delta H_{\text{transformation}}$  values but rather  $\Delta H$  values for the reaction:  $\alpha\text{-Li}_{0.33}\text{Al}_{0.33}\text{Si}_{0.66}\text{O}_2 + \text{gas (H}_2\text{O)} \rightarrow \beta\text{-Li}_x\text{Al}_x\text{Si}_{1-x}\text{O}_2 + \text{gas (Li-Al rich)}$  where  $x < 0.33$ . These findings do not agree with those of Stewart (1963, 1964) who has shown that at 2 Kbar  $P_{\text{H}_2\text{O}}$  the gaseous H<sub>2</sub>O-rich phase coexisting with lithium aluminium silicates is siliceous. This is more fully considered in a later section of this paper.

*Description of samples.* Of the three samples selected for this study, two were spodumenes (nos. 684 and 1 200)<sup>1</sup> and the third (No. 97) a gem variety, kunzite. Brief descriptions of these specimens are:

684—Spodumene, from near Keystone, South Dakota in the Black Hills pegmatite district. Light grey cleavage fragment.

1200—Spodumene, Seymour, Connecticut. Mauve cleavage fragment.

97—Kunzite, Pala, San Diego, California. Almost transparent crystal but showing very faint lilac tinges.

Prior to chemical and X-ray analyses the samples were crushed to approximately 100 mesh size and impurities removed by passing through a Franz isodynamic separator and by hand picking. Chemical analysis, optical data, and number of ions recalculated to six oxygens for these samples are given in table I. Comparison of these analyses with those listed in Deer, Howie, and

TABLE I. Spodumene analyses. All constituents determined on powders dried at 110°C. Analyst: J. Esson

Sample no.	97	684	1 200	Sample no.	97	684	1 200
<i>Numbers of ions on the basis of 6 oxygens:</i>							
SiO <sub>2</sub>	64.03	63.90	63.60	Si	1.984	1.984	1.982
Al <sub>2</sub> O <sub>3</sub> *	27.69	27.55	27.48	Al	1.032	1.008	1.012
Fe <sub>2</sub> O <sub>3</sub>	0.02	0.22	0.04	Fe <sup>3+</sup>	0.000	0.004	0.000
FeO	n.d.	<0.05	n.d.	Li	0.980	0.982	0.978
MnO	0.02	0.13	0.14	Fe <sup>2+</sup>	—	0.000	—
MgO	<0.02	<0.02	<0.02	Mn	0.000	0.004	0.004
CaO	0.04	<0.02	<0.02	Na	0.007	0.011	0.015
Na <sub>2</sub> O	0.11	0.18	0.22	Ca	0.002	0.000	0.000
K <sub>2</sub> O	<0.02	<0.02	n.d.	K	0.000	0.000	—
Li <sub>2</sub> O*	7.87	7.85	7.79	α	1.658	1.661	1.660
TiO <sub>2</sub>	n.d.	n.d.	n.d.	β	1.667	1.668	1.665
P <sub>2</sub> O <sub>5</sub>	n.d.	n.d.	n.d.	γ	1.678	1.677	1.678
H <sub>2</sub> O <sup>+</sup>	0.17	0.14	0.17	γ : [001]	24°	26°	26°
Total	99.95	99.97	99.44	D	3.109	3.156	3.123

\* — average of duplicate determinations.

Zussman (1963, p. 93) indicates that the spodumenes used in this study are very pure varieties. In all samples, the Li<sub>2</sub>O contents are higher than those listed in Deer, Howie, and Zussman and in most of the samples Fe<sub>2</sub>O<sub>3</sub>, Na<sub>2</sub>O, and K<sub>2</sub>O are lower. Sample 97 is exceptionally pure, containing 7.87% Li<sub>2</sub>O (in comparison with the theoretical value of 8.05% for pure LiAlSi<sub>2</sub>O<sub>6</sub>). The principal secondary constituents are Fe<sub>2</sub>O<sub>3</sub> in sample 684, Na<sub>2</sub>O and MnO in samples 684 and 1 200. Density measurements on these samples were determined on a Berman balance. Because of insufficient material, accurate density measurements could not be made on the β-spodumene solid solutions.

<sup>1</sup> Numbers are those of the departmental collections at the University of Western Ontario.

Table II gives the  $d$  spacings of  $\alpha$ -spodumene obtained on a Philips high-angle diffractometer with filtered Cu radiation using smear mounts and an internal silicon standard. Included in this table are the  $d$  spacings and  $hkl$  values from the A.S.T.M. index for spodumene. Table III lists the  $d$  spacings of  $\beta$ -spodumene solid solutions produced in this study. For comparison, the values determined by Skinner and Evans (1960) are included.

*Experimental methods.* All experiments were carried out in cold-seal pressure vessels (Tuttle, 1949) using the sealed tube technique of Goranson (1931). For each experiment, 30 to 40 mg. of the powdered natural spodumene, together with a constant ratio of distilled water, were placed in a sealed gold capsule. A constant powder : water ratio is required in this study because of the preferential solubility of certain components in the gas phase. At the completion

TABLE II.  $d$  Spacings for natural spodumenes. Internal Si standard, Cu- $K\alpha$ , smear mount

Sample no.	97			684			1 200			A.S.T.M. (9-468)		
$hkl$	$d$	$I^*$	$d$	$I^*$	$d$	$I^*$	$d$	$I^*$	$d$	$I^*$		
110	6.08	10	6.08	8	6.12	10	6.12	3	6.12	3		
$\bar{1}11$	4.43	3	4.42	10	4.42	8	4.38	5	4.38	5		
020	4.19	10	4.20	5	4.20	9	4.21	6	4.21	6		
111	3.439	2	3.437	1	3.444	2	3.45	4	3.45	4		
021	3.187	2	—	—	3.188	2	3.19	4	3.19	4		
220	3.050	4	3.049	1	3.051	2	3.04	1	3.04	1		
$\bar{2}21$	2.914	4	2.912	6	2.917	6	2.93	10	2.93	10		
$\bar{2}11$	—	—	—	—	2.862	1	2.87	1	2.87	1		
310	2.793	10	2.793	8	2.794	9	2.80	8	2.80	8		
130	2.670	4	2.667	2	2.669	6	2.67	1	2.67	1		
002- $\bar{1}31$	2.447	3	2.445	2	2.445	1	2.45	6	2.45	6		
221- $\bar{4}01$	2.353	1	2.348	2	2.352	2	2.35	2	2.35	2		
400- $\bar{3}13$	—	—	2.218	1	2.217	2	2.21	1	2.21	1		
$\bar{3}31$ - $\bar{4}21$	2.060	1	2.060	1	2.059	1	2.05	2	2.05	2		
330	2.034	3	2.032	1	2.034	2	2.02	1	2.02	1		
	—	—	1.929	1	1.928	2	1.928	2	1.928	2		
	1.865	3	—	—	1.828	2	1.862	4	1.862	4		
	—	—	—	—	1.837	1	1.824	1	1.824	1		
	—	—	—	—	1.739	1	1.737	1	1.737	1		
	—	—	1.647	1	—	—	1.647	1	1.647	1		
	1.524	6	1.524	1	1.526	4	1.523	3	1.523	3		
	1.460	3	—	—	—	—	1.460	4	1.460	4		
	1.398	3	—	—	—	—	1.397	2	1.397	2		
	1.330	3	—	—	—	—	1.331	4	1.331	4		
	—	—	1.212	1	—	—	—	—	—	—		
$a$	9.478 Å		9.470 Å		9.482 Å							
$b$	8.391		8.384		8.391							
$c$	5.240		5.245		5.249							
$\beta$	110.41°		110.38°		110.41°							

\* — visually estimated intensities.

TABLE III. *d*-Spacings for  $\beta$ -spodumenes. External Si standard. Cu-K $\alpha$ , smear mount

Sample no. <i>hkl</i>	97		684		1 200		LiAlSi <sub>2</sub> O <sub>6</sub> †	
	<i>d</i>	<i>I</i> *	<i>d</i>	<i>I</i> *	<i>d</i>	<i>I</i> *	<i>d</i>	<i>I</i>
101	—	—	—	—	5.76	3	5.821	3
111	4.57 <sub>0</sub>	3	4.592	2	4.579	4	4.610	5
102	3.887	8	3.897	3	3.898	8	3.920	6
201	3.47 <sub>0</sub>	10	3.473	10	3.471	10	3.487	10
210	3.36 <sub>0</sub>	3	3.36 <sub>0</sub>	2	3.359	2	3.369	1
211	3.149	3	3.152	1	3.148	4	3.167	5
103	—	—	—	—	2.797	1	2.858	1
212	2.736	1	—	—	2.733	1	2.713	1
113	2.639	1	—	—	2.639	2	2.628	3
222	2.29 <sub>0</sub>	1	2.295	1	—	—	2.304	4
213	2.251	1	2.256	1	2.255	2	2.264	4
104	—	—	—	—	2.185	1	2.191	2
312	2.100	1	2.106	1	2.106	1	2.113	4
303	1.933	2	1.935	1	1.934	2	1.938	5
400	1.875	3	1.877	2	1.877	3	1.882	6
205	1.641	1	1.644	1	1.645	2	1.646	4
324	1.54 <sub>0</sub>	1	—	—	1.54 <sub>0</sub>	1	1.543	2
<i>a</i>	7.514 <sub>6</sub>	—	7.515 <sub>0</sub>	—	7.512 <sub>8</sub>	—	7.533 <sub>2</sub>	—
<i>c</i>	9.138 <sub>5</sub>	—	9.147 <sub>3</sub>	—	9.133 <sub>2</sub>	—	9.154 <sub>0</sub>	—
wt. % SiO <sub>2</sub> ‡	69	—	68.5	—	68.8	—	64.6	—

\* — visually estimated intensities.

† Skinner and Evans, 1960.

‡ — average value of SiO<sub>2</sub> determined from graph of Skinner and Evans (1960, p. 319).

of the run, water and gas were observed when the capsule was opened indicating that the experiment had taken place under conditions of excess water. To ensure that runs had taken place in a closed system, all capsules showing any weight difference were discarded.

Temperature measurements were made with chromel–alumel thermocouples, previously calibrated at the melting point of sodium chloride (801 °C), and pressure measurements were recorded on a Bourdon tube-type gauge and are believed to be accurate to within  $\pm 4\%$ . The majority of runs were of approximately one week's duration except those at high pressures, which were shorter, and those at low pressures, where the transition is sluggish, which were longer.

The products were identified using a petrographic microscope and by X-ray diffraction methods. Optically  $\alpha$ -spodumene can be readily distinguished from  $\beta$ -spodumene by its prismatic habit,  $\gamma$ : [001] extinction angle, and higher refractive indices.

Cell parameters of spodumenes were determined on an I.B.M. 7040 computer using a programme written by Mozzi and Newall (1961) based on a least squares determination. Parameters of  $\alpha$ -spodumene are given in table II, those of  $\beta$ -spodumene in table III. This table also lists the weight percent SiO<sub>2</sub> in the  $\beta$ -spodumene solid solutions as determined from the graph (Skinner and Evans, 1960, p. 319) relating weight % SiO<sub>2</sub> and cell parameters.

## Results

*Transition curves.* Experimental results for the  $\alpha$ - $\beta$  transitions are given in table IV and plotted as  $P_{\text{H}_2\text{O}}-T$  curves in figs. 1 to 3. The slopes of the transition curves for 97 and 1 200 are similar but differ from that of 684. For samples 97, 684, and 1 200,  $dT/dP$  values are 0.028, 0.034, and 0.025 °C Kg<sup>-1</sup> cm.<sup>2</sup> respectively. The extrapolated values for transition temperatures at atmospheric pressure are 545 °C (sample 97), 530 °C (sample 684), and 550 °C (sample 1 200).

In all samples, it was found that the  $\alpha$ -spodumene did not transform to  $\beta$ -spodumene sharply but that over an interval of 5 to 25 °C both  $\alpha$  and  $\beta$ -spodumene could be detected. For Samples 97 and 1 200, this interval was

TABLE IV. Experimental data

Run	$T$	$P(\text{lb./in.}^2)$	Time	Result	Run	$T$	$P(\text{lb./in.}^2)$	Time	Result
(a) Sample no. 97:					(b) Sample no. 684:				
49	630 °C	$15 \times 10^3$	164 hr.	$\beta$	52	630 °C	$15 \times 10^3$	164 hr.	$\beta$
50	550	5	480	$\alpha$	60	630	25	188	$\beta$
57	510	11	240	$\alpha$	59	510	11	240	$\alpha$
58	630	25	188	$\beta$	61	625	30	90	$\beta$
62	600	30	146	$\alpha$	64	600	30	164	$\alpha$
63	620	27	168	$\beta + \alpha$	65	620	27	196	$\beta$
70	600	15	171	$\beta + \alpha$	68	570	10	216	$\beta + \alpha(?)$
75	600	23	150	$\beta + \alpha$	71	600	15	158	$\beta$
84	560	5	240	$\alpha + \beta$	74	610	20	155	$\beta$
88	565	15	164	$\alpha$	82	560	5	240	$\beta + \alpha$
89	585	24	140	$\alpha$	83	555	10	216	$\beta + \alpha$
90	590	20	162	$\alpha$	86	565	15	164	$\alpha$
95	570	20	563	$\alpha$	87	585	24	140	$\alpha + \beta$
97	615	35	120	$\alpha + \beta$	91	590	20	162	$\beta$
100	610	34	96	$\alpha$	105	615	33	120	$\beta + \alpha$
115	625	40	72	$\alpha + \beta$	114	630	45	75	$\alpha$
116	580	15	168	$\beta + \alpha$	126	535	5	300	$\alpha$
117	570	10	168	$\beta + \alpha$					
118	625	45	72	$\alpha$					
(c) Sample no. 1 200:									
2	600 °C	$15 \times 10^3$	112 hr.	$\beta$	36	580	10	336	$\beta$
3	725	15	112	$\beta$	37	575	15	168	$\alpha$
7	650	20	142	$\beta$	39	595	20	168	$\beta + \alpha$
19	675	10	138	$\beta$	41	610	30	112	$\alpha + \beta$
17	700	*	138	$\alpha + \beta$	42	625	40	48	$\alpha + \beta$
20	660	15	94	$\beta$	54	510	11	240	$\alpha$
22	590	15	120	$\alpha + \beta$	66	570	10	256	$\beta$
27	600	25	96	$\alpha + \beta$	72	605	20	155	$\beta + \alpha$
28	580	15	117	$\alpha + \beta$	80	560	5	480	$\alpha$
32	550	16	244	$\alpha$	120	620	40	72	$\alpha + \beta$
33	580	21	281	$\alpha$	121	605	35	115	$\alpha$
34	600	30	95	$\alpha + \beta$	125	620	45	96	$\alpha$

\* run at 1 atm.

about 25°C and for sample 684 considerably less. The curves have been drawn on the basis of the first appearance of  $\beta$ -spodumene. The most likely explanation for this lack of sharp transition is that the kinetics of the transition are sluggish. In this connection, the average length of run was about one week, but although several samples were run for much longer durations this increase did not affect the transition curves.

The monotropic nature of this transition and the partitioning of silica, lithium, and possibly aluminum between the solid and gaseous phases on either side of the transition curve do not make this transition readily amenable to experimental determination of reversibility. Until the necessary thermodynamic data are available, these curves cannot be regarded as equilibrium curves with any degree of certainty, although the close correlation between the present curves and results of Stewart (1963) (see below) suggests that equilibrium is a strong likelihood.

*Calculation of  $\Delta H$ .* Values of  $\Delta H_{\text{transformation}}$  (table V) were calculated from the Clapeyron equation:  $dT/dP = T\Delta V/\Delta H$ , whence  $\Delta H = T\Delta V dP/dT$ , where  $T$  = absolute temperature (°K) of transition,  $\Delta V$  = difference in molar volumes of  $\beta$ -spodumene solid solution and  $\alpha$ -spodumene in  $\text{cm}^3$ , and  $dT/dP$  = experimentally determined slope of transition curve in  $^{\circ}\text{K Kg}^{-1} \text{cm}^2$ .

In the calculation it has been assumed that the differences in molar volumes of the gaseous phases (of slightly different composition) are negligible. Molar volumes of  $\alpha$ -spodumenes have been calculated from their measured cell dimensions, assuming  $Z=4$  'molecules' per unit cell, and also from densities measured at room temperature; corrections for the thermal expansion of  $\alpha$ -spodumene have been determined from Skinner (1966).

For  $\beta$ -spodumene solid solutions, molar volumes have only been determined from their cell dimensions and a  $Z$ -value of 4, as insufficient material was available for accurate density measurements. Transition temperatures, molar volumes, and  $dT/dP$  values, are included in table V.

TABLE V. Summary of data for  $\alpha$  and  $\beta$  spodumenes

No.	$T_{\text{Trans}}^*$	$dT/dP^\dagger$	Molar vol. $\ddagger$ calc.			$\Delta H^\S$	
			$\alpha$		$\beta$		
			1§	2		1§	2
97	818°K	0.028	60.33	59.27	77.71	$11.891 \times 10^3$	$12.616 \times 10^3$
684	803	0.034	59.40	59.21	77.93	10.249	10.354
1 200	823	0.025	60.05	59.39	77.81	13.692	14.201

\* at 1 atm.

†  $^{\circ}\text{K.Kg}^{-1} \text{cm}^2$ .

‡ Molar volumes of  $\alpha$ -spodumenes corrected for thermal expansion using data of Skinner (1966).

§ calculated from density.

|| calculated from unit cell.

¶  $\Delta H$  for the transition in cal./mole.

The  $\Delta H$  values must be regarded as only very approximate due to the various errors involved in this calculation. There are three principal sources of error, in determination of cell parameters, of density measurements, and of  $dT/dP$  values involving temperature and pressure errors. Examination of the Clapeyron equation shows that the third of these factors is by far the most important. Based on a temperature error of  $\pm 5^\circ\text{C}$ , the value of  $\Delta H$  is only accurate to  $\pm 3\,000$  cal./mole. However, the crude  $\Delta H$  obtained by this method indicates that these values are very large in comparison to other silicate transformations, as can be predicted from the structural changes involved.

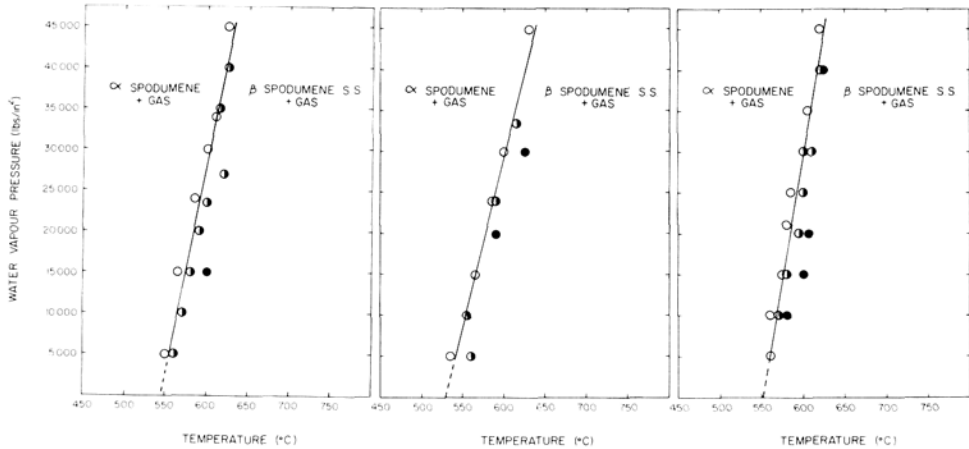
*Discussion.* The results of this study have important crystallographic and petrologic implications.

Crystallographically, the  $\alpha$ - $\beta$ -spodumene transition represents a "reconstructive" transformation (Buerger, 1951) involving two major silicate structures of radically different types that can be conveniently studied experimentally and thermodynamic values obtained from the results. Petrologically,  $\alpha$ -spodumene is the most important lithium-bearing mineral and the determination of the limits of its stability is important in the genesis of lithium pegmatites.

The spodumenes used in the present work are exceptionally pure varieties when compared with the analyses given in Deer, Howie, and Zussman (1963, p. 93). Very little data is available on cell sizes of spodumenes; the dimensions of the present samples (table II) are very similar to those given by Deer, Howie, and Zussman (1963, p. 92) although the  $b$  dimension is slightly larger in all cases, possibly as a result of the substitution of Na for Li in the structure. Stewart (1964) showed that regular variations in the cell parameters of spodumenes accompany this substitution. The cell sizes of the samples used in this study are much smaller than those reported by Scavnicar and Sabatier (1957) for a synthetic iron-bearing  $\alpha$ -spodumene obtained by heating albite with LiCl in an iron autoclave. In addition to iron, this sample may have possibly contained considerable Na replacing Li.

Samples 97 and 1 200 have very similar transformation curves (figs. 1 and 3) but are different from the transformation curve obtained for sample 684 (fig. 2). Chemically, 684 has a much higher  $\text{Fe}^{3+}$  content than the other samples (table I) suggesting that increased  $\text{Fe}^{3+}$  may increase the stability field of  $\alpha$ -spodumene at higher pressures.

The transformation temperatures for the natural spodumenes are slightly higher than the maximum of  $500^\circ\text{C}$  at  $10\,000$  lb./in.<sup>2</sup> suggested by Roy *et al.* (1950) for the  $\alpha$ - $\beta$  transformation. D. B. Stewart (personal communication) suggests that the presence of alkalis and other ions in the structure may increase the stability range of the  $\alpha$ -form. In the presence of quartz, spodumene will react to produce petalite at temperatures greater than  $550^\circ\text{C}$  at 2 Kb.  $P_{\text{H}_2\text{O}}$ , but above  $680^\circ\text{C}$  petalite becomes unstable and the reaction  $\alpha$ -spodumene + 2 quartz produces  $\beta$ -spodumene solid solutions + quartz (Stewart, 1963). Assuming that the reaction  $\alpha$ -spodumene + 2 quartz = petalite varies linearly



FIGS. 1 to 3:  $P_{\text{H}_2\text{O}}-T$  diagrams for the transformation of  $\alpha$ -spodumene;  $\circ$ ,  $\alpha$ -spodumene;  $\bullet$ ,  $\alpha$ -spodumene +  $\beta$ -spodumene solid solutions;  $\bullet$ ,  $\beta$ -spodumene solid solutions. FIG. 1 (left), sample no. 97, kunzite, Pala, California. FIG. 2 (middle), sample no. 684, Keystone, South Dakota. FIG. 3 (right), sample no. 1200, Seymour, Connecticut.

with pressure, petalite will become unstable at  $680^\circ\text{C}$  at a pressure slightly in excess of 5 Kb. Extrapolation of the  $\alpha$ - $\beta$  transition temperatures of the present study to this pressure passes within  $10^\circ\text{C}$  of Stewart's upper temperature limit of the stability of petalite. This suggests that at high pressures the addition of quartz has little effect on the  $\alpha$ - $\beta$  spodumene transition, and also suggests that the transition curves may represent a reasonable approximation to equilibrium conditions.

As might have been predicted from the large differences in molar volumes of the two forms of spodumene, the  $\Delta H$  values are very large in comparison to those of other silicates undergoing reconstructive transformations. Tuttle and Bowen (1958), using the same method as the present study, obtained a  $\Delta H$  value of 560 cal/mole for the quartz  $\rightarrow$  tridymite inversion. Isaacs and Roy (1958) give a value of  $3750 \pm 750$  cal/mole for the  $\text{LiAlSiO}_4$  (willemite-type structure)  $\rightarrow$   $\text{LiAlSiO}_4$  (high-quartz-type structure).

One surprising result of this study is the formation of silica-rich  $\beta$ -spodumene solid solutions. This suggests, but does not necessarily prove, that the coexisting gaseous phase is enriched in Li and possibly Al since the natural spodumenes are very close to stoichiometric  $\text{LiAlSi}_2\text{O}_6$ . This is apparently contrary to the findings of Stewart (1964) who has shown that the gaseous phase coexisting with lithium aluminum silicates at  $575^\circ\text{C}$  and 2000 bars contains 0.64 wt. % of dissolved solids, mainly  $\text{SiO}_2$ . Under these conditions the stable lithium aluminum silicate would be  $\alpha$ -spodumene (provided there was the correct available ratio of  $\text{Li}_2\text{O} : \text{Al}_2\text{O}_3 : \text{SiO}_2$ ), which has a tight pyroxene-type structure from which the cations cannot easily be removed. In contrast, Skinner and Evans (1960) have shown that  $\beta$ -spodumene has channels through which the

cations can readily be moved. This is one possible explanation of the silica-rich gas phase found by Stewart within the stability field of  $\alpha$ -spodumene and the Li (and Al) rich gas phase within the  $\beta$ -spodumene solid-solution stability field of the present study.

The formation of silica-rich  $\beta$ -spodumene solid solutions does not, of course, prove that the gas is necessarily enriched in Li and Al. The coexisting gas could still be enriched in silica provided a second lithium aluminosilicate mineral, such as eucryptite (LiAlSiO<sub>4</sub>), containing a lower percentage of silica than spodumene, also crystallized. There is no evidence for such a mineral in the present investigation, but the possibilities that minute amounts of such a mineral are also present cannot be disregarded.

Because  $\beta$ -spodumene has never been reported in nature, the transition values suggest either that rocks containing spodumene have crystallized at lower temperatures than the  $\alpha$ - $\beta$  transition, or that the presence of other elements raises this transition temperature to geologically improbable values. Deer, Howie, and Zussman (1963, p. 94) suggest that small amounts of Si present in spodumene analyses may represent small amounts of SiO<sub>2</sub> originally in solid solution in  $\beta$ -spodumene. However, the monotropic nature of the  $\alpha$ - $\beta$  transition make this unlikely.

*Acknowledgements.* During the course of this work the author benefited from discussions with Dr. D. B. Stewart, U.S. Geological Survey, Washington, D.C. Dr. J. M. Piotrowski, University of Western Ontario, reviewed the manuscript. Mr. R. Brigham helped with the computer analyses. Financial support was provided by a grant from the University of Western Ontario.

#### References

- BUERGER (M. J.), 1951. *Phase Transformations in Solids*, Chap. 6, p. 183.  
— 1954. *Amer. Min.*, **39**, 600.  
DEER (W. A.), HOWIE (R. A.), and ZUSSMAN (J.), 1963. *Rock-Forming Minerals*, vol. 2, Longmans, London.  
EPPLER (R. A.), GIARDINI (A. A.), and TYDINGS (J. E.), 1962. *Journ. Amer. Ceram. Soc.*, **45**, 218.  
GORANSON (R. W.), 1931. *Amer. Journ. Sci.*, **22**, 481.  
ISAACS (T.) and ROY (R.), 1958. *Geochimica Acta*, **15**, 213.  
MOZZI (R.) and NEWALL (J.), 1961. An I.B.M. 704 program for the least squares determination of lattice parameters. International Union of Crystallography.  
ROY (R.) and OSBORN (E. F.), 1949. *Journ. Amer. Chem. Soc.*, **71**, 2086 [M.A. 11-94].  
—, ROY (D.), and OSBORN (E. F.), 1950. *Journ. Amer. Ceram. Soc.*, **33**, 152.  
SCAVNICAR (S.) and SABATIER (G.), 1957. *Bull. Soc. franç. Min. Crist.*, **80**, 308.  
SKINNER (B. J.), 1966. Handbook of Physical constants (editor S. R. Clark), *Geol. Soc. Amer.*, Memoir 97.  
— and EVANS (H. T.), 1960. *Amer. Journ. Sci.*, **258-A**, 312.  
STEWART (D. B.), 1960. Rept. 21st Internat. Geol. Congress, Norden, Pt. 17, p. 15.  
— 1963a. *U.S. Geol. Surv.*, Prof. Paper 475A, p. A-142.  
— 1963b. *Geol. Soc. Amer.*, Special paper No. 76, p. 159.  
— 1964. *U.S. Geol. Surv.*, Prof. Paper 501A, p. A-159.  
TUTTLE (O. F.), 1949. *Geol. Soc. Amer., Bull.*, **60**, 1727.  
— and BOWEN (N. L.), 1958. *Geol. Soc. Amer.*, Memoir 74.  
WARREN (B. E.) and BI COE (J.), 1931. *Zeit. Krist.*, **80**, 394.

# Classification of the amphiboles

By E. J. W. WHITTAKER

Department of Geology & Mineralogy, Parks Road, Oxford

*Summary.* It is shown that the systems of classification of the calciferous and alkali amphiboles proposed by Smith and by Phillips are both equivalent to a classification in terms of the cationic charge distribution in the chains. When this is made explicit, the diagrams of these authors can be modified into a symmetrical form, which is more conveniently visualized and which is related to orthogonal axes such that the co-ordinates of the point corresponding to any composition can be readily derived from the formula. The system is applicable not only to the classification of idealized formulae of calciferous and alkali amphiboles, but to all amphiboles whether or not they correspond to the ideal classical substitutions. The concept of end-members is not appropriate to the expression of general compositions involving charge balancing substitutions in the amphiboles, but cells can be defined in the charge distribution diagram that provide unambiguous definitions of the main recognized amphibole species and of some others. The applicability of these definitions to real amphibole compositions has been tested against some two hundred published analyses covering a very wide range of composition.

THE attainment of a completely satisfactory system of classifying the compositions of the amphiboles is a matter of considerable difficulty owing to the large number of parameters involved and the fact that some replacements are simple and direct (e.g.  $Mg \equiv Fe(II)$ ), whereas others involve coupled substitutions to maintain charge balance (e.g.  $Na, Al \equiv Ca, Mg$ ). The matter is made even more difficult by the fact that some of the coupled substitutions involve addition of an ion into a vacant site in the structure as well as direct substitution. Limited parts of the system can of course be treated by simple graphical methods.

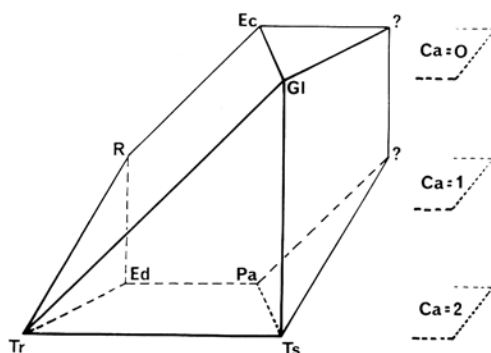


FIG. 1. The amphibole composition diagram of Smith, extended beyond the GI–Ec–Pa–Ts rectangle to include all nine possible extreme compositions.

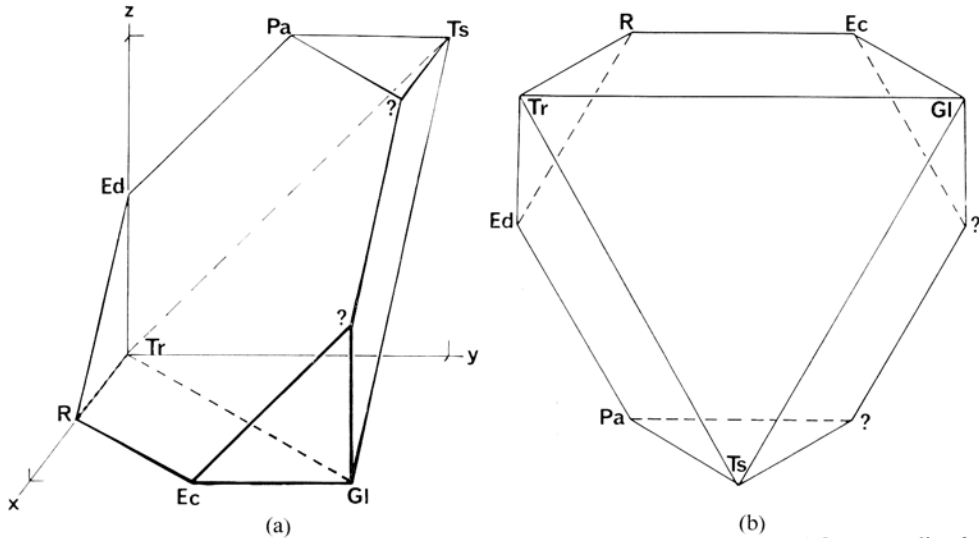


FIG. 2. (a) Amphibole composition space according to Phillips, with the solid figure outlined by joining the positions corresponding to his nine "end-members". (b) Projection of the solid figure from (a), seen down the common normal to its two large faces.

Sundius (1944) used triangular diagrams to represent some of the simpler substitutions, and in more complicated cases grouped classes of cations together at each vertex of the triangle. Winchell and Winchell (1951) used a square diagram to depict the coupled substitutions  $Mg \equiv Fe(II)$  and  $(Mg, Fe(II)), Si \equiv Al, Al$  in the anthophyllite-grunerite-gedrite range. Smith (1959) introduced a three dimensional diagram (fig. 1) to show the inter-relationships among the calc-alkali amphiboles, and Phillips (1966) has produced a system of three co-ordinates that is equivalent to another such 3-dimensional diagram (fig. 2).<sup>1</sup> The latter is a development from the 2-dimensional diagram of Phillips and Layton (1964). Zussman (priv. comm.) has also suggested a 2-dimensional diagram which can be regarded as a superposition of two planes from another 3-dimensional diagram (Fig. 3).<sup>2</sup>

At first sight the diagrams of Smith and Phillips appear very dissimilar, but in fact they are topologically equivalent to each other, and also to the 3-dimensional version of Zussman's diagram. This suggests that all three correspond to the same fundamental concept, which makes it seem worthwhile to seek a method of making this underlying unity explicit in the clearest possible way. The resulting diagram might then be rather more fundamental than just another variant among a large number of equally good (or bad) arrangements.

<sup>1</sup> The following abbreviations are used in Fig. 1 and elsewhere for mineral names or compositions: C.H.=common hornblende; Ec=eckermannite; Ed=edenite; Ek=eckrite; Gl=glaucophane; Ka=catophorite; Mb=mboziite; Pa=pargasite; R=richterite; Tr=tremolite; Ts=tschermakite; ?=un-named.

<sup>2</sup> This 3-dimensional diagram is equivalent to the one proposed by Fabriès (1966), to which the attention of the author has been drawn since the presentation of this paper.

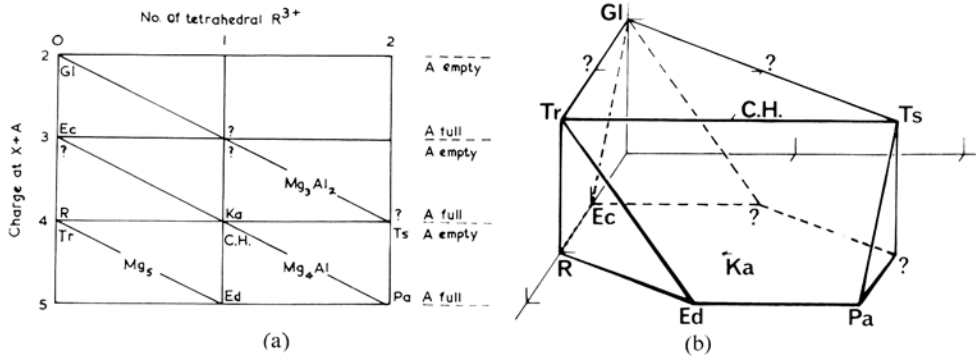


FIG. 3. (a) Two-dimensional diagram to show the interrelations of the amphiboles according to Zussman. (b) Three-dimensional version of (a) in which the upper horizontal plane corresponds to "A empty" and the lower one to "A full".

### *Comparison of the methods of Phillips and Smith*

Both authors simplify the problem in the first instance by confining attention to amphiboles containing only the ions Na, Ca, Mg, Al[6], Al[4], and Si. They assume that these are distributed in the A, X, Y, Z sites (per formula unit) as  $A = 0-1 \text{ Na}$ ;  $X = 2(\text{Na, Ca})$ ;  $Y = 3 \text{ Mg} + 2(\text{Mg, Al})$ ;  $Z = 6 \text{ Si} + 2(\text{Si, Al})$ . Phillips then takes as co-ordinates  $x = \text{Na}$  in X,  $y = \text{Al}$  in Y (i.e. Al[6]), and  $z = \text{Al}$  in Z (i.e. Al[4]). If the extreme values of  $(x, y, z)$  are joined to their neighbours this leads to the diagram shown in fig. 2, which shows a solid figure of high symmetry with nine vertices, disposed unsymmetrically with respect to the co-ordinate axes. Phillips regards the nine vertices as end-members. Seven of them can be identified with well-known amphibole names, and Phillips and Layton gave hypothetical "end-member names" to the other two. One of them is equivalent to an Mg-Al equivalent of the high-iron amphiboles taramite (Morozewicz, 1923) and mboziite (Brock, Gellatly, and von Knorring, 1964), but the other vertex does not seem to correspond to any known mineral.

Smith started from quite a different basis. He took the three charge-balancing substitutions Al[6], Al[4]  $\equiv$  Mg, Si (which converts tremolite to tschermakite), Na, Mg  $\equiv$  Al[6] (which converts tschermakite to pargasite), and Si  $\equiv$  Na, Al[4] (which converts edenite to tremolite) as the basis of a triangular diagram, truncated at the edenite-pargasite join. Perpendicular to this he erected an axis giving the number of Ca atoms in the formula. The resulting solid figure has seven vertices representing the seven well-known "end-members" of Phillips' diagram, but it can be extended, by introducing the appropriate substitutions, to include Phillips' two additional "end-members". In this extended form it is shown in fig. 1. It has no symmetry.

In the orientations shown the two diagrams appear to have little in common, but in fact corresponding "end-members" are connected in the same way in both. Each figure has two large parallel faces, one triangular (Tr-Ts-Gl) and the other hexagonal (Ec-R-Ed-Pa and the two extra vertices), though in

Phillips' diagram these are regular plane figures and in Smith's they are not. The remaining six faces consist of 3 trapezia and 3 triangles, which in Smith's diagram are of varied shapes.

Zussman's figure (fig. 3a) is based on two orthogonal axes giving charge at the  $A + X$  sites, and the number of trivalent atoms in tetrahedral sites. Its three-dimensional development (fig. 3b) introduces a third orthogonal axis giving the number of atoms in the  $A$  site (0 or 1). The solid figure, outlined by joining the established and hypothetical extreme compositions in this space, is again topologically equivalent to the diagrams of Phillips and Smith, but like Smith's figure it lacks symmetry.

#### *Derivation of a symmetrical system*

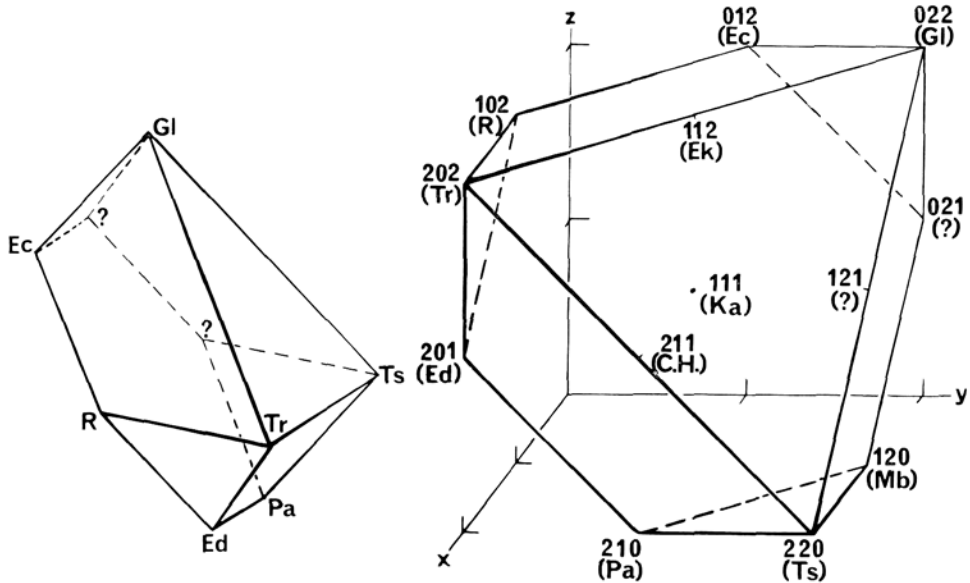
In order to derive a symmetrical figure it is necessary to avoid the use of a mixture of dissimilar co-ordinate systems as in Smith's method, and of co-ordinates which run between different limits, as has already been observed by Phillips in his modification of the co-ordinates used by Layton and Phillips.

The use of wholly triangular co-ordinates might be expected to increase the symmetry. In addition to the three charge-balancing replacements used by Smith, there are three others which he could not use in conjunction with Ca as an independent variable, because this element is involved.<sup>1</sup> These are: Na, Al[6] for Ca, Mg (which converts tremolite to glaucophane), 2Na for Ca (which converts tremolite to richterite), and Na, Si for Ca, Al[4] (which converts tschermakite to glaucophane). Use of all six of these makes the Tr-Ts-Gl triangle equilateral and the parallel hexagonal face regular, as in Phillips' diagram, and it also makes the other three triangular faces equilateral, and converts the three trapezia into the truncated bases of equilateral triangles (as one of them, Tr-Ts-Pa-Ed, was in Smith's diagram). The resulting figure (fig. 4) has trigonal symmetry with three mirror planes intersecting in the unique axis. The projection down the latter axis is identical with the corresponding projection of Phillips' diagram.

The symmetry of this form is very attractive, but by basing it on charge-balanced substitutions we have made it entirely relative. That is, we cannot express the composition of an amphibole directly but only by giving the substitutions that would convert some arbitrarily chosen "end-member" into it. We cannot express the composition uniquely in percentages of "end-member molecules", because this would require only four end-members in 3-dimensional space, and these would have to define a tetrahedron that contained all possible compositions (unless negative percentages of end-members were used). No set of four existing "end-members" satisfies this criterion. The fact that the figure is half an octahedron suggests the use of the orthogonal axes emerging

<sup>1</sup> The use of any other set of three charge-balanced substitutions with a different independent variable would produce a diagram geometrically congruent with Smith's though of course with the meaning of the vertices systematically displaced. None of them would be more useful than, or even as useful as, Smith's diagram.

at Tr, Ts, and Gl as a frame of reference, but unfortunately the co-ordinates of the vertices derived in this way are not simply related to the compositions. Furthermore, by basing the figure on the charge-balanced substitutions we have inevitably made it difficult to represent in the diagram compositions in which these are not strictly adhered to, as a result of changes in the number of protons in the structure for instance.



FIGS. 4 and 5: FIG. 4 (left). Amphibole compositions based entirely on triangular diagrams depicting the six possible charge-balancing substitutions. The figure is half of an octahedron, cut by a plane through its centre, parallel to the Gl-Tr-Ts face. FIG. 5 (right). Charge-distribution space for the amphiboles. The named species indicated have compositions corresponding to the co-ordinates against which they are placed, but are only representatives from among such species.

For all these reasons it seems desirable to achieve the same degree of symmetry, but to start from simple rectangular co-ordinates. This has already been achieved by Phillips insofar as the shape of his solid figure is concerned, but his system of co-ordinates has the drawback that the symmetry of the solid is not that of the axes, so that the symmetry is not reflected in the co-ordinates of symmetrically related points; *e.g.* Tr, Ts, Gl are represented as 000, 022, and 220. This is obviously due to the ingrained habit of mineralogists of regarding tremolite as in some sense the primary amphibole to which all others should be related. This "tremolite-centred" viewpoint can be eliminated in four ways by modification of the co-ordinates:

Tr, Ts, and Gl are placed on the axes to have co-ordinates 200, 020, and 002, or some permutation of these, and with the triangular face of the figure closer to the origin than the hexagonal face.

Tr, Ts, and Gl are placed at 200, 020, and 002, or some permutation of these, with the triangular face further from the origin than the hexagonal face; however, the other six "end-members" then no longer have simple co-ordinates related to composition, so that this orientation is unsatisfactory.

Tr, Ts, and Gl are placed at 202, 220, and 022, or some permutation of these, with the triangular face closer to the origin than the hexagonal face; this leads to the same result as the second alternative.

Tr, Ts, and Gl are placed at 202, 220, and 022 with the triangular face remote from the origin.

We obviously only need to consider the first and last alternatives further. The first requires:  $x$  = number of Na atoms at  $X$ ,  $y = 2 -$  number of Al[6], and  $z =$  number of Al[4]. It is obvious that only that permutation need be considered which associates the  $x, y, z$  co-ordinates with the  $X, Y, Z$  positions respectively. The way of defining  $y$  is only apparently unsymmetrical. If we consider the positions  $X, Y,$  and  $Z$  in their most highly charged conditions independently, then  $x, y, z$  correspond to the reductions in charge, from this starting point, that are required to give a particular composition.

The only disadvantage of this alternative is that only  $z$  can be read directly from the formula; the fourth is slightly better. It requires:  $x$  = number of Ca atoms at  $X$  ( $= 2 -$  number of Na at  $X$ ),  $y =$  number of Al[6], and  $z = 2 -$  number of Al[4] *i.e.* number of Si in excess of 6.

Here two variables can be read directly from the formula. This definition of  $x$ , when generalized to mean the number of  $M(\text{II})$  ions at  $X$ , is also more appropriate to the description of other amphiboles like anthophyllite. Here therefore each variable is the increase in charge of the site above its minimum value. It follows that the total cationic charge in the chain (*i.e.* apart from the  $A$  site) is  $42 + x + y + z$ , and the additional charge required for electrical neutrality is therefore  $4 - x - y - z$ . If positive this may be given by ions at  $A$  or by protons giving OH in excess of 2 (calculated on 24 O, OH, F), and if negative it may be given by  $\text{O}^-$  replacing  $\text{OH}^-$ . It is also possible for the first and second or first and third of these effects to occur simultaneously.

Fig. 5 shows the figure finally arrived at, in this orientation.

#### *Advantages of the proposed system of co-ordinates*

This system of co-ordinates shares the following advantages with that proposed by Phillips:

It leads to a highly symmetrical and easily remembered figure, which is easily represented by an orthogonal projection, so that for many purposes a 3-dimensional diagram is not required. None of the vertices overlaps another in the projection, and none occurs in a position that is hidden by the upper plane.

The co-ordinates of a point in the composition space are easily related to the composition.

Although the system has been developed under the simplifying assumption that  $X$  is always preferentially filled by Ca rather than Na, and that the latter

rather than the former goes preferentially to *A* when there is a choice, the procedure is not inseparable from this. In fact it provides different co-ordinate descriptions for richterite formulated on this assumption as  $\text{Na CaNaMg}_5\text{Si}_8$  and what may be described as the isomeric structure "iso-richterite"  $\text{Ca Na}_2\text{Mg}_5\text{Si}_8$ . Thus it provides a framework for expressing such differences when our structural knowledge makes such distinctions possible.

In addition, the proposed system has the following additional advantages not possessed by Phillips' proposals:

The co-ordinates have the same symmetry as the isolated solid figure.

Because it is based on composition in a way that relates directly to the more fundamental factor of charge distribution, it can easily be extended to cover various possible charge-balancing mechanisms, and to deal with the presence of ions of different charge from those considered in the derivation (*e.g.* Li and Ti at *Y*). In doing this one does not need to use Phillips' concept of "equivalent aluminium" as one is working directly with a defined physical parameter, charge. It can therefore be extended in principle to all amphiboles and does not merely apply to the idealized calc-alkali amphiboles for which it was derived. Oxy-amphiboles for example lie further from the origin than the triangular face of the sliced cube in fig. 5.

#### *The classification derived from the co-ordinate system*

The derivation of a suitable co-ordinate system is only the first step towards defining a method of classifying an amphibole composition. The second step involves the definition of boundaries between species in terms of the chosen co-ordinates. Smith did not make any proposals in this respect, and Phillips' proposals are complicated. This complication arises from his endeavour to confine named species to the nine vertices of his solid figure, and to regard these as end-members in some sense. Because of the ambiguity of representation of compositions in terms of such end-members he provides rules for the choice of sets of vertices in terms of which to describe any given composition represented within the composition space outlined by the nine vertices. These rules involve the application of a series of inequalities, because the boundaries of the corresponding regions in his composition space follow oblique planes. This is a sacrifice of the simplicity that should follow from adopting rectangular co-ordinates. Furthermore two of the ideal vertex compositions fall on a boundary plane, so that every member of such a species has to be further designated with a prefix *alk-* or *calc-*.

Very much greater simplicity is achieved if each species is defined as having a composition corresponding to a point within the cubic cell extending to  $\pm 0.5$  in each co-ordinate from the integral point which represents the ideal composition of the species. This permits the name to be assigned by simple inspection of the co-ordinates.

This system requires the use of four more names if all parts of the outlined region of fig. 4 are represented in nature, corresponding to the three mid-points

of the sides of the triangular face and the centre of the hexagonal face. Three of these are already occupied by named species, *viz.*, common hornblende (211), eckrite (112), and catophorite (111). Additional names would be required for cells whose centres lie outside the bounds of the outlined region, if and when such compositions appear to merit mineral names.

*Application of the method to real minerals*

It is much easier to classify idealized formulae than to classify real minerals. The method has therefore been tested by applying it to the 209 amphibole formulae listed, with the analyses from which they were derived, by Deer, Howie, and Zussman (1963). Of these 166 are calc-alkali amphiboles, and these are considered first.

The detailed application of the system was as follows:

The number of doubly charged atoms at  $X$  was taken to be the number of Ca atoms + any excess of  $Y$ -type atoms above 5. Then  $x$ ,  $y$ ,  $z$  were derived as:

$x$  = number of doubly charged ions at  $X$  – number of vacancies at  $X$ ;

$y$  = number of triply charged ions at  $Y$  + twice number of quadruply charged ions at  $Y$  (Ti) – number of singly charged ions at  $Y$  (Li) – twice number of vacancies at  $Y$ ;

$z$  = number of Si atoms at  $Z$  + number of vacancies at  $Z$  (assumed to be filled by  $H_4$ ) – 6.

If one accepts the idealized formulae given in table I as corresponding to the names used by Deer, Howie, and Zussman, then 100 out of the 166 fall into the expected cell of composition space centred on the co-ordinates shown in table I, the number of each being shown in brackets.

Of the remaining 66, fifteen were so close to the border of the cell corresponding to the name given, that very small errors in analysis, or even changes in the method of calculating the formula could have displaced them into it. These are therefore also indicated, after the + sign, in table I. Three more were at least isomeric with the given name, and are similarly included.

Twenty fall into nine cells without long established names (including one, the original taramite (Morozewicz 1923), which goes into 120, a cell that also corresponds to mboziite (Brook, Gellatly, and von Knorring 1964) and may perhaps therefore be regarded as named), and most of these (16) were named by Deer, Howie, and Zussman in accordance with the nearest named cell in the present system.

Nineteen appear to be wrongly named in accordance with the above ideal formulae, and are distributed as follows: 7 common hornblendes should be pargasite–hastingsite, 2 should be edenite, and one tschermakite; 3 edenites and one pargasite should be common hornblende; 2 tschermakites should be pargasite–hastingsite; 1 hastingsite should be tschermakite; 1 crossite should be catophorite; and 1 arfvedsonite should be richterite. It is considered that the existence of a system such as that presented here would help to make more systematic the naming of such doubtful and intermediate compositions.

TABLE I. Classification of 100 analyses of calc-alkali amphiboles. *n*, number of analyses falling into the cell whose co-ordinates are named.

Coords.	<i>n</i>	Name	Formula
202	(11)	tremolite-actinolite	$\text{Ca}_2(\text{Mg, Fe}^{2+})_5\text{Si}_8\text{O}_{22}(\text{OH})_2$
220	(20)	tschermakite basaltic hornblende	$\text{Ca}_2(\text{Mg, Fe}^{2+})_3\text{Al}_2\text{Si}_6\text{Al}_2\text{O}_{22}(\text{OH})_2$
022	(13 + 5)	kaersutite	$\text{NaCa}_2(\text{Mg, Fe}^{2+})_3(\text{Fe}^{3+}, \text{Al})_2\text{Si}_6\text{Al}_2\text{O}_{23}(\text{OH})$
		glaucophane	$\text{NaCa}_2(\text{Mg, Fe}^{2+})_4\text{TiSi}_6\text{Al}_2\text{O}_{22}(\text{OH})_2$
		crossite	$\text{Na}_2\text{Mg}_3\text{Al}_2\text{Si}_8\text{O}_{22}(\text{OH})_2$
		riebeckite	$\text{Na}_2(\text{Mg, Fe}^{2+})_3(\text{Fe}^{3+}, \text{Al})_2\text{Si}_8\text{O}_{22}(\text{OH})_2$
		magnesio-riebeckite (rhodusite)	$\text{Na}_2\text{Fe}^{2+}\text{Fe}^{3+}\text{Si}_8\text{O}_{22}(\text{OH})_2$
102	(4 + 3)	richterite	$\text{Na}_2\text{CaMg}_3\text{Si}_8\text{O}_{22}(\text{OH})_2$
012	(4 + 3)	eckermannite arfvedsonite	$\text{Na}_3\text{Mg}_4\text{AlSi}_8\text{O}_{22}(\text{OH})_2$
210	(17 + 6)	pargasite	$\text{NaCa}_2\text{Mg}_4\text{AlSi}_6\text{Al}_2\text{O}_{22}(\text{OH})_2$
		hastingsite	$\text{NaCa}_2(\text{Mg, Fe}^{2+})_4(\text{Fe}^{3+}, \text{Al})\text{Si}_6\text{Al}_2\text{O}_{22}(\text{OH})_2$
201	(2 + 1)	edenite	$\text{NaCa}_2\text{Mg}_5\text{Si}_7\text{AlO}_{22}(\text{OH})_2$
211	(26)	common hornblende	$\text{Ca}_2\text{Mg}_4\text{AlSi}_7\text{AlO}_{22}(\text{OH})_2$
111	(3)	catophorite	$\text{Na}_2\text{CaFe}_4^{2+}(\text{Fe}^{3+}, \text{Al})\text{Si}_7\text{AlO}_{22}(\text{OH})_2$

The remaining nine were more difficult to classify: they included four barkevikites, which is a name that cannot be identified with a cell; application of the method categorizes one as 211 (common hornblende) and two as 210 (pargasite-hastingsite); the other is of very peculiar composition corresponding to  $2\bar{1}1$ . There are also three "arfvedsonites" that do not correspond to 012; they are of highly oxy-hornblende type and may be described as oxy-riebeckites, 022. Finally two were rejected from classification because of poor analysis or unbalanced charge in the formula given.

The un-named cells that are found to be occupied have the following co-ordinates: 121 (or its isomer 021), 112, 200, 011, 230, 221, 122, 212. None of these corresponds with certainty to any of the many names listed by Hey (1950), but an amphibole of composition corresponding to 112 has been described under the name eckrite (Ravier, 1951).

When the method is applied to the 43 minerals of the anthophyllite-cummingtonite group with formulae given by Deer, Howie, and Zussman it serves to reveal our relative ignorance of the structural relations in this group. It is tempting to regard holmquistite as 022, but in fact we do not know that Li is at *X* and Al at *Y*; both might be distributed randomly, leading to charge co-ordinates<sup>1</sup> of 202. In anthophyllite, gedrite, and cummingtonite-grunerite we do not know definitely where the small amount of calcium lies in the structure. If

<sup>1</sup> Since the presentation of this paper the author has shown that holmquistite has Li at *X* and Al at *Y* (Whittaker, 1968).

TABLE II. Classification of 43 analyses of amphiboles of the anthophyllite-cummingtonite group, on the alternative assumptions that Ca lies at *X* and at *A*; *n*, number of analyses falling in the cell with the co-ordinates named

	Ca at <i>X</i>		Ca at <i>A</i>			Ca at <i>X</i>		Ca at <i>A</i>	
	Coords.	<i>n</i>	Coords.	<i>n</i>		Coords.	<i>n</i>	Coords.	<i>n</i>
Anthophyllite	202	7	202	5	Cummingtonite- grunerite	202	10	202	5
	112	1	112	1					
	212	3	212	3		201	3	201	3
			102	2		211	1	212	1
Gedrite	220	3	220	2		212	1	102	6
	210	3	210	2		102	1	111	1
	211	3	211	3					
	221	1	221	1					
			110	1					
		120	1						

we accept the formulae at face value it usually appears to be required to lie at *X*, but on structural grounds this seems unlikely and it may be at *A* with some corresponding vacancies at *X*. Dependent on the assumption made the charge co-ordinates found are as shown in table II. Thus, although the application of the method to these minerals does not suggest that any of them should have been named differently in terms of current nomenclature, it does show that there is a much greater variety of charge distribution included under the traditional names than is suggested by the usual idealized formulae, or than is tolerated within individual mineral names in the calc-alkali amphiboles.

### Conclusion

The concept of end-members in isomorphous series is a familiar one that has much to recommend it, especially when only 2 or 3 end-members are required to express a mineral composition, which can then be represented graphically along a line or on a triangular diagram. However when three independent variables are involved, as in the cationic charge distribution in the amphibole chain, a tetrahedral arrangement of four end-members is required, which is more difficult to visualize. Moreover, there does not exist any one set of four named amphibole compositions in terms of which the others could be expressed without involving negative proportions; in geometrical terms this means that, in any proposed amphibole composition space, there is no set of four named compositions that forms a tetrahedron having all other named compositions represented by points within it. In a general sense therefore, Phillips' nine "end-members" are not end-members at all in respect of the three-dimensional system required to represent the cation charge distribution. They are only end-members of the fifteen two-component substitution systems considered separately, of the three-component system Tr-Ts-Gl, or of various other ambiguously defined three- and four-component systems. Also, although the points 211 (common hornblende), 111 (cataphorite), and the points 112 and 121 in fig. 4 (and the corresponding points in Smith's and Phillips' diagrams)

can be represented in terms of mixtures of vertex compositions, they are no less necessary than the vertex compositions in adequately representing other intermediates. Furthermore 111 cannot be uniquely represented in terms of vertex compositions; it is equally (210+021), (102+120) and (012+210). Also some real amphibole compositions lie outside the limits of the idealized diagrams.

Since it has been shown that both Smith's and Phillips' classifications are equivalent to a classification of cationic charge in the chain, it is suggested that this should be recognized explicitly by the adoption of the present symmetrical system of classification, which has so many features in its favour for the classification of present, and possible future, knowledge. End-member classification will of course still remain extremely useful for the expression of other features of amphibole compositions that do not affect the distribution of cationic charge in the chain, for example  $Mg \equiv Fe^{2+}$  substitution as in the tremolite-actinolite series,  $Al \equiv Fe^{3+}$  substitution in the glaucophane-riebeckite series, and many others. Because of these many other important features of amphibole compositions it would not be possible to seek for a 1 : 1 correspondence between mineral names and cells in composition space (or rather charge-distribution space as it would be better called). Each cell may correspond to many names, but it is suggested that each name should be limited to a single cell, and delimited by the boundaries of that cell. Compositions corresponding to unnamed cells should not be referred to the nearest named one, but may be indicated by the cell co-ordinates, unless or until they are considered to merit an individual name. This should certainly always be done in discussions of theoretically possible but unrealized compositions, and would eliminate the tendency to introduce names for "hypothetical end-members".

#### References

- BROCK (P. W. G.), GELLATLY (D. C.), and VON KNORRING (O.), 1964. *Min. Mag.*, **33**, 1057.  
 DEER (W. A.), HOWIE (R. A.), and ZUSSMAN (J.), 1963. *Rock Forming Minerals*. Vol. 2. London: Longmans.  
 FABRIÈS (J.), 1966. *Compt. Rend. Acad. Sci. Paris*, **262**, sér. D, 1824.  
 HEY (M. H.), 1950. *Chemical Index of Minerals*, 1st edn, London: British Museum.  
 MOROZEWICZ (J.), 1923. *Spraw. Polsk. Inst. Geol.*, **2**, 6.  
 PHILLIPS (R.), 1966. *Min. Mag.*, **35**, 945.  
 PHILLIPS (R.) and LAYTON (W.), 1964. *Min. Mag.*, **33**, 1097.  
 RAVIER (J.), 1951. *Bull. Soc. franç. Min. Crist.*, **74**, 10.  
 SMITH (J. V.), 1959. *Amer. Min.*, **44**, 437.  
 SUNDIUS (N.), 1944. *Arsbok. Sveriges Geol. Undersökn.* **38**, no. 2.  
 WHITTAKER (E. J. W.), 1968. *Acta. Cryst.* (in press).  
 WINCHELL (A. N.) and WINCHELL (H.), 1951. *Elements of Optical Mineralogy*, Pt. 2. New York: John Wiley & Sons, Inc.

## Hydrothermal investigations and stability relations of synthetic gedrites

By TH. J. HINRICHSSEN

Mineralogisches Institut der Universität,  
355 Marburg/Lahn, Deutschhausstrasse 10,  
Germany

*Summary.* The stability relations of synthetic iron–magnesium mixed crystals of two gedrite series with different aluminium contents have been determined at a  $H_2O$ -pressure of 1 000 bars. The oxygen fugacity in the charge was controlled by buffers. The synthesis of a stable amphibole phase was possible only by substituting a small proportion of the bivalent cations by sodium. The minimum stability temperature of the amphibole phase is  $580 \pm 10^\circ C$  in both mixed crystal series investigated. These two gedrites are the iron end-members of the series: they contain no magnesium. No pure magnesium gedrite could be synthesized in experiments up to  $800^\circ C$ . The upper stability temperature of the iron-rich gedrites exceeds  $700 \pm 10^\circ C$ . At low temperatures chlorite and quartz coexist over the whole composition range. The maximum temperature of this assemblage is  $570^\circ C$  in the aluminium-poor mixed crystal series. Chlorite was found to be stable up to  $690 \pm 10^\circ C$ .

GREAT efforts have been made in recent years to clarify the stability relations of synthetic orthorhombic amphiboles. In the system  $MgO-SiO_2-H_2O$ , Fyfe (1962), using natural seed crystals, showed that anthophyllite has a stability field in the presence of water. Greenwood (1963) succeeded in determining the stability field of magnesium anthophyllite. Investigations on the magnesium-iron mixed crystals of the anthophyllite series were started by Boyd (1959). Hellner, Hinrichsen, and Seifert (1965) determined the stability fields of the magnesium–iron anthophyllites.

Attempts to synthesize the magnesium end-member of the gedrite series failed (Fawcett and Yoder, 1966), but Hellner (1964) and Hellner, Hinrichsen, and Seifert (1965) showed that it is possible to synthesize iron containing gedrites in which the magnesium and iron are partly substituted by sodium. Akella and Winkler (1966) succeeded in synthesizing gedrite from natural chlorite and quartz using a sodium-containing gedrite as seed crystal.

In this work magnesium–iron mixed crystals of two gedrites were investigated. In the first of these  $1(Mg, Fe^{2+}) + 1 Si$  are substituted by 2 Al, and in the second  $2(Mg, Fe^{2+}) + 2 Si$  are substituted by 4 Al.

*Experimental.* The starting materials were powder mixtures made from iron oxalate, magnesium oxalate, sodium carbonate, silica, and aluminium hydroxide. These powder mixtures were at first used directly in the hydrothermal runs for

synthetic or equilibrium studies. Later on the mixtures were subjected to a preliminary hydrothermal treatment at 500°C and 1 000 bars to remove CO<sub>2</sub> and CO, and the products of this treatment were used in all experiments. The pressure was 1 000 bars and the temperature 490°C to 800°C. Temperatures were controlled to  $\pm 10^\circ\text{C}$ . The oxygen fugacity was controlled by buffers, using below 570°C a magnetite-iron mixture and above 570°C a magnetite-wüstite mixture. All phase boundaries were checked by reverse reactions. The products of the runs were investigated with an X-ray diffractometer and with an optical microscope.

*Stability relations of aluminium-poor gedrite.* The hydrothermal investigations of the gedrites were started with the mixed crystal series where (Mg, Fe<sup>2+</sup>)Si is substituted by 2 Al. The general formula for the series is (Mg, Fe<sup>2+</sup>)<sub>6</sub>Al[AlSi<sub>7</sub>O<sub>22</sub>(OH)<sub>2</sub>]. Part of the magnesium and iron was substituted by 1.0 to 1.2 wt. % sodium. Fig. 1 shows the results of about 200 hydrothermal runs projected on a pseudobinary *t-x* diagram. The lowest stability temperature of the amphibole phase was found to be  $580 \pm 10^\circ\text{C}$ . The gedrite formed under these conditions contains no magnesium. The lower stability temperature of the amphibole phase rises steeply with increasing magnesium content. The gedrite with the highest magnesium content, synthesized at  $700 \pm 10^\circ\text{C}$ , had a Mg/(Mg+Fe<sup>2+</sup>) ratio of 0.7. The pure magnesium gedrite could not be synthesized. Experiments at  $800 \pm 10^\circ\text{C}$  yielded another amphibole phase of unknown composition coexisting with cordierite, enstatite and talc. This agrees with the results of Fawcett and Yoder (1962, 1966), who also found that in

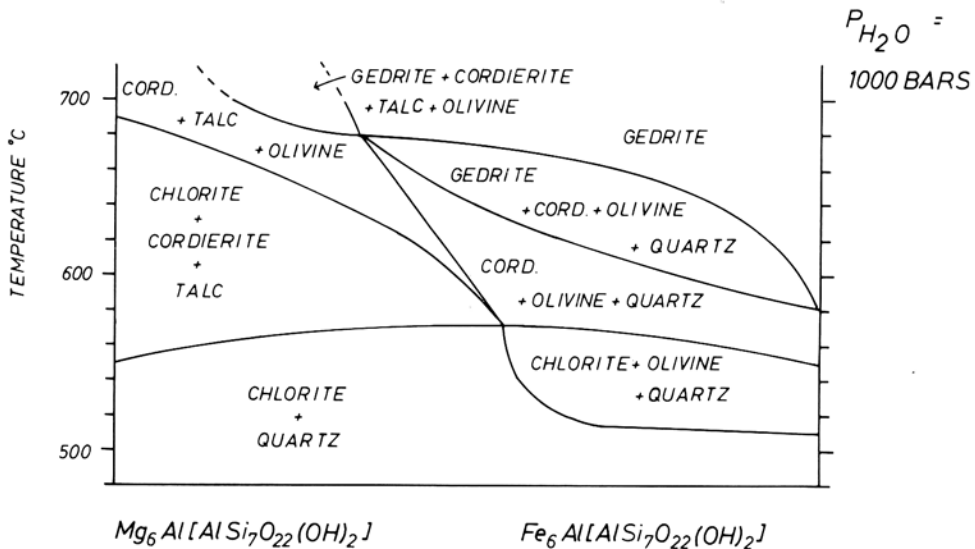


FIG. 1. *T-x* diagram for gedrites poor in aluminium.

the system  $\text{MgO-Al}_2\text{O}_3\text{-SiO}_2\text{-H}_2\text{O}$  amphiboles were formed metastably at 700 to 850 °C. In nature no pure magnesium gedrites have been found.

At lower temperatures (500 to 570 °C) a chlorite-quartz assemblage is stable over the whole composition range. The chlorites contain less aluminium than those of the clinocllore-daphnite series. The maximum stability temperature of the chlorite-quartz assemblage is  $570 \pm 10$  °C. This result supports the view of Fawcett and Yoder (1966) that the maximum temperature of the chlorite-quartz assemblage in the system  $\text{MgO-Al}_2\text{O}_3\text{-SiO}_2\text{-H}_2\text{O}$  is not reduced by substituting MgO by FeO.

At higher temperatures the magnesium-rich chlorite coexists stably with cordierite and talc up to  $690 \pm 10$  °C. Above this temperature cordierite, talc, and olivine coexist. The iron-rich chlorites decompose to give a chlorite richer in aluminium together with olivine. At even higher temperatures (above 570 °C) the chlorite becomes unstable and cordierite is formed. Two transition fields exist at higher temperature, one with gedrite, cordierite, olivine, and quartz and another with gedrite, cordierite, olivine, and talc. Above the first of these fields lies the stability field of gedrite.

*Stability relations of aluminium-rich gedrites.* In this mixed crystal series  $2(\text{Mg}, \text{Fe}^{2+}) + 2 \text{Si}$  are replaced by 4 Al, and the bivalent cations are partly substituted by 0.8 to 1.0 wt.% sodium. The general formula for the series is  $(\text{Mg}, \text{Fe}^{2+})_5\text{Al}_2[\text{Al}_2\text{Si}_6\text{O}_{22}(\text{OH})_2]$ . Fig. 2 shows the pseudobinary  $t$ - $x$  diagram of the mixed crystal series, based on the results of about 250 hydrothermal runs.

The minimum stability temperature of gedrite is again  $580 \pm 10$  °C for the

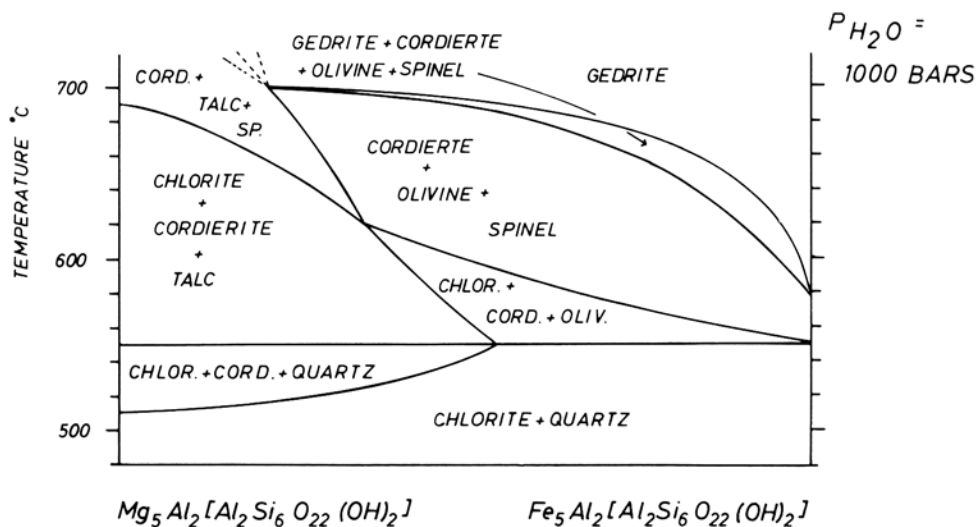


FIG. 2.  $T$ - $x$  diagram for gedrites rich in aluminium.

pure iron end-member. This phase can readily be distinguished optically from the ferroan gedrite poor in aluminium. At  $700 \pm 10^\circ\text{C}$  the magnesium-rich gedrite has a  $\text{Mg}/(\text{Mg} + \text{Fe}^{2+})$ -ratio of 0.8. If the mixture is richer in magnesium and the temperature is raised to  $800 \pm 10^\circ\text{C}$  an orthorhombic amphibole is formed, but cordierite, enstatite, and spinel form in addition.

At low temperatures (500 to  $550^\circ\text{C}$ ) chlorite and quartz coexist over the whole composition range. The chlorites contain more aluminium than those of the clinocllore-daphnite series. Chlorite and quartz are found to be stable up to  $550 \pm 10^\circ\text{C}$  provided the  $\text{Mg}/(\text{Mg} + \text{Fe}^{2+})$  ratio of the starting material is below 0.55. If the mixture is richer in magnesium the upper stability temperature is reduced, and falls to  $510 \pm 10^\circ\text{C}$  at the magnesium end of the diagram. At higher temperatures magnesium-rich mixtures yield cordierite in addition.

The iron-rich chlorite-quartz assemblage is replaced at higher temperatures by chlorite, cordierite, and olivine. When the chlorite becomes unstable, spinel is formed in addition to cordierite and olivine.

At the magnesium-rich end of the diagram the chlorite is stable together with cordierite and talc up to  $690 \pm 10^\circ\text{C}$ . At higher temperatures cordierite, talc, and spinel coexist. Cordierite, olivine, and spinel coexist on the iron-rich side of the diagram over a wide field of composition and temperature. A transition field was found below the stability field of gedrite; in this field gedrite, cordierite, olivine, and spinel coexist.

*Application to natural assemblages.* The variation in chemical composition of natural orthorhombic amphiboles is shown in fig. 3 (after Seki and Yamasaki, 1957). The field shaded with full lines indicates the range of composition of natural anthophyllite and gedrite quoted by Rabbitt (1948). Seki and Yamasaki (1957) proposed a wider field for this series, which is shaded with broken lines. The  $\text{Mg}/(\text{Mg} + \text{Fe}^{2+})$  ratio of natural anthophyllite varies from 1.0 to 0.6. The  $\text{Mg}/(\text{Mg} + \text{Fe}^{2+})$  ratio of gedrites with maximum Al-substitution varies from 0.8 to 0. The field of composition of synthetic orthorhombic amphiboles is bounded by the double line.

Anthophyllite and gedrite are typical minerals of the amphibole-hornfels facies. The first appearance of orthorhombic amphiboles characterizes the beginning of this facies. This temperature is a function of  $\text{H}_2\text{O}$ -pressure (which was not investigated) and of the bulk composition of the rock. The lower stability temperature of the pure magnesio-anthophyllite was determined by Greenwood (1963) to be  $667 \pm 8^\circ\text{C}$  at 1 000 bars  $\text{H}_2\text{O}$ -pressure. Hellner, Hinrichsen, and Seifert (1965) found a minimum stability temperature of  $520 \pm 10^\circ\text{C}$  at 1 000 bars  $\text{H}_2\text{O}$ -pressure for an anthophyllite with a  $\text{Mg}/(\text{Mg} + \text{Fe})$  ratio of 0.4. The minimum stability temperature of gedrites was found to be  $580^\circ\text{C} \pm 10^\circ\text{C}$  for the iron end member. Akella and Winkler (1966) showed, using natural material, that the gedrite becomes stable at  $548 \pm 12^\circ\text{C}$  (1 000 bars  $\text{H}_2\text{O}$ -pressure,  $(\text{Fe}^{2+} + \text{Fe}^{3+})/(\text{Fe}^{2+} + \text{Fe}^{3+} + \text{Mg})$  ratio 0.4). If one applies these data to the rocks found in nature, one can say that the lower temperature of

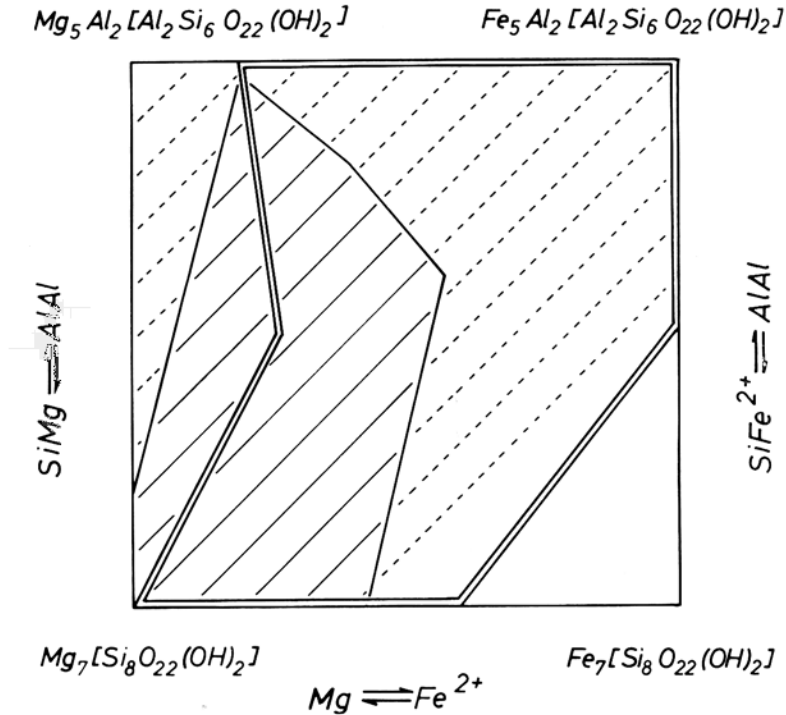


FIG. 3. Fields of composition of synthetic and natural orthorhombic amphiboles. Double lines outline the field of synthetic orthorhombic amphiboles; natural members occur in the field shaded with full lines, according to Rabbitt (1948), while Seki and Yamasaki (1957) extend their field to include the area shaded with broken lines.

the amphibole-hornfels facies lies in the range from 520°C to 580°C at 1 000 bars H<sub>2</sub>O-pressure.

An interesting result of the hydrothermal experiments is that the chlorite-quartz assemblage was found to be stable over the whole composition range of the two mix-crystal series investigated. The chlorite-quartz assemblage is characteristic for the greenschist facies. Fawcett and Yoder (1966) found that this assemblage is stable up to 570°C at 2 000 bars H<sub>2</sub>O-pressure in the system MgO-Al<sub>2</sub>O<sub>3</sub>-SiO<sub>2</sub>-H<sub>2</sub>O.

The investigations on the Mg-Fe mixed crystals of gedrites show that at 1 000 bars a Fe<sup>2+</sup>-containing chlorite can coexist with quartz up to 570 ± 10°C at a Mg/(Mg + Fe<sup>2+</sup>) ratio of 0.45. If the temperature is increased, cordierite is formed as a new phase. This mineral does not exist in the greenschist facies.

#### References

- AKELLA (J.) and WINKLER (H. G. F.), 1966. *Contr. Min. Petr.*, **12**, 1.  
 BOYD (F. R.), 1959. Hydrothermal investigations of amphiboles. In "Researches in Geochemistry" (ed. P. H. Abelson), New York.

- DEER (W. A.), HOWIE (R. A.), and ZUSSMAN (J.), 1963. *Rock-forming minerals*. 2, 211, London.
- FAWCETT (J. J.) and YODER (H. S.), 1962. *Carnegie Inst. Wash.*, Yearbook 61, 88.
- GREENWOOD (H. J.), 1963. *Journ. Petrology*, 4, 317.
- HELLNER (E.), 1964. The study of mixed crystals of minerals in metamorphic rocks. *Liverpool Geol. Soc.*, A Symposium on the Controls of Metamorphic Crystallisation. (Liverpool), Abstracts page 10.
- HELLNER (E.), HINRICHSEN (TH.), and SCHÜRMAN (K.), 1963. *Fortschr. Min.*, 41, 2, 164.
- HELLNER (E.), HINRICHSEN (TH.), and SEIFERT (F.), 1965. The study of mixed crystals of minerals in metamorphic rocks. In "The Controls of Metamorphism" (ed. W. S. Pitcher and G. W. Flinn), London.
- HOLSER (W. T.) and KENNEDY (G. C.), 1959. *Amer. Journ. Sci.*, 257, 71.
- RABBITT (J. C.), 1948. *Amer. Min.*, 33, 263.
- SEKI (Y.) and YAMASAKI (M.), 1957. *Amer. Min.*, 42, 506.
- TURNER (F. J.) and VERHOEGEN (J.), 1960. *Igneous and Metamorphic Petrology*, New York.

## Studies on synthetic alkali amphiboles

By R. PHILLIPS and G. ROWBOTHAM

Department of Geology, University of Durham

*Summary.* Optical and X-ray data are given for synthetic richterite and eckermannite. The various products formed from gels of sundiusite and miyashiroite compositions are described.

PHILLIPS and Layton (1964), in attempting to systematize the nomenclature of the calciferous and alkali amphiboles, have considered for simplicity the possible range of substitution of sodium and aluminium in the tremolite structure. These two elements were chosen as typical of the various elements that may substitute in the *A*, *X* and *Y*, *Z* positions, taking the general formula as  $AX_2Y_5Z_8O_{22}(OH)_2$ . Substitutions involving cations of similar charge and ionic radius—as for example  $Fe^{2+}$  for  $Mg^{2+}$ —were disregarded in the first instance as being trivial for the purposes of fundamental classification.

It was found that nine end-member compositions were theoretically possible, two of which, miyashiroite and sundiusite, had not previously been described. To distinguish these pure end-members of exact composition from naturally occurring minerals, it was suggested that a suffix  $\kappa$  (from Greek *καθαρος*, *pure*) be used. Thus tremolite- $\kappa$  indicates the exact chemical composition  $Ca_2Mg_5Si_8O_{22}(OH)_2$ , to which the minerals called tremolite merely approximate.

Phillips (1966) has shown how the relationships of these nine end-members may be represented on a simple diagram and has defined the alkali amphiboles as having at least 1.00 sodium atoms in the *X* position in the above general formula. This means that five of the nine end-members are classed as alkali amphiboles, namely richterite, eckermannite, glaucophane, miyashiroite, and sundiusite. The next logical step was to see if these compositions could exist as stable amphiboles and if possible to determine their stability ranges with varying temperature and pressure.

Glaucophane- $\kappa$  has been prepared by Ernst (1961) and the same author has shown that it has a pressure-dependent polymorphism. Michel-Lévy (1957) hydrothermally synthesized an amphibole approximating in chemical formula to richterite, with a composition said to be  $Na_{1.5}Ca_{0.7}Mg_{5.4}Si_8O_{22}(OH)_{3.8}$ . The mineral was synthesized from a mixture of  $MgCO_3$ ,  $CaCO_3$ ,  $Na_2CO_3$ , and  $SiO_2$  at approximately 450°C. At 580°C he also noted the appearance of pyroxene. Kohn and Comeforo (1955), Gibbs, Miller, and Shell (1962), and Saito and Ogasawara (1959) have all synthesized fluor-richterites. Eckermannite, to our knowledge, has not been hydrothermally synthesized, but fluor-eckerman-

nite and fluor-lithium eckermannite have been prepared by Eitel (1954). The type eckermannite from Norra Kärr in southern Sweden (Adamson, 1942; analysis by Sundius, 1946) contains 1.15% lithium.

Miyashiroite and sundiusite have not as yet been synthesized, nor are they known as minerals, although mboziite (Brock, Gellatly, and von Knorring, 1964) approximates to the iron analogue of sundiusite. The chemical composition is  $(\text{Na, K, Ca})_{3.03}(\text{Fe}^{2+}, \text{Mn, Mg, Fe}^{3+}, \text{Ti, Al})_{4.93}(\text{Si}_{6.20}\text{Al}_{1.80})\text{O}_{22}(\text{OH})_2$ , which gives a basic formula (Phillips and Layton, 1964) equivalent<sup>1</sup> to  $\text{Su}_{90}\text{R}_{10}$ , although there is a 78% replacement of  $\text{Mg}^{2+}$  by  $\text{Fe}^{2+}$  and an 88% replacement of  $\text{Al}^{3+}(\text{Y})$  by  $\text{Fe}^{3+}$ . No natural mineral with more than 48% miyashiroite in the basic formula is yet known to us. This is a value given by an arfvedsonite from Los Archipel, analysed by Kunitz (1930) and quoted by Sundius (1946).

### Experimental

Gels of the compositions Ec, R, Su, and M were prepared using a modification (D. L. Hamilton, personal communication) of the "organic silica-nitrate method" (Roy, 1956).

The materials used were: for  $\text{Na}_2\text{O}$ , Sodium carbonate of "Analar" grade; for  $\text{CaO}$ , Calcium carbonate of "Analar" grade; for  $\text{Al}_2\text{O}_3$ , Finely divided aluminium powder supplied by British Aluminium Co. Ltd.; for  $\text{MgO}$ , pure magnesium metal supplied by Magnesium Elektron Ltd.; and for  $\text{SiO}_2$ , tetraethylorthosilicate supplied by Monsanto Chemicals Ltd. The sealed tube method of Goranson (1931) was used in the experiments. The gels were loaded, together with 5 to 10% of water by weight, into gold or platinum capsules, depending on the pressure and temperature of the experiments. The gold capsules were not used above 950°C.

The experiments were carried out in three types of hydrothermal apparatus. The first, a conventional "cold-seal" apparatus designed by Tuttle (1949), was used for experiments at 700 to 900°C and 1 kilobar. The second, a molybdenum-0.5%-titanium vessel described by Williams (1966), was used for experiments at 885 to 1 100°C and 1 kilobar. A nimonic sheath (alloy No. 75) surrounds the vessel and is filled with argon to prevent oxidation. The pressure medium for these experiments is argon gas and the pressure is raised from cylinder pressure to the required pressure by a simple hand pump. The third type of apparatus used was an internally heated hydrothermal vessel, which is a modification of that described by Yoder (1950). The pressure medium is argon and is raised to the required pressure by two intensifiers and the temperature of the experiment. This apparatus was used for experiments at 700 to 1 000°C and 5 kilobars.

The condensed products were examined under a Zeiss petrographic microscope using white light and refractive index oils 1.590 to 1.630, depending upon the composition of the material. X-ray examination of all the samples was carried out using a Philips diffractometer with  $\text{Cu-K}\alpha$  radiation. Smear mounts were used with quartz as an internal standard. The specimens were scanned from 5° to 50°  $2\theta$  at 1° per minute for routine identification.

### Results

*Richterite- $\kappa$*  ( $\text{NaCaNaMg}_5\text{Si}_8\text{O}_{22}(\text{OH})_2$ ). Twelve runs, in which gels of composition  $\text{Na}_2\text{O} \cdot \text{CaO} \cdot 5 \text{MgO} \cdot 8 \text{SiO}_2$  were treated with excess water for 18 to 192 hours at 750 to 1 000°C and 1 to 5 kilobars, gave a product that was identified as richterite- $\kappa$ . The mineral nucleated very quickly even at the lower tempera-

<sup>1</sup> Abbreviations, used here or subsequently: Ec=eckermannite, M=miyashiroite, R=richterite, Su=sundiusite.

tures investigated, and appears to be formed stably over the whole of the above range of temperatures and pressures. At 1 075°C and 1 kilobar a pyroxene was formed. The richterite- $\kappa$  was holocrystalline. The crystals varied in size from  $50 \times 20 \mu$  to  $200 \times 70 \mu$ ; they had a prismatic habit and were occasionally twinned. All had identical optical properties. Because of preferred orientation due to a prismatic cleavage, only two refractive indices could be obtained:  $\alpha' = 1.602 \pm 0.003$  and  $\gamma' = 1.624 \pm 0.003$ . The extinction angle  $\gamma' : [001]$  was  $15 \pm 2^\circ$ , and the crystals were optically negative with a high 2 V. The refractive indices agree well with those of synthetic fluor-richterite (Kohn and Comeforo, 1955) which has  $\alpha = 1.603$ ,  $\beta = 1.614$ ,  $\gamma = 1.622$ , and those of natural richterite from Långban, Sweden (Sundius, 1946), which has  $\alpha = 1.605$  and  $\gamma = 1.627$ .

Richterite- $\kappa$  has similar optical properties to tremolite- $\kappa$ . The distinguishing features are the 2 V and extinction angle. If we assume a refractive index of 1.614 (that of fluor-richterite, *op. cit.*) the 2  $V_x$  should be  $70^\circ$ , whereas tremolite- $\kappa$  has 2  $V_x = 86^\circ$ . The extinction angle ( $\gamma : [001]$ ) of tremolite- $\kappa$  is  $21^\circ$  and that of richterite- $\kappa$  is  $15^\circ$ .

The X-ray pattern of the synthetic richterite was compared with those of two specimens of natural richterite from Långban, Sweden (table I, cols. 1 and 2).

TABLE I. X-ray powder data for (1) synthetic richterite- $\kappa$ , (2) natural richterite from Långban, Sweden, (3) natural eckermannite from Norra Kärr, Sweden, (4) synthetic glaucophane- $\kappa$  (Ernst, 1961), and (5) synthetic eckermannite- $\kappa$

1		2		3		4		5	
<i>d</i>	<i>I/I</i> <sub>0</sub>								
8.984 Å	10					9.00 Å	9		
8.485	65	8.51 Å	100	8.35 Å	100	8.38	32	8.355 Å	40
4.861	10	—	—	4.888	2	4.818	12	4.822	12
4.802	15	4.804	20	4.480	3	4.481	36	4.479	40
4.496	44	4.50	40	4.054	2	4.049	19	4.040	14
3.865	28	3.858	20	3.852	2	3.885	35	3.835	38
3.388	85	3.388	70	3.398	5	3.412	72	3.404	70
3.282	90	3.281	60	3.355	11	—	—	—	—
3.148	100	3.146	70	3.225	9	3.257	65	3.246	70
3.027	40	—	—	3.059	53	3.120	91	3.097	100
2.959	65	2.962	60	2.947	5	2.980	50	2.965	50
2.823	45	2.823	40	2.920	2	2.913	34	2.910	25
2.734	45	—	—	2.758	8	2.794	24	2.781	35
2.707	100	2.707	80	2.702	13	2.714	100	2.708	80
2.585	55	2.587	40	2.678	2	2.683	20	2.673	15
2.527	30	2.532	60	2.581	3	2.581	32	2.571	35
2.391	20	—	—	2.510	6	2.502	81	2.500	60
2.334	70	2.337	50	2.296	4	2.301	13	2.294	20
2.288	30	2.278	50	—	—	2.265	25	2.276	20
2.271	20	—	—	2.154	4	2.173	50	2.164	50
2.202	10	—	—	2.067	2	2.081	15	—	—
2.167	60	2.167	60	—	—	2.031	9	2.019	10
2.055	10	—	—	2.005	4	—	—	—	—
—	—	—	—	—	—	1.887	16	1.878	12

The small differences in pattern may be a result of the manganese oxide content of the natural specimen, which may be as high as 9%.

We are grateful to P. J. Broomfield (University of Durham) for calculation of the cell parameters of this and other amphiboles described, using a least squares programme "Cohen" on the Atlas computer at Didcot. Values for richterite- $\kappa$  are compared with synthetic tremolite- $\kappa$  (Colville, *et al.*, 1966), using the space-group notation  $C2/m$ :

Richterite- $\kappa$	$a$ 9.892 $\pm$ 0.005 Å	$b$ 17.958 $\pm$ 0.007 Å	$c$ 5.263 $\pm$ 0.002 Å	$\beta$ 104.282 $\pm$ 0.029°	$a \sin \beta$ 9.586 Å	$V$ 906.0 $\pm$ 1.0 Å <sup>3</sup>
Tremolite- $\kappa$	9.833 $\pm$ 0.005	18.054 $\pm$ 0.009	5.268 $\pm$ 0.004	104.52 $\pm$ 0.07	9.52	905.3 $\pm$ 1.0

The  $\beta$  value for richterite- $\kappa$  would be expected to be less than that of tremolite- $\kappa$ , Whittaker (1960), as Na replaces Ca in one of the M<sub>4</sub> sites. Other cell parameters do not appear to change systematically.

*Eckermannite- $\kappa$*  (NaNa<sub>2</sub>Mg<sub>4</sub>AlSi<sub>8</sub>O<sub>22</sub>(OH)<sub>2</sub>). Ten runs, in which gels of composition 3 Na<sub>2</sub>O.8 MgO.Al<sub>2</sub>O<sub>3</sub>.16 SiO<sub>2</sub> were treated with excess water for 18 to 92 hours at 770 to 1 000°C and 1 to 5 kilobars, gave mixtures of an amphibole with a talc-like mineral. The crystals of the amphibole were extremely small, and of a fibrous habit. Their maximum size was 20  $\times$  3  $\mu$  and their average length usually about 10  $\mu$ . None of the optical properties could be determined with any accuracy from such small crystals. The amphibole was considered to be a synthetic eckermannite. In table I, cols. 3 to 5, its X-ray powder pattern is compared with those of natural eckermannite from Norra Kärr in Sweden and synthetic glaucophane- $\kappa$  (Ernst, 1961). There is a close similarity between the patterns of the synthetic eckermannite and glaucophane- $\kappa$  at high  $d$  values.

The cell parameters for the synthetic eckermannite- $\kappa$  are compared below with glaucophane I and II (Ernst, 1961 and 1963).

Eckermannite- $\kappa$	$a$ 9.762 $\pm$ 0.006 Å	$b$ 17.892 $\pm$ 0.011 Å	$c$ 5.284 $\pm$ 0.006 Å	$\beta$ 103.17 $\pm$ 0.049°	$a \sin \beta$ 9.505 Å	$V$ 898.6 $\pm$ 0.8 Å <sup>3</sup>
Glaucophane- $\kappa$ (I)	9.75	17.91	5.27	102.8	9.50	897
Glaucophane- $\kappa$ (II)	9.64	17.73	5.28	103.6	9.37	877

These figures show the close similarity that would be expected from the close similarity in chemical composition.

The talc-like mineral had optical and X-ray properties very similar to those of talc. Because of its presence, the exact composition of the eckermannite is uncertain. It must be very close to the eckermannite end of the eckermannite- $\kappa$ -glaucophane- $\kappa$  join (see fig. 3 of Phillips, 1966) because the mineral is stable at 1 000°C and 1 kilobar pressure. Glaucophane breaks down to forsterite, enstatite, albite, and vapour at 835°C and 1 kilobar (Ernst, 1961). The eckermannite was stable over the whole range of temperature and pressure investigated but was rather slow to nucleate below 750°C.

*Miyashiroite- $\kappa$*  and *sundiusite- $\kappa$* . Alkali amphiboles were not among the products of runs using gels of miyashiroite- $\kappa$  composition (3 Na<sub>2</sub>O.6 MgO.3 Al<sub>2</sub>O<sub>3</sub>.14 SiO<sub>2</sub>) or sundiusite- $\kappa$  composition (Na<sub>2</sub>O.CaO.3 MgO.2 Al<sub>2</sub>O<sub>3</sub>.6 SiO<sub>2</sub>). The experiments covered a temperature range of 750 to 1 000°C at pressures

of 1 to 5 kilobars, with times of 18 to 192 hours. All runs in which the miyashiroite- $\kappa$  gel was used gave only one phase, a sodic montmorillonite. Sometimes the crystals of this clay mineral were  $200 \times 100 \mu$  and possessed straight extinction. The condensed products using a sundiusite- $\kappa$  gel were quite different; in all cases, anthophyllite, the talc-like mineral, and a sodium-calcium montmorillonite were formed. All these phases persist metastably above their upper stability limits. At 5 kilobars and  $1\ 000^\circ\text{C}$  they were still formed, but possibly as quench phases. Investigations with the miyashiroite- $\kappa$  and sundiusite- $\kappa$  compositions are continuing. In order to overcome the kinetic barrier for nucleation of these minerals, several methods are being attempted: seeding of the starting materials with natural submicroscopic alkali amphibole; seeding of the gel with the synthetic fluoride analogues of the above hydroxy minerals; and use of higher pressures. The results of these investigations will be reported later.

#### Discussion

Richterite- $\kappa$  and eckermannite- $\kappa$  are stable over a wide range of temperatures and pressures but the natural minerals of these compositions are relatively rare. Richterite occurs in metasomatic and thermal metamorphic environments that are rich in carbonates and often manganese minerals. It also occurs in some nepheline syenites (Larsen, 1942). It has recently been reported for the first time in a meteorite (Olsen, 1967).

Eckermannite is extremely rare; the type specimen was found in a foliated pectolite-eckermannite-aegirine nepheline syenite at Norra Kärr in southern Sweden (Adamson, 1942). Nayak and Neuvonen (1964) described an eckermannite from a granite associated with manganese mineralization at Goldongri, India. Imerinite from Ambatoharina, Madagascar (Lacroix, 1921) is intermediate between richterite and eckermannite in composition.

The most common chemical environment in nature in which alkali amphiboles are developed is that in which high soda is accompanied by a high iron content. The environment required for the formation of richterite and eckermannite is high soda accompanied by a high magnesium content. The rarity of these conditions in nature explains the infrequent occurrence of natural richterite and eckermannite. It is worthy of note that natural richterite and eckermannite are often manganese- or lithium-bearing and that these minerals are frequently associated with low-temperature manganese mineralization.

#### References

- ADAMSON (O. J.), 1942. *Geol. För Förh. Stockholm*, **64**, 329.  
BROCK (P. W. G.), GELLATLY (D. C.), and VON KNORRING (O.), 1964. *Min. Mag.*, **33**, 1057.  
COLVILLE (P. A.), ERNST (W. G.), and GILBERT (M. C.), 1966. *Amer. Min.*, **51**, 1727.  
EITEL (W.), 1954. Proc. Internat. Symposium on Reactivity of Solids; Gothenburg. Pt. I. p. 335.  
ERNST (W. G.), 1960. *Geochimica Acta*, **19**, 10.  
— 1961. *Amer. Journ. Sci.*, **259**, 735.

- ERNST (W. G.), 1962. *Journ. Geol.*, **70**, 689.  
— 1963. *Amer. Min.*, **48**, 241.  
GORANSON (R. W.), 1931. *Amer. Journ. Sci.*, ser. 4, **22**, 481.  
GIBBS (G. V.), MILLER (J. L.), and SHELL (H. R.), 1962. *Amer. Min.*, **47**, 75.  
KOHN (J. A.) and COMEFORO (J. E.), 1955. *Ibid.*, **40**, 410.  
KUNITZ (W.), 1930. *Neues Jahrb. Min.*, Abt. A., **60**, 171.  
LACROIX (A.), 1921. *Neues Jahrb. Min.*, Ref. **II**, 304.  
LARSEN (E. S.), 1942. *U.S. Geol. Surv. Prof. Paper* No. 197A.  
MICHEL-LÉVY (M. C.), 1957. *Bull. Soc. franç. Min. Crist.*, **80**, 297.  
NAYAK (V. K.) and NEUVONEN (K. J.), 1964. *Bull. Comm. géol. Finlande*, **35**, no. 212, 27.  
OLSEN (E.), 1967. *Science*, **156**, 61.  
PHILLIPS (R.) and LAYTON (W.), 1964. *Min. Mag.*, **33**, 1097.  
— — 1966. *Ibid.*, **35**, 945.  
ROY (R.), 1956. *Journ. Amer. Ceram. Soc.*, **39**, 145.  
SAITO (H.) and OGASAWARA (K.), 1959. *Chem. Sect.*, **62**, 976.  
SUNDIUS (N.), 1946. *Årsbok Sveriges Geol. Undersök*, **40**, no. 4.  
TUTTLE (O. F.), 1949. *Bull. Geol. Soc. Amer.*, **60**, 1727.  
WHITTAKER (E. J. W.), 1960. *Acta Cryst.*, **13**, 291.  
WILLIAMS (D. W.), 1966. *Min. Mag.*, **35**, 1003.  
YODER (H. S.), 1950. *Trans. Amer. Geophys. Union*, **31**, 827.

# Synthesis and stability field of cummingtonite

By KAY SCHÜRMAN

Mineralog. Institut, Marburg/Lahn, Germany

*Summary.* Hydrothermal investigations at  $P_{\text{H}_2\text{O}} = 1\ 000$  bars and  $P_{\text{CO}_2} = 80$  bars in a reducing atmosphere controlled by buffers were made on the Mg-Fe mixed crystals of the monoclinic cummingtonite-grunerite series. Under these conditions cummingtonite was only obtained if a small amount of CaO (2.7 wt. %) was added. This CaO content is in agreement with that of natural cummingtonites that are poor in Mn.

The stability relations of the quasi-binary section of the Mg-Fe cummingtonites are shown by a  $T$ - $x$  phase diagram. Cummingtonite with more Mg than  $\text{Mg}_{65}\text{Fe}_{35}$  has not been synthesized; the pure iron end-member grunerite was obtained over a wide temperature range from  $450^\circ\text{C} \pm 10^\circ\text{C}$  to  $595^\circ\text{C} \pm 10^\circ\text{C}$ . The lowest point of stability at  $450^\circ\text{C}$  is determined only for the pure iron end-member of the series. The low-temperature parageneses are talc + olivine, talc + olivine + quartz, and at iron-rich compositions olivine + quartz. Without any iron the paragenesis talc + olivine converts at  $645^\circ\text{C} \pm 10^\circ\text{C}$  to talc + pyroxene.

THE members of the monoclinic cummingtonite-grunerite series with the theoretical formula  $\text{Mg}_7\text{Si}_8\text{O}_{22}(\text{OH})_2$ - $\text{Fe}_7\text{Si}_8\text{O}_{22}(\text{OH})_2$  are typically found in both regionally and contact metamorphosed rocks. First attempts in synthesizing cummingtonites have been made by Boyd (1954, 1959). He obtained the monoclinic cummingtonite phase only in a few runs at temperatures above  $800^\circ\text{C}$  (at  $P_{\text{H}_2\text{O}} = 1\ 000$  bars), and he stated that this phase was metastable.

Flaschen and Osborne (1957) obtained grunerite only in short runs (24 hr.) at  $700^\circ\text{C}$  and  $12\ 500$  lb./in.<sup>2</sup> pressure together with fayalite and quartz. In longer runs the grunerite phase disappeared.

Our first attempts failed to prepare synthetic cummingtonites in the system MgO-FeO-SiO<sub>2</sub> under various water vapour pressures up to 6 000 bars and various water contents of the mixture. In nature however cummingtonite has a small CaO content from 1 to 4 wt. %. Therefore we prepared our starting materials with 2.7% CaO in addition. The presence of this CaO was sufficient to produce nuclei of cummingtonite, which continued to grow (Hellner, Hinrichsen, and Schürmann, 1963).

*Experimental methods.* The hydrothermal runs were made in closed pressure bombs (modified Morey-type) at 1 000 bars water pressure and 80 bars CO<sub>2</sub> pressure. The amount of water that has to be used for different temperatures was taken from papers by Kennedy (1950) and Holser and Kennedy (1959). The results were controlled by additional runs under hydrostatic pressure controlled by a manometer. The error in water pressure is  $\pm 50$  bars and the

error in  $\text{CO}_2$  pressure between  $450^\circ\text{C}$  and  $650^\circ\text{C}$  is  $\pm 10$  bars. This range includes the increase of  $\text{CO}_2$  pressure by increasing temperature. The error in temperature is  $\pm 5^\circ\text{C}$ .

The specimen and the iron-magnetite buffer were separated by a sealed silver tube, but a hydrogen exchange was possible (Eugster and Wones, 1962). Both together were in sealed gold tubes.

The runs lasted from 14 days to 4 months. After each run the used buffers were checked. The phases that appear in the hydrothermal runs were determined by X-ray methods using a Philips powder diffractometer and a Guinier X-ray powder camera.

Successful attempts have been made to reverse the reaction; therefore it was possible to give our quasi-binary diagram.

*Experimental results.* About 300 runs were made at various temperatures from  $400^\circ\text{C}$  to  $680^\circ\text{C}$  at constant pressure  $P_{\text{H}_2\text{O}} = 1\,000 \pm 50$  bars and  $P_{\text{CO}_2} = 80 \pm 10$  bars. In fig. 1 more than 150 points in the  $T$ - $x$  diagram are indicated by different symbols explaining the results of the phase examinations.

The stability relations of the quasi-binary section of the Mg-Fe cummingtonites are shown by a subsolidus phase diagram (fig. 2).

No cummingtonite has been synthesized in the region  $\text{Mg}_{100}\text{Fe}_0$ - $\text{Mg}_{65}\text{Fe}_{35}$ . On the pure Mg-side of the diagram the paragenesis talc + olivine is stable up to  $645^\circ\text{C} \pm 10^\circ\text{C}$ . Above this temperature talc + orthopyroxene (enstatite) becomes stable.

The lowest point in the stability field lies near  $450^\circ\text{C}$  and at the composition of the pure iron cummingtonite. This grunerite is stable up to  $595^\circ\text{C} \pm 10^\circ\text{C}$ . Above this temperature it decomposes into olivine and quartz. The low temperature parageneses are talc + olivine, talc + olivine + quartz, and at iron rich composition olivine + quartz. It is remarkable that siderite has never been found although the  $\text{CO}_2$  partial pressure is relatively high.

*Discussion.* Cummingtonite is common in regional metamorphic amphibolitic rocks. Plagioclase and hornblende are the most associated minerals. Cummingtonite and anthophyllite have the same theoretical formula. Nevertheless parageneses of these amphiboles are relatively rare in nature. Eskola and Kervinen (1936), Collins (1942), and Tilley (1936) described such occurrences. But there is a little chemical difference between these two coexisting amphiboles: cummingtonite has more Ca and Mn and usually more Fe, whereas anthophyllite has more Al and Na and usually more Mg. If we compare the experimental stability fields of these two amphiboles (anthophyllite after Hellner, Hinrichsen, and Seifert, 1965), there is a rather large field of overlapping (fig. 3). This shows that the two phases can be stable together although they have sometimes nearly the same Mg-Fe ratio. This field of overlapping corresponds to the findings of Kranck (1961). He compared a number of analyses of anthophyllite and cummingtonite and found both phases for a rather large Mg-Fe region.

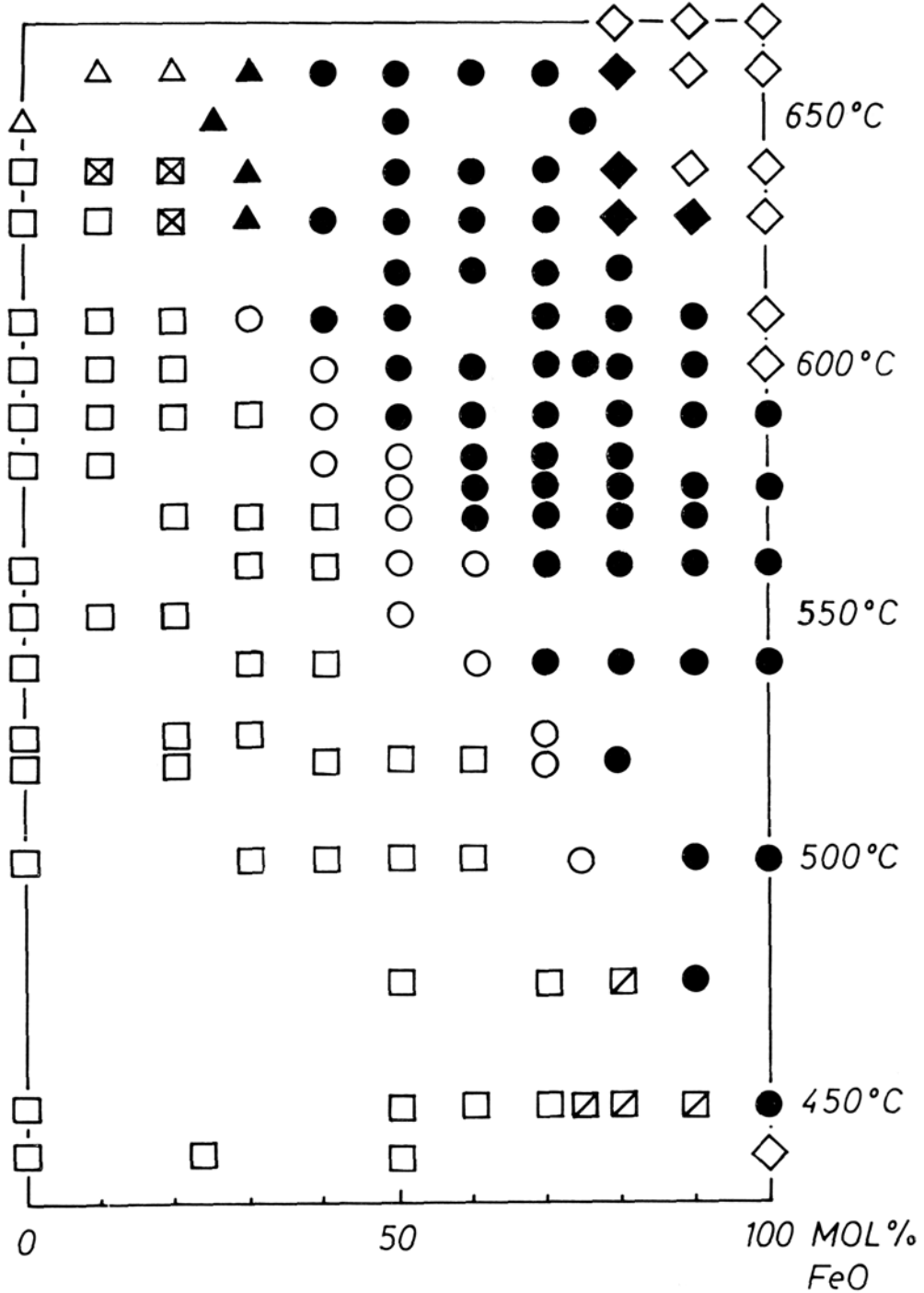


FIG. 1. Characteristic results of hydrothermal runs as a function of composition and temperature. ● cummingtonite; □ talc + olivine; ▧ talc + olivine + quartz; ○ talc + cummingtonite + olivine; ⊠ talc + pyroxene + olivine; △ talc + pyroxene; ▲ talc + pyroxene + cummingtonite; ◆ cummingtonite + olivine + quartz; ◇ olivine + quartz.

## CUMMINGTONITE (WITH 2 WEIGHT % CaO)

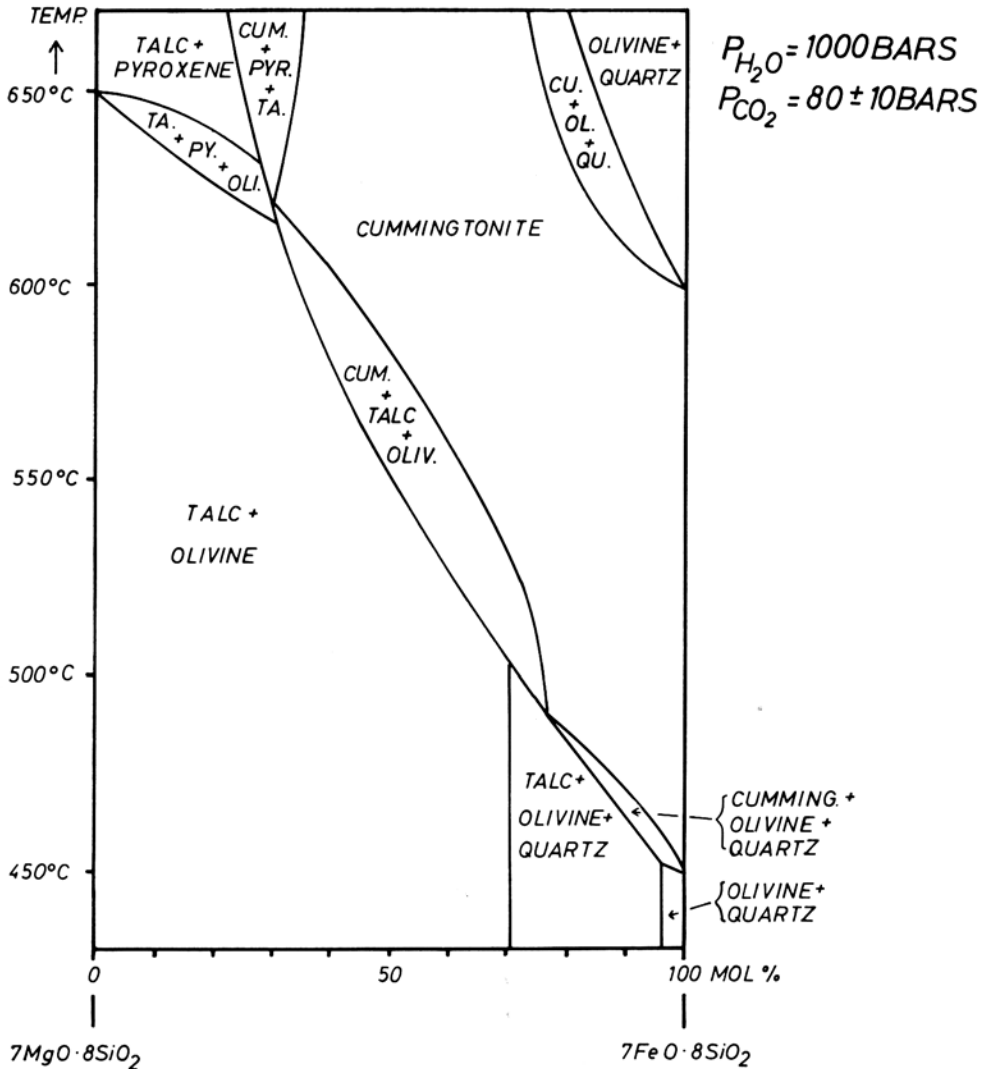


FIG. 2. Subsolidus phase diagram of the cummingtonite-grunerite series in terms of composition and temperature.

Grunerite is found in low metamorphosed zones as well as in highly metamorphosed contact rocks together with fayalite and pyroxenes. This is in good agreement with the wide temperature range from 450°C to 600°C of the determined stability field.

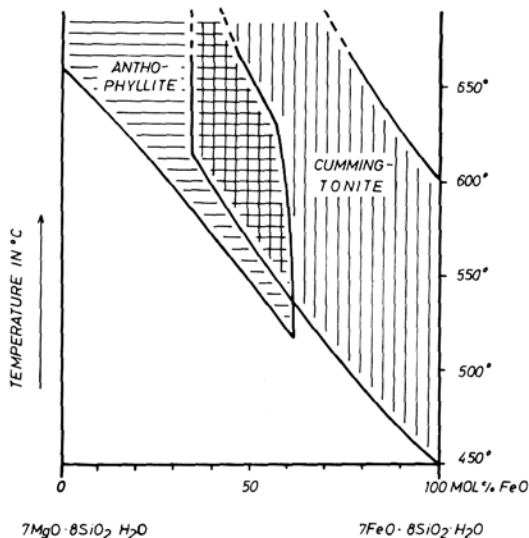


FIG. 3. Stability fields of synthetic anthophyllites and cummingtonites (anthophyllite after Hellner, Hinrichsen, and Seifert, 1965).

The variation in chemical composition of natural cummingtonites is in good agreement with our experiments. Eskola (1950) found more Ca in cummingtonites than in coexisting anthophyllites. But he stated that this fact has no relevance to the formation of the monoclinic amphibole phases. Layton and Phillips (1960) supposed that a partial occupation of the  $X$ -positions in the amphibole structure (general amphibole formula  $W_{0-1}X_2Y_5Z_8O_{22}(OH)_2$ ) by Ca, and substitution for Mg by Fe favors the monoclinic symmetry.

Mueller (1962) described a number of analyses of coexisting actinolites and cummingtonites from the Quebec Iron formation. He found a CaO content in the cummingtonites of about 0.5 wt. % and stated that this CaO content is not essential for stabilizing cummingtonites. However he conceded that the  $P$ - $T$  stability field of cummingtonites may become larger if Ca or Mn is added. It has been supposed by Klein (1964) that the maximal CaO content in the cummingtonite structure is 1.5 wt. %.

In our experimental investigations we obtained cummingtonite only in presence of CaO. Except for Mn-cummingtonite, it can be stated that CaO is necessary to obtain nuclei of cummingtonite. Up to now we have not obtained single crystals of cummingtonite large enough to check the position occupied by Ca in the structure.

#### References

- BOYD (F. R.), 1954. *Amphiboles*. Carnegie Inst. Washington Ann. Rpt. Director Geophys. Lab., no. 53, 116.  
 — 1959. Hydrothermal investigations of amphiboles. In "Researches of Geochemistry", New York, John Wiley and Sons, p. 377.

- COLLINS (R. S.), 1942. *Min. Mag.*, **26**, 254.  
ESKOLA (P.), 1950. *Amer. Min.*, **35**, 728.  
— and KERVINEN (T.), 1936. *Bull. Comm. géol. Finlande*, **115**, 475.  
EUGSTER (H. P.) and WONES (D. R.), 1962. *Journ. Petrology*, **3**, 82.  
FLASCHEN (S. S.) and OSBORNE (E. F.), 1957. *Econ Geol.*, **52**, 923.  
HELLNER (E.), HINRICHSSEN (T.), and SCHÜRMAN (K.), 1963. *Fortschr. Min.*, **41**, 164.  
— — and SEIFERT (F.), 1965. The study of mixed crystals of minerals in metamorphic rocks. In "Controls of Metamorphism", London, Oliver and Boyd, p. 155.  
HOLSER (W. T.) and KENNEDY (G. C.), 1959. *Amer. Journ. Sci.*, **257**, 71.  
KENNEDY (G. C.), *Ibid.*, **248**, 540.  
KLEIN (C., jr.), 1964. *Amer. Min.*, **49**, 963.  
KRANCK (S. H.), 1961. *Journ. Petrology*, **2**, 137.  
LAYTON (W.) and PHILLIPS (R.), 1960. *Min. Mag.*, **32**, 659.  
MUELLER (R. F.), 1962. *Geochimica Acta*, **26**, 581.  
TILLEY (C. E.), 1936. *Min. Mag.*, **24**, 331.

# On the chemical composition, properties, and mineral paragenesis of riebeckite and arfvedsonite

By V. I. KOVALENKO  
(В. И. КОВАЛЕНКО)

Institute of Geochemistry, Siberian Branch, Academy of Sciences,  
U.S.S.R., Irkutsk

*Summary.* This paper discusses the chemical composition and probable types of isomorphous replacements in the arfvedsonites and riebeckites. It attempts to correlate some optical and X-ray features with the chemical composition and genesis of these amphiboles, and to assess the influence of the main physical and chemical conditions (temperature, oxidation-reduction conditions, alkalinity) on their isomorphism.

The work is based on 85 analyses from the literature, 12 previously unpublished analyses of amphiboles from carbonatites kindly provided by L. K. Posharitskaya and E. A. Chernysheva, and 37 new analyses of amphiboles from alkali granitoids from Siberia.

## *Chemical Composition, Isomorphous, Replacements, and Some Geochemical Features of Arfvedsonites and Riebeckites*

PREVIOUSLY unpublished chemical analyses of 49 riebeckites and arfvedsonites from various rocks are shown in table II. Formulae calculated from these analyses and from 85 previously published analyses are shown in table I. These formulae are all computed to 13 cations (Borneman-Starynkevich, 1964).

These data, especially those from alkali granitoids (nos. 61–74 and 100–133), demonstrate the existence of the isomorphous series riebeckite–arfvedsonite. This is illustrated in fig. 1, which shows the inverse correlation between the parameters  $Si' = Z/(X + Y + Z)$  and  $X = (Na + K + Ca)$ . This inverse correlation is characteristic of the isomorphous series riebeckite–arfvedsonite. Calcium apparently does not participate constantly in the isomorphism, since the mean Ca contents of riebeckites and arfvedsonites do not differ substantially. Hence in this series the isomorphous replacement is of the type  $\square Na_2Fe^{3+} \rightleftharpoons Na_3Fe^{2+}$  as considered by Ernst (1962).

Fig. 1 shows the existence of all intermediate compositions between riebeckite and arfvedsonite, proving their perfect isomorphism in nature. Generally it seems reasonable to distinguish riebeckites ( $X = 2.0–2.4$ ;  $Si' = 0.532–0.520$ ), intermediate members ( $X = 2.4–2.8$ ;  $Si' = 0.519–0.505$ ), and arfvedsonites ( $X \geq 2.8$ ;  $Si' = 0.505–0.498$ ). The entrance of Ca and Al draws the isomorphism towards a position between arfvedsonite and catophorite (analyses 98 to 105) (Miyashiro, 1957). We stress that amphiboles of this isomorphous series are

TABLE I. Cation numbers (calculated to 13 (Y+Z) cations) and some general chemical parameters of alkali amphiboles.

No. Original no.† Name*	1	2	3	4	5	6	7	8	9	10	11‡	12	13	14	15	16	17	No. Original no.† Name*
	1 Rieb-Arf	2 Rieb-Arf	3 Rieb	5 Arf	6 Rieb-Arf	7 Rieb-Arf	8 Rieb-Arf	32 Rieb	33 Mg-Rieb	34 Rieb	35 Rieb	36 Rieb	37 Rieb	38 Rieb	39 Rieb	40 Rieb	41 Mg-Rieb	
Si	7.35	7.48	7.05	7.78	7.34	7.29	7.80	7.42	6.75	7.87	—	8.10	8.07	7.55	7.82	8.12	7.77	Si
Ti§	0.09	0.14	0.07	0.15	0.09	0.48	0.12	0.04	0.09	0.04	—	—	—	0.01	—	—	0.01	Ti§
Aliv	0.56	0.38	0.88	0.07	0.57	0.23	0.08	0.47	0.61	—	—	—	—	0.020	0.16	—	—	Aliv
Feiv <sup>3+</sup>	—	—	—	—	—	—	—	0.07	0.55	0.09	—	—	—	0.42	0.02	—	0.22	Feiv <sup>3+</sup>
Z	8.00	8.00	8.00	8.00	8.00	8.00	8.00	8.00	8.00	8.00	—	8.10	8.07	8.00	8.00	8.12	8.00	Z
Alvi	0.07	0.27	1.16	—	0.25	0.26	0.19	—	—	—	—	0.07	0.08	—	—	—	—	Alvi
Fevi <sup>3+</sup>	1.60	1.73	0.52	1.83	1.01	1.38	1.27	1.95	2.41	1.51	—	1.85	2.01	1.16	1.80	1.96	1.77	Fevi <sup>3+</sup>
Fe <sup>2+</sup>	3.14	2.76	2.79	3.11	3.57	2.10	3.40	1.52	1.12	2.43	—	2.50	2.39	2.80	2.01	1.65	1.05	Fe <sup>2+</sup>
Mn	—	—	—	—	0.09	0.16	0.06	—	—	—	—	—	—	0.03	0.01	—	—	Mn
Mg	0.19	0.14	0.53	0.06	0.09	1.10	0.08	1.56	1.30	1.03	—	0.47	0.47	1.02	1.23	1.19	2.18	Mg
Li	—	—	—	—	—	—	—	—	—	—	—	—	—	—	—	—	—	Li
Y	5.00	5.00	5.00	5.00	5.00	5.00	5.00	5.00	5.00	5.00	—	4.90	4.93	5.00	5.00	4.88	5.00	Y
Ca	0.67	0.17	0.28	0.49	0.51	0.46	0.17	0.34	0.19	0.12	—	0.29	0.47	0.07	0.04	0.04	0.06	Ca
Na	1.44	2.11	1.68	2.30	1.60	1.93	2.20	1.20	1.62	1.96	—	1.52	1.70	0.99	1.62	1.73	1.80	Na
K	0.25	0.37	0.33	0.43	0.33	0.17	0.31	0.08	0.03	0.06	—	0.17	0.17	0.14	0.12	0.06	0.05	K
X	2.36	2.65	2.26	3.22	2.44	2.56	2.68	1.62	1.84	2.14	—	2.81	2.34	1.20	1.78	1.83	1.91	X
OH	1.90	0.43	0.88	1.40	1.12	1.84	2.72	3.25	2.30	2.00	—	1.98	2.23	2.48	3.76	1.9	2.29	OH
F	—	—	—	—	—	—	—	—	—	—	—	—	—	—	—	—	—	F
Na/(Na+K)	0.85	0.85	0.835	0.873	0.760	0.920	0.875	0.935	0.980	0.970	—	0.900	0.910	0.873	0.940	0.965	0.972	Na/(Na+K)
f' <sub>  </sub>	0.942	0.950	0.838	0.975	0.975	0.655	0.970	0.571	0.462	0.700	—	0.840	0.835	0.730	0.616	0.580	0.324	f' <sub>  </sub>
Si' <sub>  </sub>	0.511	0.510	0.524	0.491	0.519	0.517	0.509	0.545	0.539	0.529	—	0.531	0.521	0.561	0.540	0.540	0.535	Si' <sub>  </sub>

\*Footnotes see page 269

TABLE I—Continued

No. Original no.† Name*	18	19	20	21	22	23	24	25	26	27	28	29	30	31	32	33	34	No. Original no.† Name*
	42 Mg-Rieb	43 Mg-Rieb	44 Mg-Rieb	45 Mg-Rieb	46 Mg-Rieb	47 Mg-Rieb	48 Mg-Rieb	112 Mg-Rieb-Ek	372 Ek	370 Ek	385 Ek	313 Ek	317 Mg-Arl	54/0 Ek	14/37-I Ek	11/18-I Ek	—	
Si	7.65	7.78	7.70	7.69	7.67	7.62	7.72	7.83	7.69	7.66	7.78	7.71	7.75	8.00	7.50	7.65	5.68	Si
Ti§	0.02	—	0.01	—	0.01	—	—	0.04	0.10	0.10	0.05	0.07	0.08	—	0.09	0.07	0.28	Ti§
Al <sub>v</sub>	0.03	0.12	0.09	0.08	0.07	0.38	0.05	0.13	0.21	0.24	0.12	0.22	0.17	—	0.41	0.28	2.04	Al <sub>v</sub>
Fe <sub>iv</sub> <sup>3+</sup>	0.30	0.10	0.20	0.23	0.25	—	0.23	—	—	—	0.05	—	—	—	—	—	—	Fe <sub>iv</sub> <sup>3+</sup>
Z	8.00	8.00	8.00	8.00	8.00	8.00	8.00	8.00	8.00	8.00	8.00	8.00	8.00	8.00	8.00	8.00	8.00	Z
Al <sub>v1</sub>	—	—	—	—	—	0.06	—	0.31	0.17	0.09	—	—	0.01	—	0.03	0.04	0.68	Al <sub>v1</sub>
Fe <sub>v1</sub> <sup>3+</sup>	1.31	1.63	1.61	1.84	1.53	1.66	2.03	2.03	0.89	0.91	0.19	0.35	0.35	0.54	1.07	1.29	0.65	Fe <sub>v1</sub> <sup>3+</sup>
Fe <sup>2+</sup>	0.90	0.84	0.92	0.48	0.42	0.99	0.40	0.29	0.62	0.57	0.20	0.17	0.26	0.01	0.41	0.43	0.84	Fe <sup>2+</sup>
Mn	—	0.03	0.03	0.01	0.01	—	0.03	—	0.01	0.01	0.02	0.01	0.01	0.03	—	—	0.03	Mn
Mg	2.81	2.45	2.48	2.66	3.17	2.21	2.58	3.21	3.37	3.41	4.62	4.47	4.33	4.32	3.49	3.24	2.80	Mg
Li	—	—	—	—	—	—	—	—	—	—	—	—	—	—	—	—	—	Li
Y	5.00	5.00	5.00	5.00	5.00	5.00	5.00	5.00	5.00	5.00	5.00	5.00	5.00	5.00	5.00	5.00	5.00	Y
Ca	0.11	0.06	0.26	0.03	0.39	0.34	0.40	0.20	0.57	0.67	0.97	0.91	1.03	0.56	0.30	0.43	2.15	Ca
Na	1.36	1.65	1.23	1.66	1.23	1.68	1.55	2.25	2.08	2.02	1.72	1.71	1.67	2.22	2.51	2.54	0.35	Na
K	0.20	0.06	0.04	0.08	0.08	0.05	0.03	0.08	0.18	0.19	0.24	0.23	0.21	0.14	0.08	0.16	0.34	K
X	1.67	1.77	1.53	1.77	1.70	2.07	1.98	2.53	2.83	2.88	2.93	2.85	2.91	2.92	2.89	3.13	2.84	X
OH	2.67	3.20	3.16	2.54	2.14	2.92	0.63	—	—	—	—	—	—	n.d.	n.d.	n.d.	2.33	OH
F	—	—	—	—	—	—	—	—	—	—	—	—	—	—	—	—	0.003	F
Na/(Na+K)	0.870	0.960	0.968	0.955	0.939	0.978	0.980	0.965	0.918	0.913	0.877	0.881	0.888	0.940	0.966	0.940	0.519	Na/(Na+K)
f' <sub>  </sub>	0.242	0.255	0.270	0.153	0.116	0.309	0.134	0.083	0.155	0.143	0.041	0.036	0.565	0.00	0.107	0.118	0.231	f' <sub>  </sub>
Si' <sub>  </sub>	0.542	0.541	0.549	0.541	0.542	0.530	0.531	0.515	0.503	0.501	0.501	0.502	0.502	0.502	0.502	0.496	0.505	Si' <sub>  </sub>

\*Footnotes see page 269

TABLE I—Continued

No. Original no.† Name*	35	36	37	38	39	40	42	43	44	45	46	47	48	49	50	51	52	No. Original no.† Name*
	19/70 Mg-Rieb	112/11 Ek	107/3 Mg-Rieb-Arf	Mg-Rieb	Mg-Rieb	Mg-Rieb	Mg-Rieb	Mg-Rieb	Mg-Rieb-Arf	Rieb	Ek	Mg-Rieb-Ek	I Rieb	II Mg-Rieb	III Mg-Rieb	IV Rieb-Arf	I Mg-Rieb-Ek	
Si	8.00	7.71	8.33	8.05	7.86	8.26	7.90	7.75	7.90	7.65	7.68	7.79	8.23	7.68	7.71	8.15	7.67	Si
Ti§	—	0.09	—	—	—	—	0.03	0.01	—	0.01	—	0.01	—	—	0.01	—	0.04	Ti§
Al <sub>IV</sub>	—	0.20	—	—	0.14	—	0.07	0.23	0.08	0.04	0.07	0.20	—	0.08	0.09	—	0.29	Al <sub>IV</sub>
Fe <sub>IV</sub> <sup>3+</sup>	—	—	—	—	—	—	—	—	—	—	0.25	—	—	0.24	0.19	—	—	Fe <sub>IV</sub> <sup>3+</sup>
Z	8.00	8.00	8.33	8.05	8.00	8.26	8.00	8.00	8.00	8.00	8.00	8.00	8.23	8.00	8.00	8.15	8.00	Z
Al <sub>VI</sub>	0.41	0.04	0.15	0.30	0.23	0.28	0.20	—	—	—	—	0.06	—	—	—	—	0.12	Al <sub>VI</sub>
Fe <sub>VI</sub> <sup>3+</sup>	1.63	0.70	1.71	1.61	1.65	1.35	1.61	1.53	1.07	0.72	0.74	0.86	1.87	1.83	1.61	2.21	0.69	Fe <sub>VI</sub> <sup>3+</sup>
Fe <sup>2+</sup>	1.22	0.44	0.42	1.16	0.56	0.79	0.87	0.91	0.27	0.27	0.40	0.17	1.78	0.48	0.92	2.31	0.52	Fe <sup>2+</sup>
Mn	—	0.01	0.08	—	—	—	—	—	—	—	—	—	—	—	—	—	—	Mn
Mg	1.74	3.81	2.17	2.84	2.59	2.32	2.29	2.56	3.73	4.10	3.75	3.93	1.16	2.66	2.48	0.33	3.64	Mg
Li	—	—	—	—	—	—	—	—	—	—	—	—	—	—	—	—	—	Li
Y	5.00	5.00	4.67	4.95	5.00	4.74	5.00	5.00	5.00	5.00	5.00	5.00	4.77	5.00	5.00	4.85	5.00	Y
Ca	—	0.55	0.10	0.20	0.11	0.18	0.24	0.30	0.20	0.12	0.26	—	0.21	0.05	0.26	0.22	0.27	Ca
Na	1.98	1.93	2.28	1.64	1.75	1.55	1.45	1.31	2.15	2.05	2.49	2.52	1.78	1.65	1.23	2.16	2.04	Na
K	0.07	0.32	0.32	0.11	0.10	0.09	0.07	0.03	0.32	0.03	0.17	0.13	0.01	0.08	0.04	0.10	0.27	K
X	2.05	—	2.70	1.95	1.96	1.82	1.76	1.64	2.67	2.20	2.92	2.65	2.00	1.78	1.53	2.48	2.58	X
OH	1.66	—	2.13	4.00	3.66	2.80	3.36	3.75	2.98	3.09	3.61	2.23	2.39	—	—	3.11	0.40	OH
F	0.09	—	1.28	—	—	—	—	—	—	—	—	—	—	—	—	—	—	F
Na/(Na+K)	0.965	0.858	0.877	0.938	0.945	0.945	0.955	0.975	0.870	0.985	0.933	0.950	0.992	0.955	0.966	0.955	0.882	Na/(Na+K)
f' <sub>II</sub>	0.410	0.104	0.162	0.289	0.177	0.254	0.275	0.251	0.672	0.615	0.096	0.041	0.605	0.153	0.270	0.875	0.125	f' <sub>II</sub>
Si' <sub>II</sub>	0.530	0.506	0.509	0.534	0.534	0.541	0.542	0.545	0.509	0.526	0.502	0.510	0.531	0.540	0.550	0.515	0.512	Si' <sub>II</sub>

\*Footnotes see page 269

TABLE I—Continued

No. Original no.† Name*	53	54	55	46 USNM C-498 Mg-Rieb	57	58	59	60	61	62	63	64	65	66	67	68	69	No. Original no.† Name*
	II Mg-Rieb-Ek	— Rieb	— Rieb		2 Rieb	10 Rieb	9 Rieb	1 Rieb	A9 Arf	A16 Arf	A4 Rieb-Arf	A2 Rieb-Arf	A7 Arf	A3 Arf	A8 Arf	A12 Arf	A13 Arf	
Si	7.95	8.02	7.85	7.90	7.56	7.37	7.96	8.05	7.74	7.82	7.65	7.62	8.00	7.76	7.74	7.76	7.69	Si
Ti§	0.05	—	—	0.01	0.44	0.13	0.04	—	0.15	0.18	0.13	0.21	—	0.20	0.13	0.13	0.09	Ti§
Al <sub>iv</sub>	—	—	—	0.04	—	0.50	—	—	0.07	—	0.12	0.06	—	0.04	0.01	0.11	0.11	Al <sub>iv</sub>
Fe <sub>iv</sub> <sup>3+</sup>	—	—	0.15	0.05	—	—	—	—	0.04	—	0.10	0.11	—	—	0.12	—	0.01	Fe <sub>iv</sub> <sup>3+</sup>
Z	8.00	8.02	8.00	8.00	8.00	8.00	8.00	8.05	8.00	8.00	8.00	8.00	8.00	8.00	8.00	8.00	8.00	Z
Al <sub>vi</sub>	0.65	0.03	—	—	0.14	0.13	0.11	0.49	—	0.10	—	—	0.07	0.09	—	0.07	—	Al <sub>vi</sub>
Fe <sub>vi</sub> <sup>3+</sup>	0.87	2.15	2.11	1.74	1.67	1.28	1.65	1.68	1.46	0.61	1.46	1.16	1.40	1.53	1.38	1.54	1.39	Fe <sub>vi</sub> <sup>3+</sup>
Fe <sup>2+</sup>	0.99	2.50	2.00	0.62	2.23	2.44	1.89	2.42	2.88	3.76	3.01	3.36	3.00	2.94	2.82	2.69	3.02	Fe <sup>2+</sup>
Mn	—	—	—	0.01	0.07	0.13	0.19	0.13	0.06	0.08	0.07	0.14	0.06	0.14	0.07	0.04	0.05	Mn
Mg	2.51	0.31	0.84	2.61	0.86	1.05	1.15	—	0.01	0.08	0.11	0.01	0.04	0.01	0.10	0.07	0.01	Mg
Li	—	—	—	—	—	—	—	—	0.61	—	0.33	0.34	0.34	0.27	0.60	0.69	0.64	Li
Y	5.00	4.98	5.00	5.00	5.00	5.00	5.00	5.00	5.00	5.00	5.00	5.00	5.00	5.00	5.00	5.00	5.00	Y
Ca	0.32	0.04	0.31	0.33	0.38	0.43	0.21	0.19	0.18	0.79	0.38	0.14	0.16	0.51	0.34	0.12	0.18	Ca
Na	1.89	1.81	1.32	1.86	1.30	1.41	1.46	1.83	2.49	1.93	1.98	2.27	2.74	2.10	2.44	2.76	2.73	Na
K	0.39	—	—	0.03	0.16	0.28	0.40	0.28	0.36	0.26	0.25	0.21	0.35	0.38	0.35	0.33	0.32	K
X	2.60	1.85	1.63	2.22	1.84	2.12	2.07	2.30	3.03	2.98	2.64	2.62	3.25	3.00	3.13	2.82	3.23	X
OH	0.20	2.65	4.30	0.26	3.46	2.93	2.06	2.00	1.37	1.77	1.77	1.38	1.18	1.80	1.17	1.35	1.06	OH
F	—	—	—	0.03	—	—	0.15	—	1.03	0.30	0.67	0.52	1.12	0.90	1.18	1.06	1.10	F
Na/(Na+K)	0.830	0.880	0.000	0.985	0.890	0.835	0.785	0.865	0.877	0.880	0.888	0.915	0.888	0.846	0.876	0.860	0.893	Na/(Na+K)
f <sup>  </sup>	0.284	0.88	0.704	0.102	0.722	0.696	0.620	1.00	0.996	0.980	0.915	0.950	0.933	0.995	0.966	0.975	0.995	f <sup>  </sup>
Si <sup>  </sup>	0.511	0.539	0.542	0.525	0.537	0.529	0.521	0.521	0.498	0.499	0.510	0.510	0.492	0.499	0.496	0.505	0.490	Si <sup>  </sup>

\*Footnotes see page 269

TABLE I—Continued

No. Original no.† Name*	70	71	72	73	74	75	76	77	78	79	80	81	82	83	84	85	86	No. Original no.† Name*
	A14 Arf	A15 Arf	A1 Arf	A6 Arf	A5 Rieb-Arf	1 Rieb-Arf	2 Rieb-Arf	4 Rieb	8 Mg-Rieb	9 Mg-Rieb	10 Mg-Rieb	11 Mg-Rieb	12 Mg-Rieb	13 Mg-Rieb	14 Mg-Rieb	1 Ek	2 Ek	
Si	7.70	8.06	7.70	7.73	7.60	8.01	8.13	7.78	7.93	7.69	7.85	7.40	7.81	7.64	7.66	7.92	7.92	Si
Ti§	0.06	—	0.09	0.16	0.21	—	—	—	0.04	0.16	0.01	—	—	0.01	—	—	0.03	Ti§
Aliv	0.05	—	0.05	0.11	0.17	—	—	0.20	0.03	0.15	0.14	0.46	0.08	0.07	0.08	0.08	0.05	Aliv
Feiv <sup>3+</sup>	0.19	—	0.16	—	0.02	—	—	0.02	—	—	—	0.14	0.11	0.28	0.26	—	—	Feiv <sup>3+</sup>
Z	8.00	8.06	8.00	8.00	8.00	8.01	8.13	8.00	8.00	8.00	8.00	8.00	8.00	8.00	8.00	8.00	8.00	Z
Alvi	—	0.05	—	0.07	—	0.15	0.14	—	0.55	0.20	0.17	—	—	—	—	0.86	0.15	Alvi
Fevi <sup>3+</sup>	1.33	1.61	1.45	1.61	1.64	1.96	1.23	1.85	1.61	1.47	1.77	1.35	1.53	1.40	1.90	0.24	0.89	Fevi <sup>3+</sup>
Fe <sup>2+</sup>	2.54	2.75	2.19	2.80	3.03	2.31	3.28	2.74	1.02	1.38	—	0.26	0.47	0.42	0.48	0.15	0.31	Fe <sup>2+</sup>
Mn	0.07	0.05	0.07	0.08	0.09	0.07	0.08	0.16	0.01	0.01	0.65	0.17	—	0.01	—	—	—	Mn
Mg	0.03	0.01	0.01	0.01	0.03	0.05	0.07	0.19	1.81	1.94	2.41	3.22	3.04	3.17	2.65	3.73	3.64	Mg
Li	1.06	0.40	1.31	0.43	0.30	0.34	—	—	—	—	—	—	—	—	—	—	—	Li
Y	5.00	4.94	5.00	5.00	5.00	4.99	4.87	5.00	5.00	5.00	5.00	5.00	5.00	5.00	5.00	5.00	5.00	Y
Ca	0.06	0.09	0.04	0.30	0.29	0.04	0.11	—	0.34	0.78	0.07	0.22	0.17	0.38	0.04	0.20	0.40	Ca
Na	2.85	2.70	2.62	2.23	2.11	2.43	2.76	1.82	1.74	1.44	1.87	1.72	1.37	1.23	1.65	2.43	2.21	Na
K	0.33	0.39	0.42	0.32	0.25	0.36	0.35	0.34	0.03	0.14	0.05	—	0.12	0.08	0.08	0.20	0.32	K
X	3.24	3.18	3.08	2.85	2.65	2.83	3.22	2.16	2.11	2.36	1.99	1.94	1.66	1.69	1.77	2.83	2.93	X
OH	1.14	1.39	0.41	1.48	1.69	0.95	1.40	1.20	3.26	2.44	1.54	0.72	2.05	2.11	2.51	1.99	0.81	OH
F	1.22	1.01	1.61	0.80	0.70	0.85	—	—	—	0.10	—	—	—	—	—	—	—	F
Na/(Na+K)	0.895	0.875	0.860	0.875	0.895	0.872	0.886	0.844	0.984	0.912	0.973	1.00	0.861	0.938	0.954	0.922	0.872	Na/(Na+K)
f <sup>  </sup>	0.985	0.995	0.995	0.995	0.990	0.978	0.978	0.935	0.362	0.419	0.00	0.075	0.134	0.117	0.153	0.039	0.078	f <sup>  </sup>
Si <sup>  </sup>	0.490	0.493	0.497	0.502	0.509	0.507	0.499	0.528	0.529	0.521	0.532	0.534	0.543	0.541	0.540	0.502	0.501	Si <sup>  </sup>

\*Footnotes see page 269

TABLE I—Continued

	No. Original no.† Name*	87	88	89	90	91	92	93	94	95	96	97	98 CRM 250 Cat	99 CRM 251 Cat	100 A269 Hast	101 Ir 274 Cat-Rieb	102 As 237 Rieb-Arf	103 As 236 Rieb	No. Original no.† Name*
Si		8.09	7.40	8.05	8.02	7.56	8.02	7.46	7.75	7.80	7.57	7.68	6.96	6.92	6.81	7.52	7.60	7.95	Si
Ti§		—	0.60	—	—	0.24	—	0.06	0.15	0.16	0.05	0.18	0.27	0.38	0.25	0.30	0.15	0.05	Ti§
Aliv		—	—	—	—	0.20	—	0.48	0.09	0.04	0.28	0.14	0.55	0.32	0.94	0.18	0.20	—	Aliv
Feiv <sup>3+</sup>		—	—	—	—	—	—	—	0.01	—	0.10	—	0.22	0.38	—	—	0.05	—	Feiv <sup>3+</sup>
Z		8.09	8.00	8.05	8.02	8.00	8.02	8.00	8.00	8.00	8.00	8.00	8.00	8.00	8.00	8.00	8.00	8.00	Z
Alvi		1.04	0.36	0.33	0.30	0.62	0.23	0.27	—	0.31	—	0.34	—	—	0.61	0.62	—	0.14	Alvi
Fevi <sup>3+</sup>		0.85	0.86	1.73	0.88	0.88	2.00	1.19	1.80	1.35	—	1.03	0.67	0.56	0.60	1.20	1.91	1.74	Fevi <sup>3+</sup>
Fe <sup>2+</sup>		0.32	1.15	0.45	1.50	2.14	1.99	3.48	3.08	3.22	4.90	0.13	2.59	2.83	2.25	2.53	1.43	1.47	Fe <sup>2+</sup>
Mn		0.04	0.05	0.14	0.07	0.06	0.09	—	0.06	0.10	0.10	0.99	0.12	0.14	0.09	0.14	0.15	0.06	Mn
Mg		1.98	2.58	2.13	2.12	1.30	0.33	0.06	0.06	0.02	—	2.51	1.62	1.47	1.45	0.39	1.25	1.19	Mg
Li		0.64	—	0.14	—	—	—	—	—	—	—	—	0.01	0.01	0.01	0.11	0.26	0.32	Li
Y		5.00	5.00	4.95	4.98	5.00	4.98	5.00	5.00	5.00	5.00	5.00	5.00	5.00	5.00	5.00	5.00	5.00	Y
Ca		0.04	0.51	0.04	0.56	0.47	0.96	0.36	0.49	0.21	0.65	0.63	1.13	0.94	1.88	0.80	0.34	0.19	Ca
Na		2.68	2.29	3.03	2.02	2.45	2.51	2.04	2.33	2.32	2.07	2.59	1.01	1.45	0.47	1.56	1.95	1.76	Na
K		0.42	0.35	0.26	0.39	0.35	0.32	0.60	0.43	0.31	0.51	0.04	0.22	0.26	0.19	0.30	0.22	0.25	K
X		3.14	3.15	3.33	2.97	3.33	3.79	3.00	3.25	2.84	3.23	3.26	2.36	2.65	2.54	2.66	2.51	2.20	X
OH		0.48	1.52	1.03	1.46	1.12	1.62	1.32	1.37	1.02	1.78	1.88	1.09	0.52	—	0.18	0.59	0.34	OH
F		1.16	—	1.00	0.99	—	—	—	—	1.51	—	—	—	—	—	—	—	—	F
Na/(Na+K)		0.865	0.866	0.920	0.837	0.875	0.880	0.805	0.842	0.881	0.805	0.985	0.820	0.848	0.713	0.839	0.900	0.875	Na/(Na+K)
f <sub>  </sub> <sup>1</sup>		0.139	0.309	0.173	0.413	0.620	0.855	0.980	0.980	0.965	1.00	0.049	0.958	0.954	0.617	0.868	0.535	0.963	f <sub>  </sub> <sup>1</sup>
Si <sub>  </sub> <sup>2</sup>		0.498	0.495	0.489	0.499	0.480	0.475	0.500	0.482	0.504	0.492	0.492	0.519	0.509	0.514	0.509	0.514	0.527	Si <sub>  </sub> <sup>2</sup>

\*Footnotes see page 269

TABLE I—Continued

No. Original no.† Name*	104 As 242 Rieb	105 247 Arf	106 273 Rieb	107 18 Rieb-Arf	108 246 Rieb-Arf	109 243 Rieb	110 A118 Rieb	111 A189 Rieb	112 A200 Rieb	113 A111 Rieb	114 — Rieb	115 1a Ca-Rieb	116 3a Ca-Rieb-Arf	117 4a Ca-Rieb	118 5a Rieb	119 6a Rieb-Arf	120 7a Rieb	No. Original no.† Name*
Si	7.45	7.89	8.18	6.94	7.55	7.52	7.58	7.18	7.50	7.90	7.71	7.17	7.35	7.95	7.45	7.61	7.54	Si
Ti§	0.26	0.11	—	0.47	0.14	0.19	0.09	0.32	0.09	0.09	0.08	0.09	0.07	0.05	0.08	0.08	0.09	Ti§
Al <sub>iv</sub>	0.17	—	—	0.59	0.18	0.21	0.22	0.27	0.31	0.01	0.21	0.12	0.24	—	0.21	0.27	0.26	Al <sub>iv</sub>
Fe <sub>iv</sub> <sup>3+</sup>	0.12	—	—	—	0.13	0.08	0.11	0.23	0.10	—	—	0.62	0.34	—	0.26	0.04	0.17	Fe <sub>iv</sub> <sup>3+</sup>
Z	8.00	8.00	8.18	8.00	8.00	8.00	8.00	8.00	8.00	8.00	8.00	8.00	8.00	8.00	8.00	8.00	8.00	Z
Al <sub>vi</sub>	—	0.15	0.23	0.47	—	—	—	—	—	0.41	0.36	—	—	0.10	—	—	—	Al <sub>vi</sub>
Fe <sub>vi</sub> <sup>2+</sup>	1.73	1.09	1.60	1.55	0.99	1.59	1.73	1.59	1.90	2.18	1.97	1.98	2.15	2.29	1.96	1.66	1.90	Fe <sub>vi</sub> <sup>2+</sup>
Fe <sup>2+</sup>	2.36	3.22	2.02	1.45	3.41	2.67	2.10	2.30	2.40	2.22	2.32	2.77	2.54	2.44	2.73	2.95	2.64	Fe <sup>2+</sup>
Mn	0.20	0.13	0.12	0.47	0.16	0.13	0.13	0.15	0.10	0.08	0.07	0.07	0.04	0.04	0.09	0.09	0.10	Mn
Mg	0.41	0.27	0.44	1.07	0.36	0.42	0.29	0.25	0.13	0.05	0.04	0.07	0.08	0.02	0.02	0.02	0.08	Mg
Li	0.32	0.05	0.25	—	0.13	0.19	0.75	0.71	0.47	—	0.24	0.13	0.17	0.08	0.21	0.28	0.28	Li
Y	5.00	5.00	3.00	5.00	5.00	5.00	5.00	5.00	5.00	5.00	5.00	5.00	5.00	5.00	5.00	5.00	5.00	Y
Ca	0.12	0.72	0.26	0.24	0.47	0.09	0.03	0.04	0.08	0.11	0.19	0.75	1.06	0.63	0.36	0.29	0.28	Ca
Na	1.68	1.82	1.71	2.00	1.71	1.87	1.76	2.00	1.92	1.86	1.72	1.53	1.55	1.07	1.67	2.10	1.72	Na
K	0.22	0.34	0.36	0.20	0.28	0.24	0.22	0.26	0.21	0.21	0.20	0.06	0.08	0.06	0.12	0.18	0.19	K
X	2.02	2.88	2.33	2.44	2.46	2.20	2.01	2.30	2.21	2.18	2.11	2.34	2.69	1.76	2.15	2.57	2.19	X
OH												2.14	2.26	1.79	2.25	2.02	1.77	OH
F	0.52	0.50			0.41	0.29	0.39	0.49	0.54		0.22	1.45	1.87	0.80	0.81	0.53	0.53	F
Na/(Na+K)	0.886	0.843	0.921	0.921	0.862	0.885	0.926	0.799	0.902	0.900	0.895	0.962	0.950	0.947	0.932	0.924	0.900	Na/(Na+K)
f' <sub>  </sub>	0.842	0.924	0.572	0.572	0.905	0.865	0.883	0.905	0.952	0.975	0.980	0.985	0.975	0.970	0.990	0.995	0.995	f' <sub>  </sub>
Si' <sub>  </sub>	0.530	0.501	0.517	0.517	0.514	0.522	0.529	0.518	0.521	0.525	0.529	0.521	0.509	0.541	0.528	0.512	0.525	Si' <sub>  </sub>

\*Footnotes see page 269

TABLE 1—Continued

No. Original no.† Name*	121	122	123	124	125	126	127	128	129	130	131	132	133	134	No. Original no.† Name*
	8a Rieb-Arf	9a Rieb	11a Rieb	1 Rieb	2 Ca-Rieb	10 Ca-Rieb	3 Rieb	4 Rieb	5 Rieb	6 Rieb-Arf	7 Rieb	8 Rieb	11 Rieb	5 026 Arf	
Si	7.55	7.50	7.51	7.25	7.56	7.55	7.48	7.56	7.50	7.46	7.48	7.48	7.64	7.30	Si
Ti§	0.08	0.08	0.08	0.07	0.09	0.09	0.08	0.07	0.07	0.09	0.09	0.07	0.09	0.14	Ti§
Aliv	0.26	0.32	0.35	0.29	0.31	0.30	0.39	0.35	0.38	0.35	0.26	0.34	0.28	0.56	Aliv
Feiv <sup>3+</sup>	0.11	0.10	0.06	0.39	0.04	0.06	0.03	0.03	0.05	0.10	0.17	0.11	—	—	Feiv <sup>3+</sup>
Z	8.00	8.00	8.00	8.00	8.00	8.00	8.00	8.00	8.00	8.00	8.00	8.00	8.00	8.00	Z
Alvi	—	—	—	—	—	—	—	—	—	—	—	—	—	0.17	Alvi
Fevi <sup>3+</sup>	1.68	2.02	1.90	2.09	2.54	2.03	2.22	2.12	2.26	2.45	2.03	1.86	2.27	1.27	Fevi <sup>3+</sup>
Fe <sup>2+</sup>	2.96	2.62	2.64	2.22	2.11	2.60	2.38	2.42	2.29	2.19	2.48	2.55	2.32	1.64	Fe <sup>2+</sup>
Mn	0.08	0.09	0.09	0.07	0.10	0.10	0.07	0.10	0.10	0.11	0.10	0.10	0.09	0.16	Mn
Mg	0.02	0.04	0.08	0.05	0.18	0.04	0.05	0.05	0.04	0.03	0.10	0.11	0.02	1.76	Mg
Li	0.25	0.24	0.30	0.56	—	0.24	0.29	0.30	0.31	0.22	0.29	0.37	0.30	—	Li
Y	5.00	5.00	5.00	5.00	5.00	5.00	5.00	5.00	5.00	5.00	5.00	5.00	5.00	5.00	Y
Ca	0.36	0.27	0.22	0.29	0.61	0.35	0.31	0.25	0.26	0.25	0.32	0.19	0.22	0.50	Ca
Na	1.99	1.91	1.89	1.33	1.66	1.84	1.79	1.78	1.86	2.14	1.70	1.90	1.84	2.15	Na
K	0.15	0.17	0.17	0.20	0.11	0.15	0.19	0.19	0.17	0.22	0.20	0.10	0.18	0.30	K
X	2.50	2.35	2.28	1.82	2.38	2.34	2.29	2.22	2.29	2.64	2.22	2.19	2.24	2.95	X
OH	1.95	1.72	1.68	1.90	2.60	1.72	2.13	2.28	1.74	2.53	1.78	1.98	1.94	—	OH
F	0.50	0.58	0.47	0.77	0.91	0.69	0.49	0.51	0.53	0.46	0.53	0.47	0.49	—	F
Na/(Na + K)	0.930	0.925	0.932	0.868	0.880	0.925	0.905	0.905	0.915	0.910	0.897	0.950	0.910	0.875	Na/(Na + K)
f <sub>iv</sub>	0.970	0.992	0.985	0.970	0.975	0.923	0.985	0.980	0.985	0.985	0.960	0.991	0.991	0.482	f <sub>iv</sub>
Si' <sub>iv</sub>	0.515	0.520	0.520	0.539	0.520	0.520	0.521	0.524	0.520	0.510	0.525	0.525	0.523	0.500	Si' <sub>iv</sub>

Key to tables I and II

- The cation numbers are calculated from analyses from the following sources.
- 1-7. Chumakhov (1958). 1, 2, 5, and 6 are from alkali granites, 3 from a quartz vein, and 6 and 7 from khibinites.
  - 8-24. Eliseev *et al.* (1961). 8, 9, 11-15 are from amphibole-magnetite rocks, 10, 16-21 from shale, and 46-48 from slate.
  - 25-36. From previously unpublished analyses by L. K. Pozharitskaya and E. A. Chernisheva given in Table II (all from carbonatites).
  - 38-47, 50, and 52-53. Andreev (1962). 38-47 and 50 asbestiform rhodusite and magnesio-arfvedsonite (of Andreev) and 52-53 are from skarn.
  - 48, 49, 51. Kuman (1961). 4 is crocidolite from quartzite, 49 is rhodusite, and 51 is crocidolite from quartz vein.
  - 54-56. Peacock (1928). Crocidolite.
  - 57-59. Miyashiro (1956). 57 is from nepheline syenite, 58 from syenite pegmatite, and 59 from syenite with quartz.
  - 60. Plemister *et al.* (1960). From riebeckite felsite.
  - 61-74. Borley (1963). From alkali granite (63 from alkali granite with astrophyllite).
  - 75-97. Deer, Howie, and Zussman (1965). 75 is from alkali granite, 76 from rockallite, 78, 83, 84 from slate, 79 from granulite, 80 and 82 are crocidolite, 85 from jadeite, 87, 91, and 94 from nepheline syenite, 88 from shonkinite, 89 and 97 from pegmatite, 90 from syenite pegmatite, and 92 and 95 from syenite.
  - 98-134. From previously unpublished analyses given in Table II on amphiboles from alkali granitoids from Siberia:
    - 98 from syenite of intrusive phase I of alkaline massif.
    - 99-101 from granite syenite of intrusive phase II.
    - 102, 104-106 from alkali granite of intrusive phase III.
    - 103 from alkaline granitic pegmatite of the body of granite NAC237.
    - 107 from alkali granite.
    - 108-109 from alkaline granitic pegmatite of phase IV.
    - 110-113 from albitite.
    - 114 data by Kostine.
    - 115-133 from metasomatic microcline.
    - 134 from nepheline-syenitic pegmatite.
  - 115-123 and 124-133 were taken from two sections at intervals of 0.2-0.3 m. across the contact from the metasomatic microclinites from gabbro to the alkali granites.

Notes:

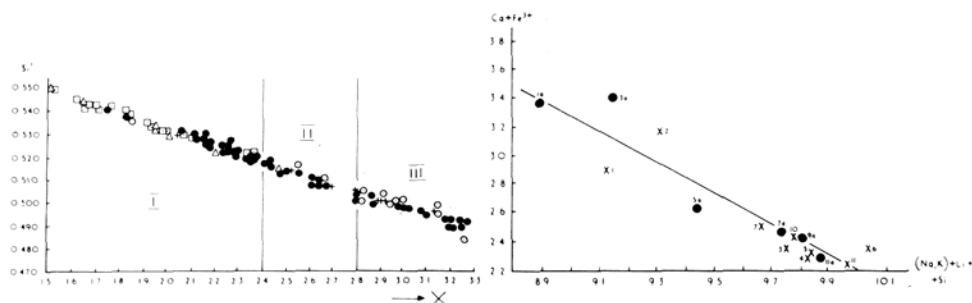
- \* The names of the amphiboles follow the terminology of Deer *et al.* (1965) and of figs. 1 and 2. Ek = eckermannite, Cat = catophorite, Arf = arfvedsonite, Rieb = riebeckite.
- † These are the numbers assigned by the original authors, as distinct from those used in this paper.
- ‡ No formula is given for No. 11 because the analysis had an anomalously high content of Si.
- § In the formulae of Nos. 15, 31, 35, 37, 60, 65, 71, 75, 76, 87, 89, 90, 103, 105, and 106 Ti is allocated to the Y group of cations.
- || f<sub>iv</sub> = Fe<sup>2+</sup>/(Fe<sup>2+</sup> + Mg) and Si'<sub>iv</sub> = Z/(X + Y + Z).

TABLE II. Chemical analysis of amphiboles 25 to 36 and 98 to 134 of Table I

No.	25	26	27	28	29	30	34	36	No.					
SiO <sub>2</sub>	54.84	53.06	52.40	55.74	55.52	55.28	38.26	54.12	SiO <sub>2</sub>					
TiO <sub>2</sub>	0.43	0.91	0.91	0.52	0.65	0.65	2.48	0.91	TiO <sub>2</sub>					
Al <sub>2</sub> O <sub>3</sub>	2.66	2.19	1.88	0.72	1.32	1.04	15.50	1.38	Al <sub>2</sub> O <sub>3</sub>					
Fe <sub>2</sub> O <sub>3</sub>	11.20	8.10	8.30	2.25	3.29	3.33	5.86	6.62	Fe <sub>2</sub> O <sub>3</sub>					
FeO	2.43	5.10	4.67	1.74	1.51	2.24	6.75	3.75	FeO					
MnO	n.d.	0.07	0.07	0.13	0.11	0.12	0.22	0.07	MnO					
MgO	15.3	15.67	15.67	22.15	21.67	20.89	12.66	17.88	MgO					
CaO	1.30	3.70	4.30	6.45	6.10	6.90	13.52	3.60	CaO					
Na <sub>2</sub> O	8.17	7.44	7.17	6.33	6.35	6.18	1.20	7.02	Na <sub>2</sub> O					
K <sub>2</sub> O	0.47	0.94	1.02	1.32	1.31	1.13	1.78	1.78	K <sub>2</sub> O					
Li <sub>2</sub> O	—	—	—	—	—	—	—	—	Li <sub>2</sub> O					
H <sub>2</sub> O	—	—	—	—	—	—	2.35	—	H <sub>2</sub> O					
F	1.57	—	—	—	—	—	0.01	1.17	F					
Others	1.59	1.78	1.81	1.09	1.13	1.31	—	—	Others					
P <sub>2</sub> O <sub>5</sub>	0.03	0.12	0.15	—	—	0.01	—	—	P <sub>2</sub> O <sub>5</sub>					
O≡F	99.99	99.08	98.36	98.44	98.96	99.08	100.59	98.30	O≡F					
Total	0.66	—	—	—	—	—	0.00	0.49	Total					
	99.33	99.08	98.35	98.44	98.96	99.08	100.59	97.81						
No.	98	99	100	101	102	103	104	105	106	107	108	109	No.	
SiO <sub>2</sub>	44.60	44.50	42.75	47.05	50.25	53.40	49.45	48.22	52.97	45.85	47.76	48.75	SiO <sub>2</sub>	
TiO <sub>2</sub>	2.29	3.27	2.25	2.50	1.44	1.11	1.28	1.51	1.36	4.10	1.20	1.56	TiO <sub>2</sub>	
Al <sub>2</sub> O <sub>3</sub>	3.10	1.68	8.74	4.40	1.27	0.74	0.96	0.74	1.27	5.94	0.96	1.17	Al <sub>2</sub> O <sub>3</sub>	
Fe <sub>2</sub> O <sub>3</sub>	7.72	8.03	5.15	10.14	17.22	15.68	16.35	9.07	13.79	13.66	9.31	14.29	Fe <sub>2</sub> O <sub>3</sub>	
FeO	19.91	21.83	17.67	19.23	10.72	11.87	18.76	23.74	15.70	11.46	25.66	20.68	FeO	
MnO	0.87	1.06	0.68	1.08	1.21	0.53	1.54	0.91	0.93	3.64	1.18	1.01	MnO	
MgO	7.01	6.38	6.41	1.64	5.61	5.39	1.82	1.11	1.92	4.72	1.50	1.79	MgO	
CaO	6.68	5.68	11.28	4.63	2.06	1.16	0.74	4.08	1.53	1.46	2.81	0.56	CaO	
Na <sub>2</sub> O	3.59	4.83	1.54	5.06	6.51	6.08	5.71	5.71	5.71	6.75	5.61	6.26	Na <sub>2</sub> O	
K <sub>2</sub> O	1.10	1.32	0.90	1.47	1.10	1.29	1.10	1.62	1.83	1.00	1.38	1.26	K <sub>2</sub> O	
Li <sub>2</sub> O	0.01	0.01	—	—	0.10	0.12	0.12	0.02	0.09	—	0.03	0.07	Li <sub>2</sub> O	
H <sub>2</sub> O	—	—	—	—	—	—	—	—	—	—	—	—	H <sub>2</sub> O	
F	1.02	—	—	—	0.71	0.95	0.54	0.95	0.67	—	—	0.59	F	
Others	2.49	2.40	2.37	2.39	0.65	2.01	2.26	2.86	2.52	2.23	2.82	2.20	Others	
P <sub>2</sub> O <sub>5</sub>	0.53	0.64	0.15	0.24	0.39	0.29	0.16	0.44	0.25	0.04	0.16	0.12	P <sub>2</sub> O <sub>5</sub>	
O≡F	100.92	101.63	99.89	99.83	99.24	100.62	100.79	100.98	100.54	100.85	100.38	100.31	O≡F	
Total	0.43	—	—	—	0.30	0.40	0.23	0.40	0.28	—	—	0.25	Total	
	100.49	101.63	99.89	99.83	98.94	100.22	100.56	100.58	100.26	100.85	100.38	100.06		
No.	110	111	112	113	114	115	116	117	118	119	120	121	No.	
SiO <sub>2</sub>	50.90	47.12	48.85	50.23	49.34	43.04	43.46	50.34	46.82	48.27	47.76	47.81	SiO <sub>2</sub>	
TiO <sub>2</sub>	0.80	2.79	0.80	0.67	0.74	0.68	0.54	0.55	0.64	0.61	0.72	0.63	TiO <sub>2</sub>	
Al <sub>2</sub> O <sub>3</sub>	1.27	1.48	1.69	2.19	3.14	0.62	1.18	0.52	1.12	1.43	1.36	1.37	Al <sub>2</sub> O <sub>3</sub>	
Fe <sub>2</sub> O <sub>3</sub>	16.37	15.79	17.41	18.34	16.84	21.01	19.57	19.27	18.43	14.31	17.45	14.98	Fe <sub>2</sub> O <sub>3</sub>	
FeO	16.85	18.09	18.76	16.84	17.75	19.91	18.00	18.48	20.29	21.83	19.91	21.83	FeO	
MnO	0.97	1.12	0.75	0.60	0.60	0.47	0.29	0.32	0.66	0.65	0.75	0.59	MnO	
MgO	1.28	1.10	0.56	0.22	0.15	0.31	0.32	0.06	0.07	0.05	0.35	0.05	MgO	
CaO	0.15	0.22	0.52	0.67	1.07	4.18	5.83	3.69	2.14	1.73	1.61	2.14	CaO	
Na <sub>2</sub> O	6.10	6.75	6.07	6.07	5.69	4.75	4.75	3.51	5.40	6.88	5.66	6.48	Na <sub>2</sub> O	
K <sub>2</sub> O	1.16	1.33	1.47	1.02	0.94	0.32	0.42	0.30	0.60	0.84	0.92	0.74	K <sub>2</sub> O	
Li <sub>2</sub> O	0.29	0.27	0.178	—	0.40	0.20	0.26	0.12	0.34	0.48	0.47	0.40	Li <sub>2</sub> O	
H <sub>2</sub> O	—	—	—	—	1.93	1.92	2.01	1.76	2.25	1.93	1.71	1.85	H <sub>2</sub> O	
F	0.83	0.94	—	—	0.46	2.76	3.50	1.60	1.60	1.06	1.06	1.0	F	
Others	2.18	3.18	2.63	4.73	1.83	—	—	—	—	—	—	—	Others	
P <sub>2</sub> O <sub>5</sub>	0.08	0.39	0.41	0.30	—	—	—	—	—	—	—	0.22	P <sub>2</sub> O <sub>5</sub>	
O≡F	99.23	100.57	100.10	101.88	100.88	100.17	100.13	100.52	100.36	100.07	99.73	100.09	O≡F	
Total	0.35	0.40	—	—	0.19	1.16	1.48	0.67	0.67	0.45	0.45	0.42	Total	
	98.88	100.17	100.10	101.88	100.69	99.01	98.65	99.85	99.69	99.62	99.28	99.67		
No.	122	123	124	125	126	127	128	129	130	131	132	133	134	No.
SiO <sub>2</sub>	47.86	48.24	47.20	46.20	47.56	47.72	48.40	48.02	46.20	47.44	48.22	48.76	47.78	SiO <sub>2</sub>
TiO <sub>2</sub>	0.64	0.64	0.79	0.71	0.66	0.68	0.54	0.54	0.66	0.74	0.60	0.78	1.25	TiO <sub>2</sub>
Al <sub>2</sub> O <sub>3</sub>	1.69	1.86	1.53	1.66	1.55	2.03	1.86	2.03	1.78	1.36	1.86	1.53	4.09	Al <sub>2</sub> O <sub>3</sub>
Fe <sub>2</sub> O <sub>3</sub>	17.95	16.75	22.33	21.66	17.61	19.07	18.20	19.65	21.66	18.66	16.86	19.39	11.09	Fe <sub>2</sub> O <sub>3</sub>
FeO	19.91	20.29	17.28	15.36	19.77	18.19	18.48	17.43	16.12	18.82	19.69	17.66	12.76	FeO
MnO	0.71	0.71	0.54	0.69	0.72	0.54	0.76	0.70	0.80	0.76	0.77	0.74	1.28	MnO
MgO	0.13	0.33	0.22	0.74	0.17	0.18	0.22	0.14	0.10	0.40	0.54	0.04	7.70	MgO
CaO	1.64	1.34	1.73	3.48	2.04	1.84	1.49	1.56	1.44	1.83	1.22	1.30	3.09	CaO
Na <sub>2</sub> O	6.25	6.25	4.46	5.18	5.99	5.88	5.88	6.14	6.87	5.55	6.37	6.08	7.23	Na <sub>2</sub> O
K <sub>2</sub> O	0.61	0.81	1.01	0.53	0.75	0.89	0.89	0.81	1.03	0.93	0.57	0.87	1.50	K <sub>2</sub> O
Li <sub>2</sub> O	0.40	0.43	—	—	0.39	0.47	0.49	0.49	0.36	0.47	0.62	0.49	—	Li <sub>2</sub> O
H <sub>2</sub> O	1.67	1.63	1.85	2.36	1.66	2.03	2.19	1.72	2.35	1.74	1.92	1.85	—	H <sub>2</sub> O
F	1.16	0.95	1.59	1.75	1.40	1.00	1.02	1.07	0.90	1.07	0.97	0.98	—	F
Others	—	—	—	—	—	—	—	—	—	—	—	—	1.73	Others
P <sub>2</sub> O <sub>5</sub>	—	—	—	—	—	—	—	—	—	—	—	—	0.07	P <sub>2</sub> O <sub>5</sub>
O≡F	100.62	100.23	100.53	100.32	100.27	100.52	100.43	100.30	100.27	99.77	100.21	100.47	99.57	O≡F
Total	0.49	0.40	0.67	0.77	0.58	0.42	0.43	0.45	0.38	0.45	0.41	0.41	—	Total
	100.13	99.83	99.86	99.55	99.69	100.10	100.00	99.85	99.89	99.32	99.80	100.06	99.57	

characteristic of the agpaitic comagmatic complex syenites → granite-syenites → alkali granites (Kovalenko *et al.*, 1965) as well as for rocks of alkali gabbro type.

The amphiboles nos. 115 to 133, table I, form a new or at least a rather rare isomorphous series in the riebeckite group, and the author is not aware of its description in the literature. The character of the isomorphism in these amphiboles is to be seen in fig. 2, demonstrating the reverse correlation of the content  $\text{Ca} + \text{Fe}^{3+}$  and  $(\text{Na}, \text{K}) + \text{Li} + \text{Si}$  in formula compositions. Hence, the isomorphism in these amphiboles is mainly according to the scheme  $(\text{Na}, \text{K})\text{Si} \rightleftharpoons \text{CaFe}^{3+}$  less  $\text{LiSi} \rightleftharpoons \text{CaFe}^{3+}$ . We propose to call this isomorphous series riebeckite  $\rightleftharpoons$  calcian riebeckite. Thus calcian riebeckite is a variety of riebeckite,

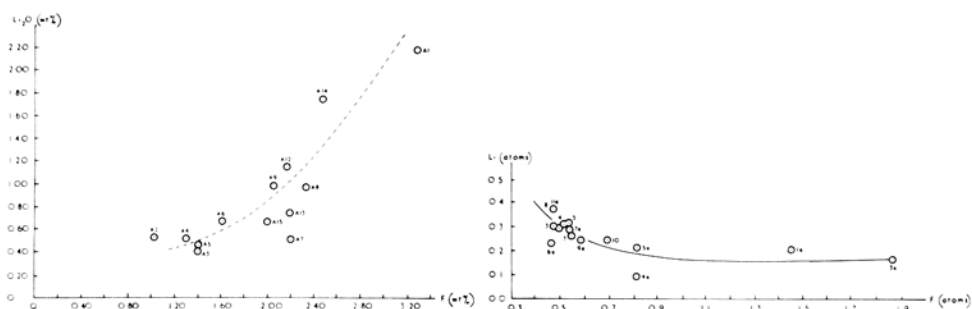


FIGS. 1 and 2: FIG. 1 (left). The compositions of the amphiboles of the Rieb-Arf type.  $X = \text{K} + \text{Na} + \text{Ca}$ ;  $\text{Si}' = Z / (X + Y + Z)$ ; I- the region of riebeckite; II- the region of middle members; III- the region of arfvedsonite. ●, amphiboles from alkaline granitoids; ○, amphiboles from nepheline syenites; □, amphiboles from iron-stones and slates; △, amphibole asbestos; +, amphiboles from carbonatites. FIG. 2 (right). The reverse correlation of the contents  $(\text{Ca} + \text{Fe}^{3+})$  and  $(\text{Na} + \text{Li} + \text{Si})$  in the formula unit of the calcian riebeckites.

in which sodium is partially replaced by calcium and a certain part of Si by  $\text{Fe}^{3+}$ . According to the data given in table I calcian riebeckite may contain up to one atom Ca in the X-group and one atom of  $\text{Fe}^{3+}$  (possibly with a small quantity of Al) in the Z-group per formula unit of amphibole. Due to the isomorphous replacement of Si by  $\text{Fe}^{3+}$  in calcian riebeckite  $\text{Fe}^{3+}$  may dominate with respect  $\text{Fe}^{2+}$ . The crystal-chemical position of Li in riebeckites and arfvedsonites deserves special consideration, as its content in these amphiboles reaches 2 or more wt. % (Borley, 1963), but the information about its behaviour in alkali amphiboles is inadequate. Unfortunately there are available only a few chemical analyses of riebeckites and arfvedsonites in which the Li content has been determined. However, even these incomplete data indicate a possibility of replacement of  $\text{Fe}^{2+}$  by Li. Thus according to the data given in table I, nos. 61 to 74 for these amphiboles from African alkalic granites (Borley, 1963), the linear correlation coefficient between the content of  $\text{Fe}^{2+}$  and Li,  $r = 0.731 \pm 0.25$ , which proves the replacement of  $\text{Fe}^{2+}$  by Li in arfvedsonites. On the other

hand, as mentioned above, Li may replace  $\text{Fe}^{3+}$  or Ca in isomorphous series from riebeckite to calcian riebeckite by taking part in a complex isomorphism  $\text{LiSi} \rightleftharpoons \text{CaFe}^{3+}$ .

Finally, there is a frequently observed correlation between the content of Li and F in riebeckites and arfvedsonites (figs. 3 and 4). This correlation may be a direct one (fig. 3) as in arfvedsonites from African alkalic granites, as well as a reverse one as in riebeckite in microclinites from Siberia (fig. 4). In a number of cases a clear correlation between Li and F content is not observed as in nos. 98 to 114 of table I for amphiboles of the comagmatic series syenite-granosyenites-alkalic-granites-pegmatites from alkalic-granites-albites. These facts prove that the correlation that is sometimes observed between Li and F is more probably due to genetic causes than to crystal-chemical ones.



FIGS. 3 and 4: FIG. 3 (left). The direct correlation between the contents of Li and F in the amphiboles from alkali granites of Africa (Borley, 1963). FIG. 4 (right). The reverse correlation between the contents of Li and F in the calcian riebeckites.

There is rather limited information about the content of other rare elements. Borley (1963) has shown that African arfvedsonites have a rather high content of  $\text{ZrO}_2$ . In table III data for rare earth and  $\text{Y}_2\text{O}_3$  contents in riebeckite-arfvedsonite from Siberia are given. As a whole, alkali amphiboles only concentrate rare earths rather weakly, so that their concentrations in these amphiboles do not appreciably exceed the Clarke of these elements in rocks (Vinogradov, 1956). Usually the lanthanons content in riebeckite and arfvedsonite exceed the  $\text{Y}_2\text{O}_3$  content.

Table III presents the ratio of  $\text{Y}_2\text{O}_3$  to the sum of  $\text{Ln}_2\text{O}_3 + \text{Y}_2\text{O}_3$  in four pairs of coexisting zircons and riebeckites in which the rare-earth spectrum is selectively ceric. In three cases it can be seen that the zircons are far more yttric than the coexisting amphibole. The full spectrum for two other amphiboles is:

Test no.	Wt. %	La	Ce	Pr	Nd	Sm	Eu	Dy	Er	Tu	Yb	Y
E21	0.138	21.24	44.38	2.54	8.90	1.41	0.35	1.82	0.68	0.42	1.22	17.03
E18	0.27	23.2	57.2	—	8.9	—	—	9.7	—	—	—	—

This shows why the concentrator-minerals (Tauson, 1961) of rare earths in alkalic granites are yttrian (Semenov, 1964) while the alkali granites are cerian (Kovalenko, 1966).

TABLE III

No.	Amphibole			Zircon		
	Ln <sub>2</sub> O <sub>3</sub>	Y <sub>2</sub> O <sub>3</sub>	Y <sub>2</sub> O <sub>3</sub>	Ln <sub>2</sub> O <sub>3</sub>	Y <sub>2</sub> O <sub>3</sub>	Y <sub>2</sub> O <sub>3</sub>
			Ln <sub>2</sub> O <sub>3</sub> +Y <sub>2</sub> O <sub>3</sub>			Ln <sub>2</sub> O <sub>3</sub> +Y <sub>2</sub> O <sub>3</sub>
246	0.17%	0.029%	0.145	3.45%	1.575%	0.313
236	0.083	0.046	0.356	2.40	1.200	0.333
200	0.12	0.023	0.161	2.00	0.700	0.259
189	0.20	0.049	0.196	1.70	1.240	0.420

*The optical properties of riebeckite and arfvedsonite*

At present it is not always possible to distinguish arfvedsonite from riebeckite by optical properties, let alone to differentiate the intermediate members of the isomorphous series. This should be expected, because the isomorphous replacements in the series arfvedsonite-eckermannite and riebeckite-magnesioriebeckite lead to more substantial changes in optical properties than do those in the series riebeckite-arfvedsonite (Deer, Howie, and Zussman, 1965). Table IV shows the optical constants of some amphiboles from Siberia, and it may be seen that they do not correlate easily with chemical composition. There are some indications of a correlation of  $\gamma$  with the F-content in arfvedsonite from Africa (Borley, 1963).

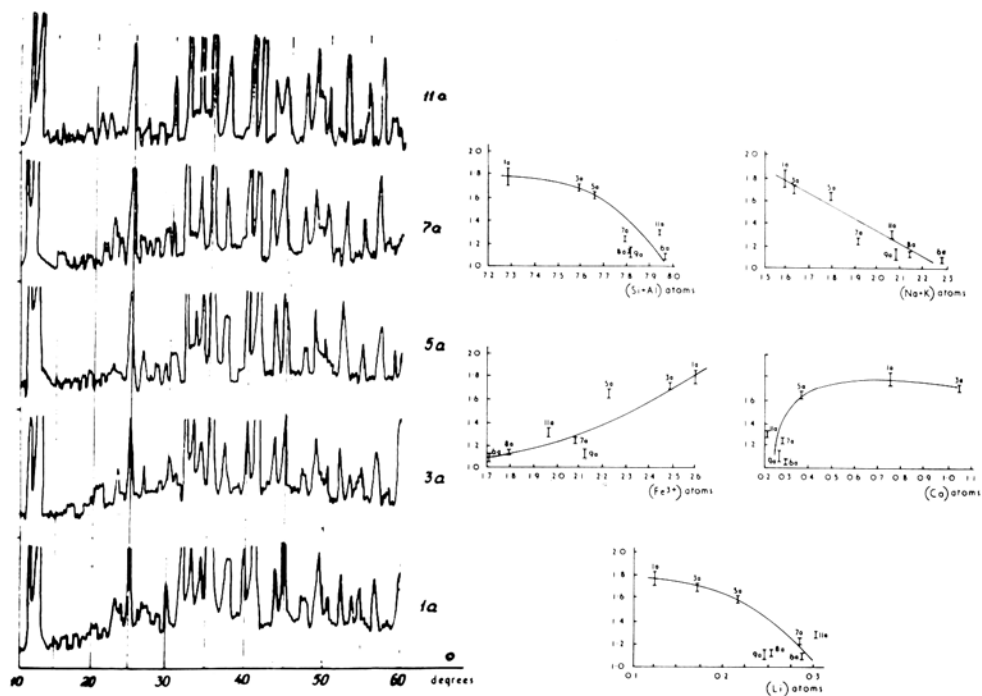
TABLE IV. The optical properties of the alkaline amphiboles from granitoids of Siberia ( $\lambda = 5890 \text{ \AA}$ );  $\gamma$  and  $\alpha$  all  $\pm 0.002$ 

no. from Table I	Description	$\gamma$	$\alpha$	$\gamma : [001]$	$2 V_x$	No. from Table I	Description	$\gamma$	$\alpha$	$\gamma : [001]$	$2 V_x$
99	Cat	1.692	1.672	+28°	52°	116	Ca-Rieb	1.708	1.696	7	80
98	Cat	1.692	1.672	+27°	50	117	Ca-Rieb	1.708	1.696	8	83
105	Arf	1.708	1.696	-9°	—	118	Ca-Rieb	1.708	1.696	8	81
101	Cat-Rieb	1.712	1.700	+25°	75°	120	Rieb	1.708	1.696	7	79
103	Mg-Rieb	1.702	1.696	-3°	70°	122	Rieb	1.708	1.696	7	85
112	Rieb	1.708	1.700	8-9°	72	123	Rieb	1.708	1.696	8	80
110	Rieb	1.708	1.700	7°	large	125	Ca-Rieb	1.708	1.700	8	81
115	Ca-Rieb	1.708	1.696	6°	80						

*The correlation of X-ray data of some alkalic amphiboles of riebeckite-  
arfvedsonite composition with their chemical composition*

There have been a number of investigations in which attempts have been made to correlate the composition of amphiboles with X-ray data (Borley, 1963; Ginsburg *et al.*, 1961). Table V gives the unit cell parameters of riebeckites, arfvedsonites, and catophorites whose chemical compositions are among nos. 98 to 133 of table I. The accuracy of these parameters ( $\Delta a = \pm 0.007$  to 0.014;  $\Delta b = \pm 0.007$  to 0.014;  $\Delta c = \pm 0.007$  to 0.014;  $\Delta \beta = \pm 0.1$  to 0.3) does

not permit a detailed discussion of the isomorphous series riebeckite–arfvedsonite. In table V there are also given the unit cell parameters for the most typical members of the isomorphous series riebeckite to calcian riebeckite. All these X-ray investigations were carried out by G. G. Afonina on the diffractometer DRON-1 with a BCV-9 Fe value. The X-radiation was registered by a scintillation counter and recorder. Although the diffraction patterns of amphiboles of the calcian riebeckite series show constant unit cell parameters, the intensity of certain reflections changes regularly (fig. 5) (the unit cell parameters were judged at lines 310; 202;  $\bar{2}02$ ; 151 with NaCl as an internal standard.)



FIGS. 5 and 6: FIG. 5 (left). X-ray data for calcian riebeckites (the numbers are from table I).

FIG. 6 (right). The dependence of the intensity of the line 041 ( $d = 3.32 \text{ \AA}$ ) on the contents of Si (with Al), K + Na, Li,  $\text{Fe}^{3+}$ , and Ca (atoms per formula unit) for calcian riebeckites.

Fig. 6 is an attempt to correlate the intensity of the line 041 ( $3.32 \text{ \AA}$ ) of the X-ray diagram with the composition of calcian riebeckite. The intensity of this line was measured by the method of Smagunova *et al.* (1964). The mean intensity values with their mean errors (2 limits) for eight amphiboles are:

No.	115	116	118	119	120	121	122	123
$i \pm 2\sigma_i$	$1.78 \pm 0.08$	$1.70 \pm 0.03$	$1.64 \pm 0.02$	$1.09 \pm 0.02$	$1.23 \pm 0.005$	$1.13 \pm 0.01$	$1.13 \pm 0.06$	$1.30 \pm 0.03$

As may be seen from fig. 6, the intensity of this line in the calcian riebeckite depends on the content of the main components Ca,  $\text{Fe}^{3+}$ , Na, Li, Si. If there

is a high content of Ca and  $\text{Fe}^{3+}$  then the intensity of line 041 is increased, but high contents of Na, Li, and Si lower its intensity.

On the basis of these data we can distinguish groups of lithian riebeckite and calcian riebeckite.

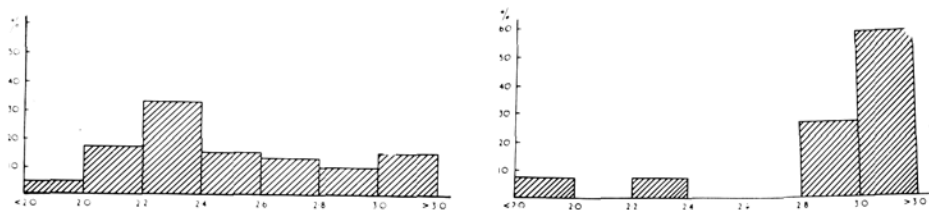
TABLE V. The parameters of the unit cell (in Å) of some alkali amphiboles from granitoids of Siberia

No.	<i>a</i>	<i>b</i>	<i>c</i>	<i>V</i>
115	9.80±0.01	18.08±0.01	5.32±0.01	103.75±0.2
118	9.80±0.01	18.08±0.01	5.34±0.01	103.75±0.2
119	9.80±0.01	18.06±0.01	5.35±0.01	103.90±0.2
120	9.79±0.08	18.08±0.01	5.34±0.01	103.77±0.2
121	9.78±0.014	18.08±0.00	5.35±0.00	103.80±0.14
122	9.80±0.01	18.07±0.01	5.35±0.01	103.83±0.2
123	9.84±0.01	18.13±0.01	5.33±0.01	103.83±0.2
113	9.82±0.01	18.04±0.01	5.32±0.01	103.80±0.2
111	9.82±0.01	18.00±0.00	5.37±0.01	103.75±0.1
112	9.82±0.01	18.03±0.01	5.36±0.00	103.87±0.1
103	9.84±0.01	18.04±0.00	5.37±0.01	103.95±0.15
105	9.89±0.00	18.08±0.01	5.35±0.00	103.58±0.11
101	9.92±0.014	18.10±0.01	5.33±0.01	103.83±0.30
99	9.96±0.00	18.22±0.01	5.31±0.01	104.42±0.10
108	9.86±0.01	18.11±0.00	5.34±0.01	103.80±0.14
102	9.823±0.007	18.065±0.007	5.32±0.01	103.93±0.2
116	9.765±0.007	18.045±0.007	5.33±0.00	103.80±0.14

*Mineral paragenesis of riebeckite–arfvedsonite, the conditions for their forming and the mineral facies of alkalic granites*

The riebeckite–arfvedsonite series is met in paragenesis with the following rock forming minerals: potassium feldspars, albite, quartz, nepheline, alkali pyroxenes, astrophyllite, fayalite, magnetite, garnets, carbonates, fluorite, cryolite, willemite, and some other rarer minerals. The distribution of the main different members of the series in different rocks is: in alkali granites and their metasomatic analogue (alkalic apogranites, Beus *et al.*, 1962) mainly ferrous members, but the presence of riebeckite or arfvedsonite is characteristic. This fact is illustrated in the histogram of fig. 7, based on all known chemical analyses of amphiboles from alkali granites. In the mineral paragenesis of nepheline-syenites riebeckite is rarer, but arfvedsonite is a rather typical amphibole (fig. 8). The related Mg analogues eckermannite, magnesioriebeckite, and soda-tremolite are widespread in carbonatites. There are numerous amphiboles of the isomorphous series riebeckite–magnesioriebeckite–glaucophane (with a transition to grunerites) in ironstones and in fibrous amphiboles (table I) (Eliseev, 1961). In some cases arfvedsonites are reported among asbestos fibres from skarns.

We consider the influence of various physico-chemical conditions on the isomorphous series riebeckite *sensu stricto* to arfvedsonite in the mineral



FIGS. 7 and 8 Variations in composition of amphiboles of the riebeckite–arfvedsonite series; abscissae, atoms in X positions: FIG. 7 (left). From alkaline granitoids. FIG. 8 (right). From nepheline syenites.

parageneses of alkali granites and the connected metasomatites and nepheline syenites.

The physico-chemical analysis of the mineral parageneses of alkalic granitoids and nepheline syenites is based on the fundamental works by D. S. Korzhinsky (1936, 1940, 1946, 1957, 1958, 1959, 1963).

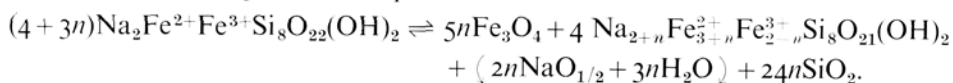
On the whole, the data of table I show the earliest and apparently highest-temperature amphiboles from alkali syenites of the early intrusive phase to be represented by cataphorites. The composition of the later amphiboles from the granite-syenites of the second phase correspond to hastingsite and cataphorite–arfvedsonite, and that of the latest from alkali granites of the third phase and their pegmatites correspond to magnesio–arfvedsonite (of Andreev), arfvedsonite, and middle members of the arfvedsonite–riebeckite series. The amphiboles from albitites are generally represented by riebeckite. Thus during the magmatic evolution of alkalic bodies with the differential late alkali granites, the following changes are observed: cataphorite  $\rightarrow$  cataphorite–arfvedsonite, hastingsite  $\rightarrow$  magnesioriebeckite, and arfvedsonite or middle members of the arfvedsonite–riebeckite series  $\rightarrow$  riebeckite. This pattern widens our understanding of the evolution of amphiboles from alkalic rocks (Yagi, 1953).

It may be assumed that variations in the series arfvedsonite–riebeckite are connected with the time evolution of the alkalic granitic magma and also with the changes of formation temperature of granitoids. The dependence of the composition of amphiboles on their conditions of genesis allows us to distinguish the alkalic granite facies possibly correlated with rare metallic ore formation.

#### *The paragenesis magnetite plus riebeckite or arfvedsonite*

The paragenesis of alkali amphibole with magnetite is observed in alkali granites. This paragenesis involves four components  $\text{Na}_2\text{O}$ ,  $\text{FeO}$ ,  $\text{Fe}_2\text{O}_3$ ,  $\text{H}_2\text{O}$  and has four degrees of freedom  $f = c + 2 - p = 4 + 2 - 2 = 4$ . At a constant pressure, the chemical potential  $\mu_{\text{H}_2\text{O}}$  will be a function of the temperature  $T$ , and  $f = 2$ , i.e. the amphibole is stable with magnetite within the limits of a definite region on the diagram  $\mu_{\text{H}_2\text{O}} - \mu_{\text{Na}_2\text{O}}$ . At a constant value of the chemical potential of oxygen, i.e. at a constant value of  $\text{FeO}/\text{Fe}_2\text{O}_3$  in the amphibole, the paragenesis of amphibole with riebeckite is characterized by a single degree

of freedom and the equilibrium mentioned can be illustrated on a diagram of  $\mu_{\text{H}_2\text{O}}$  by a series of equipotential ( $\mu_{\text{O}_2} = \text{const.}$ ) lines, the position of which is determined from the equation of reactions between those minerals, with some variations in the amphibole composition:



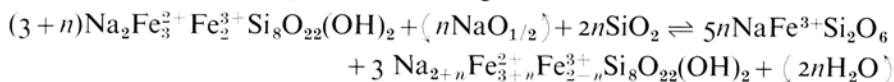
At infinitely small values of  $n$  this reaction corresponds to an equilibrium of magnetite with amphibole of a constant composition and the slope of the line of this equilibrium is  $\tan \alpha = -\Delta\text{H}_2\text{O}/\Delta\text{NaO}_{1/2} = -\frac{3}{2}$  (Marakushev, 1965). Therefore it follows that a change of amphibole composition towards arfvedsonite is possible with increase of temperature (decrease of  $\mu_{\text{H}_2\text{O}}$ ), as well as with decrease of the  $\mu_{\text{NaO}_{1/2}}$ .

As mentioned above, during the evolution of the alkalic rock evolution of Siberia the composition of amphibole of the riebeckite–arfvedsonite series varies towards riebeckite, which appears frequently in metasomatic albitites (analyses 109 to 114, table II). Though the albitites (being postmagmatic metasomatites) are of lower-temperature formations if compared with the magmatic alkali granites, the composition of their amphibole is determined not only by the temperature decrease, but also by the increase in the chemical potential of sodium. This fact is confirmed by an analysis of the ratio  $\text{Na}/(\text{Na} + \text{K})$  in the amphibole, which is characteristic of the relational changes of the chemical potentials of potassium and sodium in those rocks, in keeping with the known relation between the chemical potential of a component and its content change in a phase:  $\partial\mu_i/\partial n_i \geq 0$  (Korshinsky, 1957, Storonkin *et al.*, 1960). Thus the increase of the chemical potential of a component leads to an increase of its content in a phase. The highest ratio  $\text{Na}/(\text{Na} + \text{K})$  in riebeckite from albitites is characteristic of greater values of the chemical potential of sodium during the formation of the rock.

#### *The paragenesis aegirine plus riebeckite or arfvedsonite*

The paragenesis of alkali amphibole with alkali pyroxenes is characteristic for agpaite nepheline syenites (Iwao, 1938; Yagi, 1953; Sørensen, 1960; Deer *et al.*, 1965).

Using the same procedure as with the paragenesis alkali amphibole plus magnetite, we derive the equation of equipotential lines ( $\mu_{\text{O}_2} = \text{const.}$  at  $\text{FeO}/\text{Fe}_2\text{O}_3 = \text{const.}$ ) for the equilibrium of aegirine with riebeckite or arfvedsonite:



The slope of these lines in the co-ordinates  $\mu_{\text{NaO}_{1/2}} - \mu_{\text{H}_2\text{O}}$  is positive,  $\tan \alpha = -\Delta\text{H}_2\text{O}/\Delta\text{NaO}_{1/2} = 2n/n = 2$ ). Therefore increase of  $\mu_{\text{NaO}_{1/2}}$  and decrease of  $\mu_{\text{H}_2\text{O}}$  (increase of  $T$ ) should displace the equilibrium composition of the amphibole towards arfvedsonite.

The domination of arfvedsonite compared with riebeckite in the mineral paragenesis of nepheline syenites (fig. 8), and particularly in those of agpaitic ones, is primarily connected with a high value of  $\mu_{\text{NaO}_2}$ .

*The paragenesis riebeckite and magnesioriebeckite*

Analysis of the data in tables I and II shows that the composition of amphibole in alkali granites does not only vary within the limits of the series riebeckite–arfvedsonite. Compositions of amphibole from the isomorphous series riebeckite–magnesioriebeckite and arfvedsonite–eckermannite are also observed in alkalic granitoids (102, 103, 107, table I). The value  $\text{Fe}^{2+}/(\text{Fe}^{2+} + \text{Mg})$  of the amphiboles of these series from metamorphic rocks is due to temperature (Glagolev, 1958). On the other hand we doubt whether the variation of amphibole in alkali granites can be connected with temperature changes. Indeed, comparing the composition of amphiboles 102 and 103 from alkali granite and pegmatite from one and the same intrusive body, they have identical values

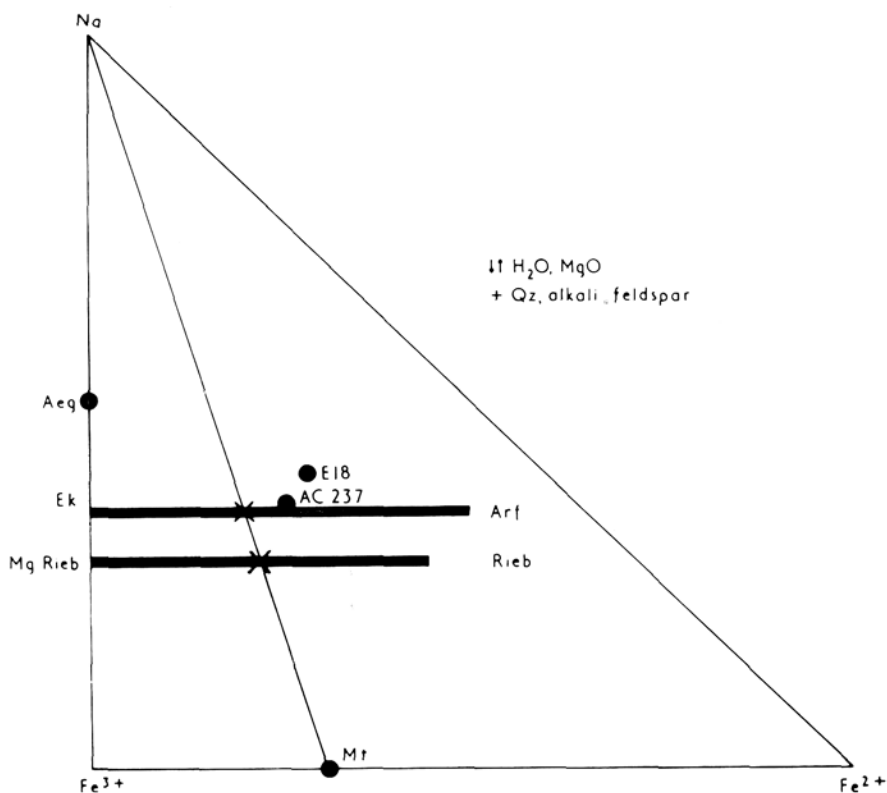
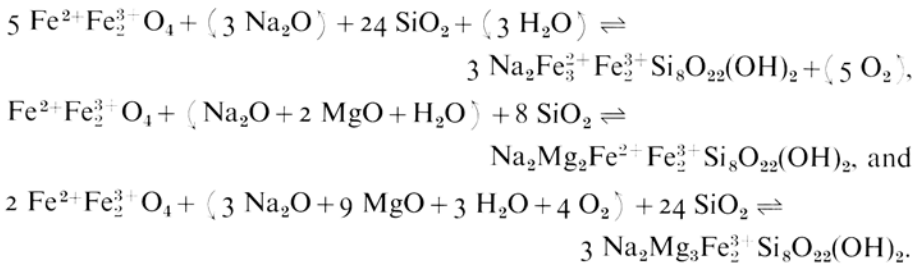


FIG. 9. Mineral paragenesis with alkali amphiboles and magnetite. Crosses mark the compositions of the amphiboles at the maximum of  $\mu_{\text{Na}}$ . Circles mark the composition with the highest content of Mg known in alkaline granites.

of  $\text{Fe}^{2+}/(\text{Fe}^{2+} + \text{Mg})$ , although their formation took place under different temperature conditions. But the value of  $\text{Fe}^{2+}/(\text{Fe}^{2+} + \text{Mg})$  of these amphiboles differs markedly from the value for alkali amphiboles from granites and pegmatites of adjacent intrusive bodies with analogous formation conditions. Therefore the value of  $\text{Fe}^{2+}/(\text{Fe}^{2+} + \text{Mg})$  of magnesian riebeckites in alkali granites must be connected with more local factors than temperature and pressure. As already pointed out (Kovalenko, 1965), the behaviour of Mg is rather mobile when the value of  $\text{Fe}^{2+}/(\text{Fe}^{2+} + \text{Mg})$  for amphibole from alkali granites (with reactional relations of amphibole and magnetite) is not due to the initial ratio in the system, but primarily depends on the  $\mu_{\text{O}_2}$  and  $\mu_{\text{Na}}$ . In fact, a system consisting of amphibole and magnetite is composed of Na, Fe,  $\text{O}_2$ , Mg, and  $\text{H}_2\text{O}$ . In this case (a perfectly mobile Mg and an inert Fe and constant temperature of  $\mu_{\text{H}_2\text{O}}$  and pressure) the system is determined by the relation of  $\mu_{\text{Na}}$  and  $\mu_{\text{O}_2}$ :  $f = c - p = 3 - 2 = 1$ .

The dependence of the amphibole composition on  $\mu_{\text{O}_2}$  and  $\mu_{\text{Na}}$  may be analysed on the composition–paragenesis diagram, fig. 9. In this case the ratio  $\text{Fe}^{2+}/\text{Fe}^{3+}$  in amphibole is determined by  $\mu_{\text{O}_2}$ , if the oxygen is believed to be a single oxidizer in the system, and this in turn determines the Mg content of the amphibole. It follows from fig. 9 that the variable ratio  $\mu_{\text{O}_2}/\mu_{\text{Na}}$  will determine the composition of amphibole coexisting with magnetite. We may say that the monovariant equilibrium line will vary its slope in the co-ordinates depending on the composition of the amphibole. The slope is determined from the following reactions (for compositions of the riebeckite–magnesioriebeckite):



The slopes of these equilibrium lines are 0.6,  $\infty$ , and  $-0.75$  respectively, a change of sign from positive to negative as a result of a compositional variation of the amphibole from riebeckite to magnesioriebeckite. This fact manifests the existence of an extreme on the equilibrium line considered (Korzhinsky, 1958, 1960). This line is characteristic of a maximum of the  $\mu_{\text{Na}_2\text{O}}$  value corresponding to a Mg/Fe ratio of 2. On the same line in the region of stability of amphibole the lines of equal value of  $\text{Fe}^{2+}/(\text{Fe}^{2+} + \text{Mg})$  may be constructed.

Fig. 9 shows that in the equilibrium magnetite plus arfvedsonite or eckermanite there is a maximum of  $\mu_{\text{Na}_2\text{O}}$  also. Calculation indicates that the composition of arfvedsonite in an extreme paragenesis with magnetite appears to be more magnesian ( $\text{Arf}_{0.75}\text{Ek}_{2.75}$ ) than the composition of an extreme riebeckite. It follows that arfvedsonite with a value of  $\text{Fe}^{2+}/(\text{Fe}^{2+} + \text{Mg}) = 0.333$  should be

rare in metasomatic and metamorphic rocks, as they need for generation a maximum high value of  $\mu_{\text{Na}_2\text{O}}$ . Lower values of  $\mu_{\text{Na}_2\text{O}}$  create either high magnesian or more ferric amphibole than the extreme composition. At the lowest values of the  $\mu_{\text{Na}_2\text{O}}$  there may appear the typical riebeckite and arfvedsonite of alkali granitoids.

Among the data above, the most magnesian composition of amphibole from alkali granites has  $\text{Fe}^{2+}/(\text{Fe}^{2+} + \text{Mg}) = 0.56$  to  $0.57$  (102, 103, 107 of tables I and II), that is, a more ferroan amphibole than the extreme composition. We suggest that this is connected with the high Fe content of the magma in alkali granites (Ernst, 1963), as well as with an extreme in the equilibrium of amphibole with magnetite.

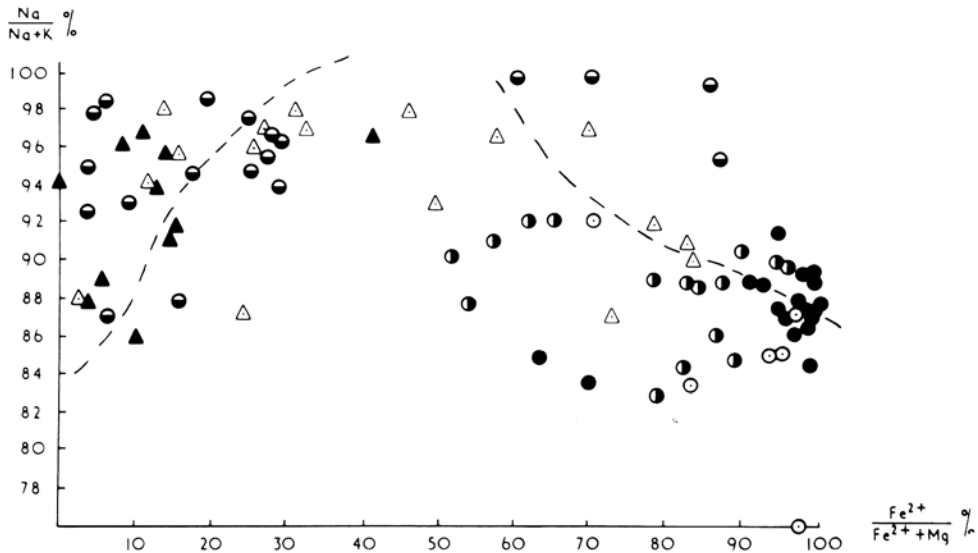


FIG. 10. The dependence of the values of  $\text{Na}/(\text{Na} + \text{K})$  and  $f = \text{Fe}^{2+}/(\text{Fe}^{2+} + \text{Mg})$  in alkaline amphiboles of the series riebeckite–magnesioriebeckite and arfvedsonite–eckermannite: ●, from alkali granites of Siberia; ●, from alkali granites of Africa (Borley, 1963); ○, from alkali granites of the Kola peninsula (Chumakov, 1958); △, from metamorphic rocks; ▲, from carbonatites; ◐, amphibole asbestos.

For estimation of the role of the theoretically obtained extreme condition in the equilibrium of amphibole with magnetite, we have taken all available analyses of riebeckite and arfvedsonite and plotted them in terms of the coordinates  $\text{Na}/(\text{Na} + \text{K})$  and  $f = \text{Fe}^{2+}/(\text{Fe}^{2+} + \text{Mg})$ , which to a first approximation may be regarded as activity indicators of sodium and oxygen (fig. 10). The diagram shows that most of the amphibole compositions are situated in the regions of high and low values of  $f = \text{Fe}^{2+}/(\text{Fe}^{2+} + \text{Mg})$ , which apparently confirms the existence of this extreme in natural formations.

*Facies and subfacies of alkalic granitoids*

Based on the above considerations table VI has been drawn up, characterizing the facies and subfacies of alkali granitoids. The mineral paragenesis of alkali granitoids is taken as a single mineral formation (Pavlenko, 1963; Kovalenko *et al.*, 1965), described as a definite association of factors of state. The mineral facies is determined by a relative constancy of a number of external conditions (intensive factors):  $T$ ,  $p$ ,  $\mu_{\text{Na}}$ ,  $\dots$ ,  $\mu_{\text{K}}$ ; but the qualitative composition of paragenesis is constant. The mineral subfacies has an absolute constancy of external conditions expressed in a constancy of minerals of variable composition (alkali amphibole).

TABLE VI. Facies and subfacies of the alkalic granitoids

Parameters	Facies and subfacies	Paragenesis and composition of the amphibole
$T$	<ul style="list-style-type: none"> <li>{ High temperature</li> <li>{ Medium temperature</li> <li>{ Low temperature</li> </ul>	<ul style="list-style-type: none"> <li>Arf + Mt + (KFS + Q)</li> <li>Arf-Rieb + Mt + (KFS + Q)</li> <li>Rieb + Mt + (KFS + Q)</li> </ul>
$T, \mu_{\text{Na}_2\text{O}}$	<ul style="list-style-type: none"> <li>{ Relatively high <math>T</math> and low <math>\mu_{\text{Na}_2\text{O}}</math></li> <li>{ Relatively low <math>T</math> and high <math>\mu_{\text{Na}_2\text{O}}</math></li> </ul>	<ul style="list-style-type: none"> <li>Arf + Mt + (KFS + Q)</li> <li>Rieb + Mt + (NaFS + Q)</li> </ul>
$\mu_{\text{O}_2}, \mu_{\text{Na}}$	<ul style="list-style-type: none"> <li>{ High <math>\mu_{\text{O}_2}</math> and <math>\mu_{\text{Na}}</math></li> <li>{ Moderate <math>\mu_{\text{O}_2}</math> and <math>\mu_{\text{Na}}</math></li> </ul> Subfacies: <ul style="list-style-type: none"> <li>{ Low <math>\mu_{\text{O}_2}</math> and <math>\mu_{\text{Na}}</math></li> <li>{ Medium <math>\mu_{\text{O}_2}</math> and <math>\mu_{\text{Na}}</math></li> <li>{ High <math>\mu_{\text{O}_2}</math> and <math>\mu_{\text{Na}}</math></li> </ul>	<ul style="list-style-type: none"> <li>Aeg + Q + (FS)</li> <li>Rieb + Q + (FS)</li> <li>Rieb<sub>0.9</sub>-Mg-Rieb<sub>0.1</sub> + Q + (FS)</li> <li>Rieb<sub>0.7</sub>-Mg-Rieb<sub>0.3</sub> + Q + (FS)</li> <li>Rieb<sub>0.6</sub>-Mg-Rieb<sub>0.4</sub> + Q + (FS)</li> </ul>

From the alkali granites of Siberia, both a high-temperature facies of amphibole granites and a relatively low-temperature facies of riebeckite granites and albitites can be specified. Besides this, the following three subfacies can be distinguished in the sequence of increase of  $\text{O}_2$  and Na activity: albitites with riebeckite, alkali granites and pegmatites with relatively magnesian alkali amphibole, and alkali granites with a maximum content of Mg.

Finally, we note that, according to experimental data (Ernst, 1963; Ivanov, 1962; Tugarinov *et al.*, 1963; Sand, Roy, and Osborn, 1957), the temperature interval of all these facies does not exceed 150 to 250 °C.

*Mineral paragenesis riebeckite plus calcian riebeckite*

The single deposit of riebeckite with calcian riebeckite the author knows is in Eastern Siberia. These amphiboles are formed in metasomatic microclinites in zones of postmagmatic interaction of alkali granites with wall rocks of gabbro type. The amphiboles with an appreciable content of calcian riebeckite

are conjugate with parts of endocontactic microclinities adjacent to wall gabbroids, and formed by a diffusional bimetasomatism of Fe, Si, Na, Ca, and Li between alkali granites and gabbro (Kovalenko *et al.*, 1966).

*Acknowledgements.* The author would like to thank Prof. L. V. Tauson for his support, S. B. Brandt for consultations, V. A. Pysarskaya, A. S. Znamenskaya, and G. Afonina for the analytical data, L. K. Pozharitskaya and E. A. Chernisheva for analyses of amphiboles, and I. I. Kolosovsky for consultations on the translation of the text into English.

#### References

- [ANDREEV (YU. U.)] Андреев (Ю. У.), 1962. Генетические типы Месторождений щелочных амфиболов-асбестов и основные принципы их прогноза и поисков. *In: Закономерности размещения полезных ископаемых.* Москва. (The location regularities of useful minerals. Moscow).
- [BEUS (A. A.), SEVEROV (E. A.), SITNIN (A. A.), and SUBBOTIN (K. D.)] Беус (А. А.), Северов (Э. А.), Ситнин (А. А.), и Субботин (К. Д.), 1962. Альбитизированные и грейзенизированные граниты (апограниты). Изд. Акад. Наук СССР. (The albitized and greisenized granites (apogranites). Moscow, Acad. Sci. U.S.S.R.).
- BORLEY (G. D.), 1963. *Min. Mag.*, **33**, 358.
- and FROST (M. T.), 1963. *Ibid.*, 646.
- [BORNEMAN-STARYNKEVICH (I. D.)] Борнеман-Старынкевич (И. Д.), 1964. Руководство по расчету формул минералов. Изд. "Наука". (Instructions for computing the formulae of minerals. "Nauka", Moscow).
- CARMICHAEL (I. S. E.), 1962. *Min. Mag.*, **33**, 86.
- [CHUMAKOV (A. A.)] Чумаков (А. А.), 1958. О происхождении щелочных гранитов Кейв. *In: Щелочные граниты Кольского полуострова.* Изд. Акад. Наук СССР. (On the origin of alkaline granites of Kiev. *In: The alkaline granites of the Kola peninsula.* Moscow, Acad. Sci. U.S.S.R.).
- DEER (W. A.), HOWIE (R. A.), and ZUSSMAN (J.), 1965. *Rock-forming minerals*, vol. 2. (Russian translation).
- [ELISEEV (N. A.), NIKOLSKII (N. P.), and KUSHEV (V. G.)] Елисеев (Н. А.), Никольский (Н. П.), и Кушев (В. Г.), 1961. Метасоматиты Криворожского рудного пояса. Изд. Акад. наук СССР. (The metasomatites of the Krivoy Rog mine belt. Moscow, Acad. Sci. U.S.S.R.).
- ERNST (W. G.), 1961. *Amer. Journ. Sci.*, **259**, 735.
- 1962. *Journ. Geol., Chicago*, **70**, 689.
- [GINZBURG (I. V.), SIDORENKO (G. A.), and ROGACHEV (D. L.)] Гинзбург (И. В.), Сидоренко (Г. А.), и Рогачев (Д. Л.), 1961. Труды Мин. Муз. Акад. Наук СССР (Trav. Mus. Min. URSS), **12**, 3.
- [GLAGOLEV (A. A.)] Глаголев (А. А.), 1958. Доклады акад. наук СССР (Compt. Rend. Acad. Sci. URSS), **119**.
- [IVANOV (I. P.)] Иванов (И. П.), 1962. О природе "альбитизирующих растворов". *In: Экспериментальные исследования в области глубинных процессов.* Изд. Акад. Наук СССР (An experimental study of the deep processes of the earth. Moscow, Acad. Sci. U.S.S.R.).
- IWAO (S.), 1939. *Japan. Journ. Geol. Geogr.*, **16**, 155.
- [KOVALENKO (V. I.)] Коваленко (В. И.), 1964. Параянезисы метасоматически измененных гранитоидов с аксессуарными тантало-ниобатами. *In: Физико-химические условия магматизма и метасоматоза.* Изд. "Наука", Новосибирск. (Paragenesis of metasomatically altered granitoids with accessory tantaloniobates. *In: Physico-chemical conditions of magmatism and metasomatism.* "Nauka", Novosibirsk).

- [—, OKLADNIKOVA (L. V.), PAVLENKO (A. S.), POPOLITOV (E. I.), and FILIPPOV (L. V.)] —, Окладникова (Л. В.), Павленко (А. С.), Пополитов (Э. И.), и Филиппов (Л. В.), 1965. Петрология среднепалеозойского комплекса гранитоидов и щелочных пород Восточной Тувы. In: Геохимия и петрология магматических и метасоматических образований. Изд. "Наука", Москва. (Geochemistry and petrology of magmatic and metasomatic formation. Nauka, Moscow).
- [—, PISARSKAYA (V. A.), and NIKOLAeva (D. Kh.)] —, Писарская (В. А.), и Николаева (Д. Х.), 1966. Доклады акад. Наук СССР (*Compt. Rend. Acad. Sci. URSS*), **169**, 1162–1165.
- [KORZHINSKIИ (D. S.)] Коржинский (Д. С.), 1936. Изв. акад. Наук СССР, сер. геол. (*Bull. Acad. Sci. URSS, sér. géol.*), No. 1.
- , 1940. Труды Инст. Геол. Наук, акад. Наук СССР (*Trans. Inst. geol., Acad. Sci. URSS*), **12**.
- , 1946. Принцип подвижности щелочей при магматических явлениях. (The principle of mobility of alkalis in magmatic phenomena.) Belyankin vol., Acad. Sci. U.S.S.R.
- , 1957. Физико-химические основы анализа парагенезисов минералов. Изд. Акад. Наук СССР (The physico-chemical principles of analyses of mineral paragenesis.) Moscow, Acad. Sci. U.S.S.R.
- , 1958. Журн. физ. Хим. (*Journ. Phys. Chem.*), **32**, 1536.
- , 1959. Доклады акад. Наук СССР (*Compt. Rend. Acad. Sci. URSS*), **128**, No. 2.
- , 1963. Теория экстремальных состояний и их значение для минеральных систем. In: Химия земной коры, Т. I (The theory of extreme states and their significance for mineral systems. In: *Chemistry of the Earth's crust*, vol. I, Moscow, Acad. Sci. U.S.S.R.).
- [KUMAN (V. E.)] Куман (В. Е.), 1960. Доклады Акад. Наук СССР (*Compt. Rend., Acad. Sci. URSS*), **131**, No. 1.
- [MARAKUSHEV (A. A.)] Маракушев (А. А.), 1965. Проблемы минеральных фаций метаморфических и метасоматических горных пород. Изд. "Наука", Москва (The problems of the mineral facies of metamorphic and metasomatic rocks. Nauka, Moscow).
- MIYASHIRO (A.), 1953. *Journ. Fac. Sci. Univ. Tokyo*, sec. 2, **2**, 57.
- [PAVLENKO (A. S.)] Павленко (А. С.), 1963. Петрология и некоторые геохимические особенности среднепалеозойского комплекса гранитоидов и щелочных пород Восточной Тувы. In: Проблемы магмы и генезиса изверженных горных пород. Москва. (Petrology and some geochemical peculiarities of the mid-paleozoic complex of granitoids and alkali rocks of Eastern Tuva. In *Problems of magma and the genesis of the eruptive rocks*. Moscow).
- PHEMISTER (J.), 1950. *Min. Mag.*, **29**, 359.
- PHILLIPS (R.), 1963. *Ibid.*, **33**, 701.
- ROWE (R. B.), 1955. *Canad. Min. Journ.*, **76**, No. 3.
- SAND (L. B.), ROY (R.), and OSBORN (E. F.), 1957. *Econ. Geol.*, **52**, 169.
- [SEMENOV (E. I.)] Семенов (Е. И.), 1964. Иттрий. Лантаноиды. In: Геохимия, минералогия и генетические типы месторождений редких элементов. Т. I, Геохимия редких элементов. Изд. "Наука", Москва. (Yttrium. Lanthanides. In *Geochemistry, mineralogy and genetic types of deposits of rare elements*, vol. I, geochemistry of rare elements. Nauka, Moscow).
- [SMAGUNOVA (A. N.), BELOVA (R. A.), AFONINA (V. P.), and LOSEV (N. F.)] Смагунова (А. Н.), Белова (Р. А.), Афонина (В. П.), и Лосев (Н. Ф.), 1964. Завод. Лаб. (Factory laboratory), ser. 4, **30**.
- SØRENSEN (H.), 1960. Report of the 21st session, Internat. Geol. Congr., part 13, 319.
- [STORONKIN (A. V.) and SHULTS (M. M.)] Сторонкин (А. В.) и Шульц (М. М.), 1960. Журн. Физ. Хим. (*Journ. Phys. Chem.*), **34**, 1928.

- SUNDIUS (N.), 1946. *Årsbok Sveriges Geol. Undersök*, **40**, No. 4.
- [TAUSON (L. V.)] Таусон (Л. В.), 1961. Геохимия редких элементов в гранитоидах. Изд. Акад. Наук СССР, Москва. (Geochemistry of rare elements in granitoids. Moscow, Acad. Sci. U.S.S.R.).
- [TUGARINOV (A. I.), PAVLENKO (A. S.), and ALEKSANDROV (I. V.)] Тугаринов (А. И.), Павленко (А. С.), и Александров (И. В.), 1963. Геохимия щелочного метасоматоза. Изд. Акад. Наук СССР, Москва. (Geochemistry of the alkaline metasomatose. Moscow, Acad. Sci. U.S.S.R.).
- TUTTLE (O. F.) and BOWEN (N. L.), 1958. *Geol. Soc. Amer., Mem.* 74.
- [VINOGRADOV (A. P.)] Виноградов (А.П.), 1956. Геохимия (Geochemistry), no. 1.
- YAGI (K.), 1957. *Bull. Geol. Soc. Amer.*, **64**, No. 7.

## On the amphiboles of the hastingsite-pargasite series

By D. P. SERDYUCHENKO  
(Д. П. Сердюченко)

*Summary* Some occurrences of metamorphic amphiboles from the Aldan, south Yakutia, are described, and their metamorphic relationships are discussed. Analyses, formulae, and optical properties are given for three pargasites, five hastingsites, and four tremolite-actinolites. The characteristics that serve to distinguish between these amphiboles are considered, and the desirability is emphasized of performing initial formula calculations for amphiboles (and other hydrous minerals) on a water-free basis.

AMONG the Archean sedimentary-metamorphic formations of the Aldan, south Yakutia, in the uppermost older Iengre (Иенгре) series, there are developed sillimanite quartzites, graphite-biotite-plagioclase or plagioclase paragneisses, and paraschists. The coloured minerals present in these are mainly diopside or diopside-hedenbergite and common hornblende, but in some layers and packets there also occur pyroxenes of the enstatite-hypersthene series. In some places they alternate conformably with forsterite-(clinohumite)-magnetite, diopside-(or augite)-magnetite bedded ores, often bearing minor (or even important) phlogopite. To the same series there are subordinated enstatite (hypersthene)-magnetite ores, changing either gradually or at sharp contacts into magnetite-forsterite (with some ceylonite) or magnetite-pargasite beds. Some of these beds, or lenses, are relatively low in magnetite and rhombic pyroxene, and contain pargasite in important quantity. In other cases iron ore packets are composed of light-coloured magnetite-pargasite layers interbedding dark-green magnetite-hastingsite ones; in thin sections one can see that colourless pargasite ( $2 V_{\gamma} 68^{\circ}$ ) overgrows, and blue-green hornblende ( $2 V_{\alpha} 82^{\circ}$ ) replaces, diopside grains.

In diopside-plagioclase schists and diopside-carbonate (calciphyre) rocks the pargasites form fine-grained disseminations or veined segregations in fissures. Locally, there are large, well-developed, single crystals and also druses. The pargasite is in close paragenetic relation with diopside. It is not rare for them to occur as aggregates and grain intergrowths, but more often the pargasite crystallizes somewhat later; sometimes inside relatively coarse pargasite crystals there are fine idiomorphic or partly idiomorphic pyroxene grains.

Some magnetite-diopside-pargasite ores have autonomous pargasite grains syngenetic to pyroxene, the latter often being replaced by pale-green pargasite, which sometimes gradually changes into greenish-blue hastingsite.

Some pyroxene-amphibole (with scapolite) paraschists are composed of

augite and green-blue hornblende (hastingsite), sometimes overgrown by pyroxene grains.

It should be noted that in almost monomineralic amphibole, magnetite–amphibole or magnetite–diopside rocks (with replacement of pyroxene by pargasite), the most developed green-blue hastingsite is confined, as a rule, to beds, packets of beds, and zones, where it is most clearly seen in large or small veined injections of light rose alaskite granites. Not infrequently in such cases large or even giant hastingsite crystals have resulted. In carbonate rocks almost devoid of iron, very big pargasite crystals develop in the same manner, associated with diopside.

There are some noteworthy cases in which finely banded diopside–tourmaline schist recrystallizes metasomatically under the influence of bedded (conformable) and intersecting veinlets of granite composition, and changes into hastingsite–tourmaline rock. In some zones the latter is enriched in phlogopite (after diopside and hastingsite) but in others (during the last low-temperature stages of recrystallization) the hastingsite is transformed into acicular or fibrous aggregates of light green actinolite. Away from this granite injection zone the conformable diopside–hastingsite schists (with phlogopite) gradually change into thin banded magnetite–pyroxene–amphibole rock. However, with the appearance of magnetite the amphibole character changes; the hastingsite ( $\gamma$  light blue,  $\beta$  green,  $\alpha$  greenish-yellow;  $\gamma$  : [001] $30^\circ$ ,  $2V_\gamma 80^\circ$ ) gives way to pargasite ( $\gamma$  pale-green,  $\beta$  light-greenish,  $\alpha$  colourless;  $\gamma$  : [001] $22^\circ$ ,  $2V_\gamma 76^\circ$ ). Thus, in some places there are observed gradual transitions from a barren ferriferous amphibole(hastingsite)-bearing zone into a magnetite one with pargasite almost devoid of iron. Investigations of the amphiboles from diopside–pargasite and diopside–hastingsite rocks and ores showed that their  $2V$  is not infrequently near  $90^\circ$  ( $86$  to  $94^\circ$ ). Some forsterite–diopside–pargasite schists, injected by pinkish-gray granite flows, become enriched in phlogopite and give transitions to hastingsite rock. Here, there are places that are composed of light green (in thin sections colourless) tremolite transformed into tremolite asbestos felt on the ends of the crystals.

Blue-green hornblende sometimes contains relics of common brown-green hornblende, but skeletal grains of hastingsite occur also among late phlogopite plates as a result of resorption.

In the Archean sedimentary-metamorphic series of the Aldan, amphibolization occurs not only by infiltration-metasomatism, but also frequently by (deuteric) autometasomatism of older pyroxenes. These are replaced under the influence of residual pore-filling hydrothermal fluids rich in volatiles ( $H_2O$ , F, Cl) and other mineral substances. In form, mechanism, and degree of development, this "uralitization" is absolutely similar to that occurring in gabbroid and other igneous rocks. L. Duparc (1908) first studied it in detail in the Urals. Autometasomatic amphibolization of pyroxene metamorphic rocks of the Aldan indicate that here (and also in magmatic bodies: Asklund, 1925; Kennedy, 1935) not only temperature and pressure but also the primary sedimentary

rock constituents and the relative proportions of particular components (for example, MgO-CaO-FeO-Al<sub>2</sub>O<sub>3</sub>) essentially decide the mineral composition (pyroxene, amphibole, mixed) of the metamorphic products. Apparently the original sediment composition should influence by right of succession the formation of common hornblende and hastingsite or pargasite in rocks of similar metamorphic facies.

The sillimanite, titanian biotite (with graphite), two-pyroxene, hypersthene-pargasite, magnetite-pargasite crystalline schists and pyroxene-pargasite calciphyres appear to have been formed in the conditions of the granulite facies of metamorphism. However, these rocks, thin or thick banded, are often intercalated rhythmically in diopside-hornblende, biotite-hornblende, epidote-hornblende schists and gneisses of the amphibolite facies. The composition of metamorphosed rocks seems to have an essential importance during the formation of mineral complexes. On the other hand, under the influence of granite injections there occurred rather large retrograde-metamorphic (partial or total) regeneration of many of the rocks of the granulite facies. The metasomatic blue-green (hastingsite) hornblende became one of the principal coloured minerals. This hornblende developed under the conditions of the amphibolite facies of metamorphism.

The successive hydrothermal formation of acicular and fibrous amphiboles of the actinolite-tremolite series appears to correspond to the greenschist facies of metamorphism. In some places it is accompanied by intensive sulphide mineralization.

Thus, in the Archean of south Yakutia, there are primary metamorphic amphiboles (common hornblendes and pargasites) and secondary metasomatic ones (blue-green hastingsites, secondary pargasites, and actinolite-tremolites). Their formation is controlled by temperature and pressure (facies of metamorphism) and also by the concentrations of the components taking part in mineral formation.

The field and laboratory studies show that there occurs a fairly gradual trend in the composition and optical properties of the hastingsite-pargasite series in the Aldan (table I).

The total alkali content (about 3%) varies insignificantly, the Fe<sup>3+</sup> and Fe<sup>2+</sup> quantity decreases to zero in the colourless, iron-free, koksharovite variety of pargasite, the importance of Mg and Al<sup>vi</sup> increases markedly, the Ca group and Al<sup>iv</sup> quantity remain almost constant, and the (OH) content is low in both types and is far from reaching (OH)<sub>2</sub> (cf. table II).

The isomorphous substitutions in this series take place almost entirely in octahedral sites according to: Al<sup>vi</sup>Mg (pargasite)  $\rightleftharpoons$  Fe<sup>3+</sup>Fe<sup>2+</sup> (hastingsite), i.e., these pargasites are constitutionally magnesian-aluminian analogues of hastingsites, and have the common formula (cf. Sundius, 1946): (Na, K)Ca<sub>2</sub>(Mg, Fe<sup>2+</sup>)<sub>4</sub>(Al, Fe<sup>3+</sup>)[Al<sub>2</sub>Si<sub>6</sub>]O<sub>22</sub>(OH)<sub>2</sub>.

Fluorine is absent in blue-green and green-blue hastingsites. There is always noticeable chlorine content in these hastingsites, whereas the F content is

characteristic for pargasites (especially in the zone of phlogopitization, cf. analysis 1). The development (on common hornblende and diopside) of metasomatic hastingsites might take place under the influence of ferrous solutions containing chloride and sulphate. The aqueous solutions containing fluorine are more important at the higher-temperature conditions of pargasite formation.

TABLE I. Chemical composition of amphiboles from south Yakutia

	Pargasites			Hastingsites				Actinolite—tremolite series				
	1	2	3	4	5	6	7	8	9	10	11	12
SiO <sub>2</sub>	40.96	44.37	43.86	40.12	38.48	43.21	40.37	43.50	50.94	53.20	56.08	57.54
TiO <sub>2</sub>	0.20	0.89	nil	0.44	0.60	0.07	2.26	2.27	0.16	nil	nil	0.10
B <sub>2</sub> O <sub>3</sub>	—	nil	0.37	nil	0.28	—	—	0.37	nil	nil	nil	0.18
Al <sub>2</sub> O <sub>3</sub>	17.84	16.88	14.20	12.83	14.46	9.05	13.35	10.77	4.82	3.61	2.06	1.00
Fe <sub>2</sub> O <sub>3</sub>	3.24	2.17	4.85	9.58	4.88	8.75	5.96	5.00	1.40	2.40	0.81	0.66
Cr <sub>2</sub> O <sub>3</sub>	—	nil	—	0.02	nil	—	nil	0.09	trace	0.01	—	nil
FeO	2.00	1.81	8.01	7.20	10.22	8.61	11.80	9.71	7.30	4.17	3.91	1.47
MnO	0.08	0.06	0.14	0.10	0.15	0.13	0.29	0.13	0.11	0.03	0.10	0.11
MgO	17.58	15.29	13.52	12.72	12.19	14.32	9.68	12.52	18.65	20.53	23.05	24.78
BaO	0.06	0.28	—	nil	nil	—	0.07	nil	0.04	—	—	no
CaO	12.53	12.98	11.60	11.28	12.22	11.70	11.64	12.31	12.71	12.22	11.52	12.74
Li <sub>2</sub> O	—	0.15	0.06	0.02	—	—	—	0.16	0.05	0.05	—	0.27
Na <sub>2</sub> O	1.70	3.80	1.55	1.30	1.50	2.26	1.92	1.92	0.58	2.48	1.02	0.32
K <sub>2</sub> O	1.90	0.76	1.05	2.68	3.06	1.03	1.28	0.43	0.80	0.57	0.46	0.12
P <sub>2</sub> O <sub>5</sub>	—	0.03	—	—	0.21	—	—	0.11	—	—	—	—
F	1.28	0.52	nil	0.02	nil	—	nil	—	—	—	—	—
Cl	0.41	0.01	0.10	0.50	0.08	0.51	0.32	0.26	1.18	trace	0.66	nil
CO <sub>2</sub>	nil	nil	nil	0.16	nil	nil	nil	0.24	0.16	0.09	0.24	0.06
S	—	0.07	0.07	—	0.03	0.06	nil	nil	—	—	—	—
H <sub>2</sub> O <sup>+</sup>	1.00	0.10	0.67	0.90	1.10	0.44	0.72	0.74	0.91	0.71	0.52	0.98
H <sub>2</sub> O <sup>-</sup>	0.04	0.14	nil	0.08	0.14	0.08	0.20	—	0.24	0.04	0.20	0.16
Total	100.82	100.31	100.05	99.95	99.60	100.22	99.86	100.53	100.05	100.11	100.63	100.49
O≡(F, Cl) <sub>2</sub>	0.63	0.21	—	0.11	0.02	0.12	0.07	0.06	0.51	0.02	0.32	0.02
2 V	100.17	100.05	100.05	99.84	99.58	100.10	99.79	100.47	99.54	100.09	100.31	100.47
γ	-64°	+60°	+56°	-80°	-74°	-69°	-83°	-82°	-85°	—	—	-88°
β	1.658	1.645	1.641	1.690	1.684	—	1.686	1.680	1.652	1.634	1.630	1.628
α	1.645	1.640	1.638	1.679	1.677	—	1.676	1.669	1.639	—	—	1.618
γ : [001]	1.641	1.635	1.634	1.666	1.666	—	1.664	1.656	1.627	1.613	1.610	1.609
	23°	20°	26°	24°	32°	26°	19°	26°	21°	19°	14°	12°

TABLE II. Atomic composition of pargasites, hastingsites, and actinolites

Anal.	Si <sup>iv</sup>	Al <sup>iv</sup>	Al <sup>vi</sup>	Fe <sup>···</sup>	Fe <sup>··</sup>	Ti	Mg	Ca	Na	K	O	OH	F
1	5.84	2.16	0.84	0.34	0.25	0.02	3.73	1.91	0.46	0.34	22.18	0.97	0.67
2	6.22	1.78	1.01	0.22	0.21	0.09	3.19	1.97	1.03	0.14	22.82	0.10	0.26
3	6.30	1.70	0.77	0.52	0.97	—	2.89	1.78	0.43	0.19	22.67	0.66	—
4	6.00	2.00	0.26	1.08	0.91	0.05	2.80	1.80	0.38	0.48	22.32	1.12	0.24
5	5.83	2.17	0.41	0.56	1.31	0.08	2.74	1.93	0.44	0.60	22.44	1.11	0.01
6	6.34	1.66	—	0.88	1.08	0.01	3.13	1.84	0.65	0.19	22.72	0.44	0.12
7	6.04	1.96	0.33	0.67	1.52	0.26	2.18	1.87	0.56	0.25	22.61	0.70	0.08
8	6.50	1.50	0.32	0.53	1.18	0.24	2.67	1.82	0.53	0.09	22.63	0.70	0.04
9	7.28	0.72	0.08	0.16	0.88	0.02	3.97	1.86	0.16	0.14	22.28	0.89	0.58
10	7.40	0.59	—	0.25	0.50	—	4.24	1.82	0.67	0.10	22.65	0.67	0.03
11	7.66	0.34	—	0.07	0.45	—	4.69	1.69	0.28	0.08	22.59	0.48	0.34
12	7.79	0.22	—	—	0.18	—	5.00	1.85	0.14	0.02	22.58	0.82	0.02

Means of the pargasites (P), of the hastingsites (H), and of the actinolites (A):

P	6.12	1.88	0.86	0.36	0.47	0.04	3.17	1.89	0.64	0.22	22.56	0.58	0.31
H	6.14	1.86	0.26	0.74	1.20	0.13	2.71	1.85	0.51	0.32	22.55	0.81	0.09
A	7.53	0.47	0.03	0.12	0.50	0.01	4.47	1.80	0.31	0.09	22.51	0.72	0.24

The  $\text{Fe}^{2+}$  and  $\text{Fe}^{3+}$  quantities in pargasites are inversely proportional to the halogen content, but their influence on the amphibole optics is offset to some extent by the simultaneous increase of Si (from analyses 1 to 3).

In the compositions of actinolite-tremolites of the same region (table I), as a result of the almost complete absence of trivalent ions in six co-ordination, the values of Si and divalent ions (mainly Mg) increase considerably. This is accompanied by a substantial reduction in the indices of refraction. The gradual changes in crystal habit (thick prisms, thin long prisms, rod-like, needle-shaped, and felt-like aggregates) and in their composition (tables I and II) show uninterrupted transitions from hastingsites to actinolites and further to tremolites. The comparison of actinolite-tremolites with hastingsite-pargasites reveals mutual heterovalent replacements such as:  $\text{SiMg} \rightarrow \text{Al}^{\text{IV}}\text{Al}^{\text{VI}}$  comprising not only octahedral groups but also tetrahedral ones. A deficiency of  $\text{H}_2\text{O}+$  has been noted by many authors in the case of amphiboles of the granulite and high-temperature zones of the amphibolite facies. It involves definite equivalent anion replacements,  $\text{O} \rightleftharpoons (\text{OH})_2$ .

When the composition and optics vary markedly it is difficult to distinguish common hornblende from hastingsite. However, there is a clear tendency:  $2V_x$  increases from common hornblendes ( $52^\circ$ ;  $64^\circ \dots$ ) to green-blue hastingsites ( $\dots 69^\circ$ ,  $84^\circ \dots$ ); in transitional hastingsite-pargasite varieties it is close to  $90^\circ$ , then becomes positive and gradually decreases in pargasites ( $2V_\gamma 82^\circ$ ,  $70^\circ$ ,  $56^\circ$ ).

The pleochroic properties of hastingsite and pargasite are similar, except that the blue ( $\gamma$ )-green ( $\beta$ )-yellow ( $\alpha$ ) tones of hastingsite are more intense, and the values of  $\gamma : [001]$  are often high (26 to  $33^\circ$ ).

The pargasites, hastingsites, and actinolites of the Aldan that have been studied contain about 1% or less of  $\text{H}_2\text{O}+$  (determined by the direct method). This value is far less than that (about 3%) corresponding to the crystal-chemical formula with  $(\text{OH})_2$ . However, some amphiboles appear to have more "high temperature" water as a result of the presence of water that is physically adsorbed on finely dispersed material and is only lost at 200 to  $400^\circ$ . If, in calculating the formula, one assumes 24 (O, OH), this leads not only to more than  $2(\text{OH})$  but also to errors in the cation numbers in the unit cell of the mineral.

Therefore, for more than 20 years, we have calculated crystal-chemical formulae of minerals such as micas, chlorites, montmorillonites, and amphiboles on the basis of the number of oxygens in the "dry" substance, excluding  $\text{H}_2\text{O}+$  in the first instance. We then subsequently determine the number of (OH)-groups by the use of the coefficient-divisor already determined. In the case of micas and montmorillonites we take 11 oxygens, for chlorites 14, and for amphiboles 23. We used this method (with 23 oxygens) to calculate the formulae of the pargasites and hastingsites (Serdyuchenko, 1954, 1960).

Estimations of the specific gravity of amphiboles from formulae calculated for 23 oxygens resulted in values closer to experimental determinations than when the formulae were recalculated on the basis of 24 (O, OH, F) (Binns, 1965).

*References*

- ASKLUND (B.), 1925. *Arsbok. Sver. geol. undersökn.*, ser. C, **17**, No. 6.
- BINNS (R. A.), 1965. *Min. Mag.*, **35**, 306.
- DUPARC (L.), 1908. *Bull. Soc. franç. Min.*, **31**, 50.
- KENNEDY (W. Q.), 1935. *Min. Mag.*, **24**, 203.
- [SERDYUCHENKO (D. P.)] Сердюченко (Д. П.), 1954. Доклады Акад. Наук. СССР (*Compt. Rend. Acad. Sci. URSS*), **96**, 1233.
- , 1960. Amphiboles from magnetite and phlogopite deposits of the Aldan. In *Iron Ores of south Yakutia*, publ. by Acad. Sci. U.S.S.R.
- SUNDIUS (N.), 1946. *Arsbok. Sver. geol. undersökn.*, ser. C, **40**, No. 4.

# Chemistry of hastingsitic amphiboles from the Marangudzi igneous complex, Southern Rhodesia

By C. M. B. HENDERSON B.Sc., Ph.D., D.I.C.

Department of Geology, Manchester University

*Summary.* The coeval silica-oversaturated and silica-undersaturated syenites from the Marangudzi igneous complex, Southern Rhodesia, contain amphiboles belonging to the iron-rich end of the solid-solution series pargasite-ferrohastingsite. Hastingsites from the undersaturated syenites have compositions approximating to  $(\text{Na, K})_{1.2}\text{Ca}_{1.9}(\text{Fe}^{2+}, \text{Mn, Mg})_{3.8}(\text{Fe}^{3+}, \text{Al, Ti})_{1.1}\text{Si}_{5.9}\text{Al}_{2.1}\text{O}_{22}(\text{OH, F})_2$ . Hastingsites from the oversaturated syenites are of distinctly different composition  $(\text{Na, K})_{0.9}\text{Ca}_{1.7}(\text{Fe}^{2+}, \text{Mn, Mg})_{4.3}(\text{Fe}^{3+}, \text{Al, Ti})_{0.8}\text{Si}_{6.5}\text{Al}_{1.5}\text{O}_{22}(\text{OH, F})_2$ . The most important differences are seen to be in Si, Al, Ca, and Na + K. The chemical compositions of the hastingsites are therefore directly related to the chemistry of the rocks in which they occur.

Amphiboles from both the undersaturated and oversaturated syenites range in composition from femaghastingsites to ferrohastingsites. In particular hastingsites from the undersaturated syenites show well developed iron-enrichment with differentiation. The colour of the hastingsites can be correlated with their relative proportions of  $\text{Fe}^{3+}$  and Ti; those with high  $\text{Fe}^{3+}$  are coloured green to blue-green while those with high Ti are coloured brown to red-brown.

THE amphiboles described in this paper come from the syenitic rocks of the Marangudzi igneous complex, Southern Rhodesia. This complex is particularly interesting in that it provides an opportunity to study the chemistry of hastingsitic amphiboles from coeval silica-oversaturated and silica-undersaturated igneous syenites. The geology and petrology of the Marangudzi complex have been fully described in the unpublished work of Rees (1960) and Gifford (1961). The complex consists of a large gabbro mass intruded by ring dykes of quartz syenite, cone sheets of nepheline syenite (nepheline monzonite, pulaskite, foyaite, and juvite) and a suite of tinguaitic dykes. The geochemistry and petrology of the complex will be published elsewhere (Henderson, in preparation), but it is relevant to give here the modal analyses of the rocks from which the amphiboles have been analysed (table I). Unfortunately no thin sections of R. 131 were available for point counting.

*Classification of hastingsitic amphiboles.* The general formula for amphiboles can be written:  $A_{0-1}X_2Y_3Z_8\text{O}_{22}(\text{OH})_2$ , where  $A = \text{Na, K}$ ;  $X = \text{Na, Ca, Mn, Mg, Fe}^{2+}$ ;  $Y = \text{Mg, Fe}^{2+}, \text{Fe}^{3+}, \text{Al, Ti, Mn}$ ;  $Z = \text{Si, Al, Ti}$ ; (OH) may be wholly or partly replaced by F and Cl. The classification of the Marangudzi amphiboles is based on the ideal hastingsite formula:  $(\text{Na, K})\text{Ca}_2(\text{Mg, Fe}^{2+})_4(\text{Al, Fe}^{3+},$

TABLE I. Modal analyses of Marangudzi rocks, (volume %)

	R.2	R.15	R.17	R.20	R.26	R.28†	R.31	R.76	R.133	R.174†	R.183	R.226	R.16	R.21	R.141	R.177	R.439	
Quartz	—	—	—	—	—	—	—	—	—	—	—	—	17.2	Tr.	6.8	8.6	3.6	Quartz
Perthite	60.0	70.7	55.7	62.8	54.2	45	72.0	69.3	73.2	65.6	65.7	65.2	50.6	64.6	81.7	79.2	73.4	Perthite
Nepheline	15.6	18.0	7.1	13.1	5.8*	40*	4.5*	8.1*	8.7	3.4*	17.0	27.7	—	—	—	—	—	Nepheline
Sodalite	4.4		1.6	5.5									—	—	—	—	—	—
Plagioclase	—	—	8.3	—	17.9	—	7.6	6.8	3.5	15.3	—	0.4	12.1	17.6	—	—	—	Plagioclase
Amphibole	19.3	9.4	25.6	17.8	21.1	9	12.8	12.8	14.0	7.9	15.1	6.7	17.6	16.0	11.1	11.3	10.7	Amphibole
Pyroxene	—	—	0.5	—	—	3	1.1	1.7	—	3.8	—	—	—	—	—	—	—	Pyroxene
Biotite	—	—	—	—	—	2	—	—	—	3.0	—	—	1.3	0.3	—	—	—	Biotite
Iron ore	0.7	1.9	0.7	0.8	0.3	1	1.5	0.8	0.6	0.7	—	—	1.2	1.5	0.3	0.4	3.8	Iron ore
Apatite	Tr	—	0.5	Tr	0.7	Tr	0.5	0.5	—	0.3	—	—	Tr	Tr	Tr	Tr	Tr	Apatite
Others	—	—	—	—	—	—	—	—	—	—	2.2	—	—	—	—	0.5	0.5	Others

\* Plus alteration products.

† Approximate modes only.

Tr=Trace amount.

*Undersaturated Rocks.*

R. 2, R. 20, R. 183 and R. 226 Foyaites  
 R. 17 Plagioclase-bearing foyaites  
 R. 15, R. 133 Microfoyaite  
 R. 26, R. 31, R. 76 Pulaskites  
 R. 28 Juvite  
 R. 131 Pseudoleucite-bearing tinguaites  
 R. 174 Nepheline monzonite

Marangudzi Complex, S. Rhodesia.

*Key to tables**Oversaturated Rocks.*

R. 16, R. 21, R. 439 Porphyritic quartz syenites } Marangudzi complex, S. Rhodesia.  
 R. 141, R. 177 Quartz syenites }

The amphiboles from each of the above rocks are identified by the respective numbers with the prefix A.

$(\text{Ti})\text{Si}_6\text{Al}_2\text{O}_{22}(\text{OH}, \text{F}, \text{Cl})_2$ . Solid solution within the hastingsite group can be considered in terms of the four end members: pargasite,  $\text{NaCa}_2\text{Mg}_4\text{AlSi}_6\text{Al}_2\text{O}_{22}(\text{OH})_2$ , ferropargasite,  $\text{NaCa}_2\text{Fe}_4^{2+}\text{AlSi}_6\text{Al}_2\text{O}_{22}(\text{OH})_2$ , hastingsite,  $\text{NaCa}_2\text{Mg}_4\text{Fe}^{3+}\text{Si}_6\text{Al}_2\text{O}_{22}(\text{OH})_2$ , and ferrohastingsite,  $\text{NaCa}_2\text{Fe}_4^{2+}\text{Fe}^{3+}\text{Si}_6\text{Al}_2\text{O}_{22}(\text{OH})_2$ .

Billings (1928) subdivided the hastingsite group on the basis of molecular proportion of  $\text{FeO}/\text{MgO}$ . Magnesiohastingsite, femaghastingsite, and ferrohastingsite were defined as having  $\text{FeO}/\text{MgO}$  ratios of respectively  $< \frac{1}{2}$ ;  $\frac{1}{2} < 2$ ;  $> 2$ . Borley and Frost (1963) subdivided hastingsites on the basis of  $\text{Fe}^{2+} \times 100 / (\text{Fe}^{2+} + \text{Mg})$  and gave the limits for magnesio-, femag-, and ferro-hastingsite as respectively 0 to 35, 35 to 65, and 65 to 100. Marangudzi hastingsites have relatively high Mn content and this has been included with  $\text{Fe}^{2+}$  to give the ratio  $(\text{Fe}^{2+} + \text{Mn}) \times 100 / (\text{Fe}^{2+} + \text{Mn} + \text{Mg})$ .

*Calculation of amphibole formulae.* One amphibole formula unit (there are two in the unit cell) contains a total of 24 anions, 22(O) and 2(OH, F, Cl). In the calculation of formulae from chemical analyses it is usual to recalculate the atomic proportions of the cations to 24(O, OH, F, Cl). It is well known that the chemical determination of  $\text{H}_2\text{O} +$  (combined water) and F are often imprecise and, in many cases, inaccurate. By recalculating an analysis to 24 anions this possible error is extended to the whole analysis, i.e. if  $\text{H}_2\text{O} +$  and F are underestimated cation numbers will be high and if  $\text{H}_2\text{O} +$  and F are overestimated they will be low. To get over this problem many people recalculate analyses on an anhydrous basis i.e. to 23(O). Phillips (1963) has criticized this procedure as it neglects the oxyamphibole type of substitution (where O replaces OH and  $\text{Fe}^{3+}$  replaces  $\text{Fe}^{2+}$ ). Binns (1965), however, considers it better to recalculate to 23(O); from knowledge of unit cell dimensions he shows that the calculated density usually agrees with the determined density much closer for recalculation to 23(O) than for recalculation to 24 anions. It is important to realise that for an amphibole with exactly 22(O) and 2(OH, F, Cl) in its formula, recalculations to 23(O) and to 24 anions give identical cation numbers. However, as (OH, F, Cl) deviates from two atoms so will the 23(O) cation numbers differ from those obtained by the 24 anion calculation. It is, therefore, misleading to compare directly amphibole formulae that have been calculated by the two different methods.

Marangudzi amphibole analyses have been recalculated to both 24 anions (table III, upper half) and 23(O) (table III, lower half) and it is interesting to note the numerical differences in cation numbers obtained for both calculations. For all amphiboles except A.28 and A.174 the (OH, F, Cl) group totals between 1.80 and 2.15; therefore these amphiboles show close agreement for the two sets of cation numbers. A.28 and A.174 have (OH, F, Cl) totalling 1.38 and 1.21 respectively and this deviation from two introduces considerable differences between the cation numbers calculated by the two different methods. Owing to the restricted amount of separated minerals it was not possible to make precise determinations for  $\text{H}_2\text{O} +$  on these two amphiboles and it seems

likely that the low totals for (OH, F, Cl) are due to  $H_2O+$  being underestimated. Under these circumstances formulae recalculated to 23(O) should be more reliable than those recalculated to 24 anions and the diagrams and discussion in this paper refer to the 23(O) formulae (table III, lower half).

*Chemistry of the amphiboles.* Eighteen amphiboles from Marangudzi rocks have been analysed, thirteen from undersaturated rocks and five from oversaturated rocks and the analyses are given in table II. Five of these analyses (A.2, A.15, A.20, A.76, and A.131) have been published by Borley and Frost (1963). Owing to confusion over its sample number the analysis of the amphibole from undersaturated rock R.131 was attributed by Borley and Frost to the quartz syenite R.141. The analysis of the amphibole that does come from R.141 is given in this paper and when the analyses of A.131 and A.141 are compared it is quite clear that A.131 comes from an undersaturated rock and A.141 from an oversaturated rock.

The chemical data show that there is a distinct difference in composition between the amphiboles from under- and oversaturated rock types. It is therefore convenient to discuss their formulae separately.

*The Z Group* contains the tetrahedrally co-ordinated<sup>1</sup> ions  $Si^{4+}$  (0.42 Å) and  $Al^{3+}$  (0.51), and where  $Si + Al$  is less than eight atoms it is assumed that  $Ti^{4+}$  (0.68) makes up the deficiency. In the undersaturated-rock amphiboles  $Si$  varies from 5.65 to 6.02 atoms, which is lower than the theoretical hastingsite formula, and this will be discussed later in the paper. The oversaturated rock amphiboles have higher  $Si$ , varying from 6.34 to 6.53 atoms, and lower  $Al$  than the above types.

*The Y group* contains the ions  $Fe^{2+}$  (0.74 Å),  $Mg^{2+}$  (0.66),  $Mn^{2+}$  (0.80),  $Fe^{3+}$  (0.64),  $Al^{3+}$ , and  $Ti^{4+}$  all in six-fold co-ordination. This group should contain a total of five atoms as required by the ideal hastingsite formula. The undersaturated-rock amphiboles have totals for  $Y$  group atoms of slightly less than five and vary from 4.84 (A.17) to 4.98 (A.28). The ideal hastingsite formula requires four atoms of ( $Fe^{2+}$ ,  $Mn$ ,  $Mg$ ) and one atom of ( $Fe^{3+}$ ,  $Al$ ,  $Ti$ ). In the undersaturated-rock amphiboles ( $Fe^{2+}$ ,  $Mg$ ,  $Mn$ ) totals less than four and varies from 3.54 (A.133) to 3.97 (A.131).  $Fe^{2+}$  shows a considerable range from 2.18 (A.17) to 3.25 (A.15) and  $Mg$  shows a corresponding decrease in amount.  $Mn$  is subordinate and increases with increasing  $Fe^{2+}$  but at a more rapid rate; thus the ratio  $Fe^{2+}/Mn$  decreases with increasing  $Fe^{2+}$  (table III, fig. 1h). The ( $Fe^{3+}$ ,  $Al$ ,  $Ti$ ) group usually totals more than one atom and its maximum is 1.38 atoms in A.133.

The oversaturated-rock amphiboles all contain an excess over five atoms in the  $Y$  group; the maximum is 5.25 in A.439. As there is a deficiency of atoms in the  $AX$  group for these amphiboles it is reasonable to assume that the excess could enter the  $X$  group replacing  $Ca$  (e.g. as in cummingtonites)—this will be

<sup>1</sup> Ionic radii given in this paper are all for six-fold co-ordination and are taken from Ahrens (1952)

TABLE II. Analyses and optical properties of Marangudzi hastingsites

	A. 2*	A. 15*	A. 17†	A. 20*	A. 26†	A. 28†	A. 31†	A. 76*	A. 131*	A. 133†	A. 174†	A. 183†	A. 226†	A. 16†	A. 21†	A. 141†	A. 177†	A. 439†	
SiO <sub>2</sub>	37.34	36.80	36.98	36.73	36.91	36.44	37.71	37.48	37.08	36.64	36.59	36.95	35.52	40.26	40.30	39.73	40.29	40.15	SiO <sub>2</sub>
TiO <sub>2</sub>	1.12	0.96	1.71	1.56	1.95	2.04	3.04	2.63	0.80	1.35	2.81	1.18	0.92	2.08	1.66	1.98	1.83	1.70	TiO <sub>2</sub>
Al <sub>2</sub> O <sub>3</sub>	10.92	10.15	13.43	12.08	13.31	13.58	11.25	11.74	11.77	13.16	14.51	12.18	13.13	9.24	8.05	7.75	7.01	8.94	Al <sub>2</sub> O <sub>3</sub>
Fe <sub>2</sub> O <sub>3</sub>	7.08	7.58	6.63	5.69	6.31	5.03	5.54	5.21	5.82	8.26	5.05	8.01	8.18	4.56	5.67	5.18	5.52	4.71	Fe <sub>2</sub> O <sub>3</sub>
MnO	20.40	23.74	16.60	21.43	17.94	17.32	19.50	19.16	22.02	18.34	16.90	19.25	18.32	22.16	19.75	27.16	27.19	21.38	MnO
MgO	0.94	1.57	0.58	0.90	0.63	0.34	0.63	0.78	1.33	0.85	0.38	0.95	1.57	0.63	0.70	0.81	0.80	0.61	MgO
CaO	4.30	1.95	5.71	3.73	5.62	6.89	5.35	5.58	3.46	4.27	6.35	3.74	4.09	5.22	6.94	2.22	2.11	6.60	CaO
Na <sub>2</sub> O	10.90	10.22	11.69	10.78	11.09	11.90	11.02	11.27	10.94	10.72	11.75	10.88	10.77	10.41	11.00	9.43	9.60	9.72	Na <sub>2</sub> O
K <sub>2</sub> O	2.87	2.94	2.39	2.68	2.47	1.76	2.29	2.25	2.54	2.63	2.09	2.56	2.57	2.13	2.10	2.16	2.19	1.94	K <sub>2</sub> O
H <sub>2</sub> O+	2.00	1.88	2.06	2.36	2.21	2.46	2.08	2.15	2.07	2.04	2.25	2.04	2.09	1.25	1.54	1.43	1.40	1.42	H <sub>2</sub> O+
F	1.03	0.98	0.81	1.06	0.82	0.45	0.88	0.82	0.87	1.03	0.40	0.94	0.79	0.52	0.59	0.94	1.04	0.65	F
Cl	1.51	2.06	2.6	1.57	2.0	1.8	1.9	1.84	1.94	2.1	1.6	2.2	2.4	2.5	2.5	2.2	1.7	2.8	Cl
Less O=F, Cl	0.10	0.05	—	0.08	—	—	—	0.16	0.14	—	—	—	—	—	—	—	—	—	Less O=F, Cl
Total	100.51	100.88	101.19	100.65	101.26	100.01	101.19	101.07	100.87	101.39	100.78	100.89	101.35	100.96	100.80	100.99	100.68	100.62	Total
α	1.701	1.710	—	1.692	1.696	1.702	1.696	1.700	—	—	—	—	—	—	1.689	1.708	1.706	1.692	α
<i>Pleochroism</i>																			
α	pale straw	pale straw	pale straw	pale straw	pale yellow	pale brown	pale brown	pale brown	—	pale straw	pale yellow-brown	pale straw	pale straw	pale brown-green	pale yellow	pale yellow	pale yellow	pale yellow	α
β	yellow-green	blue-green	yellow-green	brownish-green	brown-green	brown	green-brown	green-brown	—	yellow-green	green-brown	yellow-green	olive-green	olive-green	yellow-green	yellow-green	yellow-green	yellow-green	β
γ	deep green	deep bluish green	deep brown-green	deep green with brown tinge	deep brown-green	deep brown	very deep red-brown	deep brown	—	deep bluish green	deep brown	deep bluish green	deep bluish green	brown	deep brown green	deep brown green	brown-green	deep olive-green	γ

\* Analyst I. S. E. Carmichael (Borley and Frost, 1963).

† Analyst C. M. B. Henderson.

TABLE III. Analyses recalculated to 24 (O, OH, F, Cl) (upper half) and to 23 oxygen (lower half)

	A.2	A.15	A.17	A.20	A.26	A.28	A.31	A.76	A.131	A.133	A.174	A.183	A.226	A.16	A.21	A.141	A.177	A.439	
Si	6.00	6.00	5.78	5.89	5.79	5.79	5.95	5.92	5.97	5.77	5.75	5.88	5.79	6.37	6.37	6.42	6.54	6.34	Si
Al	2.00	1.95	2.22	2.11	2.21	2.21	2.05	2.08	2.03	2.23	2.25	2.12	2.21	1.63	1.50	1.48	1.34	1.66	Al
Ti	—	0.05	—	—	—	—	—	—	—	—	—	—	—	—	0.13	0.10	0.12	—	Ti
Z	8.00	8.00	8.00	8.00	8.00	8.00	8.00	8.00	8.00	8.00	8.00	8.00	8.00	8.00	8.00	8.00	8.00	8.00	Z
Al	0.07	—	0.25	0.18	0.26	0.33	0.04	0.11	0.20	0.21	0.44	0.17	0.24	0.09	—	—	—	—	Al
Ti	0.13	0.07	0.20	0.19	0.23	0.24	0.36	0.31	0.11	0.16	0.33	0.14	0.11	0.25	0.06	0.14	0.10	0.20	Ti
Fe <sup>3+</sup>	0.85	0.93	0.78	0.69	0.75	0.60	0.66	0.62	0.70	0.98	0.60	0.96	0.98	0.54	0.67	0.63	0.67	0.56	Fe <sup>3+</sup>
Fe <sup>2+</sup>	2.74	3.24	2.17	2.88	2.35	2.30	2.57	2.53	2.96	2.42	2.23	2.56	2.43	2.93	2.61	3.67	3.69	2.82	Fe <sup>2+</sup>
Mn	0.13	0.22	0.08	0.12	0.08	0.05	0.08	0.10	0.18	0.11	0.05	0.13	0.21	0.09	0.09	0.11	0.11	0.08	Mn
Mg	1.03	0.47	1.33	0.89	1.32	1.63	1.26	1.32	0.83	1.00	1.49	0.80	0.97	1.23	1.64	0.54	0.51	1.55	Mg
Y	4.95	4.93	4.80	4.95	4.99	5.15	4.97	4.99	4.98	4.88	5.14	4.85	4.94	5.13	5.07	5.09	5.08	5.21	Y
Ca	1.87	1.79	1.96	1.85	1.87	2.03	1.86	1.91	1.80	1.81	1.98	1.86	1.83	1.77	1.86	1.63	1.67	1.64	Ca
Na	0.89	0.93	0.73	0.83	0.75	0.54	0.70	0.69	0.79	0.80	0.64	0.79	0.79	0.65	0.64	0.68	0.69	0.59	Na
K	0.41	0.39	0.41	0.49	0.44	0.50	0.42	0.43	0.43	0.41	0.45	0.42	0.42	0.25	0.31	0.30	0.29	0.29	K
AX	3.17	3.11	3.10	3.17	3.06	3.07	2.98	3.03	3.11	3.02	3.07	3.04	2.67	2.81	2.61	2.65	2.52	2.52	AX
OH	1.10	1.07	0.84	1.13	0.86	0.48	0.92	0.86	0.93	1.08	0.41	1.00	0.83	0.55	0.62	1.01	1.12	0.69	OH
F	0.77	1.06	1.28	0.80	0.99	0.90	0.95	0.92	0.99	1.05	0.80	1.11	1.20	1.25	1.13	1.13	0.87	1.40	F
Cl	0.03	0.01	—	0.02	—	—	—	0.04	0.04	—	—	—	—	—	—	—	—	—	Cl
Total (OH)	1.90	2.14	2.12	1.95	1.85	1.38	1.87	1.83	1.96	2.13	1.21	2.11	2.03	1.80	1.87	2.14	1.99	2.09	Total (OH)
Si	5.98	6.02	5.79	5.89	5.78	5.71	5.93	5.90	5.96	5.79	5.65	5.90	5.79	6.34	6.35	6.44	6.53	6.35	Si
Al	2.02	1.96	2.21	2.11	2.22	2.29	2.07	2.10	2.04	2.21	2.35	2.10	2.21	1.66	1.50	1.48	1.34	1.65	Al
Ti	—	0.02	—	—	—	—	—	—	—	—	—	—	—	—	0.15	0.08	0.13	—	Ti
Z	8.00	8.00	8.00	8.00	8.00	8.00	8.00	8.00	8.00	8.00	8.00	8.00	8.00	8.00	8.00	8.00	8.00	8.00	Z
Al	0.04	—	0.27	0.17	0.23	0.22	0.01	0.07	0.19	0.24	0.30	0.19	0.25	0.06	—	—	—	—	Al
Ti	0.14	0.10	0.20	0.19	0.23	0.24	0.36	0.31	0.11	0.16	0.33	0.14	0.11	0.25	0.04	0.17	0.09	0.20	Ti
Fe <sup>3+</sup>	0.85	0.93	0.78	0.69	0.74	0.59	0.66	0.62	0.70	0.98	0.59	0.96	0.98	0.54	0.67	0.63	0.68	0.56	Fe <sup>3+</sup>
Y <sup>3+</sup>	1.03	1.03	1.25	1.05	1.20	1.05	1.03	1.00	1.38	1.22	1.29	1.34	0.85	0.71	0.80	0.77	0.78	0.78	Y <sup>3+</sup>
Fe <sup>2+</sup>	2.73	3.25	2.18	2.87	2.35	2.27	2.56	2.52	2.96	2.42	2.20	2.57	2.43	2.92	2.60	3.68	3.69	2.83	Fe <sup>2+</sup>
Mn	0.13	0.22	0.08	0.12	0.08	0.05	0.08	0.10	0.18	0.11	0.05	0.13	0.21	0.08	0.09	0.11	0.11	0.08	Mn
Mg	1.03	0.48	1.33	0.89	1.31	1.61	1.26	1.31	0.83	1.01	1.46	0.89	0.97	1.23	1.63	0.54	0.51	1.56	Mg
Y <sup>2+</sup>	3.89	3.95	3.59	3.88	3.74	3.93	3.90	3.93	3.97	3.54	3.71	3.59	3.61	4.23	4.32	4.33	4.31	4.47	Y <sup>2+</sup>
Y	4.92	4.98	4.84	4.93	4.94	4.98	4.93	4.93	4.97	4.92	4.93	4.88	4.95	5.08	5.03	5.13	5.08	5.25	Y
Ca	1.87	1.79	1.96	1.85	1.86	2.00	1.86	1.90	1.89	1.81	1.95	1.86	1.83	1.76	1.86	1.64	1.67	1.65	Ca
Na	0.89	0.93	0.73	0.83	0.75	0.54	0.70	0.69	0.79	0.81	0.63	0.79	0.79	0.65	0.64	0.68	0.69	0.60	Na
K	0.41	0.39	0.41	0.48	0.44	0.49	0.42	0.43	0.43	0.41	0.44	0.42	0.42	0.25	0.31	0.30	0.29	0.29	K
AX	3.17	3.11	3.10	3.16	3.05	3.03	2.98	3.02	3.11	3.03	3.02	3.07	3.04	2.66	2.81	2.62	2.65	2.54	AX
(Fe <sup>2+</sup> +Mn) <sub>100</sub>	73.6	87.9	62.8	77.1	65.0	59.0	67.9	66.7	79.1	71.6	60.6	75.2	73.2	71.0	62.3	87.6	88.2	65.2	(Fe <sup>2+</sup> +Mn) <sub>100</sub>
Fe <sup>2+</sup> +Mn+Mg	—	—	—	—	—	—	—	—	—	—	—	—	—	—	—	—	—	—	Fe <sup>2+</sup> +Mn+Mg
Fe <sup>2+</sup> /Fe <sup>3+</sup>	3.21	3.48	2.78	4.19	3.16	3.82	3.91	4.09	4.21	2.47	3.73	2.67	2.49	5.40	3.87	5.83	5.47	5.04	Fe <sup>2+</sup> /Fe <sup>3+</sup>
Fe <sup>2+</sup> /Mn	21.3	14.9	28.2	23.5	27.9	50.5	30.5	24.3	16.3	21.2	43.9	20.1	11.5	34.8	27.7	33.2	33.5	34.5	Fe <sup>2+</sup> /Mn
FeO/MgO (mole %)	2.66	6.83	1.63	3.22	1.79	1.41	2.05	3.22	5.15	2.41	1.50	2.89	2.51	2.38	1.60	6.87	7.23	1.82	FeO/MgO (mole %)

discussed in detail later. The (Fe<sup>2+</sup>, Mg, Mn) group contains more than four atoms, the maximum being 4.47 (A.439). Fe<sup>2+</sup> shows considerable variation from 2.60 (A.21) to 3.69 (A.177) and Mg shows a corresponding decrease from 1.63 (A.21) to 0.51 (A.177). Mn increases with increasing Fe<sup>2+</sup> but Fe<sup>2+</sup>/Mn remains fairly constant (table III, fig. 1h). (Fe<sup>3+</sup>, Al, Ti) totals less than one atom and shows a maximum of 0.85 in A.16.

Fe<sup>2+</sup>/Fe<sup>3+</sup> ratios in both over- and undersaturated rock amphiboles show haphazard variation but the ratio is generally higher in the former than in the latter.

The *AX* group contains the larger cations Ca<sup>2+</sup>(0.99 Å), Na<sup>+</sup>(0.97), and K<sup>+</sup>(1.33) in eight- or ten-fold co-ordination. The theoretical formula contains three atoms in this group two of which should be Ca. These two atoms are in the *X* group and Na and K enter the *A* group.

The undersaturated-rock amphiboles generally have an excess over three atoms in this group, the maximum being 3.17 in A.2. There is some correlation of Ca with Na, *i.e.* as Ca decreases Na increases. K remains fairly constant. In most of these amphiboles Na is in considerable excess over K and Na/K ratios vary up to 2. However A.28 and A.174 have much lower ratios (1.1 and 1.4) and it is interesting to note that both rocks R.28 and R.174 contain especially high K<sub>2</sub>O. R.28 contains pseudoleucites and R.174 major amounts of biotite.

In the oversaturated-rock amphiboles the *AX* group atoms always total less than three. A.21 contains higher Ca than the others but alkalis remain constant. Na/K ratios are higher than for the undersaturated rock amphiboles and are always greater than 2.

The (*OH*) group. It is relevant to discuss the composition of the OH group at this stage (see table III). The total is usually near two atoms except for R.28 and R.174. OH is fairly low with a maximum of 1.13 atoms. On the other hand F is high with a maximum of 1.40 atoms. Five of the amphiboles from the undersaturated rocks were analysed for Cl but very small amounts were found. This is surprising, especially for A.15, which comes from a rock in which the dominant feldspathoid is sodalite.

#### *Comparison with the ideal hastingsite formula*

Amphiboles from the undersaturated rocks have compositions approximating to the formula: (Na, K)<sub>1.2</sub>Ca<sub>1.9</sub>(Fe<sup>2+</sup>, Mn, Mg)<sub>3.8</sub>(Fe<sup>3+</sup>, Al, Ti)<sub>1.1</sub>Si<sub>5.9</sub>Al<sub>2.1</sub>O<sub>22</sub>(OH, F, Cl)<sub>2</sub>. The main deviation from the ideal hastingsite formula is in the high total alkali content and in the deficiency of divalent atoms in the *Y* group from the theoretical four atoms. This deviation could be attributed to the presence of a small amount of the amphibole mboziite, Na<sub>2</sub>CaFe<sub>3</sub><sup>2+</sup>Fe<sub>2</sub><sup>3+</sup>Si<sub>6</sub>Al<sub>2</sub>O<sub>22</sub>(OH)<sub>2</sub> (Brock *et al.*, 1964), in solid solution.

The oversaturated-rock amphiboles deviate considerably from the ideal

hastingsite formula and can be represented by the formula:  $(\text{Na, K})_{0.9}\text{Ca}_{1.7}(\text{Fe}^{2+}, \text{Mn, Mg})_{1.3}(\text{Fe}^{3+}, \text{Al, Ti})_{0.8}\text{Si}_{6.5}\text{Al}_{1.5}\text{O}_{22}(\text{OH, F})_2$ . This composition can be described as being a member of the hastingsite-rich end of a solid solution series with edenite ( $\text{NaCa}_2\text{Mg}_5\text{Si}_7\text{AlO}_{22}(\text{OH})_2$ ).

Phillips (1963) has devised a scheme by which the accuracy of amphibole analyses and formulae can be checked. He makes several assumptions regarding the occupancy of the various lattice sites, some of which seem to be unjustified when the Marangudzi amphiboles are investigated in detail.

He states that a deficiency in Si from six atoms in the *Z* group suggests analytical error. This limit of replacement of Si by Al (and Ti) has been accepted by most authors for a considerable time. He suggests that variation, from a total of five atoms in the *Y* group of more than 2% (*i.e.*  $\pm 0.1$  atom) and excess of Na, K, Ca in the *AX* group over three atoms both suggest analytical errors. And he recommends that an amphibole analysis is reliable if it satisfies the condition  $[\text{Na}]_X + [\text{Al}]_Z = [\text{Na}]_A + [\text{Al}]_Y$ . In this formula atoms of Na in the *A* group include K and atoms of Al in the *Y* group include  $\text{Fe}^{3+}$  and equivalent Ti (see Phillips, 1963).

Amphiboles from Marangudzi undersaturated rocks all have Si less than six atoms (except for A.15). The variation is from 5.65 (A.174) to 5.98 (A.2). The deficiency in A.174 is approximately 6% and is much greater than analytical error should be. Most published mineral analyses are presumably done by classical methods and deficiency of Si is usually attributed to loss of soluble  $\text{SiO}_2$  to the  $\text{R}_2\text{O}_3$  precipitate. Most of the Marangudzi amphiboles had  $\text{SiO}_2$  determined by the usual classical scheme (*i.e.* two dehydrations) but  $\text{SiO}_2$  on two amphiboles was determined by a combined gravimetric and colorimetric method (Jeffery and Wilson, 1960). A.17 and A.133 were determined with two dehydrations and A.17 was repeated with one dehydration; soluble  $\text{SiO}_2$  was determined colorimetrically on all three filtrates. The soluble  $\text{SiO}_2$  after two dehydrations was determined as 0.05% for A.17 and 0.06% for A.133. Total  $\text{SiO}_2$  contents were 37.06% and 36.64% respectively. Soluble  $\text{SiO}_2$  in A.17 after one dehydration was 1.71% and total  $\text{SiO}_2$  was 36.90%.

These figures show very close agreement for A.17 and it seems that as long as two dehydrations are carried out the amount of  $\text{SiO}_2$  escaping precipitation is minute. A check on the accuracy was gained by the analysis of W-1 in triplicate. The three figures determined were 52.31, 52.50 and 52.41 wt.%, an average of 52.41%. The recommended value is either 52.64% (Fleischer and Stevens, 1962) or 52.58% (Ingamells and Suhr, 1963). Dr. I. S. E. Carmichael analysed five of the Marangudzi amphiboles and his lowest Si content in the formula was 5.89 atoms for A.20. It seems that slight deficiency of Si below six atoms (and excess of Al over two atoms) can occur in the *Z* group in the amphiboles. The undersaturated rock types in which these amphiboles occur are all high in  $\text{Al}_2\text{O}_3$ , and it seems that the  $\text{Al}_2\text{O}_3$  content of the magma and its state of saturation play a decisive part in controlling the Si/Al ratio in the *Z* group of these amphiboles.

Amphiboles from Marangudzi undersaturated rocks have high total alkalis and Na+K+Ca is in slight excess of three atoms. The maximum content is 3.17 in A.2 and A.20. This excess is approximately 6% and is greater than analytical error. The same amphiboles have slight deficiencies in the Y group and it seems possible that some Ca is replacing Mg in the Y group. The excess of alkalis over one in the A group also seems to balance the excess of Al in the Z group. In the oversaturated rock amphiboles the Y group atoms total more than five. As these amphiboles have AX less than three atoms it is likely that this excess may enter the X group replacing Ca (as in cummingtonite) and this is substantiated below. It is likely that Y group elements will enter the X group in the order of preference Mn, Fe<sup>2+</sup>, Mg (Ghose, 1965).

When the reliability of the amphibole analyses is checked according to Phillips' (1963) method (i.e. [Na]<sub>X</sub>+ [Al]<sub>Z</sub>=[Na]<sub>A</sub>+ [Al]<sub>Y</sub>) it is found that the undersaturated-rock amphiboles satisfy this condition very closely (table IV). This is so even though Al>2 in Z and Na+K>1 in A. It therefore seems reasonable to accept these departures from the ideal formula as being real and not due to analytical error. In the oversaturated-rock amphiboles this condition is not satisfied because of the excess of Y group atoms over five. However, when this excess is added to the X group (as in cummingtonite) and the formulae recalculated the condition is seen to be closely satisfied (table IV). It is therefore reasonable to conclude that this excess of Y group atoms is replacing Ca in the X group.

TABLE IV Formulae recalculated to show correspondence of [Na]<sub>A</sub>+ [Al]<sub>Y</sub> with [Na]<sub>X</sub>+ [Al]<sub>Z</sub>

	[Na] <sub>A</sub> + [Al] <sub>Y</sub>	[Na] <sub>X</sub> + [Al] <sub>Z</sub>		[Na] <sub>A</sub> + [Al] <sub>Y</sub>	[Na] <sub>X</sub> + [Al] <sub>Z</sub>		[Na] <sub>A</sub> + [Al] <sub>Y</sub>	[Na] <sub>X</sub> + [Al] <sub>Z</sub>
A. 2	2.16	2.15	A. 131	2.15	2.15	A. 177	1.52	1.67
A. 15	2.17	2.17	A. 133	2.41	2.41	A. 439	1.51	2.00
A. 17	2.23	2.25	A. 174	2.41	2.40			
A. 20	2.27	2.26	A. 183	2.24	2.25	A. 16*	1.84	1.82
A. 26	2.36	2.37	A. 226	2.38	2.38	A. 21*	1.60	1.60
A. 28	2.28	2.29	A. 16	1.76	1.90	A. 141*	1.72	1.71
A. 31	2.22	2.21	A. 21	1.56	1.64	A. 177*	1.60	1.59
A. 76	2.21	2.20	A. 141	1.59	1.84	A. 439*	1.76	1.75

\* Recalculated after addition of excess ions in Y group to X group.

*Petrological considerations.* It has been shown that there are considerable differences in composition between amphiboles from the Marangudzi silica over- and undersaturated rocks. The principal differences are in the lower Si, higher Al, higher Na+K, and slightly higher Ca of the undersaturated-rock amphiboles. These differences reflect the main variations in major element composition between the two rock series.

Iron enrichment in a differentiated series of mafic minerals has been well established (e.g. Skaergaard pyroxenes). For a genetically related series of amphiboles those from early formed rocks should have smaller values for an iron-enrichment function of the type 100(Fe<sup>2+</sup>+ Mn)/(Fe<sup>2+</sup>+ Mn+ Mg) than those from progressively later-formed rocks. In the Marangudzi undersaturated rocks a differentiated suite of syenites from nepheline-monzonite-pulaskite-

foyaite-microfoyaite can be identified from their mineralogy, their major and trace element composition (Henderson, in preparation), and their order of intrusion (Rees, 1960; Gifford, 1961). The amphiboles from this rock series show increasing values for the iron-enrichment function (table III). Juvitic nepheline syenites do not fit into this differentiated rock series but their mineralogy and chemistry show them to be of early formation even though field evidence shows them to be of late intrusion. Their early formation is confirmed by A.28 having the lowest value for the iron-enrichment function.

Variations in the concentration of other elements are well shown by plotting numbers of atoms against  $100(\text{Fe}^{2+} + \text{Mn})/(\text{Fe}^{2+} + \text{Mn} + \text{Mg})$ . Fig. 1 shows the variation of Si, Al, Ca, Na, K, Ti, Mn, and  $\text{Fe}^{2+}/\text{Mn}$ . The differences in composition between amphiboles from over- and undersaturated rocks are well shown for Si, Al, Ca, Na, and K. The undersaturated-rock amphiboles show fairly regular increase of Si, Na, and Mn and decrease of Al, Ca, Ti, and  $\text{Fe}^{2+}/\text{Mn}$  with increase in  $100(\text{Fe}^{2+} + \text{Mn})/(\text{Fe}^{2+} + \text{Mn} + \text{Mg})$  (*i.e.* with differentiation)

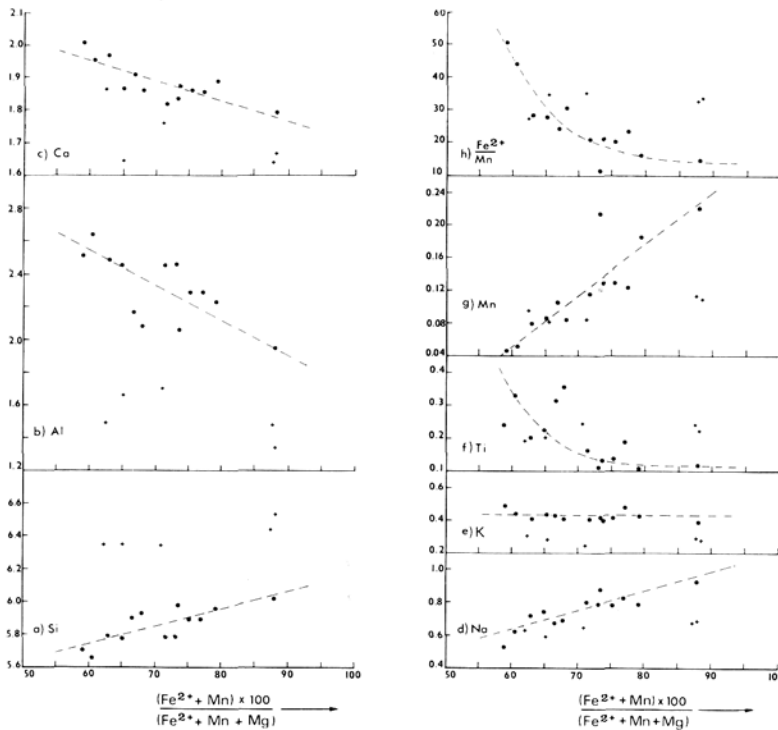


FIG. 1. Variation of Si, Al, Ca, Na, K, Ti, Mn, and  $\text{Fe}^{2+}/\text{Mn}$  with the iron enrichment function  $(\text{Fe}^{2+} + \text{Mn}) \times 100 / (\text{Fe}^{2+} + \text{Mn} + \text{Mg})$ . ● Hastingsites from Marangudzi undersaturated rocks, + hastingsites from Marangudzi oversaturated rocks. The dotted lines show the approximate trends of composition within the undersaturated rock hastingsites.

whilst K remains fairly constant. These variations are similar to those occurring in silicate magmas during differentiation. The oversaturated rock amphiboles show little sensible variation for any of these elements.

Substitution of  $\text{Fe}^{2+}$  for Mg has been used as a basis of classification for hastingsites (Billings, 1928; Borley and Frost, 1963). A differentiated suite of hastingsites could, therefore, show variation from magnesio- to femag- to ferrohastingsites. Amphiboles from Marangudzi over- and undersaturated rocks show similar ranges in  $100(\text{Fe}^{2+} + \text{Mn})/(\text{Fe}^{2+} + \text{Mn} + \text{Mg})$ : 62.3–88.2 for the former and 59.0–87.9 for the latter. Both series, therefore, range from femag- to ferrohastingsites.

Other series of genetically related hastingsites have been described from the metamorphosed calc-alkaline Adirondack granites (Buddington and Leonard, 1953) and from the alkaline Nigerian granites (Borley and Frost, 1963). Adirondack hastingsites have values for  $100(\text{Fe}^{2+} + \text{Mn})/(\text{Fe}^{2+} + \text{Mn} + \text{Mg})$  varying from 54.1–87.8, a similar range to Marangudzi amphiboles. However, Nigerian hastingsites have a higher range of values for this function and vary from 69.5–95.7. Marangudzi oversaturated-rock amphiboles are very similar in composition to those from Nigeria but contain slightly higher Si and lower Al than those from Adirondacks. However, Marangudzi undersaturated-rock amphiboles contain lower Si, higher Al, higher Na + K, and slightly higher Ca than amphiboles from the Adirondack and Nigerian granites. The Marangudzi undersaturated-rock amphiboles, therefore, show the same differences in composition from amphiboles from the oversaturated rocks of Marangudzi, Adirondacks, and Nigeria.

*Colour of amphiboles.* Over a period of years many authors have considered the relationship between the colour and chemical composition of hornblendes. Barnes (1930) heated common green hornblende at  $800^\circ\text{C}$  and transformed it to brown hornblende with almost complete oxidation of  $\text{Fe}^{2+}$  to  $\text{Fe}^{3+}$  and loss of H (as  $\text{H}_2\text{O}$ ) from the hydroxyl group. By reheating in an atmosphere of H he was able to reverse this reaction. In this case the colour was shown to be dependent on the oxidation state of the Fe; however in most natural hornblendes (including oxyhornblendes) the  $\text{Fe}^{2+}/\text{Fe}^{3+}$  is much higher than in Barnes' heated variety. The effect of oxidation state of iron on colour might therefore be less in natural minerals. Deer (1950) described phenocrysts of brown hornblende with rims of green hornblende from Glen Tilt appinites. Groundmass green hornblende was present as smaller grains and was the same composition as the rims of the phenocrysts. The green hornblende was found to have higher Si and lower Al, Ti, and  $\text{Fe}^{2+}/\text{Fe}^{3+}$  ratio than the brown variety.

Seitsaari (1953) correlated the blue-green colour of some hornblendes with their high  $\text{Fe}^{3+}/\text{Fe}^{2+}$  ratios and high  $\text{H}_2\text{O}+$  contents. Wilkinson (1961) suggested that the brown mineral barkevekite was similar in its chemical composition to  $\text{TiO}_2$ -poor green and blue-green hastingsites. However, Borley and Frost (1963) point out that some brown barkevekites have lower  $\text{TiO}_2$

contents than green hastingsites. The only difference in chemical composition seems to be that of deficiency of  $H_2O+$  in barkevekites. Whether this is real or denotes analytical error is not clear. The major factors affecting the colour of barkevekites and hastingsites are complex and are not yet understood.

Binns (1965) showed that hornblendes from a series of metamorphic rocks change colour from bluish-green to deep brown varieties with increase in metamorphic grade. He correlated the change in colour with the content of  $Fe^{3+}$  and Ti in the minerals. Thus increasing Ti and decreasing  $Fe^{3+}$  accompany colour changes from blue-green to brown.

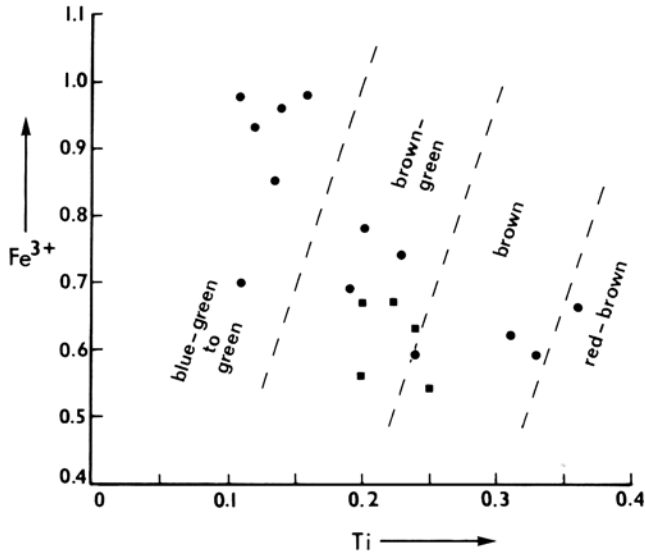


FIG. 2. Variation of  $Fe^{3+}$  with Ti and its relation to colour in the amphiboles. ● Hastingsites from Marangudzi undersaturated rocks, ■ hastingsites from Marangudzi oversaturated rocks.

Marangudzi hastingsites from undersaturated rocks show decreasing Ti with differentiation. This is accompanied by a change in colour from brown in early formed varieties to blue-green in late formed varieties. This relationship is well seen in fig. 2. There is no relationship between colour and  $Fe^{2+}/Fe^{3+}$  ratio. The amphiboles from the oversaturated rocks show little variation in Ti and are all coloured brown-green.

In this series of genetically related hastingsites the colour change can be related to variation in their content of Ti and  $Fe^{3+}$ ; it seems that high  $Fe^{3+}$  (relative to Ti) can be correlated with green or blue-green colours and high Ti (relative to  $Fe^{3+}$ ) with brown to red-brown colours. The actual mechanism controlling the colour variation must be complex and may be associated with

the presence of  $Ti^{3+}$  ions or charge transfer between Ti and Fe ions. However, this is merely speculation and is outside the scope of the present paper.

The amphiboles with strong brown pleochroism (*e.g.* A.31 and A.174) could be called barkeveekites, but it is preferable to refer to the whole series of Marangudzi amphiboles as members of the hastingsite group. Extensive variation in chemical composition occurs in this series of amphiboles and variation of only one element (*e.g.* Ti) does not warrant a separate name for individual amphiboles.

*Acknowledgements.* I would like to thank Professor W. S. MacKenzie for his useful criticisms of this paper. This research work was begun in the Geology Department, Imperial College during the tenure of a D.S.I.R. Studentship and completed in the Geology Department, Manchester University during the tenure of a N.E.R.C. Research Assistantship.

#### References

- AHRENS (L. H.), 1952. *Geochimica Acta*, **2**, 155.  
 BARNES (V. E.), 1930. *Amer. Min.*, **15**, 393.  
 BILLINGS (M.), 1928. *Ibid.*, **13**, 287.  
 BINNS (R. A.), 1965. *Min. Mag.*, **35**, 306.  
 BORLEY (G.) and FROST (M. T.), 1963. *Ibid.*, **33**, 646.  
 BROCK (P. W. G.), GELLATLY (D. C.), and VON KNORRING (O.), 1964. *Ibid.*, **33**, 1057.  
 BUDDINGTON (A. F.) and LEONARD (B. F.), 1953. *Amer. Min.*, **38**, 891.  
 DEER (W. A.), 1950. *Geol. Mag.*, **87**, 181.  
 FLEISCHER (M.) and STEVENS (R. E.), 1962. *Geochimica Acta*, **26**, 524.  
 GHOSE (S.), 1965. *Min. Mag.*, **35**, 46.  
 GIFFORD (A. C.), 1961. *The Geology of Southern Rhodesia*. Unpublished Ph.D. Thesis, University of London.  
 INGAMELLS (C. O.) and SUHR (N. H.), 1963. *Geochimica Acta*, **27**, 897.  
 JEFFERY (P. G.) and WILSON (A. D.), 1960. *Analyst*, **85**, 478.  
 PHILLIPS (R.), 1963. *Min. Mag.*, **33**, 701.  
 REES (G.), 1960. *The geology of West Marangudzi*. Unpublished Ph.D. Thesis, University of London.  
 SEITSAARI (J.), 1953. *Bull. Comm. géol. Finlande*, no. 159, 83.  
 WILKINSON (J. F. G.), 1961. *Amer. Min.*, **46**, 340.

*Appendix giving analytical methods.* The analysed amphiboles were separated from crushed and sieved material of mesh size  $-80$  to  $+120$ . Initial separation was made using the Frantz Isodynamic Separator, followed by centrifuging in Clerici solution. Final purification was made by hand picking under a binocular microscope. The separated minerals were mounted in an oil of similar refractive index to the mineral and purity was determined by counting grains. All samples except A.28 and A.174 were found to be greater than 99.5% pure; A.28 and A.174 were found to be approximately 98% pure with diopside pyroxene as the main impurity.

Classical gravimetric analysis was used in the determination of  $SiO_2$ ,  $R_2O_3$ , CaO, and MgO for all except two amphiboles. For these  $SiO_2$  was determined by a combined gravimetric and colorimetric method (Jeffery and Wilson, 1960) and  $R_2O_3$ , CaO, and MgO determined in the usual gravimetric way. Colorimetric methods were used to determine  $TiO_2$  and MnO, and alkalis were determined on the flame photometer. Total iron was determined by titration with stannous chloride, and FeO by the ammonium metavanadate method.  $H_2O+$  was determined by fusing the sample with a mixture of lead oxide and lead chromate. The water was condensed on the sides of a test-tube and collected on a weighed piece of filter paper.

For amphiboles A.28 and A.174 only a little material was available for determination of  $H_2O+$  and the results are, therefore, thought to be imprecise. F was determined by emission spectrography by measuring the intensity of the CaF bandhead at  $5291 \text{ \AA}$ ; chemically analysed amphiboles were used as standards; precision is thought to be in the region of  $\pm 15-20\%$ .

## Redox behaviour of amosite

W. E. ADDISON and J. H. SHARP\*

(Chemistry Department, University of Nottingham)

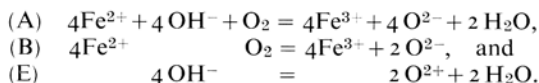
*Summary.* The oxidation of amosite (fibrous grunerite,  $\text{Fe}_{5.5}\text{Mg}_{1.5}\text{Si}_8\text{O}_{22}(\text{OH})_2$ ) proceeds by a combination of the reactions (A)  $4\text{Fe}^{2+} + 4\text{OH}^- + \text{O}_2 \rightarrow 4\text{Fe}^{3+} + 4\text{O}^{2-} + 2\text{H}_2\text{O}$  and (B)  $4\text{Fe}^{2+} + \text{O}_2 \rightarrow 4\text{Fe}^{3+} + 2\text{O}^{2-}$ , which were proposed by Addison *et al.* (1962a) to describe the oxidation of the related amphibole, crocidolite, and by Hodgson, Freeman, and Taylor (1965b) in the case of amosite. The extent of reaction (A) does not increase beyond  $550^\circ\text{C}$ , whereas that of reaction (B) increases with increasing temperature. Reaction (A) is probably limited by magnesium blocking of the electron-transfer process rather than by lack of hydroxyl groups.

When fresh or oxidized amosite is heated in hydrogen at 500 to  $600^\circ\text{C}$ , reduction of iron(III) to iron(II) occurs, but no iron(0) is produced as in the case of crocidolite. It is suggested that reduction occurs by combination of the reactions (C)  $4\text{Fe}^{3+} + 4\text{O}^{2-} + 2\text{H}_2 \rightarrow 4\text{Fe}^{2+} + 4\text{OH}^-$  and (D)  $4\text{Fe}^{3+} + 2\text{O}^{2-} + 2\text{H}_2 \rightarrow 4\text{Fe}^{2+} + 2\text{H}_2\text{O}$ , which are the converse of reactions (A) and (B) respectively. The water formed during the reduction of oxidized amosite is probably produced by reaction (D) rather than from breakdown of the amphibole.

Further discussion of the oxidation of crocidolite below  $500^\circ\text{C}$  is included; there is general agreement between the investigations of Addison *et al.* (1962a, b) and Hodgson, Freeman, and Taylor (1965a), although minor differences are discussed.

AMOSITE ( $\text{Fe}_{5.5}\text{Mg}_{1.5}\text{Si}_8\text{O}_{22}(\text{OH})_2$  approx.) is the fibrous form of the amphibole grunerite, and is of commercial importance as a form of asbestos. The oxidation, reduction, and thermal decomposition of two fibrous amphiboles, crocidolite and amosite, have been the subjects of several recent papers (Addison *et al.*, 1962a, b, c; Hodgson *et al.*, 1965a, b; Hodgson, 1965; Patterson, 1965; Patterson and O'Connor, 1966). The authors of these papers are in general agreement with respect to the experimental observations and their interpretation, except for a few relatively minor points, some of which are discussed below.

It has been shown that when amosite (Hodgson, Freeman, and Taylor, 1965b) or crocidolite (Addison *et al.*, 1962a, b; Hodgson *et al.*, 1965a) is heated in air or oxygen, three reactions can occur. These are summarized by the equations:



Hodgson, Freeman, and Taylor (1965b) have proposed the terms "dehydrogenation" and "oxygenation" for reactions (A) and (B) respectively. Dehydrogenation occurs at lower temperatures than dehydroxylation (reaction E) and is accompanied by a slight weight loss but results in no breakdown of the

\* Present address: Department of Ceramics, University of Sheffield.

structure, leading instead to the formation of an oxyamphibole. Oxygenation, however, adds anions to the material and is, therefore, accompanied by a weight gain. No water is liberated in this process.

The reduced form of crocidolite after reaction with hydrogen at 450°C appears from X-ray diffraction and infra-red spectroscopy to be an unchanged amphibole (Addison *et al.*, 1962c; Hodgson *et al.*, 1965a), yet contains iron in an oxidation state lower than two and most probably zero, perhaps concentrated near the surface. At higher temperatures the amphibole breaks down with formation of metallic iron and other phases.

The present paper describes the reactions that occur when amosite is heated in oxygen and hydrogen and compares the behaviour with that of crocidolite.

### Experimental methods and results

The sample of amosite, which was supplied by the Cape Asbestos Company, was from Penge, South Africa and is that described by Hodgson *et al.* (1965b) as PRS<sub>3</sub>. Its chemical analysis and atomic ratios are shown in table I, and correspond approximately to the formula (Na, K, Ca, Mn)<sub>0.3</sub>Fe<sub>5.3</sub>Mg<sub>1.4</sub>(Si, Al)<sub>8</sub>O<sub>22</sub>(OH)<sub>2</sub>. Two size fractions were used, *viz.* fibres approximately 5 cm in length, and fiberized material, *i.e.* after grinding to decrease the fibre length.

TABLE I. Chemical analysis and atomic ratios for amosite PRS<sub>3</sub>

	1		2	3	4			
SiO <sub>2</sub>	49.8	Si	7.88	7.92	7.88	}	7.99	Z
Al <sub>2</sub> O <sub>3</sub>	0.6	Al	0.11	0.05	0.11			
Fe <sub>2</sub> O <sub>3</sub>	0.4	Fe <sup>III</sup>	0.05	0.06	0.05			
FeO	40.1	Mg	1.41	1.45	1.41	}	5.00	Y
MgO	6.0	Fe <sup>II</sup>	5.27	5.30	3.54			
MnO	0.5				1.73	}	2.02	X
CaO	1.0	Mn	0.07	0.07	0.07			
Na <sub>2</sub> O	0.09	Ca	0.17	0.15	0.17			
K <sub>2</sub> O	0.12	Na	0.03	0.03	0.03			
CO <sub>2</sub>	0.2	K	0.02	0.03	0.02			
H <sub>2</sub> O <sup>+105</sup>	2.0	H	2.11	1.99				

1. Chemical analysis. H<sub>2</sub>O<sup>+105</sup> is likely to result in a high value for H (Addison *et al.*, 1962a, p. 1468; Hodgson *et al.*, 1965b, p. 462). Analyst, W. Bennis.
2. Atomic ratios calculated from col. 1, based on total O = 24. CO<sub>2</sub> in col. 1 was assumed to be produced from Fe<sub>0.8</sub>Mg<sub>0.2</sub>CO<sub>3</sub> (Hodgson *et al.*, 1965b, p. 447).
3. Mean atomic ratios for 10 specimens of amosite from the Penge area (Hodgson *et al.*, 1965b, p. 447).
4. A possible allocation of atoms to sites.

The methods of studying the oxidation and reduction reactions were described by Addison *et al.* (1962a). In each experiment, a weighed sample was treated with either oxygen or hydrogen at a fixed temperature and pressure (about 0.5 atmospheres), usually until apparent equilibrium was reached. The volume of gas sorbed and the amount of water liberated were determined. The reaction

of oxygen was studied only with the original amosite, but that of hydrogen was studied both with the original amosite and with material that had been oxidized in a previous run. The results are listed in table II.

The colour of the fibres changed from grey-white to brown on oxidation and reverted to grey-white on subsequent heating in hydrogen. Infrared spectra showed the presence of hydroxyl groups in all samples that had been heated in hydrogen.

TABLE II. Oxidation and reduction of amosite

Gas	Sample	Temperature (°C)	Gas uptake* (ml./g.)	Fe oxidized or reduced† (atoms/mole)	Molar water yield‡ (mole/mole)
O <sub>2</sub>	amosite (5 cm. lengths)	450	0.76	0.13	—
O <sub>2</sub>	amosite (5 cm. lengths)	550	4.00	0.68	—
O <sub>2</sub>	amosite (5 cm. lengths)	610	8.08§	1.38	1.14
O <sub>2</sub>	amosite (fiberized)	450	4.20	0.72	—
O <sub>2</sub>	amosite (fiberized)	550	9.57	1.63	1.44
O <sub>2</sub>	amosite (fiberized)	610	16.19	2.76	0.82
H <sub>2</sub>	amosite (5 cm. lengths)	615	2.06	0.18	—
H <sub>2</sub>	oxidized amosite (fiberized)	550	19.03	1.62	0.45
H <sub>2</sub>	oxidized amosite (fiberized)	610	40.33	3.43	0.67

\* ml. O<sub>2</sub> or H<sub>2</sub> at N. T. P./g. amosite.

† Atoms of Fe oxidized or reduced/mole of amosite, assuming that Fe<sup>II</sup> and Fe<sup>III</sup> are the only oxidation states involved, and that 1 "mole" of amosite contains the formula weight, 953.7.

‡ Moles of H<sub>2</sub>O liberated per mole of O<sub>2</sub> or H<sub>2</sub> sorbed.

§ After 30 days, reaction apparently complete.

|| After 3 days, reaction not complete.

### Discussion

*Oxidation of amosite.* It can be seen from the data of table II that the extent of oxidation of amosite increases both with increasing temperature and with decreasing particle size. The amounts of water formed during the oxidations are in accordance with the proposition (Hodgson *et al.*, 1965c) that oxidation proceeds by a combination of dehydrogenation (reaction A) and oxygenation (reaction B); a molar water yield of 2.00 is expected from the former process, whereas no water is produced by the latter.

The molar water yield from fiberized amosite oxidized at 550°C was 1.44, indicating that 72% of the oxygen uptake was due to dehydrogenation and 28% to oxygenation, whereas at 610°C 41% was due to dehydrogenation and 59% to oxygenation. From these values it may be calculated that, for fiberized material, the number of Fe<sup>2+</sup> ions per mole of amosite oxidized through the

dehydrogenation reaction is 1.17 at 550°C and 1.13<sup>1</sup> at 610°C. These figures suggest that dehydrogenation reaches a maximum extent, which is independent of increasing temperature. On the other hand, the total oxygen uptake and, therefore, that due to oxygenation increase with increasing temperature.

This upper limit to dehydrogenation is not caused by deficiency of iron(II) or hydroxyl groups. A possible explanation is provided by the magnesium blocking hypothesis (Addison *et al.*, 1962a), which is discussed below.

*Reduction of amosite.* When fresh amosite was heated in hydrogen at 610°C a slight reaction occurred in which iron(III) was reduced to iron(II). In spite of the high iron content, the amount of hydrogen reacting was very small, so that there is no evidence for the formation of any iron in an oxidation state lower than II, as when crocidolite is heated in hydrogen (Addison and Sharp, 1962c).

Similarly when oxidized amosite is heated in hydrogen the uptake is about that calculated to reduce the iron(III) to iron(II), including not only that formed in the oxidation, but also that present initially and that produced by fiberization. It may seem that the production of water is evidence for a breakdown of the amphibole structure, but an alternative explanation is considered more likely. It was shown above that oxygenation is more extensive in the oxidation of amosite than in that of crocidolite. Just as the reaction (C)  $4 \text{Fe}^{3+} + 4 \text{O}^{2-} + 2 \text{H}_2 \rightarrow 4 \text{Fe}^{2+} + 4 \text{OH}^-$  is the converse of dehydrogenation (reaction A), so the reaction (D)  $4 \text{Fe}^{3+} + 2 \text{O}^{2-} + 2 \text{H}_2 \rightarrow 4 \text{Fe}^{2+} + 2 \text{H}_2\text{O}$  is the converse of oxygenation. Reaction (D) describes the mechanism by which the additional oxide ions produced on oxygenation are removed on reduction, with the formation of water, and could account for the molar water yields listed in table II. These additional oxide ions are present, not in the amphibole structure, but in other phases.

#### *Further discussion of the oxidation of crocidolite*

As stated above, the investigations of the oxidation of crocidolite by Addison *et al.* (1962a, b) and by Hodgson *et al.* (1965a, b) are in good agreement. There are two items of disagreement: Hodgson *et al.*, suggest, firstly that oxygenation does not occur below 600°C and secondly that lack of hydroxyl groups, rather than magnesium blocking, limits the extent of oxidation at 450°C in the case of the South African specimens that were studied.

On the basis of careful determinations of the amount of water produced, Addison *et al.* (1962a) proposed that oxygenation occurs to a small extent at 450°C. The molar water yields were always around 1.9 whereas reaction (A) predicts 2.0; hence it was proposed that further oxidation occurred by reaction (B). An oxygen uptake due to oxygenation of about 0.6 ml./g. would account for the low molar water yields. Hodgson *et al.* (1965a), who used different techniques, were unable to obtain evidence for this small amount of oxygenation.

<sup>1</sup> This figure would have been slightly higher had the reaction been allowed to continue for more than 3 days.

To determine whether oxygenation can occur at 450°C in the absence of dehydrogenation, a sample of crocidolite anhydride was oxidized. It was prepared by heating South African crocidolite at 600°C *in vacuo* for 48 hours and reacted at 450°C with 1.98 ml. O<sub>2</sub>/g., which is equivalent to 0.33 atoms of iron oxidized/mole. No water was produced during the oxidation. Although this experiment seems to support the hypothesis that oxygenation of fresh crocidolite can occur below 500°C, it is likely that crocidolite anhydride, which must contain many defects, will undergo oxygenation more readily than fresh crocidolite.

*The magnesium blocking hypothesis.* This hypothesis was proposed by Addison *et al.* (1962a) to explain the incomplete oxidation of iron(II) in South African crocidolite at 450°C. It was suggested that oxidation is limited not by lack of hydroxyl groups but by the occupation of adjacent  $M_1$  sites by magnesium ions, which prevent the transfer of electrons from iron(II) ions in the interior of the structure to iron(III) ions on the surface, where it is likely that dehydrogenation takes place.

The principal evidence for the hypothesis was the observation that fiberized crocidolite (which was partially oxidized during the grinding process) reacted with more oxygen than unfiberized crocidolite. Secondly, an inverse relation was observed between the uptake of oxygen and the magnesium content of three South African crocidolites. However, it has been shown by Hodgson *et al.* (1965a) that the dehydrogenation of South African crocidolite proceeds until all (or nearly all) hydroxyl groups have reacted and that further reaction proceeds by oxygenation. Magnesium blocking may prevent dehydrogenation, which involves the migration of electrons, but not oxygenation, which involves the migration of ions. It seems then that fiberized crocidolite may react to a greater extent than unfiberized crocidolite because its larger surface area permits further oxygenation.

The oxidation of Bolivian crocidolite, on the other hand, appears to stop at 450°C before all hydroxyl groups have been removed (Addison *et al.*, 1962a). This material has a higher Mg(II) and lower Fe(II) content than the South African specimens, so that it seems to be a genuine example of dehydrogenation prevented by magnesium blocking rather than by lack of hydroxyl groups.

Hodgson *et al.* (1965b) invoked the hypothesis to account for the relative stability to dehydrogenation of amosite, which has a higher magnesium content than crocidolite. In crocidolite, however, the  $M_1$  sites are mostly occupied by sodium (Whittaker, 1949), whereas they contain mostly iron(II) in cummingtonite (Ghose, 1961, 1965; Fisher, 1966), and presumably in grunerite and amosite also. Since the iron(III) cation is relatively small, it is unlikely that an amphibole containing appreciable quantities of iron(III) in the  $M_1$  sites would be stable. It is possible, however, that a few ions of iron(III) could have a transient existence in  $M_1$  sites in order to maintain the electron transfer process. To form a complete block, it would be necessary to have either four cations

other than iron together in the adjacent  $M_1$  and  $M_4$  sites or three cations other than iron in the  $M_2$  and  $M_3$  sites, as shown in fig. 1. Ghose (1961, 1965) and Fisher (1966) suggest that there is ordering in the cummingtonite-grunerite series that favours the concentration of magnesium at  $M_2$ , thereby increasing the possibility of three adjacent magnesium ions in the two  $M_2$  and the  $M_3$  sites.

This factor, coupled with the considerable change in crystal (lattice) energy associated with the change in composition, make it difficult to generalize about the relative ease of oxidation of crocidolite and amosite. Such considerations, however, are of no importance when samples of different particle size but of the same composition are compared. The number of atoms of iron(II) converted to iron(III) by dehydrogenation of fiberized amosite is much greater than that of 5 cm. lengths at all three temperatures investigated. This is in accordance with the magnesium-blocking hypothesis, since the process of fiberization increases the possibility of electrons released from iron(II) ions in the interior of the amphibole reaching iron(III) ions on the surface without encountering any magnesium blocks.

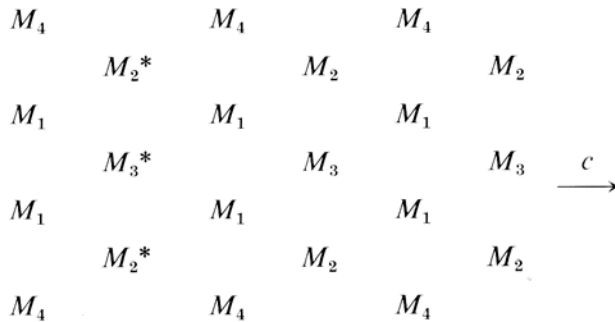


FIG. 1. Ribbon of cations in amphibole;  $M^*$  = cation other than Fe(II) or Fe(III) (usually Mg).

The electrical conductivity of crocidolite falls as Fe(II) is replaced by Mg(II) (Littler and Williams, 1965). This seems to support the hypothesis since it indicates that the probability of transfer of an electron from an iron(II) ion in the structure to an iron(III) ion on the surface is reduced by the presence of additional magnesium ions. However, the position is more complicated than the simple hypothesis illustrated in fig. 1; although the conduction depends on the presence of Fe(II)–Fe(III) pairs it does not depend on a continuous series of such pairs, since the electron can “jump” around a single magnesium block.

Finally, it should be emphasized that the hypothesis refers only to the *extent* of dehydrogenation and cannot account for the *temperature* at which the reaction commences.

*Acknowledgements.* The authors wish to thank Prof. H. F. W. Taylor and Dr. A. D. White for helpful discussions, the directors of Cape Asbestos Company Ltd. for financial support and the supply of samples, and the Department of Scientific and Industrial Research for a grant for J. H. S.

*References*

- ADDISON (C. C.), ADDISON (W. E.), NEAL (G. H.), and SHARP (J. H.), 1962a. *Journ. Chem. Soc.*, 1468.
- ADDISON (W. E.), NEAL (G. H.), and SHARP (J. H.), 1962b. *Ibid.*, 1472.
- and SHARP (J. H.), 1962c. *Ibid.*, 3693.
- FISHER (K. F.), 1966. *Amer. Min.*, **51**, 814.
- GHOSE (S.), 1961. *Acta Cryst.*, **14**, 622.
- , 1965. *Min. Mag.*, **35**, 46.
- HODGSON (A. A.), 1965. *Ibid.*, 291.
- , FREEMAN (A. G.), and TAYLOR (H. F. W.), 1965a. *Ibid.*, **35**, 5.
- — —, 1965b. *Ibid.*, 445.
- LITTLER (J. G. F.) and WILLIAMS (R. J. P.), 1965. *Journ. Chem. Soc.*, 6368.
- PATTERSON (J. H.), 1965. *Min. Mag.*, **35**, 31.
- and O'CONNOR (D. J.), 1966. *Aust. Journ. Chem.*, **19**, 1155.
- WHITTAKER (E. J. W.), 1949. *Acta Cryst.*, **2**, 312.

## The alkalic amphibole of the Lueshe carbonatite

By H. JANS and P. DE BÉTHUNE

Laboratory for Petrography,  
Louvain University, Belgium

*Summary.* Chemical, optical, and X-ray data on this amphibole are reported.

THIS alkalic amphibole, which has been mentioned in some earlier publications under the name of borgniezite, has been recognized in albite-aegirine rocks (sometimes with microcline); it is sometimes segregated in diffuse bands (metasomatic veins?). These rocks represent the eastern-country rock of the Lueshe carbonatite body in the province of Kivu, in the Republic of Congo, and have probably undergone strong alkaline metasomatism. A similar amphibole occurs exceptionally in the carbonatite itself. (A. Meyer and P. de Béthune, 1960). Its analysis and properties are given on p. 313.

This intermediate amphibole is related to richterites by high Ca-content in *X*, to magnesioriebeckite by vacant places (low *A*-content), to magnesioarfvedsonite by its  $\text{Fe}^{3+}$ -content in *Y*.

The values of the indices are those of an amphibole with a content of Mg of about 3 in the formula. The rather low birefringence is common in many alkalic amphiboles. The crossed axial plane dispersion or crossite orientation, combined with a rather small optic axial angle, are typical for a transition from magnesium-rich to iron-rich alkalic amphiboles. Large extinction angles are common in magnesioriebeckites, magnesioarfvedsonites, eckermannite, and some richterites. The pleochroism is typical for alkalic amphiboles; the discrepancy in orientation between the indicatrix and the absorption axes is discussed in the paper by P. de Béthune and H. Jans (1968). Optically and chemically it can be related to torendrikite, *sensu* Miyashiro (1957).

We experienced, like many others, difficulty in the determination of optical properties, due to strong dispersion, strong absorption, and anomalous extinction. We obtained excellent and clear images (and photographs) by using oil-immersion objectives and a set of monochromatic interference filters on sections selected with the Fedorov stage. In thicker sections the phenomena due to biabsorption become very distinct: incomplete extinction of sections perpendicular to an optic axis but with appreciable dichroism, polarization phenomena without analyser and even without both polarizers, eoptic figures. One should bear in mind, in all such cases, that the optics of strongly bi-absorbant crystals are much more complicated than those of transparent ones.

TABLE. Analysis and properties of an amphibole from the Lueshe carbonatite

SiO <sub>2</sub>	54.86	Si	7.865	} Z = 7.990
Al <sub>2</sub> O <sub>3</sub>	0.74	Al	0.125	
TiO <sub>2</sub>	0.33	Ti	0.035	} Y = 5.126
Fe <sub>2</sub> O <sub>3</sub>	10.70	Fe <sup>3+</sup>	1.154	
FeO	6.07	Fe <sup>2+</sup>	0.727	
MgO	15.03	Mg	3.210	
MnO	0.22	Mn	0.026	} X = 2.000
CaO	4.74	Ca	0.728	
Na <sub>2</sub> O	5.09	Na	1.246	} A = 0.264
K <sub>2</sub> O	0.53	K	0.096	
H <sub>2</sub> O <sup>+</sup>	1.73	O	22.336	} 24.000
H <sub>2</sub> O <sup>-</sup>	0.01	OH	1.664	
Total	100.05			

Analyst: Pentti Ojanperä

*Optical properties*

A. Analysed specimen B. Larger crystals from same locality

$\alpha$ 1.651	$\gamma$ 1.661	$\alpha$ 1.643	$\gamma$ 1.653
$\delta$ 0.010 (Na)		$\delta$ 0.010 (Na)	
2 V <sub><math>\alpha</math></sub> variable (O.A.P. $\perp$ 010), 25°-53°		2 V <sub><math>\alpha</math></sub> 38° blue (O.A.P. 010), nearly uniaxial green-yellow, 26°-30° red (O.A.P. $\perp$ 010)	

$\alpha$ : [001]	$\alpha$ : [001]	another specimen
{ blue 52°	{ blue 20°	40°
{ yellow 55°	{ yellow 26°	45°
{ red 58°	{ red 31°	49°

$\gamma = b$  (crossite orientation)       $\beta = b$  for blue to green-yellow,  $\gamma = b$  for yellow to red

*Physical properties other than optical:*

Density measured: 3.12, calculated 3.11  
 Hardness: between 5 and 6  
 Cleavage: {110} perfect, (110): (1 $\bar{1}$ 0) = 55° 40'; {010} parting frequent  
 Crystal faces: {110} nearly always present, (010) frequent  
 Crystal habit: elongated prismatical  
 Magnetic susceptibility:  $\chi = 28.4 \cdot 10^{-6}$  e.m.u. measured by means of the Frantz isodynamic separator. This value is in excellent agreement with the Vernon formula and diagram for iron-bearing amphiboles (Amer. Min. 1961, 46, 1141), the total of MnO, FeO, and Fe<sub>2</sub>O<sub>3</sub> (calculated as FeO) amounting in our case to 15.92 wt. %

Very strong bisectrix dispersion, strong horizontal dispersion, 2 V<sub>r</sub> > 2 V<sub>v</sub>

Extreme bisectrix dispersion, striking crossed-axial-plane dispersion, combined with strong inclined and horizontal dispersion

Pleochroism related to crystallographic and not to indicatrix axes is distinct in pale yellow  $\perp b$  and  $c$ , blue green  $\parallel c$ , grayish violet  $\parallel b$  absorption violet > blue green > yellow

*Unit cell:*

Orientation I2/m	Orientation C2/m
a 9.98 ± 0.04 Å	a 9.86 Å
b 18.07 ± 0.06 Å	b 18.07 Å
c 5.33 ± 0.02 Å	c 5.33 Å
$\beta$ 106.8° ± 0.4°	$\beta$ 104.3°

*Acknowledgements.* The authors wish to thank Prof. Th. G. Sahama for some data, and for his interest in this work.

*References*

- DE BÉTHUNE (P.) and JANS (H.), 1968. This vol., p. 315.  
MEYER (A.) and DE BÉTHUNE (P.), 1960. *Proc. Intern. Geol. Congress*, 21st Session, part 13, p. 304.  
MIYASHIRO (H.), 1957. *Journ. Fac. Sci. Univ. Tokyo*, **11**, 68.

## On the pleochroic formula of alkali amphiboles

By P. DE BÉTHUNE and H. JANS

Laboratory for Petrography,  
Louvain University, Belgium

*Summary.* The greenish-blue-violet-yellow pleochroism of these amphiboles should be referred to crystallographic axes and not to the axes of optical symmetry.

THE observations reported here relate to a "blue" amphibole, which is briefly described in another paper in this volume (H. Jans and P. de Béthune, 1967).

The pleochroism of this mineral as seen in thin section varies between tender shades of greenish blue, violet, and pale yellow, similar to those of glaucophane; some neutral greyish green tints occur also. These three colours fit in the general scheme of pleochroism of alkalic amphiboles where three colours are usually recognized as, for example: pale yellowish green, blue green, and greyish violet; pale yellow, blue green, and violet; pale brownish yellow, deep blue green, and deep yellowish green; almost colourless, blue, and purple; etc.

As one of us recognized quite a number of years ago (P. de Béthune, 1952) the colours should not be related to the axes of the indicatrix, as is usually done, but to three mutually perpendicular absorption axes. Similar observations have been made by Murgoci (1922), DeNaeyer (1924), De Roever (1947), Shoda (1956), and Miyashiro and Iwasaki (1957). It has been known for many years (e.g. Laspeyres, 1880), that in crystals of monoclinic or orthorhombic symmetry the absorption axes will not, in general, coincide with the axes of the indicatrix; this is fully discussed by Pockels (1906), but although referred to by Tutton (1922), it is overlooked in many modern texts on crystal optics.

The pleochroic scheme in our minerals is:

Light vibrating parallel to the axis of symmetry of the monoclinic crystals,  $b[010]$ , gives a violet colour.

Light vibrating parallel to  $c[001]$ , defined by the intersecting cleavages, gives a greenish blue colour.

The third axis, perpendicular to  $b$  and  $c$  and to the hexagonal rings in the amphibole chains, corresponds to no particular crystallographic axis. Light vibrating parallel to this axis undergoes minimal absorption and shows a pale yellowish tint or is almost colourless.

This scheme has been found to be consistently valid, not only for the Lueshe amphibole, but also for the other examples of blue amphiboles investigated.

It goes without saying that the coincidence of one absorption axis with the  $[001]$  crystallographic axis is accidental, as is the zero extinction angle and the  $\gamma(=\beta)$  pleochroism of most biotites. The surfaces for refractive indices and for

absorption are only coincident as far as is imposed by symmetry. It is therefore natural to assign absorption colours to absorption axes and not to indicatrix axes as is usually done. A complete analysis, taking these theoretical concepts into consideration is beyond the reach of ordinary polarizing equipment. The following discussion will indicate how the phenomena can be observed under the microscope.

The typical colours are those relative to the light-rays vibrating parallel to the absorption axes as defined above. In any section taken at random, the two rays vibrating along the directions of extinction show colours that are a mixture of the axial colours. If we chose a section where the direction of vibration coincides with, or approximates to, the axes of absorption, colours typical of these axes can be observed. Many such sections may be found in a thin section and oriented exactly on the Fedorov stage. This allows the rigorous investigation of the three principal sections (fig.).

The (100) section contains the absorption axes  $[010]$  and  $[001]$ . The rays vibrate parallel to these axes, and the resulting colours are therefore violet parallel to  $[010]$  and blue-green parallel to  $[001]$ .

The basal sections, perpendicular to  $[001]$ , contain  $[010]$  and the normal to (100); the rays vibrate parallel to these axes and the resulting colours are therefore violet parallel to  $[010]$  and pale yellow parallel to the normal to (100).

The (010) sections call for more detailed remarks. These sections contain the plane of symmetry of the crystals and two of the principal indices; they are one of the most important sections as far as birefringence is concerned. With regard to pleochroism we must distinguish two cases:

The first case is that of minerals with a small extinction angle like glaucophane (G1 on fig.), where the rays vibrate nearly parallel to the  $[001]$  and  $\perp(100)$  absorption axes. The colours shown by light vibrating along these directions differ only very slightly from the colours typical for these axes. The difference is hardly noticeable and the discrepancy with the usual way of expressing the pleochroic formula is not evident. This explains why the phenomenon with which we are concerned has escaped general attention.

In the second case, however, as exemplified by the Lueshe amphibole (L on fig.), the extinction angle is large and the vibration directions have a greater inclination to the absorption axes. The colour of light vibrating at an angle to these axes will be compounded according to the degree of inclination; the resulting colour is a neutral greyish green tint, intermediate between bluish-green and pale yellow. In so far as the extinction angle approximates to  $45^\circ$ , the second position of extinction is almost symmetrical and will show nearly the same tint; accordingly, such sections show very little pleochroism, if any, when the section is rotated with regard to the polarizer. These (010) sections, which are significant from other points of view, are thus quite dull, as far as pleochroism is concerned. In this second case one cannot therefore place the section with one absorption axis along the polarizer vibration direction and then repeat with the other axial direction. These sections are devoid of significance in this connection.

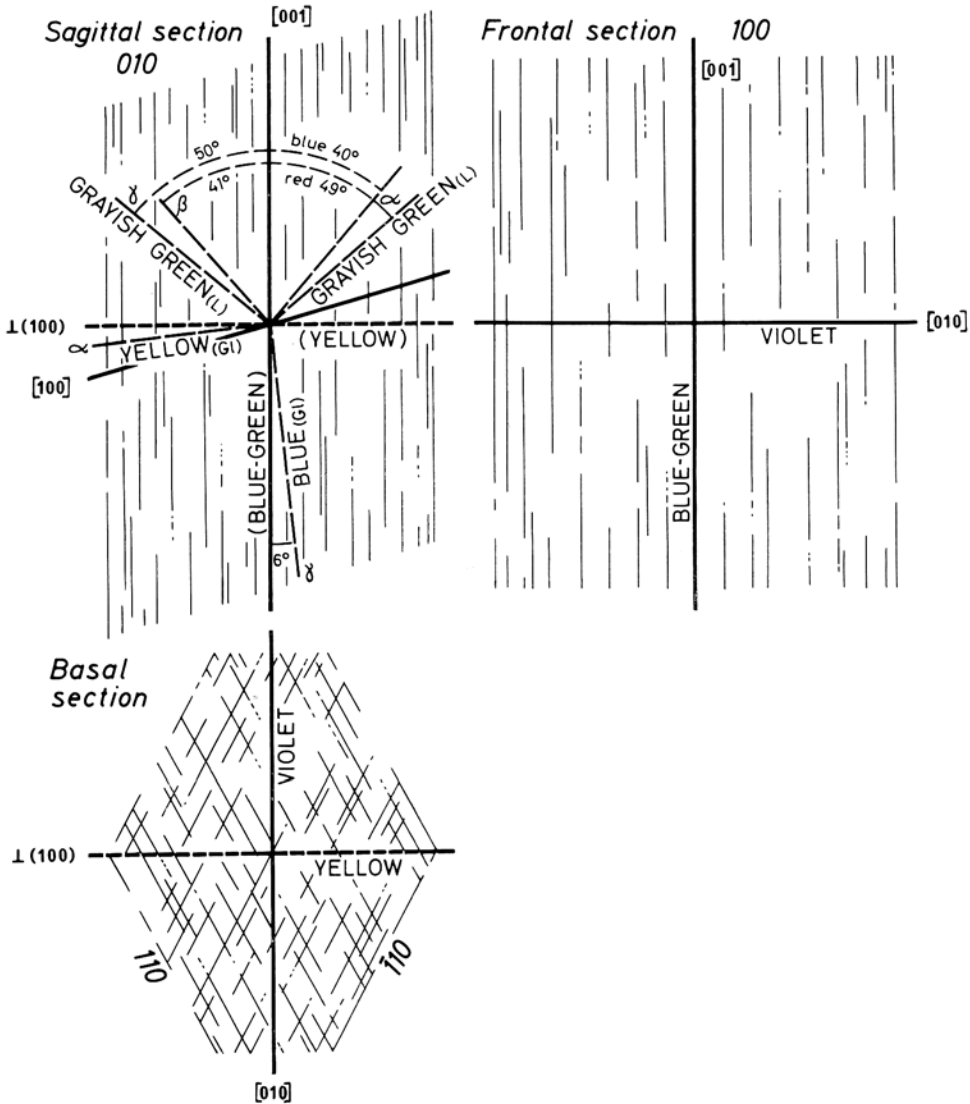


FIG. Orientation of the indicatrix and of the absorption ellipsoid in the Lueshe alkali amphibole.

Of course, besides the three principal sections described above, we find a full array of random sections where the pleochroism varies from somewhat greenish pale yellow or somewhat greyish violet to neutral greyish blue-green.

These observations call for a few general remarks:

The difficulty of relating the pleochroic colours of blue amphiboles to the principal indices  $\alpha$ ,  $\beta$ , and  $\gamma$  is well known. The pleochroic formulae tabulated in

any textbook of optical mineralogy (*e.g.* Winchell and Winchell, 1951) will show that there is no coherence between a particular colour and a particular index; the colours wander almost randomly from one column to the others, without any apparent rule. This may be partly due of course to the vagaries of the optical orientation; with crossed dispersion  $\beta$  changes even in position according to the wavelength. On the contrary, when the colours are related to the absorption axes, as defined here, the discrepancy disappears in every one of the cases that we have been able to investigate.

Our work has been limited, however, to a few alkali amphiboles only. It should be extended in order to find out if the explanation holds in other cases. The literature is deceptive in this respect, as the colours are usually related to the indices. An investigation of enough individual examples of alkali amphiboles should be undertaken to find out if this leads to a more coherent pleochroic formula for this group of minerals.

Augites are not pleochroic enough, and more strongly pleochroic minerals such as hornblende or aegirine have a small extinction angle, but other groups of monoclinic minerals with large extinction angles should be investigated with this view in mind, in order to find out if the explanation can be generalized.

If this explanation is found to hold in general it would mean that the absorption axes are unrelated to the indicatrix but are fundamentally related to the crystal structure. The pleochroic formula should therefore be expressed with regard to this structure rather than with respect to the axes of the optical indicatrix.

#### References

- DE BÉTHUNE (P.), 1952. *Mem. Inst. Géol.*, Univ. Louvain, **16**, 277.  
 DENAEYER (M.-E.), 1924. *Bull. Soc. franç. Min.*, **47**, 32.  
 DE ROEVER (W. P.), 1947. *Igneous and metamorphic rocks in eastern central Celebes*. Amsterdam. Pp. 65 ff.  
 JANS (H.) and DE BÉTHUNE (P.), 1968. This vol., p. 312.  
 LASPEYRES (H.), 1880. *Zeits. Kryst. Min.*, **4**, 454.  
 MIYASHIRE (A.) and IWASAKI (M.), 1957. *Journ. Geol. Soc. Japan*, **63**, 698 [M.A. 14-145].  
 MURGOCI (C.), 1922. *Compt. Rend. Acad. Sci. Paris*, **175**, 372.  
 POCKELS (F.), 1906. *Lehrbuch der Kristalloptik*. Leipzig. Pp. 363 ff.  
 SHODA (T.), 1956. *Min. Journ. Japan*, **2**, 39.  
 TUTTON (A. E. H.), 1922. *Crystallography and Practical Crystal Measurement*. 2nd edn (Macmillan, London), vol. 2, p. 1114.  
 WINCHELL (A. N.) and WINCHELL (H.), 1951. *Elements of Optical Mineralogy*, Part 2, p. 442.

## Some aspects of the chemical compositions of nonalkaline monoclinic pyroxenes from effusive rocks

By G. V. ГВАХАРИЯ  
(Г. В. Гвахария)

Geological Institute,  
Academy of Sciences of the Georgian SSR,  
Tbilisi, Georgia, U.S.S.R.

*Summary.* Chemical analyses and optical data are given for pyroxenes (essentially diopside-augites) from the effusive rocks of the Georgian SSR. Within a given formation, pyroxenes occurring as phenocrysts contain less iron than those of the matrix, and where the phenocrysts are zoned, iron contents rise on passing towards the edges of the crystal. The pyroxenes first separating from the magma are thus relatively low in iron, but as crystallization proceeds, the iron contents increase. The pyroxene compositions also depend on the nature of the region in which vulcanism occurred. The alkali contents of those from the geosynclinal regions are low or very low, but tend to increase as crystallization proceeds; vulcanism associated with the rigid-block substratum, in contrast, yields pyroxenes richer in alkalis. The two types of region also differ in the post-volcanic stage of mineralization, and especially in the zeolites produced, which are calciferous in the first case, and alkali-rich in the second.

A WIDE range of investigations has recently been carried out by the author and his associates into the pyroxenes that are so widely and variously represented in the area of the Georgian SSR. Their presence as rock-forming minerals is most marked in products of effusive vulcanism, which, in Georgia, began with the Middle Jurassic and, with some intervals, continued well into the Quaternary. Dzotsenidze (1948) and Skhirtladze (1958) were responsible for the petrographic study of effusive vulcanism in Georgia; rock-forming pyroxenes and amphiboles were studied by Gvakhariya *et al.* (1965).

The present paper deals with two specific problems, namely the evolution of the pyroxene content within a single lava-flow, and the relations between the pyroxene content and the conditions under which the effusive rocks containing it were formed.

Broadly conceived experimental investigations aimed at relating the optical properties of pyroxenes to their compositions do not permit the precise determination of chemical composition by this means. The systems discussed by Tomita (1934), Hess (1949), Veselovskaya (1950), Barth (1951), Tsvetkov (1951), Kuno (1955) and others fail to cover the great variety of chemical elements taking part in the isomorphous replacements of pyroxenes that significantly

affect their optical properties.<sup>1</sup> Nonetheless, the general pattern of optical properties permits the diagnosis of pyroxenes within a given group, and also the comparison of the chemical compositions of the various generations within a single lava-flow.

In the effusive formations of Georgia, two generations of pyroxenes stand out sharply, though this figure must be considerably increased if distinctive zones of dissimilar content, as observed here in zonal augites, are treated as separate generations. This view is held by some investigators. The two sharply-defined generations are macrocrystalline phenocrysts, which have grown freely, and microlites of the matrix.

In Georgia, mainly in Eocene eruptive products of andesitic-basaltic composition, single crystals of augite frequently attain a size of 2 to 3 cm and very interesting coalescent, intumescent, and interpenetrating twins are found.

Table I gives chemical analyses, optical properties, and atomic ratios for some Georgian augites. The analyses conform essentially with the composition of diopside-augite. Analyses 1 to 3 are for phenocrysts of diopside-augite from Eocene effusions; in them (FeO + Fe<sub>2</sub>O<sub>3</sub>) is 9 to 10% and alkalis are practically absent. Analysis 4, also for a diopside-augite from a Middle Eocene effusive formation, is not for a phenocryst but for microlites picked out by electromagnetic and electrostatic separation after extraction of the phenocrysts, with subsequent heavy-liquid separation of monomineralic fractions, which were checked by X-ray diffraction. The sum (FeO + Fe<sub>2</sub>O<sub>3</sub>) is in this case 13.79%. Comparison of analyses 1 to 3 with analysis 4 shows that augites of the matrix, when the latter is of the same formation, contain considerably more iron than do the augite phenocrysts.

In the phenocrysts themselves, several generations can frequently be distinguished, differing in degree of idiomorphism and colour. In all cases where measurement of optical constants was possible, idiomorphic grains proved less ferruginous than xenomorphic ones. The following are data from a thin section:

Type of grain	$2V_\gamma$	$\gamma : [001]$	Colour	Generation
Idiomorphic	56°	46°	Light	1st
Less idiomorphic	59°	48°	Darker	2nd
Xenomorphic	62°	48°	Dark	3rd

Microscopic study of a large number of thin sections showed that in zoned crystals the colour always becomes more intense on passing from the centre to the margins, with a pronounced trend towards a rise in refractive indices. In one section of a zoned crystal, it proved possible to measure the optical constants: the internal zone had  $2V_\gamma 52^\circ$ ,  $\gamma : [001] 42^\circ$ , while the outer zone had  $2V_\gamma 60^\circ$ ,  $\gamma : [001] 42^\circ$ .

<sup>1</sup> Petrov, in an editorial footnote to the Russian edition of Deer, Howie, and Zussman's (1965) handbook, rightly points out that the optical properties of pyroxenes are apparently linked with the degree of order in their structures. Study of the phenomena attendant on this state will, in the author's view, greatly aid the solution of a number of physico-chemical, structural, petrological, and geological problems.

TABLE I. Chemical analyses, optical properties, and atomic ratios for some Georgian augites. Nos. 1 to 4 from Gvakhariya *et al.* (1965), anal. V. I. Kobiashvili; no. 5 from Dzotsenidze (1948), anal. O. F. Razmadze; no. 6 from D. S. Belyankin, 1914.

	1	2	3	4	5	6
SiO <sub>2</sub>	49.98	48.93	49.24	48.17	47.36	48.21
TiO <sub>2</sub>	0.55	0.60	0.60	0.79	1.05	0.75
Al <sub>2</sub> O <sub>3</sub>	5.14	5.55	3.81	1.75	2.01	3.17
Fe <sub>2</sub> O <sub>3</sub>	3.78	5.02	4.81	7.73	4.70	3.52
FeO	5.20	3.29	5.82	6.06	7.94	6.87
MnO	0.11	0.09	0.14	0.11	0.21	0.15
CaO	20.68	21.93	21.54	19.43	20.07	19.24
MgO	13.90	14.26	13.79	15.59	14.76	15.48
K <sub>2</sub> O	traces	traces	traces	traces	0.66	0.39
Na <sub>2</sub> O	traces	traces	traces	0.25	1.02	1.32
H <sub>2</sub> O - 110°	0.16	0.17	0.02	0.14	0.42	0.75
H <sub>2</sub> O + 110°	0.20	0.09	0.10	0.09	0.08	2.01
Total	99.70	99.93	99.87	100.11	100.28	101.86
α	1.673	1.698	1.684	1.690		
			1.676			
γ	1.702	1.719	1.711	1.716		
γ : [001]	40-44°	45-48°	42-45°	42-48°	47°	
2 V <sub>γ</sub>	54-56°	55-64°	52-60°	50°	58°	47-55°
			0.027			
γ-α	0.029	0.021	0.026	0.026		

No. of ions in terms of 6 oxygen:

Si	1.851	1.81	1.841	1.81	1.815	1.76
Al	0.149	0.19	0.159	0.08	0.092	0.13
Fe <sup>3+</sup>	—	—	—	0.11	0.133	0.10
Al	0.075	0.054	0.006	—	—	—
Fe <sup>3+</sup>	0.106	0.137	0.134	0.11	0.04	—
Ti	0.015	0.017	0.018	0.025	0.03	0.02
Mg	0.766	0.787	0.768	0.88	0.84	0.84
Fe <sup>2+</sup>	0.159	0.102	0.181	0.20	0.133	0.21
Mn	0.002	0.002	0.004	—	0.008	—
Ca	0.819	0.869	0.862	0.78	0.817	0.75
K	—	—	—	—	0.032	0.02
Na	—	—	—	0.02	0.072	0.08
Mg	41.41	41.53	39.49	44.67	45.90	46.67
Fe	14.32	12.61	16.19	15.74	9.45	11.66
Ca	44.27	45.86	44.32	39.59	44.65	41.67

1. Augite from augite-porphyrite, Dagva (Upper Eocene).
2. Augite from andesite-basalt, Zvare (Middle Eocene).
3. Augite from globular lavas, Tashiscari (Middle Eocene).
4. Augite from the augite porphyrite matrix, Mt. Rabat, Akhaltsikhe (Middle Eocene).
5. Augite from augite-labradorite porphyrite, Mt. Bakhmaro (Upper Eocene).
6. Augite from diabase, Vesh-Tskharo (Middle Jurassic).

All the above data show that magnesium-lime diopside-augites were the first to crystallize from the magma, and that they were followed later by augites that were progressively richer in iron and apparently in alkalis. As has just been seen, this regularity is in evidence in crystal growth as well.

The second problem that will be discussed here concerns the connection between the chemical composition of the pyroxenes and that of the magma, taking into account the geological conditions under which the outpouring of the latter took place.

As was shown by Dzotsenidze (1948), vulcanism related to the geosynclinal areas (geosyncline of the southern slope of the main Caucasus range, the Adzhara

–Trialeti geosyncline) is represented in Georgia by rocks of the calc-alkali series, while vulcanism related to the rigid block substratum was in the nature of central-type outflows and rich in alkalis. The distinction between these two groups of rocks extends to the pyroxenes they contain. Analyses 1 to 4 (table I) are for augites of rocks of andesitic–basaltic composition confined to the Adzhara–Trialeti geosyncline; analyses 5 and 6 are for pyroxenes from rocks of the transitional zone between the geosynclinal area and the rigid block substratum. In the former case, pyroxenes are represented by diopside–augites in which the presence of alkalis is restricted to traces or to mere decimals of 1%, whereas in pyroxenes of the transitional zone (analyses 5 and 6) the alkali contents exceed 1.5%. While this does not change the essentially diopsidic character of the augites, potassium is nevertheless present in their compositions.

Gvakhariya *et al.* (1952), while studying the zeolites of Georgia, showed that there was a connection between postvolcanic mineralization and the composition of the parental lavas. In the one case typically calciferous zeolites were found such as thomsonite, stilbite, laumontite, and heulandite, and in the other case, zeolites rich in sodium (natrolite, analcime). In rocks of the transitional zone both types of zeolites were met with, the calciferous zeolites invariably showing some content of alkalis.

#### References

- BARTH (T. F. W.), 1949. *Norsk. Geol. Tids.*, **29**, 218.
- [BELYANKIN (D. S.)] Белянкин (Д. С.), 1914. К петрографии Архотского тоннеля. Геол. иссл. в области перев. жел. дороги глав. Кавказ. хребет. С.П.-Б. On the petrography of the Avkhotsk Tunnel. Geological study in the region of the railway line across the main Caucasian range. St. Petersburg.
- DEER (W. A.), HOWIE (R. A.), and ZUSSMAN (J.) Дир (У. А.), Хауи (Р. А.), и Зусман (Дж.), 1965. Пороодообраз. Мин. (transl. of *Rock-forming minerals*; ed. V. P. Petrov), vol. 2.
- [DZOTSENIDZE (G. S.)] Дзотсенидзе (Г. С.), 1948. Домиоц. эффузив. вулкан. Грузии. Монография по. 1, Акад. Наук Грузии. ССР, Инст. Геол. Мин. (Monograph no. 1, Acad. Sci. Georgian SSR, Inst. Geol. Min.)
- [GVAKHARIYA (G. V.)] Гвахария (Г. В.), 1952. Цеолиты Грузии. *Ibid.*, no. 3.
- [—, VEZIRISHVILI (E. K.), BAGRATISHVILI (T. D.), MANVELIDZE (R. M.), and AKHVLEDIANI (R. A.)] —, Везиришвили (Е. К.), Багратишвили (Т. Д.), Манвелидзе (Р. М.), и Ахвледиани (Р. А.), 1965. Матер. Мин. Грузии (пироксены и амфиболы). Акад. Наук Грузн. ССР, Инст. Геол. Мин. (*Materials for a mineralogy of Georgia (amphiboles and pyroxenes)*). Acad. Sci. Georgian SSR, Inst. Geol. Min.).
- HESS (H. H.), 1949. *Amer. Min.*, **34**, 621.
- KUNO (H.), 1955. *Amer. Min.*, **40**, 70.
- [SKHIRTLDZE (N. M.)] Схиртладзе (Н. М.), 1958. Постпалеоген. эффузив. вулканизм Грузии. Монография по. 8, Акад. Наук Грузии. ССР, Геол. Инст. (Monograph no. 8, Acad. Sci. Georgian SSR, Inst. Geol.)
- ТОМИТА (I.), 1934. *Journ. Shanghai Sci. Inst.*, sect. 2, 7, 41.
- [TsvETKOV (A. I.)] Цветков (А.И.), 1951. Труды Инст. Геол. Наук, (Trans. *Inst. Geol.*), **138**.
- [VESELOVSKAYA (M. M.)] Веселовская (М. М.), 1950. Труды Инст. Геол. (Trans. *Inst. Géol.*), **86**.

## Phase transitions of enstatite in the Earth's mantle

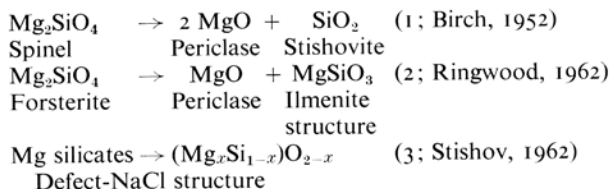
By V. A. KIRKINSKIИ  
(В. А. Киркинский)

Institute of Geology and Geophysics,  
U.S.S.R. Academy of Sciences, Akademgorodok,  
Novosibirsk 90, Siberia, U.S.S.R.

*Summary.* Various models of the mineral composition of the mantle, all of which satisfy the geophysical evidence, are considered from the viewpoint of thermodynamic equilibria at high temperatures and pressures. The reaction of periclase with stishovite to give an ilmenite form of  $MgSiO_3$  is considered and the changes in volume and in isobaric-isothermal potential evaluated. Calculations indicate that this form of  $MgSiO_3$  is unstable relative to periclase and stishovite at depths below 600 to 800 km. They do not support the view that a magnesium iron silicate with a defect-NaCl structure occurs in the mantle. Di-positive iron and magnesium replace each other isomorphously in all layers of the mantle. A sequence of transformations in the C-layer is proposed, on the basis of thermodynamic calculations, which accords with the geophysical evidence. It is suggested that, in the D-layer, stishovite occurs in equilibrium with (Mg, Fe)O of either periclase or caesium chloride structure.

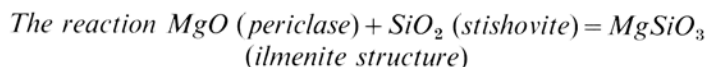
ACCORDING to present views oxygen, silicon, magnesium, and iron are the major constituents of the Earth's mantle, the average composition of which lies between those of forsterite and enstatite with 10 to 20% fayalite and ferrosilite.<sup>1</sup> It follows that knowledge of the phase transitions of enstatite, and also of equilibrium phase relations in the system  $MgO-FeO-SiO_2$  at high temperatures and pressures, is necessary for an understanding of the constitution of the mantle. Many hypotheses have been proposed regarding polymorphic transformations in the mantle, and particularly in its C-layer, but the nature of the phases present under the prevailing high pressures is still not definitely known.

According to the calculations of Ringwood (1962b), confirmed recently by experiment (Sclar, Carrison, and Schwartz, 1964), enstatite decomposes into forsterite plus stishovite under thermodynamic conditions corresponding to a depth of nearly 400 km. At 600 km. forsterite must transform to spinel, as predicted by Bernal (1936). For the transitions of  $Mg_2SiO_4$  with the spinel structure in the lower part of the C-layer, the following reactions have been proposed:

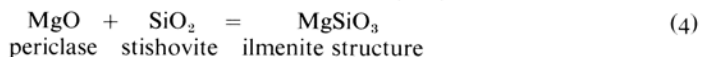


<sup>1</sup> See Green and Ringwood (1963), Levin (1955), Ringwood (1962a and b), and Vinogradov (1959a and b).

All three models are compatible with geophysical evidence of the increase in density with depth. Let us consider these models from the point of view of thermodynamic equilibrium at high temperatures and pressures.

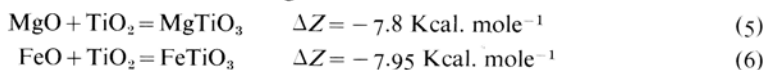


To compare the stabilities of the associations (periclase + stishovite) and (periclase + MgSiO<sub>3</sub> with the ilmenite structure) we shall estimate the volume effect and the change of isobaric-isothermal potential ( $\Delta Z$ ) for the reaction:



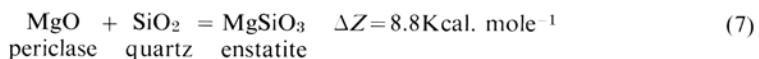
As noted by Ringwood (1962b), reactions of the type:  $AO$  (NaCl structure) +  $BO_2$  (rutile structure)  $\rightarrow ABO_3$  (ilmenite structure), where  $A = \text{Mg, Fe, Co, Ni, Mn, or Cd}$ , and  $B = \text{Ti or Ge}$ , are accompanied by an increase in volume ( $\Delta V$ ) of 1.5 to 4.0%.  $\Delta V$  for reaction (4) will not be less than for the reaction between MgO and GeO<sub>2</sub> (rutile structure), for which  $\Delta V = 4\%$ , because of the greater difference in size between the Mg<sup>2+</sup> and Si<sup>4+</sup> ions. As all the cations taking part in reaction (4) occupy octahedral sites, the compressibilities of the initial and final phases are approximately equal and  $\Delta V$  will decrease proportionally to the weighted mean compressibility of periclase and stishovite, determined in (1). On this basis, it can be calculated that the increase in volume in reaction (4) at 200 to 300 Kbar is approximately 1.1 cm<sup>3</sup> mole<sup>-1</sup>.

The isobaric-isothermal potential for (4) can be estimated from the values for the analogous reactions in which Mg and Fe titanates are formed:



For reaction (5) the change in  $\Delta Z$  with temperature can be calculated using Kirchoff's equation and the dependence of heat capacity on temperature reported by Zefirova (1965). This gives a value of 5.9 Kcal mole<sup>-1</sup> for  $\Delta Z$  at 1800°K for reaction (5). Energies of formation of complex oxides from simple ones are known to increase with the difference between their ionic radii or their polarizing properties;  $\Delta Z$  for MgO–SiO<sub>2</sub> reaction must therefore be somewhat higher than for reactions (5) and (6).

Another, independent way for estimating  $\Delta Z$  for reaction (4) is based on comparison with the reaction:



$\Delta Z$  for reaction (4) differs from  $\Delta Z$  for reaction (7) by ( $\Delta Z' + \Delta Z''$ ), where  $\Delta Z'$  and  $\Delta Z''$  are the changes in isobaric-isothermal potential for the quartz–stishovite and MgSiO<sub>3</sub>(ilmenite structure)–enstatite transformations. These values are not known, but it can be supposed that  $\Delta Z' \approx -\Delta Z''$ , as in the first case the energy change is associated with transition of Si<sup>4+</sup> ions from fourfold to sixfold co-ordination, and in the second case with the reverse transition.

$\Delta Z$  for reaction (4) should therefore not differ greatly from  $\Delta Z$  for reaction (7).

The above calculations suggest that for formation of  $\text{MgSiO}_3$  by reaction (4)  $\Delta Z$  will be around 6 to 8 kcal. mole<sup>-1</sup> at 1 800 to 3 000°K. In order to estimate the pressure corresponding to equilibrium in reaction (4) at the temperatures of the C-layer, we shall use the formula:  $p = -\Delta G_t/\Delta V$ , where  $\Delta G_t$  is the free energy of reaction at zero pressure and  $t$  is the temperature in the C-layer. If we now put  $\Delta Z = \Delta G_t$ , we find that the assemblage of periclase and stishovite will be stable relative to  $\text{MgSiO}_3$  with the ilmenite structure at pressures above 200 to 300 Kbar. This pressure is reached at a depth of 600 to 800 Km. Thus, there will be a transitional layer in which  $\text{Mg}_2\text{SiO}_4$  with the spinel structure decomposes into a mixture of periclase and stishovite. For  $\text{MgSiO}_3$  with the ilmenite structure, a narrow stability region is possible at depths of 600 to 800 Km.

*The hypothesis of a magnesium silicate of defect-NaCl structure*

Let us now consider the possibility of the existence in the mantle of a homogeneous magnesium silicate having a defect-NaCl structure, *i.e.* a phase consisting of close-packed oxide ions with magnesium, iron, and silicon ions in octahedral holes. This phase could also be described as a solid solution of widely variable composition, formed from  $\text{MgO}$ ,  $\text{SiO}_2$ , and also  $\text{FeO}$ .

To evaluate the minimum possible heat of mixing ( $\Delta H_{\text{mix}}$ ) between periclase and stishovite, we estimated the difference in unit cell volume for  $\text{MgO}$  and  $\text{SiO}_2$ . Proceeding from the data of Altshuller *et al.* (1965) on the compressibilities of periclase and stishovite at 0 to 4 000°K and pressures up to 2 500 Kbar, it can be calculated that at pressures of 400 to 1 000 Kbar this difference amounts to 43 to 49% of the smaller unit-cell volume ( $\text{SiO}_2$ ). This difference is greater than in the system  $\text{MgO-TiO}_2$ , which is analogous in crystal structure and chemical bond type, for which it is 19%. Therefore the heat of mixing between  $\text{MgO}$  and  $\text{SiO}_2$  (stishovite) must be greater, and the mixing much less than between periclase and rutile; the latter, according to Conghanour and de Prose (1953) does not exceed 0.1–0.2%. Hence we find that the heat of mixing between periclase and stishovite is not less than 25 Kcal. mole<sup>-1</sup>.

Various authors have estimated the temperatures in the deepest parts of the C-layer at 1 850 to 3 000°C (Gutenberg, 1963). The limits of miscibility in the  $\text{MgO-SiO}_2$  system at these temperatures can be calculated from the formula:  $c_1/c_2 = \exp[-\Delta H_{\text{mix}}(1/RT_1 - 1/RT_2)]$ , where  $c_1$  and  $c_2$  are limits of concentration at temperatures  $T_1$  and  $T_2$ ,  $R$  is the gas constant, and  $\Delta H_{\text{mix}}$  the heat of mixing. This gives  $c_2 = 2.4\%$  at  $T_2 = 3 000^\circ\text{K}$ , and  $c_2 = 3.4\%$  at  $T_2 = 3 400^\circ\text{K}$ . Even at 4 000°K the limiting concentration in the solid solution will not be more than 11%. Therefore, at the temperatures existing in the transitional layer and the upper parts of the D-layer, the isomorphous miscibility of components in the system  $\text{MgO-TiO}_2$  cannot exceed a few percent, and miscibility in the  $\text{MgO-SiO}_2$  system is likely to be still lower.

Let us now consider how the pressure, which is equal to 300 to 400 Kbar at

a depth of 800 to 1 000 Km, influences the miscibility of the components. The effect of pressure on isomorphous miscibility has been earlier considered by the present author (Kirkinskii, 1965, 1966). It has been shown that, in systems with the same cation co-ordination numbers, positive deviations from volume additivity usually take place, *i.e.*, increase in pressure favours the decomposition of the solid solutions. The extent of the decrease in miscibility at a given pressure  $p$  can be approximately estimated using the Planck–Van Laar equation, if the difference in the compressibilities of the solid phases is neglected:  $C_p/C_{p0} = \exp(-\Delta V(p-p_0)/RT)$ , where  $\Delta V$  is the volume change corresponding to solution of one mole of the component under consideration, *i.e.* the difference between the partial molar volume of this component when present in the solid solution and its volume when present as a pure compound.

$\Delta V$  for the formation of a solid solution  $(\text{Mg}_x\text{Si}_{1-x})\text{O}_{2-x}$  cannot be less than for the formation of  $\text{MgSiO}_3$  with the ilmenite structure, as the disordered arrangement of cations in the octahedral holes results in a more open structure. Thus  $\Delta V = 1.1$  to  $1.2 \text{ cm}^3 \text{ mole}^{-1}$ . Substituting this value, and putting  $T = 3\,000^\circ\text{K}$ , we find that at a pressure of 360 to 380 Kbar (*i.e.* a depth of 900 to 1 000 Km) the miscibility of the components will decrease by a factor of 4 or 5, and that at a pressure corresponding to a depth of 2 000 Km it will decrease by a factor of 60 to 70. Thus the highest possible miscibility of periclase and stishovite in the lowest part of the transitional layer will be only 1 to 2%.

On the basis of these data it can also be shown that at the geothermal-geobaric coefficients that exist in the *D*-layer of the mantle the miscibility of  $\text{MgO}$  and  $\text{SiO}_2$  will continue to decrease with depth, and that in the lower parts of the *D*-layer the extent of miscibility will be less than at depths of 900 to 1 000 Km. It must be emphasized that all assumptions in these calculations were made in such a way as to over- rather than underestimate the extent of miscibility. Thus the model of the Earth's mantle that is founded on the hypothesis of a homogeneous magnesium silicate with a defect- $\text{NaCl}$  type structure is not correct.

#### *Phase equilibria in the MgO–SiO<sub>2</sub> system*

The fig. shows schematically phase equilibria in the system  $\text{MgO}$ – $\text{SiO}_2$  as a function of pressure or depth. The phase boundaries are approximate, particularly at the highest pressures. The diagram gives a picture of the phase transformations that occur at either increasing depths in the mantle for any given ratio of  $\text{MgO}$  to  $\text{SiO}_2$ , or, approximately, of  $(\text{Mg}, \text{Fe})\text{O}$  to  $\text{SiO}_2$ . Although the extent of miscibility of  $\text{MgO}$  and  $\text{SiO}_2$  is insignificant, the calculations show that corresponding compounds of  $\text{Mg}^{2+}$  and  $\text{Fe}^{2+}$  are completely miscible at depths extending to the boundary of the Earth's core.

Direct experiments of many authors have shown that the pressures of transition to denser phases for Fe (or Ni) compounds differ considerably from those observed for isomorphous Mg compounds. With pyroxenes and olivines, the differences may amount to dozens of kilobars. Comparable differences may well occur for the formation of minerals of ilmenite structure, and for reactions of

decomposition into simple oxides. A second important cause of considerable spread in transition pressures is the positive slope of these pressures as a function of temperature; for example, for the decomposition of enstatite into forsterite and stishovite, Sclar and coworkers (1964) give the equation  $P = (97.5 \pm 5) + 0.027T$ . The geothermal  $P$ - $T$  curve thus intersects the equilibrium curves of  $P$ - $T$  diagrams at small angles, and the spread in transition pressures for solid solutions containing Mg and Fe is thereby increased. Other kinds of isomorphous substitution may also be significant in this respect. Iron substitution may even reverse the sequence of transitions found with the magnesium minerals.

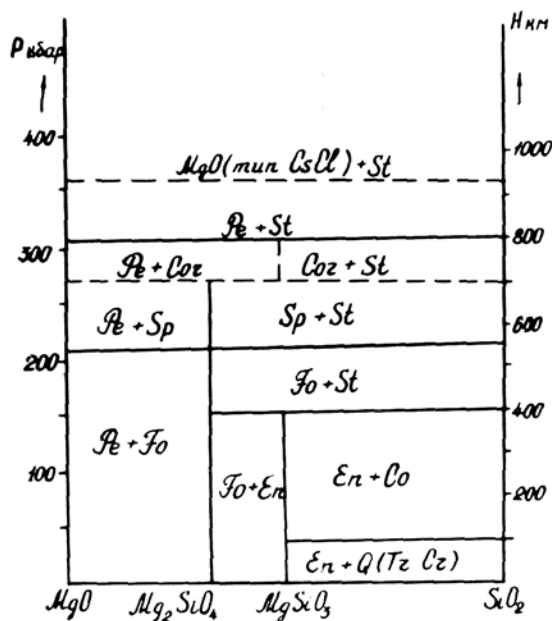


FIG. Suggested equilibria in the system MgO-SiO<sub>2</sub> as a function of pressure or depth. Pe=periclase, Fo=forsterite, En=enstatite, Q=quartz, Tr=tridymite, Cr=cristobalite, Co=coesite, St=stishovite, Sp=Mg<sub>2</sub>SiO<sub>4</sub> with the spinel structure, Il=MgSiO<sub>3</sub> with the ilmenite structure. Doubtful transitions are shown by broken lines.

These factors can explain the absence of sharp changes in the velocity of seismic waves within the mantle and the thickness of the layer over which these velocities change abnormally rapidly with depth. They remove the main objection to the hypothesis of polymorphism in the transitional layer of the mantle.

#### References

- [ALTSHULLER (L. V.), TRUNIN (R. F.), and СИМАКОВ (G. V.)] Алтшуллер (Л. В.), Трунин (Р. Ф.), и Симаков (Г. В.), 1965. Физика Земли (*Physics of the Earth*), no. 10, 1.  
 BERNAL (J. D.), 1936. *Observatory*, 59, 268.  
 BIRCH (F.), 1952. *Journ. Geophys. Res.*, 57, 227.

- CONGHANOUR (L. W.) and DE PROSSE (V. A.), 1953. *Journ. Res. Nat. Bur. Stand.*, **51**, 85.
- GREEN (D. H.) and RINGWOOD (A. E.), 1963. *Journ. Geophys. Res.*, **68**.\*
- [GUTENBERG (B.)] Гутенберг (Б.), 1965. Физ. Земн. Недр. ИЛ (*Physics of the earth's interior*).
- [KIRKINSKII (V. A.)] Клркинский (В. А.), 1965. Геол. Геофиз. (*Geology and Geophysics*), по. 3.
- , 1966. Геохимия (*Geochemistry*), 303.
- [LEVIN (B. YU.)] Левин (Б. Ю.), 1955. Состав Земли. (*Composition of the earth*) Труды Геофиз. Инст. (*Proc. Geophys. Inst.*), по. 26, 153.
- RINGWOOD (A. E.), 1962a. *Journ. Geophys. Res.*, **67**, 857.
- , 1962b. *Ibid.*, 4473.
- SCLAR (C. B.), CARRISON (L. C.), and SCHWARTZ (C. M.), 1964. *Ibid.*, **69**, 325.
- [STISHOV (S. M.)] Стишов (С. М.), 1962. Геохимия (*Geochemistry*), 989.
- [ZEFIROVA (A. P.), ed.] Зефирова (А. П.), ред., 1965. Термодинам. Свойст. Неорг. Веществ. (*Thermodynamic properties of inorganic compounds*. Publ. Atomizdat.
- [VINOGRADOV (A. P.)] Виноградов (А. П.), 1959a. Изв. Акад. Наук СССР, Сер. геол. (*Bull. Acad. Sci. URSS, ser. géol.*), по. 10, 5.
- , 1959b. Химическая Эволюция Земли. (*Chemical Evolution of the Earth*). Publ. Acad. Sci. USSR.

\* As this journal has no index, the Editor has not been able to add a page-reference.

# Über Kosmochlor (Ureyit)

A. NEUHAUS

Min. Inst. der Universität, Bonn

*Summary.* X-ray and optical data and electron-probe analyses show that ureyite (Fron­del and Klein, 1965) is identical with cosmochlore (kosmochlor; Laspeyres, 1897).

IN 1897 berichtete H. Laspeyres<sup>1</sup> dass er aus der zum Teil ziemlich dicken Rostrinde eines 12.5 kg schweren Toluca Meteoriten der Bonner Mineralien­sammlung kleine gestreckt-tafelige Kriställchen eines tief-smaragdgrünen, durch­ichtigen Minerals isoliert habe, das mit keinem bis dahin bekannten terre­strischen oder meteoritischen Minerale ident sei. Die chemische Analyse ergab ein sehr Cr-reiches Silikat, doch war die verfügbare Probemenge (0.0033 g.) für eine zuverlässige quantitative Analyse zu gering. Laspeyres gab diesem Mineral, wegen seiner meteoritischen Herkunft und seiner grünen Farbe, den Namen "Kosmochlor", modifiziert von E. S. Dana<sup>2</sup> zu Cosmochlore.

1965 berichteten Fron­del und Klein<sup>3</sup>, dass auch sie aus einem Toluca-Meteoriten (vgl. aus Meteoriten von Coahuila und Hex River Mountains) Kriställchen eines smaragdgrünen durchsichtigen Minerals von ähnlichem Wuchs und ähnlicher Grösse isoliert haben, wie von Laspeyres für Kosmochlor beschrieben. Letztere Verff. identifizierten dieses Mineral mittels Röntgen­analyse, Optik, und Mikrosonde als das Cr-Analogue des Jadeits.

Da Fron­del und Klein nach den Angaben von Laspeyres von der Identität ihrer Mineralart mit Laspeyres Kosmochlor nicht überzeugt waren, gaben sie ihrer Kristallart, in Ehrung des bekannten Meteoritenforschers und Chemikers H. C. Urey, den neuen Namen Ureyit.

Im Rahmen von Untersuchungen des Bonner Mineralogischen Instituts über das Druckverhalten der trockenen Tektosilikate und der Alkalipyroxene<sup>4</sup> ist seit längerem auch über das System Jadeit-NaCrSi<sub>2</sub>O<sub>6</sub> gearbeitet worden. Im Rahmen dieser Arbeiten interessierte naturgemäß auch Laspeyres' Kos­mochlor. Tatsächlich fand sich unter den geretteten Beständen der Bonner Meteoritensammlung ein Glasröhrchen mit einer Aufschrift von Laspeyres Hand: Kosmochlor, größter vermessener Kristall, mit einem einzigen dicktafligen Kosmochlor-Kriställchen (0.3 × 0.25 mm<sup>2</sup> Tafelfläche). Dieser Kristall wurde

<sup>1</sup> H. Laspeyres, Zeits. Kryst. Min., 1897, 27, 586-600.

<sup>2</sup> E. S. Dana, Syst. Min., 6th edn, App. I, p. 20 (1899).

<sup>3</sup> C. Fron­del u. C. Klein jr., Science, 1965, 149, 742-744.

<sup>4</sup> A. Neuhaus, C. Ballhausen, H. J. Meyer, u. R. Steffen, Jahrbuch 1965 des Landesamtes für Forschung des Landes Nordrhein-Westfalen, 546 (1965).

röntgenographisch, optisch, und mittels Mikrosonde untersucht. Er erwies sich zweifelsfrei als  $\text{NaCrSi}_2\text{O}_6$  mit mäßigem diadochen Austausch  $\text{NaCr-CaMg}$  (Näheres vgl. unten). Im folgenden seien zunächst die entscheidenden Unterlagen von Laspeyres zusammengestellt und anschließend die eigenen Beweise für die  $\text{NaCrSi}_2\text{O}_6$ -Natur des Kosmochlor mitgeteilt.

*Die Untersuchungsergebnisse von Laspeyres.* Ausgangsmasse waren 585 g der leicht abblätternden sekundären Rostrinde des Bonner Toluca-Meteoriten. Hiervon waren in  $\text{HCl}$  und  $\text{HNO}_3$  (konz. u. verd., heiss u. kalt) 1.61 g unlöslich (vorwiegend Plagioklas, allg. Augit und Quarz), und hiervon auch in Flußsäure unlöslich: 0.0073 g. Dieser in allen Säuren unlösliche Rest bestand praktisch nur aus einzelnen oder aggregierten eckigen, gestrecktaflichen, teils hypidionormphen, smaragdgrünen, durchsichtigen Kriställchen bis max. 0.35 mm Kantenlänge. Von der Gesamtausbeute von 0.0073 g wurden 0.0040 g für kristallographisch-optische Untersuchungen, für Belegzwecke für auswärtige Fachinteressenten und für das Bonner Museum verwendet. Der verbleibende Rest von 0.0033 g wurde für eine quantitative (!) nass-chemische Analyse geopfert.

Die kristallographisch-optischen Untersuchungen wiesen auf ein Augitartiges Mineral. Im einzelnen: Optisch zweiachsig; stark doppelbrechend und stark pleochroitisch: tiefsmaragdgrün–mittelgelbgrün; Härte  $\approx 6$  (Feldspathärte); mehrere Längsspaltbarkeiten; Symmetrie wahrscheinlich monoklin; triklin jedoch nicht ganz ausgeschlossen.

Chemische Analyse: Die in allen Säuren unlöslichen smaragdgrünen Kriställchen waren in Sodaschmelze vollständig aufschliessbar. Einzelergebnisse sind:

0.00105 g $\text{SiO}_2$	= 31.8 Gew. % = 45.8 Mol %
0.00030 g $\text{Al}_2\text{O}_3$	= ?
0.00130 g $\text{Cr}_2\text{O}_3$	= 39.9 Gew. % = 22.4 Mol %
0.00030 g $\text{Fe}_2\text{O}_3$	= ?
0.00020 g $\text{CaO}$	= *)
0.00015 g $\text{MgO}$	= *)
0.00330 g	

Vergegenwärtigt man sich die sehr geringen absoluten Gewichtsmengen und die mit den Methoden und Analysenwaagen der damaligen Zeit erreichbaren Analysengenauigkeiten, so dürfte klar sein, dass die Analysenwerte für  $\text{CaO}$  und  $\text{MgO}$  irreal sind und nicht einmal die Existenz dieser Komponenten im Kosmochlor beweisen. Starke Vorbehalte sind ferner gegenüber den Analysenzahlen für  $\text{Al}_2\text{O}_3$  und  $\text{Fe}_2\text{O}_3$  am Platze, jedenfalls hinsichtlich ihres quantitativen Wertes. Es verbleiben somit für eine reale Diskussion nur die Analysenzahlen für  $\text{SiO}_2$  und  $\text{Cr}_2\text{O}_3$ . Aber selbst sie sind, bei den äusserst geringen absoluten Mengen (1.05 mg. für  $\text{SiO}_2$  bzw. 1.3 mg. für  $\text{Cr}_2\text{O}_3$ ), mit einer sehr breiten Fehlergrenze zu versehen.

\* Von Laspeyres selbst bezweifelt.

Da Laspeyres, trotz mehrfacher eigener Hinweise auf eine mögliche Pyroxennatur seiner neuen Mineralart, offenbar keinerlei Probe auf Na ausgeführt hat, ja nicht einmal einen Na-Gehalt als möglich diskutiert, so kann mit Sicherheit nur eine Verbindung abgeleitet werden, die  $\text{Cr}_2\text{O}_3$  und  $\text{SiO}_2$  im Mol-Verhältnis 1 :  $\approx 2$  enthält. Das ist ein Mol-Verhältnis, das wenig für, angesichts der grossen Fehlergrenze der Analysenwerte aber auch nicht unbedingt gegen einen Pyroxen spricht.

Man kann verstehen, dass die vorstehend aufgezeigten Unsicherheiten, vor allem hinsichtlich der chemischen Zusammensetzung des Kosmochlors, Frondel und Klein (3) dazu geführt haben, an der Identität ihres smaragdgrünen Toluca-Minerals mit dem Kosmochlor zu zweifeln. Sie glaubten daher für das von ihnen aus dem Toluca-Meteoriten isolierte Mineral den Namen Ureyit vorschlagen zu sollen.

### *Neue Untersuchungen am Kosmochlor<sup>1</sup>*

*Röntgenuntersuchungen.* Von Laspeyres "Original-Kosmochlor" wurde aus Sicherheitsgründen und zwecks Durchführung von mikroskopischen Untersuchungen (Lichtbrechungsmessungen, Spaltverhalten, usw.) zunächst ein kleinerer Teil vorsichtig abgetrennt. Die Teilung erfolgte sehr scharf nach einer guten Spaltbarkeit, die sich späterhin als  $\parallel [001]$  erwies. Der verbleibende grössere Teil wurde für die folgenden Röntgenuntersuchungen benutzt. Er war gestreckt-tafelig mit  $[001]$  als Längsachse. Grösse:  $\approx 0.25 \times \approx 0.15$  mm Tafelfläche. Mit diesem letzteren Kristall wurden, nach polarisationsoptischer Vororientierung, zunächst Dreh- und Weissenberg-Aufnahmen um  $[001]$  angefertigt, sodann, zur Kontrolle und Verschärfung des Wertes für  $a$ , auch Dreh- und Weissenberg-Aufnahmen um  $[100]$ . Alle Aufnahmen waren gut scharf und erwiesen den Einkristallcharakter des untersuchten Kosmochlorkristalls (vgl. auch unten). Die aus den Röntgen-Aufnahmen errechneten Zellendaten sind in Tab. I verzeichnet. Sie sind, wie ein Vergleich zeigt, mit jenen des Ureyits praktisch völlig ident.

Zum Vergleich des Kosmochlor-Ureyits mit der reinen  $\text{NaCr}[\text{Si}_2\text{O}_6]$ -Phase wurden in Tab. I auch die Zellendaten synthetischer Produkte aufgeführt; Werte von Frondel u. Klein und die Zellendaten eines eigenen hydrothermalen (4) Syntheseproduktes (dargestellt bei  $P \approx 3\,000$  at.,  $T \approx 600^\circ\text{C}$ ). Die Zellenbestimmung erfolgte in diesem Fall mittels Pulvermethoden und zwar mittels Guinier-Diffraktometeraufnahmen mit Auswertung nach einem, im eigenen Institut entwickelten neuen Rechenprogramm zur Indizierung von Diagrammen niedrigsymmetrischer Strukturen.<sup>2</sup>

Kosmochlor und Ureyit sind gemäss Tab. I nach Zellengrösse unter sich praktisch gleich. Entsprechendes gilt für die zwei  $\text{NaCr}(\text{Si}_2\text{O}_6)$ -Synthesen unter

<sup>1</sup> Eine ausführliche Darstellung erfolgt zusammen mit I. Abs-Wurmbach an anderer Stelle.

<sup>2</sup> Eine ausführliche Behandlung dieses Auswerte-Verfahrens folgt unter E. A. Jumpertz und R. Klar.

TABELLE I. Zellendaten und chemischen Analysen für Kosmochlor, Ureyit, und  $\text{NaCrSi}_2\text{O}_6$ .

	1.	2.	3.	4.	5.	6.	7.	8.
<i>a</i>	9.54 <sub>5</sub> Å	9.56 <sub>0</sub> Å	9.550 ± 0.016 Å	9.582 ± 0.004 Å	SiO <sub>2</sub>	45.8	63.4	60
<i>b</i>	8.76 <sub>1</sub>	8.74 <sub>6</sub>	8.712 ± 0.007	8.717 ± 0.002	Al <sub>2</sub> O <sub>3</sub>	—	—	66.66 <sub>7</sub>
<i>c</i>	5.26 <sub>5</sub>	5.27 <sub>0</sub>	5.273 ± 0.008	5.271 ± 0.002	Cr <sub>2</sub> O <sub>3</sub>	22.4	10.11	14
$\beta$	107.4°	107.38°	107.44 ± 0.16°	107.43 ± 0.03°	Fe <sub>2</sub> O <sub>3</sub>	?	0.175	—
<i>V</i>	420.2	420.6	418.6 ± 1.4 Å <sup>3</sup>	420.0 ± 0.35 Å <sup>3</sup>	MgO	?	9.1	6
Symm.	$(C_2/c)$	$C_2/c$	$C_2/c$	$(C_2/c)$	CaO	?	4.49	7
					Na <sub>2</sub> O	n.d.	12.7	13
								16.66 <sub>7</sub>

1. Kosmochlor, Toluca Meteorit; Laspeyres Kristall; Messdaten nach E. A. Jumpertz und P. Otten, Bonn, Min. Inst. (Einkristallbestimmungen).
2. Ureyit, Coahuila Meteorit (Frondel und Klein, 1965).
3.  $\text{NaCrSi}_2\text{O}_6$ , synthetisch (Frondel und Klein, 1965).
4.  $\text{NaCrSi}_2\text{O}_6$ , synthetisch; Präparat von I. Abs-Wurmbach; Röntgendaten nach E. A. Jumpertz und R. Klar, Bonn, Min. Inst. (Pulverbestimmungen).
5. Kosmochlor, Toluca Meteorit; nass-chemische Analyse mit 0.0033 g Probenmenge (Laspeyres, 1897).
6. Ureyite, Toluca Meteorit; Mikroanalyse mittels Elektronen-Mikrosonde (Appl. Research Lab. Instr.: Frondel und Klein, 1965).
7. Kosmochlor, Toluca Meteorit; Laspeyres Kristall, Mikroanalyse mittels Cameca Mikrosonde; die Mol%-Werte wurden bestimmt durch Impulszahlen-Verhältnis gegen synth.  $\text{NaCrSi}_2\text{O}_6$  bzw. Diopsid als Norm. Die Werte wurden auf Untergrund korrigiert. Betriebsdaten: 20 KV, 100 nA; 100 sec Zählzeit, C-Schicht 50 Å. Fe and Al konnten nicht mit Sicherheit nachgewiesen werden.
8.  $\text{NaCrSi}_2\text{O}_6$ , theoretisch.

sich (über die geringe Abweichung der *a*-Perioden kann zur Zeit noch nichts ausgesagt werden). Geringe aber doch zweifelsfreie Unterschiede weisen jedoch die *b*-Perioden der zwei Naturkristalle gegenüber den zwei Synthesen auf. Und zwar sind die *b*-Perioden beider Naturkristalle deutlich grösser als die *b*-Werte beider Synthesen. Die Ursache dieser systematischen Abweichung dürfte, wie der weiter unten folgende Analysenbefund zeigt (Tab. I), in einem mässigen diadochen Austausch NaCr–CaMg zu suchen sein.

*Untersuchungen mittels Mikrosonde.*<sup>1</sup> Beide Bruchstücke des zerteilten Originalkristalls von Laspeyres wurden getrennt der Untersuchung mittels einer Mikrosonde unterworfen. Das Analysenergebnis zeigt Tab. I. Es besagt: Kosmochlor ist chemisch ein ziemlich reiner  $\text{NaCrSi}_2\text{O}_6$  mit mässigem Austausch NaCr–CaMg. Fe und Al konnten nicht nachgewiesen werden. Kosmochlor und Ureyit stimmen also nicht nur hinsichtlich der Hauptkomponenten Na, Cr, Si, sondern auch hinsichtlich Art und Menge der Nebenkomponten gut überein.

*Mikroskopische Untersuchungen am Kosmochlor.* Das für die Röntgenanalyse benutzte, gestreckt taflige Bruchstück des Kosmochlors wurde durch Drehen (in halb-verdicktem Kanadabalsam) um die röntgenographisch als [001] ausgewiesene Längsachse nacheinander mit (100) und (010) parallel zum Mikroskopisch eingestellt.

Die orthoskopische Untersuchung dieser beiden Schnittlagen ergab: Für (100)-Schnittlage: gerade Auslöschung mit  $\alpha'$  = mittelhellgelbgrün || [001] (morphologische Längsachse) und  $\gamma'$  = tiefsmaragdgrün  $\perp$  [001]. Für (010)-Schnittlage: schiefe Auslöschung mit  $\alpha$  : [001]  $\approx 21^\circ$ ; Pleochroismus:  $\alpha$  = mittelhellgelbgrün,  $\gamma$  = tiefsmaragdgrün.

Die konoskopische Untersuchung ergab: AE || (010);  $\gamma'$  der orthoskopischen Untersuchung von (100) ist somit  $\beta$  || [010];  $\gamma$  = IIM-L; optischer Charakter also negativ.

<sup>1</sup> Cameca-Mikrosonde.

Die optische Charakteristik des Kosmochlors entspricht also sehr nahe jener des Ägirins bzw. des Ägirin-reichen Ägirinaugits und unterscheidet sich von der optischen Charakteristik der meisten Clinopyroxene durch die neg. Längszone mit  $\alpha = I.M-L$ .

Diese optischen Feststellungen stehen mit Laspeyres Angaben in vollem Einklang und vervollständigen sie. Sie stimmen, abgesehen von einer Vertauschung der Absorptionsangaben  $\parallel [100]$  und  $[010]$ , auch mit den optischen Befunden von Frondel u. Klein überein. Eine Erklärung der teilweisen Abweichung der Absorptionsachsen kann nicht gegeben werden.

Kosmochlor und Ureyit sind nach allen vorstehenden Ergebnissen also zweifelsfrei *identische Minerale* (Die Arbeiten werden fortgesetzt).

## Summaries of other papers presented in Symposium II

**On synthetic lithium pyroxenes and related compounds.** By W. L. BROWN, Dept. of Geology, The University, Manchester 13.

The synthesis of compounds of general formula  $\text{LiM}^{3+}\text{Si}_2\text{O}_6$  has been attempted for a series of trivalent cations—Al, Ga, and the transition elements Sc, V, Cr, Mn, and Fe—by dry heating of oxide mixes at ordinary pressure and temperatures up to 1 000 °C, and also hydrothermally at lower temperatures and high pressures. Synthetic pyroxenes of probable space group  $C2/c$  or compounds of so-called “ $\beta$ -spodumene” type (tetragonal stuffed keatite derivatives) were generally obtained (in some cases both), though other structures were obtained from some elements.

Lattice constants were measured for both the pyroxene and stuffed keatite structures and for related natural compounds. They show a regular variation with trivalent cation size (using the ionic radii of Goldschmidt). The molar volume change from the dense pyroxene structure to the more open keatite derivative is very large.

**The crystal structures of the ferrosilite ( $\text{FeSiO}_3$ ) polymorphs.** By C. W. BURNHAM, Dept. of Geological Sciences, Harvard University, Cambridge, Massachusetts.

Synthetic clinoferrosilite ( $P2_1/c$ ,  $a$  9.709,  $b$  9.087,  $c$  5.228, all  $\pm 0.001$  Å,  $\beta$  108.432°  $\pm 0.004$ °,  $Z$  8) is isostructural with clinoenstatite, and has two crystallographically distinct silicate chains with mean tetrahedral Si–O distances of 1.623 Å and 1.635 Å. Both metal sites are occupied by  $\text{Fe}^{2+}$ ; the  $M_2$  (=Ca in diopside) octahedron has a mean Fe–O distance of 2.224 Å, and is distorted by two long distances (2.444 and 2.587 Å) to chain-linking oxygens, while the more regular  $M_1$  (=Mg in diopside) octahedron has a mean Fe–O distance of 2.137 Å. Orthoferrosilite ( $Pbca$ ,  $a$  18.431  $\pm 0.004$  Å,  $b$  9.080  $\pm 0.002$  Å,  $c$  5.238  $\pm 0.001$  Å,  $Z$  16) is likewise structurally analogous to orthoenstatite. The two independent silicate tetrahedra have mean Si–O distances of 1.624 Å and 1.614 Å. The mean Fe–O distances are 2.240 Å in the distorted  $M_2$  octahedra and 2.145 Å in the  $M_1$  octahedra. In both structures Si–O bonds to chain-linking oxygens are significantly longer than those to other oxygens. Neither structure exhibits evidence of octahedral shared-edge contraction; O–O distances along shared octahedral edges are 2.8 Å or greater. At the present level of refinement ( $R_{\text{CFS}} = 4.3\%$ ,  $R_{\text{OFS}} = 5.1\%$ ), isotropic thermal parameters,  $B$ , for all atoms in orthoferrosilite are two to three times larger than those for corresponding atoms in clinoferrosilite.

Ferrosilite III is triclinic with  $a$  6.634  $\pm 0.001$  Å,  $b$  7.472  $\pm 0.001$  Å,  $c$  22.610  $\pm 0.002$  Å,  $\alpha$  115.294°,  $\beta$  80.649°,  $\gamma$  95.423°, all  $\pm 0.006$ °. Relationships between this cell and those of the pyroxenoids have led to the suggestion that ferrosilite III is a pyroxenoid with silicate chains running parallel to  $c$  that repeat after every nine tetrahedra. The structure is now being analysed with this hypothesis in mind.

**Amphibole cation site disorder.** By G. V. GIBBS, Dept. of Geological Sciences, Virginia Polytechnic Institute, Blacksburg, Virginia, and C. T. PREWITT, Department of Geology and Geophysics, Massachusetts Institute of Technology, Cambridge 39, Massachusetts.

Recent least-squares refinements of riebeckite (I), synthetic magnesio-richterite (II) and sodium cobalt amphibole (III) reveal that there is a definite correlation between cation order-

ing and apparent thermal vibration parameters. In general, when cations of appreciably different radii statistically occupy an  $M$  site, their temperature factors as well as those of the co-ordinating anions are larger than those recorded for sites containing cations of similar radii. For example,  $M_1$  of (III) contains both sodium and cobalt as determined by population density refinement. The isotropic  $B$  is 1.3 as compared with 0.5 for the remaining  $M$  sites, which contain only cobalt. In (I),  $M_3$  shows a similar relation for the statistical distribution of lithium, ferrous iron, and aluminium.

It is apparent that one cannot assume that the temperature factors will be identical for all  $M$  sites. In addition, the usual mathematical model should be modified to account for two centres of electron density in the disordered  $M_1$  site containing cations of different sizes.

In these amphiboles, the  $A$  site cation is statistically displaced about 0.1/2,0 revealing that the symmetry of a particular cell is not compatible with the centrosymmetric space group  $C2/m$ . In the fluorine-containing amphiboles, (I) and (II), the displacement appears to be normal to  $b$  whereas in the hydroxyl one (III) it is parallel to  $b$ .

**Effect of pressure on the incongruent melting of acmite.** By M. C. GILBERT, Geophysical Laboratory, 2801 Upton Street, N.W., Washington, D.C.20008, U.S.A.

In the presence of hematite+magnetite, acmite,  $\text{NaFe}^{3+}\text{Si}_2\text{O}_6$ , melts incongruently to hematite+magnetite+liquid over the pressure range 10 to 40 Kb as determined in the single-stage, piston-cylinder apparatus. No polymorphic changes were detected. The slope changes from approximately  $17^\circ\text{C/Kb}$  at 10 Kb (m.p. =  $1\ 175^\circ \pm 20^\circ\text{C}$ ) to  $9^\circ\text{C/Kb}$  at 40 Kb (m.p. =  $1\ 537^\circ \pm 10^\circ\text{C}$ ). Compared to the melting of jadeite,  $\text{NaAlSi}_2\text{O}_6$ , the substitution of  $\text{Fe}^{3+}$  for Al in acmite raises its melting temperature  $70^\circ\text{C}$  at 30 Kb and  $20^\circ\text{C}$  at 40 Kb. Strong control of oxygen fugacity on acmite melting is indicated by runs in graphite and iron capsules where the beginning of melting is lowered 250 to  $350^\circ\text{C}$  and the slope is lowered to about  $8^\circ\text{C/Kb}$  over the range of 10 to 30 Kb. Cell parameters of acmite synthesized in an iron capsule in a 30-minute run,  $a\ 9.659 \pm 0.005\ \text{\AA}$ ,  $b\ 8.803 \pm 0.005\ \text{\AA}$ ,  $c\ 5.292 \pm 0.005$ ,  $\beta\ 107.57 + 0.05^\circ$ , volume  $428.9 \pm 0.2\ \text{\AA}^3$ , compared to the microcrystalline starting material,  $a\ 9.660 \pm 0.005\ \text{\AA}$ ,  $b\ 8.804 \pm 0.005\ \text{\AA}$ ,  $c\ 5.289 \pm 0.005\ \text{\AA}$ ,  $\beta\ 107.33 \pm 0.05^\circ$ , volume  $429.4 \pm 0.3\ \text{\AA}^3$ , show essentially no difference suggesting little acmite-ferrosilite solid solution.

**The join hedenbergite-ferrosilite at high pressures and temperatures.** By D. H. LINDSLEY, Geophysical Laboratory, 2801 Upton Street, N.W., Washington, D.C.20008, U.S.A.

Experiments on the join hedenbergite-ferrosilite at pressures up to 40 Kb yield the following information:

The temperature of the hedenbergitic-clinopyroxene-wollastonite solid solution (pyroxenoid) transition is pressure dependent:  $dT/dP = 23^\circ\text{C/Kb}$  for  $\text{CaFeSi}_2\text{O}_6$ ; evidence of this inversion in the Skaergaard intrusion may thus reflect a low total pressure during crystallization. A complete solid-solution series of clinopyroxenes exists above ca. 17.5 Kb, the pressure at which pure  $\text{FeSiO}_3$  becomes stable; the solidus is not intersected by a miscibility gap; no evidence was found for the existence of a sub-solidus miscibility gap, although that possibility cannot be ruled out on the basis of the present data. A complete range of pyroxenoids can be synthesized along the hedenbergite-ferrosilite join, but there is no one pressure at which the pyroxenoid form is stable throughout the join; an abrupt change in powder X-ray diffraction patterns at  $\text{Fs}_{75}\text{Wo}_{25}$  may reflect the transition from wollastonite solid solutions (dreierketten?) to the ferrosilite-III form (neunerketten). Refractive indices of both the clinopyroxene and pyroxenoid modifications appear to show continuous variation along the

join. Pressures in excess of 30 Kb are required to stabilize orthoferrosilite containing 5 mole%  $\text{CaSiO}_3$ .

Experiments were performed using iron capsules in a solid-medium piston-and-cylinder pressure apparatus.

**On the exsolution phenomena in pyroxenes.** By N. MORIMOTO, Institute of Scientific and Industrial Research, Osaka University, Higashiasaka, Sakai, Osaka, Japan.

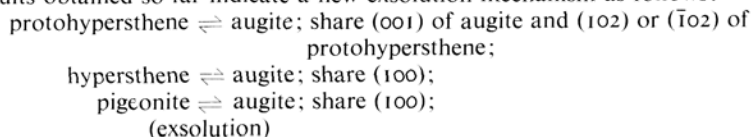
The exsolution phenomena commonly occurring in augite, pigeonite, and orthopyroxenes have been studied by many people. The opinion as to their nature given by Poldervaart and Hess (1951), based on the phase relations of the  $\text{MgSiO}_3$ - $\text{FeSiO}_3$  system after Bowen and Schairer (1935), had been widely accepted.

Sclar *et al.* (1964) discovered a new phase relation for  $\text{MgSiO}_3$  and proved that clinostatite is stable at below 540°C, 1 atm. The phase relations of the  $\text{MgSiO}_3$ - $\text{FeSiO}_3$  system, however, have not been revealed. In order to elucidate the exsolution phenomena on the basis of the possible phase relations of the  $\text{MgSiO}_3$ - $\text{FeSiO}_3$ - $\text{CaSiO}_3$  system, X-ray study of the exsolution textures of augite and pigeonite has been carried out.

The specimens studied are pigeonite in the Moore County meteorite; augite in EG 4526A rock, Skaergaard; pigeonite and augite in andesite, Hakone Volcano (No. 14, Kuno, 1955); pigeonite in basalt, Ō-Sima Island (No. 8, Kuno, 1955); pigeonite in andesite, Hakone Volcano (No. 12, Kuno, 1955), and pigeonite, Mull.

They were studied by the precession method. The chemical compositions of hosts and exsolved products were obtained graphically from their  $a \sin \beta$  and  $b$  values (Brown, 1960).

The results obtained so far indicate a new exsolution mechanism as follows:



where protohypersthene is assumed to have a similar structure to protoenstatite (Smith, 1959).

When protohypersthene is cooled rapidly without enough exsolution of the Ca component, it inverts to pigeonite and exsolves augite parallel to (100). Two augites exsolved in pigeonite (Moore Co.) and two pigeonites in augite (Skaergaard) are well explained by this exsolution mechanism. If protohypersthene exsolves enough Ca component as augite, it inverts to hypersthene. This is the case of inverted pigeonite.

Pigeonite inverted from protohypersthene can be distinguished from that inverted from hypersthene or that exsolved in augite at low temperature by the content of Ca component.

**The oriented transformation johannsenite  $\rightarrow$  bustamite.** By N. MORIMOTO, K. KOTO, and T. SHINOHARA, Institute of Scientific and Industrial Research, Osaka University, Higashiasaka, Sakai, Osaka, Japan.

Details of the oriented transformation, johannsenite  $\rightarrow$  bustamite, have been studied by the single crystal X-ray method, in order to elucidate the transformation mechanism in silicate chain structures in general. Single crystals of johannsenite were heated at 900°C in a silica tube. The product is a mixture of johannsenite and bustamite and the orientation of the derived bustamite has been determined; the sheets of close-packed oxygen atoms of johannsenite makes an angle of 4.5° with those of bustamite and [012] of johannsenite coincides with [111] of bustamite. This orientation shows that a dense zone of large cations and silicon atoms in johannsenite is preserved in the transformation.

These results are interpreted on the basis of the preservation of the close-packed framework of oxygen atoms along the dense zone of the cations and silicon atoms in johannsenite in the transformation. The difference in direction of  $\text{SiO}_3$  chains and in the ordering of Ca and Mn atoms in johannsenite and bustamite structures provides direct evidence of the migration of large cations as well as silicon atoms during the transformation.

The oriented transformation, rhodonite  $\rightarrow$  wollastonite described by Dent Glasser and Glasser, can be better explained by this principle deduced from the johannsenite  $\rightarrow$  bustamite transition than by the simple preservation of the close-packed framework of oxygen atoms.

**Variations in the composition of pigeonite from Mount Wellington, Tasmania, and the Skaergaard Intrusion, East Greenland.** By I. D. MUIR, Department of Mineralogy and Petrology, Downing Place, Cambridge, England, and R. G. BURNS, Department of Chemistry, Victoria University of Wellington, Wellington, New Zealand.

Variations in the compositions and optical properties of uninverted pigeonites from the Mt. Wellington Sill and the layered series of the Skaergaard Intrusion are reported. Analyses for Ca, Mg, Fe, Al, Si, and Ti have been carried out using the electronprobe microanalyser. New data are also presented for the pyroxenes from the Beaver Bay Diabase, Minnesota.

**Physical properties of synthetic and natural pyroxenes in the system diopside-hedenbergite-acmite.** By J. NOLAN.

Unit-cell dimensions and the indices of refraction  $\alpha$  and in some cases  $\gamma$  have been measured for synthetic pyroxenes in the system  $\text{CaMgSi}_2\text{O}_6$ - $\text{CaFeSi}_2\text{O}_6$ - $\text{NaFeSi}_2\text{O}_6$ , which have been crystallized and annealed on the Ni-NiO oxygen-buffer curve at  $700^\circ\text{C}$  and a total pressure of 2 Kb. The data presented confirm the numerous postulates that a complete solid-solution series does exist in the subsolidus region of the "ternary" system. The unit-cell dimensions show a systematic linear change with composition between the three end members. The data for the unit-cell dimensions of the end members are: diopside,  $a=9.748$ ,  $b=8.924$ ,  $c=5.251$ ,  $\beta=105.79^\circ$ ; hedenbergite,  $a=9.841$ ,  $b=9.027$ ,  $c=5.247$ ,  $\beta=104.79^\circ$ ; acmite,  $a=9.658$ ,  $b=8.795$ ,  $c=5.294$ ,  $\beta=107.42^\circ$  ( $a$ ,  $b$ , and  $c$  are considered to be within  $\pm 0.005 \text{ \AA}$  and the angle  $\beta$  to be within  $\pm 0.05^\circ$ ). The indices of refraction for the end members are in complete agreement with the published data. The computed cell parameters for a series of analysed natural alkali pyroxenes have been compared with the data for the synthetic pyroxenes and the agreement was found to be very close. A method is presented for the determination of alkali pyroxenes using a combination of the  $b$  unit-cell dimension and the refractive indices.

**The distribution of amphibole basic formula compositions.** By R. PHILLIPS, Department of Geology, University Science Laboratories, South Road, Durham, England.

The major compositional affinities of an amphibole are best appreciated by knowing what is termed a basic atomic formula. Parameters derived from the basic formula can be plotted in a three dimensional compositional space. Results of the examination of a large number of analyses are given.

**Synthetic amphiboles in the system  $\text{Na}_2\text{O}$ - $\text{MgO}$ - $\text{SiO}_2$ - $\text{H}_2\text{O}$  and their significance for the chemistry of natural amphiboles.** By W. SCHREYER and F. SEIFERT, Min. Inst. Universität Kiel, 23 Kiel, Olshausenstrasse 40/60, Germany.

In accordance with the earlier synthesis of a fluor-bearing soda richterite (Gibbs *et al.*, 1962) an amphibole of the composition  $\text{Na}_2\text{Mg}_6[\text{Si}_8\text{O}_{22}](\text{OH})_2$  was synthesized hydrothermally. This phase was found to represent one end member of a binary series of amphibole solid

solutions in the system  $\text{Na}_2\text{O}-\text{MgO}-\text{SiO}_2-\text{H}_2\text{O}$  extending to a more sodium-rich end member,  $\text{Na}_4\text{Mg}_4[\text{Si}_8\text{O}_{20}(\text{OH})_2](\text{OH})_2$ . This series of solid solutions is due to the substitution  $\text{Na}^+ + \text{OH}^- \rightleftharpoons \text{Mg}^{+2} + \text{O}^{-2}$ , which suggests that the amphibole structure can accommodate more than three large cations, and that some oxygens of the tetrahedral chains may be replaced by hydroxyl groups. The present results are in agreement with unusually high  $\text{H}_2\text{O}^+$  values of many natural amphiboles (*e.g.* Zussman, 1955), and they yield an explanation for the occasional reports of (Na + K + Ca) contents in excess of 3.00 per formula unit in some natural richterites, eckermannites, and arfvedsonites. The inferred differences in OH-content of the two synthetic end members was confirmed by weight-loss determination.

The stability relations of the amphibole series in the system investigated as determined so far as 1 000 bars  $P_{\text{H}_2\text{O}}$  are as follows:  $\text{Na}_2\text{Mg}_6[\text{Si}_8\text{O}_{22}](\text{OH})_2$  has the highest upper stability, melting incongruently to forsterite, an osumilite-type phase, and liquid at  $965 \pm 20^\circ\text{C}$ . Solid solutions towards  $\text{Na}_4\text{Mg}_4[\text{Si}_8\text{O}_{20}(\text{OH})_2](\text{OH})_2$  melt at successively lower temperatures, and this phase itself at  $770 \pm 10^\circ\text{C}$  yielding less sodium-rich amphiboles plus liquid. Forsterite in these compositions does not appear below  $950 \pm 10^\circ\text{C}$ . The lower stability limit of the series seems to decrease with increasing Na-contents of the amphiboles, undetermined phyllosilicates phases appearing instead.

**X-ray powder diffraction data on orthopyroxenes.** By D. A. STEPHENSON, J. V. SMITH, Department of Geophysical Sciences, University of Chicago, Chicago, Illinois, and R. A. HOWIE, Department of Geology, King's College, Strand, London W.C.2. England.

The indices 004 assigned to a powder diffraction peak of orthopyroxenes by Ramberg and DeVore (1951), and accepted by later workers, are incorrect. The *hko* indices are correct. Thus the *a* and *b* dimensions in the literature are correct, while the *c* dimensions are wrong. Complete indexing of the powder patterns of orthopyroxenes has been made with the aid of intensities from single-crystal photographs. Many diffraction intensities change rapidly with the Mg/Fe ratio, and it is necessary to use different groups of reflections in least-squares refinements of the cell dimensions. Cell dimensions for the specimens re-analysed by microprobe techniques by Howie and Smith (1966) are reported. Although the Mg/Fe ratio exercises the major control on the cell dimensions, the minor substituents Al and Ca have significant effects.

**Temperatures of equilibrium of amphiboles and pyroxenes in magmatic, metamorphic, and metamorphic rocks.** By L. L. PERCHUK (Л. Л. Перчук).

From the reported experimental data (Orville, 1963; Debrom *et al.*, 1961; Iiyama *et al.*, 1963), the excess and relative thermodynamic functions for alkali feldspar, nepheline, and plagioclase were calculated and isotherms of distribution of Na between these minerals and aqueous solutions were derived. Using these data as a basis the natural parageneses alkali-feldspar + plagioclase + nepheline + amphibole for rocks of moderate depth of formation were studied and temperatures of equilibria determined. From the data obtained, the isotherms (450 to 700°C) of Ca distribution in coexisting amphiboles and plagioclases were calculated. The approximate computation of excess thermodynamic functions for amphiboles (for isomorphism  $\text{Ca} \rightleftharpoons \text{Na} + \text{K}$ ) allowed the extrapolation to 1 300° and 350° and the plotting of a corresponding diagram.

Employing this diagram, the compositions of coexisting amphiboles, plagioclases, clinopyroxene and orthopyroxenes (Cpx and Opx) were studied, which permitted the derivation of the isotherms of distribution for Mg in equilibria amphibole-clinopyroxene, amphibole-orthopyroxene, and clinopyroxene-orthopyroxene (excluding equilibrium with pigeonite).

The temperature evaluation of mineral equilibria was carried out using the reported compositions of coexisting amphiboles and pyroxenes. Our own data were also used.

The greatest temperature range (400 to 1 300°C) was found for igneous rocks. In effusive rocks, depending on their composition, the temperatures of equilibria from 850 to 1 300° and higher were determined. For most intrusions of granitoids and nepheline syenites, the temperatures of equilibria were found to be 700 to 400°, but the principal bulk of data covers the range 600 to 400°. These relatively low values show that in most of rocks from the granite and syenite massives, the temperature of mineral equilibria were determined in the auto-metamorphic stage.

For metasomatic carbonatites and albitites, the temperatures of equilibria apply to the range 380 to 500°, but for apatite rocks containing phlogopite, clinopyroxene, and amphibole, the temperatures are as high as 700°.

In metamorphic rocks, the temperature boundaries of the principal facies are sufficiently clearly defined as: granulite facies, 650 to 900°; amphibolite facies, 510 to 650°; epidote-amphibolite facies, 400 to 510°.

The temperatures of mineral equilibria in charnockites are very stable, being 660 to 710° (India, Africa, the Ukraine, Eastern Siberia).

The boundary between granulitic and amphibolitic facies can be clearly distinguished at 650 to 660°. Below this temperature orthopyroxene was found to be unstable, except highly ferrous varieties in granites, for which the temperature of equilibria is as low as 600 to 500°C.

The parageneses of amphiboles and pyroxenes from eclogites and glaucophane schists were given a special study. Pressure, along with temperature, appeared to have a considerable effect on distribution coefficient of magnesium ( $K_{Mg}^{\text{pl}}$ ) between these minerals. Allowing for pressure, the following temperatures of equilibria were obtained: eclogites and garnet pyroxenites (without epidote and clinozoisite), 590 to 900°C, glaucophane schists, 350 to 450°.

## **Titles and authors of other papers presented in open sessions at the meeting**

### *General lectures*

- The relation of lattice dynamics to chemical bonding . . . . . W. Cochran  
Theory of chemical valence and its relation to bonding in silicates  
D. J. W. Cruickshank

### *Methods in reflected light*

- On the question of measuring the reflectivity of ore minerals  
M. S. Bessmertnaya and L. A. Loginova (М. С. Бессмертная и Л. А.  
ЛОГИНОВА)  
Analyses of the dependence of mineral hardness on composition by the method  
of micro-indentation . . . . . S. I. Lebedeva (С. И. Лебедева).  
Dispersion of the reflectivity in some minerals of the type  $Cu_3XS_4$  . . . . . C. LÉvy  
Towards diagnosis of lead sulpho-antimonides  
N. N. Mozgova, Yu. S. Borodaev, A. D. Rakcheev, and S. S. Borishanskaya  
(Н. Н. Мозгова, Ю. С. Бородаев, А. Д. Ракчеев, и С. С.  
Боришанская)  
Colour measurements in ore microscopy . . . . . H. Piller  
Electron micro-probe study of minerals of the linnaeite group from the Raipas  
formation, Finnmark . . . . . F. M. Vokes

### *Crystal structures*

- The average structure of a topologically monoclinic adularia and a refinement  
of the structure of orthoclase . . . . . A. A. Colville and P. H. Ribbe  
The crystal structure of stilbite . . . . . E. Galli and G. Gottardi  
The crystal structure of walstromite ( $Ca_2BaSi_3O_9$ )  
L. S. Dent Glasser and F. P. Glasser  
The crystal structure of 3T muscovite . . . . . N. Guven and C. W. Burnham  
The crystal structure of heated Guilford cordierite  
E. P. Meagher and G. V. Gibbs  
The crystal structure of grandidierite . . . . . D. A. Stephenson and P. B. Moore

### *Synthetic minerals*

- Chemical composition and synthesis of transition-metal lead silicates: the  
melanotektite–kentrolite series . . . . . F. P. Glasser and L. S. Dent Glasser

## Ternary solid solution in the feldspar system

D. L. Hamilton and W. S. Mackenzie

Phase equilibrium studies in the system  $\text{KAlSi}_3\text{O}_8$ - $\text{NaAlSi}_3\text{O}_8$ - $\text{CaAl}_2\text{Si}_2\text{O}_8$ - $\text{SiO}_2$ - $\text{H}_2\text{O}$  . . . . . R. S. JamesStability of substituted  $\text{Al}_2\text{SiO}_5$  minerals . . . . . R. G. J. StrensFeldspar-liquid equilibria in peralkaline acid liquids; an experimental study  
R. N. Thompson*New minerals*

Pendletonite, a new mineral from California . . . . . J. Murdoch

Rosenhahnite, a new hydrous calcium silicate from Mendocino Co., California  
A. Pabst, E. B. Gross, and J. T. Alfors*Rock minerals*The parageneses of ilvaite . . . . . P. Bartholomé and F. Dimanche  
Fe contents of aluminium silicate polymorphs

G. A. Chinner, C. R. Knowles, and J. V. Smith

Thermal behaviour of  $\beta$ -uranophane . . . . . W. G. R. de Camargo

Optical determination of water content in vaterite

J. D. H. Donnay and G. Donnay

On the crystallochemical alterations of tri-octahedral and di-octahedral micas  
in sedimentary rocks

V. A. Drits, A. G. Kossovskaya, and V. D. Shutov (В. А. Дриц, А. Г. Коссовская, и В. Д. ШУТОВ)

Original polytypic modifications of sheet silicates

V. A. Drits, B. B. Zvyagin, and S. V. Soboleva (В. А. Дрлц, Б. Б. ЗвЯгин, и С. В. Соболева)

Sulphur mineralogy in agraitic nepheline syenites

V. I. Gerasimovsky (В. И. Герасимовский)

On the role of copper and silver in the lead-bismuth sulpho-salts

A. A. Godovikov (А. А. Годовиков)

Iron-titanium oxides in a suite of alkaline volcanic rocks from Tenerife

S. E. Haggerty, G. D. Borley, and M. J. Abbott

Electron microprobe studies of the role of titanium in garnets . . . . . T. Isaacs

Sulphurization of magnetite . . . . . G. Kullerud and G. Donnay

Cell dimensions of olivines . . . . . S. J. Louisnathan and J. V. Smith

The thermoluminescence of minerals

L. N. Ovchinnikov and V. G. Maksenov (Л. Н. Овчинников и В. Г. Максенов)

The iron content of melilite . . . . . Th. G. Sahama

The sodalite group of minerals . . . . . D. Taylor

Secondary minerals produced by weathering of the Wolf Creek meteorite

J. S. White, Jr., E. P. Henderson, and B. H. Mason

*Petrology*

- Potash-rich volcanic rocks from Southern Spain . . . . . G. D. Borley  
 On graphical representation and appraisal of the strength of association  
 F. Chayes
- A micro-probe study of the prehistoric tholeiitic lava lake of Makaopuhi,  
 Hawaii . . . . . B. W. Evans and J. G. Moore
- The factors determining the acidity–basicity in the processes of endogenetic  
 mineral formation . . . . . D. S. Korzhinski (Д. С. Коржинский)
- Petrological interpretations of crystallochemical characteristics of minerals  
 from selected igneous and metamorphic rocks . . . . . H. C. Liese
- Aspects of distribution of ions, and the diadochic relations among silicon,  
 titanium, and aluminium in co-existing ferromagnesian minerals  
 S. K. Saxena
- Migmatites from Bangalore, India  
 B. L. Sreenivas, R. Srinivasan, G. Srinivas, and T. R. Gopinath
- The syn-metamorphic emplacement of gabbro at Hasvik, Söröy, Norway  
 B. A. Sturt
- Use of the opaque minerals in petrogenetic studies of basalts  
 N. D. Watkins and S. E. Haggerty

*Miscellaneous*

- Ten years of service in the conservation of mineral species  
 C. Guillemin and P. Sainfeld
- Transmitted-light interference microscopy in mineralogy . . . . . A. F. Hallimond
- X-ray diffraction of minerals at high pressures and temperatures  
 H. O. A. Meyer
- On chemistry and crystal symmetry . . . . . A. S. P. Rao

## Topographical Index

### EUROPE

#### Norway (Norge)

Kongsberg, fluorite, 145

#### Sweden (Sverige)

Långban, Värmland, richterite, 249

Norra Kärr, Årjang, Värmland, eckermanite, 28

#### Germany (Deutschland)

Albtal, Schwarzwald, feldspar, 117

Hesselbach, Bavaria, fluorite, 145

Wölsendorf, Schwarzenfeld, Bavaria, fluorite, 145

#### Austria (Österreich)

Ankogel, Salzburg, feldspar, 117

Gross-Eibenstein, feldspar, quartz, 117

Kollmitzberg, feldspar, quartz, 117

Naarntal, Perg, feldspar, quartz, 117

Pulgarn, plagioclase, 117

St Oswald, Freistadt, feldspar, quartz, 117

Weitersfelden, feldspar, quartz, 117

Wernberg, Villach, feldspar, 117

#### England

Alston, Cumberland, galena, 110

Sherburn Hill colliery, Durham, galena, 110

#### France

Bellericq mine, Orpierre, Gap, Hautes-Alpes, galena, 140

La Gardette, Isère, quartz, 54

#### Spain (España)

Minas del Pinneo, fluorite, 145

Sierra Morena, Seville, hornblende, 204

#### Switzerland (Helvetia)

St Gotthard, quartz, 63

#### Yugoslavia (Jugoslavija)

Stari Trg mine, Trepča, galena, 110

### U.S.S.R.

Kola peninsula, baryte, 1

Tators, Caucasus, blende, galena, pyrite, 140

Urals, quartz, 123, 131

Kazakhstan, amblygonite, 1

Tyuya Muyun, Kirgizia, baryte, 1

Pamir, Tadzhikistan, quartz, 131

Slyudyanka, Irkutsk, calcite, baryte, 1

Aldan, Yakutia, actinolite, hastingsite, pargasite, 285

Tetyukhe, Primorskii Krai, danburite, 6

#### Georgian S.S.R.

Dagva, augite, 319

Mt Bakhmaro, augite, 319

Mt Rabat, augite, 319

Tashiskari, augite, 319

Vesha-Tekharo, augite, 319

Zvaro, augite, 319

### ASIA

#### Japan (Nippon)

Akiu mine, Miyagi Prefecture, pyrite, 63

Chichibu mine, Saitama Prefecture, pyrite, 63

Donsuiwa mine, Fukushima Prefecture, quartz, 63

Hanaoka mine, Akita Prefecture, pyrite, 63

Ichikawa, Fukushima Prefecture, quartz, 63

Kambe mine, Nara Prefecture, pyrite, 63

Kamikita mine, Aomori Prefecture, pyrite, 63

Kofu, Yamanashi Prefecture, quartz, 63

Komatsu mine, Ishikawa Prefecture, pyrite, 63

Kwaduzu mine, Shimoda township, Shidzoka Prefecture, inesite, 22

Mizusawa, Akita Prefecture, pyrite, 63

Naegi, Gifu Prefecture, quartz, 63

Ogosawara Island, Tokyo, pyrite, 63

Ogoya mine, Ishikawa Prefecture, pyrite, 63

Osarizawa mine, Akita Prefecture, pyrite, 63

Tsunatori mine, Iwate Prefecture, pyrite, 63

## AFRICA

- Lueshe, Kivu, Congo, amphibole (borgniezite), 312, 315  
 Marangudzi, Rhodesia, syenite, hastingsite, 291  
 Penge, South Africa, amosite, 305

## AMERICA

**Greenland**

- Skaergaard, pigeonite, 337

**Canada**

- Grenville, Quebec, phlogopite, 85

**U.S.A.**

- Beaver Bay, Lake County, Minnesota, pyroxene, 338  
 Custer Mountain mine, Custer County, South Dakota, lithiophilite, 22  
 Franklin, Sussex County, New Jersey, glaucochroite, leucophoenicite, tephroite, 22

- Keystone, Pennington County, Black Hills, South Dakota, spodumene, 222

- Moose mine, Gilpin County, Colorado, rhodochrosite, 22

- Pala, San Diego, California, spodumene, 222

- Seymour, New Haven, Connecticut, spodumene, 222

- Sterling Hill, Sussex County, New Jersey, sussexite, 22

- White Picacho district, Yavapai County, Arizona, lithiophilite, 22

## AUSTRALIA

**New South Wales**

- Budthingeroo, metadiabase, amphibole, plagioclase, 189

- North mine, Broken Hill, rhodonite, 22

**Tasmania**

- Mt Wellington, pigeonite, 338

## Alphabetical Index

Names of Authors are printed in SMALL CAPITALS, Subjects in lower-case roman, Localities in *italics*.

- Absorption ellipsoid, orientation of in alkali amphiboles, 315  
Absorption spectra of manganese minerals, interpretation of, 22  
Acmite, synthetic, cell dimensions, 335, 337; effect of pressure on melting, 335  
Actinolite, crystal-field stabilization energy and ordering of iron in, 170; *Yakutia*, anal., opt., 285  
ADDISON (W. E.) and SHARP (J. H.), Redox behaviour of amosite, 305  
Aegirine, definition of, 212  
Aegirine-diopside redefined, 212  
Aegirine-hedenbergite redefined, 212  
*Akiu mine, Miyagi Prefecture, Japan*, pyrite, 63  
*Albtal, Schwarzwald, Germany*, feldspar, 117  
*Aldan, Yakutia, U.S.S.R.*, actinolite, hastingsite, hornblende, pargasite, 285  
*Alston, Cumberland, England*, galena, 110  
Amblygonite, *Kazakhstan*, electron paramagnetic resonance spectrum, 1  
Amosite, *South Africa*, anal., oxidation and reduction, 305  
Amphiboles, magnetic susceptibility of, observed and calculated, 184; variation of composition with metamorphic grade, 189; distribution of Mg and Fe between pyroxenes and, 338; classification of, 232  
Amphibole, synthetic NaCo, structure, 334  
Amphibolite facies, temperature boundary, 338  
*Ankogel, Salzburg, Austria*, feldspar, 117  
Anthophyllite, crystal-field stabilization energy and ordering of iron in, 170  
Arfvedsonite, high-alkali, 337; *Russia*, anal., opt., cell-dimensions, paragenesis, 261  
ARMING (H.) and PREISINGER (A.), Inclusions of gases in minerals, 117  
Arsenic, bond strengths in, 6  
Augite, definition of, 212; *Georgian S.S.R.*, anal., opt., 319  
BABKINE (J.), BOLFA (J.), REITHLER (J. C.) and ZELLER (C.), Étude magnétique de pyroxènes et d'amphiboles, 184  
BANCROFT (G. MICHAEL) and BURNS (R. G.), Applications of the Mössbauer effect to mineralogy, 36  
BANFIELD (J.) and SEAGER (A. F.), Crystal growth of galena, 110  
Baryte, *Kola, Slyudyanka, and Tyuya Muyun*, electron paramagnetic resonance spectrum, 1  
*Beaver Bay, Minnesota*, pyroxenes, 337  
*Bellericq mine, Orpierre, Gap, Hautes-Alpes, France*, galena, 140  
BENNS (W.), anal. by, 305  
BERSHOV (L. V.) and MARFUNIN (A. S.), Paramagnetic resonance of electron-hole centres, 1  
BIENFAIT (M.) and KERN (R.), Thermodynamique et cinétique de formation d'une texture par nucléation dans un champ de tension, 153  
BOLFA (J.), see BABKINE (J.), 184  
Bonding, degree of covalent in Mn minerals, deduced from absorption spectra, 22  
Bonding forces in minerals, strength of, 6  
Borgniezite, *Congo*, anal., opt., x-ray, 312, 315  
Boron nitride, cubic, morphology, crystal growth, 43  
BROWN (W. L.), On synthetic lithium pyroxenes and related compounds (abstr.), 334  
Brucite, bond strengths in, 6  
*Budthingeroo, New South Wales*, meta-diabase, amphiboles, plagioclase, 189  
BUERGER (M. J.) and DOLLASE (W. A.), The possible bonding between aluminium atoms in rhodizite and other crystals (abstr.), 169

- BURNHAM (W.), The crystal structures of the ferrosilite ( $\text{FeSiO}_3$ ) polymorphs (abstr.), 334
- BURNS (ROGER G.), Crystal-field phenomena and iron enrichments in pyroxenes and amphiboles, 170; see also BANCROFT (G. M.), 36, and MUIR (I. D.), 337
- Bustamite, oriented transformation of johannsenite to, 336
- Calcite, *Slyudyanka*, electron paramagnetic resonance spectrum of, 1
- Chalcocite, bond strengths in, 6
- Chalcostibite, bond strengths in, 6
- CHERNISHEVA (E. A.), *anal.* by, 261
- CHERNYSHEVA (V. F.), see TATARSKY (V. B.), 123
- Chichibu mine, Saitama Prefecture, Japan*, pyrite, 63
- Cinnabar, bond strengths in, 6
- Clinoamphiboles, classification, 232; synthetic with  $(A+X) > 3$  and  $\text{OH} > 2$ , 337; *Congo*, *anal.*, opt., cell-dimensions, 312; *Congo*, pleochroism, orientation of absorption ellipsoid in, 315
- Clinoferrosilite, crystal structure, 334; solid solutions with hedenbergite at high temperature and pressure, 335
- Clinopyroxenes, classification, 212; variation of cell-dimensions and optics with composition, 337
- Cosmochlore, synthetic and from *Coahuila* and *Toluca* meteorites, *anal.*, opt., cell-dimensions, 323
- Covellite, bond strengths in, 6
- Crystal-field spectra of manganese minerals, 22
- Crystal habit, classification, dependence on genetic conditions, 100
- Cummingtonite, crystal-field stabilization energy and ordering of iron in, 170; location of iron in structure from Mössbauer effect, 36; synthesis, stability field, 255
- Custer Mountain mine, Custer County, South Dakota*, lithiophilite, 22
- Dagva, Georgian S.S.R.*, augite, 319
- Danburite, *Tetyukhe*, electron paramagnetic resonance spectrum of, 1
- DE BÉTHUNE (P.) and JANS (H.), On the pleochroic formula of alkali amphiboles, 315; see also JANS (H.), 312
- Deerite, symmetry of coordination of iron in, from Mössbauer effect, 36
- Dendritic growth in lead-zinc ores, 140
- Diamond, synthetic, morphology, crystal growth, 43; *Africa*, oriented inclusions in, 163, 169
- Diaspore, bond strengths in, 6
- Diopside, bond strengths in, 6; crystal-field stabilization energy and ordering of iron in, 170; synthetic, cell-dimensions, 337
- Dislocation strain, effect on crystal morphology, 13
- Distribution of Fe and Mg between co-existing orthopyroxenes, clinopyroxenes, and amphiboles, 338
- DOLLASE (W.), see BUERGER (M. J.), 169
- Donsuiwa mine, Fukushima Prefecture, Japan*, quartz, 63
- Eckermannite, synthesis, opt., cell-dimensions, X-ray, 249; high-alkali, 337; *Sweden*, X-ray, 249
- EDGAR (A. D.), The  $\alpha$ - $\beta$ - $\text{LiAlSi}_2\text{O}_6$  (spodumene) transition from 5 000 to 45 000  $\text{lb/in}^2$   $P_{\text{H}_2\text{O}}$ , 222
- Electron paramagnetic resonance spectra, 1
- Electron-hole colour centres, 1
- ENDO (Y.) and SUNAGAWA (I.), Macro- and micro-morphology of quartz and pyrite, 63
- Enstatite, inclusions of in diamond, *Africa*, 163; stability of in the upper mantle, 337
- Epidote-amphibolite facies, temperature boundaries of, 338
- ESSON (J.), *anal.* by, 222
- FABRIÈS (J.), Nature des hornblendes et types de métamorphisme, 204
- Fassaite, definition of, 212
- Feldspar, *Austria* and *Germany*, gaseous inclusions in, 117
- Ferrosilite, see Ferrosilite-III, Clinoferrosilite, Orthoferrosilite
- Ferrosilite-III (anorthic), 335; crystal structure of, 334
- Fluorite, *Germany*, *Norway*, *Spain*, and synthetic, trace elements, colour, and fluorescence in, 145
- FRANK-KAMENETSKY (V. A.) and KAMENTSEV (I. E.), Substitutional and interstitial impurities in quartz and their mineralogical significance, 131

- Franklin, New Jersey*, glaucophroite, leuco-phoenicite, and tephroite, 22
- Galena, Cumberland, Durham, and Yugoslavia*, crystal growth of, 110; *France*, skeletal growths, 140
- Garnet, inclusion of in diamond, *Africa*, 163
- Gedrite, synthesis, stability in relation to composition, 243
- GIBBS (G. V.) and PREWITT (C. T.), Amphibole cation site disorder (abstr.), 334
- Gibbsite, bond strengths in, 6
- GIELISSE (P. J.), Growth of diamond and cubic boron nitride from multi-component systems, 43
- GILBERT (M. C.), Effect of pressure on the incongruent melting of acmite (abstr.), 335
- GINZBURG (I. V.), An attempt to rationalize the classification of natural pyroxenes of space-group  $C2/c$ , 212
- Glaucophroite, *New Jersey*, absorption spectrum, 22
- Granulite facies, temperature boundaries of, 338
- Greenschist facies, stability of chlorite and quartz under hydrothermal conditions, 243
- Grenville, Quebec*, phlogopite, 85
- Gross-Eibenstein, Austria*, feldspar and quartz, 117
- Grunerite, crystal-field stabilization energy and ordering of iron in, 170; location of iron in structure from Mössbauer effect, 36; synthesis, stability field, 255; see also Amosite.
- GVAKHARIA (G. V.), Some aspects of the chemical compositions of nonalkaline monoclinic pyroxenes from effusive rocks, 319
- Hanaoka mine, Akita Prefecture, Japan*, pyrite, 63
- HARRIS (J. W.), The relative orientation of solid mineral inclusions in diamond, 163
- HARTMAN (P.), Comparison between theoretical and observed morphology of crystals with the rutile type structure, 94
- Hastingsite, *Rhodesia*, anal., opt., 291; *Yakutia*, anal., opt., 285
- Hedenbergite, crystal-field stabilization energy and ordering of iron in, 170; solid solutions with clinoferrosilite at high temperature and pressure, 335; synthetic, cell-dimensions, 337
- HENDERSON (C. M. B.), Chemistry of hastingsitic amphiboles from the *Marangudzi* igneous complex, *Southern Rhodesia*, 291
- HENRIQUES (R.), The crystal structure of olivine with reference to inclusions in diamond, 169
- Hesselbach, Bavaria*, fluorite, 145
- HINRICHSSEN (TH. J.), Hydrothermal investigations and stability relations of synthetic gedrites, 243
- Hornblende, change in composition with grade of metamorphism, 189, 204; *New South Wales*, anal., opt., trace elements, 189; *Spain*, anal., opt., cell-dimensions, 204
- HOWIE (R. A.), see STEPHENSON (D. A.), 338
- Howieite, symmetry of coordination of Fe in from Mössbauer effect, 36
- Hübnerite, synthetic, absorption spectrum, 22
- Ichikawa, Fukushima Prefecture, Japan*, quartz, 63
- Ilesite, synthetic, absorption spectrum, 22
- Inesite, *Japan*, absorption spectrum, 22
- Jadeite defined, 212
- JANS (H.) and DE BÉTHUNE (P.), The alkali amphibole of the *Lueshe* carbonatite, 312; see also DE BÉTHUNE (P.), 315
- Johannsenite, definition of, 212; oriented transformation to bustamite, 337
- Kambe mine, Nara Prefecture, Japan*, pyrite, 63
- KAMENTSEV (I. E.), see FRANK-KAMENETSKY (V. A.), 131
- Kamikita mine, Aomori Prefecture, Japan*, pyrite, 63
- Kazakhstan*, amblygonite, 1
- KEESTER (KENNETH L.) and WHITE (W. B.), Crystal-field spectra and chemical bonding in manganese minerals, 22
- Keystone, Black Hills, South Dakota*, spodumene, 222
- KIRKINSKII (V. A.), Phase transitions of enstatite in the Earth's mantle, 329
- KOBIASHVILI, anal. by, 319

- Kofu, Yamanashi Prefecture, Japan*, quartz, 63
- Kola, U.S.S.R.*, baryte, 1
- Kollmitzberg, Austria*, feldspar and quartz, 117
- Komatsu mine, Ishikawa Prefecture, Japan*, pyrite, 63
- Kongsberg, Norway*, fluorite, 145
- Kosmochlor, see Cosmochlore, 323
- KOSTOV (IVAN), Notation and genetic significance of crystal habit, 100
- KOTO (K.), see MORIMOTO (N.), 337
- KOVALENKO (V. I.), On the chemical composition, properties, and mineral paragenesis of riebeckite and arfvedsonite, 261
- KRETZ (R.), Growth of phlogopite crystals in marble from *Quebec*, 85
- Kunzite, see Spodumene
- Kwaduzu mine, Shimoda township, Shidzoka Prefecture, Japan*, inesite, 22
- La Gardette, Isère, France*, quartz, 54
- Långban, Värmland, Sweden*, richterite, 249
- LECKEBUSCH (R.), see NEUHAUS (A.), 145
- Leucophoenicite, *New Jersey*, absorption spectrum, 22
- LINDSLEY (D. H.), The join hedenbergite-ferrosilite at high pressures and temperatures (abstr.), 335
- Litharge, bond strengths in, 6
- Lithophilite, *Arizona* and *South Dakota*, absorption spectrum, 22
- Lithium silicates of type  $LiM^{3+}Si_2O_6$ , 334
- Lueshe, Kivu, Congo*, Clino-amphibole, 312, 315
- MACARA (BRENDA J.), The use of amphiboles to illustrate trends in contact metamorphism, 189
- Magnesiorichterite, cation disorder in, 334; synthesis, 337
- Manganese minerals, absorption spectra and degree of covalent bonding, 22
- Manganosite, synthetic, absorption spectrum, 22
- Marangudzi, Southern Rhodesia*, syenites, hastingsite, 291
- MARFUNIN (A. S.), see BERSHOV (L. V.), 1
- Margarite, bond strengths in, 6
- Metadiabase, *New South Wales*, mode, amphiboles in, in relation to metamorphic grade, 189
- Minas del Pinneo, Spain*, fluorite, 145
- Miyoshiroite, attempt at synthesis, 249
- Mizusawa, Akita prefecture, Japan*, pyrite, 63
- Moose mine, Gilpin County, Colorado*, rhodochrosite, 22
- MORIMOTO (N.), On the exsolution phenomena in pyroxenes (abstr.), 336; —, KOTO (K.) and SHINOHARA (T.), The oriented transformation johannsenite → bustamite, 336
- Mössbauer effect, applications to mineralogy, 36
- Mount Bakhmaro, Georgian S.S.R.*, augite, 319
- Mount Rabat, Georgian S.S.R.*, augite, 319
- Mount Wellington, Tasmania*, pyroxene, 338
- MUIR (I. D.) and BURNS (R. G.), Variations in the composition of pigeonite from *Mount Wellington, Tasmania*, and the *Skaergaard* intrusion, *East Greenland*, 337
- Muscovite, bond strengths in, 6
- Naarntal, Perg, Austria*, feldspar and quartz, 117
- Naegi, Gifu Prefecture, Japan*, quartz, 63
- NEUHAUS (A.) Über Kosmochlor (Ureyit), 323; —, RECKER (K.), and LECKEBUSCH (R.), Vergleichende Untersuchungen der Farb- und Lumineszenzeigenschaften natürlicher und gezüchteter, definiert dotierter Fluorite, 145
- NOLAN (J.), Physical properties of synthetic and natural pyroxenes in the system diopside-hedenbergite-acmite (abstr.), 337
- Norra Kärr, Årjang, Värmland, Sweden*, eckermannite, 249
- North mine, Broken Hill, New South Wales*, rhodonite, 22
- Nucleation in a field of tension, 153
- Ogasawara Island, Tokyo, Japan*, pyrite, 63
- Ogoya mine, Ishikawa Prefecture, Japan*, pyrite, 63
- Olivine, as oriented inclusions in diamond, *Africa*, 163, 169
- Omphacite defined, 212
- Orthoferrosilite, crystal structure, 334

- Orthopyroxenes, composition and cell-dimensions, 338; crystal-field stabilization energies and ordering of iron in, 170  
*Osarizawa mine, Akita Prefecture, Japan*, pyrite, 63
- Pala, San Diego, California*, spodumene, 222
- Pamir, U.S.S.R.*, quartz, 131
- Pargasite, *New South Wales*, anal., opt., trace elements, 189; *Yakutia*, anal., opt., 285
- Pendletonite, a new mineral [name only], 341
- Penge, South Africa*, amosite, 305
- PERCHUK (L. L.), Temperatures of equilibrium of amphiboles and pyroxenes in magmatic, metasomatic, and metamorphic rocks (abstr.), 338
- PHILLIPS (R.), The distribution of amphibole basic formula compositions, 337; — and ROWBOTHAM (G.), Studies on synthetic alkali amphiboles, 249
- Phlogopite, *Quebec*, morphology, development in marble, 85
- Pigeonite, crystal-field stabilization energy and ordering of iron in, 170; *Greenland, Minnesota, and Tasmania*, anal., opt., 337
- Plagioclase, *Austria*, gaseous inclusions in, 117
- POTY (L.), La croissance du quartz lamellaire sur l'exemple des cristaux de *La Gardette (Isère, France)*, 54
- POVARENENYKH (A. S.), The strength of bonding forces in mineral structures, 6
- POZHARITSKAYA (L. K.), anal. by, 261
- PREWITT (C. T.), see GIBBS, (G. V.), 334
- PREISINGER (A.), see ARMING (H.), 117
- Pulgarn, Austria*, plagioclase, 117
- Pyrite, *Japan*, surface structure of faces, 63
- Pyrophanite, synthetic, absorption spectrum, 22
- Pyroxenes, distribution of Mg and Fe between ortho-, clino- and amphibole, 338; magnetic susceptibility of, observed and calculated, 184; mechanism of exsolution in, 336; see also Clinopyroxene, Orthopyroxene
- Quartz, *Austria*, gaseous inclusions in, 117; *Isère*, lamellar growth regulated by adsorbed impurities, 54; *Japan, Switzerland*, and synthetic, surface structure of faces, 63; *Pamir, Urals*, and synthetic, impurities and cell-dimensions, 131; *Urals* and synthetic, refractive indices, 123
- Quenselite, bond strengths in, 6
- RADKEVICH (A. O.), The geochemical significance of dendritic-skeletal crystallization in polymetallic ore deposition processes, 140
- RECKER (K.), see NEUHAUS (A.), 145
- REITHLER (J. C.), see BABKINE (J.), 184
- Rhodizite, crystal structure (abstr.), 169
- Rhodochrosite, *Colorado*, absorption spectrum, 22
- Rhodonite, *New South Wales*, absorption spectrum, 22
- Richterite, synthesis, opt., cell-dimensions, 249; *Sweden*, X-ray, 249; high-alkali, 337; see also Magnesiorichterite
- Riebeckite, infra-red pleochroism, 20; cation disorder, 334; *Russia*, anal., opt., cell-dimensions, paragenesis, 261
- Rochelle salt, growth rates of, 169
- ROWBOTHAM (G.), see PHILLIPS (R.), 249
- Rosenhahnite, a new mineral [name only], 341
- Rutile, bond strengths in, 6; — structure, theoretical and observed morphology of crystals with, influence of impurities, 94
- St Gotthard, Switzerland*, quartz, 63
- St Oswald, Freistadt, Austria*, feldspar and quartz, 117
- SCHLICHTA (P. J.), The influence of dislocation-strain energy on crystal morphology, 13
- SCHNEER (C. J.) and SILVA (R.), Vectorial growth rates, statistical morphology, and the internal structure of crystals, 169
- SCHREYER (W.) and SEIFERT (F.), Synthetic amphiboles in the system  $\text{Na}_2\text{O}-\text{MgO}-\text{SiO}_2-\text{H}_2\text{O}$  and their significance for the chemistry of the natural amphiboles, 337
- SCHÜRSMANN (KAY), Synthesis and stability field of cummingtonite, 255
- SEAGER (A. F.), see BANFIELD (J.), 110
- SEIFERT (F.), see SCHREYER (W.), 337
- SERDYUCHENKO (D. P.), On the amphiboles of the hastingsite-pargasite series, 285
- Seymour, Connecticut*, spodumene, 222
- SHARP (J. H.), see ADDISON (W. E.), 305
- Sherburn Hill colliery, Durham*, galena, 110

- SHINOHARA (T.), see MORIMOTO (N.), 336  
*Sierra Morena, Seville, Spain*, hornblende, 204
- SILVA (R.), see SCHNEER (C. J.), 169  
*Skaergaard, East Greenland*, pigeonite, 337  
*Slyudyanka, Irkutsk*, baryte, calcite, 1
- SMITH (J. V.), see STEPHENSON (D. A.), 338
- Spodumene, synthesis, 334; (=  $\alpha$ -spodumene), transition to  $\beta$ -spodumene, 222; *California, Connecticut, and South Dakota*, anal., opt., X-ray, 222
- $\beta$ -spodumene, synthesis, 334; formation from  $\alpha$ -spodumene, Si-rich solid solutions, 222
- Stari Trg mine, Trepča, Yugoslavia*, galena, 110
- STEPHENSON (D. A.), SMITH (J. V.) and HOWIE (R. A.), X-ray powder diffraction data on orthopyroxenes (abstr.), 338  
*Sterling Hill, New Jersey*, sussexite, 22
- Stibnite, bond strengths in, 6
- SUNAGAWA (I.), see ENDO (Y.), 63
- Sundiusite, attempt at synthesis, 249
- Sussexite, *New Jersey*, absorption spectrum, 22
- Syenites, *Rhodesia*, modal anal., variation of amphiboles in, 291
- System  $\text{CaFeSi}_2\text{O}_6$ - $\text{FeSiO}_3$  at high pressures, 335
- System  $\text{CaMgSi}_2\text{O}_6$ - $\text{CaFeSi}_2\text{O}_6$ - $\text{NaFeSi}_2\text{O}_6$ , 337
- System  $\text{MgO}$ - $\text{FeO}$ - $\text{SiO}_2$  at high pressures, 329
- System  $\text{Na}_2\text{O}$ - $\text{MgO}$ - $\text{SiO}_2$ - $\text{H}_2\text{O}$ , 337
- Tashiskari, Georgian S.S.R.*, augite, 319
- TATARSKY (V. B.), and CHERNYSHEVA (V. F.), An investigation of natural and synthetic quartz by the Hilger-Chance refractometer, 123
- Tators, north Caucasus*, blende, galena, pyrite, 140
- Tephroite, *New Jersey*, absorption spectrum, 22
- Tetyukhe, Primorskii Krai, U.S.S.R.*, danburite, 1
- Topaz, infra-red pleochroism, 20
- Topotactic reaction johannsenite  $\rightarrow$  bustamite, 336
- Tremolite, bond strengths in, 6; crystal-field stabilization energy and ordering of iron in, 170; *Yakutia*, anal., opt., 285; aluminian, *New South Wales*, anal., opt., trace elements, 189
- Tsunatori mine, Iwate Prefecture, Japan*, pyrite, 63
- Tyuya Muyun, Kirghzia*, baryte, 1
- Urals*, quartz, 123, 131
- Ureyite, see Cosmochlore
- Vesha-Tekharo, Georgian S.S.R.*, augite, 319
- Weitersfelden, Austria*, feldspar and quartz, 117
- Wernberg, Villach, Austria*, feldspar, 117
- White Picacho district, Yavapai County, Arizona*, lithiophilite, 22
- WHITE (WILLIAM B.), see KEESTER (K. L.), 22
- WHITTAKER (E. J. W.), Classification of the amphiboles, 232
- Wölsendorf, Schwarzenfeld, Bavaria*, fluorite, 145
- X-ray powder data: eckermannite, 251; richterite, 251; spodumene, 225;  $\beta$ -spodumene, 226
- ZELLER (C.), see BABKINE (J.), 184
- ZEMANN (J.), Measurement and interpretation of infra-red pleochroism in minerals, 20
- Zussmanite, symmetry of coordination of Fe in, from Mössbauer effect, 37
- Zvaro, Georgian S.S.R.*, augite, 319